Centre for Doctoral Training in Medical Device and Health Technologies

Department of Biomedical Engineering

Development of novel antioxidant drug-free coronary artery stent coatings

Daniel Longhorn

A Thesis submitted in fulfilment of the requirements for the degree of Doctor of Engineering

2023

Declaration of authorship

This thesis is the result of the author's original research. It has been composed by the author and has not been previously submitted for examination which has led to the award of a degree.

Signed: 

Date: 25th Apr 2023

Abstract

Drug eluting stents have significantly improved patient outcomes since their introduction to widespread clinical practice in the early 2000s, but significant complications remain including restenosis and thrombosis. These issues become particularly apparent in the late and very late stages after stent placement (>12 & 24 months), although the cause can be linked to the initial response of the vessel to stenting and failure to achieve complete re-endothelialisation. Oxidative stress offers a target for controlling the early vessel healing response and dampening pro-atherogenic inflammatory stresses.

Oxidation and activation of the enzyme Ca2+/calmodulin-dependent protein kinase II (CaMKII), a pivotal molecular switch in the transition between heath and disease in the cardiovascular system, may play a crucial role in vessel pathology following stenting. Inducing a pro-healing response by targeting oxidation and specifically CaMKII oxidation represents a novel approach that may thus improve patient outcomes.

Due to their redox-sensitive chemistry, conducting polymers may be capable of acting as scavengers of reactive oxygen species (ROS) and eliciting antioxidant benefit. Polypyrrole (PPy) presents a suitable coating due to its established biocompatibility and ability to be generated using electropolymerisation. This study aimed to reliably generate uniform PPy coatings by electropolymerisation and determine their ROS scavenging capacity. Furthermore, this study explored the response of vascular cells to PPy coatings and their effect on ROS generation and CaMKII activation.

In this study, electropolymerisation was found to be effective at generating PPy films on stainless steel wires and strips under potentiostatic and galvanostatic conditions. Scanning electron microscopy, cyclic voltammetry and electrical impedance spectroscopy were used to show that 1.3 V applied voltage and 0.5 mA maintained current were optimal for generating PPy-coated wires over 10 minutes.

All PPy coatings generated by electropolymerisation were found to demonstrate high DPPH (2,2-diphenyl-1-picrylhydrazyl) scavenging capacity, with coatings generated potentiostatically at 1.3 V also exhibiting significant scavenging activity against biologically relevant ROS.

PPy coatings were found to allow endothelial cell attachment and proliferation. The benefit of PPy on ROS generation and CaMKII activation was more limited, with no significant reduction in ROS generation in PPy-attached human coronary artery endothelial cells (HCAEC) compared with stainless steel and tissue culture plastic (TCP)-attached cells, but

PPy-coated strips generated galvanostatically at 1 mA were found to significantly decrease TNFα (tissue necrotic factor-alpha)-stimulated CaMKII oxidation in HCAECs (TCP: 1.93±0.19, vs. 1 mA: 0.75±0.06; mean fold-change c.f. unstimulated TCP attached-HCAECs, two-way ANOVA with post-hoc Sidak, $p<0.05$, $n=4$).

The results of this study establish the potential benefit of PPy as a novel antioxidant and therefore demonstrate the need for continued investigation of this material in coronary artery stent applications.

Acknowledgements

Firstly, and sincerely, I would like to whole-heartedly thank my supervisors, Dr Christopher McCormick and Dr Susan Currie, for giving me the opportunity to undertake this Doctoral research project. The work included in this thesis was a collaborative effort and wouldn't have been possible without their support, guidance, and trust. Their enthusiasm to support the project saw them take the roles of mentor, advisor and eagle-eyed scrutinisers, but their humour, character and warmth allowed them to support me personally and make the academic process a more joyful experience. I would like to extend this appreciation to all the other students in the McCormick and Currie research groups, especially, Calum, Craig, Justine, Alyssa and Keelin.

I would also like to thank EPSRC and the CDT in Medical Devices and Health Technologies for providing the funding to complete this project and extend these thanks to Carol McInnes personally for her administrative support and organisational wisdom.

There are numerous individuals that provided support for this project including the Plevin and Cunningham research groups at the Strathclyde Institute of Pharmacy & Biomedical Sciences. I would like to give special thanks to Katie Henderson for her technical support in the Department of Biomedical Engineering and her commitment for getting research back after the Coronavirus disruption, Graeme Mackenzie for his technical microscopy support, generosity and kindness, Katy McIntosh for technical support in the Strathclyde Institute of Pharmacy & Biomedical Sciences, Dr James Cobley for sharing his knowledge of redox chemistry.

A special thanks to my flatmate of 3 years and fellow EngD student, Dan, for his support and friendship, especially during the Coronavirus lockdowns, and for re-grounding me during the many troughs that come with a PhD project. Similarly, I would like to extend this gratitude to my closest friends, Lily and Clodagh, Freddie and Nicole for their encouragement and for reliably providing laughter and joy when I needed it most. I would also like to thank everyone who helped make Glasgow my home and the greatest place to live – I'll be back!

Finally, I give my greatest appreciation to my family, in particular my mum and my grandparents, for their encouragement, without which I couldn't have achieved this, nor would I be in the position to. Their pride is all the motivation needed.

Introduction and Study Overview

Atherosclerosis and coronary artery heart disease represent a significant health risk particularly in populations with aging demographics and with high prevalence of risk factors such as obesity, smoking, stress, and air pollution. This presents increasing burden to health systems globally (British Heart Foundation, 2019).

The introduction of balloon angioplasty, and later coronary artery stenting, provided a minimally invasive process by which the symptoms of atherosclerosis could be alleviated. These new processes however introduced new complexities and complications such as in stent restenosis and thrombosis (Yeh, et al. 2017).

The advancement of drug eluting stent technology reduced the incidence of complications after coronary intervention, but the mechanism of action of the eluted drugs inhibited vascular healing in parallel with preventing smooth muscle cell infiltration (Koppara, et al. 2015). Healing of the coronary endothelium is key to promoting long-term vessel health after stent placement (Finn, et al, 2007).

After any traumatic injury, including stent placement, inflammatory and reactive species stress are increased locally around the trauma site. After stent placement, the initiation of this process can be considered a trigger for the pathogenesis of restenosis (Inoue, et al. 2011). The process of inflammation and reactive stress is complex, but driven by some key proteins that act as intracellular mediators within inflammatory cells and also vascular cells. Calcium (Ca^{2+}) calmodulin-dependent protein kinase II (CaMKII) activation, via oxidation, has been linked to cardiac hypertrophy, and in vascular cells excessive activation of this protein is linked with oxidative stress and endothelial dysfunction (House & Singer, 2008). This study aims to consider new stent coatings that may dampen this inflammation and reactive species stress; promoting a pro-healing environment and arterial re-endothelialisation.

Conducting polymers present a material that could be utilised as an anti-oxidative stent coating. Their redox active chemistry allows them to be fabricated into thin coatings on a metallic substrate and also presents a potential chemical means for scavenging reactive species (Guimard, et al. 2007). In this study, the electropolymerisation of one such conducting polymer, polypyrrole, will be characterised to assess the suitability of the material and process in a coronary artery stent coating application. Furthermore, the scavenging capacity of the polymer will be assessed chemically and biologically to determine their radical scavenging capacity.

Finally, optimised polypyrrole coatings will be assessed in an *in vitro* cell culture model to determine whether this scavenging activity offers a benefit to adherent human vascular cells, and whether the benefit is mediated through targeting of CaMKII activation.

Chapter 1 – Background and Literature Review

This chapter explores the clinical background of cardiovascular disease and atherosclerosis, the current technologies for treatment, the persistent challenges for stenting and complications following implantation, novel targets for promoting pro-healing responses and new stent coating technologies to target these novel pathways. Cardiovascular disease is increasing in incidence leading to further burden on healthcare systems. It arises due to an accumulation of fatty pro-inflammatory lesions in the coronary arteries, narrowing the vessels and restricting blood flow. This depletion in blood flow to the heart leads to increasing risk of myocardial infarction without treatment.

Drug eluting stents (DES) have become the dominant approach for treating atherosclerosis over bare metal stents and the more invasive approach of bypass grafting. The introduction of drug eluting stents has reduced the rates of complications, such as thrombosis and in-stent restenosis, particularly in the short term due to the release of anti-proliferative drugs that prevent smooth muscle cell luminal infiltration (Yeh, et al. 2017). Long term complications remain, particularly from 24 months after stent placement (Kandzari, et al. 2011). Anti-proliferative drugs prevent smooth muscle cell infiltration but negatively impact endothelial cell function, limiting vascular healing and re-endothelialisation. Achieving re-endothelialisation remains the biggest correlator for long term vessel health after stent placement (Finn, et al, 2007). Novel approaches, such as the use of pro-healing designs, new elution drugs and bioresorbables, have had limited clinical efficacy and poor market uptake resulting in commercial failure.

The long term complications of drug eluting stents encourages the exploration of alternative approaches to stenting that promote re-endothelialisation. Calcium (Ca^{2+}) calmodulin-dependent protein kinase II (CaMKII) is a key mediator in health and disease and overactivation of the protein has been shown to shift cells towards pathology in many disease states (House & Singer, 2008). Excessive CaMKII activation in endothelial cells is associated with dysfunction and in smooth muscle cells, the protein is associated with proliferation; two responses relevant to stent restenosis (Toussaint, et al. 2015). Oxidative stress presents another novel target in the vessel and has been shown to increase significantly after stent placement.

Oxidation persistently activates CaMKII (Anderson, 2015). Endothelial cells are sensitive to oxidative stress causing apoptosis and increased recruitment of inflammatory cells to the stent location and oxidation in smooth muscle cells pushes a shift towards synthetic activity (Ebenebe, et al. 2018).

Targeting oxidative stress has shown mixed results with traditional antioxidants (Watt, et al. 2008), but conducting polymers may provide a new strategy by providing a material that responds to oxidative stress locally in the vessel. These polymers have established biocompatibility in other applications, a simple polymerisation process and their redox active chemistry has demonstrated antioxidant activity in chemically synthesised polypyrrole (Atah, et al. 2006).

This chapter presents the five key aims for the subsequent, which are met and explored in the subsequent chapters:

Aim 1: To reliably develop appropriate polypyrrole coatings by electropolymerisation in a range of coating formats/structures to allow use with a variety of assays and techniques. These coatings and the electropolymerisation will be characterised. (Chapter 2).

Aim 2: To measure and quantify antioxidant capacity of PPy coatings and 316L SS uncoated samples with a range of relevant ROS and nitric oxide. (Chapter 3).

Aim 3: To identify a biological *in vitro* model for the assessment of polypyrrole coatings and assays to quantify PPy's biological antioxidant potential. (Chapter 4).

Aim 4: To develop the biological cell-based model in relevant endothelial and smooth muscle cell types. (Chapter 5).

Aim 5: To identify biological antioxidant effects of PPy coatings in ECs and SMCs. Investigate any possible inhibitory effect on CaMKII that PPy coatings may have and identify any downstream consequences. (Chapter 5).

Chapter 2 – Generation and Characterisation of Polypyrrole Coatings

Polypyrrole can be generated by electropolymerisation to generate uniform coatings, this can be leveraged to reliability make stent coatings. Dopant ions are required to stabilise conducting polymers during electropolymerisation. Sodium salicylate is an anti-inflammatory drug which may offer benefits to the vascular environment, in addition to polypyrrole's antioxidant potential. Salicylate has been shown to function as a dopant for polypyrrole electropolymerisation, with coatings which when exposed to solution elute the salicylate dopant into the surrounding environment (Arbizzani, et al. 2007). The conditions to generate optimal coatings are not well characterised and vary depending on the electropolymerisation method, such as electrode materials, geometry, dopant concentration and solvent.

In this chapter, various electropolymerisation methods were used to generate polypyrrole-salicylate coatings and these coatings were characterised using scanning electron microscopy, electrochemical impedance spectroscopy, cyclic voltammetry and Fourier transform infrared spectroscopy. The elution of salicylate from polypyrrole coatings was also quantified and characterised.

The study shows that both potentiostatic and galvanostatic electropolymerisation approaches can be utilised to generate uniform polypyrrole coatings using a salicylate dopant on stainless steel wires and strips. By controlling electropolymerisation at a fixed voltage, 1.1 V (wires) and 1.3 V (strips), or current, 0.5 mA (wires) and 2 mA (strips), polypyrrole coatings can be quickly and reliably generated that exhibit no evidence of overoxidation. Drug elution kinetics from these coatings however is rapid, and therefore this application may be limited without demonstrable antioxidant benefits.

Chapter 3 – Assessing Polypyrrole Antioxidant Capacity

Conducting polymer's redox active structure suggest propensity for radical scavenging capacity. This has been demonstrated in chemically synthesised polypyrrole and conducting polymer nanoparticles, where the oxidative state of the generated polymer is tightly controlled (Hsu, et al. 2010). The antioxidant activity of electropolymerised polypyrrole has not been widely considered and has not been assessed when using salicylate as a dopant.

In this chapter, polypyrrole coatings generated under different electropolymerisation methods were assessed for broad antioxidant activity using DPPH and for specific scavenging capacity against superoxide, nitric oxide and peroxyl radicals, and hydrogen peroxide.

These chemical assays demonstrated that polypyrrole coatings possess strong antioxidant activity with high radical scavenging capacity which persisted after repeated oxidative challenge. Broad antioxidant activity was demonstrated by all polypyrrole coatings tested, but specific radical scavenging activity against biologically relevant species was dependent on the electropolymerisation method. A summary of the antioxidant activity demonstrated by different polypyrrole coatings is presented in Chapter 6. Polypyrrole broad antioxidant activity and specific scavenging was tested before and after salicylate elution and showed that antioxidant activity was not dependent on the dopant.

This study presents evidence of electropolymerised polypyrrole antioxidant activity that goes beyond what has been established in the literature, and the use of chemical assays for specific reactive species is shown as a novel and efficient method for screening for new materials.

Chapter 4 – *In vitro* model development

The use of antioxidants as a therapeutic approach for reducing the occurrence of in-stent restenosis has had limited efficacy when delivered systemically, via oral administration, or locally, via drug eluting platforms on stents (Watt, et al. 2013). Therefore, the use of any new antioxidant approach should be carefully considered and supported by significant feasibility data. Standard testing approaches are performed using in vivo test methods, typically utilising porcine models as this best reflect the biological response after human implantation.

This study uses human umbilical vein endothelial cells (HUVEC) with common analytical and imaging-based techniques, such as immunoblotting and acridine orange staining, to develop an *in vitro* method for assessing cell inflammation, CaMKII activation, adhesion and proliferation.

The techniques used in this chapter were shown to be effective at assessing CaMKII oxidation and P65 phosphorylation and HUVEC attachment. Further improvements to the methods are identified to improve method suitability for assessing cellular proliferation and measuring oxidative stress. Furthermore, stimulation with IL-1β and TNFα, two cytokines relevant in the

vessel after stent placement, were found to significantly increase inflammatory and oxidative stress in HUVECs.

Chapter 5 – *In vitro* characterisation of endothelial cell response to polypyrrole surfaces in the presence of oxidative stress

Despite the strong evidence of suitability for an in vitro model presented in Chapter 4, the use of HUVECs is not optimal and it was therefore required to establish a model more relevant to the post-implantation environment. Human coronary artery endothelial cells (HCAEC) were deemed to provide a model to assess the biological effects of interventions in vitro that better reflects the post-implantation environment. It was also unclear how the approach developed in Chapter 4 translates to assessing experimental PPy samples.

In this chapter, the method approach developed in Chapter 4 was utilised to assess the effects of PPy samples on HCAECs, with a focus on oxidative stress, P65 phosphorylation and CaMKII oxidation. The results of Chapter 4 were verified in HCAECs and IL-1β and TNFα were similarly found to significantly increase inflammatory and oxidative stress. TNFα was used in the final model due to its correlation to in-stent restenosis clinically. The relevance of the model to the human pathological environmental offers benefits over the porcine in vivo models without the complexity of performing animal studies.

Cells cultured on PPy generated by galvanostatic electropolymerisation showed no significant difference in oxidative stress, and a significant reduction in CaMKII after TNFα simulation vs. cells cultured on tissue culture plastic. Interestingly, cells cultured on PPy generated by potentiostatic electropolymerisation did not experience the same antioxidant benefit despite the coatings comparable behaviour when assessed using chemical cell-free assays in Chapter 3.

The novel findings of this study are unprecedented as the effect of conducting polymers on CaMKII has not been assessed in the literature, nor has the use of in vitro cell-based assays to assess electropolymerised PPy antioxidant activity in human cells been documented previously.

Chapter 6 – Discussion

This chapter summarises the findings of Chapter 2 – 5 and provides further consideration of the differences in electropolymerised polypyrrole coatings generated in these studies and how these differences may result in the observed antioxidant activities and resulting biological response by HCAECs.

Overall, this study provides new insight into the potential applications of polypyrrole, guidance for reliably generating uniform coatings on stainless steel substrates using potentiostatic and galvanostatic electropolymerisation, and a method for screening anti-inflammatory or anti-oxidant biomaterial coating technologies prior to commencing in vivo experimentation. These findings culminate in the finding that PPy coatings are capable of providing an attachment and pro-proliferative substrate for endothelial cells which may suppress excessive CaMKII activation associated with oxidation.

This final chapter also establishes areas of improvement for the study and focus areas for future work, including further refinement of the electropolymerisation process to improve mechanical properties and characterisation of polypyrrole antioxidant activity after exposure to more complex physiological fluids, such as blood. Ultimately, this study supports the continued investigation and characterisation of electrochemically generated polypyrrole.

List of Abbreviations

AAPH	2,2'-Azobis(2-amidinopropane) dihydrochloride
ABTS	2,2′-azino-bis(3-ethylbenzothiazoline-6-sulfonic acid)
AFM	Atomic force microscopy
AKT	Protein kinase B
ANOVA	Analysis of variants
ATR	Attentuation total reflection
BMS	Bare metal stents
BSA	Bovine serum albumin
CABG	Coronary artery bypass grafting
CaMKII	Calcium/Calmodulin-dependent protein kinase II
CE	Counter elecrode
CHD	Coronary heart disease
CP	Conducting polymers
CV	Cyclic voltammetry
DAPI	4′,6-diamidino-2-phenylindole
DAPT	Dual anti-platelet therapy
DCF	Dichlorodihydrofluorescein
DCFDA	2',7'-dichlorodihydrofluorescein diacetate
DES	Drug eluting stents
DMSO	Dimethyl sulphoxide
DPPH	2,2-diphenyl-1-picrylhydrazyl
EC	Endothelial cell
ECM	Extracellular Matrix
EGM-2	Endothelial growth medium-2
EIS	Electrochemical impedance spectroscopy
eNOS	Endothelial nitric oxide synthase
EO	Ethylene oxide
ERK 1/2	Extracellular signal-regulated kinase 1/2
FITC	Fluorescein isothiocyanate
FTIR	Fourier transform infrared spectroscopy
GSH	Glutathione
HAT	Hydrogen atom transfer
HCAEC	Human coronary artery endothelial cell
HCASMC	Human coronary artery smooth muscle cell
HSF1	Heat shock factor 1
HUVEC	Human umbilical vein endothelial cell
IFNγ	Interferon-gamma
IKK	inhibitory – κB kinase
IL-1	Interleukin-1
IL-1β	Interleukin-1 beta
IL-6	Interleukin-6
ISR	In stent restenosis
JNK	c-Jun N-terminal kinases
LTCC	L-type calcium channels
MMP	Matrix metalloproteinase
mTOR	Mammalian target of rapamycin
MTT	3-(4,5-Dimethylthiazol-2-yl)-2,5-Diphenyltetrazolium Bromide
mtROS	Mitochondrial reactive oxygen species
NaSa	Sodium salicylate
NaTS	Sodium toluene sulphonate
NBT	Nitro blue tetrazolium

NO	Nitric oxide
eNOS	Endothelial nitric oxide synthase
iNOS/NOS2	Inducible nitric oxide synthase
NF-κB	Nuclear factor-kappa B
NOX	NADPH oxidase
NSAID	Non-steroidal anti-inflammatory drug
OCP	Open circuit potential
ORAC	Oxygen radical absorbance capacity
OxCaMKII	Oxidised-CaMKII
Ox-LDL	Oxidised low-density lipoprotein
PANI	Polyaniline
PBS	Phosphate buffered saline
PCA	Principle component analysis
pCaMKII	Phosphorylated-CaMKII
PCI	Percutaneous coronary intervention
PCET	Proton-coupled electron transfer
PEDOT	Poly (3,4-ethylenedioxythiophene)
PLB	Phospholamban
PPy	Polypyrrole
pP65	Phosphorylated-P65
PT	Polythiophene
PTCA	Percutaneous transluminal coronary angioplasty
Py	Pyrrole
RE	Reference electrode
ROS	Reactive oxygen species
RyR	Ryanodine receptor
Sa	Salicylate
SA	Surface area
SDS-PAGE	Sodium dodecyl sulfate–polyacrylamide gel electrophoresis
SEM	Scanning electron microscopy
S.E.M.	Standard error of the mean
SERCA	sarco/endoplasmic reticulum Ca^{2+} ATPase
SET	Single electron transfer
SMC	Smooth muscle cell
SNP	Sodium nitroprusside
SOD	Superoxide dismutase
SS	Stainless steel
TBHP	Tert-Butyl hydroperoxide
TCP	Tissue culture plastic
TLR4	Toll like receptor 4
TNFα	Tissue necrotic factor-alpha
VEGF	Vascular endothelial growth factor
VSMC	Vascular smooth muscle cell
vWF	Von Willibrand factor
WE	Working electrode
XO	Xanthine oxidase
XPS	X-ray photoelectron spectroscopy

Contents

Figures

Supplementary Figures

Tables

1. Background and Literature Review

As outlined in the Introduction and Study Overview, the incidence of cardiovascular disease is increasing and whilst drug eluting stent technologies have improved clinical outcomes, late complications persist and the technology underdelivers for certain vulnerable patient groups, such as diabetics.

Conducting polymers present an alternative stent coating material that may offer antioxidant capabilities, dampening the inflammatory and reactive stress response after stent placement. This study assesses the potential for conducting polymer coatings to be generated by electropolymerisation, assesses their antioxidant capacity, and considered the biological effect of this antioxidant activity on vascular cells and intracellular proteins.

Chapter 1 outlines the clinical background of coronary heart disease (CHD) and the use of coronary stenting. Existing treatments and technologies are introduced along with their complications and associated issues that require intervention. The need for further research and innovation in coronary stents will thus be conveyed. This chapter also begins to explore the role of oxidative stress and Calcium/Calmodulin-dependent protein kinase II (CaMKII) in vascular biology and how this may be used to inform the development of novel coronary stenting technologies. As part of this, the chemistry of conducting polymers and their current use in biomedical engineering will also be introduced. Electropolymerisation will be explored as a potential means of generating conducting polymer stent coatings. This chapter will conclude by summarising the rationale for the study and presenting its main aims and objectives.

1.1. Cardiovascular Anatomy

Although stenting is not limited to the coronary artery, atherosclerosis is most common in these vessels leading to coronary heart disease. For this reason, this study will focus the application of novel stent coatings in these vessels. This section will outline the structure of coronary arteries, and arteries in general, along with their specific role in the heart. Where a point is made elsewhere in this report in relation to applications in other vessels, the specific application will be clearly outlined.

1.1.1. Coronary Arteries in Relation to the Heart

The coronary arteries transport blood from the aorta, through openings in the aortic valve, to the muscles of the heart. This delivery of oxygenated blood allows systolic contraction, which generates pressure to push blood from the heart to the aorta and pulmonary artery.

The anatomy of the coronary vessels in relation to the heart is shown in Figure 1.1. From the aorta, the coronary arteries compose of two major vessels, the left and right coronary arteries. These continue to branch to supply blood to a significant area of the heart surface. The left coronary artery supports the left side of the heart, providing circulation to the essential organs and the peripheral cardiovascular system, and the right coronary artery supports the left side of the heart, providing circulation to the pulmonary cardiovascular system.

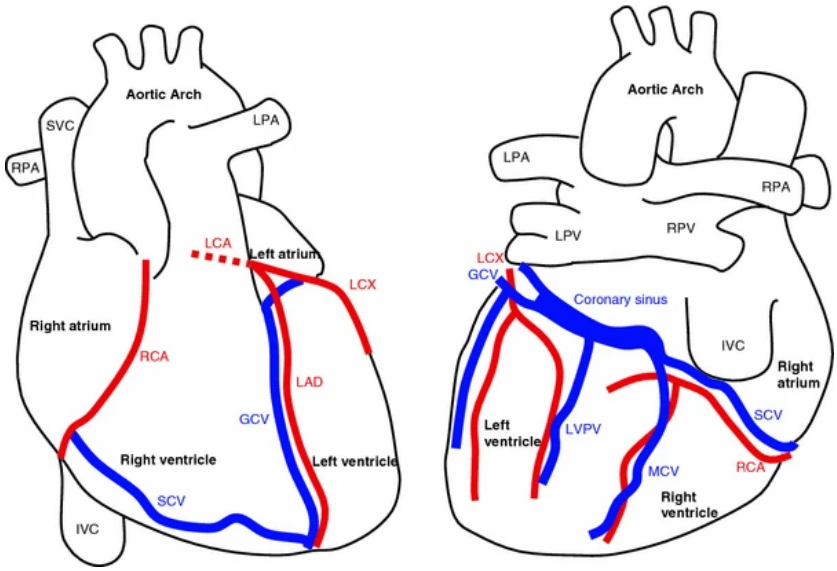

Figure 1.1. Anatomy of the heart from anterior and posterior aspects. Coronary arteries: left coronary artery (LCA), left circumflex (LCX), left anterior descending (LAD), right coronary artery (RCA). Coronary veins: coronary sinus (CS), great cardiac vein (GCV), middle cardiac vein (MCV), small cardiac vein (SCV), left ventricular posterior vein (LVPV). Pulmonary vessels: left and right pulmonary arteries (LPA/RPA), left and right pulmonary veins (LPV/RPV). Vena cava: superior vena cava (SVC), inferior vena cava (IVC). (reproduced from Lee & Smith, 2012).

1.1.2. Structural Anatomy of the Coronary Arteries

Coronary artery structure is comparable to the structure of all arteries and an overview of this structure is shown by the diagram in Figure 1.2. The structure wall is made of three distinguishable layers, the tunica intima, the tunica media, and the tunica adventitia. The internal hollow space of the lumen provides the volume for blood to be transported through.

The tunica intima consists of a single layer of endothelial cells that line the internal luminal space, with a layer of loose connective tissue beneath the endothelial cells consisting of elastin and collagen fibres.

The tunica media sits behind the tunica intima and consists of smooth muscle cells, elastin and collagen. This layer is critical to the muscular response of the vessel. The thickness of this layer is variable for different vessel sizes and the proportion elastic tissue also changes to influence the elastic response of larger vessels. This layer is particularly relevant in the pathogenesis of atherosclerosis and re-stenosis (see Section 1.2.2. and 1.3.2.)

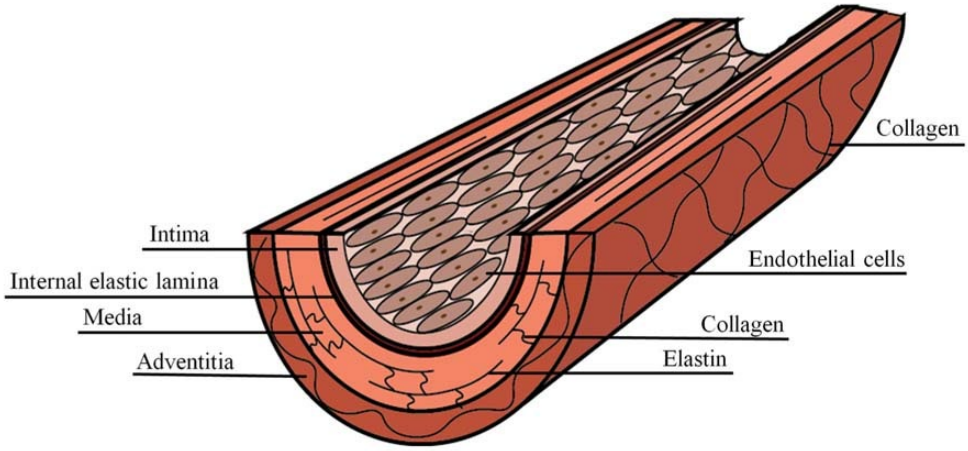

Figure 1.2. Cross-sectional structure of arteries. The overall layered structure shown here applies to all major arteries including coronary arteries. (reproduced from Kohn, *et al.* 2015).

1.2. Cardiovascular Disease

Coronary stenting is a well-established clinical intervention for the treatment of coronary heart disease. Coronary heart disease is one type of cardiovascular disease, which collectively are a leading cause of mortality in economically developed nations. Overall, cardiovascular disease leads to 27% of deaths in the UK, with this issue being particularly acute in Scotland. Despite a reduction in the number of deaths caused by cardiovascular disease by nearly 50% from 1969 to 2017, there remains an annual total cost of £19 billion per year to the UK economy (British Heart Foundation, 2019).

1.2.1. Coronary Heart Disease

Coronary heart disease (CHD) is the most prevalent and fatal cardiovascular disease. Patients with CHD will often display symptoms such as angina and shortness of breath, although many patients will only become aware of the disease after a major incident such as myocardial infarction or acute heart failure. The symptoms and mortality associated with CHD are the result of the gradual and chronic build-up of fatty plaques in the patient's coronary arteries. The resulting narrowing leads to a loss of perfusion to the conductive tissues of the heart. This build-up of plaques within the arterial walls is known as atherosclerosis and the progression of this disease can take decades before reaching a clinically identifiable and symptomatic stage.

1.2.2. Plaque Formation

Atherosclerosis is the development of fatty and calcified plaques within the vessel walls, specifically the tunica media, of arteries. These plaques can either be stable or vulnerable; both types contribute to a high risk of myocardial infarction, but vulnerable, unstable plaque increases the risk, since rupture is likely to lead to coronary thrombosis (Finn, et al. 2010).

The formation of an atherosclerotic lesion is believed to be initiated by oxidised low-density lipoprotein (ox-LDL) – harmful cholesterol that is modified by reactive oxygen species (ROS), increasing its potency. Risk factors that increase the likelihood of developing atherosclerosis include: a high cholesterol diet, high blood pressure and diabetes. Ox-LDL's presence in the

vessel induces atherosclerosis by activating endothelial cells, inducing macrophage-foam cell conversion and stimulating smooth muscle cell proliferation and infiltration (Gao, et al. 2017).

Development of an atherosclerotic lesion is a multicellular process adding to the complexity of this condition. The first apparent stage of atherosclerosis is the formation of a fatty streak within the vessel intima; consisting of an accumulation of lipids and lipoproteins, initiating a pro-inflammatory local environment. Dysfunction and activation of endothelial cells promotes the attachment and subsequent transmigration of monocytes. Once monocytes have entered the fatty intimal space, they differentiate to form phagocytic macrophages. Ideally, these cells would be able clear the accumulation of lipoproteins, however they are unable to phagocytise the modified ox-LDL and therefore it collects within the macrophages. This accumulation of ox-LDL in the macrophages results in their transformation into localised foam cells (Sakakura, et al. 2013).

In some respects, the development of atherosclerosis may be considered an inflammatory disease, since after initiation propagation occurs largely through maladaptive and excessive inflammatory responses. The continued amassing of foam cells in the lesion area acts as a source of pro-inflammatory stimulation which drives the progression of the disease, ultimately promoting the migration of smooth muscle cells into the intima and resulting in necrotic tissue damage. The resultant atheroma now carries substantial clinical risk through ischaemia and plaque rupture risk (Raggi, et al. 2018).

Early atherosclerosis can manifest as positive or negative remodelling of the vessel. During positive remodelling, the overall size of the vessel increases during plaque formation. This overall increase is vessel diameter allows the luminal diameter to be maintained and atherosclerotic positive remodelling as little impact on flow dynamics of blood through the artery. By contrast, negative remodelling involves shrinkage of the luminal space as the lesion size increases. This dramatically decreases the flow of blood through the lumen, changing the fluid dynamics of the vessel and resultant shear forces on the endothelium. This remodelling poses a greater clinical risk to the patient. The reduction in lumen size and reduction is blood flow can be estimated using angiography and is given by the fractional flow reserve, where 1 represents uninterrupted flow and 0 represents a complete vessel blockage.

Figure 1.3. illustrates the relevant cellular components and factors involved in driving progression of the atherosclerotic lesion. This clearly highlights the roles for key factors already identified, such as endothelial cell-mediated monocyte recruitment, macrophage-associated pro-inflammatory signalling and foam cell generation. It also further indicates the role of the immune response in disease progression, with the lymphocyte T-helper cells

responding to pro-inflammatory signalling by releasing interferon-gamma (IFNγ) which will act to further embed the pathophysiological state.

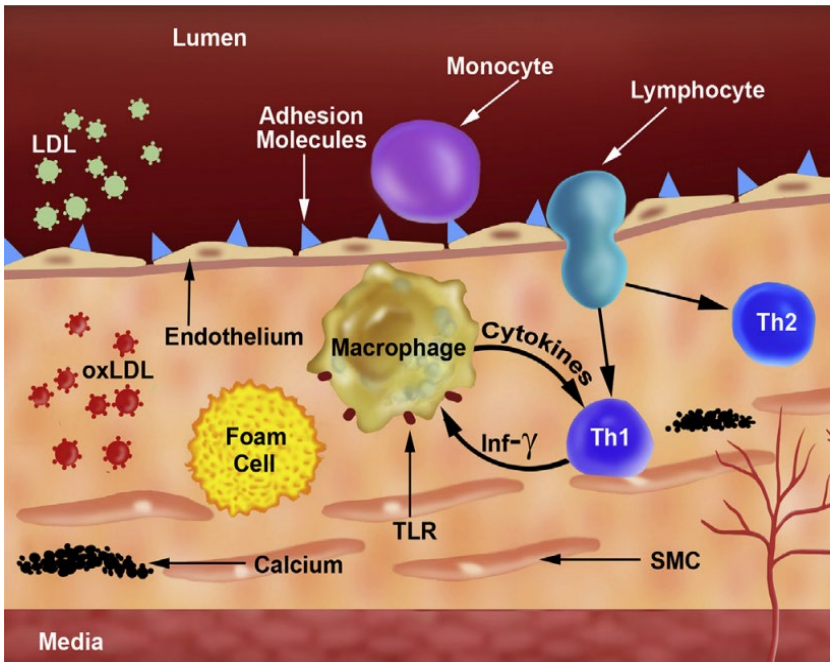

Figure 1.3. Cellular constituents and factors in the progression of atherosclerosis. LDL: low-density lipoproteins; Inf-γ: interferon-gamma; MMPs: matrix metalloproteinases; SMC: smooth muscle cells; Th1: lymphocyte T-helper 1; Th2: lymphocyte T-helper 2; TLR: toll like receptor (reproduced from Raggi, et al. 2018)

Atherosclerosis is a long-standing disease, which has been the subject of many decades of research. Consequently, there is substantial clinical and academic understanding of its causes and consequences. Such research has provided important insights that have helped inform the development of preventative strategies aimed at slowing the progression of this disease.

1.3. Surgical Intervention

Late-stage atherosclerosis has been identified as an urgent clinical issue and if left untreated carries severe life-threatening prognoses. Once established, lifestyle changes and pharmacological intervention are incapable of reversing the disease but may be capable of stopping the progression. Once life threatening, surgical intervention will be required. This can take the form of highly invasive coronary artery bypass grafting, or minimally invasive percutaneously coronary intervention – including stent placement.

1.3.1. Coronary Artery Bypass Grafts

The first routine surgical treatment for coronary heart disease was coronary artery bypass grafting (CABG). This intervention, pioneered in the 1960s by Robert Goetz, grew in use at the start of the 1980s and continues to be the preferred treatment choice for some CHD patient groups (Melly, et al. 2018). CABG involves open-heart surgery to access the heart and the blood supply is restored to the ischaemic cardiac tissues using autografts; this typically involves mammary artery or vein grafts that are sutured between the aorta and the diseased coronary artery.

Grafting using the left internal mammary or left anterior descending arteries are considered gold standard, but venous grafts may be considered if the patient's arterial sites are inappropriate for grafting. Venous grafts do however suffer from accelerated atherosclerosis driven by macrophage infiltration (Jannati, et al. 2019).

Since CABG procedures utilise autologous tissues, they have a unique set of advantages and disadvantages over percutaneous coronary interventions (PCI). Firstly, the autologous approach limits the inflammatory response to the graft. Furthermore, the grafts are placed to completely bypass the sclerotic vessel, therefore initially fully restoring blood flow to the region. Despite its advantages, the use of coronary stents has increased significantly and the proportion of patients undergoing CABG continues to reduce (Batnagar, et al. 2016). The surgical procedure of carrying out this procedure is highly invasive and involved – limiting patient suitability. Also, patients with atherosclerotic coronary vessels often do not have any adequate healthy and suitable donor vessels. Moreover, narrowing of the graft vessels may occur after placement, thereby requiring further intervention (Gaudino, et al. 2017). Despite these drawbacks, CABG may still be used for some patients with complex diseases where it is

preferred by the surgical team, such as where there is a significant risk of sclerotic lesion rupture of multiple sites of sclerosis across the coronary vessels (Yerokun, et al. 2016).

1.3.2. Percutaneous Transluminal Coronary Angioplasty

The significant risks associated with CABG led to the development of less invasive techniques. Percutaneous transluminal coronary angioplasty (PTCA) or balloon angioplasty is a procedure used to widen the blocked lumen after atherosclerosis. Here, the vessel is stretched using a balloon which is administered to the site by catheterisation - typically via the femoral artery, but also via the brachial or radial arteries. The balloon is navigated to the coronary arteries from the catheterisation site using a guidewire.

PTCA can be carried out more rapidly than more invasive treatments and typically under regional anaesthetic and mild sedation. Within the operating theatre, angiography allows the cardiologist to visualise the vessels while the heart is pumping, assisting with locating the blocked vessel and navigating the catheter tip and balloon.

The clear advantage of this technique is the accelerated recovery for the patient (van Domburg, et al. 2002). Firstly, a significantly invasive operation is replaced with catheterisation, reducing infection risk. Also, augmenting the existing tissue by balloon expansion eliminates the need for grafting of autologous tissue or placement of a medical device. This has the benefit of reducing the inflammatory response and need for healing in the locality of the intervention. However, there are significant drawbacks to this treatment, meaning that modern use of PTCA alone is not routine. In particular, PTCA is often not sufficient to fully regain a functional lumen, with the intrinsic elasticity of the vessel increasing the risk of acute arterial recoil in some patients. More commonly, a progressive remodelling of the vessel wall takes place (restenosis) leading to a reduction in lumen area, with approximately 32% of PTCA patients ultimately requiring revascularisation in the first year after surgery (van Domburg, et al. 2002).

1.3.3. Bare Metal Stents

Recurrent atherosclerosis and the emergence of restenosis necessitated a further development in the clinical treatment. Bare metal stents (BMS) were developed to mechanically prevent elastic recoil after PTCA. The use of PTCA and the placement of a stent is termed percutaneous coronary intervention (PCI). These devices have high radial and axial strength to prevent mechanical failure and appropriate radial stiffness to retain the vessel

lumen (Noad, et al. 2014). BMS are placed in the vessel immediately after angioplasty and expanded by the balloon inflation, therefore PTCA is an essential component of the stent implantation process. The process of catheterisation and navigation using guidewires is comparable for stent placement and balloon angioplasty, including surgical percutaneous entry points. An overview of the stent implantation is shown in Figure 1.4.

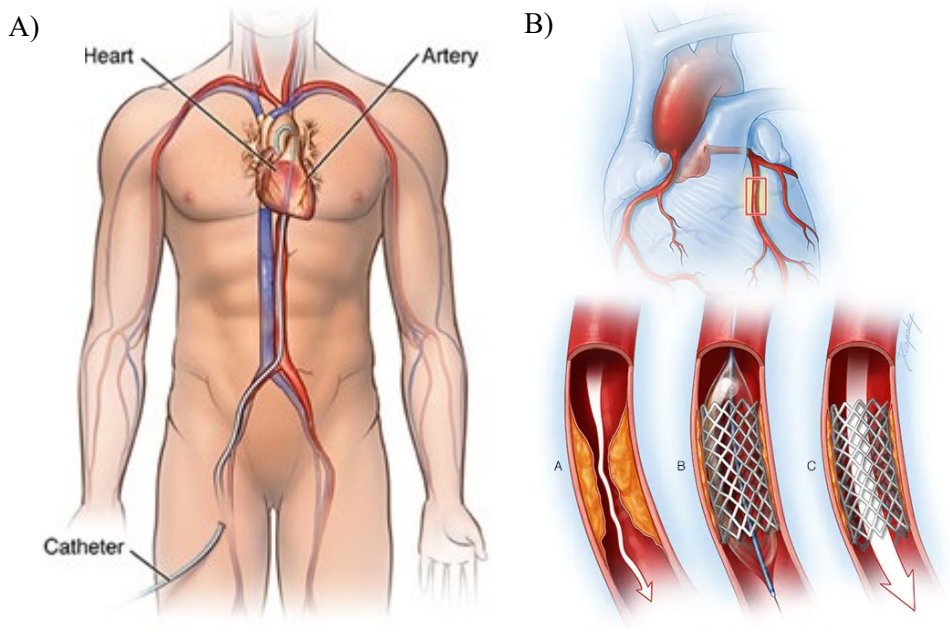

Figure 1.4. Surgical insertion process of percutaneous transluminal coronary angioplasty including: A) catheterisation [image reproduced from https://www.hopkinsmedicine .org/-/media/images/health/2_-treatment/cardiovascular/coronary-artery-disease-treatment], and B) stent expansion and placement [image reproduced from https://www.mayoclinic.org/-/media/kcms/gbs/patient-consumer/images/2013/11/15/17/37/].

All stents typically have a structure of connected rings that consist of struts that are shaped to allow for expansion, as shown in Figure 1.5.

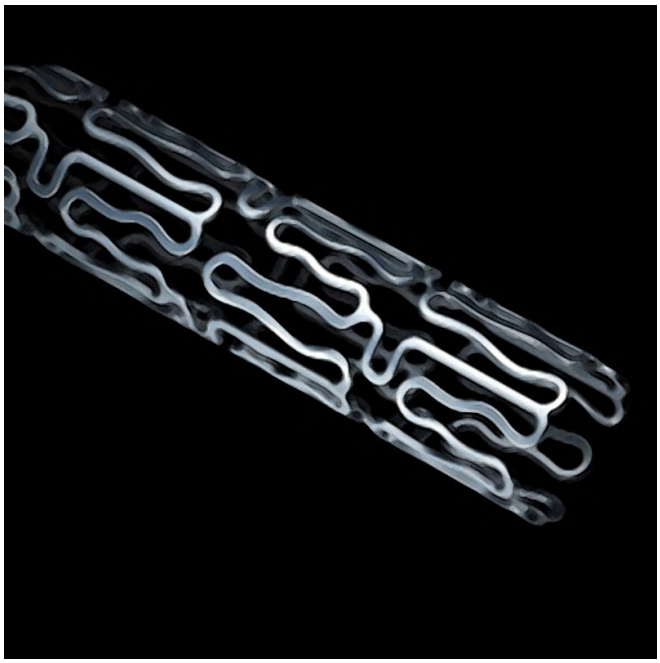

Figure 1.5. Example structure of a Co-Cr BMS (Vision, Abbott Vascular). Here, structured rings of coiled metal are visible with struts acting as connectors between the rings. [www.incathlab.com]

The struts of bare metal stents typically are between 100-150 μm for stainless steel designs and 60-100 μm for newer Co-Cr designs. Furthermore, the struts can vary in cross-sectional geometry with some early stents deploying a simple square geometry; this was succeeded by designs with more rounded corners or cylindrical struts. Co-Cr alloys were a major development in materials design for stent applications as use of this alloy allowed for the strut, and overall size of the stent, to be reduced while maintaining, or even improving the mechanical performance.

Restenosis rates were initially very high (up to 40%), leaving a significant risk of lumen loss and this complication was particularly difficult to resolve due to the presence of the inflexible metal stent embedded in the neointima (Buccheri, et al. 2017). The Benestent I clinical trial comparing the early Palmaz-Schatz stainless steel BMS with PTCA found no significant differences in clinical outcomes for the two patient groups, demonstrating the lack of significant development BMS offered (Kienmeneij, et al. 2001). Smaller and optimally shaped struts improved the clinical outcomes for stenting (Pache, et al. 2003), but major complications and risks remain when using any bare metal stents. After a one-year follow-up, the STRESS I trial found no significant differences in the outcomes of patients treated with BMS and PTCA,

but this one year follow-up likely missed issues associated with late thrombosis and restenosis and acknowledges its statistical and selection criteria weaknesses (George, et al. 1998). More modern opinion however supports the advances that BMS offered over balloon angioplasty and suggests that BMS presented a safe intervention strategy that overall reduced restenosis risk and the need for repeat revascularisation (Rathore, 2010).

1.3.4. Drug Eluting Stents

First Generation Drug Eluting Stents

The inherent drawbacks of both PTCA and BMS use further demonstrated the need for new treatment options and improved device options. Drug eluting stents (DES) were developed to mitigate some of these issues. Most DES have the same design features: a metal stent base structure, a polymer coating – acting as a drug delivery platform, and an anti-proliferative drug.

The first DES (CYPHER, Cordis) was first implanted in 1999, but became widely used after first regulatory approval in 2002. This device improved on BMS by coating 316L SS with multiple polymer layers loaded with sirolimus – an immunosuppressive and anti-proliferative macrolide. Sirolimus inclusion prevented the worst neointimal formation by suppressing smooth muscle cell proliferation and subsequent infiltration into the lumen. Sirolimus works by inhibiting the activation of mammalian target of rapamycin (mTOR) - a cell cycle-specific protein kinase, completely suppressing proliferation by arresting the cell cycle at G1 (Sehgal, 2003). The main issue associated with the use of an anti-proliferative is the lack of specificity, and off target effects, particularly the suppression of endothelial cell proliferation and recovery.

Although sirolimus was the first drug used with stents, paclitaxel was another drug used in first generation DES (Taxus, Boston Scientific). Paclitaxel DES comprised coatings with a single styrene-based polymer layer, again to a 316L SS substrate, loaded with paclitaxel. Like sirolimus, paclitaxel works as an anti-proliferative agent to supress neointimal formation and has uses in anti-cancer therapies. Instead of targeting mTOR, paclitaxel works by stabilising microtubules and preventing cell division (Weaver, 2014). The delayed endothelial healing attributes of sirolimus DES remain when using paclitaxel DES.

Despite the decrease in incidence of in-stent restenosis around stent placement, first generation DES were associated with an increase in late and very late thrombosis. Early thrombosis is

characterised as occurring within 1 month of placement; this can be easily prevented by administering dual anti-platelet therapy (DAPT) but occurs in roughly 1% of cases where DES or BMS are used. Similarly rates of late stent thrombosis – defined as occurring within 12 months after stent placement, were comparable with BMS and first-generation DES, but use of these DES necessitated longer and more stringent administration of DAPT (Sudhir, et al. 2013). Very late stent thrombosis demonstrated the most striking difference with BMS. This thrombosis, defined as occurring from 12 months after stent placement, had significantly higher incidence with CYPHER and Taxus stents vs. 316 L SS BMS and increased risk of very late stent thrombosis by 82% (Varenhorst, et al. 2018).

Second Generation DES

The development of second-generation DES brought many changes over the first generation. Firstly, 316L SS was replaced with Co-Cr alloys, allowing for thinner struts to be used in the designs therefore reducing the initial trauma and impact. Importantly, sirolimus and paclitaxel were replaced by sirolimus-analogues everolimus and zotarolimus. These drugs mimic sirolimus action of inhibiting mTOR activation, while reducing associated side-effects. Everolimus improves on sirolimus by being more selective to mTOR complex 1; sirolimus also inhibited mTOR complex 2, leading to activation of the kinase Akt and disrupting normal glucose metabolism, this is largely responsible for sirolimus' immunosuppressant effects (Kirchner, et al. 2004). Zoratolimus has been used exclusively with drug eluting stents after the development of Endeavour stents (Medtronic) and its therapeutic mechanism is largely comparable to everolimus.

Multiple clinical studies have demonstrated the superior performance of second-generation DES and these devices have almost entirely eliminated the use of first-generation DES. The RESOLUTE global trial assessing the efficacy of Resolute (Medtronic) zotarolimus eluting stents, but also using Xience everolimus eluting stents, found that both second-generation DES offered superior efficacy to both CYPHER and Taxus first-generation DES. The trial reported a reduction in early and late myocardial infarction, and very late stent thrombosis, but no significant difference in late stent thrombosis rates (Yeh, et al. 2017).

When all major adverse coronary events (MACE) measures are considered, treatment with zotarolimus or everolimus appears superior, however in-stent restenosis alone is found to be significantly higher with these devices. A 5-year follow up of the ENDEAVOR III trial of Endeavor stents found incidents of angiographic evidence of restenosis to be 3 times higher with these devices vs. CYPHER DES (Kandzari, et al. 2011). This has been confirmed in

further studies (Maeng, et al. 2012), but the progression of the restenosis is believed to be slowed in zotarolimus eluting stents.

Overall, second-generation DES significantly improved the overall efficacy of stenting and improved outcomes for PCI, dramatically increasing its use in the clinic. Despite this, issues remain, particularly the incidence of long term in-stent restenosis and the requirement for long courses of DAPT after placement.

Third generation DES

With second-generation DES many of the most significant disadvantages of DES and PCI were resolved. Third-generation DES were therefore developed to further improve and refine these designs. Engineering improvements, rather than pharmacological changes, mark the major changes in these new devices as everolimus and zotarolimus continue to be used.

One such stent, Promus Element (Boston Scientic), was engineered to improve stent deployment and outcomes by reducing the stent strut thickness and replacing Co-Cr alloys with Pt-Cr alloys, while maintaining everolimus elution. Pt-Cr alloys improved on Co-Cr with better radiopacity, mechanical properties and removed cobalt that may have led to sensitivities in some patients. The PLATINUM clinical trial assessed the efficacy of these devices and after 5 years found they were in no way inferior to Co-Cr everolimus-eluting stents in terms of clinical outcomes (Kelly, et al. 2017). Considering the advantages to surgeons of using these devices, this clinical data shows promise in their use.

Another development in this set of devices is the use of biodegradable polymer coatings as drug carriers. The Yukon Choice (Translumina) sirolimus-eluting stent is a clear example of this innovation. Here, a biodegradable polymer drug-carrier is used with a microporous textured 316L SS structure. The ISAR TEST 4 trial found that after 10 years, although there was little benefit in outcomes within the early period after stenting (<1 yr), the Yukon Choice stent resulted in lower very late stent thrombosis and overall improved outcomes at 10 year – comparable to permanent polymer everolimus-eluting stents (Kufner, et al. 2019).

Although engineering changes represent most major changes to DES, biolimus-eluting stents demonstrates that innovation is ongoing in the use of pharmacological agents for DES. BioFreedom (Biosensors Europe) is the leading biolimus-eluting stents and combines the novel drug with engineering changes to achieve a polymer and carrier-free drug-elution system (Mauler-Wittwer & Garot, 2021). This allows DAPT to be shorted and shows comparable long-term outcomes to other third generation DES (Vlachojannis, et al. 2017).

Despite improvements afforded by stent development and clinical use, the guidance for stent placement is still targeted to specific patient groups and implantation should be well planned to treat symptoms and alleviate symptoms in vessels where there is a clear benefit over the risks. One such group is for patients where angiography is used, and a fractional flow reserve greater than 0.8 is observed and the lesion is found to be stable; these patients are not recommended to undergo PCI as the risks continue to outweigh the potential benefit (Lawton, et al. 2022).

1.3.5. Innovation in Stent Design

Third-generation DES have significantly improved the clinical outcomes of coronary interventions, but side effects still remain and innovative approaches are continually being considered to reduce these. This becomes particularly important for some uniquely disadvantaged patients, such as: children and young adults, and patients with diabetes. These patients are among those recommended in the AHA guidelines not to undergo PCI (Lawton, et al. 2022).

In the case of children and young patients, research has focussed on development of bioresorbable stents; these are typically magnesium alloys or biodegradable polymers, but this loss of mechanical properties requires the stent struts to be larger in diameter (120-150 μm) (Iqbal, 2014). These design compromises, specifically around mechanical properties, along with the longevity of any therapeutic benefit are the major issues associated with these stents. Overall, early clinical data is mixed, and the ABSORB II trial showed that a bioresorbable stent scaffold demonstrated non-inferiority to second-generation DES, but admitted that this reassuring clinical data will be insufficient to move clinicians away from well-established conventions (Di Mario & Caiazzo, 2015).

Despite the potential benefits offered by bioresorbable stent technologies, the Absorb product launched by Abbott and FDA approved in 2016 was commercially unsuccessful and suspended sales in 2017. Further data has shown that the use of this bioresorbable technology increased the incidence of thrombosis at all stages, with significant increases in the very late stage, likely due to its large stent strut size (150 μm) (Pradhan, et al. 2019). Biotronik (Switzerland) are the leading manufacturer of metallic resorbable designs but clinical data is limited compared with Abbott's Absorb.

A more relevant innovation to this study is the use of endothelial progenitor cell capture to increase and speed up re-endothelialisation. These devices used CD34 antigen to capture

progenitor cells that would ideally differentiate into endothelial cells to promote rapid healing (Leopold, 2013). Furthermore, this strategy has been combined with sirolimus to create hybrid DES (Ndunda, et al. 2020). Unfortunately, multiple studies found these devices failed at their intended aims and lead to significantly increased failure events vs. DES. Despite these failures, rapid and complete re-endothelialisation remains a key goal for all stent technologies.

The limited success of novel designs highlights the need for emerging technologies to be supported by robust and long-term clinical data.

1.4. Post-operative Events

In order to logically and specifically target vascular healing to improve coronary stenting outcomes, it is necessary to consider the cellular events and physiological processes that occur after stent placement. It is important to identify the normal process of healing, then crucially define the cellular and multicellular changes that characterise the shift to pathology or lack of healing.

1.4.1. Healing after Coronary Stenting

Identifying a normal physiological response to stenting is difficult for a number of reasons. Firstly, as with all immune responses, the duration and degree of the response will vary between individuals. This is further limited by a lack of systematic clinical data, since many clinical trials focus on specific devices or record very closely defined clinical observations. Another weakness in the literature is that data is typically normalised to set follow-up times (e.g. 9, 24 and 48 months), and observations are limited by the imaging and surveillance techniques deployed.

Nevertheless, *in vivo* animal studies and human clinical follow-ups give indications to the process of re-endothelialisation and this can be confirmed with autopsy data. During surgery, denudation of the endothelium occurs with a high proportion of the endothelial layer completely removed. Ideally, the endothelial cells will proliferate and quickly restore the integrity of the lumen. There is no set time by which re-endothelialisation must occur, but it is widely believed that complete re-endothelialisation between 1 and 12 months after stent placement will significantly reduce the risk of restenosis (Finn, et al, 2007). This link has been established in autopsy studies, with a strong negative correlation between % of uncovered stent and neointimal thickness observed ($r=-0.60$, $p<0.005$) (Nakazawa, et al. 2008). Interestingly, the correlation between neointimal formation and stent coverage was stronger than between neointimal formation and implant duration; suggesting stent coverage is the major driver in restenosis.

The aim for re-endothelialisation within 1 month is challenging, as it aligns closely with the initial drug release period commonly observed with DES (Finn, et al. 2007). Swine models are the preferred *in vivo* model for restenosis, with 7 days healing in swine reflecting 1 month in human. In this model BMS (316L and Co-Cr), unlike DES, were found to reliably promote re-

endothelialisation by day 7 despite no difference being observed at day 1; confirming BMS allow endothelial proliferation after the initial cell attachment (Perez de Prado, et al. 2011).

With the use of DES, it is thought that the endothelial population is unable to recover due to the rapid release of anti-proliferative agents leading to the inhibition of mTOR in both endothelial and smooth muscle cells. This has two key negative effects in endothelial cells: the loss of vascular endothelial growth factor (VEGF) and suppressed activation of endothelial nitric oxide synthase (eNOS), leading to reduced nitric oxide availability (Cornelissen & Vogt, 2018). VEGF and eNOS are key drivers in many endothelial signalling pathways and a critical in promoting proliferation. This has also been shown to further impair endothelial function, so any endothelial barrier is incapable of regulating the underlying smooth muscle (Koppara, et al. 2015). This was further demonstrated by Habib & Finn (2015), in a rabbit model of sirolimus-eluting stents and BMS re-endothelialisation, where BMS were found to encourage a healthy endothelial phenotype; marked by increased CD 31 expression and high cell-cell barrier integrity. They suggested from this research that many stented vessels do not recover within the 2-year window of DAPT.

1.4.2. Restenosis

Restenosis can be described as the recurrence of vascular narrowing after PTCA or stenting, leading to the re-emergence of symptomatic disease. Compared with atherosclerosis, in-stent restenosis is not well understood. Despite major differences in the diseases, atherosclerosis may provide insight into the mechanism of restenosis and highlight potential therapeutic targets.

Restenosis is often defined by the tissue response which can be split into three pathological mechanisms or stages: i) elastic recoil, ii) vascular remodelling and iii) neointimal hyperplasia (Buccheri, et al. 2016). This characterisation is however more appropriate for PCTA interventions, since elastic recoil and vascular remodelling are largely eliminated after stent placement. A more useful characterisation of restenosis is made by Weintraub, (2007) when considering the inflammatory response in parallel with the process of neointimal hyperplasia. In this definition, more emphasis is given to the cellular responses, which can be split into four stages: i) thrombosis, ii) inflammation, iii) proliferation and iv) extracellular matrix production. In this definition, the inflammatory disease progression of atherosclerosis can be more closely paralleled with restenosis. This process is summarised in Figure 1.6.

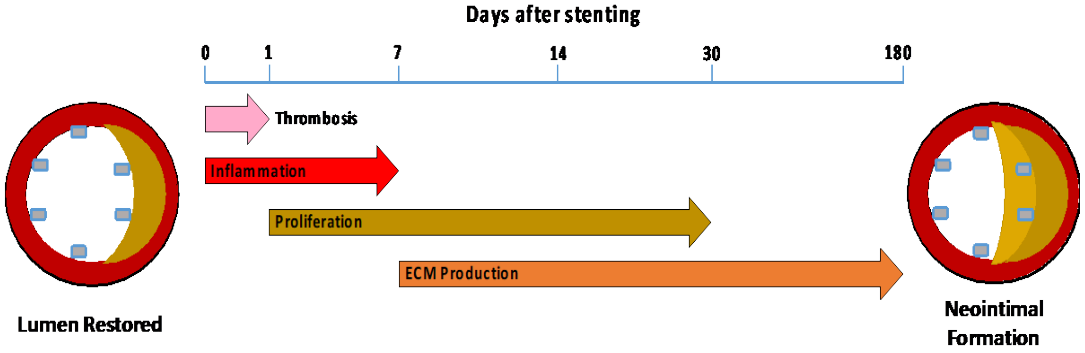

Figure 1.6. Timeline showing the events associated with pathological healing after stent placement, culminating in the development of restenosis. Adapted from: (Weintraub, 2007).

Thrombosis

The initial cellular response to mechanical injury and the denudation of the endothelium is thrombosis. This occurs in the first 24 hours after stent placement and should not be confused with in-stent thrombosis which is the clinical complication of vascular occlusion by thrombus formation. This is an important stage of healing for initiating and modulating the inflammatory response and therefore occurs in both healthy and restenosis timelines. The exposed tunica intima expresses factors to promote the attachment and recruitment of platelets and leukocytes. This process is rapid, highly localised and has been found to be highly dependent on the technique of stenting rather than the type of stent (Sakr, et al. 2016). Overall, this makes thrombosis a difficult process to target to reduce restenosis.

Inflammation

The inflammation stage of restenosis begins in the first 24 hours with thrombosis, but typically continues for at least 7 days. Here, the recruited leukocytes and activated platelets propagate the process through the upregulation of adhesion molecules and the release of pro-inflammatory cytokines, such as Interleukin-1 (IL-1), IL-6 and TGF-ß (Inoue, et al. 2011). Although crucial to the progression of restenosis, neointimal formation does not occur during the inflammatory stage and follow-up data from DES use in patients has shown that neointimal formation is typically initiated at day 7 (Chaabane, et al. 2013). This stage of restenosis is not targeted by current therapies including DES, but if properly regulated the progression of restenosis could be limited or inhibited entirely.

Proliferation

After inflammation and driven by the release of the pro-inflammatory cytokines, proliferation and migration of SMCs within the tunica media, and towards the tunica intima, occurs. This can begin within the first 7 days of the inflammation stage, and typically proceeds for 30 days after stent placement. This stage of restenosis is the inhibitory target of DES and although SMC proliferation is controlled, the underlying causes of restenosis are not eliminated by this approach.

Extracellular Matrix Production

Although characterised as neointimal formation, the initial proliferation of SMCs into the lumen does not characterise the neointimal formation observed in patients with chronic inflammation. After the proliferation of SMCs, between 1 and 6 months after stent placement, the extracellular matrix is modified and expanded by the migratory cells. It is worth noting that although this is typical within the first 6 months after stent placement, it can occur slowly and develop further into the long-term.

Significantly, these smooth muscle cells begin a process of activation and display a synthetic SMC phenotype (Kibos, et al. 2007). These cells then produce the extracellular components, predominantly: proteoglycans, collagen I and III and matrix metalloproteinases (MMPs), the proportions of which, do not reflect normal ECM. Importantly, the MMPs that are released allow the SMCs to continue to remodel the neointima and surrounding vessel walls (Chaabane, et al. 2013). The continuing infiltration of SMCs and expansion of the ECM proceeds to reduce the lumen diameter created by the stent placement. In contrast to atherosclerosis, this process typically occurs rapidly and without frequent clinical surveillance, symptoms may go unnoticed until late stages of progression.

1.5. Reactive Species

Reactive oxygen species (ROS) are a group of biological relevant chemicals with oxygen acting as the highly reactive electron donor/acceptor, they are collectively known along with reactive nitrogen species (RNS) as reactive species (RS or RNOS). ROS can be split into two categories: radical ROS and non-radical ROS (typically peroxides, but also including peroxynitrite). Importantly, ROS chemical behaviour is not determined exclusively by whether they are a radical or not. For example, superoxide ($\bullet O_2^-$) and hydroxyl (•OH) are both radicals but superoxide has relatively low reactivity, whereas hydroxyl has extremely high reactivity and will attack and modify most biological structures (Collin, 2019).

Although focus will be given in this study to ROS as mediators of cellular dysfunction, under normal circumstances ROS have significant and beneficial physiological roles. For example, the ability of immunocytes to controllably generate significant concentrations of ROS, via NADPH oxidase, is important in the innate immune response (Panday, et al. 2015), and ROS expression in the epithelium/endothelium promotes the recruitment of T cells during infection (Roy, et al. 2017). When not stressed by infection, ROS controlled at low levels have an important role in vascular cells in signal transduction by acting as second messengers (Taverne, et al. 2013). Low levels of ROS are produced during oxidative phosphorylation, a critical by-product of aerobic respiration and are therefore a critical component of vascular homeostatic (Nolfi-Donegan, et al. 2020).

ROS may be endogenous or exogenous in source. Endogenous ROS originate in the cytoplasm or the mitochondria with dominant sources including NADPH oxidase, mitochondria electron chain transfer, uncoupled endothelial nitric oxide synthase and xanthine oxidase (Munzel, et al. 2017). Exogenous sources present significant risk factors for disease and there is some evidence linking these sources more closely to cardiac disease than dysregulation of endogenous ROS (Sudgen & Clerk, 2006). These species may originate from environmental pollution, lifestyle origins such as tobacco smoke and recreational drug use. Despite the links between exogenous ROS sources in the pathogenesis of long term disease, dysregulation of, and excessive expression of, endogenous ROS has been shown to be a major patient risk factor after surgical interventions including PCI (Mathis, et al. 2022).

In normal biological systems, antioxidants work to moderate the oxidative state of the cell against excessive ROS or control their effects. There are a number of antioxidant systems that exist throughout the body and their abundance and mechanisms of action vary. Fundamentally however, antioxidants act as reducing agents and a negative feedback system against the

generation of ROS. Another mechanism employed by the mitochondria to moderate ROS production is to organise the electron transfer chain into supercomplexes, this provides an energetic advantage for non-ROS generating reactions leadings to fewer ROS generated (Novack, et al. 2020). The ubiquity of antioxidant systems in the cell, compartmentation of cell, and organisation of proteins illustrates the tight control on ROS in the cell.

1.5.1. Oxidative Stress

Oxidative stress is a term that encompasses both ROS and antioxidants and describes the pathological environment where there is an increased production of ROS or depletion of antioxidant defences. Oxidative stress in the short term may occur as a result of many physiological biochemical reactions, particularly oxidative phosphorylation during aerobic respiration. ROS production can be upregulated as an important mediator of immune response and controlled short-term increases in ROS has also been identified as a key regulator of signalling cascades in many cell types, including fibroblasts, endothelial cells, cardiac myocytes and smooth muscle cells (Pham-Huy, et al. 2008). In these scenarios, oxidative stress is observed to have an important physiological role and is highly controlled by antioxidant systems. Whereas, long-term oxidative stress has a clear pathological effect and is implicated in diabetes mellitus, cardiovascular diseases, many neurodegenerative diseases and cancers (Liguori, et al. 2018).

There are many ROS, but some are key in healthy and pathological vascular chemistry. These are shown in Figure 1.7. In this study, a strong focus will be given to superoxide and the reasons for this will be explored thoroughly. Superoxide is an abundant free radical as it is generated by NADPH oxidase in response to aerobic respiration. In normal physiological conditions it has little negative consequences as it is quickly eliminated by superoxide dismutase (SOD). Despite being a free radical, it has relatively weak reactivity but in the process of dismutation hydrogen peroxide is formed. As shown, hydrogen peroxide has fully paired electrons, but nonetheless is highly reactive and if concentrated could have cytotoxic effects on its own; or more notably, can be converted to hydroxyl radicals. In normal healthy conditions hydrogen peroxide will be reduced by glutathione peroxidase and catalase. Hydroxyl radicals have extremely strong reactivity and react strongly to modify lipids and proteins with potentially deleterious effects. From these reactions, peroxyl radicals can be formed which similarly can react strongly (Liguori, et al. 2018). Although superoxide should be regulated, in pathological conditions it can react with nitric oxide (NO) to form peroxynitrite. This decreases the availability of NO and increases the potential for damage as

peroxynitrite is more reactive than superoxide. Alternatively, superoxide may react with Fe-S clusters in proteins leading to a loss of protein tertiary structural integrity (Murphy, et al. 2022).

The downstream reactions of reactive species are critical when considering their propensity to damage the cell. Another factor to consider is the species stability or half-life, for species that have small half-lives where localisation is tightly controlled, there is low risk of cellular damage. Hydroxyl radicals have a very low half-live (approximately 1 ns), superoxide and singlet oxygen also have low half-lives, albeit considerably longer than hydroxyl (approximately <4 μs), but hydrogen peroxide has a significantly longer half-life (approximately 1 ms) (Das & Roychoudhury, 2014). This extended half-life allows hydrogen peroxide to diffuse further around the cell, or out of the cell, potentially triggering damaging reaction cascades. Due to the different reaction pathways, importance and stability of different ROS species, in this study assessment of broad ROS scavenging capacity will be supported by assessment of antioxidant activity against specific species.

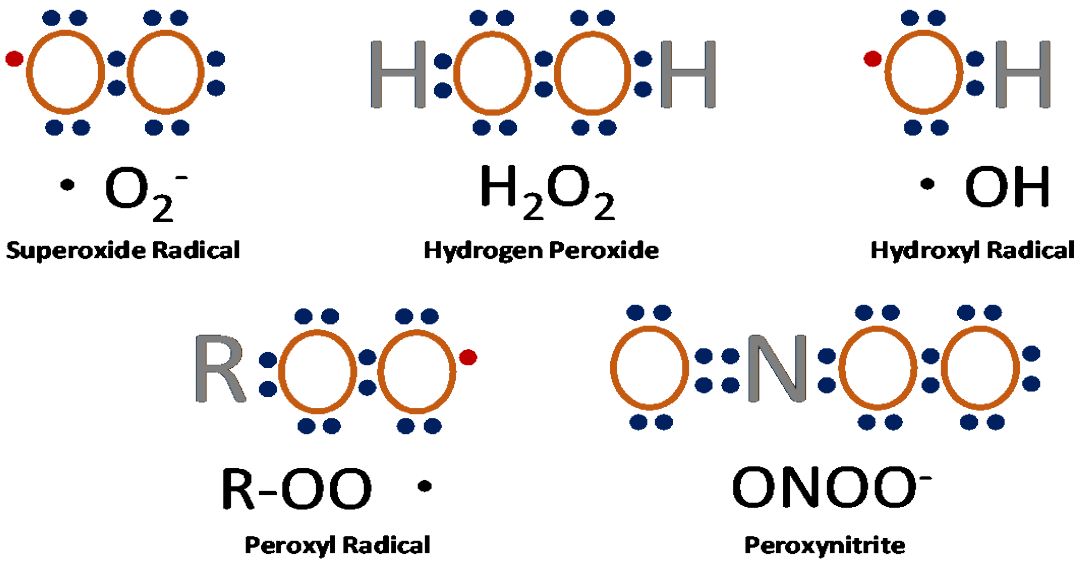

Figure 1.7. Chemical diagrams of biologically relevant ROS showing the outer electron distribution. For peroxyl radicals, R represents any protein or lipid structure carrying the peroxyl radical.

Given the breadth of ROS in terms of abundance, generation, individual reaction mechanism and effects, the use of the term oxidative stress is disputed and widely discouraged. Frequently,

oxidative stress has been used in the literature unconditionally as a pathogenic concept and many studies fail to explore the range of species or relevant pathways in question, therefore failing to properly characterise the cellular redox state (Lichtenberg & Pinchuk, 2015). In this study, the term oxidative stress will be used, but will be conditioned by defining the reactive species of interest and by discussing the limitations of any assays used.

1.5.2. Reactive Nitrogen Species

When considering redox signalling by reference to oxidative stress and ROS, nitric oxide (NO) may be overlooked. NO is a key mediator of endothelial function, but may be considered a reactive nitrogen species (RNS) alongside peroxynitrite. Overall, a consensus across cardiovascular research suggests that NO provides a strong vasoprotective effect and increasing NO production or availability offers potential treatment for atherosclerosis (Förstermann, et al. 2017). Considering the similarities between atherosclerosis and restenosis, this therapeutic effect may be relevant.

Like superoxide and other reactive oxygen species, nitric oxide can react with other entities. NO reacts with hydrogen sulphide (H_2S) to form nitroxyl radicals, these can be converted back to NO by superoxide dismutase, but also nitroxyl radicals independently have a positive effect in vascular cells by vasodilation, ROS scavenging and inhibition of inflammation (Sun, et al. 2020). NO reacts with thiol groups of cysteine residues on proteins to form S-nitrothiols. This nitrosylation reaction effects protein activity and the impact of this will depend on the protein target, the rate of reaction and regulation or reversal. S-nitrosylation is a known regulator of ryanodine receptor, matrix metalloprotein-9, and glutathione, with dysregulation a risk factor in atherosclerois and stroke and atrial fibrillation (Maron, et al. 2013). It is worth noting that NO does not readily react with thiol groups, and instead this reaction occurs through generation of a nitrosonium (NO^+) radical after NO reacts with a transition metal or other ROS, therefore S-nitrosylation is most common in high oxidative stress environments.

Despite the positive benefit of nitroxyl radicals, dysregulation of NO activity leading to reactive nitrogen stress is associated with endothelial dysfunction much in the same way as oxidative stress due to the ready generation of peroxynitrite radicals (Salisbury & Bronas, 2015).

1.5.3. Oxidative Stress in Endothelial Cells

Overall, the role of oxidative stress in cardiovascular disease has been widely reported, and already this report has identified the significance of oxidised-LDL in the progression of atherosclerosis. Hypertension is another disease that has been linked to oxidative stress in the form of NOS dysfunction, which in turn is specifically linked to endothelial dysfunction. Silva, et al. (2012) showed that uncoupling of NOS led to reduced-NO bioavailability and increased superoxide generation, ultimately forming peroxynitrite; which was shown to directly dysregulate calcium signalling in the underlying smooth muscle cells of hypertensive rats.

In endothelial cells (ECs), there is a strong potential for high concentrations of superoxide to be generated due to the quantities of enzymatic generators present. In addition to NOS, ECs express four isoforms of NADPH oxidase (NOX 1, 2, 4 and 5), with all but NOX 4 producing superoxide radicals (NOX 4 produces hydrogen peroxide) (Pignatelli, et al. 2018). Furthermore, mitochondrial ROS (mtROS) has been implicated in endothelial dysfunction and despite cellular compartmentalisation, a high degree of cross-talk between the mitochondrial and cytosolic generators of ROS has been identified (Gracia, et al. 2017). In this case, mtROS and NOX interact, generating an oxidative cycle that shifts the oxidative state to pathology and resulting in significant peroxynitrite generation. This peroxynitrite is responsible for uncoupling NOS by oxidising BH_4, a cofactor of eNOS; generating a positive feedback loop guiding the cell to apoptosis. Nitrotyrosine is formed when tyrosine is modified by ROS intermediates, including peroxynitrite and therefore is a useful marker since ROS half-lives make them difficult to measure directly (Ahsan, 2013). This suggests a relevant measure that can identify the shift from physiological signalling to pathological stress.

Lum & Roebuck, (2001) explored the effects of superoxide- and hydrogen peroxide-derived oxidative stress and found inflammatory signalling (via NF- κB) and leukocyte recruitment to be upregulated, as suggested in the atherosclerotic-oxidative stress models. Furthermore, this oxidative stress significantly increased the intracellular calcium concentration, associated calcium signalling and directly activated a number of protein kinases, such as: protein kinase C, mitogen-activated protein kinase and tyrosine kinases.

1.5.4. Oxidative Stress in Smooth Muscle Cells

Although ECs would appear to be the key target of any therapeutic effect in minimising oxidative stress, re-endothelialisation following stenting would likely take 30 days or more to complete and therefore the anti-proliferative effects of DES would need to replicated, albeit in a targeted way, during this extended period. Like ECs, smooth muscle cells (SMCs) have a high capacity to generate their own ROS, expressing the same four isoforms of NADPH oxidase (Pignatelli, et al. 2018). They are also highly responsive to ROS that can diffuse out from endothelial cells and therefore act as paracrine signals, in particular peroxynitrite.

Similar to their effects in ECs, ROS have a concentration-dependent effect in SMCs and at low cytosolic levels have an important regulatory effect in vascular homeostasis. Unlike ECs, hydrogen peroxide is the key ROS that can be up-regulated in SMCs to pathological levels (Shimokawa, 2013). At low levels, hydrogen peroxide has been found to suppress migration and differentiation (Byon, et al. 2016). Hydrogen peroxide can be generated by a number of routes, including dismutation by SOD, but in SMCs, the key driver of H_2O_2 concentration is the hyper-expression and activation of xanthine oxidase; where hydrogen peroxide forms an intermediate in the reaction of xanthine to uric acid. Pathological hydrogen peroxide production has been found to promote proliferation by activating inflammatory pathways associated with: 3-kinase, protein kinase B (AKT), extracellular-regulated kinase (ERK), c-Jun N-terminal kinases (JNK), and MAPK (Byon, et al. 2016).

Cyclophilin A is a small (20 kDa) protein that is produced in vascular SMCs, but importantly also targets SMCs, via the CyPA receptor. Cyclophilin A production, is highly dependent on oxidative signalling and is secreted via VAMP2 vesicles. Downstream signalling of CyPA binding activates AKT and ERK 1/2, which exacerbates the hydrogen peroxide-induced stress pushing the cells to proliferate (Satoh, et al. 2010). This autocrine and paracrine signalling feedback loop suggests why SMCs are sensitive to hydrogen peroxide and unable to restore a physiological phenotype. So critical to SMC pathology and coronary artery disease, cyclophilin A can be used clinically as a diagnostic biomarker and even to predict disease risk (Ohtsuki, et al. 2017).

This mechanism of hydrogen peroxide-induced oxidative damage suggests a therapeutic route for any novel antioxidant to mitigate SMC proliferation, but the differences with EC oxidation-induced pathology clearly demonstrates the importance of developing a broad antioxidant.

1.5.5. Oxidative Stress after Stent Placement

Oxidative stress has a clear pathological role in atherosclerosis and a potential role in restenosis can be proposed based on the specific pathological changes in ECs and SMCs and their relevance in disease progression. All PCI, including PTCA, induce significant oxidative stress. Kochiadakis, et al. (2010), found that in human clinical trials that the use of BMS resulted in oxidative stress, as measured by blood total peroxides. After, 24 and 48 h following stent placement blood peroxide levels were significantly elevated versus the baseline measurements. This oxidative stress, as measured systemically, was not significantly elevated after 1-month post stent placement, suggesting that the oxidative state around the BMS returned to normal, but the increase in total peroxides at 48 h correlated with late luminal loss at 6 months ($r = 0.58$).

Adversely, the use of DES generated the highest level of superoxide radicals compared with both BMS and PTCA, leading to a measurable decrease in NO bioavailability (Juni, et al. 2013). Despite positive anti-proliferative effects on SMCs, paclitaxel and sirolimus both stimulated superoxide generation through enhanced NOX activity and stimulatory effects on mitochondrial ROS generation. Compared with the first-generation DES drugs, everolimus appeared to have favourable effects but still induced significant oxidative stress when assessed by *in vitro* laboratory tests, such as: SOD and lipid peroxidation assays (Suyani, et al. 2009).

1.5.6. Oxidative Stress and Diabetes

Diabetic patients experience higher overall levels of systemic oxidative stress; this is due to a direct stimulatory effect of glucose on ECs to generate superoxide radicals along with indirect effects mediated via increased inflammatory signalling (Wright Jr, et al. 2006). In a cardiovascular context, this leaves diabetic patients particularly vulnerable to oxidative damage and reduced NO associated effects.

Patients with diabetes mellitus are associated with lower event-free survival and with the use of BMS this was found to represent a significant increase in the incidence of restenosis (37.5 vs. 28.3%; diabetes vs. nondiabetic patients, $p < 0.001$) (Elezi, et al. 1998). Although beneficial, glucose control is clinically challenging and has not eliminated the increased risks that patients with diabetes are exposed to (Kuroda, et al. 2016).

There is little clinical data that specifically compares the effectiveness of BMS vs. DES in diabetic patients, but a meta-analysis of randomised clinical trials found that the DES elucidate a beneficial response in terms of decreased late lumen loss and target lesion revascularisation (Boyden, et al. 2007). This benefit was however diminished in comparison with the benefits in non-diabetic patients and the study only followed patients until 9 months therefore had limited data to make judgements around in-stent thrombosis.

Overall, evidence in the literature supports a pathogenic role for oxidation and outlines cellular pathways which could be utilised therapeutically in both major vascular cell types. Furthermore, oxidative stress in response to stenting and a role in restenosis is evident and diabetic patients present a particularly vulnerable patient group in need of novel approaches to stent design and function.

1.5.7. Cardiovascular Cellular Targets for Oxidative Stress

Chemical species that are implicated in oxidative stress are capable of causing damage through post-translation modification of proteins at cysteine and methionine residues. Proteins that have exposed cysteine and methionine residues are therefore highly vulnerable to oxidative modification and damage. As previously identified, targets of oxidative stress vary depending on the oxidant species, but include G proteins and G-protein coupled receptors, apoptosis signalling kinase-1, ERK1/2 and JNK (Senoner & Dichtl, 2019).

Highly pro-oxidant species, such as peroxynitrite, are also capable of attacking DNA and lipids (Bartsch & Nair, 2006). DNA damage is implicated in cancer, or in extreme damage may induce cellular apoptosis. Lipid peroxidation may lead to increased cell membrane permeability and modify membrane-bound enzymes, but also lipid degradation products may further enhance ROS-associated DNA damage.

Calcium signalling is critical in many cardiovascular physiological processes and ROS are capable of modifying these processes. ROS is capable of directly enhancing calcium signalling through modification of the ryanodine receptor (RyR) via oxidation of thiol groups, leading to opening of these channels and associated Ca^{2+} release. Indirectly, oxidative stress may increase intracellular calcium release via Ca^{2+}/calmodulin dependent protein kinase II (CaMKII) activation which then targets RyR. CaMKII is directly activated in the presence of ROS through oxidation at methionine sites (Luczak & Anderson, 2014). This is discussed further in Section 1.7.

1.5.8. Antioxidant Strategies

The investigation of antioxidants for the inhibition of restenosis and improvemed PCI outcomes is not, in itself, novel, with multiple animal studies and clinical trials having been undertaken (Watt, et al. 2008). Unfortunately, the efficacy of antioxidants has been varied. This is likely due to the complexities of antioxidant therapies, with differing drugs, delivery routes and durations being used between studies. Antioxidants can be administered locally through drug elution from the surface of a stent or balloon catheter, or systemically via oral and intravenous routes. These therapies can be administered for various durations and antioxidants will vary greatly in terms of target species and mechanism of action. Such differences between studies, make interpretation of the data challenging and further research is thus required in order to enhance understanding of the potential positive and deleterious effects of anti-oxidant therapies.

Succinobucol, a derivative of probucol is approved anti-hyperlipidemic drug, is a known antioxidant with anti-platelet effects (Houston, et al. 2016). When delivered locally by DES, succinobucol was found to promote significant neointimal formation and inflammation vs. BMS in a porcine model and this was linked to cytotoxic effects associated with succinobucol (Watt, et al. 2013). When administered orally in clinical trials, both succinobucol and probucol, decreased the incidence of restenosis and major adverse events, but succinobucol was associated with fewer side effects (Tardif, et al. 2003; Liu, et al. 2015). These studies only carried out patient follow-ups for up to 6 months after stent implantation however and did not measure systemic oxidative stress markers, so these positive effects cannot be directly associated with reduced oxidative stress. They do however indicate the positive potential of targeted antioxidant use.

A consideration for local delivery via DES, and not to unique to the use of antioxidant drugs, is the effectiveness of these devices to administer sufficiently high and sustained doses to achieve robust clinical efficacy. McKittrick, et al. (2015) described how atherosclerosis in the stented vessel can limit the effectiveness of vessel uptake as lipids within the vessel wall impeded sirolimus, paclitaxel and everolimus transport, resulting in these drugs failing to reach their respective cellular targets (Tzafriri, et al. 2010).

Probucol has also been studied directly as a useful component for DES platforms. Steigerwald, et al. (2009) assessed the effects of probucol incorporation into different polymeric release

platforms. Firstly, due to its lipophilic properties, incorporations of probucol into rapamycin-eluting stents, prolonged drug release. Furthermore, it was hoped its antioxidant and anti-proliferative effect would lead to a direct anti-restenotic response *in vivo*. In Steigerwald's study, all coatings containing probucol were shown to exhibit acceptable biocompatibility but were not found to offer a significant benefit in reducing inflammation or improving re-endothelialisation after stent placement. Unfortunately, the use of probucol containing coatings also led to a significant increase in fibrin deposition compared with BMS.

The use of probucol and succinobucol and the observations of poor clinical performance do not rule out the use of antioxidants, but suggest that antioxidant benefits should may need to be better controlled and targeted. Probucol is known to scavenge superoxide and preserve nitric oxide bioavailability – two species assumed to be critical in restenosis (Bridges, et al. 1991; Jiang, et al. 2002). Therefore, it will be necessary to consider a wider range of ROS, the scavenging rates and downstream effect of scavenging.

More biologically relevant antioxidant systems have been explored and demonstrate more favourable outcomes. Durand, et al. (2005) upregulated SOD and catalase in rabbits to reduce oxidative stress after balloon angioplasty. Treated rabbits showed improved outcomes and significantly lower incidence of restenosis, suggesting reduction in superoxide- and hydrogen peroxide-induced stress could improve clinical outcomes after stenting. When considering exogenous dietary antioxidants, folic acid, a known broad antioxidant, has been administered orally after BMS placement and was found to reduce restenosis, but only in diabetic patients with highly elevated oxidative stress markers prior to stent placement (Lange, et al. 2004).

A major limitation of current antioxidant approaches is that, unlike endogenous antioxidant systems, administered antioxidants are inherently non-selective and produce indiscriminate radical scavenging action. This lack of specific action may have a harmful effect since disproportionate removal of ROS may limit its physiological role, ultimately promoting disease (Schmidt, et al. 2015). It is important to consider appropriate targets of antioxidant action, for example superoxide radicals in the endothelium and extracellular space, where extracellular SOD activity is found to be diminished in atherosclerosis and possibly restenosis (Rees, et al. 2008), and hydrogen peroxide in smooth muscle cells, which are uniquely vulnerable to hydrogen peroxide-mediated stress (Shimokawa, 2013).

A further factor to consider is the appropriate antioxidant strength or capacity of a therapeutic to offer a beneficial effect. These criteria are complicated by the varied outcomes of PCI clinically that suggests patients' responses to stent placement vary significantly. This is demonstrated by the findings presented by Kochiadakis, et al. (2009) and Juni, et al. (2013),

that type and magnitude of ROS generation after stent placement varied between patients and depending on the surgical intervention made and type of stent placed. An inappropriately high antioxidant activity may over-scavenge ROS leading to a more reducing environment that could prevent ideal physiological healing of the vessel and as such, a single level of antioxidant capacity may not be appropriate for all.

A stent coating based technology that does not rely on drug elution may alleviate some of these concerns since it's antioxidant activity would be responsive to the physiological environment and only scavenge species closely neighbouring the coatings. This responsive approach to scavenging means that ROS not neighbouring the stent are preserved, this introduces risk, but may also maintain a basal beneficial environmental with low concentrations of ROS for controlled physiological reactions.

Identifying the pathological oxidative stress levels associated with ISR *in vivo* presents further unique difficulties since ROS are highly reactive and unstable and therefore their presence in samples is transitory. This instability prevents reliable or accurate direct measurement of ROS from clinical samples, therefore measures of human oxidative stress from post-operative clinical samples rely on stable compounds or indirect measures. In animal models, some ROS may be directly measured such as superoxide generation, or the expression of proteins critical to oxidative signalling, such as NOS or SOD, can be asssessed through PCR-based assays (Juni, et al. 2013). Major clinical assays for the detection of oxidative stress measure the downstream products of oxidation, such as oxidised DNA, proteins or lipids, or alternatively measure antioxidant markers such as SOD, vitamin C and E, or glutathione (Vichova & Motovska, 2013). When compared against assays used in animal models or available for *in vitro* experiments, these techniques do not offer robust and thorough analysis or representation of the specific localised oxidative state.

1.6. Calcium/calmodulin dependent protein kinase II

Ca^{2+}/calmodulin dependent protein kinase II (CaMKII) is an enzyme that exists as different isoforms, and within each isoform, there are a number of variants that may exist. CaMKII is a protein kinase that specifically phosphorylates the hydroxyl group of serine and threonine residues. The protein exists as a complex of 12 monomer subunits, which assemble into 2 six-monomer rings that in a parallel arrangement form a dodecameric multimeric structure. This is facilitated by an association domain at the C-terminal of each monomeric subunit.

Each subunit of CaMKII contains the same 3 functional domains. Firstly, the association or structural domain as mentioned. Secondly, the kinase or catalytic domain, situated at the N-terminal of each peptide; and finally, the regulatory domain situated in between the two other domains between amino acid 273 and 314 (Griffith, 2004). In this study, the regulatory domain is of significant importance since changes in this region determine the fate of CaMKII.

CaMKII has four major isoforms: alpha (CaMKIIα), beta (CaMKIIβ), delta (CaMKIIδ) and gamma (CaMKIIγ). Each CaMKII has the same mechanistic function, but they are uniquely uncoded within the nucleus, and differ in role due to differences in expression across relevant tissue types. Within the cardiovascular system, CaMKIIδ and CaMKIIγ are the predominant isoforms and therefore are of unique interest (Ebenebe, et al. 2017).

Within the cell, CaMKII can be cytosolic or nuclear localised. CaMKII is most commonly present in the cytosol, and localisation is dependent on the isoform variants and is also affected by post-translational modification. For example, $CaMKII\delta_C$ is cytosolic, whereas $CaMKII\delta_B$ is localised to the nucleus (Mollova, et al. 2015). The ability of CaMKIIδ to be present in the cytosol or the nucleus allows it to interact with many cellular protein pathways and also directly target gene expression, giving it broad impact over cell physiology. Although, CaMKII is not membrane bound, many targets of the protein are, and therefore CaMKII is often visualised localising around membrane structures. This co-localisation also modulates CaMKII activity (Tsui, et al. 2005).

Although oxidative stress as a whole has been implicated in promoting vascular remodelling and restenosis, there are several specific signalling pathways that are thought to promote restenosis. CaMKIIδ is one protein that is involved in numerous such signalling pathways and its activation has been shown to drive neointimal formation and vascular remodelling (House & Singer, 2008). In this section, CaMKII's activation and vascular function will be considered

in terms of exploring it's appropriateness as a novel therapeutic target of any antioxidant treatment.

1.6.1. CaMKII Activation

CaMKII has a strong structural-functional relationship. In its unmodified, basal confirmation, the association and regulatory domains have an important functional role of blocking the kinase domain and therefore inhibiting its activity. This association is known as autoinhibition. Direct activation occurs when calmodulin, in the presence of Ca^{2+}, binds to the regulatory domain leading to a confirmation change that exposes the kinase domain, therefore allowing the catalytic activity. Calmodulin is a small (18 kDa) protein that activates with a cellular influx of calcium by binding up to 4 Ca^{2+} ions, leading to a a change in protein confirmation and kinetics. The ability to bind up to 4 calcium ions makes calmodulin a very capable molecular detector of increasing calcium concentrations. Experimental and modelling data suggests that the catalytic activity of any CaMKII subunit is proportional to the number of Ca^{2+} ions carried by the bound calmodulin (Pepke, et al. 2010). This further demonstrates the highly refined responsiveness of CaMKII to changing intracellular Ca^{2+} concentrations.

Calmodulin's sensitivity to Ca^{2+} makes it a critical second messenger of calcium signalling in response to inflammation and apoptosis. Intracellular calcium concentrations rapidly increase upon release from the endoplasmic reticulum in endothelial cells, or the sarcoplasmic reticulum in muscle cells, or the mitochondria in all cells. Release of calcium from the sarcoplasmic reticulum occurs through ryanodine receptor activation by high levels of luminal calcium and is a normal part of muscular contraction (Filippini, et al. 2019), but in both the endo/sarcoplasmic reticuli, the ryanodine receptor is vulnerable to oxidative modification leading to calcium leakage (Zima & Mazurek, 2016).

After direct activation, via Ca^{2+}/calmodulin binding, the regulatory domain is further exposed and further activation can occur through 2 major events. Firstly, CaMKII is capable of phosphorylating itself; in this event, highly active CaMKII kinase groups on one subunit can phosphorylate a threonine residue on neighbouring subunits. This modification to the neighbouring regulatory domain at T287 causes the subunit, and therefore CaMKII, to become perpetually active since charge changes in the regulatory domain prevent the subunit from returning to its inactive conformation. (Rellos, et al. 2010). This mechanism of persistent activation is known as autophosphorylation and this event is summarised, along with other forms of CaMKII activation in Figure 1.8. In the autophosphorylated state, CaMKII more

readily migrates into the nuclear space allowing it to target signalling at a gene expression level and therefore increase its targets (Mollava, et al. 2015).

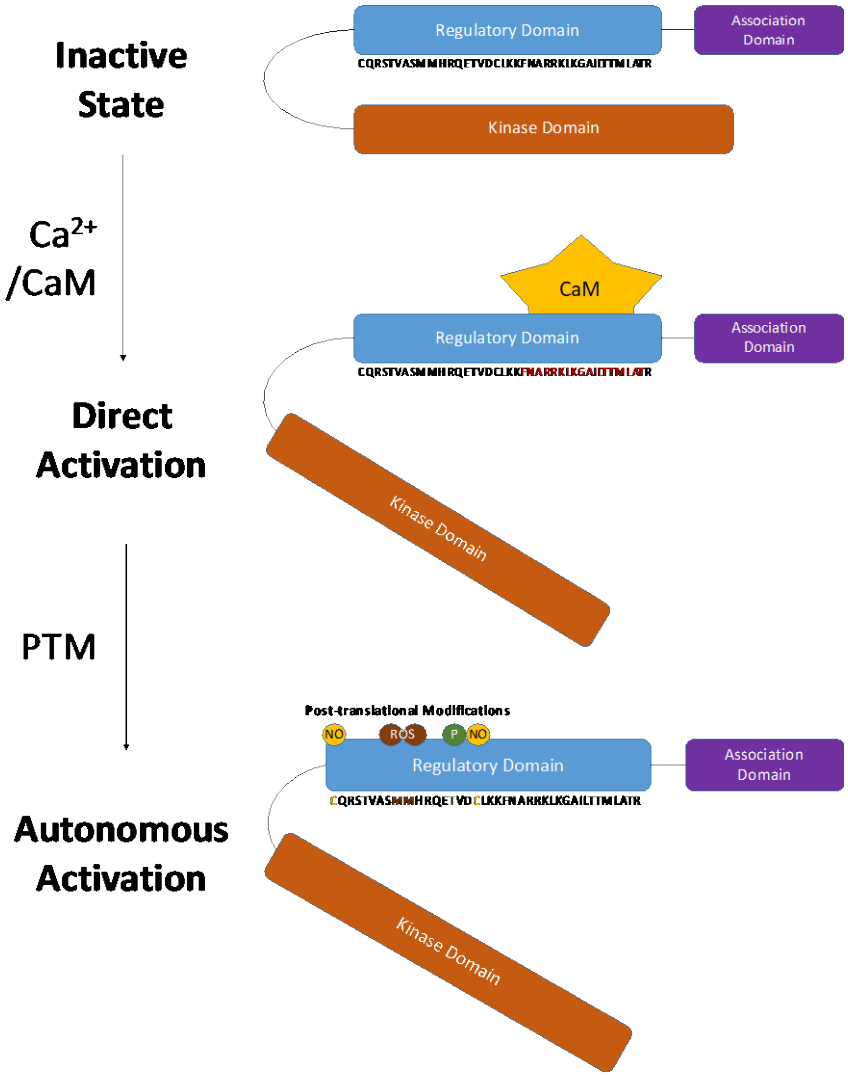

Figure 1.8. Illustration of a CaMKII functional subunit, showing the relevant mechanisms for activation. Figure adapted from: (Erickson, 2014).

The other major mechanism leading to persistent activation is when the regulatory domain is modified by other exogenous factors, mainly reactive oxygen and nitrogen species. Oxidation, specifically via hydrogen peroxide stress, has been shown to directly activate CaMKII independent of Ca^{2+}/CaM, in a similar way to CaMKII autophosphorylation (Erickson, et al. 2008). The requirement for initial Ca^{2+}/CaM binding in oxidative activation has been identified and this directly mirrors autophosphorylation. The need for direct activation appears to be in

exposing methionine residues in the regulatory domain that are susceptible to oxidative attack, these are: M281 and M282, with M282 modification leading to the most enhanced activation. Akin to autophosphorylation, oxidation leads to high levels of sustained activity that is likely relevant in CaMKII-associated pathology. CaMKII may be particularly vulnerable to oxidation as methionine residues that are in close to phosphorylation sites, as is the case within the CaMKII regulatory domain, have been shown to be preferentially oxidised in the presence of ROS (Veredas, et al. 2017).

Modification by reactive nitrogen species may be highly relevant to cardiovascular function in response to restenosis, given the role of nitric oxide in endothelial physiological and the shift to peroxynitrite generation in pathology. Interestingly, the effects of S-Nitrosylation on CaMKII are arguably more sophisticated than both oxidation and phosphorylation. Furthermore, this modification is more novel than other types of activation, and hasn't been explored thoroughly in a wider disease context.

Erickson, et al. (2015), identified S-Nitrosylation as having both an enhancing and dampening effect on CaMKII activation. This occurs because there are two cysteine residues that may be nitrosylated. Nitrosylation at C290 induces activation of the enzyme, whereas nitrosylation at C273 inhibits kinase activity. Both sites are within the CaMKII regulatory domain, but it has been suggested that the fate of CaMKII S-Nitrosylation is likely decided by whether Ca^{2+}/CaM is bound. If nitrosylation occurs before Ca^{2+}/CaM binding, modification at the C273 is favoured and this prevents Ca^{2+}/CaM binding and therefore CaMKII activation. Interestingly, C273 is unique to the delta-isoform of CaMKII suggesting its role in modifying the protein is highly specific to cardiovascular tissues expressing predominantly this isoform. The effect of activation at C290 is far more analogous to oxidation, since it autonomously activates the protein and also increases the regulatory domain's affinity for bound CaM. This modification of CaMKII may suggest a target for peroxynitrite in endothelial cells where intracellular calcium levels are high.

1.6.2. CaMKII Targets

As a kinase, CaMKII's effects come from its ability to phosphorylate downstream targets. CaMKIIα is arguably the most studied isoform due to its abundance in neuronal tissues and significant functions in the brain, but CaMKIIδ has been extensively studied for its role in cardiac health and disease. Far more research has been conducted on the heart than in the vasculature. There is abundant evidence that CaMKIIδ plays a pivotal role in the transition to

cardiac disease and there are now a number of pharmaceutical companies working on selective CaMKII inhibitors. It seems reasonable to predict that a similar scenario exists in the vasculature where sustained activation of CaMKII is linked with pathological remodelling and disease. This could have relevance to the remodelling that is observed following stent placement.

Targets of CaMKIIδ are widespread throughout a number of different cell types and include the ryanodine receptor (RyR), L-type calcium channels (LTCC), phospholamban (PLB), myofilaments, histone deacetylase 4 and other sodium and calcium transport channels (Wood, et al. 2018). The majority of these targets have calcium signalling-associated effects but the targeting of nuclear proteins may also suggest a transcriptional role for CaMKII. In cardiomyocytes, where targets are important regulators of contractility and membrane transport (RyR, LTCC and PLB), CaMKII is mostly localised around T-tubules (Zhang, 2017).

This demonstrates the limited emphasis this cardiac work can be given in context to the non-contractile cells in the wider cardiovascular system. Figure 1.9. illustrates the known localisation and targets of CaMKII in human cardiomyocytes. In these cells, CaMKII has a broad functional role due to its wide range of targets. Cytosolic CaMKII can phosphorylate the ryanodine receptor and phospholamban on the exterior sarcoplasmic reticulum membrane to facilitate the upregulation of calcium transport, or target pro-inflammatory proteins in the cytosol, such as p53, IκB kinase and calcineurin. Many of these activated pro-inflammatory proteins translocate to the nucleus where they activate protein transcription, which in turn promotes cellular disfunction and hypertrophy. CaMKII can also act directly in the nucleus to phosphorylate histone deacetylases and transcription factors, such as GATA4 and Heat shock factor 1 (HSF1). This can lead to pathological hypertrophy and disfunction, but some specific nuclear activity can also have a beneficial physiological function (Gray & Brown, 2014).

An important role in sensing and reacting to changing redox states has been suggested for CaMKII in cardiomyocytes. This has clear consequences in the events leading to restenosis, and if this signalling is to occur in endothelial and smooth muscle cells could suggest a mechanism by which CaMKII activity can be modulated for therapeutic benefit. Erickson, et al. (2011), suggests that CaMKII acts to connect multiple oxidative stress driven pathways and progress certain downstream effects, in particular Ca^{2+} overload in apoptosis, calcineurin in hypertrophy and integrates several transport channels in arrhythmias.

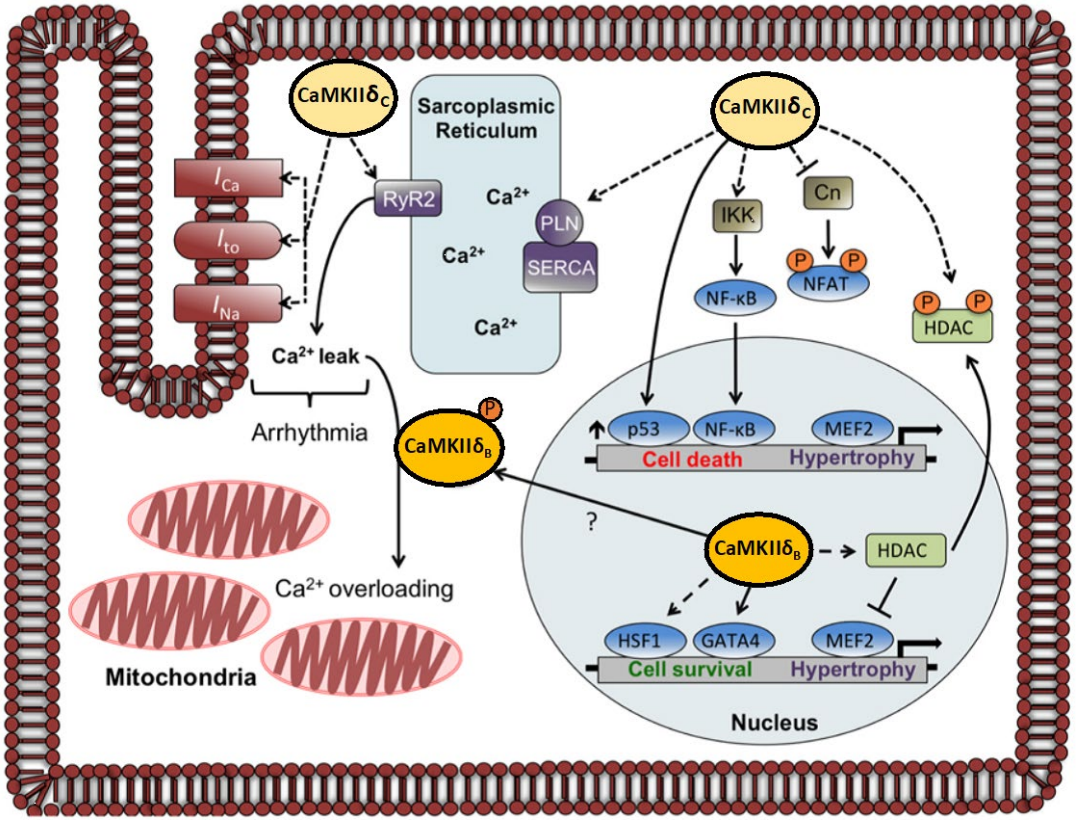

Figure 1.9. Diagram showing the localisation of CaMKIIδ in cardiomyocytes. Here, two subtypes of CaMKIIδ are shown (CaMKIIδ$_B$ and CaMKIIδ$_C$). In cardiomyocytes, CaMKIIδ is shown to act on cytosolic, nuclear, sarcoplasmic and mitochondrial targets, giving the protein a wide degree of functionality. Phosphorylation of the CaMKIIδ protein increases its activity and can change its cellular localisation. Figure adapted from: (Gray & Brown, 2014).

1.6.3. CaMKII in Cardiac Pathology

CaMKII is implicated in a range of cardiac pathologies including hypertrophy, cardiomyopathy and arrhythmias. Central to many diseases is inflammation and CaMKII has been identified as a key mediator of inflammatory stress in both contractile and structural cell types in the heart. CaMKII activation in cardiomyocytes, especially via oxidation, enhances pro-inflammatory signalling via the NF-κB pathway, but also results in histone deacetylase phosphosphorylation and p38 MAPK activation (Rusciano, et al. 2019). This has an initial pro-inflammatory effect, but also a secondary sustained effect through enhancing the production and secretion of tissue necrotic factor-alpha (TNFα), IL-1 and other cytokines. These further activate CaMKII directly and through enhanced autophosphorylation, and stimulate the mitochondria to generate ROS; ultimately forming a positive feedback loop driving disease. Similarly, in cardiac fibroblasts - which do not directly contribute to cardiac contractility but have a major role in maintaining the extracellular matrix, CaMKIIδ has been shown to directly interact with the individual inhibitory –κB kinase (IKK) to enhance NF-κB signalling; and oxidative stress via hydrogen peroxide stimulation was capable of inducing this effect (Martin, et al. 2018).

Oxidation appears to play a central role in many cardiac pathologies and in the case of myocardial infarction in mice, the infarct region shows significantly increased myocardial oxidised CaMKII in the first 24 h after the event. This has been linked to ROS generation stimulated through the activation of toll like receptor 4 (TLR4) and ischaemic injury (Anderson, 2015). Although it is important not to directly translate this finding to atherosclerosis and restenosis, high TLR4 expression has been shown in atherosclerosis, although ischaemic injury is unlikely to be relevant in many cases of restenosis (Li & Sun, 2007). It has also been described how the high activity of oxidised CaMKII in these mice led to hyperactivation of inflammatory signalling and increased incidence of hypertrophy (Anderson, 2015). This prevented recovery after infarction. The relevance in restenosis is unclear, but this mechanism of CaMKII-induced hypertrophy may extend to vascular smooth muscle cells and suggests routes of action to consider.

1.6.4. CaMKII in Vascular Pathology

Compared with the considerable evidence for a clear role in cardiac pathologies, less is clear about the significance of CaMKII in vascular disease. Fundamentally there are obstacles in determining a role for CaMKII after stenting, since there are no reported studies where intracellular calcium specifically has been monitored in vascular cells either after stenting or in the event of restenosis.

It is worth noting that there are key differences when considering the role of CaMKII in vascular pathology and cardiac pathology. Firstly, cardiac pathology is driven by overactivation of CaMKII in cardiac fibroblasts (McCluskey, et al. 2019) and cardiomyocytes (Mollova, et al. 2015). The function and structure of these cells is dissimilar to endothelial cells and vascular smooth muscle cells, and it is likely that CaMKII-associated pathways will not translate directly into these cells. However, the effects of excessive CaMKII activity in cardiac cells is hypertrophy and migration and this behaviour is particularly relevant to smooth muscle cells in the rapid progress of restenosis.

Therefore, CaMKII activity warrants consideration in this novel application. In this section, the role and targets of CaMKII are discussed in both endothelial cells and vascular smooth muscle cells.

Endothelial Cells

CaMKIIδ has been found to be highly expressed in mice and rat ECs, and fundamentally regulates intracellular Ca^{2+} dynamics by encouraging either endoplasmic reticulum Ca^{2+} release or uptake (Toussaint, et al. 2015). Under normal conditions, this function gives it a regulatory physiological role and further research has demonstrated CaMKII's involvement in regulating vascular permeability, cell barrier functions and migration. A key driver of CaMKII activation is thrombin, ECs are likely to be highly exposed to thrombin during the thrombosis and inflammation stages of healing after stent placement. This however is complicated by the finding that treating ECs with CaMKII inhibitor KN-93 before thrombosis treatment impaired endothelial permeability, suggesting CaMKII has a supportive role and this was linked to reduced ERK activation (Toussaint, et al. 2016).

The ERK signalling pathway is closely related with, and can activate directly, the NF-κB pathway. In rat aortic endothelial cells, activation of the NF-κB pathway and wider inflammatory signalling has been found to be closely associated with aging (McCluskey, et al. 2019). This study identified oxidative stress, acting through CaMKII stimulation, as a likely culprit for this increased inflammatory signalling and cellular dysregulation.

Although initially considered in the context of hypertension, the role of CaMKII in the regulation of eNOS is highly relevant to restenosis and other diseases where oxidation status is directly relevant. Evidence suggests that CaMKII can phosphorylate eNOS directly, or indirectly activate eNOS via its Ca^{2+}-dependant mechanism of activation through enhanced intracellular calcium release (Murthy, et al. 2017). CaMKII activation promotes NO production by eNOS, suggesting a positive effect. Unfortunately, the stimulation in this study is very acute (<15 minutes), and its long-term consequences are not considered. Furthermore, only CaMKII activation via phosphorylation is explored and no consideration of the effects of a possible feedback loop via CaMKII S-Nitrosylation is given. Further evidence exists suggesting that eNOS upregulation is possible via both phosphorylation or oxidation, but in the event of oxidative activation cellular increases in peroxynitrite concentration are associated, suggesting a pathological role (Cai, et al. 2008). The two fates of NO in the endothelium may go some way to explaining the dualistic effects of CaMKII activation observed in these cells. To understand CaMKII's function in endothelial cells, significance must be given to the type of activation and along with overall levels of activation.

CaMKII is directly associated with other mediators of oxidative signalling in endothelial cells. NOX5 is a calcium-dependent NADPH oxidase isoform and is a major generator of superoxide radicals (Panday, et al. 2015; Touyz, et al. 2019). Less is understood about the role of NOX5 in endothelial cells compared with the more abundantly expressed NOX1, 2 and 4 isoforms, but NOX5 is known to be expressed in these cells (BelAiba, et al. 2007). NOX5 activation in endothelial cells has been shown to promote proliferation, which would improve re-endothelialisation, but CaMKII has been shown to mediate phosphorylation and hyper-activation of NOX5, which may lead to excessive oxidative stress in a positive feedback loop (Panday, et al. 2011). This presents another pathway and target that reveals CaMKII's dualistic effects.

The localisation of CaMKII in vascular endothelial cells is presented in Figure 1.10. Here, CaMKII is shown as a cytosolic enzyme with multiple targets in the cytoplasm, but with the capacity to also target endoplasmic membrane bound proteins, such as phospholamban (PLN) and sarco/endoplasmic reticulum Ca^{2+} ATPase (SERCA), and mitochondria proteins, in turn increasing cytochrome C release and mitochondrial hyperpolarization (Ebenebe, et al. 2018; Toussaint, et al. 2016). The mobile cytosolic role for CaMKII represents the current consensus for CaMKII function in vascular endothelial cells, but the understanding of new roles continues to evolve. A critical role in controlling endothelial barrier strength by regulating

tight junctions has been suggested for CaMKII and in this role, specific localisation close to the cell membrane has been shown (Shiomi, et al. 2015).

Overall, the role of CaMKII in the ECs is complex since it positively affects NO generation and promotes migration, but negatively influences permeability and may induce apoptosis. It remains unclear how useful a target CaMKII might be reversing pathological effects in ECs because of these two opposing effects, and it must be carefully considered whether inhibiting or downregulating CaMKII in these cells would do more harm than good.

Smooth Muscle Cells

In SMCs, CaMKII targets many of the same pathways or substrates as in ECs, but with a far more physiological role, and activation associated with proliferation, migration and hypertrophy (Toussaint, et al. 2016). Calmodulin is also abundant in smooth muscle cells as activated calmodulin plays a role in controlling contractility (Tansey, et al. 1994). In smooth muscle cells, the CaMKII pathway has been shown to respond to platelet-deprived growth factor, fetal bovine serum and TNFα (Toussaint, et al. 2016).

ERK 1/2 play a critical role in mediating SMC proliferation, implicated in atherosclerosis and restenosis, and in SMCs CaMKII has been shown to activate ERK directly (Cipolletta, et al. 2010). ERK was previously implicated in the central pathological role of hydrogen peroxide in vascular SMCs and this has been further demonstrated following CaMKII targeting. Bouallegue, et al. (2009) found that knockdown of CaMKII with siRNA in primary rat SMCs attenuated hydrogen peroxide induced ERK phosphorylation. Similar effects were seen with CaMKII inhibition, via KN-93. This directly suggests that the hydrogen peroxide and CaMKII pathways are closely linked, possibly even CaMKII dependent, and identifies CaMKII as a therapeutic tool in reducing SMC proliferation.

As with ECs, CaMKII was found to directly mediate NOX5 activation in SMCs (Panday, et al. 2011). In SMCs, increased NOX5 activation was not only found to increase oxidative stress but was also implicated in driving contractility loss in these cells resulting in proliferation and migration (Furmanik, et al. 2020). This study indicated the expression of NOX5 in synthetic SMCs present in human atherosclerotic lesions, demonstrating its clinical relevance. Overall, NOX5's calcium-dependence and CaMKII-mediated hyper-activation presents a target linking calcium and oxidative signalling, and a potential driver in EC and SMC pathology.

Unlike ECs, SMCs express inducible NOS (iNOS). Importantly, the activation of iNOS is completely Ca^{2+}-independent, unlike eNOS. CaMKII directly regulates iNOS activity through phosphorylation at a transcriptional or post-translation state, leading to either increased

transcription and enzyme production, or enzyme inhibition (Jones, et al. 2007). Since iNOS offers a useful antioxidant protection for SMCs, CaMKII action inhibiting this activity is likely to have a negative effect. Cytosolic inhibitory action was associated with high levels of CaMKII activation, while nuclear activity was found in a basal state, therefore suggesting this effect may be related to the pathophysiological switch in CaMKII function at high activity levels. Although useful when considering oxidative stress, the role of iNOS in SMCs is unlikely to be as critical as eNOS in ECs, since hydrogen peroxide is implicated as the main driver of disease in these cells.

The localisation and targets of CaMKII in vascular smooth muscle cells is highlighted in Figure 1.10. Through similar action to the endothelial CaMKII, it is shown that in smooth muscle cells, cytosolic CaMKII can act on cytoplasmic, sarcoplasmic and mitochondrial targets to impart multiple physiological effects. In these cells, CaMKII is also known to have a clearer nuclear function in phosphorylating Raf1, an important promoter of proliferation and can also directly target membrane bound L-type Ca^{2+} channels promoting calcium influx leading to changes in migration and contractility (Toussaint, et al. 2016).

Overall, oxidised-CaMKII controls redox balance in these cells and CaMKII contributes to ROS generation through enhanced mitochondrial activity (Anderson, 2015). This suggests that CaMKII has a central role in a positive feedback system pushing the cells towards pathology.

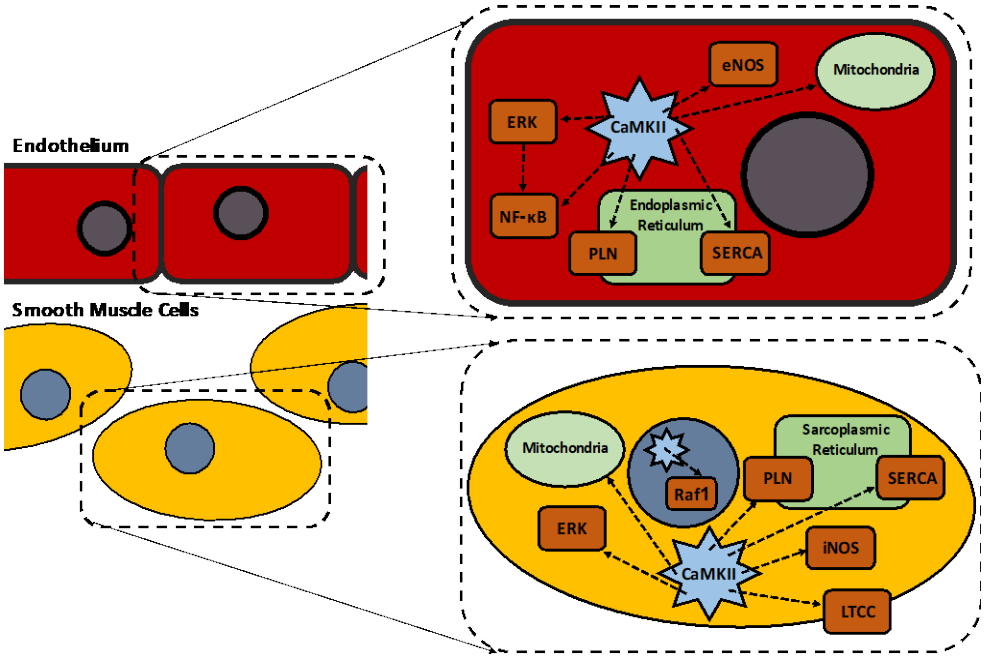

Figure 1.10. Diagram showing the localisation and major targets of CaMKIIδ in arterial endothelial and smooth muscle cells. In endothelial cells, CaMKIIδ is shown to act on cytosolic, endoplasmic and mitochondrial targets, leading to a number of different physiological outcomes. Similarly, CaMKIIδ can act on cytosolic, sarcoplasmic, mitochondrial and nuclear targets, instigating a variety of physiological effects. In both cell types, CaMKII activation is associated with migration, proliferation and apoptosis. Figure adapted from: (Ebenebe, et al. 2018 & Toussaint, et al. 2016).

1.6.5. CaMKII in Diabetes

Diabetes has been identified as in important contributor to the healing response after stent placement and it is also known to have an influence on CaMKII. An important contributor in the relationship between diabetes and CaMKII is the ability for hyperglycaemia to activate CaMKII via O-GlcNAcylation, this association has limited influence on restenosis since blood glucose should be closely monitored and interventions made accordingly after stent placement. However, the unique oxidative stress experienced by diabetic patients remains and targeting CaMKII to reduce activation in diabetic mice has shown improved outcomes in cardiac pathologies such as arrhythmias, hypertrophy and reduced overall levels of inflammation (Hegyi, et al. 2019). The role of glucose and diabetes remains highly novel and the likely significance of CaMKII in the cardiovascular function of diabetics will become more clear over time.

1.7. Conducting Polymers

Currently, the majority of patients undergoing PCI are treated using DES. It has been shown that this approach has significant limitations and is unsuitable for some key patient groups, such as those with diabetes mellitus and significant atherosclerosis. In patients who are suitable for DES platement, issues around very late restenosis and thrombosis remain, and materials used in DES platforms may trigger specific immune responses or hypersensitivity (Otsuka, et al. 2015). Furthermore, the DES platforms have manufacturing limitations with polymer dipping or spraying generating patchy or excessively thick coatings (Okner, et al. 2009). As such, there is opportunity for new materials or fabrication approaches to be developed that provide improved manufacturing reliability and provides biological benefits, such as antioxidant benefits or targeting of specific key biological mediators.

Conducting polymers are organic compounds with conductive metallic-like electrical properties. They are formed of repeated monomer units, arranged in long chains, typically with a hydrocarbon backbone. As a class of materials, they can be highly varied in terms of properties and many different conducting polymers exist, which can be divided into the 3 sub-groups shown in Figure 1.11.

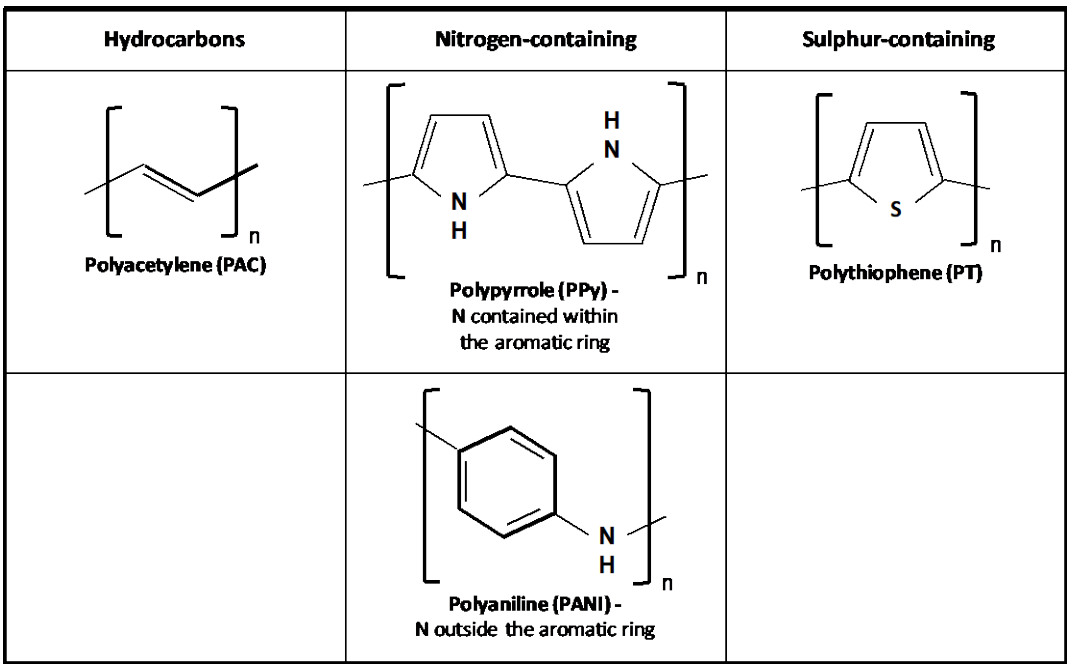

Figure 1.11. Chemical structures of repeat units of simple and common conducting polymers. Conducting polymers can be grouped based on the presence of nitrogen or sulphur within their chemical structure. The unique properties of conducting polymers can be associated with their chemical structure.

Firstly, the simplest conducting polymers are the hydrocarbons, including polyacetylenes and polyvinyls. These polymers have garnered little interest in biomedical applications and their use is not widely reported within the scientific literature. Then, there are sulphur-coating conducting polymers, such as: polythiophene (PT) and poly (3,4-ethylenedioxythiophene) (PEDOT). These polymers, especially PEDOT, have more widespread interest and have been studied in cardiovascular, orthopaedic and neurological applications. These applications of PEDOT have been selected due to its reliable electrical and degradation properties (Boehler, et al. 2019). Finally, and of most interest to this study, are the nitrogen-containing conducting polymers, such as: polypyrrole (PPy) and polyaniline (PANI). These are by far the most well studied conducting polymers and their behaviour and properties are well established within the literature (Nidhin, et al. 2016).

Many monomers of conducting polymers have aromatic rings within their structure, and this includes both PPy and PANI, with their main chemical difference being the position of their nitrogen atom within or out with the aromatic ring. The aromatic ring within many monomers is important as an electron pool that allows for the polymer chains to form.

An important consideration in the chemistry and particularly the electrical properties of conducting polymers, is the concept of doping. Doping is the alteration of the electron chemistry of a conducting polymer, by removal of an electron (p-doping), or addition of an electron (n-doping). This is typically achieved through the use of a chemical dopant, often a salt. In their neutral state, conducting polymers show very little electrical conductivity. However, upon doping, their conductivity increases significantly, along with other important properties such as: mechanical properties, wettability and optical properties (Das & Prusty, 2012).

1.7.1. Fabrication of Conducting Polymers

Conducting polymers, in a doped state, can be synthesised through 2 main methods. Chemical synthesis routes are commonly used and may readily occur or require the addition of heat or other initiators to occur. In the case of PPy, chemical synthesis readily occurs in solution with the addition of an oxidant (e.g. ferric chloride) and a surfactant (e.g. sodium dodecyl sulphate), resulting in a strong exothermic reaction producing granular PPy (Yussuf, et al. 2018). This is a relatively straightforward approach for generating conducting polymers and generates a high yield of product. Despite widespread use in research, this technique has

very little control and the resulting product is highly variable and in more complex reactions, the purity of the conducting polymer will be diminished.

Electrochemical synthesis is the other major route for fabricating conducting polymers and unlike chemical synthesis is highly controllable and produces conducting polymer films with a high degree of purity, albeit at far lower yields (Guimard, et al. 2007). For use as a novel stent coating, low yield can be accepted since purity will be critical and the intrinsic ability for this process to directly deposit films on metallic substrates makes it highly appropriate to generating stent coatings.

1.7.2. Conducting Polymer Applications

Since the properties of conducting polymers may offer typical benefits of both polymeric and metallic materials, widespread interest has gathered about the potential uses of these materials. This has led to biosensors, tissue engineering and neural probes forming the dominant applications of conducting polymers in bioengineering (Guimard, et al. 2007). In all these applications, conducting polymers were found to demonstrate suitable biocompatibility and, PPy was used in every application area. This demonstrates its widespread potential. In a wider context, conducting polymer use has been focussed in electronics, sensors, fuel cells and catalysts. The use of these compounds as catalysts may be relevant, since it is driven specifically by conducting polymer's unique ability to participate in redox reactions (Das & Prusty, 2012).

In the context of stent coatings, PPy has been considered as a stent coating for a controllable drug matrix and shown to be capable of delivering a controlled dose rate of paclitaxel over 30 days (Okner, et al. 2009). Arbizzani, et al. (2007) specifically considered conducting polymers synthesised through electropolymerisation for their high controllability, with PPy selected for its reported biocompatibility and simplicity of electropolymerisation synthesis route; it is only synthesised through n-doping. N-doping made PPy a suitable carrier of anionic drugs: sodium salicylate (NaSa) and sodium naproxene (NaNp). Arbizzani, et al. concluded that electropolymerisation presented a useful method for fabricated uniform stent coatings on platinum discs with predictable and controllable drug-elution properties.

The use of PPy for stent coatings was further investigated in the application of drug-elution for biodegradable iron stents. Here, biodegradable iron was coated with PPy-salicylate films by electropolymerisation. Increasing concentrations of salicylate incorporated into these films was found to result in the formation of rougher topographies and impede the coatings

electroactive properties, suggesting that dopant concentration must be limited to control polymer properties (Cysewska, et al. 2019). It is unclear the intent of this study as standard electropolymerised PPy is not considered biodegradable and therefore would not be expected to degrade alongside the iron stent substrate. Overall, this study found with Arbizzani, et al. that electropolymerisation of polypyrrole generated highly controllable and predictable films that would be appropriate for stent coatings, but no consideration was given in either study for endothelial compatibility or novel uses for conducting polymers outside of adapting current DES approaches.

Although standard conducting polymer films do not degrade in biological environments, biodegradable materials have been generated using polypyrrole and PEDOT. PEDOT is typically used for this by generating co-polymers with polylactic acid and polycaprolactone (Jadoun, et al. 2014). Biodegradable co-polymers of PPy have been synthesised with polyethylene glycol and polylactic acid (Shustak, et al. 2007). In all cases, these polymers are generated through chemical synthesis, are limited to nanoparticles, have limited demonstration of degradation rates and unclear biocompatibility and are therefore are currently unsuitable for coronary artery applications, either as a drug elution vehicle or potential antioxidant.

1.7.3. Conducting Polymers as Antioxidants

Antioxidant effects can be exerted through three mechanisms that act to reduce the oxidant. These are hydrogen atom transfer (HAT), single electron transfer (SET) and proton-coupled electron transfer (PCET). In HAT, a hydrogen atom is donated to the oxidant in a single step, typically from a O-H, or N-H group. In SET, an electron moves from the antioxidant to the electron-deficient oxidant; this may be a simple electron donation or could lead to the formation of a σ-bond. PCET is a more complex, single-step mechanism and is a less commonly reported mechanism. This process is similar to HAT, but differs because the electron and proton are transferred as separate chemical species and they are donated to the oxidant at different energy levels. Multiple factors may influence the antioxidant potential of a compound, but ionisation energy for SET and bond dissociation enthalpy for HAT are considered to have the greatest impact (Liang & Kitts, 2014).

In biological systems, many of the critical ROS, e.g. superoxide radicals, can be scavenged by either HAT or SET, but some specific radicals are limited in reactivity to one reduction mechanism. In particular, hydroxyl and peroxyl radicals require hydrogen transfer to occur, while nitric oxide reactivity is dependent on electron transfer (Foti, 2007; Everett, et al. 1995).

Ascorbic acid is highlighted as a beneficial supplementary antioxidant for its ability to provide broad antioxidant effects through HAT, SET and PCET.

Polyaniline

Antioxidant activity has been identified in polyaniline, but reporting of this property has been complicated by the number of oxidative states that PANI can exist in. PANI can be p- and n-doped, resulting in 3 oxidation states. When fully oxidised (p-doped), PANI exists as pernigraniline. When reduced (n-doped), PANI exists as leucoemeraldine. In a mixed or neutral state, emeraldine polyaniline can display both oxidative and reductive behaviours and is further complicated as it can be doped with hydrogen to form the electrically conductive emeraldine salt (Albuquerque, et al. 2004).

In the emeraldine base form, antioxidant activity has been shown though a DPPH assay, which showed that DPPH radicals protonated the PANI base forming a visible green emeraldine salt (Gizdavic-Nikolaidis, et al. 2004). The DPPH assay however is a mixed-mode colourmetric assay as the DPPH radical can be reduced by either HAT or SET, and despite studying the reaction kinetics closely, this study was unable to define the mechanism for PANI antioxidant activity. Unfortunately, the reduced (n-doped) form of PANI, leucoemeraldine, that would be more comparable to other conducting polymers has not been studied thoroughly.

Antioxidant chemistry within the aniline monomer has been considered and suggests interesting changes that result from the polymerisation process. Unlike PANI, the aniline monomer was incapable of scavenging DPPH, but highly capable at scavenging hydrogen peroxide – an oxygen species that is highly dependent on SET-related reduction (Bendary, et al. 2013). It is surprising that aniline readily demonstrated SET, but was unable to scavenge DPPH, since this assay is well documented as a broad mixed-mode mechanism. This study suggests that polymerisation allows HAT to occur from the amino group by “activating” the N-H bond through reduction in the dissociation energy. Additional research demonstrates that PANI does not lose its ability to react with hydrogen peroxide, further demonstrating that PANI is capable of antioxidant activity by SET and HAT (Gu & Chen, 2008).

Overall, there is clear evidence that polyaniline presents a strong and broad potential antioxidant coating. The complexities of PANI synthesis and multiple oxidation states however make it difficult to identify an ideal use for polyaniline as an antioxidant. This is further limited by the lack of a clear mechanistic action for PANI and further work needs to be carried out to clarify the importance of PANI oxidation and examine its effectiveness with a broader range of relevant ROS.

Polypyrrole

The antioxidant activity of polypyrrole is less well characterised than those conducting polymers described above. The research that does exist has generally focused on PPy nanotubes, with these structures likely to demonstrate behaviour that is highly different to electropolymerised films. In nanotubes, DPPH was used to assess antioxidant activity and PPy was found to be a capable scavenger of DPPH (Upadhyay, 2014). When examining the reaction kinetics, this study found that the reaction displayed two clear processes; indicative of SET (fast reaction) and HAT (slow reaction), but it is unclear whether this characteristic is unique to nanotubes.

Hsu, et al. (2010) studied PANI, PPy and PEDOT powders that were chemically-synthesised using an ABTS-radical assay and found all conducting polymers displayed antioxidant capacity. This assay measures reduction in ABTS-radical absorbance in a similar way to DPPH, and similarly is a mixed-mode measure. This study concluded that PANI showed the highest antioxidant capacity, followed by PPy and all conducting polymers showed improved antioxidant properties in their reduced, n-doped states.

Maclean, et al. (2008) modelled bond energies as a means of analysing the antioxidant ability of a number of pyrroles and related chemical structures, but importantly not polypyrrole. Pyrroles were found to be capable antioxidants, and HAT was commonly observed among the different chemicals. SET was also observed, but not among all the pyrroles studied, suggesting a need for specific chemical conditions. In particular, solvent and methodology-associated effects were noted by the authors as inducing SET and this may not occur under less artificial conditions. Other research has identified bond dissociation energy close to the hydroxyl groups of organic acids, which are known, albeit weak antioxidants (de Oliveira, et al. 2010). This further indicates the potential for pyrrole to engage in HAT, as shown in Figure 1.12.

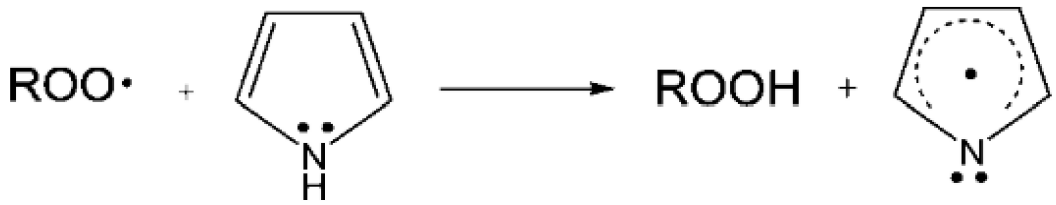

Figure 1.12. Proposed hydrogen atom transfer mechanism of antioxidant activity for pyrrole-containing chemicals. Adapted from: (Maclean, et al. 2008)

Interestingly, the N-H bond as an antioxidant source has precedent in human biology, where bilirubin acts as an endogenous antioxidant for vascular endothelial cells against hydroxyl and peroxyl radicals (Ziberna, et al. 2016). Bilirubin contains 2 pure pyrrole groups and 2 further N-containing groups and it has been shown that these pyrrole groups give bilirubin its capacity to scavenge peroxyl radicals through HAT (Chepelev, et al. 2006).

In both PANI and PPy, robust evidence of specific antioxidant activity is lacking due to the widespread use of DPPH. It will be necessary in this study to address this gay by investigating PPy reactivity with specific biological radicals before progressing to a cell-based model.

1.7.4. Conducting Polymer Biocompatibility

When considering biocompatibility, special consideration should be given to the specific tissue requirements within the intended applications. For coronary stents, these requirements are: low thrombogenicity, good coating stability and integrity and the coating must allow endothelial attachment and normal physiological function (Jeewandara, et al. 2014).

Haemocompatibility of conducting polymers has been shown in both PANI and PPy. In PANI, the thrombogenic response to both the base and salt forms of the polymer is similar to polystyrene when measured in terms of platelet adhesion (Humpolíček, et al. 2015). Furthermore, PANI has been shown to have no significant effect on clotting time *in vitro* (Skopalova, et al 2019). PPy displayed no haemolytic issues *in vitro* and did not induce coagulation when assessing coagulation time vs. untreated plasma (Zhang, et al. 2001).

Cell attachment is essential in promoting restenosis and for conducting polymers, cell attachment has been assessed in a number of clinical contexts. Cardiac myoblasts have been cultured on PANI and were found to show significantly reduced attachment on these surfaces vs. tissue culture polystyrene (92% attachment vs. TCP), but proliferated at a comparable rate (Bidez, et al. 2006).

In terms of cell adhesion, the biocompatibility of PPy has been widely recorded and summarised in a review by Ateh, et al. (2006) that for many cell types, PPy surfaces show cell attachment and proliferation potential similar to glass surfaces (Atah, et al. 2006). This is contrasted however by previous research showing that cell attachment to PPy is highly dependent on the material's oxidation state, with only n-doped PPy surfaces allowing attachment and spreading (Wong, et al. 1994). This study also found that changing the

oxidative state of the polymer, changed the organisation of the polymer and the surface topography of the coating. The precise relationship between the oxidative state and cell adhesion remains to be clarified, but may be due to protein interactions or lipophilic effects; however, this suggests that any changes of the PPy surface chemically through redox reactions due to ROS scavenging must be carefully considered.

Humpolíček, et al. (2018) studied cell viability of fibroblasts, indirectly exposed (non-attached) to PANI and PPy powders in both the base and salt (n-doped) forms, using MTT assays. The oxidation state of each sample was shown to have a significant effect on cytotoxicity, with PPy showing no cytotoxic effects in the basic form compared with mild cytotoxicity with PANI salt. The base oxidation states induced higher cytotoxic effects with more polymers, resulting in severe cytotoxicity.

The use of conducting polymers in cardiovascular applications and the effects of conducting polymers on endothelial cells in particular is not well established. Endothelial proliferation on PPy-coated polyester fibres has been assessed and PPy was found to display reduced cell attachment vs. gelatin coated polystyrene and allowed no proliferation over 1 week (Zhang, et al. 2001). Unfortunately, this study modified their PPy samples' structures by plasma treatment or phosphonylation (the chemical addition of a phosphonate group) to improve bonding with the underlying polyester fibres, and so its relevance to the present investigation is unclear.

Although it is essential for PPy to demonstrate biocompatibility in a stent application context and accordingly needs to provide exhibit a positive effect on endothelial cells, due to the aim to limit restenosis, it is not desirable for this high cytocompatibility to be matched with vascular smooth muscle cells. Ideally, any PPy coating used in stent applications will not present a cytotoxic stimulus for the adjacent SMCs, but similarly won't promote proliferation and luminal migration. There are few studies exploring the effects of PPy films on SMCs, but Stewart, et al. (2012). examined the response of human aortic SMCs to PPy coatings and found that PPy coatings doped with heparin suppressed proliferation whilst allowing adherent cells to retain phenotypes after 6 days. The use of toluene sulfonate and nitrate dopants similarly inhibited proliferation, but cells on these surfaces were visibly less spread after 6 days, so it is clear these effects were heavily dopant specific.

Overall, biocompatibility relevant to coronary stents has not been well explored for conducting polymers, and areas that are relevant such as haemocompatibility have used various measures that makes interpretation of results challenging. Specific endothelial and smooth muscle cell compatibility has not been explored in detail and the effect of these compounds on cell

signalling is unknown. Furthermore, all of these studies discussed used chemically-synthesised conducting polymers, which is in contract to the electropolymerized form that holds greatest potential for stent applications.

1.8. Electropolymerisation

As previously stated, electropolymerisation is a synthesis route for conducting polymers and is suitable for any conducting polymer that can be oxidised in the presence of a potential to form a radical, such as PPy, PANI and PEDOT. Electropolymerisation has a number of advantages over chemical synthesis since the technique is capable of producing thin uniform films directly onto a substrate surface in a single process (Guimard, et al. 2007). Unlike chemical synthesis, doping occurs directly during the electropolymerisation process, leading to the incorporation of anions or entrapment of useful pharmacological agents. Importantly, electropolymerised PPy films have been found to show very high adherence to the underlying working electrode and did not demonstrate any fragmentation upon deformation, despite the previously reported brittle nature of PPy films (Sahebzadeh, 2016). This clearly demonstrates the suitability of electropolymerised PPy films as novel stent coatings.

1.8.1 Electropolymerisation Mechanisms

A widely accepted reaction mechanism for the electropolymerisation of pyrrole was first reported by Diaz, et al. (1983) and is summarised, along with other proposed mechanisms, by Sadki, et al. (2000). The Diaz mechanism of pyrrole electropolymerisation can be considered an electrochemically-induced variation of classic free radical addition and is described in eight distinct steps. This process is outlined in Figure 1.13

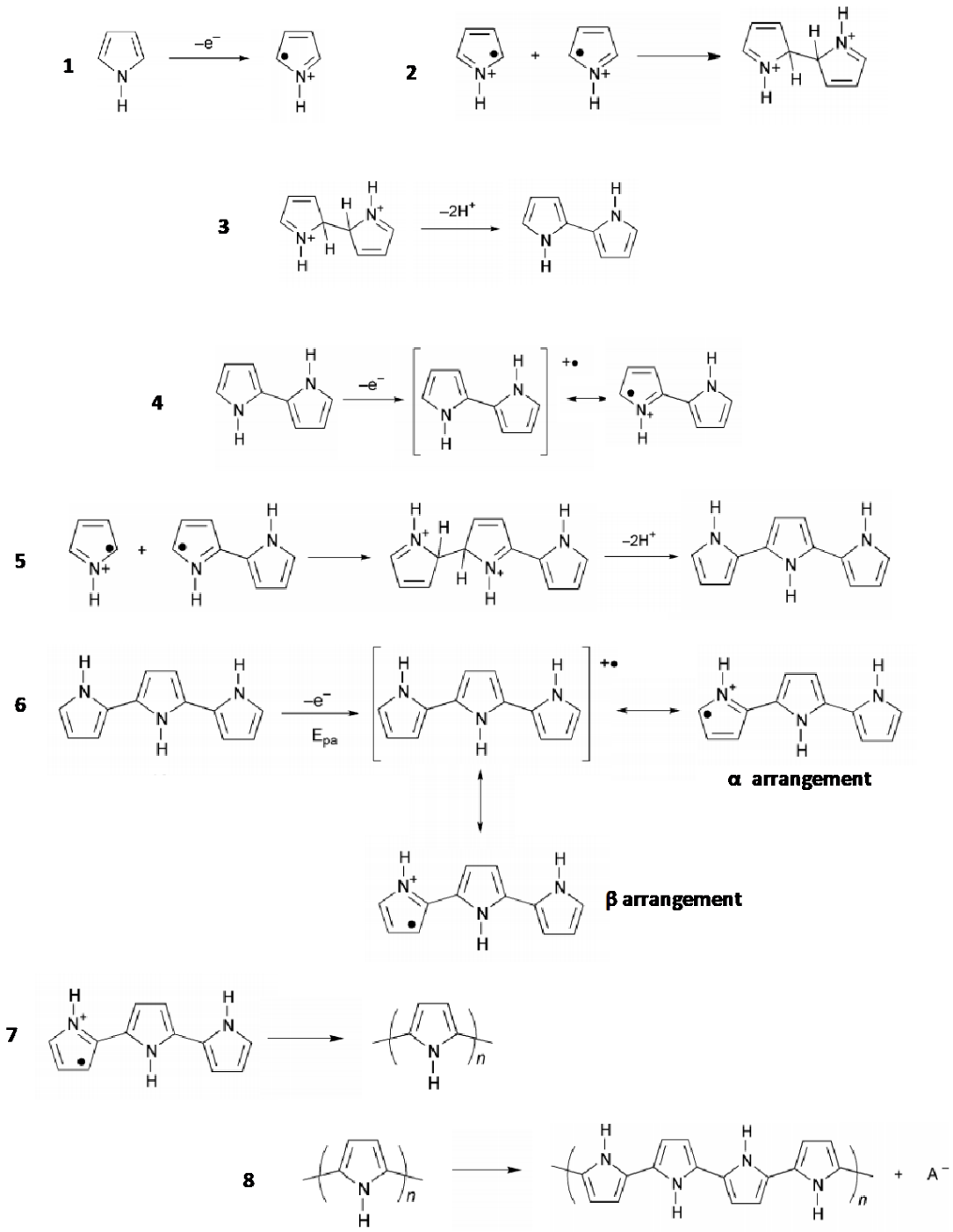

Figure 1.13. Diaz mechanism for pyrrole electropolymerisation. Adapted from: (Sadki, et al. 2000).

In the Diaz mechanism, electropolymerisation is initiated by the oxidation, loss of an electron, of the pyrrole monomer due to an applied potential at the working electrode. The oxidation reaction causes the formation of a pyrrole radical cation at the working electrode surface (step

1). The high concentration of pyrrole radicals generated at the electrode surface promotes dimerization of the radicals (step 2) leading to the formation of the dication form of pyrrole.

This cation is highly unstable due to the hydrogen atoms around the covalent bond formed in step 2. The cation therefore passively loses these two protons from the dimer, generating a stable dimer at the working electrode surface (step 3). The delocalised electrons from the bonded pyrrole radicals are now shared over two aromatic rings, reducing the dimer's oxidation potential. The causes oxidation to be favoured in the pyrrole dimer compared with the pyrrole monomer (step 4), but the resulting dimer cation radical is less reactive than the monomer radical. Due to the reduced reactivity of the dimer cation, the reaction is favoured for these species to react with a monomer radical cation, rather than with another dimer. This leads to addition of single pyrrole radicals in a reaction that closely resembles classical free radical addition (step 5). This trimer cation then deprotonates to form a stable neutral trimer.

The trimer can be further oxidised to form a radical ion (step 6). The reaction of the trimer can however propagate in two arrangements, in the alpha arrangement, this results in highly linear crystalline polymer formation, but in the beta arrangement the resulting polymer is more amorphous. In virgin pyrrole electropolymerisation, both of these reactions can occur and the step wise addition is repeated leading to the formation of a semi-crystalline polymer film (step 7). Finally, the conducting polymer backbone carries a positive charge that needs to be balanced by the incorporation of the dopant (step 8). The dopant therefore makes up approximately 35% of the final polymer weight (Sadki, et al. 2000).

Although the Diaz mechanism has been most widely reported, alternative mechanism's for PPy electropolymerisation have a also been proposed. The Kim mechanism proposes that the reaction is initiated by the loss of two electrons and a proton from the pyrrole monomer to form a pyrrole intermediate (Kim, et al. 1988). This intermediate can then form a dimer with the neutral pyrrole monomer and the reaction is further propagated by the pyrrole intermediate. Although this mechanism has been supported through experimental data, it is less widely reported than the Diaz mechanism, which has been applied and validated more widely in the literature.

The Pletcher mechanism is a further mechanism for the electropolymerisation reaction and in many ways is very similar to the Diaz mechanism. In this reaction, the oxidised pyrrole cation reacts directly with the neutral pyrrole monomer and this propagates the reaction (Asavapiriyanont, et al. 1984). This mechanism disputed as it has been applied successfully to explain changes in the electropolymerisation reaction with increased pyrrole concentration, but radical-monomer reaction would likely have a prohibitive activation energy.

The Reynold mechanism is a further mechanism of oxidative electropolymerisation, but this mechanism is only applied to electropolymerisation in the presence of perchlorate, tetrafluoroborate and hexafluorophosphate ions as dopants (Qiu & Reynolds, 1992). These dopants will not be used in this study. As such, this mechanism will not be discussed here.

In this study, the Diaz mechanism will be accepted when considering the electropolymerisation process, thereby allowing estimation of the amount of polymer and dopant contained within the PPy films.

1.8.2. Types of Electropolymerisation

As outlined above, electropolymerisation results from oxidation of monomers, radical generation and subsequent step-wise polymerisation. The oxidation of the monomer which triggers the reaction process can be initiated through different electrode set ups. These are potentiostatic, galvanostatic or potentiodynamic configurations. In a potentiostatic configuration, the working electrode potential is controlled at a constant voltage throughout the reaction process and during galvanostatic electropolymerisation, the working current is controlled throughout the process. Potentiodynamic electropolymerisation differs as the voltage is ramped up repeatedly throughout the process.

Static conditions are easiest to set-up, control and understand. Potentiostatic conditions have the benefit of better control on the electrochemical state of the conducting polymer, since the applied potential can be set close to the oxidation point of the monomer and maintained throughout. Therefore, this technique is preferred if the application requires good oxidation control and the effect of voltage on polymer properties are well understood. Galvanostatic conditions offer lower control of the voltage conditions that the polymer is exposed to, but it typically results in better polymerisation efficiency and lower coating times for the same mass/thickness and is less sensitive to changes in the experimental circuit set-up which may impact the open circuit potential (Fernandez, et al. 2002).

Potentiodynamic conditions are also common and allow for better control to generate complex surface topographies and control the electrochemical state of the polymer as the cell is allowed to cycle between oxidative and reductive states. These rapid changes in physical and electrochemical properties can have negative impacts on the final bulk properties of the polymer and the set-up and number of variables make this process more difficult to perform and interpret (Sharma, et al. 2012).

To demonstrate the capability of conducting polymers for antioxidant scavenging, static electropolymerisation conditions are sufficient in generating conducting polymer coatings with controlled oxidation, using potentiostatic modes, or high volume generation with lower control, using galvanostatic modes.

1.8.3. Dopants

Synthesis of PPy is frequently achieved using electropolymerisation and a vast array of uses for this material are emerging. As a result, many dopants have been used in electropolymerisation to obtain coatings tailored for their specific purposes. It is important that a focus is given to dopants that are medically relevant and have been established as non-cytotoxic to endothelial cells at the relevant concentrations.

When considering PPy as a potential coating alternative for DES, sodium toluenesulphonate (NaTS), NaSa and NaNp have been used as dopants for electropolymerisation (Arbizzani, et al. 2007). All of these dopants are of a medium-large size (160.11 – 252.24 g/mol), but NaTS is a widely reported dopant for electrochemical synthesis of polypyrrole, whereas NaSa and NaNp are anionic anti-inflammatory drugs that are not commonly used for electropolymerisation. Although PPy was successfully electropolymerised with each dopant and drugs were subsequently eluted, the use of anionic drugs was limited by the precipitation of these drugs around the working electrode. Electropolymerisation of Py gives rise to the release of approximately 2 mol of protons per mol of Py that is incorporated into the polymer, causing a loss of solubility in the dopant associated with their acid forms compared with the salts, resulting in the high precipitation. The effect is less prominent in NaSa compared with NaNp, since salicylic acid has greater solubility compared with naproxen (approximately 3000 times greater).

Dopants may have a direct or indirect effect on the biocompatibility of PPy coatings with the endothelium and underlying smooth muscle. Although it is not directly relevant to the cardiovascular system, potentially osteoinductive PPy coatings have been developed using chondroitin sulphate as a dopant. These coatings however were not found to enhance biocompatibility and were inferior in many important regards compared with NaTS-doped PPy. This is likely due to the indirect cellular effects associated with NaTS, resulting from differences in surface topography and wettability (Fahlgren, et al. 2015). There are a wide range of potential therapeutics that could be incorporated to directly improve NO

bioavailability or enhance endothelial cell adhesion, but any changes in electropolymerisation should be carefully considered.

Since the antioxidant potential of PPy has not been widely investigated, the effects of the dopant on antioxidant activity remain to be elucidated. Dopant effects have been investigated in PANI. Nand, et al. (2011), found that chloride-doped PANI exhibited significantly higher DPPH scavenging compared with persulphate-doped PANI and both coatings lost significant scavenging capacity when the dopant was chemically removed. The effect was not found to correlate with conductivity or surface area differences that may arise from the variation in the polymerisation reactions.

Salicylate anions have been shown to allow electropolymerisation of PPy and its safety is established through its known anti-proliferative and anti-inflammatory use, suggesting it to be a highly appropriate dopant for generating novel antioxidant PPy coatings (Marra, et al. 2000). It is however necessary in this study to consider the specific effects salicylate may impart on polypyrrole-salicylate coating's antioxidant capacity, or any innate antioxidant capacity of salicylate.

1.8.4. Salicylate as an Antioxidant

If used as a dopant in the electropolymerisation of PPy, salicylate may provide an antioxidant role through direct scavenging capacity of ROS, or indirectly through its effects on the PPy chemistry. It is important to consider the direct antioxidant capacity of any dopant to ensure that any observed effects of PPy result directly from the polymer structure and not from eluted aqueous dopant ions.

As previously stated, sodium salicylate (NaSa) has known anti-inflammatory effects and is the salt form of salicylic acid. In endothelial cells, sodium salicylate has been shown to reduce proliferation at concentrations above 10 μM, and at lower concentrations, reduce the secretion of von Willibrand Factor and C-reactive protein (Shtivelband, et al. 2003; Shahidi, et al. 2014). Similarly, salicylate has been shown to inhibit VMSC proliferation, but this assessed at concentrations from 100 μM (Muñoz, et al. 2011). Marra, et al. (2000) also assessed the effect of salicylate and only observed anti-proliferative effects at concentrations above 1 mM. It is therefore unlikely that salicylate elution will be capable of delivering a selective benefit to endothelial cell proliferation and resulting pro-healing response.

Acetylsalicylic acid (aspirin), a modified form of salicylic acid, is a routinely used painkiller and non-steroidal anti-inflammatory drug (NSAID). Aspirin and other NSAIDs have been shown to demonstrate antioxidant effects *in vivo*, but in these studies the observed effects were linked to downregulation of inflammatory pathways that generate ROS rather than direct ROS scavenging by the drugs (Demirci, et al. 2014; Milatovic, et al. 2011). When considering the direct scavenging of ROS by aspirin and other NSAIDs, it is important to note the diversity in chemistries within this group of drugs. Figure 1.14. shows the chemical structure of sodium salicylate alongside three types of NSAIDs: aspirin, ibuprofen and tolmetin. Tolmetin is not a NSAID that can be used to alleviate inflammatory pain associated with rheumatoid arthritis and gout, but that is not routinely proscribed for pain management. It is included here for consideration since it is derived from pyrrole, as such its ROS scavenging capacity could be suggestive of other pyrrole chemistries.

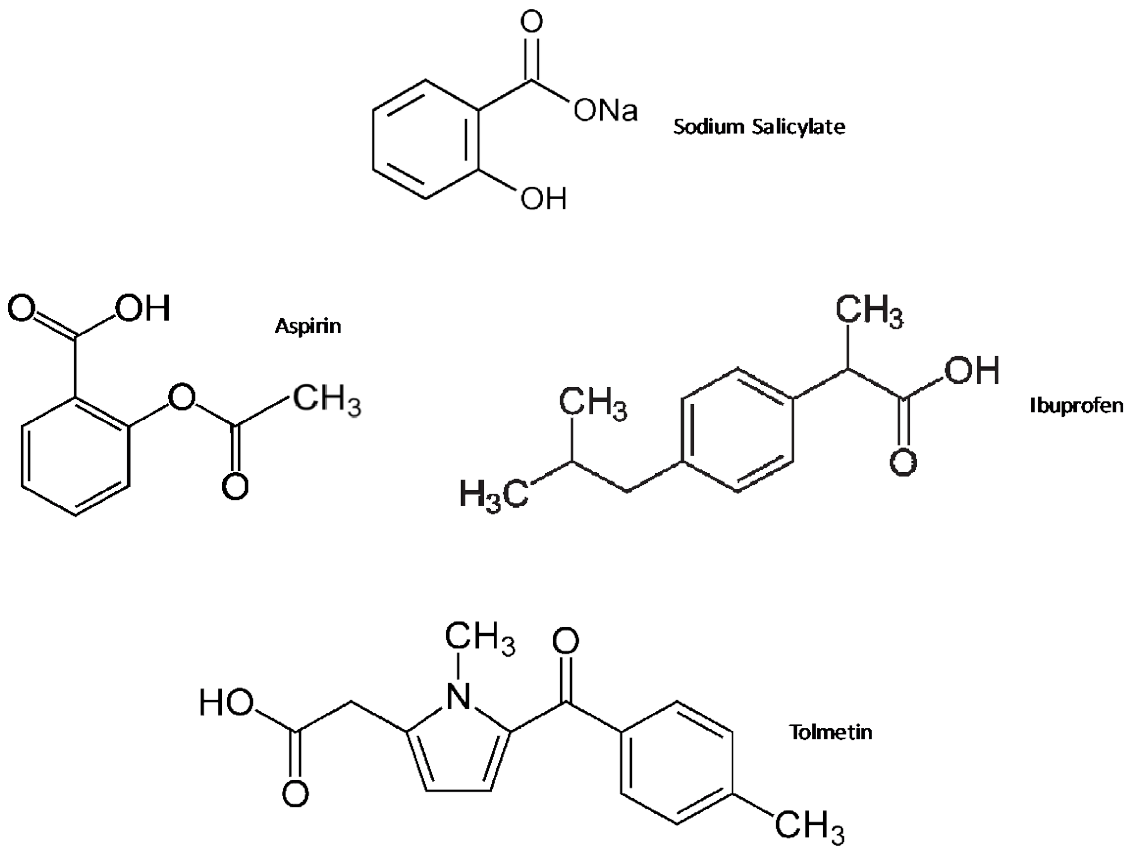

Figure 1.14. Chemical structures of sodium salicylate and non-steroidal anti-inflammatory drugs: aspirin, ibuprofen and tolmetin. Adapted from: (Costa, et al. 2013).

Since the reducing power of antioxidants is typically achieved through HAT or SET, the chemical structure of compounds may be indicative of their antioxidant power and suggest a mechanism of action. All of the chemicals shown in Figure 1.13. contain a phenolic ring structure, which have the potential to act as antioxidants due to the stability given by the delocalised ring of electrons. This structure is likely to allow for SET. Aspirin, ibuprofen and tolmetin all possess carbonyl (CO with a double bond) and hydroxy (OH) groups. Carbonyl groups contain an electron-rich double bond and this may promote scavenging of nucleophilic ROS, such as superoxide radicals (Milenković, et al. 2017). The hydroxy groups may also offer some antioxidant potential through HAT, especially in these highly polar carboxylic acid arrangements, but it is worth noting that the antioxidant potential of hydroxy groups has been mostly consider in flavonoids, which are chemically dissimilar to these NSAIDs (Musialik, et al. 2008). Tolmetin has the most complex chemical structure of the NSAIDs shown, as it also contains the previously mentioned pyrrole group and a true carbonyl group that is independent of a carboxylic acid group. Unlike the pyrrole monomer, the pyrrole group in tolmetin is attached to a methyl group rather than a single H, this potentially changes its potential for HAT.

Chemical structure alone cannot indicate the potency of a suspected antioxidant. Solecka, et al. (2014) investigated a number of carboxyl and hydroxyl containing compounds and found subtle differences in functional group arrangement could significantly impact the chemical's ROS scavenging activity. NSAIDs have been studied to determine some of their radical scavenging capacity and studies have highlighted the differences in types of ROS scavenged and strength of the reducing power. Shi, et al. (1999) showed that *in vitro* aspirin can act as a capable scavenger of hydroxyl radicals, but this antioxidant effect was not extended to superoxide radicals and hydrogen peroxide, which were not scavenged. Despite possessing similarities in functional groups, ibuprofen has been shown to demonstrate no *in vitro* ROS scavenging capacity (Costa, et al. 2013). In contrast, tolmetin has been shown to be a capable scavenger of hydroxyl radicals, and also singlet oxygen, superoxide and peroxyl radicals (Kladna, et al. 2005).

In terms of sodium salicylate, the antioxidant activity has been shown to match many of the properties demonstrated by aspirin. Sodium salicylate is a highly capable scavenger of hydroxyl radicals, resulting in the formation of a dihydroxybenzoic acid adduct, by displacing a hydrogen atom on the phenolic ring via electrophilic substitution (Amann & Peskar, 2002). This reaction, leading to radical adduct formation of a relatively stable species, is typical for highly oxidising species, such as hydroxyl radicals and can be considered a type of SET

process. Similarly, the capacity of salicylate to be nitrated by highly oxidising nitrogen species, such as peroxynitrite, is achieved through the same electrophilic substitution process (Ramezanian, et al. 1996). In fact, the hydroxylation of sodium salicylate is reliable and strong enough that sodium salicylate can be used as a fluorescent probe in the detection of hydroxyl radicals *in vivo* (Yang, et al. 2010).

Although sodium salicylate, like aspirin, is an effective scavenger of hydroxyl radicals, this does not clarify whether sodium salicylate has the capacity to scavenge ROS with a lesser oxidising power. Kimura, (1997) found some evidence that sodium salicylate can act as a scavenger for superoxide, but this was only observed when using concentrations higher than 10 mM, suggesting only weak antioxidant capacity for superoxide. The same study found no evidence of hydrogen peroxide scavenging by sodium salicylate at any concentrations. Salicylic acid is more widely studied and has been shown to promote hydrogen peroxide scavenging in various cell types, but this has been linked predominantly to interactions between SA and GSH, rather than direct scavenging effects (Herrera-Vásquez, et al. 2015). It is worth noting that in certain physiological conditions, hydrogen peroxide can generate hydroxyl radicals, via Fenton reactions, and as such, hydroxyl scavengers may offer an indirect protective effect against hydrogen peroxide (Thomas, et al. 2013). A study into the structural-activity relationships in salicylic acid found that the structure of salicylic acid does not favour oxidation, as the hydroxy groups are restricted by a high bond dissociation energy, and the electrons within its aromatic ring are less likely to be donated when compared against Trolox, a known anti-oxidant (Borges, et al. 2014).

The use of sodium salicylate as an anti-inflammatory and anti-oxidant drug has been shown to be effective in reducing pathological effects associated with oxidative stress. Along with scavenging hydroxyl radicals, this includes: upregulation of nitric oxide, increased synthesis of lipoxin, inhibition of neutrophil oxidative burst and inhibition of NF-κB signalling (Baltazar, et al. 2011). These effects may be downstream consequences of hydroxyl radical scavenging and unique interactions between salicylate and pro-inflammatory proteins were demonstrated at high concentrations, with potential for severe adverse effects. If delivered systemically, salicylate can generate pathological effects in the liver by activating mitochondria and interfering with transition metals in the respiratory chain, to promote oxidative stress (Battaglia, et al. 2005). If used as a dopant for generating PPy stent coatings, systemic salicylate exposure should be minimised through local drug delivery, and there remains the opportunity to modify these coatings with different dopants, or the use of undoped polymer coatings.

1.9. Study Rationale, Aims and Objectives

Coronary DES devices remain the most commonly used for treating CHD and designs for these devices are continuously being refined. 3rd generation DES continue to carry significant risk in the form of restenosis, especially at late and very late stages (Kelly, et al. 2017). Despite device improvements, these recurrent issues around restenosis suggest the anti-proliferative strategy may be limited. Here, we have identified oxidative stress and failed re-endothelialisation as potential key drivers in the progression of neointimal formation and restenosis (Juni, et al. 2013; Nakazawa, et al. 2008).

The role of oxidative stress in cardiovascular disease is complex and diverse, and the significance of oxidation in disease is continually becoming more apparent. Pro-oxidants have many important physiological targets and the effects of oxidative stress are complicated since ROS are important mediators of physiological signalling at low and controlled concentrations.

If controlled therapeutically early after stent placement, oxidative signalling could be moderated and utilised at the inflammatory stage of healing to promote healing and improve patient outcomes. This approach becomes particularly relevant in patients where oxidative stress is less controlled physiologically and inflammatory signalling is easily exacerbated, such as diabetic patients – where current DES approaches are less effective.

It is therefore necessary to identify antioxidant agents that will dampen oxidative stress, without disrupting physiological signalling. Previous pharmacological attempts at utilising antioxidants had limited success and largely failed to balance antioxidant action and physiological signalling due to dosing issues (Watt, et al. 2008). By controlling oxidative signalling, re-endothelialisation may be improved by enhancing endothelial cell proliferation, but other factors must also be considered such as, stent surface topography and wettability. It remains to be understood what effect controlling inflammatory and oxidative stress will have on the cellular responses to PPy coatings and this study will aim to explore the role of inflammation and oxidation in vascular physiology by assessing these measures in a cell-based model.

CaMKII presents a potentially critical mediator in the switch between physiological redox signalling and pathophysiological signalling associated with oxidative stress. The role of CaMKII activation, via oxidation, in other relevant cardiovascular diseases is clear, but in restenosis CaMKII oxidation has not been widely considered and therefore is not specifically implicated as a driver of this disease. CaMKII activation in ECs and SMCs is linked with permeability, migration and hypertrophy (Toussaint, et al. 2016). As such, the potential links

in CaMKII activation and progression of restenosis are clear. In this study, the role of CaMKII will be considered and its interactions and dependence on oxidative signalling in ECs and SMCs will be explored.

Conducting polymers offer a novel alternative to systemic antioxidant use and DES. PPy and PANI have been considered for use as stent coating materials because of their wide use and current varied applications. For its demonstrated relevant and strong biocompatility, PPy presents a useful potential stent coating material. When compared with PANI, PPy's antioxidant potential is unclear and this needs to be fully characterised. For any conducting polymer, it is unknown how antioxidant activity at the stent surface would translate to therapeutic action on cells attached to the surface or whether the use of conducting polymer coatings would impart an inhibitory effect on SMCs in the underlying vascular tissues. For its established biocompatibility and well understood electropolymerisation reaction, PPy will be explored as a novel antioxidant stent coating in this study. The use of PPy as a coronary artery stent coating is highly novel and this study will aim to explore the capacity of PPy as an antioxidant in this application further. Furthermore, electropolymerisation is an established synthesis route for PPy but it's capability for generating uniform coating for stent applications has not been established and this study will aim to assess and characterise this process for generating PPy films.

Currently, the efficacy of coronary stents is typically validated using animal models, such as porcine models of in-stent restenosis. In this study, biological responses of ECs and SMCs to PPy coatings will be explored using *in vitro* techniques. Any biological model will need to be adaptable to incorporate coated substrates and allow for the effects of oxidative stress to be explored and CaMKII to be considered. There are limited existing cell-based approaches that can be easily adapted to incorporate coated metallic substrates. This study will aim to develop a cell-based *in vitro* model and assess its appropriateness and effectiveness in testing the biological antioxidant capabilities of PPy coatings.

The aims of this study can be divided into 5 broad themes that will be explored in this study and presented in separate chapters:

Aim 1: To reliably develop appropriate polypyrrole coatings by electropolymerisation in a range of coating formats/structures to allow use with a variety of assays and techniques. These coatings and the electropolymerisation will be characterised. (Chapter 2).

Aim 2: To measure and quantify antioxidant capacity of PPy coatings and 316L SS uncoated samples with a range of relevant ROS and nitric oxide. (Chapter 3).

Aim 3: To identify a biological *in vitro* model for the assessment of polypyrrole coatings and assays to quantify PPy's biological antioxidant potential. (Chapter 4).

Aim 4: To develop the biological cell-based model in relevant endothelial and smooth muscle cell types. (Chapter 5).

Aim 5: To identify biological antioxidant effects of PPy coatings in ECs and SMCs. Investigate any possible inhibitory effect on CaMKII that PPy coatings may have and identify any downstream consequences. (Chapter 5).

2. Generation and Characterisation of Polypyrrole Coatings

Chapter 2 will explore the first aim of this study – generating polypyrrole (PPy) coatings by electropolymerisation and characterising their basic physical and chemical properties. Firstly, the specific context of this chapter will be highlighted and the key objectives outlined. The experimental methods and materials used to achieve these objectives will be clearly stated and described. This will be followed by the results detailing the main outcomes of the experimental investigations, which will lastly be followed by an in-depth discussion of these findings.

2.1. Background and Objectives

PPy has been considered for a variety of biomedical applications with notable success (Guimard, et al. 2007). It has been investigated as an alternative to traditional DES coatings (Arbizzani, et al. 2007; Okner, et al. 2007), although only Arbizzani, et al. considered the use of salicylate as a dopant and neither study explored the influence of electropolymerisation conditions on PPy generation nor the antioxidant capacity of the coatings generated. The potential utility of PPy as a novel targeted antioxidant therapy in the application of stent coatings thus remains to be fully explored.

As a conducting polymer, PPy can be generated by chemical and electrochemical synthesis, and electropolymerisation can be achieved by different methods. Unlike chemical synthesis, electropolymerisation is highly appropriate for generating reliable and uniform conducting polymer coatings on electrically conductive substrates (Guimard, et al. 2007), but there is debate about the optimal electropolymerisation conditions and the potential impact that these have on the coating's redox chemistry (Losito, et al. 1994). Thus, further research is necessary if the electropolymerisation process is to be optimised for stent coatings. Conducting polymers can exist in a doped, or undoped state, with previous work indicating that dopant incorporation during electropolymersation and subsequent release can be used to provide local drug release. Arbizzani et al, (2007) used sodium salicylate as a dopant during electropolymerisation of pyrrole, with this anti-inflammatory compound being released upon incubation of the resultant coating. The therapeutic potential of such release remains to be determined. and the release of dopants in solution can be considered as a drug release effect.

The overall aim of this study has been to generate PPy coatings with potential to promote accelerated endothelial healing whilst limiting restenosis. The surface characteristics of a stent coating play a potentially important role in both processes, with this having been the subject of considerable prior work (Mani, et al. 2007; Korei, et al. 2022). The surface characteristics of PPy coatings are variable, with variation in the electropolymerisation shown to significantly influence surface roughness (Chikouche, et al. 2014). There is substantial evidence to suggest that surface roughness is a critical factor in determining how endothelial cells will respond to a surface (Chung, et al. 2003). The oxidation of conducting polymers may also play a considerable role in the biocompatibility of these coatings (Humpolíček, et al. 2018), and this can be determined for PPy coatings using FTIR and cyclic voltammetry, although this has not been investigated in the context of stent coatings.

As the first steps towards achieving the overall aim of the wider study, the following objectives were identified:

1. Optimise the electropolymerisation process of PPy synthesis, to reliably generate uniform coatings on stainless steel substrates.
2. Characterise the surface morphology of the PPy-coatings, using SEM to identify significant topographical features.
3. Quantify the salicylate dopant contained in PPy coatings, identifying the drug-release profile and consider the effectiveness and impact of electrochemical dopant discharge on the PPy coating's topographical features.
4. Explore the electrochemical properties of PPy coatings using cyclic voltammetry and determine their redox state using FTIR. Consider over-oxidation and identify the conditions for this effect and strategies to mitigate this.

In this chapter, the key data collected in pursuit of the above objectives will be presented and analysed.

2.2. Materials and Methods

2.2.1. Materials and Equipment

Material/Equipment	Supplier
Stainless Steel (316L wires and plates)	Goodfellow Cambridge Ltd, UK
Ag/AgCl Reference Electrode (KR5)	ThermoFisher Scientific, UK
Potentiostat/Galvanostat	Metrohm Autolab
UV-Spectrophotometer (UV-2401PC)	Shimadzu, Japan
MultiSkan Go Plate reader	ThermoFisher Scientific, UK
Scanning Electron Microscope (TM-1000)	Hitachi
Spectrophotometer (ThermoSpectronic BioMate 5)	ThermoFisher Scientific, UK
Spectrum 2 Fourier Transform Infrared Spectrometer	PerkinElmer, UK

2.2.2. Chemicals

Chemical	Supplier	Catalogue Number
Pyrrole (98% solution)	Sigma Aldrich, UK	131709
Sodium Salicylate	Sigma Aldrich, UK	S3007
Phosphate Buffered Saline (PBS) tablets	Oxoid, UK	BR0014G

2.2.3. Sample Preparation

In this study, medical grade 316L stainless steel (316L SS), that has been widely used in BMS and DES designs (Mani, et al. 2007), was used as working electrodes and as a substrate for PPy electropolymerisation. 316L SS was purchased as 1 mm and 200 µm diameter wires and 0.5 mm thick foil. Wires were cut to a length of 30 mm and the foil was cut into 30 x 5 mm strips. Before use, any protective film was removed and samples were rinsed in absolute ethanol and allowed to air-dry.

2.2.4. Electropolymerisation

The electropolymerisation procedures used were based on a previously reported methodology (Arbizzani, et al. 2007; Zhou & Heinze, 1999). Electropolymerisation monomer solution was prepared in deionised water containing 0.1 M pyrrole (Py) and 0.1 M sodium salicylate (NaSa). The electropolymerisation was performed in either potentiostatic or galvanostatic mode using a potentiostat, programmed and monitored with NOVA software (Metrohm).

Potentiostatic Electropolymerisation

As established in Chapter 1, Section 1.8.2., potentiostatic electropolymerisation can be used to generate conducting polymer coatings on a working electrode substrate by applying a constant voltage to the circuit which is above the oxidative potential of the conducting polymer monomer. Since potentiostatic conditions can be defined against the open circuit potential of the set-up, more control can be gained over the oxidative state of the conducting polymer by using this technique, but it can be slow compared to other electropolymerisation approaches.

A three-electrode cell arrangement was set up for potentiostatic electropolymerisation, with the stainless steel wire or foil acting as the working electrode, a 1 mm platinum wire counter electrode and an Ag/AgCl reference electrode (KR5). The incorporation of the reference electrode allows the open circuit potential to be established. Working and counter electrodes were cleaned with ethanol before the first experiment and again with deionised water before each coating cycle was carried out. Electropolymerisation was carried out on ice, using an ice bath, in a 100 ml beaker containing 60 ml of the electropolymerisation monomer solution, as shown in Figure 2.1.

The electropolymerisation conditions were first optimised for applied voltage and time. Based on previously reported methods (Su & Iroh, 1997) and previous experimental optimisations, a series of fixed voltages were initially investigated between +0.9-1.5 V, with coating duration of between 1 and 10 minutes examined. In each case, the voltage was controlled against the reference electrode and maintained constant against the open circuit potential (OCP).

For both wires and strips, optimal conditions were identified as +1.1 or 1.3 V voltage applied for 10 minutes and these were used throughout the remainder of the study unless stated otherwise. When changing the electropolymerisation set-up, such as changing working electrode geometry, it is important to consider the impact on electropolymerisation efficiency by factors such as ohmic drop (this is explored further in 2.4.3.). Ideally, the circuit will be adapted by increasing the counter electrode proportionally, but in this study the Pt wire counter electrode was found to be sufficient to support electropolymerisation on stainless steel strips.

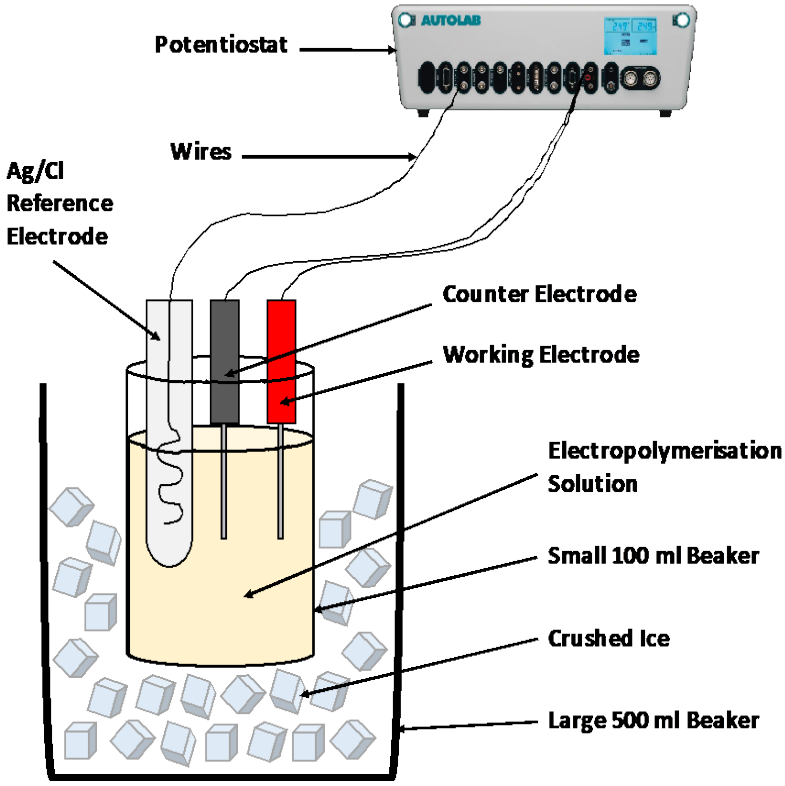

Figure 2.1. Representation of the experimental set-up for the potentiostatic electropolymerisation of PPy coatings. Working electrode – 200 μm, 1 mm wire, or 30x5 mm 316L SS strips. Counter electrode – Pt wire. Electropolymerisation solution contained pyrrole and sodium salicylate dissolved in water.

Galvanostatic Electropolymerisation

Like potentiostatic electropolymerisation, galvanostatic conditions are another technique for generating conducting polymer coatings on a working electrode substrate. During galvanostatic electropolymerisation, the current of the circuit is maintained in order to generate voltages above the oxidation potential of the monomer to initiate polymerisation. This approach provides fast polymerisation reactions with a more uniform rate of coatings formation, but the variable circuit voltage reduces the control over monomer oxidation and resulting coating oxidation state.

A two-electrode cell arrangement was set up for galvanostatic electropolymerisation, with the stainless steel wire (200 μm diameter only) or strip acting as the working electrode, a 1 mm platinum wire counter electrode. The reference electrode is not required for galvanostatic electropolymerisation since the use of current control removes the need to obtain the open circuit potential. All electrodes were cleaned with ethanol before the first experiment and again with deionised water before each coating cycle was carried out. Electropolymerisation was carried out on ice in a 100 ml beaker containing 60 ml of the electropolymerisation monomer solution, as shown in Figure 2.2.

The electropolymerisation conditions were optimised for applied current. Current was initially applied between 0.1 and 1 mA for 200 μm wires (charge density: 0.53 – 5.30 $mA.cm^{-2}$). For wires, optimal conditions were identified as 0.5 mA (change density: 2.65 $mA.cm^{-2}$) applied for 10 minutes.

Unlike potentiostatic electropolymerisation where the applied conditions for coating wires were able to be applied successfully to stainless steel strips, it was necessary to re-optimise and reduce the charge density applied when coatings strips. An initial range of 1 and 8 mA (charge density: 0.33 – 2.66 $mA.cm^{-2}$) was applied with optimal conditions identified at 1 and 2 mA (change density: 0.33 – 0.67 $mA.cm^{-2}$) applied for 10 minutes, and these conditions were used throughout this study. This approach of re-optimisation to the electropolymerisation could further me applied to other working electrode geometries, such as full stent structures.

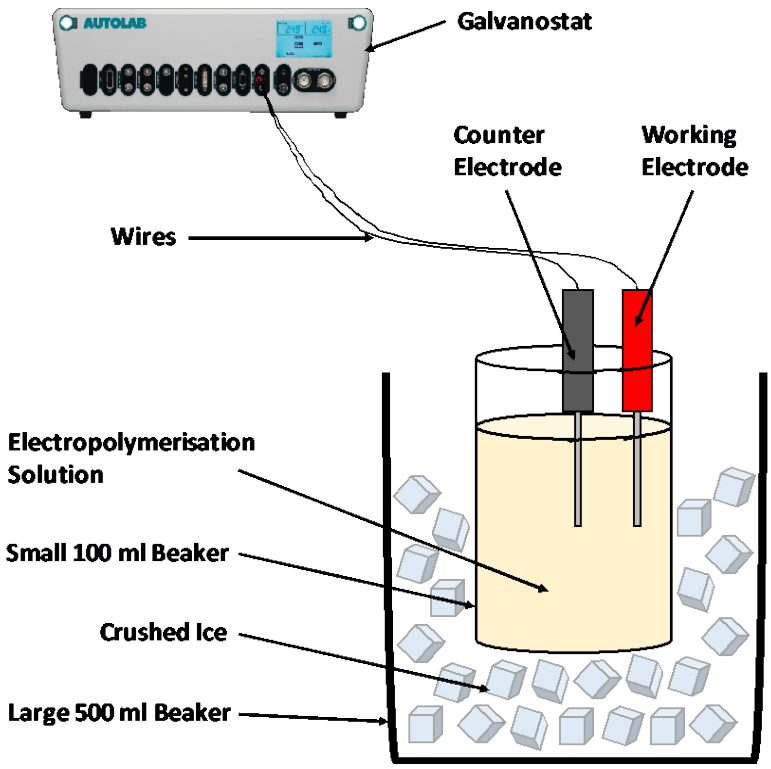

Figure 2.2. Representation of the experimental set-up for the galvanostatic electropolymerisation of PPy coatings. Working electrode – 200 µm, 1 mm wire, or 30x5 mm 316L SS strips. Counter electrode – Pt wire. Electropolymerisation solution contained pyrrole and sodium salicylate dissolved in water.

By utilising both potentiostatic and galvanostatic electropolymerisation in this study it is possible to generated a variety of coatings of different thickness and ideally different oxidative states. Differences in coatings could also be achieved by modifying other variables, such as dopant type and concentration, but these have further potential to significantly impact other coating properties such as morphology, as shown in Section 2.3.5. All coated samples, potentiostatic and galvanostatic, were left to air-dry at room temperature overnight and stored for up to 1 week in 1.5 ml Eppendorf tubes (wires) or 7 ml glass vials (strips).

2.2.5. Microscopy

Scanning electron microscopy (SEM) was used to characterise the electropolymerised PPy coatings and assess their gross surface morphology. SEM images were obtained using a benchtop scanning electron microscope (Hitachi TM-1000). Samples were mounted on stainless steel discs with carbon tape and imaged directly at a fixed accelerating voltage. Samples were imaged at 400 and 2000x magnification and exported as jpeg files.

Scanning electron microscopy provides a detailed visualisation of the surface morphology. It is not intended in this study as an assessment of surface topography or to provide a quantification of the mean surface roughness. The use of terms such as rough, flat, and uniform in this study are included as qualitative descriptors of the visual characteristics of the surface and this data should not be interpreted as indicative of the sample's surface topography.

2.2.6. Salicylate Release Assay

Salicylate release from the PPy coatings was assessed to investigate any differences in doping and elution kinetics between PPy coatings and as one method to quantify the electropolymerisation reaction efficiency. PPy-coated stainless steel wires were stored in Eppendorf tubes containing 1 ml PBS and incubated at 37°C/120 rpm for 7 days. The PBS solution was replaced at 1, 2, 4, 24, 48, and 168 h intervals and stored at -20°C. Salicylate elution was determined by measuring absorbance at 297 nm against blank PBS (MultiskanGO, Thermo Fisher). A study by Dasgupta, et al. (2015), confirms the presence of the salicylate absorbance peak at 297 nm. A calibration curve of salicylate-PBS standard solutions (0.01 - 3 mM) was prepared, allowing quantification of the salicylate within the experimental samples to be calculated. Where concentrations of eluted salicylate were in excess of the saturation level of the spectrophotometer, Sa-PBS solutions were diluted before reading absorbance and final concentrations calculated accordingly.

In vitro release data was modelled using a previously developed MATLAB programme to assess the diffusion-associated release kinetics for each coating (Quirk, 2021). This programme is capable of modelling both single phase and biphasic diffusion and works by fitting multiple fast and slow diffusion coefficients and identifies the best fit for the available data. This is performed using a Crank-Nicolson scheme to solve the diffusion equations.

Finally, the app plots the release data along with the best-fit estimate data. The approach of using mathematical modelling using single and biphasic drug elution dynamics has long been established for drug eluting stents (McGinty, 2014).

2.2.7. Electrochemical Salicylate Dischange

In addition to passive elution of the incorporated salicylate dopant from PPy coatings, the efficiency and impact of electrochemically stimulated release was also assessed. Electrochemically driven eluted should provides an efficient method for removing the dopant from the coating to generate drug-free coatings and may also be used to change the electrochemical state of the PPy coating.

Electrochemical salicylate elution was performed by applying a -0.75 V potential to the PPy coated working electrode after the electropolymerisation process. This process was adapted from previous electrochemical elution procedures recorded by Cysewska, et al. 2016. This step was performed using the same electropolymerisation set up as described in Sections 2.2.4. and the same buffer solution, with the applied voltage delivered for 10 minutes.

Quantification of salicylate remaining in the coatings after electrochemical elution was performed using the salicylate release assay as described above in Section 2.2.6.

2.2.8. Electrochemical Impedance Spectroscopy

Electrical impedance spectroscopy (EIS) was used to characterise the overall electrochemical properties of coated samples and to provide insight into the surface properties of the PPy coatings and the effects of salicylate elution on these. EIS was performed using the two-electrode cell arrangement with the PPy coated samples used as the working electrode and Pt wire used as the counter electrode as outlined for galvanostatic electropolymerisation in Section 2.2.4. PPy samples were tested after air-drying overnight. EIS was carried out using the same potentiostat system used previously, with NOVA software being used to complete Frequency Response Analysis measurements. All EIS measurements were made in PBS solution at 50 mV and a frequency range of 1 Hz – 100 kHz.

Elution effects of salicylate were assessed by performing electrochemical impedance spectroscopy on the PPy coatings every 5 minutes for 1 hour. At the time of testing, salicylate

release assays performed as per Section 2.2.6. had been performed on all coatings and demonstrated that a significant proportion of the salicylate dopant is released within one hour of PBS immersion.

EIS data can be used to generate Nyquist plots by plotting the negative imaginary impedance (Z'') against the real part of impedance (Z'). These plots can be used to determine the charge transfer resistance, which is shown by the diameter of the semi-circle in the higher frequency domain of the Nyquist plot. Warburg impedance is shown by a 45º gradient on a Nyquist plot. A Bode plot can also be obtained by plotting phase shift or the modulus of impedance against frequency. Phase shift represents the bulk resistance and capacitance behaviour of the sample, with resistor behaviour represented as a 0º shift and capacitor behaviour represented by a -90º shift. Warburg impedance can also be more easily be observed from this data, evidenced by a phase shift of -45º.

Ideally, PPy coatings should exhibit a simple impedance profile with 3 discrete phases: a Randles circuit behaviour at high frequencies with a Warburg section at intermediate frequencies, and a purely capacitive behaviour, due to the redox capacitance, in the low frequency range (Gutiérrez Pineda, et al. 2018). This profile is easily identifiable using the Nyquist plot or the phase shift Bode plot. Additionally, if the coating exhibits this profile, the EIS data provides a quantifiable measure of charge transfer resistance, electrolyte resistance, the double layer capacitance and the Warburg impedance constant. This is shown in Figure 2.3.

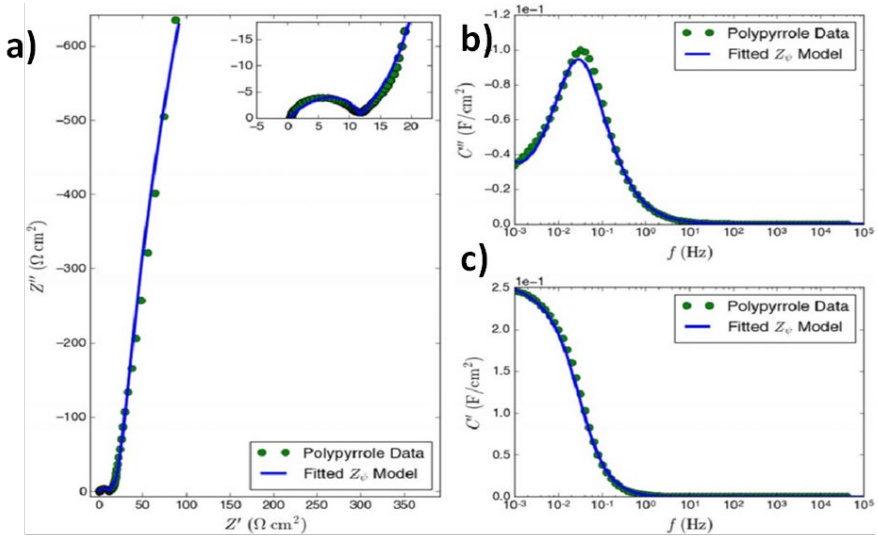

Figure 2.3. Representative Nyquist (panel a) and Bode plots (panels b and c) for Polypyrrole and other conducting polymers from previously reported literature. This data shown are for polypyrrole-chloride coatings generated by potentiodynamic electropolymerisation on porous carbon electrodes, but are representative of typical of polypyrrole coatings displaying Randle circuit characteristics and exhibiting double layer capacitance (adapted from Hasyim & Rajagopalan, 2020).

2.2.9. Cyclic Voltammetry

Cyclic voltammetry (CV) was used to assess the redox state of PPy coatings. CV was performed after samples were coated and allowed to air-dry overnight. CV was carried out using the potentiostatic, with NOVA software controlling the chronoamperometry function. A three-electrode cell was set-up as described for the "potentiostatic electropolymerisation" procedure, with PBS (prepared from tablets) used as the CV solution. Parameters for cyclic voltammetry were adapted from previous studies (Shi & Zhitomirsky, 2010), with a scan rate of 20 mV.s^{-1} and a voltage range of 0 and +0.8 V vs. the reference electrode. Voltammograms were obtained for 20 cycles and cycles 1, 3, 5, 10 and 20 are shown in the data for improved legibility.

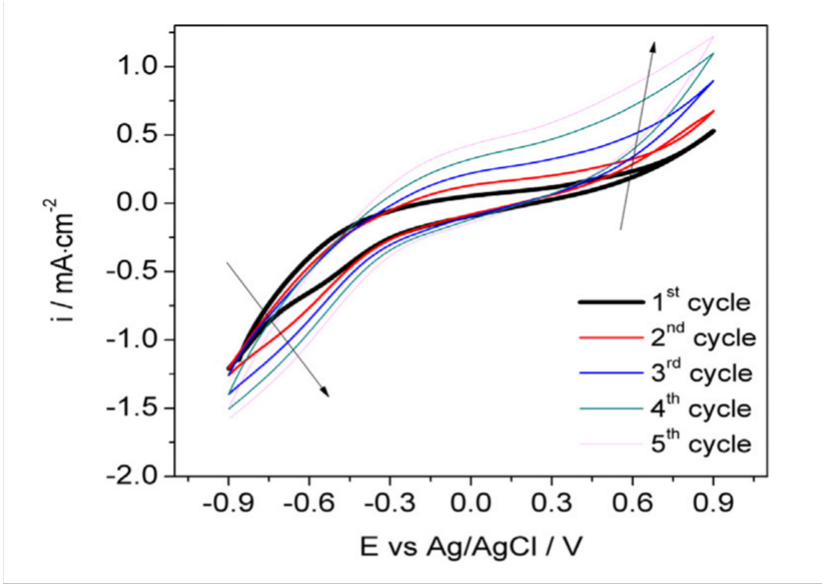

Figure 2.4. Representative cyclic voltammogram for PPy and sodium salicylate films from previously reported literature showing oxidative peaks after consecutive cycles at +0.9 V (vs. Ag/AgCl) and reduction peaks after consecutive cycles at +0.9 V (vs. Ag/AgCl) (adapted from Cysewska, et al. 2016).

Figure 2.4. shows a typical cyclic voltammogram obtained for PPy coated doped with sodium salicylate. During cyclic voltammetry, voltage is cycled within a specified rate at a selected scan rate. During these cycles, changes in current are recorded and oxidation and reduction peaks can indicate the redox response of the polymer or changes in the polymer chemistry. Scan rates, the electrolyte and the potential range affect the voltammogram. Slower scan rates allow more diffusion of large electrolytes, such as dopants, and as such, using multiple scan rates can indicate the contribution of the dopant on the electrochemical responses of a conducting polymer coating.

2.2.10. Fourier Transform Infrared Spectroscopy

Fourier transform infrared spectroscopy (FTIR) was used to identify differences in the functional groups of PPy coatings. FTIR was performed using an attenuation total refraction (ATR) Fourier transform spectrometer. Dry PPy-coated stainless steel strips were mounted to the FTIR crystal and spectra obtained in the range of 4000-400 cm^{-1}. Three independent samples were analysed per electropolymerisation condition. For each sample, spectra were obtained from three areas across the length of the strip. Data presented is representative of the

mean spectra for each sample after baseline correction. Overoxidised strips were also assessed using FTIR and generated by galvanostatic electropolymerisation for 10 minutes at 1 mA followed by 20 cycles of CV at a 0-+1.5 V potential range.

Principle Component Analysis was performed using MATLAB and a proprietary script (Baker, M. [personal communication]).

2.2.11. Statistical Analysis

During electropolymerisation, changes in current (potentiostatic) or voltage (galvanostatic) were recorded and are shown as average changes against time. Variation within the electropolymerisation procedure is not represented graphically, but is discussed separately. All averages shown are representative of the mean data, and where error bars are included they represent ± one standard error of the mean (S.E.M). Graphs were created using GraphPad Prism 9 and regression and correlation analysis was performed using the built-in tools within this software programme. Specific curve fitting procedures used are described for the data in section 3.3. Statistical analysis was also performed using GraphPad Prism, and the statistical tests performed are outlined for the data in section 2.3.

2.3. Results

The following results are structured around the objectives of this study and will therefore be presented and described separately. The key results will then be discussed together in the context of the overall aim of this chapter in section 3.4.

2.3.1. Generation of PPy-coated wires by potentiostatic and galvanostatic electropolymerisation

Initially, 1 mm 316L SS wires were used to perform preliminary optimisation of the potentiostatic electropolymerisation process. 1 mm wires were selected for ease of initial use and to generate clearly visible coatings to assess the electropolymerisation efficiency. Electropolymerisation was performed at applied voltages between 0.9 and 1.5 V, with the current responses at the working electrode shown in Supplementary Figure S2.1.

Potentiostatic Electropolymerisation

200 µm wires were used following 1 mm wire optimisation, a more relevant model for coronary stent struts. Applied voltages in the range of 1.1 – 1.5 V were used to generate PPy coatings on the thinner wires, with 0.9 V disregarded due to its inefficiency in generating PPy on 1 mm wires.

Figure 2.5. shows the outcomes of potentiostatic electropolymerisation of PPy on 200 µm wire, with the current/time profiles shown in panel a and SEM micrographs in panel b. On 200 µm wires, 1.1 V applied voltages appear to be effective for generating PPy coatings. This is shown in the current/time profile by a rapid, albeit slower than observed for +1.3 V, rise in current followed by a plateau. SEM showed these coatings to have a consistent morphology across the surface, with no underlying 316L SS visible. The PPy coatings showed a round and globular, or often termed “cauliflower”, morphology.

Coatings generated at +1.3 V and +1.5 V demonstrated similar current/time profiles to each other. A very short and substantial increase in current was recorded quickly (within the first 50 s), followed by a clear drop in current over the rest of the cycle. This contrasts with the current/time profile observed for +1.1 V (200 µm) and 1 mm coatings. Due to the similarity between +1.3 and +1.5 V coatings, SEM micrographs were not obtained for 1.5 V coatings.

SEM revealed globular features on the cauliflower PPy structure of +1.3 V coatings, resulting in less visibly uniform that was not visible to the naked eye.

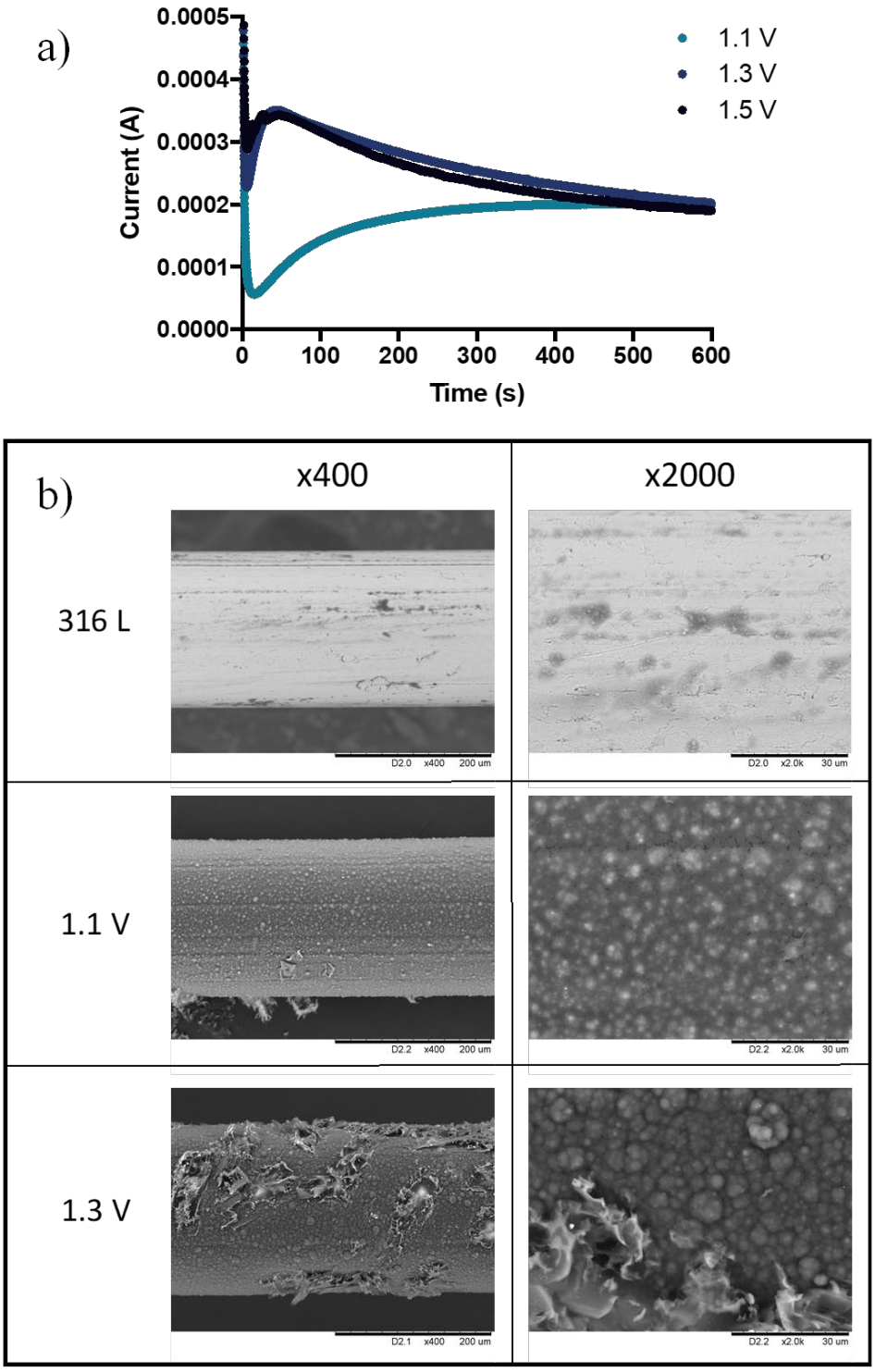

Figure 2.5. a) Current-time profiles for potentiostatic electropolymerisation of pyrrole on 200 µm 316L SS wires, coated for 10 minutes over a range of applied voltages between +1.1 and +1.5 V. b) SEM micrographs of potentiostatic electropolymerised polypyrrole films and uncoated 316 L SS. Images are representative of 3 repeat samples.

SEM was also performed on uncoated 316L SS wire samples and showed the wires to have overall a regular surface finish, but with some pits and cracking apparent over the length of the surface. These surface defects are not apparent on PPy-coated wires, suggesting potentiostatic electropolymerisation, especially at 1.1 V, may be useful for generating very regular and homogeneous films. It is important to achieve homogeneous uniform coatings as this should increase the potential for generating predictable outcomes when assessing the properties of PPy as a potential stent coating.

When translating the technology to stent applications however, it may be necessary to adapt the coating structure to elicit the intended biological effect. For example, it may be beneficial to apply different coatings, or no coating, to the luminal aspect of the stent structure to improve the thrombogenic properties of the stent, but the outer PPy coated surface should still be uniform. For this study therefore, where the aim is only to assess PPy antioxidant potential, it is ideal to generate uniform coatings.

Galvanostatic Electropolymerisation

Galvanostatic electropolymerisation was considered as an alternative method for generating PPy coating to improve coating to coating variability sometimes observed under potentiostatic conditions. Constant current was maintained for coatings at a range of 0.1 and 1 mA, equivalent to a charge density of 0.53 – 5.30 $mA.cm^{-2}$ for the 200 µm wires. This range was based on previously reported data in the literature (Shi & Zhitomirsky, 2010) and preliminary work carried out by other researchers in the laboratory (Morgan, 2018). Changes in voltage were recorded during the polymerisation process and shown in Figure 2.6. (panel a), alongside SEM micrographs of the galvanostatic PPy coatings generated (panel b).

At each current, PPy polymerisation was observed, with visible black coatings present on samples generated at all three conditions. 0.1 mA appeared to generate thinner and less consistent coatings than the 1 mA coatings, which had large visible crystalline structures on their surface. The voltage/time profiles for these coatings are similar between 0.1 and 0.5 mA-generated coatings, showing consistent voltage throughout the cycle, after initial passivation. This is in contrast to 1 mA-generated coatings, which exhibited a very strong increase in voltage during electropolymerisation.

SEM micrographs show the cauliflower PPy morphology to be present on samples generated at all three conditions and confirm the presence of the large crystalline features on the surface

of these coatings. In comparison with coatings generated under potentiostatic conditions, 0.1 mA coatings appear to have a visibly flatter morphology, with less texture from the typical 'cauliflower' topography apparent than both 1.1 and 1.3 V coatings. Whereas, 0.5 mA coatings appear to be more textured than the 0.1 mA and 1.1 V coatings, and are comparable to the 1.3 V coatings, but with improved regularity and consistency across the length of the sample.

Like potentiostatic electropolymerisation, the galvanostatic electropolymerisation conditions determine the coating characteristics, but the voltage/time profiles are less clear to interpret making it more difficult to use this to estimate PPy coatings behaviour. Nonetheless, the different PPy films generated by potentiostatic and galvanostatic electropolymerisation present useful model surfaces for studying the responses of cells to PPy films with varied topographies.

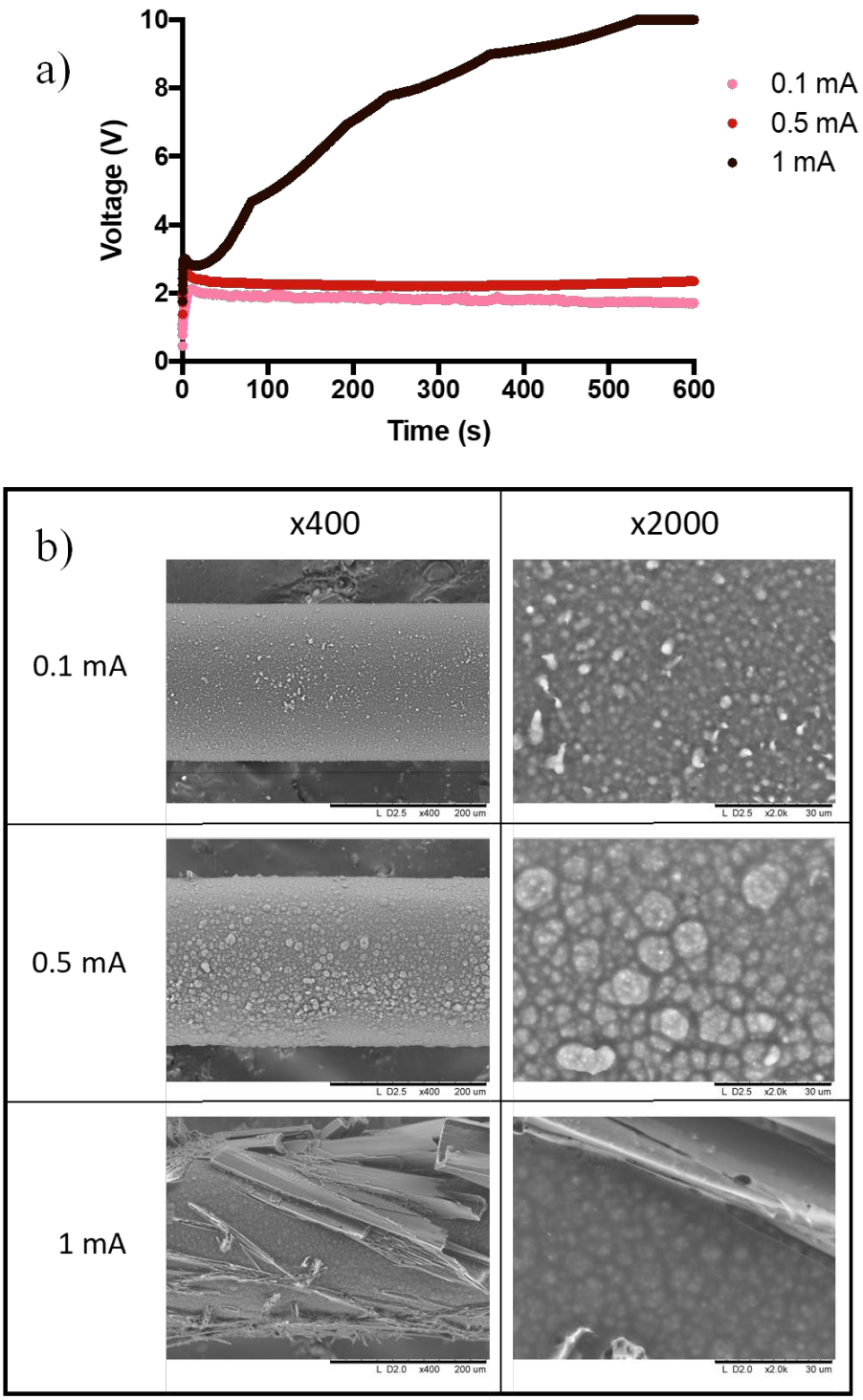

Figure 2.6. a) Current-time profiles for galvanostatic electropolymerisation of pyrrole on 200 µm 316L SS wires, coated for 10 minutes over a range of maintained currents between 0.1 and 1 mA. Data is representative of the average profile from 3 samples. b) SEM micrographs of galvanostatic electropolymerised polypyrrole films. Images are representative of 3 repeat samples.

The thickness of PPy coatings generated by potentiostatic and galvanostatic electropolymerisation were also estimated using ImageJ to measure the coated wire diameter. Mass was also measured using an analytic balance and substracting the average stainless steel wire mass (7.3 mg). Due to the low resolution of the balance and the very small mass of the coating, these measurements have very high variance and therefore only provide estimates of the coating mass. However, the data shows that under both potentiostatic and galvanostatic conditions, increasing the applied voltage or current was found to increase coating thickness and mass.

Table 2.1. Estimated mean mass and thickness of coatings generated by potentiostatic and galvanostatic electropolymerisation. All means are taken from 3 independent coating samples and shown with standard error of the mean.

Electropolymerisation Conditions	Mean coating mass ± S.E.M. (µg)	Mean coating thickness ± S.E.M. (µm)
1.1 V	83.3 ± 72.7	8.3 ± 1.7
1.3 V	183.3 ± 60.09	16.7 ± 4.4
0.1 mA	33.3 ± 44.1	3.3 ± 1.7
0.5 mA	166.7 ± 16.7	16.7 ± 1.7
1 mA	466.7 ± 33.3	45.0 ± 2.9

2.3.2. Generation of PPy-coated strips by potentiostatic and galvanostatic electropolymerisation

Strips were coated as alternative platform for PPy films. This was necessary for use with biological assays where increased surface areas would be important to achieve reliable results. Moreover, the planar surface of the strips readily permits microscopic evaluation of cell adhesion, thereby reducing the complexity associated with analysis of curved wire surfaces. Electropolymerisation of 316L SS strips was carried out following the same procedure as coating wires, and characterised by current/voltage-time profiles and SEM to assess electropolymerisation efficiency.

Potentiostatic Electropolymerisation

Based on the electropolymerisation of 200 µm wires, 316L SS strips were coated at applied voltages of 1.1 and 1.3 V for 10 minutes. Figure 2.7. shows the average current/time profile of electropolymerisation of the strips (panel a) and corresponding SEM micrographs (panel b). The current/time profile for strips shares many similarities of that observed when coating wires. Applying 1.1 V led to an increase in current with time, although slower than observed with wires. Application of 1.3 V led to a marked increase in current at a more rapid rate to 1.1 V coatings within the first 100 s, followed by a plateau and a small loss of current in the second half of the cycle. The recorded current was approximately ten-fold greater for the coated strips compared with the 200 µm coated wires, possibly reflecting the increased surface area when using the strips as the working electrode. Based on a coating length of 20 mm, the surface area of 200 µm wires is significantly lower at 12.48 mm^2 than the surface area of strips at 200 mm^2. This results in a change in the working to counter electrode surface area ratio from approximately 0.2 for the SS wires to 3.2 for SS strips.

Uncoated 316L SS samples were imaged and the grain boundaries of the steel surface are clearly visible. Potentiostatic electropolymerisation was capable of generating films of PPy on strips at 1.1 and 1.3 V, but this process was found to be highly variable between samples. When compared with coated 200 µm wires, both coated strips have a less textured surface morphology and a flatter cauliflower morphology. Crystal formation was visible on 1.3 V coated samples as thin elongated crystals and this is also evident in the SEM micrographs (Figure 2.7. (panel b)).

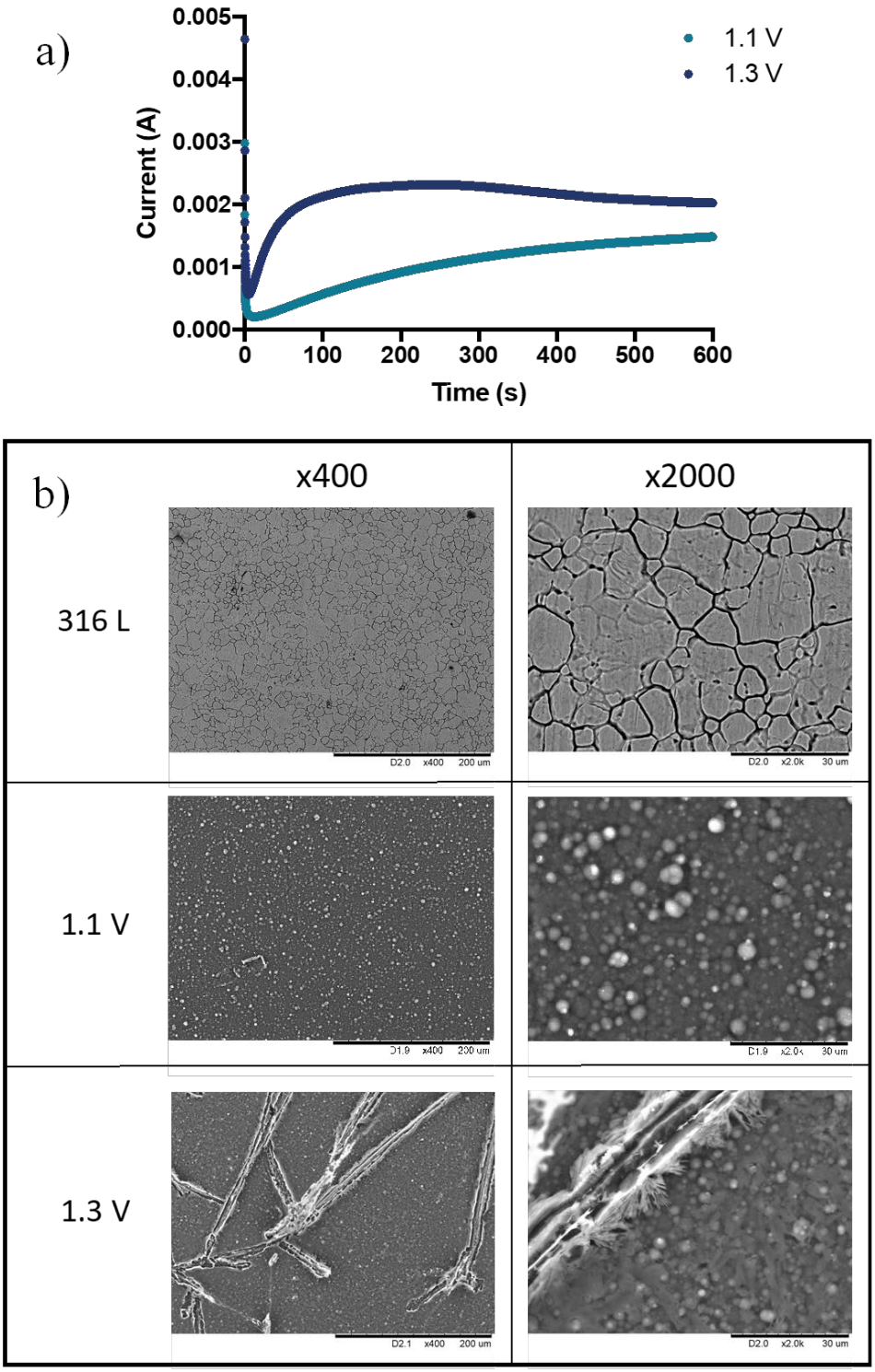

Figure 2.7. a) Current-time profiles for potentiostatic electropolymerisation of pyrrole on 30 x 5 mm 316L SS strips, coated for 10 minutes at +1.1 and 1.3 V. Data is representative of the average profile from 3 samples. b) SEM micrographs of potentiostatic electropolymerised polypyrrole films and uncoated 316 L SS strips. Images are representative of 3 repeat samples.

Galvanostatic Electropolymerisation

PPy coated wires were generated by galvanostatic electropolymerisation at maintained currents between 0.5 and 8 mA. 8 mA was selected based on charge density of 2.65 $mA.cm^{-2}$, as identified when coating 200 µm wires at 0.5 mA. Smaller currents were applied after 8 mA was found to be inappropriate for generating coatings with 316L SS strips due to the very high formation of crystalline surface structures during electropolymerisation as shown in Figure 2.8. (panel b).

The voltage/time profiles of PPy-coated strips are shown in Figure 2.8. (panel a) and the overall profile mirrors that observed when generating PPy coatings on wires. When considered alongside the SEM micrographs shown in Figure 2.8. (panel b), it is clear that applied currents above 2 mA are not appropriate for generating optimal coatings. Firstly, although 2.65 $mA.cm^{-2}$ was found to be an ideal charge density for 200 µm wires, strips generated at 2.65 $mA.cm^{-2}$ (8 mA) showed very rapid increases in voltage during electropolymerisation and surfaces saturated with surface precipitate. Strips coated at 2 and 4 mA also showed very high levels of surface precipitation on their surface, although the associated voltage/time profiles did not show the same increase in voltage during the electropolymerisation cycle.

0.5 and 1 mA conditions generated PPy coatings free of crystalline surface precipitation and their voltage/time profiles show a sustained voltage at approximately 2 V throughout the electropolymerisation cycle. This matches closely with the ideal profile for 200 µm wires coated at 0.5 mA, suggesting that 2 V is a suitable target voltage level to generate PPy without salicylate precipitation under galvanostatic conditions. SEM micrographs show very poor consistency on 0.5 mA coatings with large areas where the steel grain boundaries are still visible. 1 mA coatings were more consistent, but it is worth noting that the surface morphology appears very visibly flat with no obvious cauliflower morphology. This is notably different to the galvanostatic coatings generated on wires and less textured than potentiostatic coated strips. This data however suggests 1 mA is an appropriate applied current for generating PPy-coated wires over 10 minutes.

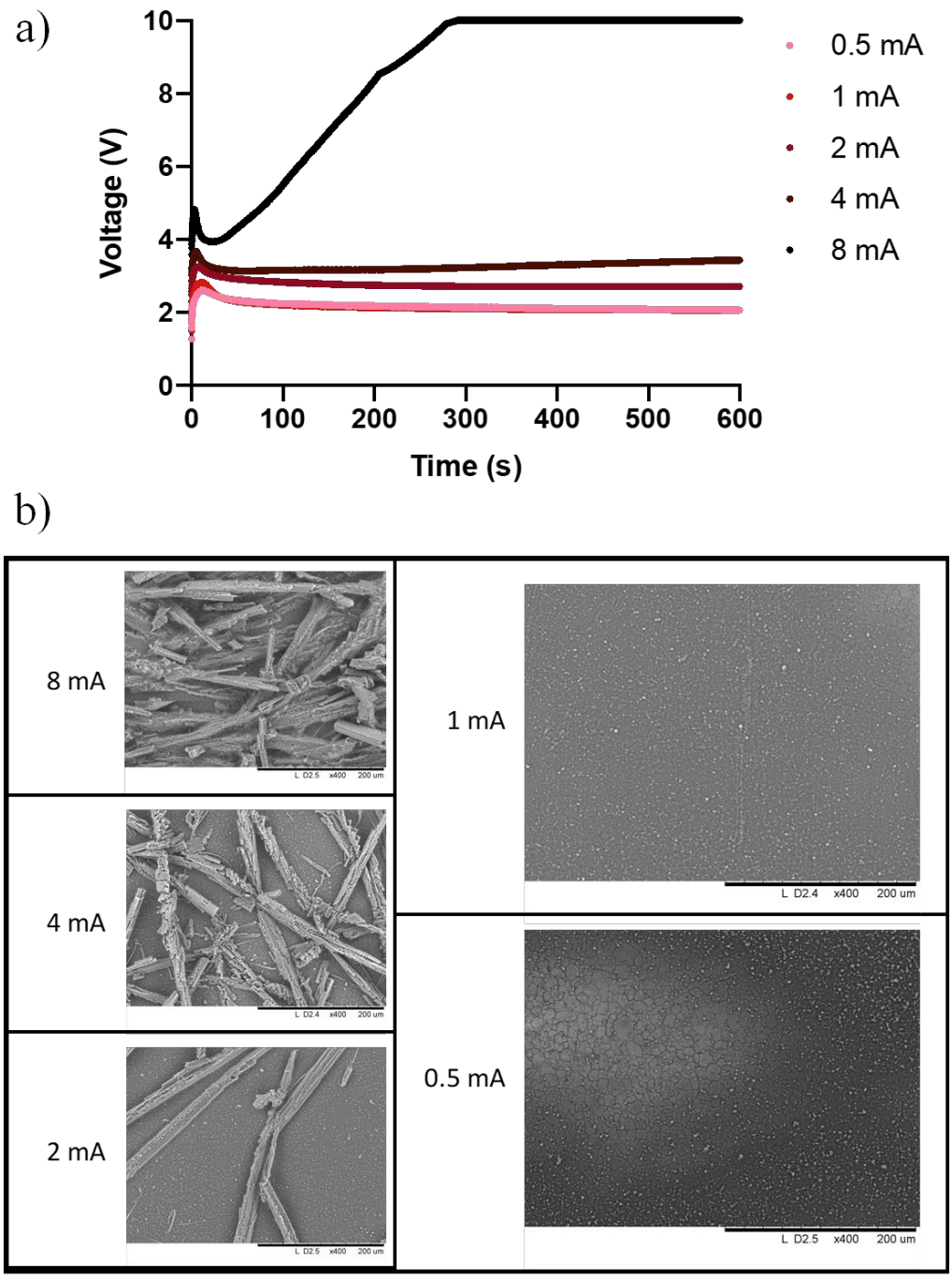

Figure 2.8. a) Current-time profiles for galvanostatic electropolymerisation of pyrrole on 30 x 5 mm 316L SS strips, coated for 10 minutes over a range of maintained currents between 0.5 and 8 mA. Data is representative of the average profile from 3 samples. b) SEM micrographs of galvanostatic electropolymerised polypyrrole films. Images are representative of 3 repeat samples.

2.3.3. Passive dopant elution from PPy-coating wires

Dopant release from PPy coatings was assessed by quantifying salicylate release into PBS over 7 days. From this *in vitro* data, a MATLAB application (developed previously; Quirk, 2021) was used to characterise the dopant release kinetics from PPy samples. Active electrochemical discharge through application of a negative potential discharge cycle was also assessed as a process for rapidly removing salicylate from the PPy films.

Before quantifying salicylate release from PPy-coated 316L SS, a salicylate-PBS standard curve (0.1 mM – 10 M) was obtained on a plate reader. Absorbance spectra were obtained in the range of 250 and 350 nm. Supplementary Figure S2.2 shows the absorbance spectra recorded using the microplate reader and absorbance values for different concentrations at 296.5 nm. This shows the plate reader to be sensitive <30 mM at detecting salicylate quantities in PBS, whilst providing improved efficiency and throughput compared with other techniques, such as UV-spectrophotometry.

Although +1.1 V potentiostatically generated, and 0.5 mA galvanostatically generated 200 µm wires were identified previously as the most suitable PPy coatings in terms of uniformity, surface morphology and lack of precipitation, +1.3 V, 0.1 and 1 mA coatings are also considered here to provide comparisons to better determine the impact of electropolymerisation on salicylate elution.

Salicylate release from PPy coatings generated potentiostatically is shown in Figure 2.9. and coatings generated galvanostatically in Figure 2.10. Non-linear regression was modelled using a MATLAB app for fitting single phase and biphasic diffusion coefficients to *in vitro* elution data (Quirk, 2021). Both +1.1 and 1.3 V coatings have similar release profiles. Both coatings released salicylate rapidly within the first 24 hours before the salicylate release slowed, suggesting the majority, if not all, of the salicylate is removed from the PPy coatings by 7 days. Coatings generated at +1.3 V were found to elute significantly more salicylate over 7 days vs. +1.1 V coatings when compared using an unpaired t test (1.3 V: 264.4±25.7 µg vs. 1.1 V: 149.0±30.0 µg; mean±S.E.M., $p<0.05$, n=4). The difference between the coatings was apparent from 1 h elution and throughout the 7-day release.

The effect of potentiostatic electropolymerisation on total salicylate eluted from PPy coatings was assessed by modelling the linear regression fit of eluted salicylate mass at 168 h and

current at the end of the 10 minute potentiostatic cycle and the peak current during electropolymerisation. The linear regression fit for final current vs. eluted salicylate is shown graphically in Figure 2.9. (panel c). A strong and significant positive correlation was observed for these two variables ($r=0.859$, $p<0.01$) with some variation from the linear fit observed ($r^2 = 0.738$). The regression fit for peak current is shown in Figure 2.9. (panel d) and shows a positive correlation between the two variables ($r=0.731$, $p<0.05$) with a weaker fit than observed when correlating salicylate elution with final current ($r^2 = 0.535$).

Dopant release from galvanostatic coatings again showed a significant difference in the overall salicylate eluted at different currents when compared by a one-way ANOVA (0.1 mA: 46.2±4.3 µg, 0.5 mA: 256.6±31.6 µg, 1mA: 696.2±15.9 µg; mean±S.E.M., $p<0.05$, $n=4$). 0.1 mA coatings eluted very low quantities of salicylate, reflecting the thin and irregular coatings seen by SEM, whereas 1 mA coatings released the highest quantity of salicylate, reflecting the significant precipitation observed on these coatings. Like, coatings generated by potentiostatic electropolymerisation, these differences are apparent within the first hour of elution and throughout the 7-day release period.

Coatings generated potentiostatically at +1.3 V and galvanostatically at 0.5 mA have similar cauliflower surface morphologies as demonstrated by SEM and the total salicylate eluted from these coatings was not significantly different when compared using an unpaired t test (1.3 V: 264.4±25.7 µg vs. 0.5 mA: 256.6±31.6 µg; mean±S.E.M., $p>0.05$, $n=4$).

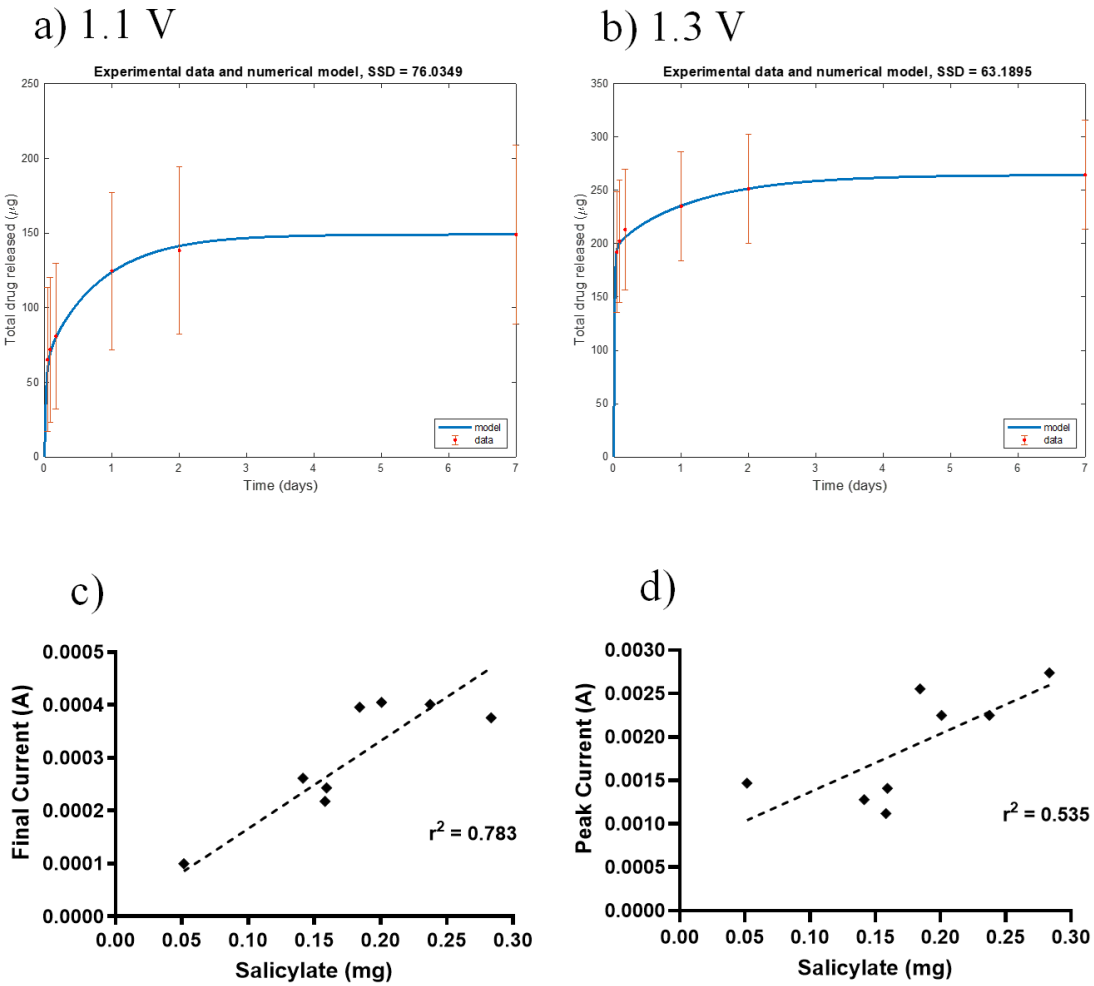

Figure 2.9. In vitro salicylate release over 7 days from potentiostatic electropolymerised polypyrrole coatings generated for 10 minutes with an applied voltage of a) 1.1 or b) 1.3 V. (n=4; mean ±SD, trendline fit calculated using MATLAB model for biphasic diffusion) c) Correlation of salicylate release from potentiostatic coatings shown in a, vs. final current during electropolymerisation, showing a significant positive correlation ($r=0.859$, $p<0.01$). d) Correlation of salicylate release from potentiostatic coatings shown in a, vs. peak current during electropolymerisation, showing a significant positive correlation ($r=0.731$, $p<0.05$).

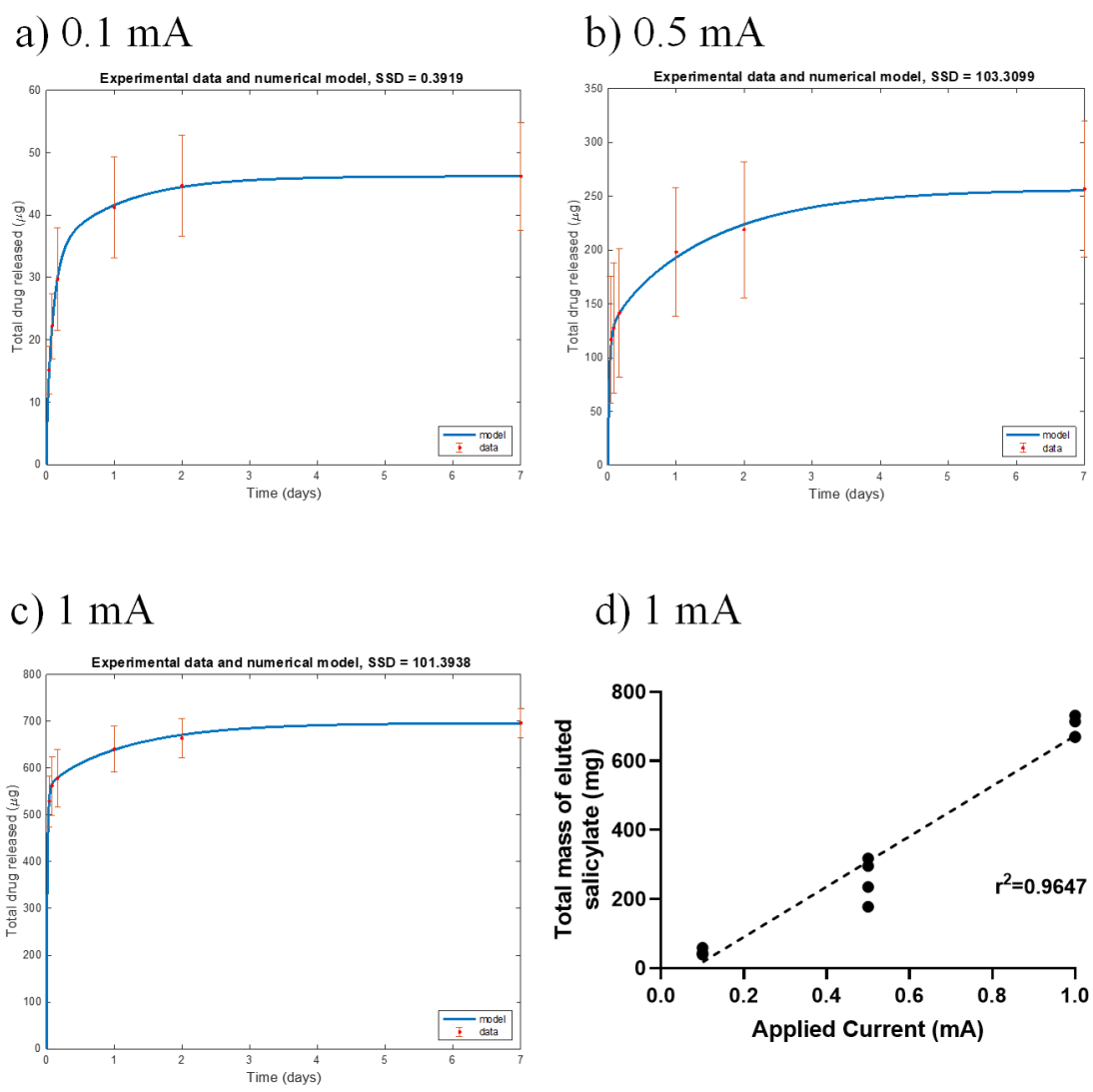

Figure 2.10. In vitro salicylate release over 7 days from galvanostatic electropolymerised polypyrrole coatings generated for 10 minutes with an applied voltage of a) 0.1, b) 0.5 and c) 1 mA. (n=4; mean ±SD, trendline fit calculated using MATLAB model for biphasic diffusion). Panel d shows the total mass of salicylate plotted against the applied current for galvanostatic electropolymerisation. This shows a strong linear correlation (r^2=0.9647).

In order to further understand the mechanisms driving salicylate elution, the diffusion coefficients driving the release kinetics for each coating were estimated using the previously developed MATLAB code (Quirk, 2021). Briefly, this code describes diffusion based release from a single phase or a two phase system. It uses the release data to estimate the effective diffusion coefficient in each case. Clear differences in the estimates were observed and are shown in Table 2.2.

For all PPy coatings, the MATLAB programme established that biphasic elution exhibited the closest statistical fit to the *in vitro* data. Coatings generated by potentiostatic electropolymerisation at 1.3 V and galvanostatic electropolymerisation at 0.5 mA had slower elution properties than coatings generated by galvanostatic electropolymerisation at 1 mA. The 1.3 V and 0.5 mA coatings possessed comparable biphasic diffusion coefficients, with estimated D1 (+1.3 V: $7.1x10^{-10,}$ 0.5 mA: $7.0x10^{-10}$) and D2 (+1.3 V: $1.5x10^{-11,}$ 0.5 mA: $2.5x10^{-11}$), although these coatings did have different F values, 0.71 and 0.42 respectively. Release from coatings generated by potentiostatic electropolymerisation at +1.1 V and galvanostatic electropolymerisation at 0.1 mA was markedly slower D1 (+1.1 V: $5.7x10^{-11,}$ 0.1 mA: $5.2x10^{-12}$) and D2 (+1.1 V: $3.3x10^{-12,}$ 0.1 mA: $9.0x10^{-13}$). 1 mA galvanostatic coatings exhibited the fastest elution, with the highest diffusion coefficient and F value (D1: $5.1x10^{-9}$, D2: $1.4x10^{-10}$, F: 0.78). The fit of these values to the *in vitro* data can be seen in Figures 2.6 & 2.7.

Table 2.2. Average diffusion coefficients and F values for salicylate elution from PPy coatings into PBS. D1 values represent the initial fast phase of diffusion and D2 values represent the secondary slow phase of diffusion. F values represent the fraction of elution that fast elution contributes to total drug release. Values were estimated using a MATLAB model and experimental data shown in Figure 2.6. & 2.7.

	D1	D2	F
1.1 V	$5.7x10^{-11}$	$3.3x10^{-12}$	0.35
1.3 V	$7.1x10^{-10}$	$1.5x10^{-11}$	0.71
0.1 mA	$5.2x10^{-12}$	$9x10^{-13}$	0.68
0.5 mA	$7.0x10^{-10}$	$2.5x10^{-11}$	0.43
1 mA	$5.1x10^{-9}$	$1.4x10^{-10}$	0.78

2.3.4. Electrochemical dopant elution from PPy-coating wires

Salicylate was electrochemically eluted from PPy coatings after potentiostatic and galvanostatic electropolymerisation by applying a -0.75 V discharge cycle for 10 minutes. Current/time profiles were recorded and coatings were characterised after salicylate elution using SEM. The efficiency of this was assessed by quantifying the mass of salicylate eluted from PPy coatings after 7 days. This is shown in Figures 2.11. & 2.12.

When -0.75 V was applied to PPy coatings generated by potentiostatic electropolymerisation, an initial negative current was observed followed rapidly by a loss in conductivity. Both 1.1 and 1.3 V coatings lost conductivity, as indicated by the very low current recorded, within the first two minutes of the electrochemical discharge cycle. Coatings generated at 1.1 V displayed a more negative current peak and faster loss of conductivity than 1.3 V samples. SEM imaging of 1.1 and 1.3 V PPy-coated samples after electrochemical elution did not show any obvious difference compared with samples that were not electrochemically modified. 1.1 V samples imaged were found to be more consistent than coatings without discharge, but all were within the normal variation seen for 1.1 V coatings. 1.3 V samples retain their cauliflower morphology and salicylate precipitation remains visible on the coating surface, suggesting electrochemical elution was not effective at removing salicylate precipitate.

Quantification of salicylate released into PBS from samples with, and without, electrochemical elution shows a mean reduction of total salicylate present in samples after application of the -0.75 V discharge cycle. As previously shown, 1.3 V samples contain a greater mass of salicylate compared with 1.1 V samples, but after electrochemical elution when compared by an unpaired t test, no significant difference in salicylate elution was observed between these samples after 7 days elution in PBS (1.1 V: 72.0±11.2 µg vs. 1.3 V: 106.8±11.3 µg; mean±S.E.M., $p>0.05$, $n=3$). Electrochemical elution was however not found to significantly reduce the total mass of salicylate in +1.1 V coatings (without Sa discharge: 72.0±11.2 µg vs. after Sa discharge: 106.8±11.3 µg; mean±S.E.M., $p>0.05$, $n=3$). Despite limited effectiveness with 1.1 V coatings, electrochemical elution was successful at significantly reducing the mass of salicylate contained in +1.3 V coatings (without Sa discharge: 226.5±22.0 µg vs. after Sa discharge: 106.9±11.3 µg; mean±S.E.M., $p>0.01$, $n=4$).

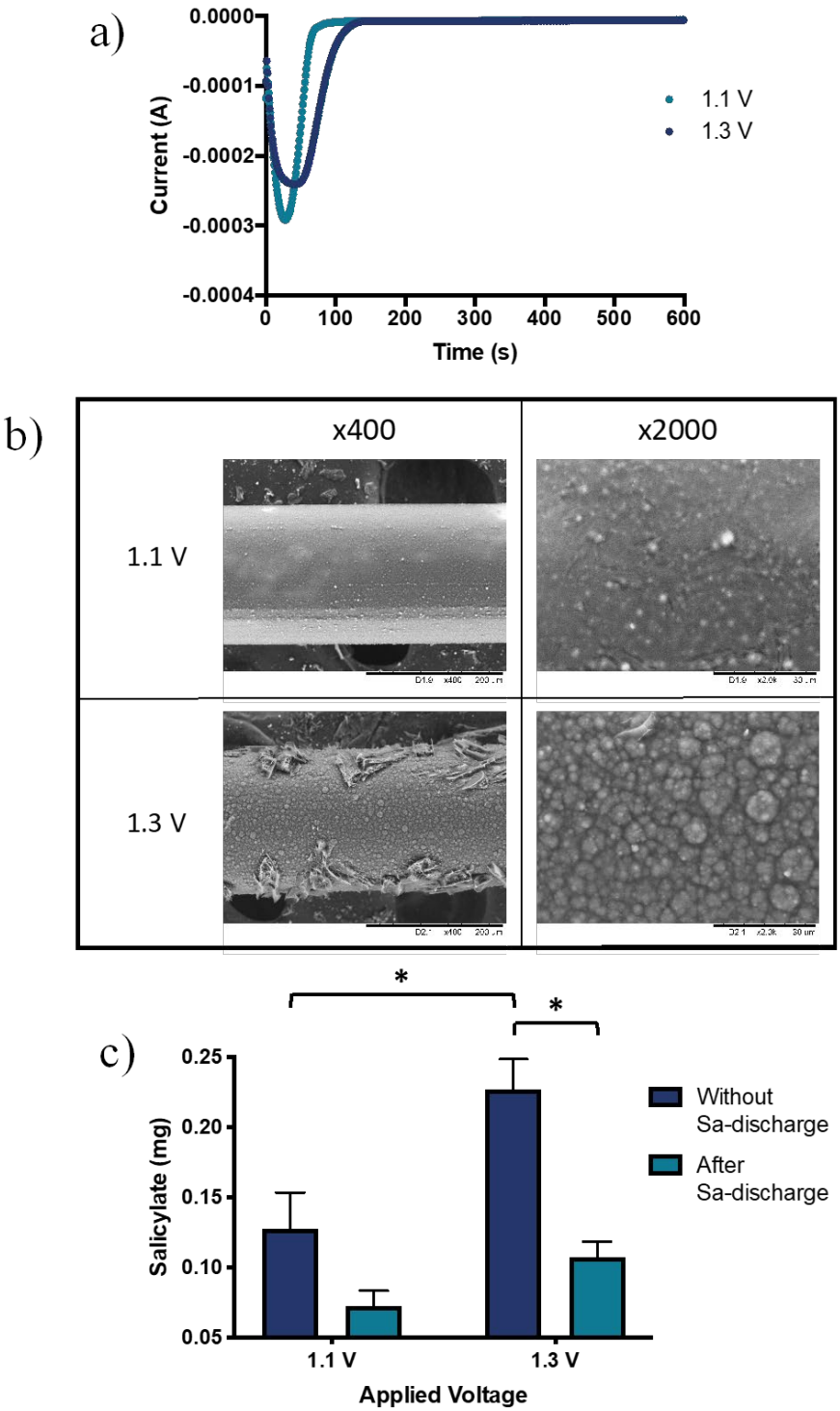

Figure 2.11. a) Average current-time profiles for the electrochemical discharge of salicylate from 200 µm potentiostatic electropolymerised polypyrrole-coated wires upon application of a 10 minute -0.75 V voltage. b) SEM micrographs of potentiostatic polypyrrole-coated wires after electrochemical discharge of salicylate. Images are representative of 3 repeat samples. c) Average mass of salicylate released from potentiostatic polypyrrole after 7 day elution in PBS, with or without electrochemical salicylate discharge. (mean±S.E.M, n=3,* $p<0.05$).

The response of coatings generated by galvanostatic electropolymerisation to a -0.75 V discharge cycle contrasted with the behaviour observed with coatings generated by potentiostatic electropolymerisation. Upon application of the -0.75 V discharge voltage, 0.5 and 1 mA coatings displayed different electrical responses to this step. Coatings generated at 0.5 mA showed a similar response to potentiostatic coatings, but coatings generated at 1 mA did not show a rapid peak, instead there was a slow decrease in current, with a much shallower peak apparent around 500 s, followed by a return towards 0 A. Unlike the other coatings, the current of 1 mA coatings did not reach ~0 A by the end of the cycle, indicating a slower and incomplete loss of conductivity with the 1 mA coatings.

SEM micrographs of the coatings show no apparent visible differences in the coating morphology caused by the discharge step. 0.5 mA coatings appeared to be regular, with highly textured surface topographies. Overall, 1 mA coatings retained the same surface topography and there were no changes to the presence of salicylate precipitate, with large crystalline structure retained on the surface. The x400 magnification image shown in Figure 2.12. (panel b) does however show fracturing of the PPy coating exposing the underlying stainless steel substrate. This was not atypical for wires coated at 1 mA conditions and therefore is not believed to be associated with the addition of electrochemical discharge. Instead, this indicates the mechanical vulnerabilities of coatings exhibiting significant levels of precipitate and highlights the need to control this to avoid unwanted events such as fracturing or the coating becoming thrombogenic. This fracturing was no observed with coatings free of salicylate precipitation.

Salicylate elution from discharged 0.5 and 1 mA samples showed no significant loss in the mass of dopant contained by each coating compared with samples that did not undergo electrochemical discharge (0.5 mA: without Sa discharge 247.0±19.0 µg vs. after Sa discharge 168.0±8.0 µg; 1.3 V: without Sa discharge 807.0±19.0 µg vs. after Sa discharge 735.0±49.0 µg; mean±S.E.M., $p>0.05$, $n=4$). This contrasts the observations made with potentiostatic coatings that electrochemical discharge reduced the mass of salicylate eluted from the coatings.

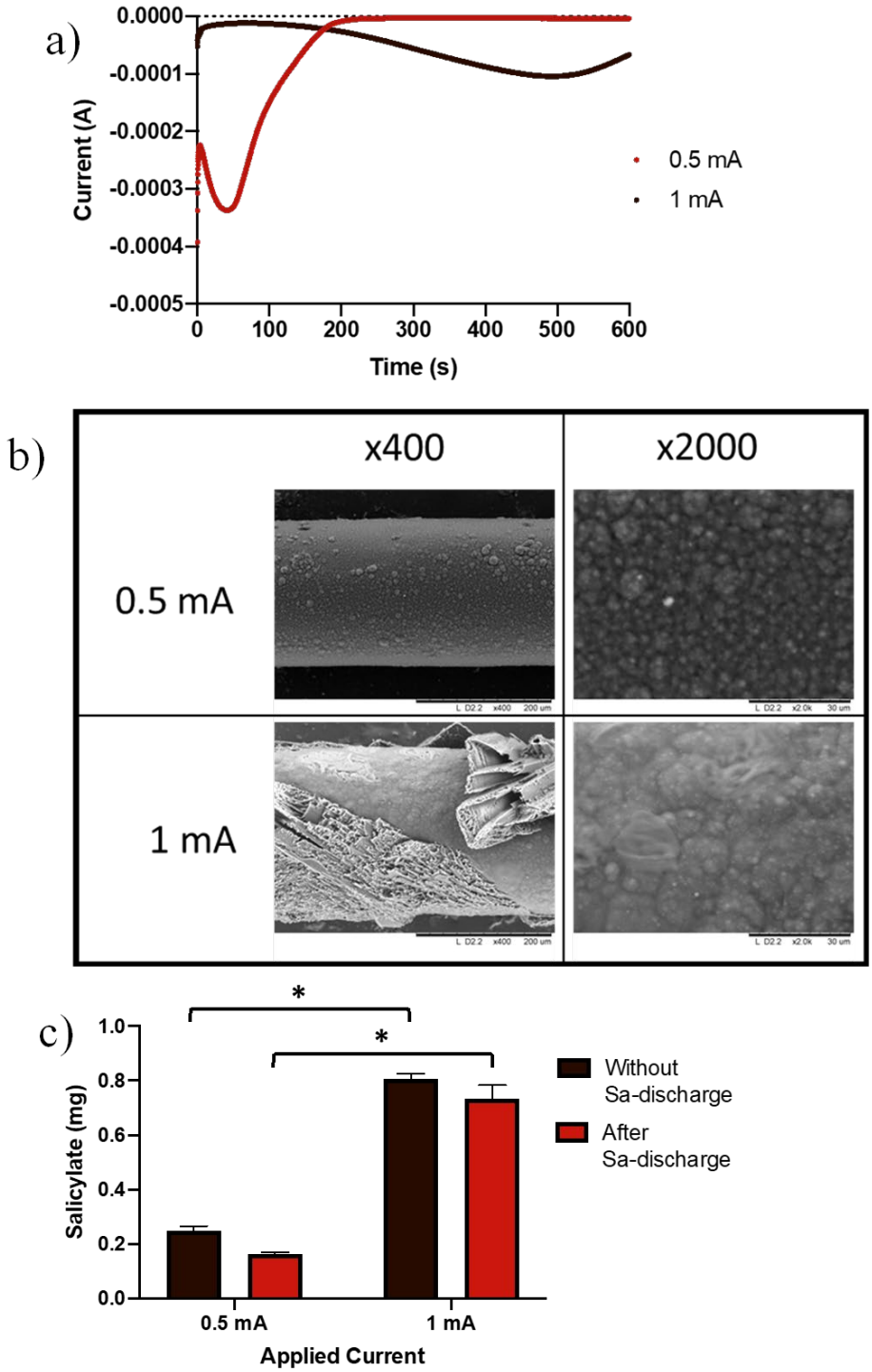

Figure 2.12. a) Average current-time profiles for the electrochemical discharge of salicylate from 200 µm galvanostatic electropolymerised polypyrrole-coated wires upon application of a 10 minute -0.75 V voltage. b) SEM micrographs of galvanostatic polypyrrole-coated wires after electrochemical discharge of salicylate. Images are representative of 3 repeat samples. c) Average mass of salicylate released from galvanostatic polypyrrole after 7 day elution in PBS, with or without electrochemical salicylate discharge.

2.3.5. Effect of dopant concentration on polypyrrole generation

The effect of increased salicylate concentration on the electropolymerisation process and subsequent dopant elution was assessed. Increased salicylate (0.5 M) and pyrrole (0.25 M) concentrations were based on previously reported electropolymerisation procedures (González, et al. 2019; Gutiérrez Pineda, et al. 2018).

Effect of increased dopant concentration on electropolymerisation

Electropolymerisation with solutions containing 0.5 M salicylate was performed potentiostatically (at 1.1 and 1.3 V) and galvanostatically (0.1 and 0.5 mA) with standard (0.1 M) and increased (0.5 M) concentrations of pyrrole. When potentiostatic electropolymerisation was attempted with 0.1 M pyrrole, increased salicylate inhibited the generation of PPy at both applied voltages, leading to formation of patchy coatings. This is shown in Figure 2.13. This low polymerisation rate is supported in the current/time profile, which confirms there was no marked increase in current for either condition during the electropolymerisation cycle.

This is contrasted in coatings generated in electropolymerisation solution containing increased concentrations of both pyrrole and salicylate. In these coatings, there is a noticeable change in current throughout the electropolymerisation cycle, and this is reflected in the SEM micrographs of these coatings showing considerable formation of coatings with a microtubular morphology. There is no discernible difference in the microtubular morphologies generated at the different applied voltages and the current of the coatings is comparable at the end of the electropolymerisation process.

Under all conditions, galvanostatic electropolymerisation was incapable of generating coatings with a microtubular morphology. These are shown in Figure 2.14. At standard concentrations of pyrrole with increased salicylate, 0.1 mA galvanostatic electropolymerisation generated uneven PPy coatings, but increased salicylate promoted precipitation in 0.5 mA coatings as shown by very large crystal structures visible on the coating surface. Increased pyrrole concentrations improved galvanostatic electropolymerisation and generated coatings with comparable morphologies to PPy coatings generated from 0.1 M Py and salicylate solutions. The absence of microtubes on galvanostatic coatings suggests that pyrrole and salicylate concentrations alone do not determine this morphology and electrochemical conditions influence the generation of this microtubular topography.

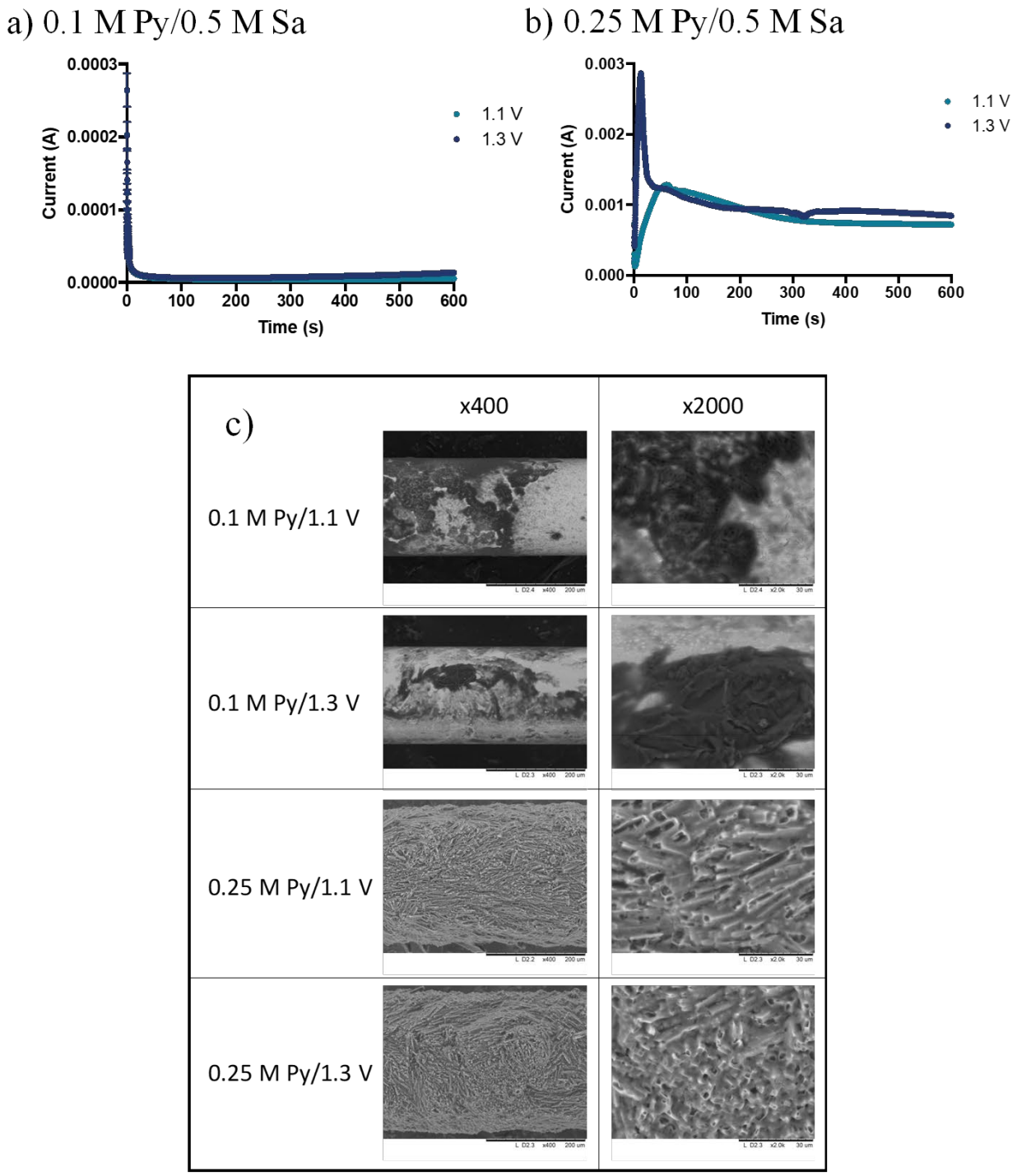

Figure 2.13. a) Average current-time profiles for potentiostatic electropolymerisation of pyrrole on 200 µm 316L SS wires, coated for 10 minutes at applied voltages of 1.1 and 1.3 V, with 0.1 M Py and 0.5 M Sa. b) Average current-time profiles for potentiostatic electropolymerisation of pyrrole on 200 µm 316L SS wires, coated for 10 minutes at applied voltages of 1.1 and 1.3 V, with 0.25 M Py and 0.5 M Sa. c) SEM micrographs of potentiostatic electropolymerised polypyrrole films generated with increased salicylate concentrations. Images are representative of 3 repeat samples.

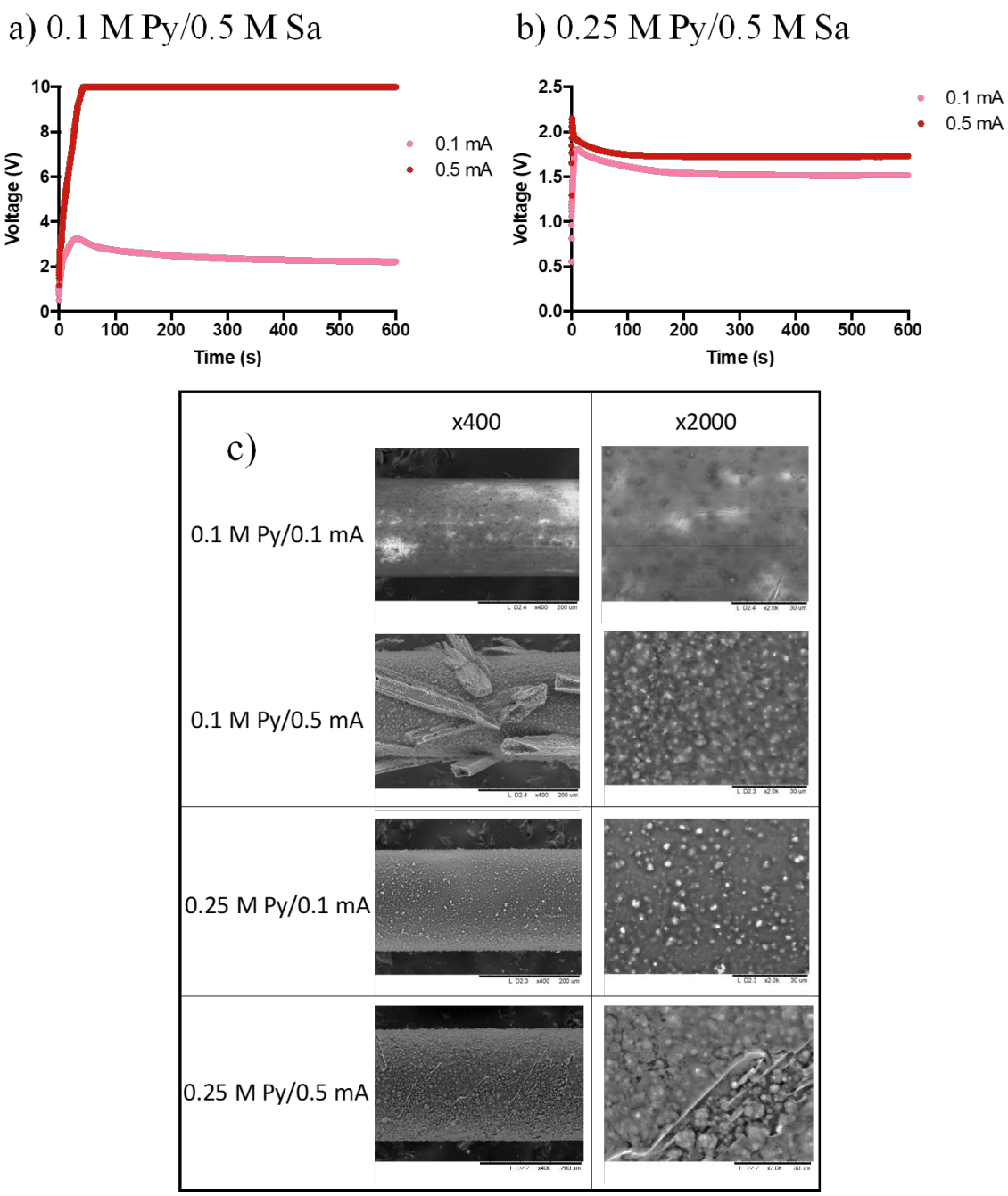

Figure 2.14. a) Average current-time profiles for galvanostatic electropolymerisation of pyrrole on 200 µm 316L SS wires, coated for 10 minutes at applied current of 0.1 and 0.5 mA, with 0.1 M Py and 0.5 M Sa. b) Average current-time profiles for galvanostatic electropolymerisation of pyrrole on 200 µm 316L SS wires, coated for 10 minutes at applied current of 0.1 and 0.5 mA, with 0.25 M Py and 0.5 M Sa. c) SEM micrographs of galvanostatic static electropolymerised polypyrrole films generated with increased salicylate concentrations. Images are representative of 3 repeat samples.

Effect of increased dopant concentration on elution

Of the coatings generated from electropolymerisation solutions containing increased salicylate concentrations, only coatings generated by potentiostatic electropolymerisation with increased pyrrole monomer concentrations were assessed. All other coatings were not considered due to their poor quality and none exhibited the microtubular morphology of interest. Salicylate elution from these coatings was compared with PPy generated from 0.1 M Py and salicylate (1.3 V and 0.5 mA).

Figure 2.15. shows the absolute and relative cumulative salicylate from PPy coatings. Both microtubular coatings generated at 1.1 and 1.3 V eluted significantly greater masses of salicylate at all time intervals than coatings generated by potentiostatic, or galvanostatic, electropolymerisation with 0.1 M salicylate (approximately 5x the mass of salicylate eluted from both 0.5 M coatings compared with 0.5 mA coatings). When compared using an unpaired t test, there was no significant difference between the total mass of eluted from 0.5 M salicylate coatings generated at 1.1 and 1.3 V (1258.3±73.9 vs. 1331.5±81.8 µg; mean±S.E.M., $p>0.05$, n=4).

The elution of salicylate from the coatings generated with standard electropolymerisation solution and at 1.3 V with increased salicylate was presented as cumulative percentages release relative to total release. Microtubular coatings exhibited faster elution than both coatings generated from standard Py/Sa solution. The 1.3 V microtubular coating eluted the majority of salicylate within the first hour (79.6±1.2% eluted vs. total at 168 h ±S.E.M., n=4) and almost all within 4 hours (92.0±0.5% eluted vs. total at 168 h ±S.E.M., n=4).

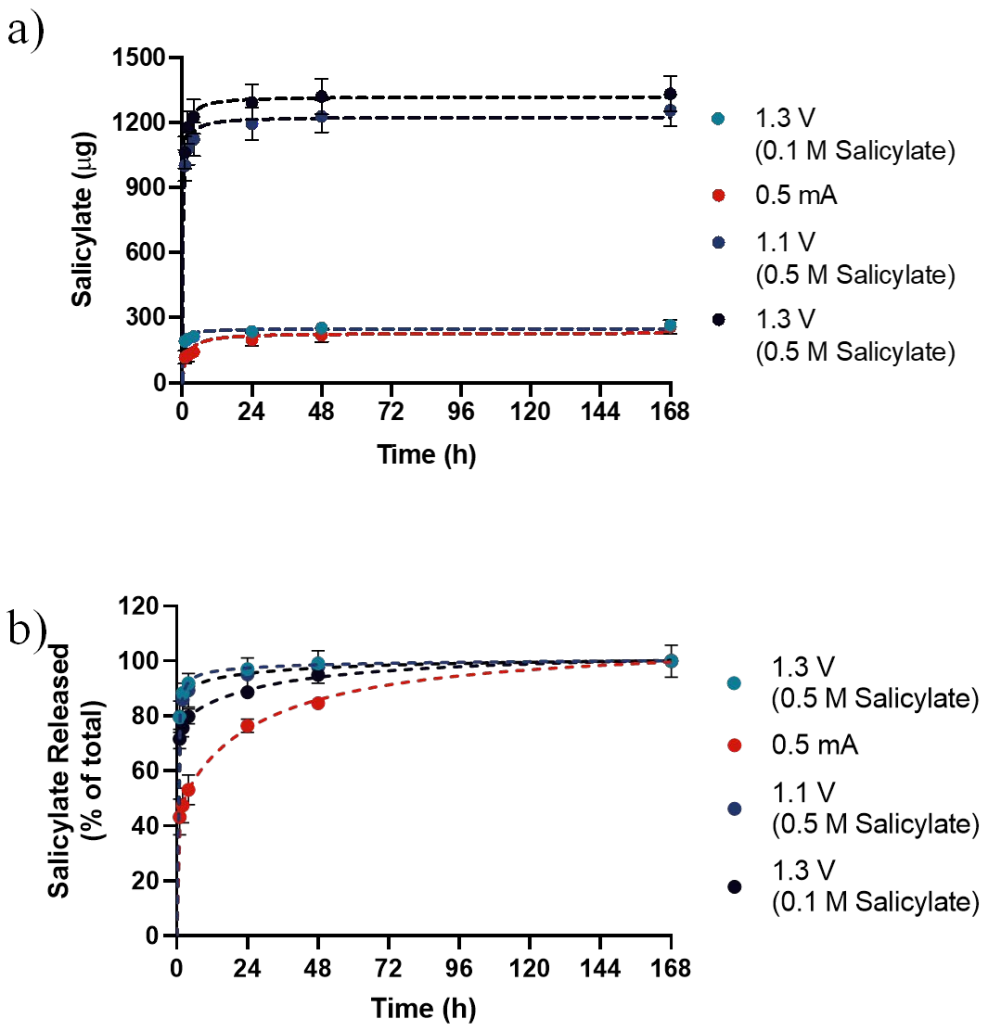

Figure 2.15. a) In vitro salicylate release over 7 days from potentiostatic electropolymerised polypyrrole coatings generated for 10 minutes with an applied voltage of 1.1 or 1.3 V, with 0.25 M Py and 0.5 M Sa. (mean±S.E.M, n=4) and comparison of salicylate release over 7 days from potentiostatic and galvanostatic electropolymerised polypyrrole coatings with 0.1 M Sa. b) Salicylate release profiles of coatings shown in panel a, presented as percentrage release (mean±S.E.M, n=4). Hyperbola trendlines fit using GraphPad Prism 9.

2.3.6. Electrochemical Impedance Spectroscopy of Polypyrrole Coatings

Electrochemical impedance spectroscopy (EIS) was used to assess electrochemical differences between coatings on 200 µm SS wires and also the effect of passive elution on each coating for the first hour of dopant release. Impedance measurements were taken every 5 minutes up to 1 h. Changes were represented using Nyquist and Bode (phase shift) plots as they were found to show the most significant differences between coatings and changes resulting from elution. The impedance modulus is not shown here since it did not reveal clear differences between coatings and or after elution.

The changes in Nyquist plot and phase shift for PPy coatings generated by potentiostatic electropolymerisation at 1.1 and 1.3 V are shown in Figure 2.16. From the Nyquist plots, 1.1 V coatings exhibit an obvious circular arc corresponding to charge transfer resistance in the high frequency region, behaviour not observed with 1.3 V coatings. After the charge resistance region, there is a higher gradient for 1.1 V than 1.3V coatings, leading to lower Z' values. The phase shift data shows that 1.3 V coatings lack a distinct peak in lower frequency domain (<10 kHz) with phase maintained around -45º Warburg impedance. At higher frequencies (>10 kHz), resistance behaviour dominates and the phase shift drops toward 15º for both potentiostatic samples. When considering the effect of salicylate elution, EIS plots for 1.3 V coatings remain stable over observed duration, but 1.1 V coatings exhibit an increase in phase shift below 10 kHz, loss of charge transfer resistance and Warburg impedance characteristics.

The changes in Nyquist plot and phase shift for PPy coatings generated by galvanostatic electropolymerisation at 0.1, 0.5 and 1 mA are shown in Figure 2.17. Before elution, all galvanostatic coatings demonstrate similar EIS responses and the Nyquist plots show that charge transfer resistance decreases with increasing applied current during electropolymerisation. After each circular arc, there is a high gradient observed relating to mass transport response of salicylate leading to the lowest Z' for 1 mA coatings. All galvanostatic coatings have similar high frequency (>10 kHz) drop in phase shift as observed with potentiostatic coatings. Although 1 mA coatings have a much lower peak at 10 kHz (approx. -30º), whereas other coatings have -45º peak, suggesting an absence in Warburg transition between charge transfer and mass transport in 1 mA coatings.

At low frequencies, coatings are comparable and demonstrate capacitive behaviour. When considering the effect of elution, EIS plots for 0.5 and 1 mA coatings remain mostly stable over duration of measurements, but significant changes in Nyquist and phase shift were observed with 0.1 mA coatings. There was a complete loss of charge transfer resistance in favour of mass transport response with a corresponding increase in Z''. There was also a loss of low frequency phase shift capacitance behaviour towards Warburg impedance (<100 Hz), which increases up to 10 kHz.

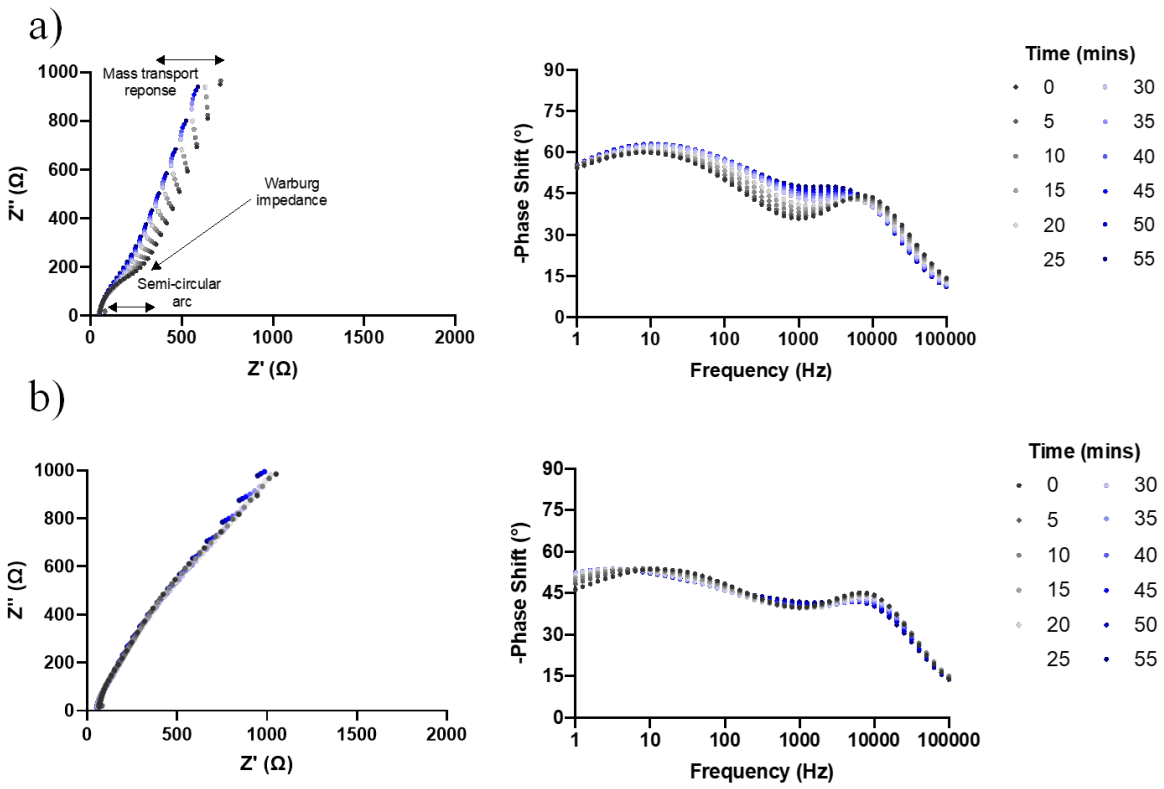

Figure 2.16. Nyquist and Bode plots for PPy coatings generated by potentiostatic electropolymerisation at a) 1.1 V, and b) 1.3 V obtained from electrochemical impedance spectroscopy. Data is representative of mean averages from 3 repeat measurements.

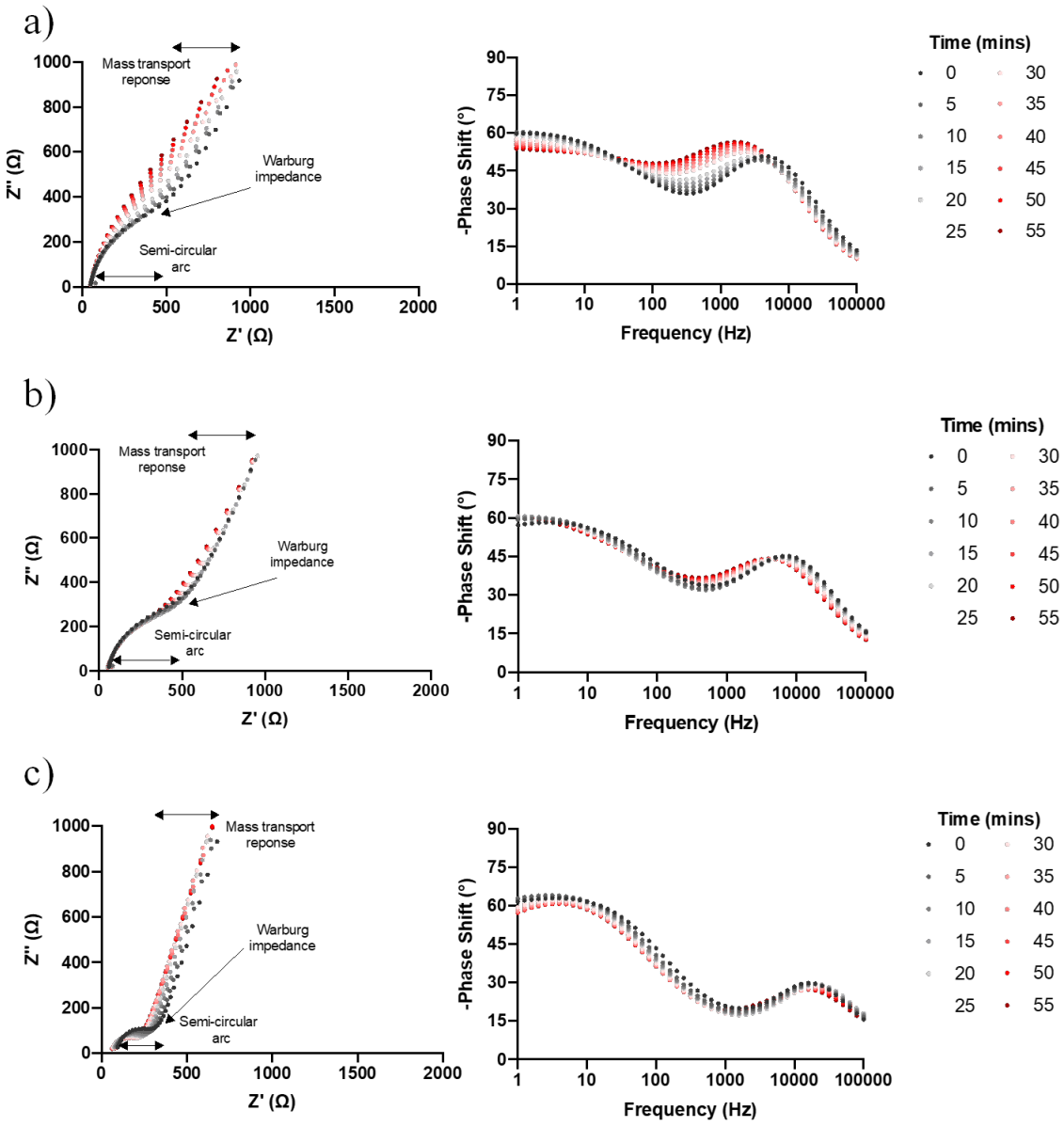

Figure 2.17. Nyquist and Bode plots for PPy coatings generated by galvanostatic electropolymerisation at a) 0.1 mA, b) 0.5 mA, and c) 1 mA obtained from electrochemical impedance spectroscopy. Data is representative of mean averages from 3 repeat measurements.

2.3.7. Cyclic Voltammetry of Polypyrrole Coatings

In addition to EIS, cyclic voltammetry (CV) was performed to further characterise the electrochemical properties of PPy coated 200 µm SS wires and identify any differences in oxidative state of PPy resulting from different electropolymerisation conditions.

Initially, the potential range applied was optimised with 1.3 V potentiostatic coatings by gradually adjusting the voltage window until an oxidation peak was identified at +0.8 V. This 0 - +0.8 V potential range was then used for all subsequent experiments and the resulting cyclic voltammograms are shown in Figure 2.18. CV was performed on uncoated 200 µm SS wires to provide a baseline measurement. Under the conditions used, 316L SS possessed an initial oxidation peak at approximately +0.6 V, which was almost completely lost in subsequent cycles. After CV, wires appeared dull indicating the presence of a thick oxide layer. No reduction reactions were observed with 316L samples.

CV showed differences in the electrochemical properties of potentiostatic PPy coatings. 1.1 V coatings exhibited an initial oxidation peak, which did not change over subsequent cycles and a reduction peak which increased with repeated cycles. At cycle 20, this led to a symmetrical oxidation and reduction peak (±43 µA). 1.3 V coatings exhibited a low oxidation peak at +0.8 V, which increased over repeated cycles, particularly between cycle 5 and 10. Reduction peaks are prominent during cycles 10 and 20, but unlike at cycle 20 with 1.1 V coatings, these are not equal in magnitude (-60 µA and 87 µA).

CV also highlighted more prominent differences with galvanostatic coatings. 0.1 mA coatings were very dissimilar to other potentiostatic and galvanostatic coatings, with a very high initial oxidation peak at approximately +0.6 V, comparable with oxidation peak for SS wires, which continued until cycle 10. At cycle 10 and 20, there was a flattening of the voltammogram but high oxidation persists and unlike other PPy samples, no reduction was observed. 0.5 mA coatings exhibited a low initial oxidation peak, which increased over subsequent cycles and reduction peaks that also increased on cycling, which are almost equal in magnitude to the oxidation peak at cycle 20 (-85 µA and 94 µA). At cycle 20, the oxidation sweep (from 0 to +0.8 V) shows a distinct box shape, which is most prominent in the 0.5 mA samples. 1 mA coatings exhibit similarities to 0.5 mA coatings, but with higher oxidations and reduction peaks (-100 µA and 125 µA) and loss of the box shape response. The 1 mA voltammogram closely resembles the observations made for 1.3 V potentiostatic coatings.

Potentiodynamic electropolymerisation was also used to identify the oxidation peak of pyrrole using the standard electropolymerisation solution over increasing voltage windows (0 - +0.8, 1.1 and 1.3 V). These are shown in Supplementary Figure S2.3. No visible PPy formation was visible on wires up to +0.8 V. PPy formation was visible after 1.1 V and 1.3 V procedures, with thin patchy coatings generated with cycles up to 1.1 V and thicker coatings generated with after 1.3 V cycles. The oxidation of pyrrole is visible in cycle 1 by a peak at +980 mV when cycles up to +1.1 V were applied, and this oxidation peak shifted slightly to +990 mV when cycles up to +1.3 V were applied. No further oxidation peaks were observed with either condition.

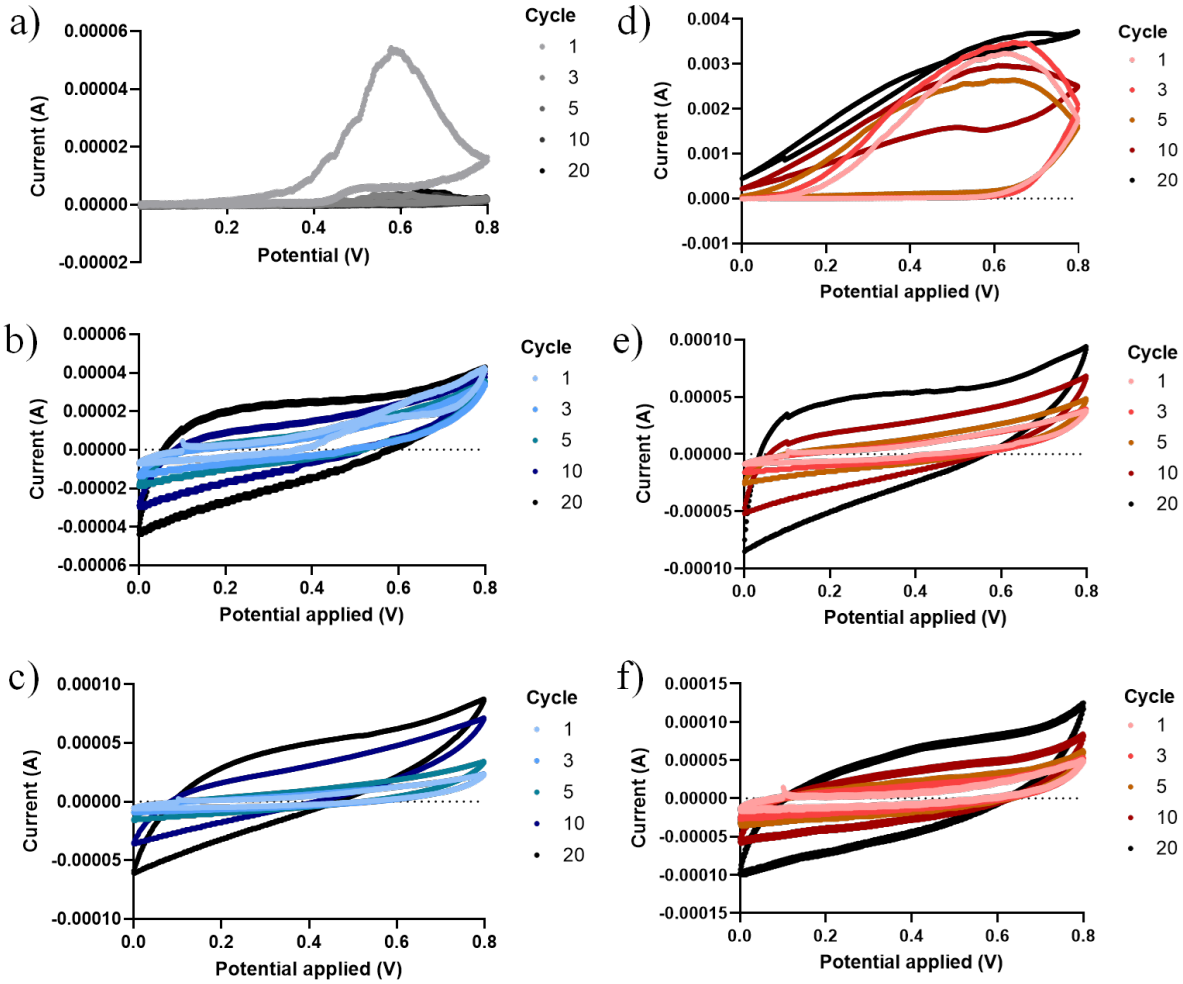

Figure 2.18. Cyclic voltammogram of uncoated and PPy coatings generated on 200 µm diameter SS wires at the following conditions: a) uncoated , b) 1.1 V, c) 1.3 V potentiostatic, d) 0.1 mA, e) 0.5 mA, and f) 1 mA galvanostatic. Each graph represents a single coating. Voltammmograms were obtained by applying a 0 - +0.8 V voltage range against an Ag/AgCl reference electrode in PBS. For simplicity, only cycles 1, 3 ,5 , 10 and 20 are shown on each graph.

2.3.8. Fourier Transform Infrared Spectroscopy of Polypyrrole Coatings

Finally, FTIR was used to identify differences in the chemistry of PPy coatings generated under the different conditions used. PPy coatings were generated on 316L SS strips to give a large surface area for analysis. The spectra obtained for PPy coatings generated by potentiostatic and galvanostatic electropolymerisation are shown in Figure 2.19. Detailed spectra are shown in Supplementary Figure S2.4 & S2.5.

Due to interference by the salicylate dopant and any surface salicylate precipitate, it was difficult to analyse the PPy spectra and identify any specific differences. Sodium salicylate is an organic dopant and as such has a number of peaks in the 700-2000 cm^{-1} range. Salicylate has been previously shown to have strong identifiable peaks at: 1386 and 1652-70 cm^{-1} resulting from symmetric and asymmetric C=O stretching, 1558 – 1610 cm^{-1} from the C=C phenolic ring region, 1444-1503 cm^{-1} resulting from C-C stretching, O-H and C-OH phenolic bending and stretching is observed at 1324 and 1156-1296 cm^{-1} respectively, and 700-759 cm^{-1} attributed to =C-H bending (Trivedi, et al. 2015). These peaks, which were observed in all PPy spectra, created a large amount of noise, potentially obscuring PPy peaks.

Another issue is demonstrated by the high absorbance in the 700 - 2000 cm^{-1} range observed with 316L SS control samples, resulting from the highly reflective surface. This interference likely contributed more to the spectra obtained for thinner +1.1 V potentiostatic coatings and 1 mA galvanostatic coatings.

As with sodium salicylate, characteristic peaks associated with PPy have previously been identified and are as follows: 811 – 910 cm^{-1} resulting from C-H wagging, 1487- 1560 cm^{-1} attributed to C=C phenolic ring stretching, and 1315 and 1685 cm^{-1} corresponding to C-N and C=N bonds respectively (Chougule, et al. 2011). Peaks in these regions were observed for all PPy coatings, with some exceptions. Coatings generated by potentiostatic electropolymerisation at +1.3 V did not exhibit a distinct C-N peak around 1315 cm^{-1}. Coatings generated by galvanostatic electropolymerisation at 1 mA possessed only one weak C=C stretching peak at 1509 cm^{-1}. Overoxidised films were also obtained from 1 mA coatings and also analysed, this spectrum, shown in Supplementary Figure S2.6, was distinct from the normal 1 mA PPy coatings, with the loss of peaks around 900, 1080 and 1400 cm^{-1}, and formation of unique peaks around 750, 1200, 1580 and 1700 cm^{-1}.

Visually, spectra obtained for 2 mA galvanostatic and +1.1 V potentiostatic coatings shared a high degree of features, whereas 1 mA galvanostatic and +1.3 V potentiostatic coatings were visually distinct from the other PPy spectra. A PCA statistical test was performed to compare the PPy and uncoated spectra and shown in Supplementary Figure S2.7. There was very high variation observed between the different PPy coatings, although 1 mA and +1.1 V coatings were the most comparable. Across all samples, except 1 mA coatings, the spectra for each coating type were tightly grouped, suggesting there is strong uniformity and the chemical structure is consistent over the surface.

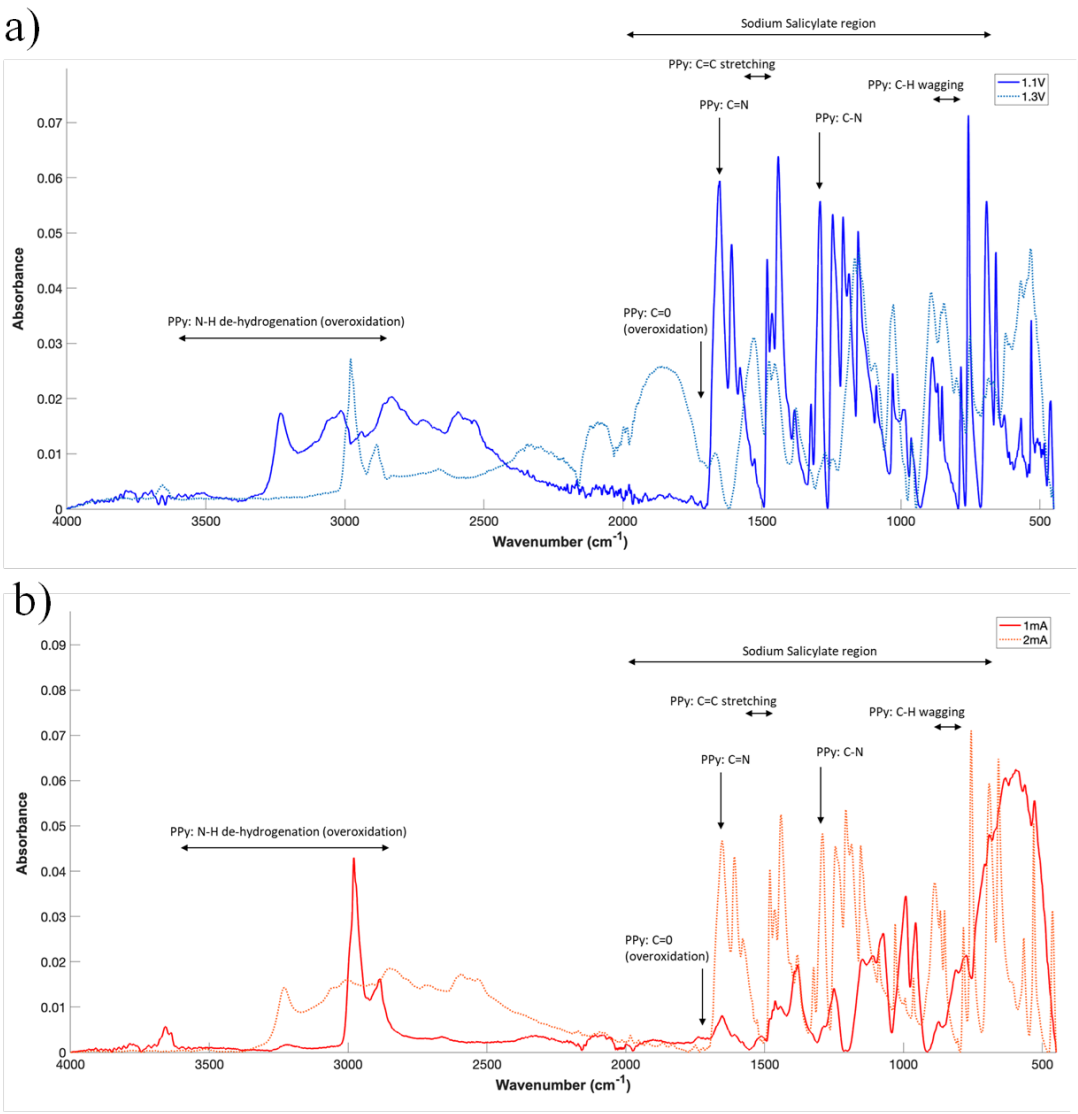

Figure 2.19. FTIR spectra for PPy coated strips generated by a) potentiostatic or b) galvanostatic electropolymerisation. Spectra were obtained in the 450 – 4000 cm^{-1} frequency range and a baseline correction applied before plotting. Each spectra is representation of an average of 3 scan areas from 3 independent coatings.

2.4. Discussion

The synthesis of PPy by electropolymerisation to generate films and coatings has been demonstrated for many uses, but there has been very little investigation of this approach for stent coatings or indeed in wider medical device applications. It has been established that electropolymerisation can generate PPy coated wires on stainless steel electrodes (Arbizzani, et al. 2007; Okner, et al. 2007), but these studies were limited in considering the effects of different electropolymerisation conditions and did not assess the oxidative state of the coatings generated. This chapter therefore explores the electropolymerisation factors, such as maintained voltage, applied current and dopant concentration on influencing the generation of PPy coatings with a view to identifying the optimal conditions for the production of stent coatings. The results in this chapter are discussed in relation to these key parameters and compared to previous studies and established data.

2.4.1. Effect of electropolymerisation conditions on the generation of PPy coated wires

Electropolymerisation voltage

In this study, potentiostatic electropolymerisation was initially used to generate PPy coatings. This was performed on 200 μm diameter 316L SS wires at +1.1-1.5 V (vs. the Ag/AgCl reference electrode) as shown in Figure 2.5. It was observed that PPy was generated on each coating, with thicker more uniform coatings generated at 1.3 V compared to 1.1 V. At the higher 1.5 V condition, PPy formation did not visibly improve, but an increase in the incidence and degree of salicylate surface precipitation was observed. At 1.3 and 1.5 V, the current-time profile changes compared with 1.1 V coatings, possibly because of salicylate crystal formation, or potentially due to PPy overoxidation. Characterisation techniques were used to determine the cause of this effect, see Section 3.4.2. for further discussion of this effect.

It is difficult to compare the electropolymerisation conditions used in this study to previous studies, as there are few reported uses of potentiostatic electropolymerisation with 316L SS working electrodes and 0.1 M Py and NaSa solution used. Furthermore, where similar materials are used, the current-time profile and SEM micrographs frequently not presented. A comparable study by Arbizzani, et al. (2007) used +0.8 and 0.9 V applied potentials to efficiently generate PPy/Sa coatings but used Pt as the working electrode. Similarly, Gutierrez Pineda, et al. (2015) used +0.8 V applied potentials to generate Py/Sa coatings on SS working

electrodes but used 0.25 M Py concentrations. PPy coatings have also been generated at lower applied voltages used to successfully generate coatings using Sa as a dopant, but this study used a copper working electrode (Annibaldi, et al. 2012).

Some differences may arise from the use of a wire Pt counter electrode in this present study, potentially resulting in comparably low counter electrode surface area. Of the three previous studies however, Arbizzani, et al. and Annibaldi, et al. both use Pt wire CEs, whilst the counter electrode material used is not reported by Gutierrez Pineda, et al. Furthermore, it is worth noting that using applied voltages lower than +1.1 V was not attempted with 200 µm wire due to the inefficiency in preliminary optimisation work with 1 mm wires and so applied voltages less than +1.1 V may have been sufficient.

Electropolymerisation current

In addition to potentiostatic electropolymerisation, galvanostatic electropolymerisation was used to generate PPy/Sa coatings as shown in Figure 2.6. An initial maintained current range of 0.1-1 mA was used based on results from a previous study (Morgan, 2017). Across this range, there was a substantial difference between the PPy coatings generated. 0.1 mA led to thin coatings with variable uniformity, 0.5 mA currents led to thicker coatings and 1 mA led to substantial Sa precipitation over the coating surface. Overall, 0.1 mA was insufficient to reliably generate PPy coatings over a 10-minute electropolymerisation time, whereas 0.5 mA produced optimal consistent coatings with no obvious precipitate visible at the surface when assessed using SEM.

As observed with increasing the applied voltage when generating coatings by potentiostatic electropolymerisation, increasing current increased the efficiency of polymerisation allowing thicker coatings to be generated over the same time. This did however lead to undesirable issues including high Sa precipitation and increased variability.

When reporting electropolymerisation conditions, the maintained current used for galvanostatic electropolymerisation is often given as a charge density, where the current is normalised over the working electrode surface area. Since the surface area of the working electrode is used, 0.1, 0.5 and 1 mA currents can be converted to charge densities of 0.53, 2.65 and 5.30 $mA.cm^{-2}$. These values are comparable to galvanostatic electropolymerisation conditions used in other studies. Cysewska, et al. (2014), used a 2.5 $mA.cm^{-2}$ charge density to reliably generate PPy/Sa coatings on iron electrodes, that did not show evidence of

overoxidation. This compares favourably to the 0.5 mA/2.65 mA.cm^{-2} coatings in this study. In addition, Cysewska, et al. (2016), demonstrated that in a 0.1 M NaSa solution, PPy coatings could tolerate charge densities up to approximately 4 mA.cm^{-2} before undergoing overoxidation. This suggests that 1 mA coatings may undergo some overoxidation during electropolymerisation, although the difference resulting from using an Fe vs. 316L SS working electrode is unclear. Shi & Zhitomirsky, (2010), generated PPy/Sa coatings at 1 mA.cm^{-2}, demonstrating that coatings can be generated reliably at lower maintained currents, but perhaps not as low as the 0.1 mA condition used in this study over a 10-minute duration.
The voltage-time profile of PPy electropolymerisation is well defined in the literature, as this profile is reflected in the data presented in this study (Rahman & Ba-Shammakh, 2004). The initial peak observed reflects passivation of the electrode and is comparable to the initial low current during potentiostatic electropolymerisation. Passivation of the electrode is key to ensure good coating stability, which in turn improves the coating's mechanical properties. Cysewska, et al. (2014) identified the passivation peak for PPy/Sa on Fe electrodes as approximately +2.2 V, which is lower than, but comparable to the +2.8 V passivation peak for 0.5 mA coatings in this study, but again it is unclear what impact the different WE and RE materials and surface areas have on this.

Despite generating thicker coatings, the use of higher charge densities has been shown to lead to poorer mechanical properties and corrosion resistance (Cysewska, et al. 2015). This may justify the use of longer deposition times with lower maintained currents for the present study. Increasing charge density has been shown to correlate with increases in film thickness but not in a predictable linear way and such increases also increase the generated PPy particle size resulting in reduced film density due to lower particle packing (Nozaki, et al. 2009). The effect on other coating properties is unclear. Monitoring particle size could provide another route of assessing PPy coating, as there are clear visual difference between the PPy coatings generated by potentiostatic and galvanostatic electropolymerisation in this study.

Film thickness may also play a critical role in determining coating antioxidant properties since film thickness has been shown to correlate with oxidation activation energy. Otero & Martinez, (2011), found that activation energy was highest at 4 µm coatings and decreased for either thinner or thicker coatings. This is likely to be dopant dependent and therefore this value is unlikely to relate to our work. Overall, the improved coating efficiency with higher electropolymerisation current is complex and must be balanced with minimising potential

overoxidation and it's impact on coating mechanical properties and potential inhibition of antioxidant capacity.

Electropolymerisation time

In this study, electropolymerisation duration was largely fixed at 10 minutes, with one-minute electropolymerisation durations used for potentiostatic electropolymerisation to assess the impact of electropolymerisation time on subsequent antioxidant activity. This is explored further in Chapter 3. Overall, 10 minutes was sufficient to generate reproducible coatings with potentiostatic and galvanostatic electropolymerisation, except for at the lower 0.1 mA maintained voltage. Other than the one-minute timepoint, which was not sufficient for generating thick and consistent coatings, the effect of using shorter durations and the change in coating thickness over time is unclear in this study.

The use of a 10-minute electropolymerisation is consistent with prior reports in the literature. Shi & Zhitomirsky, (2010) & Gutierrez Pineda, et al. (2015) both use this duration when generating PPy/Sa coatings. Alternatively, shorter durations may be used as demonstrated by Arbizzani, et al. (2007), where durations as low as 20 seconds were used to generate PPy/Sa coatings. Longer times have also been reported and shown to be successful, for example 20 minutes (Cysewska, et al. 2014), and 1 hour (Hosseini, et al. 2010).

Time alone, as with voltage or current, is not shown to determine PPy properties, but is a strong contributing factor. Increasing time does increase PPy generation and as such presents a simple means of controlling PPy coating thickness without changing other parameters. Furthermore, once characterised time may offer the best parameter to modify or alter the PPy coating process since current and voltage are complex, particularly when generating coatings where precipitation or overoxidation is suspected to occur, for example 1.3 V potentiostatic and 1 mA galvanostatic coatings in this study.

2.4.2. Optimal electropolymerisation conditions for generating polypyrrole coated wires

Optimal electropolymerisation conditions will depend greatly on the desired properties of the PPy coating to be generated for a given target application. For use as an antioxidant stent coating, this would primarily require a coating with suitable mechanical properties and surface topography to aid endothelial compatibility, in addition to suitable chemical and antioxidant properties. The generation of repeatable coatings with controllable film thickness and without oxidation, is associated with a rapid fall in current during electropolymerisation, followed by an initial rapid increase and then for the current to rise uniformly over the electropolymerisation cycle, this allows for the generation of coatings with predictable properties and film thickness and reduces or eliminates the influence of overoxidation. This process can be divided into three chemical phases: passivation, nucleation, and chain growth (Mindroiu, et al. 2009).

Under optimal conditions, these three stages would also be observed under galvanostatic polymerisation, but with voltage initially spiking during passivation, followed by a rapid drop correlating with nucleation and the initial oxidation of pyrrole, but unlike for potentiostatic electropolymerisation chain growth would be shown by a plateau in voltage. (Rahman & Ba-Shammakh, 2004).

In the present study, these optimal electropolymerisation profiles were observed with coatings generated by potentiostatic electropolymerisation at 1.1 V and galvanostatic electropolymerisation at 0.5 mA. To a lesser extent, coating galvanostatically at 0.1 mA exhibited this ideal profile, but these coatings were not consistent, highlighting the need to also factor in electropolymerisation time. Rahman & Ba-Shammakh, (2004) also noted the impact of temperature on electropolymerisation, with higher temperatures increasing the time required for sufficient electrode passivation and polymer nucleation leading to a reduction in electropolymerisation efficiency. In this study, temperature was kept low at approximately 4-8°C to minimise these effects.

Under both electropolymerisation methods, there were deviations from this ideal profile, firstly with potentiostatic electropolymerisation at 1.3 and 1.5 V and then with galvanostatic electropolymerisation at 1 mA. This is suspected to arise from either overoxidation, salicylate

precipitation or a combination of the two effects. These two mechanisms are discussed in more detail below:

Overoxidation or Sa-precipitation – two proposed mechanisms:

1. Overoxidation – leads to loss of electrical conductivity, resulting to an increase in electrical resistance (Holze, 2022). This results in the observed loss of measured current (potentiostatic) or increased voltage (galvanostatic).
2. Salicylate precipitation – very rapid passivation and pyrrole oxidation. The resulting concentration of sodium salicylate at the electrode surface exceeds its solubility limit (Arbizzani, et al. 2007). This results in localised precipitation at the electrode surface. Sodium salicylate or salicylic acid precipitation insulates the electrode, blocking electron transport, increasing resistance, and decreasing the current flow through the working electrode (Tischchenko, et al. 2002). This results in the observed loss of measured current (potentiostatic) or increased voltage (galvanostatic).

Arbizzani, et al. (2007), observed dopant precipitation when generating PPy coatings by electropolymerisation resulting in the formation of visible salt crystals on the coating surface, albeit with sodium naproxene and not with sodium salicylate. It is worth remembering that Arbizzani, et al. used a far shorter electropolymerisation time, which may not have allowed high salicylate precipitation. As noted by Arbizzani, et al., the solubility limit of sodium salicylate is much greater than for salicylic acid (approximately 50 times greater), therefore acidification at the working electrode surface could significantly promote precipitation.

As highlighted, the surface morphology and topography are key coating properties. Surface morphology can be defined as the shape of the surface features as assessed in this study by SEM. All 0.1 M coatings display a characteristic cauliflower morphology, albeit with some coatings (1.3 V and 1 mA) showing surfaces with visible salicylate precipitation. Overoxidation has been shown to be associated with a loss in cauliflower morphology and the appearance of a more obvious macroporous features (Marchesi, et al. 2011). Topography is associated with morphology but is discrete and can be defined by the surface roughness which can be compared using statistical techniques. This would be easier to assess using AFM, which has not been utilised in this study. Previously, work in the laboratory has used AFM to assess PPy topography and found the topography to compare closely with some DES, in particular Yukon®, which have significantly greater surface roughness properties compared with Xience

or Taxus devices, although in that study the rougher Yukon® devices were found to be less favourable than smooth DES surfaces (Morgan, 2017).

2.4.3. Effect of electropolymerisation conditions on the generation of PPy coated strips

Electropolymerisation voltage

Coating 316L SS strips was identified as a compromise for use with in-vitro cell models to provide a larger surface area and a flat surface to aid with microscopy. Ideally, these coatings would not be used, as they do not directly reflect the coated wires, which are more comparable to coronary stent struts. Discs would provide an ideal platform for cell culture, but this was avoided because the change in geometry would require significant re-optimisation.

Potentiostatic electropolymerisation of SS strips was achieved using the same 1.1 and 1.3 V applied voltages as used for coating wires as shown in Figure 2.7. Overall, potentiostatic electropolymerisation was less efficient on SS strips compared with wires, but over a 10-minute duration both applied voltages could generate uniform coating. Coatings generated at 1.1 V were more variable when using a strip working electrode. Coatings generated at 1.3 V exhibited more salicylate precipitation on the surface than coated wires, but this was variable and not widespread across the coating surface. At both applied voltages, the PPy morphology obtained on coated strips appeared visually flatter than coated wires, with a more granular morphology rather than a distinctive ‘cauliflower’ morphology.

The observed decrease in electropolymerisation efficiency likely resulted from the change in working electrode surface area, with the 316L SS strips having a surface area 16-times greater than the 200µm wires. Similarly, when 1 mm wires were replaced with 200µm wires, there was a significant improvement in electropolymerisation efficiency resulting in the generation of more uniform coatings. The increase in WE surface area and resultant reduction in CE SA to WE SA ratio leads to ohmic potential drop (iR drop). iR drop can be defined as the resistance of the media and electrodes during the flow of electric current through the cells and uncompensated ohmic resistance resulting from high resistance at the working electrode leading to a reduction in the actual electropolymerisation voltage applied (Oelßner, et al. 2006).

The effect of iR drop on a cell can be calculated by the equation Ep = Ea – iRu, where Ep = the actual polarising electropolymerisation voltage, Ea = the intended applied electropolymerisation voltage, i = the polymerisation current passing through the cell, and Ru = the ohmic resistance of the working electrode current path (driven by the electrolyte solution and the WE surface) (Oelßner, et al. 2006). This highlights the significant impact resulting from a change in the WE geometry. Improved electropolymerisation efficiency may be achieved by estimating iR effects and compensating accordingly, through the use of a Luggin capillary to decrease WE/RE distance or changing the dopant to reduce electrolyte resistance. Alternatively, a larger Pt counter electrode could be used, to restore an WE to CE SA ratio, where the CE SA is greater than the WE SA.

Electropolymerisation current

Galvanostatic electropolymerisation was also used to generate PPy coatings on SS strips, but unlike voltage for potentiostatic electropolymerisation, the applied current used was not completely identical when coating strips. Instead, because of the 16-times increase in WE surface area, the required maintained current to achieve the same 2.65 $mA.cm^{-2}$ that was optimal for wires coated at 0.5 mA was calculated. 8 mA was therefore initially attempted. Likely due to the iR drop effects, this was not found to be successful, with generated coatings having very high surface salicylate precipitation. The maintained current was subsequently reduced until 1 and 2 mA were identified as suitable currents, although some precipitation was still observed on coatings generated at 2 mA. This is demonstrated in Figure 2.8.

This reduction in the required current compared with the anticipated 8 mA represents a substantial difference in optimal change densities for coating wires and strips, 2.65 and 0.33 $mA.cm^{-2}$ respectively. This highlights the importance of optimising the electropolymerisation conditions when changing the parameters of the electropolymerisation cell.

Compared with strips generated by potentiostatic electropolymerisation, coating consistency and reproducibility was qualitatively higher with galvanostatic electropolymerisation. Overall however, all PPy on coated strips exhibited worse mechanical stability than coated wires, with delamination of the coating common during subsequent experiments. This, along with the shallower peak observed on the voltage-time plots, suggests poor passivation of the electrode under these conditions. In future, this could be improved by applying a pre-passivation step before the addition of the pyrrole monomer, based on Ashrafi, et al. 2003.

Other than with 8 mA coatings, coated strips exhibited less electrochemical evidence of overoxidation than SS wires coated at 1 mA. It is also worth noting that 4 mA coatings, which exhibited very high precipitation, did not show the same increases in voltage during electropolymerisation as 1 mA wires or 8 mA coated strips, suggesting that this effect is more likely a result of overoxidation. The lower electropolymerisation efficiency of strips therefore also supports that a slower reaction over a longer duration may be used to counteract undesirable observations with coated wires.

2.4.4. Dopant elution from PPy-coating wires

In vitro salicylate release from PPy-coated 200 μm wires generated by potentiostatic and galvanostatic electropolymerisation at 1.1 and 1.3 V, and 0.1, 0.5 and 1 mA, was assessed over a 7 day period into PBS. This is shown in Supplementary Figure S2.2. A microplate absorbance reader used to measure salicylate concentration at each time point.

All coatings eluted the vast majority (>75%) of salicylate dopant within the first 24 hours. The total mass of salicylate eluted was characteristic for each coating, with the lowest elution recorded from thinner 0.1 mA and 1.1 V coatings and the greatest elution from thicker 1 mA coatings. 0.5 mA and 1.3 V coatings had comparable film thicknesses and morphology and this similarity continued with both coatings eluting approximately 250 μg of salicylate, although 1.3 V coatings appear to elute the dopant more rapidly.

For potentiostatic coatings, the mass of eluted salicylate was plotted against the current at the end of the electropolymerisation voltage, and these were found to closely correlate. It has already been established that current can provide an indirect estimate of coating thickness. It therefore follows that this would relate to salicylate elution. Due to the issue of current falling after initial nucleation with 1.3 V coatings, it may be expected to be more appropriate to plot peak current rather than final current, but Figure 2.9. shows that this was not observed with a weaker correlation between peak current and eluted salicylate than final current and salicylate elution. Although the release of salicylate dopant from PPy coatings has been demonstrated (Arbizzani, et al. 2007), the potentially tunability of this effect through monitoring or altering the current hasn't been demonstrated.

To quantify, and to improve the understanding of the data, the release kinetics were modelled using a previously developed MATLAB code to approximate the diffusion coefficients.

Single-phase and biphasic diffusion models have been previously used to describe small molecule release from polymeric implant coatings (McGinty 2014 and McKittrick, 2019), with the most appropriate model being governed by physicochemical properties of the coating. Given that there has been little prior characterisation of this aspect of polypyrrole coatings, it was therefore decided to use both models to fit all data sets in this present study. It is clear from this analysis, that all coatings were found to exhibit biphasic diffusion properties, although single phase models were also found to closely fit 1.1 V potentiostatic and 0.1 mA coating data sets. For biphasic release, D1 represents initial fast diffusion, in this case likely due to surface salicylate solubility, and D2 represents slower secondary diffusion, likely due to diffusion of the dopant from the polymer matrix. The F value defines the proportion of release driven by fast D1 diffusion.

The estimated diffusion coefficients confirm the release kinetics observed, with 1 mA coatings exhibiting considerably faster elution driven primarily by fast D1 elution, and 0.1 mA exhibit the slowest release and although they similarly have a high F value, the calculated D1 and D2 values are similar. This data confirms that 0.5 mA and 1.3 V coatings have similar salicylate elution properties, with highly comparable D1 and D2 values. Between the two coatings, there is variation in the F value, with elution from 1.3 V coatings driven predominantly by D1 elution, explaining the increased elution rate in these coatings at 24 h. This is most likely driven by the increased precipitate formation occurring on the 1.3 V coatings as observed by SEM. As expected, 1.1 V coatings have D1 and D2 values between the two extremes observed, but were found to have the lowest F value, further demonstrating the low precipitation of salicylate on these coatings. Overall, the MATLAB analysis provides a simple method for quantifying and obtaining mechanistic insights into the elution characteristics of the different PPy-Sa coatings.

The diffusion coefficients for dopant release from PPy have been found to increase sharply as a result of overoxidation, although this is highly dependent on the dopant used due to unique ionic transport effects (Mostany & Scharifker, 1997). It is clear that high D1 and F values may result from high surface precipitation, but increased D2 could be more representative of overoxidation, specifically for 1 mA coatings with significantly faster elution kinetics. Arbizzani, et al. (2007) assessed the elution of Sa dopant from PPy coatings and found that Sa is eluted rapidly within the first 24 hours, with elution complete by 48 hours. This is comparable to the drug release observed from the coatings produced in this present study. The same study did however show that other relevant anti-inflammatory dopants, including

naproxene, could be released more slowly from the PPy matrix resulting in release up to 30 days.

The intention of our PPy coatings is as a passive therapeutic antioxidant, but the ability to incorporate drugs as a dopant may add to the potential utility of these coatings as novel DES platforms. To offer therapeutic benefit and match current DES release kinetics, it is estimated that PPy should offer at least 3 weeks of drug release to adequately target SMC hyperproliferation which is known to begin within 24 hours after stent placement and continue for up to several weeks thereafter (Livingston & Tan, 2019). Therefore, with salicylate these coatings only target the acute phase and would not provide adequate kinetics, but it is unclear how effective they would be for use with more relevant mTOR inhibitors.

Over 7 days, passive salicylate elution into PBS was found to be effective at releasing all salicylate from the coating. Electrochemical discharge for 10 minutes at -0.75 V was attempted as an alternative mechanism to de-dope the polymer, as previously described by Gonzales, et al. 2019. For both potentiostatic coatings, as shown in Figure 2.11, and 0.5 mA galvanostatic coatings, as shown in Figure 2.12, this resulted in a near total loss of current, suggesting a loss of conductivity resulting from the loss of the dopant. When attempting to elute salicylate from PPy generated galvanostatically at 1 mA, coatings exhibited a slower loss of current, which after 10 minutes, at the end of the electrochemical discharge step, did not approach 0 A. The ability to tune surface conductivity with drug release properties may offer another mechanism for controlling or promoting positive behaviour in adherent cells, as has been shown for other conductive surfaces (Choi, et al. 2015).

When assessing the efficiency of this release mechanism, it was found to be effective with potentiostatic coatings, particularly 1.3 V coatings, resulting in a significant decrease in salicylate content of the 1.3 V coatings. This was however not observed with galvanostatic coatings, where no significant decrease in salicylate content was observed. This was expected for 1 mA coatings due to the high contribution of precipitate and the apparent inefficiency shown by the current-time profile. The ineffectiveness of this technique for de-doping the 0.5 mA samples is however unclear. It is also surprising that this technique had a significant effect on 1.3 V coatings since high precipitation, as shown in the SEM micrographs, remains on the surface after the discharge cycle.

2.4.5. Effect of increased dopant concentration on electropolymerisation and PPy generation

In addition to generating coatings using solution containing 0.1 M Py and NaSa, electropolymerisation was also attempted using solutions containing 0.1 or 0.25 Py and 0.5 M NaSa. This was used to assess the capability of dopant concentration to modify PPy surface morphology, with the current-time profiles and corresponding SEM micrographs shown in Figure 2.13. for potentiostatic electropolymerisation and Figure 2.14. for galvanostatic electropolymerisation.

At the electropolymerisation conditions used in this study, 0.25 M Py and 0.5 M Sa solutions were found to promote electropolymerisation resulting in the formation of thick coatings with microtubular structures. There were significant differences in the electropolymerisation profiles, with very short passivation followed by very rapid nucleation for coatings generating at +1.3 V, this was followed by a drop in current. During electropolymerisation at +1.1 V, nucleation was longer with a lower drop in current. Based on SEM micrographs however, this difference did not have a noticeable effect on the resulting coating topography. A lack of strong nucleation and slow chain growth resulted in patchy coating formation when using 0.1 M Py and 0.5 M NaSa solutions.

Electropolymerisation was observed when using the same solutions with galvanostatic electropolymerisation, although coatings generated 0.1 M Py and 0.5 M NaSa solution at 0.1 mA lacked uniformity and large salicylate crystals were formed at 0.5 mA. When using 0.25 M Py and 0.5 M NaSa, PPy coatings were reliably obtained, with normal passivation, nucleation and chain growth, but no microtubular topography was observed. This suggests that the formation of microtubular PPy structures is highly dependent on electropolymerisation conditions in addition to monomer and dopant concentrations.

These results are comparable to results reported in the literature. Gonzalez, et al. (2013), used 0.5 and 0.1 M Sa with 0.25 M Py and found only 0.5 M Sa to generate microtubular structures and 0.1 M Sa to generate typical globular morphologies. One concern with the microtubular morphology is whether it represents a change in the PPy macrostructure, an artefact of very high salicylate precipitation or the result of polymerisation occurring in precipitate crystal boundaries. Gutiérrez Pineda, et al. (2018) found that before microtubes are formed, PPy polymerisation begins by forming coatings with cauliflower morphology. This suggests that salicylate precipitation likely contributes to the formation of the tubular structures or act as a

scaffold for their formation. Yang, et al. (2007) reported that methyl orange precipitates on the working electrode could act as a tubular template for the electropolymerisation of PPy nanotubes.

Chemical synthesis has been shown to be capable of generating PPy with a tubular structure and interestingly, dual-phase structure with both tubular and cauliflower structures were generated (Liu & Wan, 2001). Images of these structures were however more fibrous rather than tubular and the regularity observed in our electropolymerized films was not present. Further characterisation of the tubular coatings may be achieved using impedance spectroscopy or X-ray diffraction to characterise the crystallinity of the polymer structure.

Dopant release was assessed from these coatings and compared against globular PPy coatings generated potentiostatically at 1.3 V and galvanostatically at 0.5 mA from 0.1 M solutions. The tubular structures exhibited significantly greater total salicylate incorporation and faster elution properties as shown in Figure 2.15. The increased salicylate mass is indicative of the thickness of these coatings but may also indicate the high presence of precipitated Sa acting as a scaffold. Similarly, the very high elution rate may be driven by solubilisation of a Sa scaffold, or result from the very high PPy surface area.

In terms of the appropriateness of these films as a stent coating, it is unlikely that these thin tubular structures would offer suitable mechanical properties. Furthermore, it has been established that topographical features in the region of 4.8 and 9.9 μm are beneficial to endothelial cells (Suarez, et al. 2020). Although the diameter of the microtubes may lie within this range, the amplitude of any feature should not exceed 2 μm and due to the thickness of these coatings, it is likely that the microtubes exceed this depth. If PPy is to be considered as a matrix for drug eluting stent platforms, it will be necessary to balance the control of the topography to encourage endothelial cell attachment (Suarez, et al. 2020) and proliferation whilst reducing the surface area of the coating to moderate drug elution and prolong the elution phase. Alternative approach could be to target the surface topography of the coating to different regions of the stent, for example the luminal aspect may be textured to encourage endothelial coverage whereas the outer surface could be designed to optimise and prolong drug elution to the underlying smooth muscle cells.

2.4.6. Electrical Impedance Spectroscopy of Polypyrrole-coated wires

Time-current/voltage profiles and other basic characterisation, including microscopy and drug elution, provided some insight into the characteristics of the PPy coatings generated on SS wires and strips. These techniques alone however could not fully indicate the oxidative state of the polymers. Furthermore, these techniques indicate that coatings generated by potentiostatic electropolymerisation at 1.3 V were near-identical to coatings generated by galvanostatic electropolymerisation at 0.5 mA on 200 μm wires. EIS, CV and FTIR were therefore utilised to provide further characterisation of the coating's electrochemical and chemical states.

EIS was carried out on PPy coated wires in PBS electrolyte based on previously reported methodology (Ramanavicius, et al. 2010). Although based on this methodology, the EIS frequency range was extended up to 100 kHz in this present study.

Using EIS, differences were observed between the potentiostatic and galvanostatic PPy coatings, as demonstrated in Figure 2.16. & Figure 2.17. respectively. The charge transfer resistance of each coating can be estimated by the width of the semi-circular feature in the high-frequency domain of each Nyquist plot. High charge transfer resistance was observed for thinner galvanostatic coatings generated at 0.1 and 0.5mA. Moderate resistance was observed for potentiostatic coatings generated at 1.1 V coatings and low resistance for 1 mA galvanostatic coatings. The circular feature was largely lost for 1.3 V potentiostatic coatings indicating very low resistance charge transfer resistance.

Phase-shift differences between coatings were also observed and were most apparent at 1 kHz. In the Bode plots of phase-shift, there was a dual-peak pattern observed for all 5 PPy coatings. This may result from the combination of having two interfaces – electrolyte-PPy, and PPy-WE. This trough around 1 kHz may therefore represent the inflexion between fast (electron-driven) and slow (electrolyte diffusion-driven) transport kinetics. The phase-shaft at this inflexion point was comparable for 0.1, 0.5 mA galvanostatic and 1.1 V potentiostatic coatings at approximately 30°. For 1.3 V potentiostatic coatings however, this point was closer to 45° reflecting that this effect was coincident with the Warburg impedance point, which was obscured in these Nyquist plots due to the lack of any semi-circular arc in the high frequency domain. Finally, for 1 mA galvanostatic coatings, this point was far lower on the bode plot

around 15° indicating far more resistance-driven behaviour, likely due to the high amount of Sa precipitant.

These effects were also assessed over 1 h to monitor the effect of Sa elution. There was a greater time/elution dependency for thinner coatings observed, with notable changes in the Bode plots observed for 1.1 V potentiostatic and 0.1 mA galvanostatic coatings. Although there is a lower less mass of salicylate released from these coatings, it is likely this represents a higher relative elution in this 1 h range and the elution is driven solely by the dopant compared to precipitate elution in thicker coatings. This cannot easily be compared to elution data, as for the thicker coatings, the solubility of precipitate obscures the elution rate at the early time points.

In these coatings, where elution had a notable impact on phase shift, the majority of the effect is observed, as expected, in the low frequency range, but beginning from approximately 1 kHz. This further supports the idea that this trough represents the beginning of slow diffusion kinetics on the impedance measurements. Overall, low EIS dependence on elution was observed in the thicker, more uniform PPy coatings generated potentiostatically at 1.3 V or galvanostatically at 0.5 and 1 mA.

Gutiérrez Pineda, et al. (2018), defined the ideal impedance response of an electroactive polymer film as “a separate Randles circuit behaviour at high frequencies with a Warburg section at intermediate frequencies, and a purely capacitive behaviour, due to the redox capacitance, in the low frequency range.” None of the PPy coatings generated in this study completely met all the outlined criteria, but 1.1 potentiostatic and 0.1 and 0.5 mA galvanostatic coatings demonstrated the key transitions in behaviour defined here.

The effect on PPy oxidative state on the resulting impedance characteristics is not well reported in the literature. In reduced states, the high-frequency semi-circular arc has been shown to be increased compared with oxidised coatings (Mostany & Scharifker, 1997). No PPy coatings used in this study are believed to be in a reduced state, although it is worth noting that charge transfer resistance was increased in 1.1 V and 0.1 mA coatings after dopant elution. This effect has also been confirmed in PANI coatings and is believed to be a result of changes in polymer chain structure (Dalmolin, et al. 2005).

Overoxidation specifically has been shown to lead to an increase in PPy coating resistance, due to the insertion of large anions into the polymer chains (Marchesi, et al. 2011). This can be observed in the Nyquist plots observed by an increase/stretching of the semi-circular arc. Among the coatings generated in this present study, 1 mA galvanostatic coatings are suspected of being the most likely to be overoxidised. However, these coatings in fact had the lowest charge transfer resistance (if +1.3 V coatings are excluded), suggesting that these coatings were not overoxidised during electopolymerisation. Interestingly, for other CP, such as PEDOT, overoxidation has been shown to reduce electron transfer resistance (Zalka, et al 2017).

It is worth noting that improvements could be made to improve the ability to interpret this EIS data. As with potentiometry, iR drop also effects impedance measurements. This interference is predominantly in low frequency domain making it harder to observe or characterise the double-layer capacitance effects and semi-circular arc at lower frequencies (Shah, et al. 2018).

2.4.7. Cyclic Voltammetry of Polypyrrole-coated wires

Cyclic voltammetry was also performed on PPy coated wires in PBS electrolyte to characterise their electrochemical behaviour. This was based on previously established methodology (Cysewska, et al. 2016), although the voltage window was optimised for bare 316L SS to limit the window at the oxidation and reduction peaks of water. This was initially found to be approximately -0.2 V – +0.6 V, but 0.0 – +0.8 V was chosen as the final window as oxidation was the primary focus of this study and the water window was found to be extended when using PPy as the WE.

When applying this extended voltage range to SS samples, an irreversible strong oxidation peak was observed during the first cycle and subsequently lost due to the oxidation of the surface and formation of an oxide layer as demonstrated in Figure 2.18. (panel a). A similar oxidation peak was also observed for 0.1 mA wires, likely due to their thinness and the underlying substrate being in contact with the electrolyte. This is observed in Figure 2.18. (panel d). All other PPy samples exhibited some reversible oxidation and reduction behaviour. Generally, the magnitude of these oxidation and reduction peaks equilibrated after 20 cycles, indicating that efficient transport of dopant was occurring. The magnitude of oxidation and reduction did not equilibrate however for 1.3 V (Figure 2.18. (panel c)) and 1 mA (Figure 2.18. (panel f)) coatings, likely due to Salicylate precipitate, making these coatings incapable

of de-doping during the cycle time. The could be alleviated by using a slower scan rate, but also shows that this technique is capable of quickly indicating salicylate presence without the need for SEM.

Coatings generated by galvanostatic electropolymerisation at 1 mA exhibited a higher oxidation capacity over 0.5 mA and potentiostatic coatings. 0.5 mA (Figure 2.18. (panel e)) and 1.3 V coatings exhibited comparable oxidative capacity under the conditions tested, reinforcing the observed similarities between these coatings, but 1.1 V (Figure 2.18. (panel b)) coatings were more rapidly oxidised in cycle 1. This may indicate a greater propensity for these coatings to be readily oxidised, which may result in beneficial antioxidant properties, although that is yet to be determined. Gizdavic-Nikolaidi, et al. (2004), demonstrated that the oxidation capacity of PPy is directly related to its ability to scavenge DPPH radicals. The ability of the PPy coatings generated in this chapter to scavenge DPPH radicals will be explored further in Chapter 3.

One strong indicator of overoxidation when using CV to assess PPy is the reversibility of oxidation and reduction. Cycling of these states has been shown to be lost after PPy undergoes overoxidation, (Levi, et al. 2002). In addition to EIS, this further supports that 1.3 V potentiostatic and 1 mA galavanostatic coatings are not overoxidised.

It is difficult to compare CV data with published findings as there is a wide range of different factors or conditions used, such as scan rate, electrolyte, and voltage window. Furthermore, many studies using CV utilise this technique as part of potentiodynamic electropolymerisation using the pyrrole monomer. These studies are beneficial however for showing that pyrrole oxidation occurs at +0.8 V (vs. Ag/AgCl RE) (El Jaouhari, et al. 2017).

Shi & Zhitomirsky, (2010) used alkaline conditions and a broader voltage range to assess the specific capacitance of PPy-Sa coatings, and found coatings containing salicylate to exhibit poor capacitance behaviour. This may clarify the lack of pure capacitance behaviour observed with PPy coatings by EIS. Unfortunately, Shi & Zhitomirsky did not use EIS and the conditions used prevent direct comparison as the data in this study does exhibit an idealised “box shape” voltammogram.

Cysewska, et al. (2016), used CV to assess PPy-Sa coatings on iron substrates using a salicylate electrolyte buffered in PBS. There are therefore many similarities to this work but

it is not directly comparable, especially since the voltage range was extended to -0.9 V - +0.9 V. Cysewska, et al. did however observe similar increases in oxidation and reduction magnitude after repeat cycles, albeit with a wider and lower skew to reduction, likely due to the extended voltage range, which equilibrated after approximately 20 cycles. Furthermore, Cysewska, et al. found that this cycling capacity was lost in overoxidised samples.

Gonzales, et al. (2019) similarly observed that PPy on 316L SS could cycle salicylate without overoxidation up to 600 mV, but unfortunately this study used PPy with a microtubular topography only, making such coatings more likely respond to salicylate transport differently due to the increase in surface area.

2.4.8. Fourier Transform Infrared Spectroscopy of Polypyrrole-coated strips

Unlike EIS and CV, FTIR spectroscopy was performed on PPy coated strips. Strips were favoured over coated wires to provide a sufficient flat surface area for obtaining reliable measurements. This prevents exact comparisons between FTIR and EIS or CV, but electropolymerisation of coated strips was previously optimisised to reflect the coatings obtained on SS wires. Unlike EIS and CV, this technique was also primarily used to ascertain the chemical composition of the PPy coatings.

FTIR spectroscopy, as expected, confirmed the presence of PPy in each electropolymerised coatings. This is summarised in Figure 2.19 and demonstrated further in Supplementary Figures S2.4-2.7. It was however difficult to identify precise peaks, especially in the low region below 2000 cm^{-1}, due to the interference of the salicylate dopant. Improved characterisation of the PPy coatings could therefore be gained if FTIR spectroscopy were repeated after salicylate elution or de-doping.

Principal component analysis (PCA) was performed on spectra to allow the statistical comparison of PPy-Sa spectra and to assess differences between the coatings, but the low sample size used in this dataset gives this analysis low statistical power. PCA works by assessing each wavelength in the spectra discretely and weighting these based on their standard deviation. By weighting by standard deviation, PCA can identify principal components of the data, in this case, wavelengths with high variation. The data sets are then plotted based on how strongly these principal components are exhibited in the specta.

Within sample groups on the PCA graph however, there is generally low variability, excluding overoxidised coatings, which were highly variable, and some variability with 1 mA galvanostatic coatings. Thinner 1 mA and 1.1 V coatings would be expected to produce more variability due to less uniformity across the film surface, but this is not observed for +1.1 V potentiostatic coatings. Interestingly 1.1 V coatings are comparable to 2 mA coating which were suspected to be the most likely to be overoxidised, further suggesting that these coatings did not undergo overoxidation during electropolymerisation. Reassuringly, overoxidised coatings were dissimilar from other PPy coatings, giving confidence that the overoxidation process alters 1 mA coatings and the other PPy coatings do not show strong evidence of overoxidation.

Li & Qian, (2000), demonstrated that overoxidation could be identified by a peak at 1700 cm^{-1} resulting from the formation of C=O bonds in the pyrrole ring, and less distinctly by a loss in the 2800-3700 cm^{-1} absorbance peak resulting from the de-hydrogenation of N-H. In the overoxidised coatings generated by cyclic voltammetry, a peak at 1700 cm^{-1} is acquired and no discrete peaks are observed in the 2800-3700 cm^{-1} range. This further suggests that these coatings were overoxidised and provide a good positive control for overoxidation. For all other coatings, there was no discrete peak at 1700 cm^{-1}, but high interference from the Sa dopant did result to other peaks at adjacent wavelengths. Furthermore, all other PPy coatings also had at least one other peak in the 2800-3700 cm^{-1} range, further indicating that these coatings had not undergone overoxidation.

Although not considered in the study, FTIR spectroscopy could be used to assess chemical changes arising from PPy oxidative challenge in a physiological or therapeutic context. The dehydrogenation of PPy, as measured by the loss of the 2800-3700 cm^{-1} peak could be used to assess the ability of PPy to act as an antioxidant by hydrogen atom transfer.

2.5. Conclusions

In conclusion, the results in this chapter demonstrate that PPy can be reliably generated from pyrrole-salicylate solution using electropolymerisation to form uniform coatings with a 10 minute electropolymerisation time. The ability of electropolymerisation to generated PPy coatings was demonstrated on both 316L SS wires and strips.

When exploring the effect of electropolymerisation conditions PPy generation, increased potentiostatic voltage and galvanostatic current was found to increase coatings thickness and dopant incorporation. The ability to increase PPy generation was however shown to be limited at higher potentiostatic and galvanostatic conditions due to the formation of salicylate precipitation observed by SEM on the coating surface. After electropolymerisation, the incorporated salicylate dopant can be rapidly eluted when incubated in PBS. This presents the opportunity to utilise PPy as a DES platform.

EIS, CV and FTIR showed no indication of the occurrence of overoxidation during electropolymerisation. This suggests that the salicylate precipitation is responsible for the observed increased in coating resistance during potentiostatic and galvanostatic electropolymerisation of 200 µm wires at 1.3 V and 1 mA respectively. Based on uniformity, topographical properties and electrochemical characterisation alone, coatings generated at 1.3 V by potentiostatic electropolymerisation and 1 mA by galvanostatic electropolymerisation represent the optimal conditions for further investigation in this study.

3. Assessing Polypyrrole Antioxidant Capacity

Chapter 3 will explore the second major aim of this study, characterising the antioxidant activity of PPy-coated SS samples. Coatings were challenged with some of the key pro-oxidant species previously outlined in section 1.8. The background will firstly be outlined and the key objectives of this chapter will be defined. This will be followed by the experimental methods and materials used to achieve these objectives. The main outcomes and results of this investigation will be presented, and this chapter will conclude with an in- depth discussion highlighting the significance of these findings.

3.1. Background and Aims

Antioxidant approaches have previously been shown to improve PCI outcomes and reduce restenosis, although negative results have also been reported (Watt, et al. 2008). These studies however have focussed on pharmaceutical approaches, with oral and local DES delivery used, which has ultimately produced limited success with no antioxidant eluting stent being routinely used clinically.

For example, succinobucol failed to minimise stenting risks and these limitations were linked to pharmacological side effects, arising from fast elution kinetic resulting in localised high concentrations of the drug and the resulting toxicity to endothelial cells as well as smooth muscle cells (Watt, et al. 2013). This study demonstrates that an antioxidant approach of minimising restenosis must promote re-endothelialisation. Furthermore, probucol has been used as an alternative antioxidant drug for stent coating elution, but where used alongside sirolimus, show no significant advantage over zoratolimus 3rd-generation DES in clinical trials at a 10-year follow up (Kufner, et al. 2020).

Chemically synthesised conducting polymers, in powder form, have demonstrated specific antioxidant capacity in response to DPPH and ABTS radicals (Hsu, et al. 2010; Zare, et al. 2014), but there are no reports regarding the antioxidant behaviour of electrochemically synthesised polypyrrole (PPy) coated onto metal substrates.

The potential of antioxidants as a therapeutic after stent placement has been considered and shows some limited promise. The generation of PPy chemically with antioxidant activity has been demonstrated and the ability for electropolymerisation to generate PPy films has been

characterised. There is however a potential to establish whether an antioxidant capacity can be delivered by conducting polymers in a more specific targeted way, considering reactive oxygen species (ROS) relevant to the intended application.

Antioxidants act to reduce oxidising species, such as superoxide, hydrogen peroxide, peroxynitrite. This action is typically achieved, via hydrogen atom transfer (HAT) or single electron transfer (SET) (Foti, 2007). All PCI procedures have been shown to generate oxidative stress after surgery, with stent placement resulting in the higher elevated levels of superoxide radicals and hydrogen peroxide than balloon angioplasty (Juni, et al. 2013; Kochiadakis, et al. 2010). Therefore, the fundamental chemistry of any PPy coating and resulting mechanism of antioxidant action, will contribute to its therapeutic potential and how it may target relevant ROS. At present, it is unclear whether, or how, electropolymerisation may influence PPy's antioxidant capacity and this must be considered.

The application of electropolymerised polypyrrole as a therapeutic through targeted reactive species scavenging, achieved by use of a stenting coating is novel and may present a new and not yet considered application for this category of materials.

The work detailed in this chapter aims to address this knowledge gap, by addressing the following five objectives:

1. Characterise the antioxidant capacity of a range of electropolymerised PPy coatings.
2. Investigate the longevity of PPy antioxidant capacity in the presence and absence of repeated oxidative challenge.
3. Investigate the influence of electropolymerisation variables, such as applied voltage, current, electropolymerisation duration and dopant elution on antioxidant capacity.
4. Determine the scavenging capacity of pyrrole monomer and salicylate solution.
5. Determine the scavenging activity of PPy-coated samples against relevant ROS: peroxyl, hydrogen peroxide, superoxide and nitric oxide.

3.2. Materials and Methods

3.2.1. Materials and Equipment

Material/Equipment	Supplier
Stainless Steel (316L wires and plates)	Goodfellow Cambridge Ltd, UK
Ag/AgCl Reference Electrode (KR5)	ThermoFisher Scientific, UK
Potentiostat/Galvanostat	Metrohm Autolab, UK
POLARstar Omega Plate reader	BMG LABTECH, UK
FlexStation3 Plate reader	Molecular Devices, UK
Spectrophotometer (ThermoSpectronic BioMate 5)	ThermoFisher Scientific, UK

3.2.2. Chemicals

Chemical	Supplier	Catalogue Number
Pyrrole (98% solution)	Sigma Aldrich, UK	131709
Sodium Salicylate	Sigma Aldrich, UK	S3007
Phosphate Buffered Saline (PBS) tablets	Oxoid, UK	BR0014G
Absolute Ethanol	VWR, UK	20821.296
2,2-diphenyl-1-picrylhydrazyl (DPPH) powder	Sigma Aldrich, UK	D9132
Probucol powder	Sigma Aldrich, UK	P9672
Hypoxanthine powder	Sigma Aldrich, UK	H9377
Xanthine Oxidase from Bovine milk (grade III in solution)	Sigma Aldrich, UK	X4500
Nitrotetrazolium Blue chloride (NBT) powder	Sigma Aldrich, UK	93862
Fluorescein Sodium Salt powder	Sigma Aldrich, UK	30181
Sodium nitroprusside dihydrate granules	Sigma Aldrich, UK	567538
L-ascorbic acid powder	Sigma Aldrich, UK	A92902
Hydrogen peroxide (30% solution)	Santa Cruz, US	sc-203336
2,2′-Azobis(2-methylpropionamidine) dihydrochloride (AAPH) granules	Sigma Aldrich, UK	440914
(±)-6-Hydroxy-2,5,7,8-tetramethylchromane-2-carboxylic acid (TROLOX) powder	Sigma Aldrich, UK	238813

3.2.3. Sample Preparation and Electropolymerisation

Sample were prepared using the methodology described in sections 2.2.3. (potentiostatic electropolymerisation) and 2.2.4. (galvanostatic electropolymerisation). Both 316L SS wires (Ø=100 μm) and strips (30 x 5 mm) were used.

3.2.4. Broad Antioxidant Assay (DPPH)

The antioxidant activity of the PPy coatings was assessed by evaluating the scavenging activity of 2,2-diphenyl-1-picrylhydrazyl (DPPH) free radicals as previously described (Ebrahimiasl, et al. 2015), but with some minor changes. 2 mg of DPPH was dissolved in 20 ml of ethanol to prepare a DPPH stock solution (254 µM). PPy-coated samples were transferred to 1.5 ml Eppendorf tubes. 750 µl of ethanol and 250 µl of DPPH solution was then added to each tube, producing a final DPPH concentration of 64 µM (approx. Abs_{517nm}=1). Uncoated 316L SS wire (Ø=100 µm) in 64 µM DPPH reagent, DPPH reagent alone and probucol (0.005 - 1 mM) standard solutions were used as controls. Probucol has known broad antioxidant properties, making it a suitable positive control for this type of chemical radical scavenging assay (Kuzuya & Kuzuya, 1993). The reaction was left to progress in dark conditions for up to 24 h at room temperature and 8 and 24 h were identified as suitable incubation times when studying fixed solid chemicals. The absorbance was measured at 517 nm (ThermoSpectronic BioMate 5) after incubation, and used to calculate percentage of antioxidant activity, using the following formula:

$$\%(Antioxidant\ Activity) = 100 - \left(\frac{\left(Abs_{sample} - Abs_{blank}\right) \times 100}{Abs_{control}}\right)$$

To assess longer term antioxidant capabilities of the coatings, samples were repeatedly exposed to DPPH. This was carried out by exposing wires for an initial period of 24 h, measuring absorbance at 517 nm, reintroducing the samples into new DPPH solution and repeating the technique until a 96 h interval was reached.

Alternatively, to assess how the coatings' antioxidant activity would respond to cell culture and simulated physiological conditions, coated wires were stored in PBS and incubated in a shaking incubator for 24 to 120 h at 37°C/120rpm before exposing to DPPH for 24 h and measuring 517 nm absorbance. Similarly, DPPH scavenging was determined after storing samples in endothelial cell growth medium-2 (Lonza) for up to 72 h at 37°C/5% CO_2. The different DPPH assay approaches used to estimate antioxidant capacity, longevity and stability are summarised in Figure 3.1.

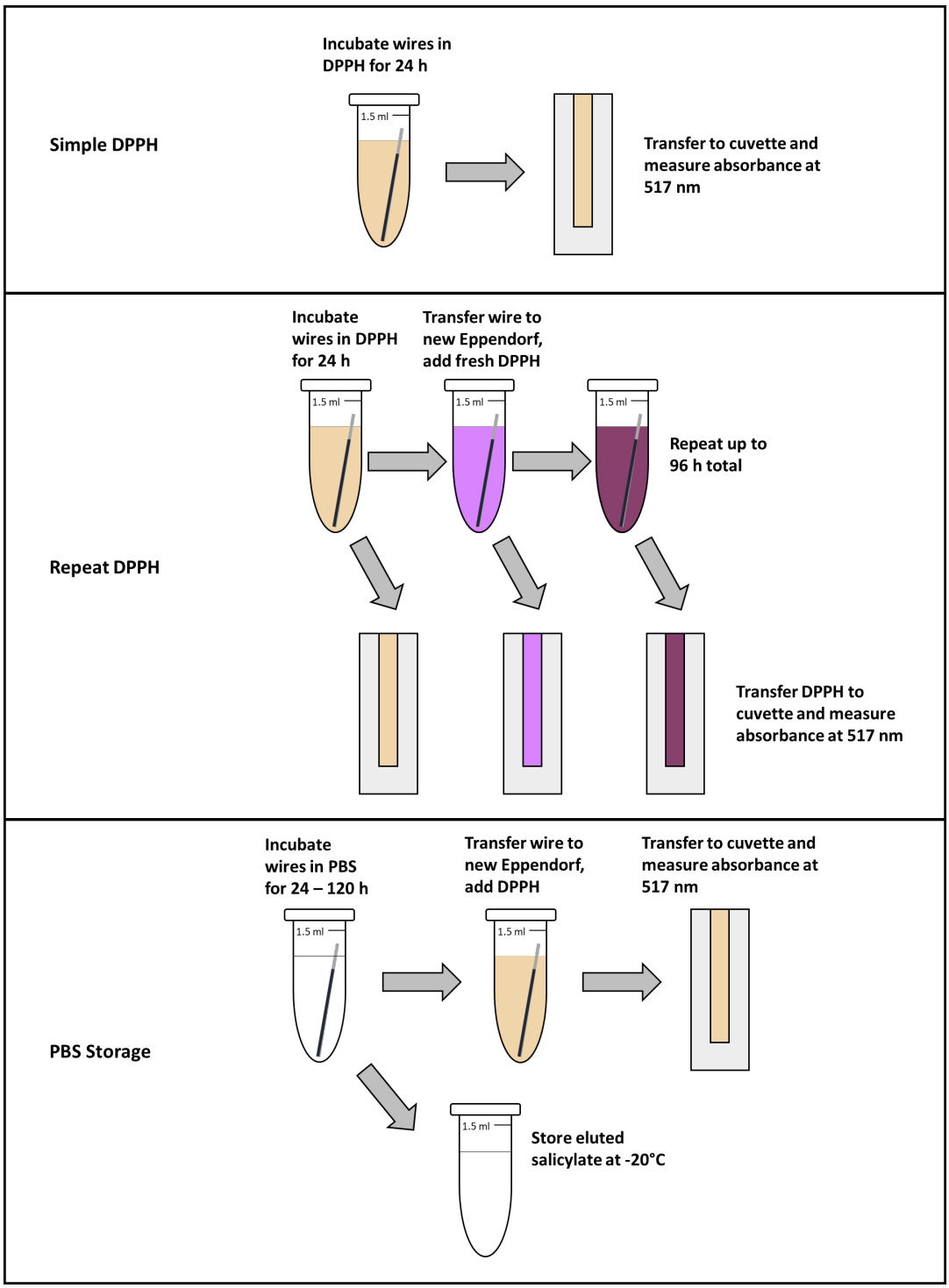

Figure 3.1. Summary of the different approaches taken to assess overall antioxidant capacity, longevity and stability based on the DPPH assay. A simple DPPH assay, with 24 h incubation, was used to assess the antioxidant capacity of uncoated and PPy-coated wires. Repeated DPPH assays were used as a measure of the longevity of a sample's antioxidant activity, and PBS incubation was used to simulate physiological conditions, which acted as a measure of the stability of a sample's antioxidant effects.

3.2.5. Superoxide Scavenging Assay

Superoxide radical scavenging capacity was assessed in coated and uncoated samples using an enzymatic superoxide protocol adapted from Liu, et al. (2009). Firstly, an assay buffer was prepared in PBS containing 500 µM nitroblue tetrazolium chloride (NBT), a well-documented detector of superoxide radicals; and 0.1 U/ml xanthine oxidase (XO), an enzyme that converts hypoxanthine to generate superoxide radicals. The assay was optimised to determine the optimal hypoxanthine concentration, which was determined to be 0.1 mM.

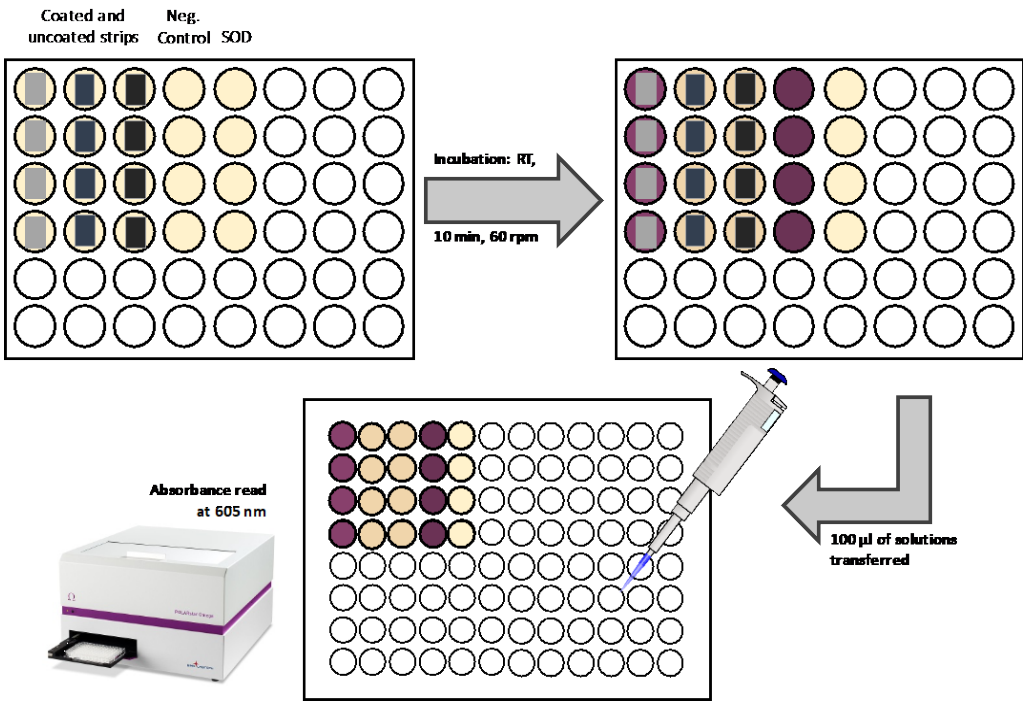

Figure 3.2. Summary of the approach taken to quantify the superoxide scavenging capacity of PPy-coated and uncoated SS strips. Similar approaches of using 8x5 mm strips and transferring the assay buffer to a new 96-well plate before reading absorbance was also taken with the ORAC, hydrogen peroxide and nitric oxide scavenging assays. Superoxide dismutase (SOD, 1000U/ml solution) was used as a positive control for superoxide scavenging and blank (PBS only) solvent was used as the negative control for scavenging.

Polypyrrole monomer (final concentrations: 30 µM – 30 mM) and aqueous salicylate (final concentrations: 30 µM – 30 mM) were assessed in 96-well clear plates in 90 µl assay buffer. This was based on the mass of salicylate eluted from 1.3 V potentiostatic and 0.5 mA galavanostatic coatings. the estimated concentrations of both pyrrole and salicylate are shown in Table 3.1. A wider concentration range was selected around the estimated concentrations

for different elution from 1.1 V potentiostatic and 0.1 and 1 mA galvanostatic coatings, and also to account for lower concentration during elution and higher concentration locally at the coating-buffer interface.

Table 3.1. Estimated salicylate and pyrrole mass and concentration in 1 ml PBS, based on the *in vitro* elution of salicylate from 1.3 V potentiostatic and 0.5 mA galvanostatic coatings established in Chapter 2. Pyrrole mass was estimated based on the established principle by Sadki, et al. 2000, that dopant mass contributes approximately 35% mass to the total PPy-Sa coating.

Approximate mass of salicylate eluted from 1.3 V potentiostatic and 0.5 mA galvanostatic PPy coatings	**Approximate mass of polypyrrole based on a dopant mass being 35% of total coating mass (Sadki, et al. 2000)**
250 µg	460 µg
Corresponding salicylate concentration based on elution into 1 ml of PBS	**Corresponding pyrrole concentration based on elution of salicylate into 1 ml of PBS**
1.56 mM	4.86 mM

The superoxide generation was initiated by the addition of 10 µl 0.1 mM hypoxanthine-PBS solution. Superoxide dismutase (1000 U/ml) was used as a positive control. Immediately after initiating the reaction, absorbance kinetics were measured every 30 seconds over a 10-minute interval at 605 nm with a microplate reader (POLARstar).

Due to the limitations of photometric assays, which require transmission of the light path through the well plate, superoxide scavenging capacity of coated and uncoated strips could not be assessed kinetically. Instead, 8 x 5 mm strip samples were placed in 48-well plates and 190 µl of assay buffer added. 20 µl 0.1 mM hypoxanthine solution was added to initiate the reaction and the samples were incubated at room temperature on a shaking platform (60 rpm) for 10 minutes. Immediately after incubation, the reaction solution (100 µl) was transferred to a clear 96-well plate and endpoint absorbance measured using a microplate reader (FlexStation). This process is summarised in Figure 3.2.

For all samples, kinetic and endpoint, superoxide scavenging capacity was calculated and presented as a percentage inhibiton vs. SOD control. XO oxidase activity was also confirmed by monitoring the formation of uric acid kinetically at 295 nm.

3.2.6. Oxygen Radical Antioxidant Capacity (ORAC) Assay

A standardised ORAC assay obtained from BMG Labtech was followed for this study to measure specific peroxyl radical scavenging capacity. Firstly, an assay buffer was prepared in PBS containing 10 nM fluorescein sodium salt, a fluorescent probe that reacts with peroxyl radicals. In a black-walled 96 well plate, 25 µl of experimental samples - polypyrrole monomer (final concentrations: 30 µM – 30 mM) and aqueous salicylate (final concentrations: 30 µM – 30 mM) - were added with 150 µl assay buffer. Sample blanks were also recorded in separate wells containing 25 µl samples and 150 µl PBS. A Trolox (0.6125 – 25 µM) standard curve was set up on each plate in the same way as experimental samples to be used as a positive control, but also to be used for calculations and to normalise between experiments. Trolox, a vitamin E analogue, has been shown to be a reliable dose-dependent scavenger of peroxyl radicals and is routinely used as standardised equivalent measure of antioxidant activity in the literature (Price, et al. 2006).

Plates were incubated at 37°C in foil for 15 minutes and peroxyl radical generation was initiated by the addition of 25 µl, 240 mM 2,2'-azobis(2-amidino-propane) dihydrochloride (AAPH) to each well with a multichannel pipette. AAPH produces peroxyl radicals by thermal decomposition and after initiation, the solutions must be maintained at 37°C with the plate reader incubator (POLARstar). Immediately after adding AAPH, fluorescence kinetics ($\lambda_{excitation}$ =485 nm, $\lambda_{emission}$ =520 nm) were recorded at 1 minute intervals for 80 minutes using a microplate reader (POLARstar).

Loss of fluorescent signal was calculated by plotting relative fluorescence of each sample vs. the first recorded signal for each sample. Peroxyl scavenging capacity was derived from these values by converting the relative fluorescence of each sample at t = 50 minutes to an equivalent Trolox dose using the standard curve. 50 minutes was selected as it was found to show a good linear relationship between Trolox concentration and loss of fluorescence during optimisation of the assay.

Due to the limitations of photometric assays, peroxyl scavenging capacity of coated and uncoated strips could not be assessed kinetically. Instead, 8 x 5 mm strip samples were placed in 48-well plates and 150 µl assay buffer added. 25 µl of experimental samples used in the standardised protocol was replaced with 25 µl PBS, and the reaction was initiated with 25 µl, 240 mM AAPH. A Trolox standard curve was also set up in the 48-well plate. Samples were

incubated with the ORAC assay components in foil at 37°C for 50 minutes before transferring to a black-walled 96-well plate and reading endpoint fluorescence ($\lambda_{excitation}$ =485 nm, $\lambda_{emission}$ =520 nm). Peroxyl scavenging capacity was again calculated by converting the endpoint fluorescence values to equivalent Trolox doses.

3.2.7. Hydrogen Peroxide Scavenging Assay

Hydrogen peroxide scavenging activity of the monomer, salicylate dopant and the ascorbic acid positive control was assessed using an established and previously described protocol (Al-Amiery, et al. 2015). This protocol was then adapted for the inclusion of uncoated and PPy-coated 316L SS strips to assess the hydrogen peroxide scavenging capacity of these substrates relative to the positive control.

For this assay, the pyrrole monomer and aqueous salicylate stocks were prepared in PBS for the final assay concentrations (30 µM – 30 mM). A stock solution of ascorbic acid was also prepared in PBS for use at the 10 mM final concentration. 0.5 ml of these solutions, along with a 0.5 ml PBS negative control were added separately to 0.5 ml of hydrogen peroxide solution in PBS (final concentration 40 mM). The reaction was allowed to incubate at room temperature for 10 minutes before measuring absorbance at 230 nm using a plate reader (FlexStation 3). Background readings were obtained for PBS containing no hydrogen peroxide and each experimental sample to remove sample 230 nm absorbance effects.

Relevant background readings were subtracted from the data and percentage hydrogen peroxide scavenged was calculated using the following formula:

$$\%(H_2O_2\ Scavenging\ Activity) = \left(\frac{Abs_{peroxide} - Abs_{sample}}{Abs_{peroxide}}\right) \times 100$$

Where solid samples were tested, samples (5 x 8 mm strips) were incubated in 40 mM hydrogen peroxide solutions in a 48-well plate for 10 minutes and the reaction buffer was transferred to a 96-well plate to measure the absorbance. Negative and positive controls were also obtained using this method, mirroring the approach taken for the superoxide scavenging assay.

3.2.8. Nitric Oxide Scavenging Assay

Nitric oxide scavenging activity of samples was measured following a previously reported protocol, with major changes in the chemicals used (Patel, et al. 2010). Nitric oxide generation was initiated by incubating samples in a sodium nitroprusside reaction buffer. Pyrrole monomer and aqueous salicylate (final concentrations: 30 µM – 30 mM) were incubated with 1 ml, 10 mM sodium nitroprusside in PBS for 30 minutes at room temperature. 5 mM ascorbic acid and blank PBS were used as positive and negative controls respectively. After incubation, 100 µl of the reaction buffer was transferred to a 96-well plate and 100 µl of modified Griess reagent was added to each well. The Griess reaction was allowed to develop for 30 minutes at room temperature before 546 nm absorbance was measured using a plate reader (FlexStation 3). Pyrrole and salicylate background absorbance was also recorded.

This assay does not directly measure the scavenging of nitric oxide, instead it measures the inhibition of nitrite generation, and this is used as a proportional measure. To calculate the percentage inhibition, relevant background absorbances were subtracted and the percentage scavenging was calculated using the following formula:

$$\%(NO\ Scavenging\ Activity) = \left(\frac{Abs_{PBS\ control} - Abs_{sample}}{Abs_{PBS\ control}}\right) \times 100$$

316L SS and PPy-coated samples were assessed using the same protocol, using the required adaptions as outlined in the superoxide and hydrogen peroxide scavenging assay protocols.

3.3. Results

3.3.1. Broad antioxidant capacity of electropolymerised polypyrrole

The DPPH assay was used as a quick and simple, broad assessment of potential antioxidant activity in PPy-coated 316L SS wires. Although well documented, this assay is typically used with samples in solution. For this reason, it was critical to assess the suitability of this assay to determine the antioxidant activity of PPy coatings reliably and quantitatively. Figure 3.3. shows the antioxidant activity of probucol at a range of concentrations (5 µM – 1 mM) after incubation at room temperature (30 minutes – 24 hours). Probucol demonstrated a concentration-dependent antioxidant effect with no change with incubation time. These results suggest incubation times of 24 h are appropriate for calculating broad antioxidant capacity and 200 µM probucol to be a suitable positive control for this assay.

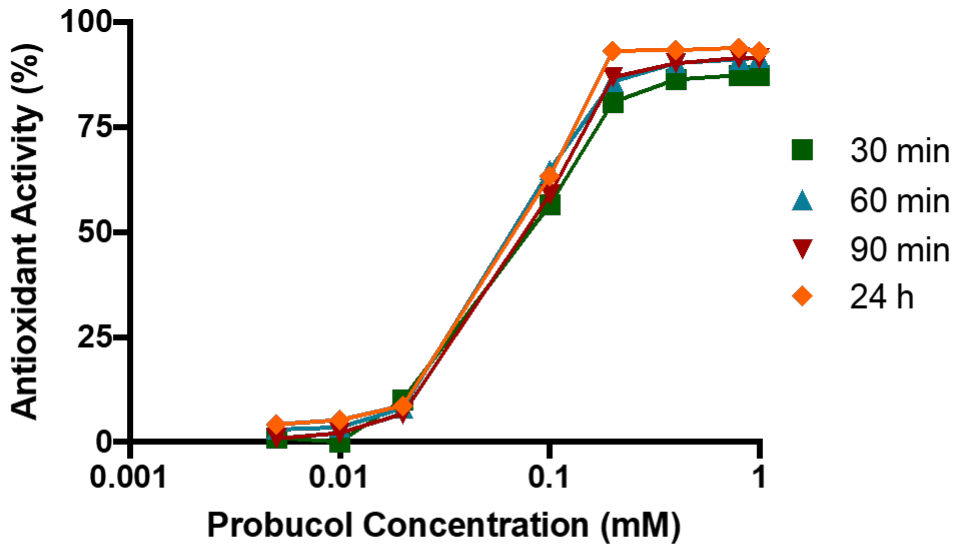

Figure 3.3. DPPH scavenging activity of probucol standards (5 µM – 1 mM), incubated for fixed times between 30 minutes – 24 h (n=1).

The antioxidant activity of PPy coatings was first assessed on the 1 mm 316L SS wires, with significant DPPH scavenging activity observed for coatings generated at 1.3 and 1.5 V for 10 minutes. This is shown in Supplementary Figure S3.1. Subsequently, 200 µm SS wires were coated at an applied voltage range of 1.1 and 1.5 V and this is shown in Figure 3.4. Panel a

shows that significant broad antioxidant activity was observed for all 200 µm wires coated by potentiostatic electropolymerisation (1.1 V: 63.5±14.3, 1.3 V: 86.9±3.2, 1.5 V: 83.4±4.7 vs. Uncoated: 0.63±0.29; %mean±S.E.M, $p<0.001$, n=3, one-way ANOVA with post-hoc Tukey). Panel b shows the relationship between current at the end of the electropolymerisation cycles and antioxidant activity with a strong correlation observed between these two variables (r^2 = 0. 9049, hyperbola fit). 1.5 V coatings were removed from subsequent experiments due to similarities to 1.3 V coatings highlighted in this data and Chapter 2.

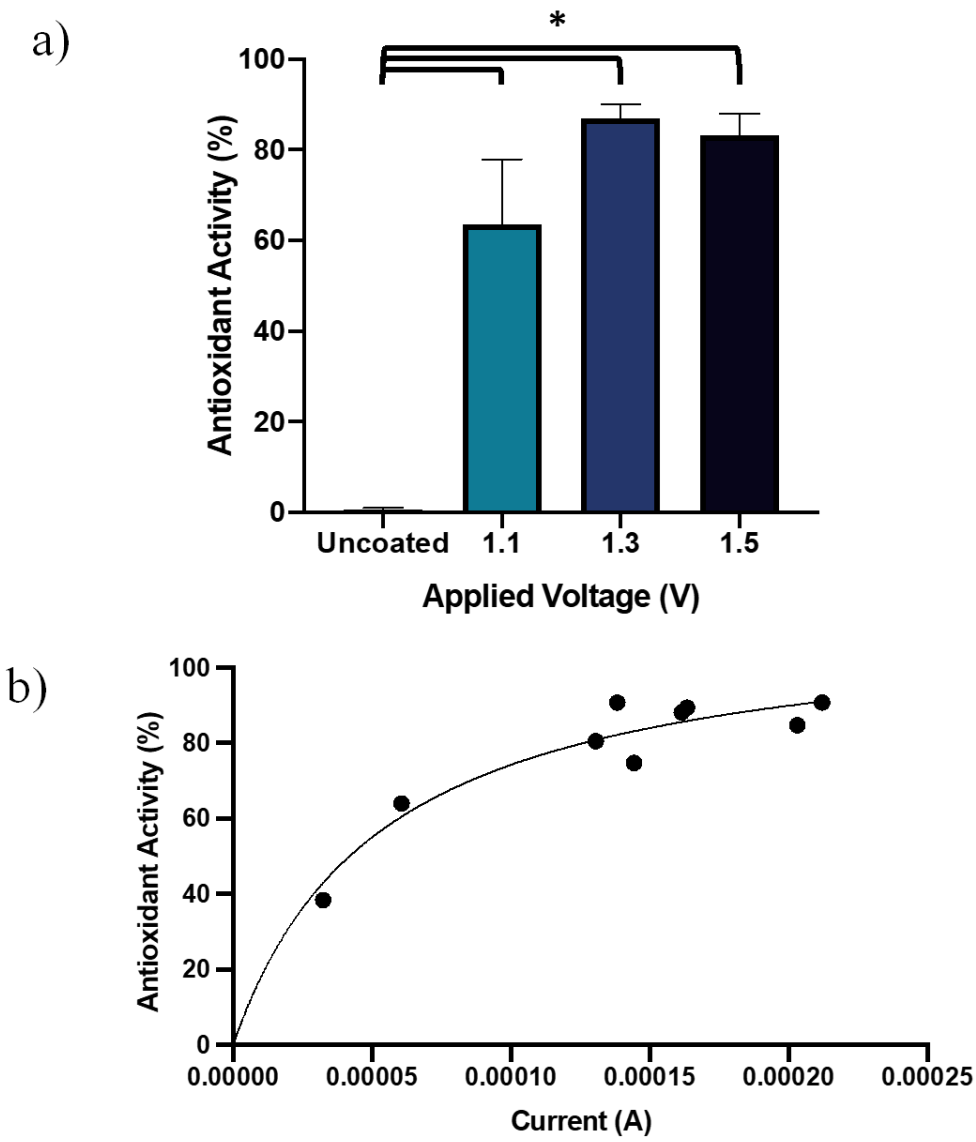

Figure 3.4. a) DPPH scavenging activity of potentiostatic electropolymerised PPy on 200 µm wires after 24 h incubation, showing strong antioxidant potential (mean±S.E.M, n=3, *$p<0.05$). b) Correlation between DPPH scavenging activity of 200 µm coated wires and terminal current during electropolymerisation (r^2 = 0.9049). As with 1 mm wires, current at the end of the electropolymerisation process correlates strongly with the DPPH scavenging capacity of 200 µm PPy-coated wires.

Although 24 h was used as the initial incubation time, a DPPH time course was used to assess the temporal stability of antioxidant properties of 1.1 V coated wires, uncoated 316 L SS wires and 200 µM probucol and is shown in Figure 3.5 panel a. It showed that solid antioxidants

require longer incubation periods in a stable radical assay, such as DPPH, than soluble antioxidants like probucol.

Uncoated 316L SS wires demonstrated little scavenging capacity, whereas probucol demonstrated very rapid antioxidant activity, with the reaction completing within the 3 hours and showing activity greater than observed with PPy coatings at 24 h (93.1% vs. 78.7%, n=3, $p<0.05$, t-test). Due to this time-dependency of the DPPH assay, scavenging capacities of 1.1 and 1.3 V coatings were compared at 8 and 24 h and shown in Figure 3.5 panel b.

At 8 and 24 h, two-way ANOVA and post-hoc Tukey tests were used to assess difference within the time point groups and showed no significant difference between the two PPy coatings. At 8 h, PPy demonstrated significant antioxidant capacity over the 316 L SS control (1.1 V: 47.4±5.2, 1.3 V: 45.0±3.1 vs. Uncoated: 1.8±0.6; %mean±S.E.M, $p<0.001$, n=3) and this continued at 24 h (1.1 V: 85.8±1.8, 1.3 V: 86.9±3.2 vs. Uncoated: 0.6±0.3; %mean±S.E.M, $p<0.001$, n=3). The difference between 8 h and 24 h was assessed using the same two-way ANOVA, but using post-hoc Sidak tests to assess differences between the time points and PPy samples demonstrated a comparable significant increase in antioxidant activity from 8 to 24 h ($p<0.001$), with no change in the SS control ($p>0.05$).

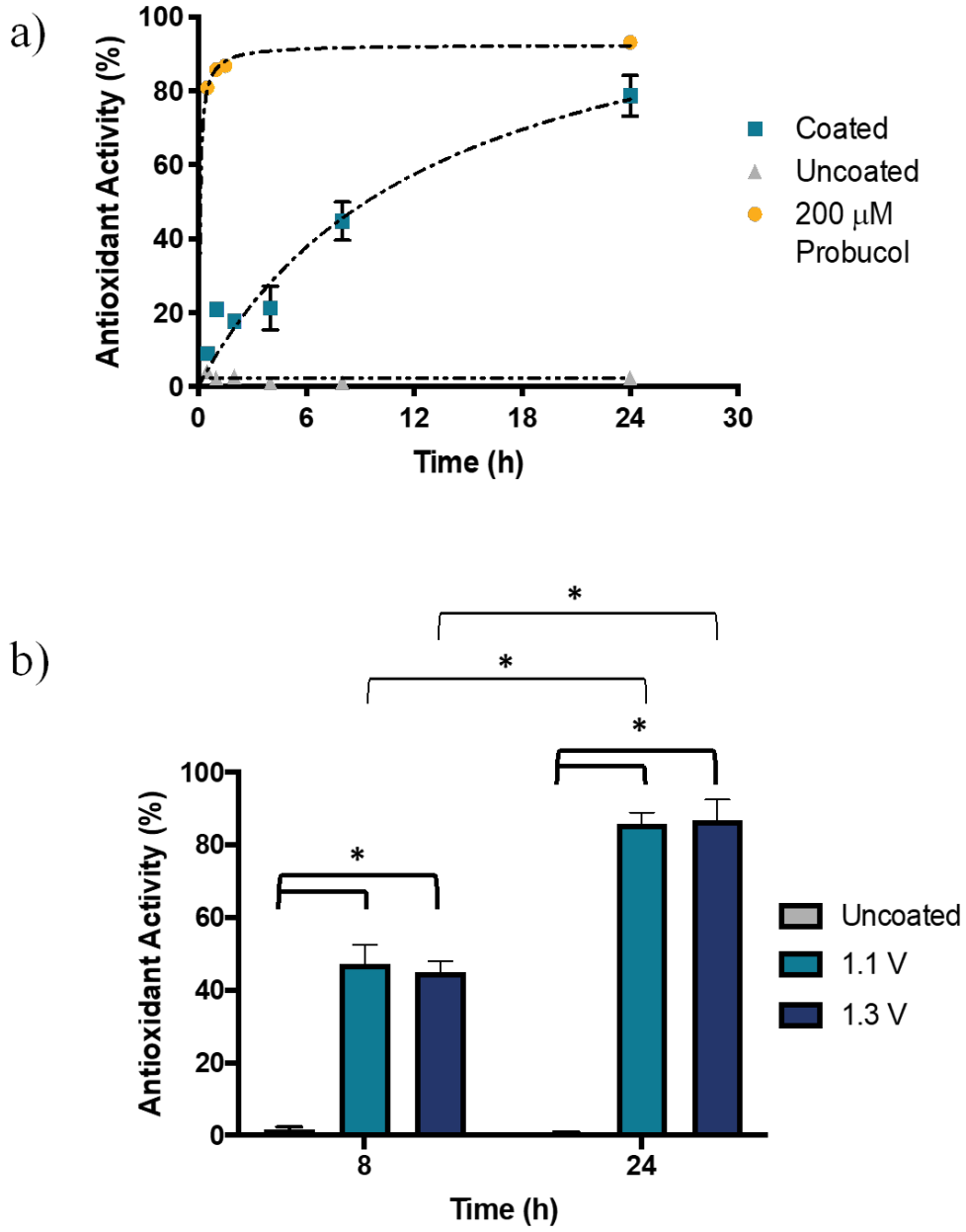

Figure 3.5. a) DPPH scavenging activity of 1.1V potentiostatic electropolymerised PPy coated 200 µm wires, uncoated 316L SS wires and 200 µM probucol over a 24 hr period, demonstrating a slower scavenging by PPy than probucol. Uncoated SS data was fitted with a linear trendline, whilst data for PPy coatings and probucol were fitted with hyperbolic trendline. b) DPPH scavenging activity of potentiostatic electropolymerised PPy coatings after 8 and 24 h incubation periods, showing no significant difference in DPPH scavenging between 1.1 and 1.3 V coatings at either time point and a significant increase from 8 h to 24 h (mean±S.E.M, n=3, *$p<0.05$).

After identifying the broad scavenging capacity of potentiostatic PPy coatings, potentiostatic and galvanostatic coatings were assessed to determine the longevity and stability of their

antioxidant activity. To assess the longevity of the antioxidant properties, coatings were repeatedly challenged with DPPH solution at 24 h intervals, with the absorbance measured after each interval to quantify the loss in antioxidant capacity. The antioxidant activity of potentiostatic coatings after repeated DPPH challenge is shown in Figure 3.6. (panel a). Challenged wires are compared against control wires that were stored in ethanol without challenge for 4 days before performing a DPPH assay. Both PPy coatings showed a linear depletion in the antioxidant activity after repeated challenge, but coatings generated at 1.3 V appear to better retain their antioxidant activity (1.1 V: gradient = -0.68 vs. 1.3 V: gradient = -0.39), with higher, albeit non-significant, antioxidant activity observed at 96 h vs. 1.1 V coatings (54.1±3.5 vs. 39.8±5.3, %mean±S.E.M, $p>0.05$, n=4). This loss is shown to be a result of repeated DPPH challenge as scavenging capacity was retained by the unchallenged controls.

To assess the stability and retention of broad antioxidant capacity in physiological conditions, coated wires were stored in PBS for fixed times up to 120 h before assessing DPPH scavenging. The loss in antioxidant activity of these coatings is shown in Figure 3.6. (panel b). Exposing coatings to PBS incubation had a marked effect on the scavenging capacity of potentiostatic PPy coatings with less than 20% capacity remaining at 120 h, with 1.1 V coatings falling to 16.8±1.5% and +1.3 V coatings falling to 12.7±2.1% ($p<0.001$, n=3). Both coatings generated at 1.1 and 1.3 V were similarly affected by PBS incubation with no significant differences in antioxidant activity when compared using a t-test ($p>0.05$). A greater effect on the loss of antioxidant activity is observed at 96 h after PBS incubation than after repeated challenge as demonstrated when comparing 1.1 V coatings (PBS storage: 19.7±3.4 vs. DPPH challenge: 39.8±5.3; %mean±S.E.M, $p<0.05$, n=3). The loss of antioxidant activity in PBS shows a strong linear loss (1.1 V: gradient = -0.50, $r^2 = 0.8311$; 1.3 V: gradient = -0.61, $r^2 = 0.9377$).

Coatings generated by galvanostatic electropolymerisation displayed noticeably different antioxidant behaviour to potentiostatic coatings in terms of longevity and stability, with a very rapid loss of antioxidant activity observed for coatings generated at 0.1 mA and no significant loss in antioxidant activity observed for coatings generated at 1 mA after repeated oxidative challenge. This is shown in Figure 3.6. (panel c). Coatings generated at 0.5 mA showed similar responses in antioxidant properties to coatings generated by potentiostatic galvanostatic, but the loss observed was slower (gradient = -0.24), although still significant to antioxidant capacity (83.7±3.3 at 24 h, vs. 64.7±2.8 at 96 h; %mean±S.E.M, $p<0.01$, n=4).

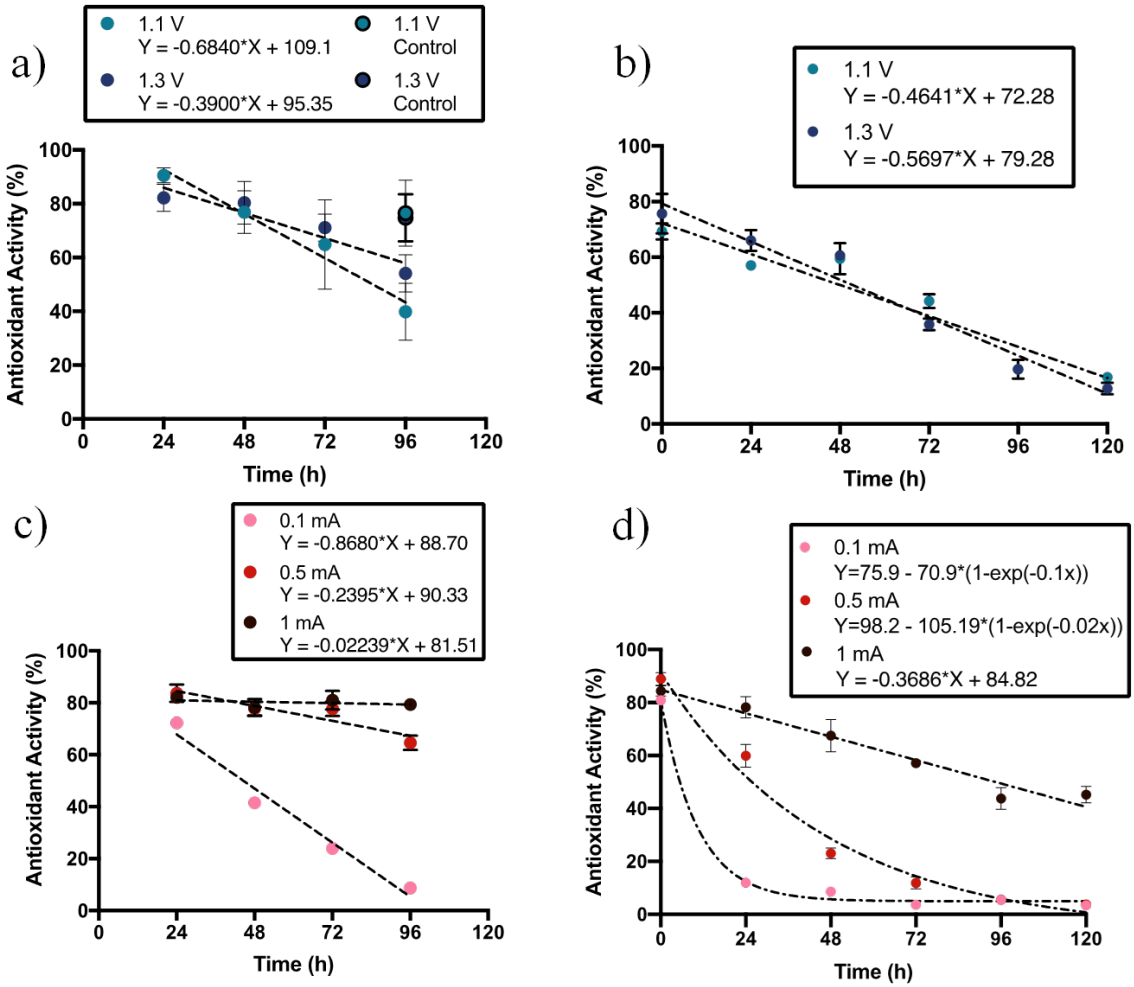

Figure 3.6. a) DPPH scavenging of potentiostatic electropolymerised PPy coatings, after repeated challenge with DPPH for 24 h intervals and control samples that were stored in ethanol for 4 day before DPPH exposure. b) DPPH scavenging of potentiostatic electropolymerised PPy coatings after incubation in PBS at 37ºC/120rpm for up to 5 days. c) DPPH scavenging of galvanostatic electropolymerised PPy coatings, after repeated challenge.. d) DPPH scavenging of galvanostatic electropolymerised PPy coatings after incubation in PBS. All PPy coatings demonstrate a linear loss in DPPH scavenging activity after repeated oxidative challenge. Linear loss in scavenging capacity is observed after PBS incubation with potentiostatic and 1 mA galvanostatic coatings, but 0.1 and 0.5 mA showed a exponential loss in scavenging capacity. (mean±S.E.M, n=3).

As with potentiostatic coatings, PBS incubation had a more detrimental effect on galvanostatic PPy coatings than repeated oxidative challenge, but the loss was not linear for all samples. This is shown in Figure 3.6. (panel d). Despite having similar DPPH scavenging capacity before incubation (0.1 mA: 80.9±1.7, 0.5 mA: 88.9±2.4, 1 mA: 84.4±1.9; %mean±S.E.M, $p>0.05$, n=3), coatings generated at 1 mA showed a linear depletion (gradient = -0.37) in

antioxidant capacity after PBS incubation, but retained high activity at 120 h, whereas coatings generated at 0.1 and 0.5 mA showed a rapid exponential decay in their antioxidant capacity with PBS incubation. After 120 h, this resulted in a significant loss in both 0.1 and 0.5 mA coatings when compared against the 1 mA samples (0.1 mA: 3.4±1.7, 0.5 mA: 3.7±0.6, vs. 1 mA: 45.2±3.2; %mean±S.E.M, $p>0.001$, n=3, ANOVA with post-hoc Tukey test).

3.3.2. Effect of dopant and electropolymerisation on DPPH scavenging capacity

As well as considering the influence of current on the antioxidant activity on PPy coatings generated by potentiostatic electropolymerisation, the contribution of the dopant and electropolymerisation time on antioxidant activity were also considered. Firstly, a DPPH assay was performed with 1 mM salicylate to identify any interference by the dopant based on the elution data collected for PPy coated samples in Chapter 2. This assay was carried out over multiple time points and the results of this assay in Figure 3.7 (panel a) shows that the salicylate dopant does not act directly as a broad antioxidant.

As presented in Chapter 2, a -0.75 V discharge step can significantly reduce the mass of salicylate contained within some PPy coatings. PPy coatings generated by potentiostatic electiopolymerisation after electrochemical Sa-depletion were found to retain their antioxidant properties, as shown in Figure 3.7 (panel b), with no significant difference between coatings with or without electrochemical discharge (1.1 V: 82.0±5.1 vs. 91.1±1.9; 1.3 V: 84.3±2.0 vs. 93.1±1.1, respectively; mean±S.E.M, $p>0.05$, n=3, two-way ANOVA with uncorrected Fisher's LSD post-hoc test). This process was repeated with galvanostatic coatings, Figure 3.7 (panel c), and similarly electrochemical discharge did not lead to a loss of DPPH scavenging capacity, with no significant difference with or without electrochemical discharge (0.5 mA: 84.5±1.6 vs. 91.0±1.5; 1 mA: 88.1±1.9 vs. 90.9±2.1, respectively; %mean±S.E.M, $p>0.05$, n=3). Across all sample types, it was observed that average DPPH scavenging increased with electrochemical discharge, although this was not statistically significant.

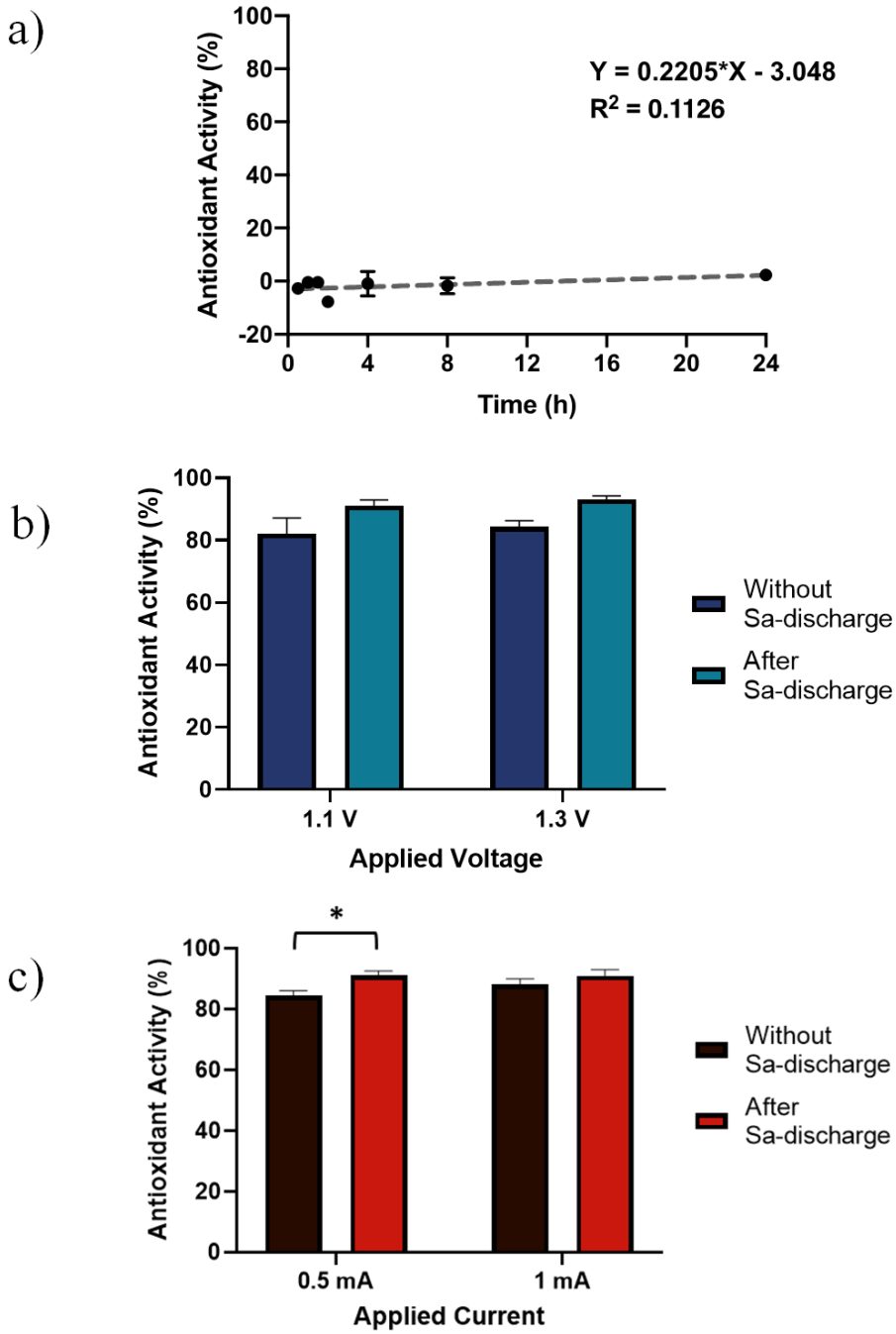

Figure 3.7. a) DPPH scavenging activity of aqueous salicylate (1 mM) over 24 h. b) DPPH scavenging of potentiostatic electropolymerised PPy coatings after electrochemical salicylate discharge (-0.75 V for 10 minutes) and control samples. c) DPPH scavenging of galvanostatic electropolymerised PPy coatings after electrochemical salicylate discharge (-0.75 V for 10 minutes) and control samples. The addition of a electrochemical salicylate elution step did not significantly affect DPPH scavenging capacity (mean±S.E.M, n=3).

The effect of the current level observed during electropolymerisation on antioxidant properties of PPy was assessed by generating samples at the same applied voltages but with reduced 1 minute electropolymerisation time. Figure 3.8. (panel a) shows the average current-time profiles of the coatings generated for 1 and 10 minutes showing similar characteristics between the 1 and 10 minute coatings. After electropolymerisation, 1.3 V coatings (1 minute) had the highest current value, while 1.1 V coatings (1 minute) had the lowest current value.

The antioxidant activity of these coatings is shown in Figure 3.8 (panel b). Despite having the highest current, 1.3 V coatings (1 minute) did not demonstrate the highest levels of antioxidant activity, although the differences in antioxidant activity between these coatings and coatings generated for 10 minutes were not significant (1.3 V/1 min: 53.4±6.7, 1.1 V/ 10 min: 69.3±2.9 and 1.3 V/10 min: 75.7±7.1; %; mean±S.E.M, $p>0.05$, n=3, one-way ANOVA with post-hoc Tukey). 1.1 V coatings (1 minute) demonstrated the lowest level of antioxidant activity and this was significantly lower than the activity demonstrated by the 10 minute coatings (21.9±9.7%, vs. 1.1 V/ 10 min, and 1.3 V/10 min; mean±S.E.M, $p<0.005$, n=3). It was however not significantly different from the coatings generated at +1.3 V for 1 minute ($p>0.05$).

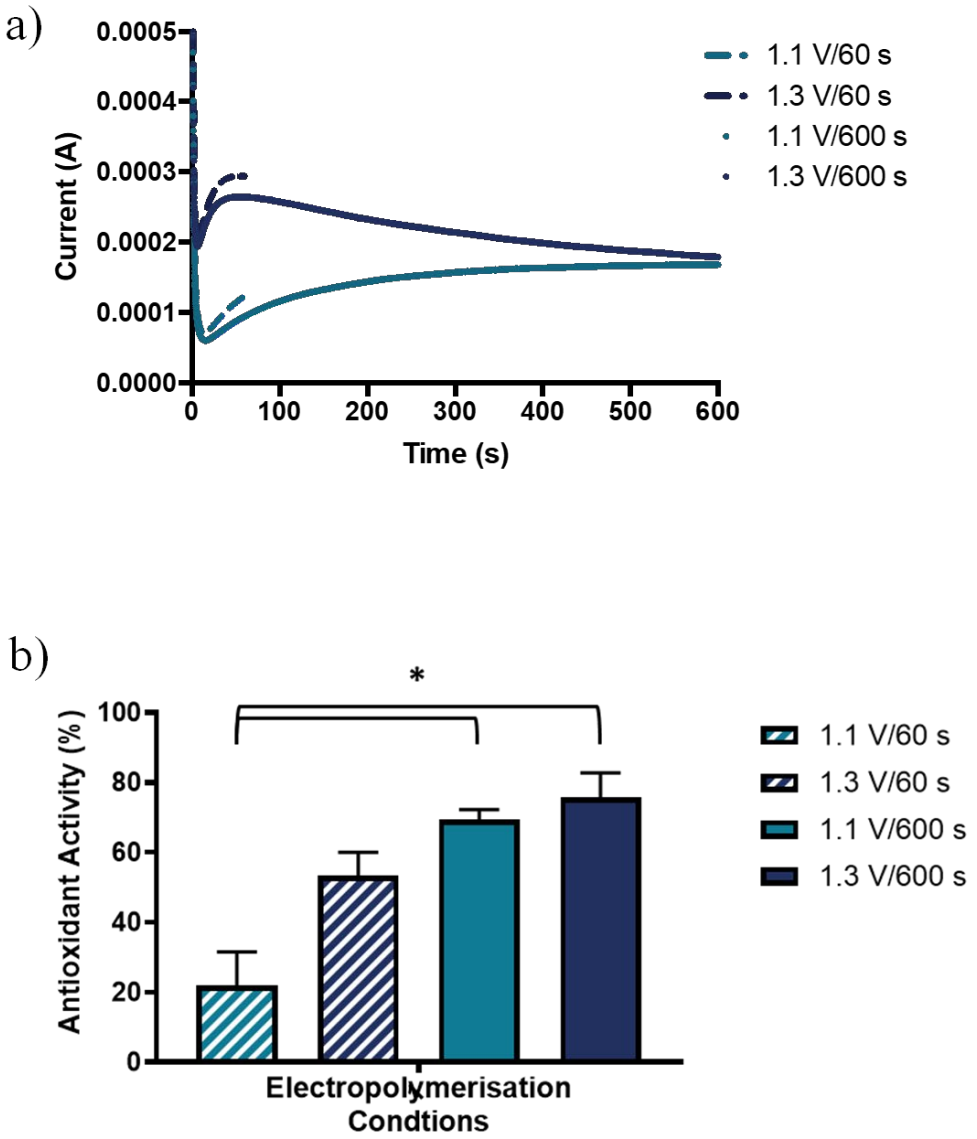

Figure 3.8. a) Current-time profiles for the potentiostatic electropolymerisation of wires at 1.1 and 1.3 V applied voltages for 1 or 10 minutes. b) DPPH scavenging of potentiostatic electropolymerised PPy coatings, coated for 1 or 10 minutes (mean±S.E.M, n=3, *$p<0.05$). The reduction in DPPH scavenging capacity by PPy coatings generated for 1 minutes suggests that coating time, and not current alone, is a determining factor in PPy antioxidant activity.

3.3.3. Superoxide radical scavenging capacity of electropolymerised polypyrrole

After characterising the broad antioxidant properties of PPy, the antioxidant activity against biologically relevant ROS was assessed. The enzymatic superoxide assay used in this study has precedent (Liu, et al. 2008), but has not been widely used with solid substrates. There are also several chemical components used in this assay to generate and detect superoxide radicals and it was important to optimise this assay before use with PPy coatings. Supplementary Figure S3.2. shows the results obtained upon optimising the superoxide scavenging assay for hypoxanthine and SOD. From this data, 1 and 2 μM hypoxanthine were identified as the most suitable initiator concentrations, and 1 μM was selected since it was sufficient in reliably inducing superoxide generation that is detectable. In this study, it was decided that 100 U SOD would be used as a positive control (for antioxidant activity) for its high effectiveness at inhibiting the reaction.

Pyrrole monomer and salicylate in solution were investigated individually. When assessing these chemicals, absorbance was recorded every 30 seconds and results are presented here by the individual data points as average linear regression fits in Figure 3.9. Figure 3.9. (panel a) shows the change in 605 nm absorbance over 10 minutes in the presence of pyrrole monomer (30 μM – 30 mM). Here, there is no loss in absorbance rise in the presence of any concentration of pyrrole and the increase is comparable with the xanthine oxidase control, suggesting no scavenging activity by the pyrrole monomer. Figure 3.9. (panel b) shows the 605 nm change in the presence of aqueous salicylate (30 μM – 30 mM). Similar to the pyrrole monomer, the rise was comparable with xanthine oxidase for all salicylate concentration, suggesting that salicylate in solution is incapable of scavenging superoxide radicals in this assay. In both figures, the presence of the superoxide dismutase inhibits the increase in 605 nm absorbance demonstrating it's antioxidant capacity for scavenging superoxide in this assay.

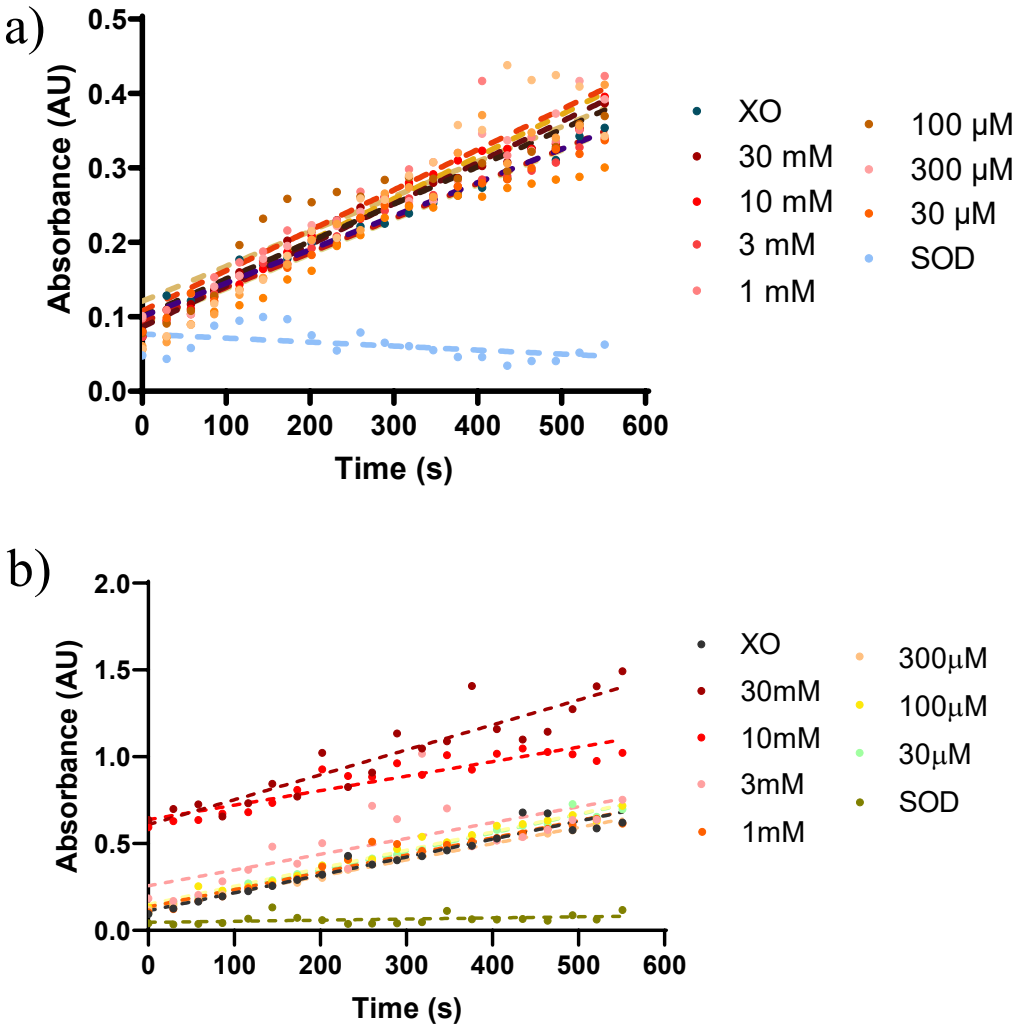

Figure 3.9. a) Superoxide scavenging assay kinetics in the presence of pyrrole monomer in PBS (30 µM – 30 mM), showing that pyrrole does not demonstrate any superoxide radical scavenging capacity. b) Superoxide scavenging assay kinetics in the presence of aqueous sodium salicylate in PBS (30 µM – 30 mM), showing that salicylate alone does not demonstrate any superoxide radical scavenging capacity. Salicylate solutions (>3 mM) led to increased absorbance due to the inability of hypoxanthine to dissolve rapidly in these solutions.

Due to limitations in using solid substrates with this assay to measure superoxide scavenging kinetically, endpoint absorbance was used to calculate the percentage of superoxide radicals scavenged and this is shown in Figure 3.10. This however does not allow the rate of the scavenging reaction to be determined. Coated samples generated by potentiostatic

electropolymerisation at 1.1 and 1.3 V, with and without an electrochemical discharge cycle, were tested and this is shown in Figure 3.10. (panel a). These samples demonstrated strong superoxide scavenging capacity, with significant activity by all samples when compared against the blank control (Blank: 0.0±2.0, vs. 1.1V: 33.2±6.2, 1.1V(-Sa): 46.8±5.4, 1.3V: 48.4±4.9, and 1.3V(-Sa): 75.1±6.9; $p<0.001$, n=4, One-way ANOVA with post-hoc Tukey). The bare 316L SS did not demonstrate significant scavenging potential (Blank, vs. 316LSS: 14.8±2.3; $p>0.05$, n=4), although 1.1V coated samples did not demonstrate a significant improvement compared with these samples ($p>0.05$). All other coated samples demonstrated a significant improvement compared to 316L SS ($p<0.005$).

Average scavenging capacity increased across both potentiostatic samples, but only significantly with the 1.3 V samples after electrochemical discharge (1.3V, vs. 1.3V(-Sa); $p<0.01$). No significant difference was observed between the 1.1 and 1.3 V coated samples ($p>0.05$), but after applying electrochemical discharge, a significant difference in the scavenging capacity of the two coatings was observed (1.1V(-Sa), vs. 1.3V(-Sa); $p<0.005$).

Coated samples generated by galvanostatic electropolymerisation at 1 and 2 mA, with and without an electrochemical discharge cycle, were also tested and this is shown in Figure 3.10. (panel b). Unlike potentiostatic coatings, strong superoxide scavenging capacity was not observed with galvanostatic coatings, with only 2 mA coatings showing significant potential compared with the blank control (Blank: 0.0±2.0, vs. 2mA: 55.0±9.; $p<0.001$, n=4, One-way ANOVA with post-hoc Tukey), although this was not significant against the 316L SS control (2 mA, vs. 316L SS: 14.8±2.3; $p>0.05$). No significant scavenging capacity was demonstrated by any other sample (Blank, vs. 1mA: 33.8±4.4, 1mA(-Sa): 16.4±8.6, and 2mA(-Sa): -13.9±21.1; $p>0.05$, n=4, One-way ANOVA with post-hoc Tukey).

When considering the effect of electrochemical discharge, the only significant effect observed was a substantial and complete loss in the scavenging capacity of the 2 mA coatings after discharge (2mA, vs. 2mA(-Sa); $p<0.001$, n=4, One-way ANOVA with post-hoc Tukey).

Although all coated samples demonstrated significantly lower scavenging capacity than the SOD control (SOD: 100.7±1.0, vs. coated samples; $p<0.001$), these results support that PPy coatings generated by potentiostatic electropolymerisation are capable of reliably scavenging superoxide radical and samples generated at 2 mA by galvanostatic electropolymerisation may demonstrate some scavenging potential.

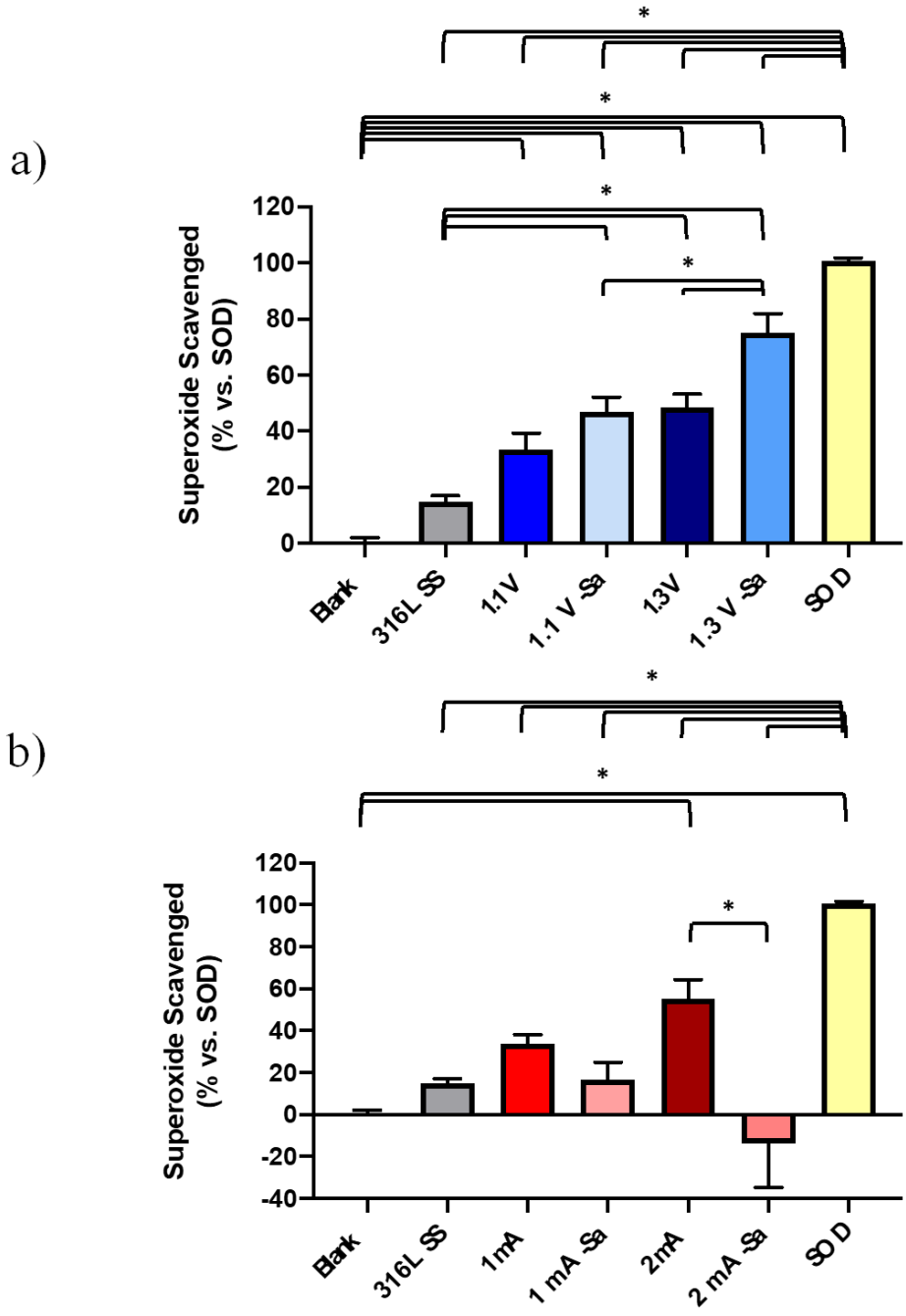

Figure 3.10. a) Superoxide scavenging by potentiostatic electropolymerised PPy-coated 316L SS strips, with and without an electrochemical discharge cycle (-Sa), showing significant superoxide scavenging capacity by both all coated samples, when compared with the blank control. b) Superoxide scavenging by galvanostatic electropolymerised PPy-coated 316L SS strips, with and without an electrochemical discharge cycle (-Sa), showing significant superoxide scavenging capacity by 2 mA coated samples, when compared with the blank control (mean±S.E.M, n=4, *$p<0.05$).

3.3.4. Nitric oxide radical scavenging capacity of electropolymerised polypyrrole

Nitric oxide is another key ROS for its role as a mediator of endothelial cell function. Assay conditions were optimised for suitable SNP (nitric oxide donor), and L-ascorbic acid concentrations prior to assessing the unknown NO scavenging capacity of experimental samples. Supplementary Figure S3.3. shows the results obtained upon optimising the nitric oxide assay for SNP, and L-ascorbic acid. To ensure reliable measurement, 5 mM SNP was chosen as the optimal concentration of generator for use in this assay. The concentration of the L-ascorbic acid positive control was then optimised, and 10 mM was deemed to be an effective and appropriate positive control.

Once optimised, the nitric oxide scavenging capacity of the pyrrole monomer and aqueous salicylate were assessed. The scavenging capacity of pyrrole is shown in Figure 3.11. (panel a). At all concentrations tested, pyrrole was not found to demonstrate any significant scavenging capacity over the blank control (0 mM: 0.0±3.6, vs. 0.03 mM: -1.1±5.9, 0.1 mM: 9.1±0.9, 0.3 mM: 11.5±0.6, 1 mM: 11.7±1.5, 3 mM: 9.9±1.4, 10 mM: 7.3±1.8, 30 mM: 0.0±0.5, mean(%scavenged) ± S.E.M, $p>0.05$, $n=3$, ANOVA with post-hoc Tukey). Similarly, salicylate was not found to possess any significant NO scavenging capacity when compared to the blank control (0 mM: 0.0±4.5, vs. 0.03 mM: 0.7±0.7, 0.1 mM: 3.4±5.0, 0.3 mM: 7.6±4.1, 1 mM: 1.6±1.8, 3 mM: 11.8±8.1, 10 mM: 5.8±5.8, 30 mM: -0.2±2.0, mean(%scavenged) ± S.E.M, $p>0.05$, $n=3$, ANOVA with post-hoc Tukey), as shown in Figure 3.11. (panel b).

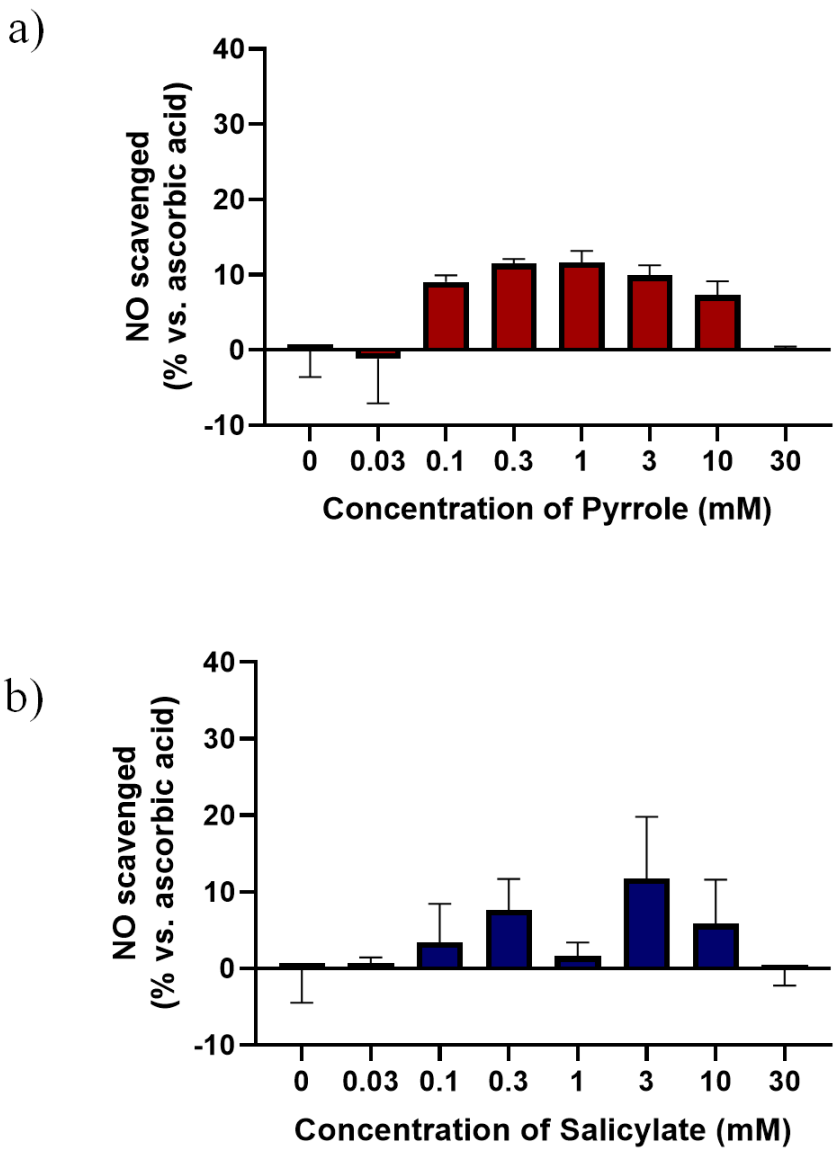

Figure 3.11. a) Nitric oxide radical scavenging capacity of pyrrole monomer in PBS solution (0.03-30 mM) presented as the % of NO scavenged relative to the postive control, showing no statistically significant NO scavenging capacity. b) Nitric oxide radical scavenging capacity of aqueous salicylate (0.03-30 mM) presented as the % of NO scavenged relative to the postive control, showing no statistically significant NO scavenging capacity (mean±S.E.M, n=3).

After assessing the scavenging capacity of the pyrrole monomer and aqueous salicylate using the nitric oxide scavenging assay, the scavenging capacity of PPy-coated strips was a

measured. This is shown in Figure 3.12. Coated samples generated by potentiostatic electropolymerisation at 1.1 and 1.3 V, with and without an electrochemical discharge cycle, were tested with 316L SS samples and this is shown in Figure 3.12. (panel a). All samples coated by potentiostatic electropolymerisation were found to demonstrate significant scavenging capacity when compared with the 316L SS control (Blank: 0.0±13.4, and 316LSS: -12.8±5.1, vs. 1.1V: 43.5±2.9, 1.1V(-Sa): 50.0±1.5, 1.3V: 44.4±4.0, and 1.3V(-Sa): 55.3±1.1; $p<0.001$, n=4, One-way ANOVA with post-hoc Tukey). Uncoated 316L SS samples did not scavenge nitric oxide (Blank, vs. 316LSS; $p>0.05$, n=4, One-way ANOVA with post-hoc Tukey). There was no statistical difference observed between coatings with or without an electrochemical discharge sample (1.1V, vs. 1.1V(-Sa); 1.3V, vs. 1.3V(-Sa); $p>0.05$).

Coated samples generated by galvanostatic electropolymerisation at 1 and 2 mA, with and without an electrochemical discharge cycle, were tested and shown in Figure 3.12. (panel b) and showed similar nitric oxide scavenging properties as potentiostatic samples. All galvanostatic samples demonstrated significant scavenging capacity compared with both the blank and 316L SS controls (Blank: 0.0±13.4, and 316L SS: -12.8±5.1, vs. 1mA: 57.0±4.7, 1mA(-Sa): 48.1±1.9, 2mA: 41.5±1.8, and 2mA(-Sa): 45.9±6.7; $p<0.001$, n=4, One-way ANOVA with post-hoc Tukey). When comparing each coating condition, electrochemical discharge was also found not to significantly affect scavenging capacity (1mA, vs. 1mA(-Sa); 2mA, vs. 2mA(-Sa); $p>0.05$).

As with superoxide scavenging, all coated samples demonstrated significant lower scavenging capacity when compared with the positive control (ascorbic acid: 100.0±0.7, vs. coated samples; $p<0.005$), but overall PPy-coated strips are shown to be capable scavengers of nitric oxide.

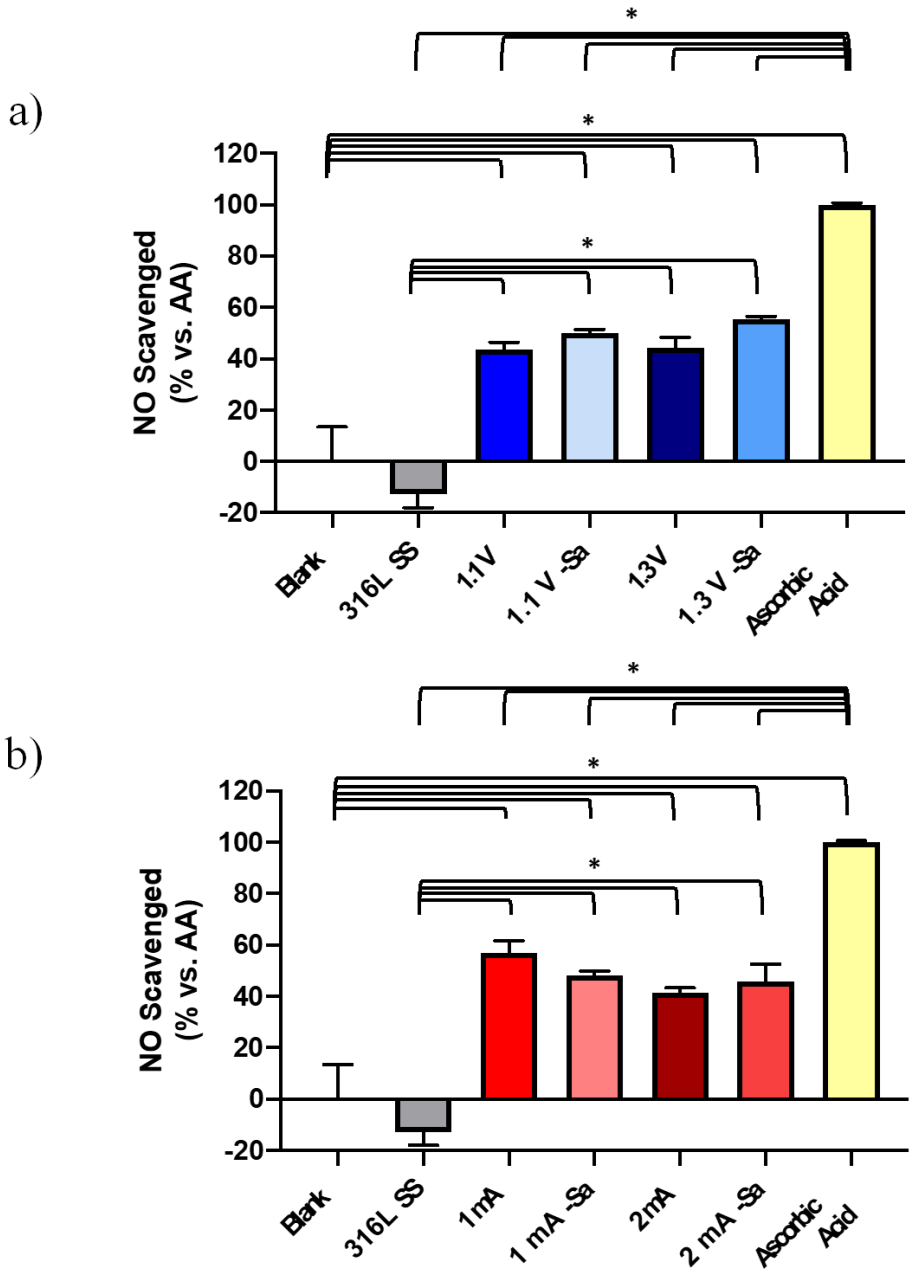

Figure 3.12. a) Nitric oxide scavenging by potentiostatic electropolymerised PPy-coated 316L SS strips, with and without an electrochemical discharge cycle (-Sa), showing significant nitric oxide scavenging capacity by both 1.1 and 1.3 V coated samples, before and after Sa discharge, when compared with the 316L SS control. b) Nitric oxide scavenging by galvanostatic electropolymerised PPy-coated 316L SS strips, with and without an electrochemical discharge cycle, showing significant nitric oxide scavenging capacity by both 1 mA and 2 mA coated samples, before and after Sa discharge, when compared with the 316L SS control (mean±S.E.M, n=4, *$p<0.05$).

3.3.5. Hydrogen peroxide scavenging capacity of electropolymerised polypyrrole

Before assessing the hydrogen peroxide scavenging capacity of PPy, the assay was first optimised with the L-ascorbic acid positive control, hydrogen peroxide concentration and incubation time. This is shown in Supplementary Figure S3.4. 40 mM hydrogen peroxide use led to a clear dose-dependent scavenging response with ascorbic acid after 10 minutes and was chosen to maximise the ROS challenge on the monomer, dopant and PPy samples. 10 mM ascorbic acid was found to be an appropriate and reliable positive control in this assay.

The hydrogen peroxide scavenging capacity of the pyrrole monomer and aqueous salicylate were assessed in solution using the optimised assay conditions and hydrogen peroxide scavenging capacity was observed for both chemicals. This is shown in Figure 3.13. Pyrrole (0.03 – 30 mM) demonstrated a concentration dependent increase in hydrogen peroxide scavenging, but significant scavenging capacity was only observed at the highest 30 mM concentration (30 mM: 70.2±15.6, vs. 0 mM: 0.0±2.5; mean(%scavenged) ± S.E.M, $p>0.05$, n=3, ANOVA with post-hoc Tukey). In contrast, significant scavenging capacity was observed at lower concentrations, 3 and 10 mM, with the aqueous salicylate (3 mM: 62.8±15.1, and 10 mM: 77.1±18.9; mean(%scavenged) ± S.E.M, $p>0.05$, n=3, ANOVA with post-hoc Tukey). Both pyrrole and salicylate exhibited high absorbance at 240 nm and this effect was very high with the aqueous salicylate preventing accurate measures being obtained for the 30 mM salicylate.

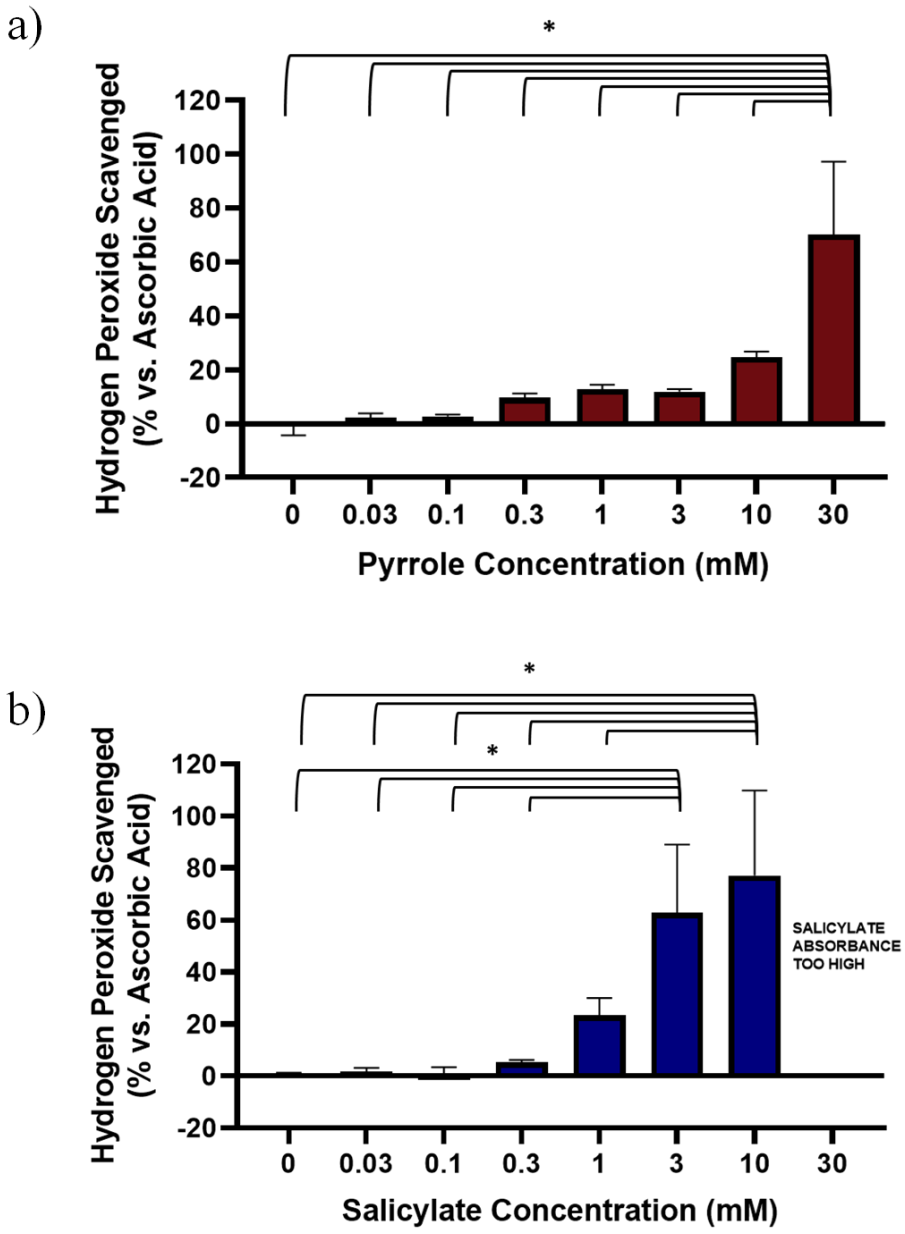

Figure 3.13. a) Hydrogen peroxide radical scavenging capacity of pyrrole monomer in PBS solution (0.03-30 mM), with 30 mM pyrrole demonstrating significant peroxide scavenging capacity. b) Hydrogen peroxide radical scavenging capacity of aqueous salicylate (0.03-30 mM), with 3 and 10 mM demonstrating significant peroxide scavenging capacity. Scavenging capacity of 30 mM could not be calculated as background 240 nm absorbance was to high. (mean % hydrogen peroxide scavenged±S.E.M, n=3, *$p<0.05$, one-way ANOVA with post-hoc Dunnett's. test)

The hydrogen peroxide scavenging capacity of potentiostatic and galvanostatic coated PPy strips was assessed and shown in Figure 3.14. Potentiostatic coatings generated at +1.3V demonstrated very high peroxide scavenging (1.3 V: 68.5±3.2, vs. Ascorbic Acid: 100.0±2.8; $p>0.05$, n=3), but no significant scavenging was observed with 1.1 V coatings (1.1 V: 2.0±15.4, vs. 316L: 4.7±0.6; $p>0.05$, n=3). This scavenging activity was unchanged by electrochemical salicylate elution, with no significant difference observed with or without a discharge cycle (1.1 V vs. 1.1 V -Sa: 3.6±8.5, and 1.3 V vs. 1.3 V -Sa: 96.1±4.9; $p>0.05$, n=3, One-way ANOVA with post-hoc Tukey).

Galvanostatic coatings demonstrated similar hydrogen scavenging capacities, with very high peroxide scavenging by coatings generated at 2 mA (2 mA: 94.5±3.0, vs. Ascorbic Acid: 100.0±5.0; $p>0.05$, n=4), but little scavenging by 1 mA coatings (1 mA: 19.8±5.2 vs. 316L: 4.7±0.6; $p>0.05$, n=4). This scavenging activity was again unchanged after Sa elution, with no significant difference observed (1 mA vs. 1 mA - Sa: 17.5±7.6, and 2 mA vs. 2 mA -Sa: 77.1±6.8; $p>0.05$, n=4, One-way ANOVA with post-hoc Tukey).

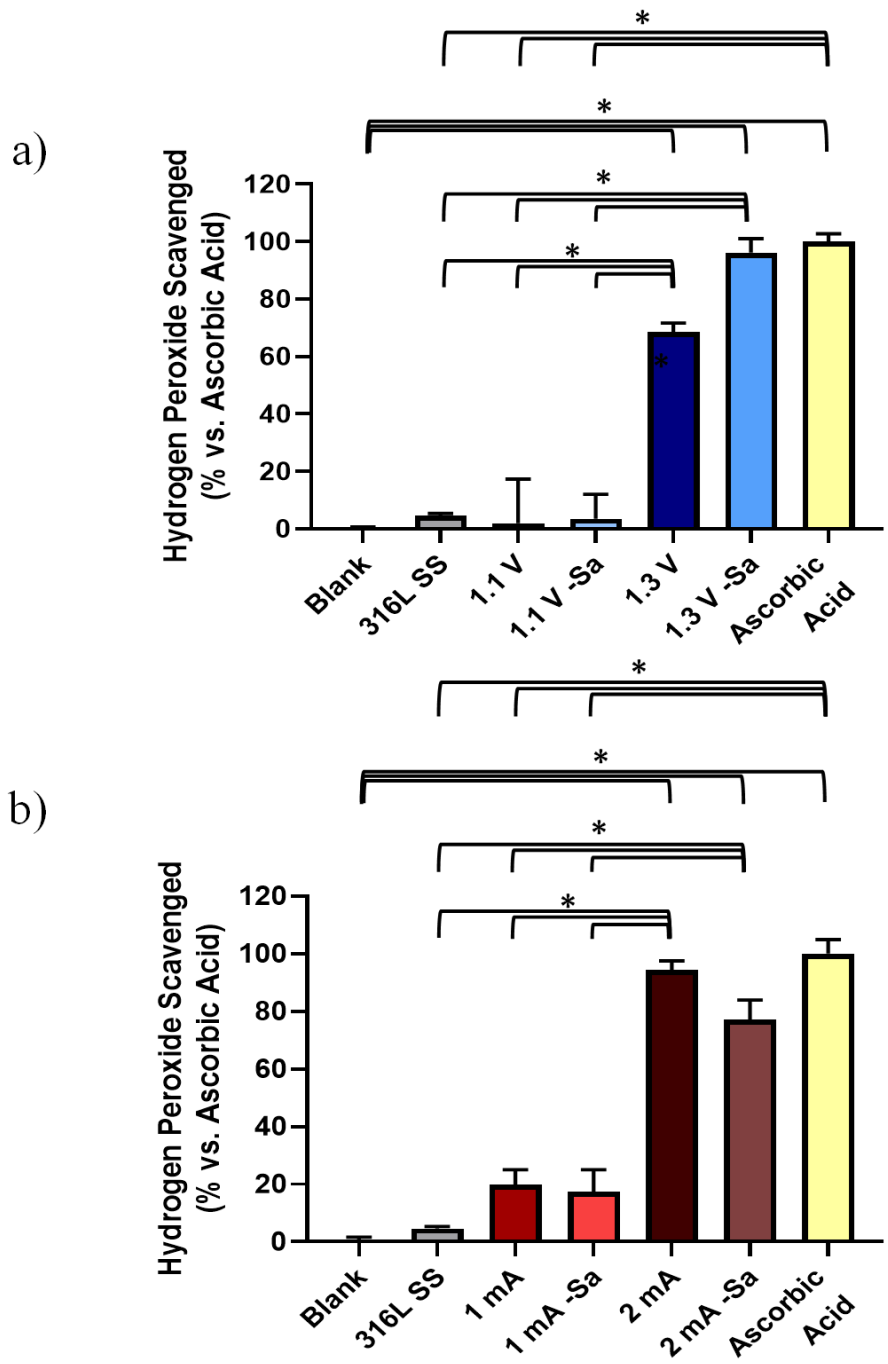

Figure 3.14. a) Hydrogen peroxide scavenging by potentiostatic electropolymerised PPy-coated 316L SS strips, with and without an electrochemical discharge cycle (-Sa), showing significant peroxide scavenging capacity by 1.3 V coated samples, before and after Sa discharge, when compared with the 316L SS control. b) Hydrogen peroxide scavenging by galvanostatic electropolymerised PPy-coated 316L SS strips, with and without an electrochemical discharge cycle, showing significant peroxide scavenging capacity by 2 mA coated samples, before and after Sa discharge, when compared with the 316L SS control (mean±S.E.M, n=4, *$p<0.05$).

3.3.6. Peroxyl radical scavenging capacity of electropolymerised polypyrrole

Trolox is a highly capable scavenger of peroxyl radicals – which are measured by the ORAC assay. When characterising antioxidants using the ORAC assay, equivalent Trolox doses may be used to quantify a substance's relative peroxyl scavenging capacity. This is less feasible when using PPy coatings as their opacity prevents kinetic fluorescence measurements. Supplementary Figure S3.5. shows the loss of fluorescence with a standard curve of increasing increasing Trolox concentrations (0.6125 – 25 μM). At 50- and 60-minutes, Trolox concentration and relative fluorescence show a linear correlation. 50 minutes was selected as the optimal incubation time for ORAC assays with PPy coatings due to the strong linear correlation between trolex concentration and relative fluoresence ($r^2 = 0.9505$).

Before measuring the peroxyl scavenging capacity of PPy-coatings, peroxyl scavenging potential of pyrrole monomer and aqueous salicylate were measured kinetically using the ORAC assay. This measurement is more robust and informative than measuring at a fixed point and is suitable because both chemicals are relatively soluble in PBS. Figure 3.15. (panel a) shows the average fluorescence loss in the presence of pyrrole monomer (30 μM – 30 mM). This data shows that in the presence of pyrrole there is a clear concentration-dependent inhibition in the loss of fluorescence, suggesting the pyrrole monomer is capable of proportionally scavenging peroxyl radicals, although 30 mM pyrrole led to an increase in fluorescence preventing an equivalent Trolox dose being obtained. Figure 3.15. (panel b) shows the effect of salicylate (30 μM – 30 mM). Except for 30 μM salicylate samples, salicylate prevented fluorescence loss, suggesting salicylate is a highly capable peroxyl scavenger at concentrations about 30 μM.

Equivalent Trolox doses for this data is shown in Figure 3.15. (panels c & d). As expected, pyrrole shows a clear concentration-dependent peroxyl scavenging capacity. Salicylate did not show the same concentration-dependent increase with peroxyl scavenging capacity appearing saturated at concentrations above 0.1 mM. The equivalent Trolox dose data may be used to compare the scavenging capacity of chemicals and suggests that high concentrations of pyrrole monomer (3 and 10 mM) demonstrate the highest peroxyl scavenging capacity.

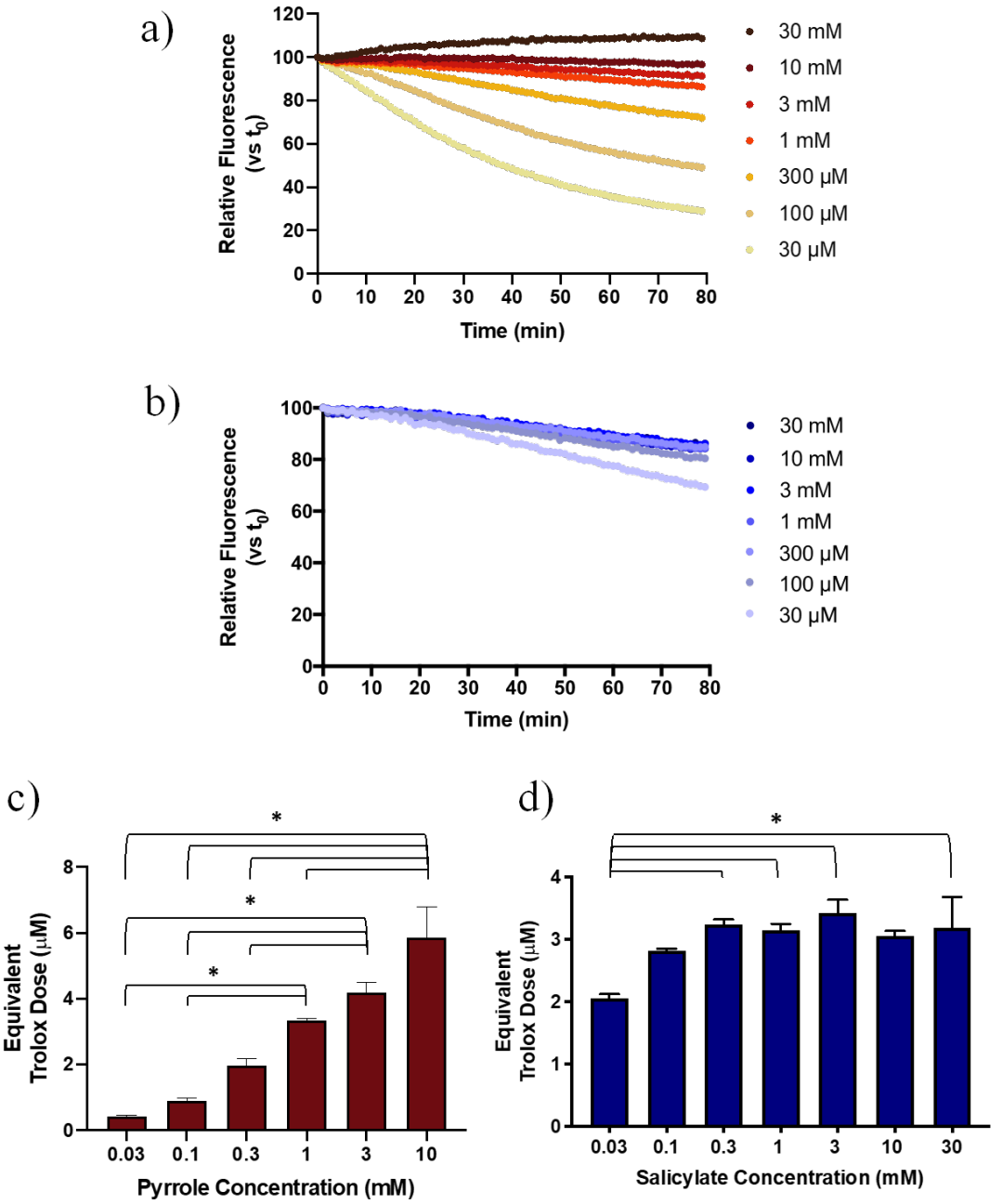

Figure 3.15. a) Loss of fluorescence due to peroxyl radical generation in the presence of increasing pyrrole monomer concentrations (30 µM – 30 mM) in PBS. b) Loss of fluorescence due to peroxyl radical generation in the presence of increasing sodium salicylate concentrations (30 µM – 30 mM) in PBS. c) Peroxyl radical scavenging capacity of pyrrole monomer presented as equivalent Trolox doses, showing a clear increasing concentration-dependent response. d) Peroxyl radical scavenging capacity of sodium salicylate presented as equivalent Trolox doses, showing peroxyl scavenging at all concentrations used (mean±S.E.M, n=3, *$p<0.05$, one-way ANOVA with post-hoc Tukey test).

The peroxyl radical scavenging capacity of potentiostatic and galvanostatic coated PPy strips was assessed and shown in Figure 3.16. Equivalent trolox doses were not estimated for the data and antioxidant activity was instead presented as percentage of peroxyl scavenged vs. the 10 μM trolox positive control. Strong peroxyl scavenging was demonstrated by 1.1 and 1.3 V coatings (1.1 V: 66.5±2.9; 1.3 V: 58.8±2.9 vs. 316L: 8.7±4.6; $p<0.001$, n=3). A significant loss in peroxyl scavenging capacity was observed after electrochemical salicylate elution (1.1 V vs. 1.1 V -Sa: 8.2±1.3; and 1.3 V vs. 1.3 V -Sa: 9.0±2.3; $p<0.001$, n=4, One-way ANOVA with post-hoc Tukey).

Similar behaviour was observed with galvanostatic coatings, with good peroxyl scavenging by coatings generated at 1 and 2 mA coatings (1 mA: 54.9±1.8; 2 mA: 63.8±6.1, vs. 316L: 8.7±4.6; $p<0.001$, n=3). This scavenging activity was again depleted after Sa elution, resulting in a significant loss in scavenging capacity (1 mA vs. 1 mA - Sa: 26.3±0.9, and 2 mA vs. 2 mA -Sa: 4.1±2.3; $p<0.01$, n=4, One-way ANOVA with post-hoc Tukey).

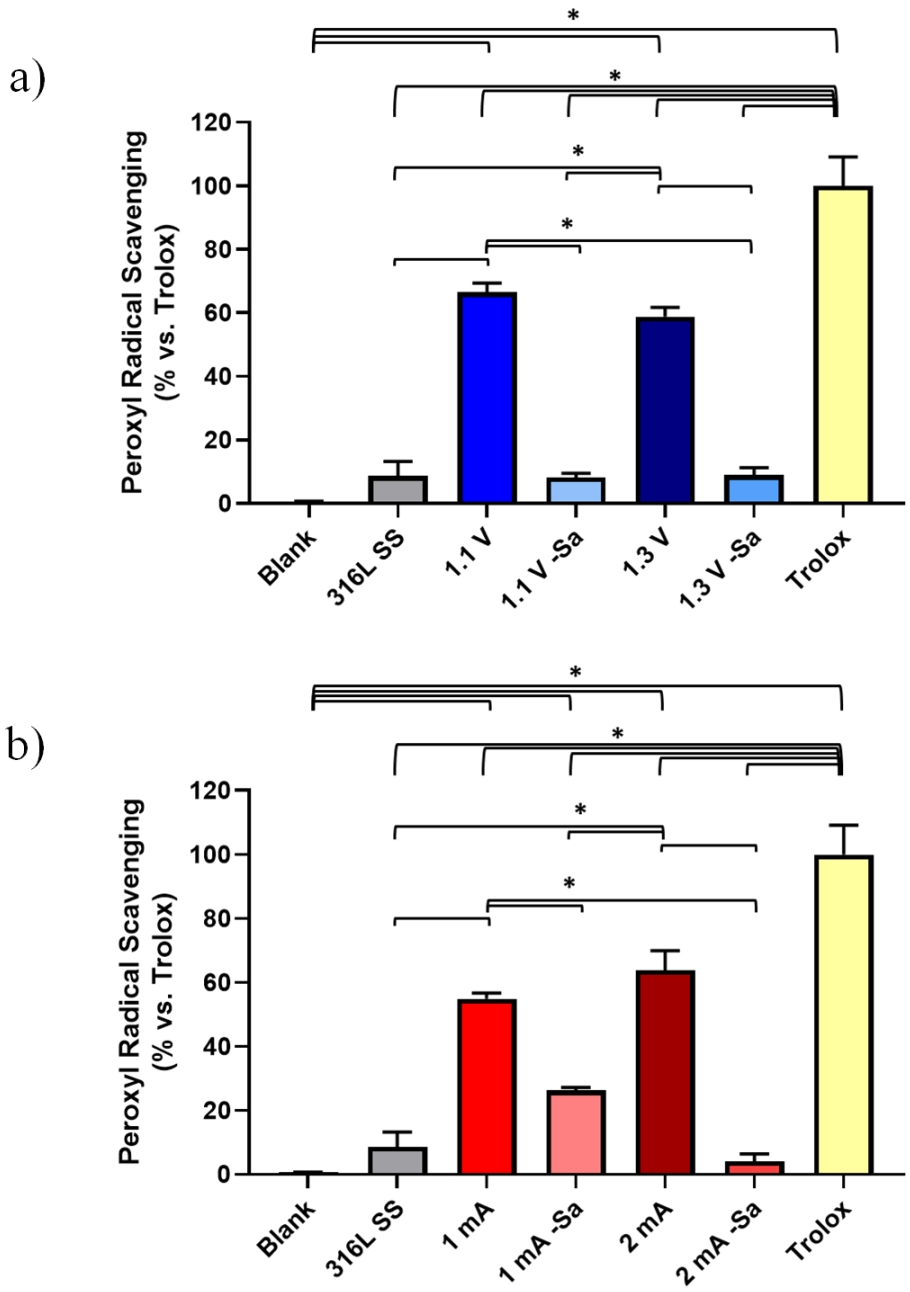

Figure 3.16. a) Peroxyl scavenging by potentiostatic electropolymerised PPy-coated 316L SS strips, with and without an electrochemical discharge cycle (-Sa), demonstrating significant peroxyl scavenging capacity by both 1.1 and 1.3 V coated samples, before Sa discharge, when compared with the 316L SS control. b) Peroxyl scavenging by galvanostatic electropolymerised PPy-coated 316L SS strips, with and without an electrochemical discharge cycle, demonstrating significant peroxyl scavenging capacity by both 1 mA and 2 mA coated samples, before Sa discharge, when compared with the 316L SS control (mean±S.E.M, n=4, *$p<0.05$).

3.4. Discussion

Polypyrrole has numerous current applications and its ability to demonstrate biocompatibility in a wide range of contexts has been established (Ateh, et al. 2006). The antioxidant activity of conducting polymers is more ambiguous within the scientific literature and no work has been carried out to study its potential as an antioxidant stent coating. Here, the results presented in this chapter are discussed in terms of their significant to the use of PPy as an antioxidant and comparisons to previously established studies. Furthermore, this discussion will also explore what potential ROS scavenging offers for PPy in a biological context before these potential effects are explored further in Chapters 4 & 5.

3.4.1. Optimisation of the DPPH assay

When assessing the broad antioxidant capacity of PPy-coated samples, incubation time was found to increase the amount of DPPH scavenged for both probucol and PPy coated wires, but this was most prominent for the coated wire samples. It was found that the 30-minute incubation in DPPH solution was insufficient for determining the full capacity of the coated samples as shown in Figure 3.5. This may be due to different reaction kinetic when using a solid sample compared with the aqueous probucol. For this reason, 24 h incubation was required for assessing differences in the PPy-coated samples.

Hsu, et al. (2008) assessed the DPPH scavenging capacity of PPy, but as with much of the previously reported work, used chemically synthesised PPy powders were used. This reduces the limitation of slow diffusion rates when using coatings strips by increasing the available surface area. 24 h incubation times were used, but in this work, the reaction was further promoted by shaking the PPy powders and assay agents for the first 6 h. When comparing the DPPH scavenging at 6 h and 24 h, this study found the majority of scavenging occurred in the first 6 h when shaking was incorporated, but a significant increase in DPPH scavenging was observed up to 24 h. Another factor worth considering when assessing these coatings with chemicals assays, is that the surface area of PPy coatings is likely high due to the cauliflower morphology that has been shown through SEM imaging. It is unclear how much of the surface is available to freely participate in the DPPH reduction reaction.

The ability of PPy coatings to scavenge significant quantities of DPPH within 1 h of incubation and continue to scavenge DPPH up to, and beyond, 24 hours demonstrates the rapid potential

for PPy coatings to offer an antioxidant ability quickly after implantation. The ability to quickly scavenge may also allow the coatings to respond to increased oxidative stress during the inflammatory stages of healing occurring quickly after stent placement and extending up to 7 days in duration (Weintraub, et al. 2007). The responsiveness of the coating to DPPH may not be representative of different ROS and is considered for the specific ROS species explored in this study.

3.4.2. Broad antioxidant capacity of electropolymerised polypyrrole

PPy is shown in this study to be a capable scavenger of DPPH, but it is also shown that this effect is dependent on the electropolymerisation conditions. The DPPH scavenging capacity of PPy coatings was shown to increase on average with increased applied voltage, as demonstrated in Figure 3.4, suggesting this improves the antioxidant properties of the coatings generated. This effect may also arise from increased applied voltage improving the electropolymerisation efficiency resulting in thicker PPy coatings.

When plotting the terminal current of electropolymerisation against the antioxidant activity, a strong hyperbola fit was observed showing that the two factors correlate, as demonstrated in Figure 3.4. The increase in current during electropolymerisation is a result of PPy generation on the working electrode and therefore this value has been shown to correspond well with the PPy film thickness at the end of the electropolymerisation cycle (Ansari, 2006). Since the current provides a measure of film thickness, it may indicate that increasing film thickness improves antioxidant properties. At lower currents, increases in current have a very high impact on antioxidant activity, but increases at higher currents have less impact, suggesting that improvements in antioxidant capacity are limited once a certain thickness is reached. Where the plateau begins, the coating is likely more consistent in thickness and across the length of the wire and any extra thickness does not contribute to antioxidant activity as antioxidant activity is fundamentally a surface property (Vasile, 2018). Bulk properties may however contribute to other aspects of the coating's biocompatibility.

Issues arise when 200 μm wires are used since the current response of PPy during electropolymerisation at 1.3 V shows an early peak before slowly falling. This was previously suggested in Chapter 2 of this present study to result from Sa-precipitation or overoxidation. It would be expected that film thickness increases or stay constant during coating and may

indicate that current is not directly proportional to PPy film thickness when overoxidation or precipitation is suspected.

When assessing the time-dependent scavenging capacity of PPy, as observed in Figure 3.5, a fast increase in DPPH scavenging was observed before 8 h, after which the rate of increase slows towards 24 h. This data may suggest that a HAT mechanism of antioxidant activity is taking place, since this mechanism is limited by the number of available hydrogen sites at the coating surface. Based on this mechanism of action, the rate of change may decrease due to three potential factors: 1. As the reaction proceeds, the activation energy necessary to reduce DPPH increases as the number of H-sites is depleted, 2. Number of H-sites depletes as the reaction proceeds, this reduces the chance of diffusion-driven collisions occurring, or 3. Between 8 and 24 h, the reaction is complete and there are no H-sites available to scavenge DPPH.

Scavenging capacity of 1.1 and 1.3 V potentiostatic coatings was assessed at 8 h and 24 h and a significant difference in DPPH scavenging was observed, suggesting the rate of scavenging between the samples is comparable. This supports the use of 24 h incubation time to assess overall DPPH scavenging capacity of PPy coated samples but illustrates the need to assess repeated oxidative challenge in the coatings as a robust measure of total DPPH scavenging capacity.

The effect of repeated oxidative challenge and PBS storage is shown in Figure 3.6. Panel a in this figure shows the depletion of DPPH scavenging capacity after repeated exposure with coatings generated by potentiostatic electropolymerisation. The continued capacity for DPPH scavenging with repeated challenge shows that at 24 h sites for HAT remain and supports the theory that as sites are lost, the required activation energy for HAT increases and number of collusions decreases, leading to a loss in the rate of DPPH scavenging. Conversely, this theory neglects the potential contribution of SET to DPPH scavenging. If PPy is reducing DPPH via SET, it may be incorporated as a dopant, resulting in stabilisation of the PPy polymer and the linear loss in DPPH scavenging observed (Hristeac, et al. 2006). The controls used here support the observation of a depletion in DPPH capacity and show that ethanol alone is not responsible, although it does contribute marginally. Coatings generated at 1.3 V may be more depletion resistant, as suggested by the lower linear gradient and the higher activity at 96 h. This is likely a result of thicker coatings being generated, leading to a greater mass of PPy to scavenge DPPH.

Fig 3.6 Panel b shows the effects of PBS storage on potentiostatic coatings. Here, there is a significant linear loss in activity, which is greater for both samples than the loss observed with DPPH exposure. This is surprising since there should be no oxidative challenge in PBS and pH should be closely controlled. The loss in scavenging capacity indicates a poor response of PPy coated samples to flow or 37ºC temperatures, either of which would greatly limit PPy's appropriateness for biomedical applications. There are no studies considering the antioxidant capacity of PPy under physiological conditions, but PPy is known to demonstrate suitable mechanical properties (Balint, et al. 2014). However, electrochemically synthesised films are known to be less crystalline than other forms of PPy with lower mechanical properties but are known to demonstrate thermal stability, with a glass transition temperature far in excess of the 37ºC required for stent coatings (Foroughi, et al. 2010; Yussuf, et al. 2018).

Galvanostatic coatings were also assessed with the effects of repeated challenge shown in Figure 3.6 panel c. Galvanostatic coatings showed similar broad scavenging potential as potentiostatic coatings. This observation, along with previously published work using chemically synthesised PPy suggest that this antioxidant behaviour is an innate material property of PPy, rather than resulting from the synthesis route. As observed from the time-voltage plots in chapter 3, there are obvious differences between the galvanostatic coatings used in this study with 0.5 mA shown to display the optimal topography, reliability in generation and demonstrating high retention of DPPH scavenging capacity. In contrast, 0.1 mA coatings suffer from very rapid and complete depletion. This supports the initial observation that patchy and thin coatings, possess inferior antioxidant properties through reduced PPy film thickness. 1 mA coatings were the only coatings assessed to not show any depletion in DPPH scavenging, despite the high precipitation present on these surfaces. This suggests that a significant mass of PPy is generated, at these conditions despite the precipitation effects.

The effects of PBS storage on galvanostatic coatings are shown in Figure 3.6 panel d. Unlike previous data highlighting similarities in the antioxidant properties of potentiostatic and galvanostatic coatings, there are significant differences in stability of their antioxidant properties. 1 mA coatings show strong retention of their antioxidant properties, with a smaller linear loss than potentiostatic coatings, but both 0.1 and 0.5 mA coatings suffered from an exponential decay in properties after PBS incubation. This more profound effect of PBS on

these coating's antioxidant properties suggests a potential weakness of the 0.5 mA coatings in long-term use.

One limitation of this study is that the consideration of stability is limited to 5 days in a non-challenged (PBS only) medium. *In vivo*, even without significant oxidative challenge, the stent will encounter a more challenging environment with blood, flow and cellular interactions. Furthermore, the period of 5 days aligns well with the peak of the inflammatory response expected after stent placement where oxidative stress is expected to be at its highest but is far shorter than the elution longevity achieved by modern DES – 120 days for full elution and high elution to align with peak SMC proliferation up to 30 days (Perkins, et al. 2009). It is worth noting that these modern DES typically achieve re-endothelialisation with 28 days, therefore this is a reasonable target for a therapeutic longevity when utilising a pro-healing strategy and design.

Future studies could explore the longevity and stability of the coatings further by developing more appropriate stent models and exploring the stability and capacity of PPy antioxidant effects over a longer period, up to, and beyond 28 days.

3.4.3. Effect of dopant and electropolymerisation on DPPH scavenging capacity

The initial data shows that PPy demonstrates potential as a broad antioxidant with some coatings showing activity that is retained after repeated oxidative challenge and after physiologically relevant PBS incubation. It was important to also consider what factors may contribute to this activity or may act to modify the level of scavenging capacity.

Firstly, the role of the salicylate dopant was assessed. Sodium salicylate is an anti-inflammatory drug, which is known to react with hydroxyl radicals, and thus may mask the DPPH scavenging capacity of PPy (Sharma, et al. 2013). The DPPH scavenging capacity of sodium salicylate (1 mM in ethanol) was assessed over 24 h, as was the scavenging capacity of potentiostatic and galvanostatic coatings with and without electrochemical discharge, and there was no evidence that salicylate is responsible for the broad scavenging activity observed with PPy coatings. This is shown in Figure 3.7. This indicates that although salicylate is a capable scavenger of hydroxyl radicals, this activity may not extend to DPPH radicals.

Although salicylate alone does not demonstrate broad antioxidant capacity when assessed using DPPH, it could have a role by modifying the electrochemical properties or influencing the redox potential of the polymer. DPPH scavenging by PPy after electrochemical discharge suggests that salicylate does not play a contributing role with improved average scavenging capacity after electrochemical discharge. It is worth noting that the addition of an electrochemical discharge step did not fully remove the salicylate dopant, but it led to a marked decrease in the mass of salicylate within all coatings. If salicylate were contributing to broad antioxidant activity therefore, the loss of salicylate should lead to reduction in scavenging capacity; this however is not observed. Reduction of PPy, leading to a complete loss of the dopant has been shown to significantly improve the DPPH scavenging activity of PPy powders (Hsu, et al. 2008).

Electropolymerisation time was assessed by generating samples at 1.1 and 1.3 V for 1 minute and 10 minutes resulting in three sets of coatings with comparable currents (1.1V/60s, 1.1V/600s, and 1.3V/600s) and one set of coatings with a higher current (1.3V/60s). If current was a determining factor of antioxidant activity, it would be expected that 1.3V/60s coatings would demonstrate the highest level of DPPH scavenging capacity. This was however not observed, as demonstrated in Figure 3.8, with 10 minute coatings demonstrating the highest scavenging capacity. From the DPPH data, it is shown that current alone does not correlate with antioxidant activity, as film thickness is associated with both current and electropolymerisation When considering antioxidant activity, it is therefore important to consider coating time, applied voltage, the potential for overoxidation and the redox state of the coating.

3.4.4. Superoxide radical scavenging capacity of electropolymerised polypyrrole

The superoxide scavenging assay used in this study was adapted from methods previously reported (Liu, et al. 2009). The methods reported by Liu, et al. (2009) were initially tested but issues resulting from the low solubility of hypoxanthine required the reoptimisation of this assay. Accordingly, hypoxanthine concentration was reduced to 1 uM and this was not found to limit the reliability or sensitivity of the assay.

The modified superoxide assay was applied to assess the superoxide scavenging potential of both the pyrrole monomer and aqueous salicylate. As with the DPPH assay, this superoxide scavenging assay should be considered a broad, albeit specific and biologically relevant assay, since superoxide has been shown to be reduced by both HAT and SET (Li, et al. 2018). Characterising the antioxidant activity of the pyrrole monomer allows the contribution of the N-H group to be assessed, but it is possible that changes in the chemical structure during electropolymerisation may also aid N-H dissociation or SET by pyrrole or PPy may also contribute. In this study, pyrrole monomer did not demonstrate any strong potential for superoxide scavenging, indicating that the monomer is not a capable scavenger of superoxide, as shown in Figure 3.9 (panel a).

Salicylate similarly indicated no significant superoxide scavenging activity at any concentration tested as shown in Figure 3.9 (panel b). One issue encountered was that high concentrations (10 and 30 mM) of salicylate were associated with solubility issues and corresponding absorbance issues. In contrast to pyrrole, salicylate is not chemically modified during the electropolymerisation process, therefore, the lack of scavenging in this assay suggests it will not contribute to superoxide scavenging when used as a dopant.

Unlike the monomer and dopant, PPy strips possess significant superoxide scavenging capacity over both the blank and uncoated SS, although this is electropolymerisation condition dependent, as demonstrated in Figure 3.10. It is also worth noting again that PPy strip scavenging capability was determined using an endpoint absorbance measurement, rather than kinetic readings taken for pyrrole and salicylate solutions, and therefore gives no indication of scavenging reaction rate. A further limitation of the fixed endpoint assay is that the superoxide control efficacy cannot be determined with the same confidence since there is no initial absorbance reading other than the blank control.

Samples generated by potentiostatic electropolymerisation appear to demonstrate good superoxide scavenging capacity. The effect of electrochemical elution on the coatings mirrored that observed with the DPPH assay, with average superoxide scavenging increasing for both samples and significantly with samples coated at +1.3 V. In contrast, samples coated by galvanostatic electropolymerisation were not found to demonstrate significant superoxide scavenging capacities. Electrochemical elution also did not improve the scavenging activity, instead resulting in loss of average scavenging for both coatings and significant depletion for the 2 mA coatings. This deleterious effect was not observed in the DPPH data. It is worth

noting that the coating protocol was reoptimized for use with the strips and 1/2 mA strips may not be directly comparable to 0.5/1 mA wires.

316L strips demonstrated some superoxide scavenging ability, although statistically comparable to the blank. This may arise if the presence of the strips disrupts the shaking causing inhibition or slowing of the reaction. This is however speculative, and SS may be a weak superoxide scavenger, but there is no evidence in the literature to indicate where SS is capable of scavenging superoxide radicals.

This data suggests that a change occurs during the electrochemical synthesis of the polymer that allows the polymer to scavenge superoxide. Superoxide has been previously shown to react with polypyrrole. Lei & Martin, (1995) reported that superoxide can react with undoped PPy by deprotonation of the pyrrole nitrogen, in a mechanism akin to HAT. Interestingly, the resulting PPy had improved electrical conductivity suggesting that the reduced superoxide radical acts as a dopant, but this study uses pristine, completely undoped PPy, which is not comparable to the coatings used in this current study. The mechanism was supported more recently, when Maruthapandi, et al. (2020) demonstrated the capacity of PPy to undergo deprotonation, but also re-protonation. The reversibility of wider oxygen interactions with PPy has been explored with PPy electrodes (Wu, et al. 2007). The level of deprotonation and superoxide incorporation can be measuring using FTIR because the imine group has a distinct peak in the range 1640-1690 cm^{-1}, presenting a method to measure the total superoxide scavenging capacity of the coatings.

One major weakness of this assay is that superoxide can react rapidly and interact with the solvent or oxygen to form other ROS with stronger oxidising power and it is unclear how this could interfere with either the NBT or PPy (Liang & Kitts, 2014). Wider conclusions cannot be inferred since superoxide radicals have relatively low oxidising power when compared with other ROS, such as peroxyl radicals and hydrogen peroxide; resulting in poor reactivity.

3.4.5. Nitric Oxide radical scavenging capacity of electropolymerised polypyrrole

The nitric oxide scavenging assay used in this study was adapted from a method previously reported by Patel, et al. (2010). This assay was optimised for SNP and the ascorbic acid positive control concentration and 5 mM SNP and 10 mM ascorbic acid were found to be suitable concentrations.

The optimised NO scavenging assay was used to determine the scavenging activity of the pyrrole monomer and the salicylate dopant within the concentration range 30 µM – 30 mM, as shown in Figure 3.11. Under the conditions tested, neither pyrrole nor aqueous salicylate demonstrated any significant NO scavenging capacity. Like superoxide, NO is a weak oxidising agent that can be reduced by both HAT and SET (Lancaster, 2015). Therefore, this assay can only be used to measure NO scavenging and does not imply any mechanism of action. The lack of NO scavenging capacity by pyrrole and salicylate is comparable to that of superoxide scavenging and may be suggestive of both chemical's lack of capacity to scavenge less oxidising ROS. One key difference between these assays however is that NO can behave as both a nitrogen and oxygen radical, and this may affect its ability to react differently compared with superoxide (Dröge, 2002). There is a lack of studies assessing the *in vitro* scavenging capacity of pyrrole, but the drug tolmetin is derived from pyrrole and the scavenging potential of this drug has been assessed. It shares structural similarities with pyrrole, although it does not have a lone H-group, which is instead replaced by a methyl group. As with pyrrole in this study, tolmetin was not found to scavenge superoxide radicals, but unlike pyrrole, it was capable of scavenging NO (Fernandes, et al. 2004).

Using this assay, both potentiostatic and galvanostatic PPy coatings demonstrated significant NO scavenging capacity over the blank and 316L SS controls, as shown in Figure 3.12. As with the chemical superoxide scavenging assay, this assay only indicates the relative capacity of the coatings to scavenge NO at the 2.5 h timepoint. Therefore, it does not indicate the total scavenging capacity of the PPy coatings, nor does it suggest any differences in reaction kinetics. However, this data does strongly suggest that the electropolymerized PPy coatings tested do demonstrate strong NO scavenging potential. 316L samples demonstrated no capacity to scavenging NO, and in these experiments, it can also be observed that SNP incubation with 316L samples lead to negative relative NO scavenging, although this was not significant. With both coatings generated by potentiostatic and galvanostatic

electropolymerisation, electropolymerisation conditions and the addition of electrochemical Sa-elution were not found to impact on NO scavenging capacity.

As with the superoxide assays, the positive control demonstrated significantly greater scavenging than all coatings, and similarly is to be expected since this has been optimised for maximal effect. Although this assay is often considered non-competitive in that no other antioxidant is present in the assay buffer, the solid and fixed nature of the strip also means it may be a competitive reaction and so in reality the coatings compete with the spontaneous degradation of NO (Gülçin, 2012).

The antioxidant capacity of polypyrrole, that is not present in the monomer, further suggests that the structural differences of polypyrrole, or the electropolymerisation process, provides a chemical mechanism by which NO scavenging can occur. The uniformity of NO scavenging potential by different PPy coatings contrasts superoxide scavenging and may indicate that the scavenging capacity of coatings is different in response to the two radical species. It also suggests that the loss of superoxide scavenging capacity observed with galvanostatic coating after electrochemical elution is not associated with complete structural degradation since NO scavenging is maintained.

3.4.6. Hydrogen peroxide scavenging capacity of electropolymerised polypyrrole

The hydrogen peroxide scavenging assay used in this study was adapted from a method previously reported by Al-Amiery, et al. (2015) and optimised for hydrogen peroxide and L-ascorbic acid concentrations, and incubation time. 10 mM L-ascorbic acid and 40 mM hydrogen peroxide were selected as the suitable concentrations and 10-minute incubation was shown to be sufficient at detecting differences in scavenging capacity.

The hydrogen peroxide scavenging capacity of the pyrrole monomer and aqueous salicylate dopant was assessed and in contrast to results for superoxide and nitric oxide, both chemicals were capable of scavenging hydrogen peroxide, as demonstrated in Figure 3.13. This however was only found to be significant at high concentrations, with 30 mM pyrrole and 3 and 10 mM salicylate demonstrating hydrogen peroxide reducing activity. The concentration of pyrrole found to be capable of peroxide scavenging is much higher than if crudely estimated in the

coatings (approximately 1 mM). This is also true of the salicylate which as a dopant is estimated from elution data to be incorporated at lower concentrations (<1 mM).

The potential for peroxide scavenging with pyrrole is not surprising, since it has long been known to be oxidised by hydrogen peroxide, but this reaction is highly pH dependent and occurs slowly with oxidation favouring acidic conditions (Bocchi, et al. 1970).

Although the scavenging capacity of sodium salicylate is not reported, salicylic acid has been shown to not reduce hydrogen peroxide (Sroka & Cisowski, 2003). Since the two chemicals are closely related, it would be expected that sodium salicylate does not have peroxide reduction capacity, but the results of this study contradict this assumption. As noted, one drawback of this assay was the high background absorbance at 230 nm, preventing quantification of the highest salicylate concentrations. This may also have led to loss of sensitivity in the assay as concentrations increased.

Despite the scavenging capacity observed in the pyrrole monomer, scavenging activity by potentiostatic polypyrrole coatings was restricted to +1.3 V coatings, with no scavenging by 1.1 V coatings. This can be observed in Figure 3.14. (panel a). Similarly, scavenging capacity of galvanostatic coatings was restricted to 2 mA coatings, although some, albeit not significant, scavenging was observed with 1 mA coatings. This can be observed in Figure 3.14. (panel b). With both potentiostatic and galvanostatic coatings, scavenging capacity was retained after salicylate elution suggesting that salicylate and polymer oxidative state were not determining hydrogen peroxide scavenging.

It is suspected that +1.3 V potentiostatic and 2 mA galvanostatic coatings are likely to be overoxidised. The unique scavenging by these coatings may indicate that this activity is unique to overoxidised PPy coatings. The ability to scavenge hydrogen peroxide in phenolic acids, has been strongly correlated with the number of hydroxyl groups on a compound, this would indicate that hydrogen peroxide reduction favours HAT (Sroka & Cisowski, 2003). The major biological antioxidant responsible for reducing hydrogen peroxide is glutathione. Glutathione promotes hydrogen peroxide decomposition by donating a hydrogen atom and forming a dimer with another oxidised glutathione to stabilise itself. This demonstrates another example of hydrogen peroxide reduction through HAT (Lubos, et al. 2011). In both acidic and basic conditions, overoxidation has been shown to lead to a loss in some N-H group within the

polymer chain (Li & Qian, 1999). This loss would suggest a reduced capacity for HAT which contradicts the observations made with this assay.

3.4.7. Peroxyl radical scavenging capacity of electropolymerised polypyrrole

The peroxyl radical scavenging assay used in this study was based on the ORAC assay outlined by BMG Labtech and was optimised for use with kinetic and endpoint measurements. Trolox standards, AAPH and sodium fluorescein were all used at concentrations reported and 50 minutes was identified as the optimal incubation time for endpoint measurements.

Both pyrrole and sodium salicylate demonstrated peroxyl radical scavenging capacity when assessed using the ORAC assay, as observed in Figure 3.15. In this assay, peroxyl radicals are only scavenged via HAT, suggesting both chemicals can provide an antioxidant benefit through this route. This was not observed with other species, but peroxyl radicals have greater oxidising potential. The pyrrole monomer demonstrated a clear concentration-dependent antioxidant effect, with HAT likely offered by the N-H group although the neighbouring carbon groups are also susceptible to electrophilic attack (Hunjan, et al. 2021). The antioxidant effect of salicylate is less clear, with no clear increase with higher concentrations. The chemistry of salicylate presents multiple functional groups for HAT (Rodríguez-Santiago, et al. 1999). When comparing the equivalent Trolox doses of pyrrole and salicylate, pyrrole achieved higher doses, suggesting it is a more capable scavenger of peroxyl radicals. At 1 mM, which is approximately proportional to PPy coatings, significant scavenging is achieved by pyrrole.

All PPy coatings were found to scavenge peroxyl radicals when assessed with the ORAC assay, as demonstrated in Figure 3.16. The scavenging capacity was comparable for all coatings, at approximately 60% and all coatings exhibited a significant loss of scavenging activity after electrochemical elution. This suggests that scavenging activity is dependent on salicylate, or more likely the electrochemical state of the polypyrrole film.

As previously suggested, overoxidised films would be expected to exhibit lower HAT-associated antioxidant capacities due to a reduced number N-H groups, but this is not observed with 1.3 V potentiostatic and 2 mA galvanostatic coatings, further suggesting that these coatings are either not overoxidised, or overoxidation does not have a significant detrimental

effect on the number of HAT-capable functional groups. The role of electrochemical discharge is however more predictable, as reduction of the polymer coating leads to deprotonation, which is more likely to lead to a significant loss of HAT-capable functional groups (Kim, et al. 2020). HAT-capable functional groups. This is likely responsible for the loss of peroxyl radical scavenging capacity observed here.

3.4.8. Limitations and other considerations

All assays used here are predominantly performed under static conditions. There was some effort made to incorporate some flow into the assay methodology by using a shaking platform for superoxide and nitric oxide assays, but this does not mirror the flow and resultant stresses in the coronary artery. It is important for PPy to be capable of scavenging ROS not only under static conditions, but also in high flow scenarios. This is particularly important, since increased blood flow in the coronary artery has been shown to correlate with increased levels of oxidative stress (Fong, et al. 2010). Therefore, scavenging is likely to be most beneficial in vessels with high flow rates, but it is unclear how PPy scavenging capacity would be affected by flow. It is possible that high flow rates and slow reaction kinetics may result in lower scavenging capacity as high flow rates may not facilitate scavenging reactions by restricting ROS exposure time.

In addition to antioxidant considerations, there are other impacts that flow may have on the use of PPy as a coronary artery stent coating. Firstly, many coatings, particularly those generated potentiostatically at 1.3 V experienced significant delamination from the stainless steel substrate, this is likely to be exaggerated under flow conditions. Furthermore, although the morphology of PPy coatings has been shown to be uniform, the topographical roughness of the coatings hasn't been assessed and it is unclear whether the coatings will be non-thrombogenic, especially in a high flow rate, high shear stress environment (Han, et al. 2022).

Another consideration is that predicting the scavenging activity of polypyrrole based on the antioxidant activity of the monomer is complicated since the pyrrole functional groups are fundamentally changed during the polymerisation reaction. During polymerisation changes in electronegativity to the monomer unit occur which is highly dependent on the dopant, but this is a weak determining factor in antioxidant activity and bond dissociation energy (Mahmood, et al. 2012). The most significant issue in translating these scavenging effects to a biological

environment is that the effect of a fixed antioxidant stent coatings on cellular and mitochondrial oxidative stresses remains unclear.

3.4.9. Biological potential for polypyrrole coatings

The potential of polypyrrole to scavenge superoxide, nitric oxide, hydrogen peroxide and peroxyl presents opportunity for polypyrrole to act as a therapeutic antioxidant in a biological context. In particular, superoxide and nitric oxide present highly relevant species in the physiology of endothelial cells and pathophysiology of atherosclerosis (Li, et al. 2014). Hydrogen peroxide also presents a key species in driving vascular smooth muscle cell dysfunction (Misra, et al. 2008).

Although the opportunity for biological antioxidant activity by polypyrrole is identified by these assays, the *in vivo* and *in vitro* relevance of chemical assays is limited. *In vivo* physiological environments present a mixed ROS system which introduces complexity due to the interactions of different antioxidants and oxidative species. These assays also fail to assess the scavenging activity against some key biological ROS, including hydroxyl and peroxynitrite (Pacher & Szabo, 2006), although the potential impact on peroxynitrite is indirectly assessed since scavenging against superoxide and nitric oxide should proportionally supress peroxynitrite generation.

In vitro and *in vivo* environments present scenarios where coatings compete with endogenous antioxidant systems, and only superoxide and nitric oxide assays used here include competing species. Due to the endpoint measures used in these assays, it also remains unclear what the total capacities of antioxidant activity by polypyrrole under physiological conditions are. One strategy to improve the assays is to optimise positive controls to utilise the most relevant endogenous systems and at relevant concentrations.

Furthermore, along with competition with endogeneous antioxidants and flow rate, blood may present other interferents that inhibit scavenging activity. Protein attachment is another factor that is not considered by these *in vitro* assays. PPy is known to allow good protein adsorption (Fonner, et al. 2008) and this interaction is critical to encourage endothelial attachment and the desired pro-healing response. The attachment of proteins may however limit PPy's scavenging capacity by acting as a blocking interface between the coating surface and blood or attached cells. Due to the novelty of PPy use as a stent coating and antioxidant, this hasn't

been considered in the literature, but the inference of non-specific protein binding is a common issue experienced when developing implantable biosensors (Contreras-Naranjo & Aguilar, 2019).

Although this study demonstrates the chemical capacity for PPy coatings to scavenge specific biologically relevant ROS, the translation of this ability, along with the effect on nearby endothelial and smooth muscle cells is unclear. With a simple coating, the scavenging capacity of the PPy will be offered to any nearby cells, especially those that are directly adhered. Depending on the specific scavenging capacity of PPy coatings, the effect on EC and SMCs may differ. This is advantageous for a pro-healing design if the scavenging profile restores a vascular environment which promotes endothelial healing and supresses smooth muscle cells proliferation.

It may not be possible to achieve such a balance with one type of PPy coating, and this study has demonstrated that the electropolymerisation method and dopant state of the polymer provides opportunities to tailor the PPy properties. If the ideal scavenging profile to promote endothelial healing, such as one that readily scavenges superoxide but possesses minimal nitric oxide scavenging ability, does not align with the necessary profile to suppress SMC proliferation, such as one that readily scavenges hydrogen peroxide, electropolymerisation may offer a convenient mechanism to utilise a two-stage fabrication process where the intramural and intraluminal surfaces are independently coated.

Due to the potential need for cells to be attached to the coating surface, the efficacy of antioxidant scavenging at suppressing smooth muscle cell proliferation, which will ideally not migrate towards the luminal space may be limited. In this case, a two-stage fabrication approach may also allow further tuneability to drug elution properties if required.

3.5. Conclusions

In conclusion, the broad antioxidant activity of PPy coatings has been demonstrated in this study through the use of DPPH assays, which supports the established findings in the literature. This antioxidant activity of these coatings was shown to be long lasting after repeated challenge that withstands incubation in PBS after 7 days. This scavenging capacity is also retained after electrochemical discharge of salicylate dopant in all PPy coatings studied.

Assays were used to assess the scavenging capacity of samples against superoxide, nitric oxide, hydrogen peroxide and peroxyl radicals. Antioxidant activity was observed for the pyrrole monomer and salicylate dopant against hydrogen peroxide and peroxyl radicals.

For potentiostatic coatings generated at 1.1 V, scavenging activity was observed against superoxide, nitric oxide and peroxyl, but only before electrochemical Sa-discharge. For potentiostatic coatings generated at 1.3 V, scavenging capacity was observed against all species but only for peroxyl before electrochemical Sa-discharge. For galvanostatic coatings generated at 1 mA, scavenging capacity was only observed against nitric oxide. Finally, for galvanostatic coatings generated at 2 mA, scavenging capacity was observed against all species but only against superoxide and peroxyl before electrochemical Sa-discharge.

Overall, this demonstrates the strong potential for PPy to act as a novel therapeutic antioxidant. The longevity of DPPH scavenging along with the ability to significantly scavenge biologically relevant ROS using assays with relatively short incubation times (1h) demonstrate the potential ability for PPy coatings to rapidly respond to changing physiological environments *in vivo*. Further experiments must be undertaken to see how this translates to a biological benefit in adherent vascular cells and this is explored in the following chapters.

4. *In vitro* model development

Chapter 4 explores the third aim of this study – developing an initial biological model for the assessment of polypyrrole (PPy) coatings generated in Chapters 2 and 3, and identifying appropriate assays, as outlined in 1.8. This chapter will begin by outlining the background of this study, and the key objectives of this chapter will then be clearly presented. The experimental methodology and materials used will be described. The results of this work will be presented in line with the objectives of this study and key findings will be highlighted. Finally, this chapter will conclude with an in-depth discussion highlighting the significance of these results and considering its relevance with previous findings.

4.1. Background and Aims

Traumatic injury during percutaneous coronary intervention (PCI) causes the denudation of endothelial cells when placing stents and failure for the vessel to quickly heal and restore the endothelium increases the likelihood of complications, particularly in-stent restenosis (ISR) (Nakazawa, et al. 2008). Accordingly, re-endothelialisation remains a key strategy for minimising risks and improving stent outcomes.

Oxidative stress is increasingly implicated in the pathology of ISR through its effects on endothelial cells as pathological superoxide signalling may prevent proliferation, migration and induce apoptosis (Juni, et al. 2013). Furthermore, current DES induce significantly higher levels of reactive oxygen species (ROS) than BMS and modulating the generation of these species, particularly superoxide has been shown to improve re-endothelialisation (He, et al. 2019). Cytokines, such as IL-1β and TNFα, are known to have strong pro-inflammatory effects and the treatment of endothelial cells with these agents may provide an experimental system for modelling diseases associated with inflammatory and oxidative stress (Tousoulis, et al. 2016). In this chapter, the aim of developing a relevant biological model was addressed using human umbilical vein endothelial cells (HUVECs) with the intention of validating and improving this model in more physiologically relevant cell types, e.g. human coronary artery endothelial and smooth muscle cells.

Increased expression and activation of Ca^{2+}/calmodulin dependent protein kinase II (CaMKII) has a known pathological role in cardiac diseases that may reflect a similar potential role in the pathology of the vascular system. Targeting the expression and/or activity of CaMKII may offer a potential route for modulating oxidative stress and improving the function of

endothelial cells after stenting. It is however unclear whether the protein is highly expressed in endothelial cells, particularly HUVECs, and how, or whether, stimulation with pro-inflammatory cytokines affects CaMKII activation, via increased oxidative stress.

The aim of this investigation can be separated and defined by five objectives that are outlined below:

1. Assess the effects of TNFα and IL-1β stimulation on HUVEC viability and pro-inflammatory signalling.
2. Assess the effects of TNFα, IL-1β and hydrogen peroxide stimulation on ROS generation in HUVECs.
3. Establish the expression of CaMKII in HUVECs and evaluate the effects of stimulation on phosphorylation and oxidation induced CaMKII activation.
4. Determine the suitability of PPy-coated strips for use in an in-vitro biological model.
5. Consider and quantify the effects of PPy and 316L surfaces on basic HUVEC attachment and proliferation.

4.2. Materials and Methods

4.2.1. Materials and Equipment

Material/Equipment	Supplier
Stainless Steel (316L wires and plates)	Goodfellow Cambridge Ltd, UK
Ag/AgCl Reference Electrode (KR5)	ThermoFisher Scientific, UK
Potentiostat/Galvanostat	Metrohm Autolab, UK
Nikon Eclipse E600 Optical Microscopy	Nikon, Japan
POLARstar Omega Plate reader	BMG LABTECH, UK
FlexStation3 Plate reader	Molecular Devices, UK
Plate reader	BioRad, UK
Human Umbilical Vein Endothelial Cells (HUVEC)	Lonza, Switzerland
Invitrogen Western Blot System	ThermoFisher Scientific, UK
Nitrocellulose	GE Healthcare, US
Autoradiography film	Santa Cruz Biotechnology, US
Calibrated Densitometer	BioRad, UK

4.2.2. Chemicals

Chemical	Supplier	Catalogue Number
Pyrrole (98% solution)	Sigma Aldrich, UK	131709
Sodium Salicylate	Sigma Aldrich, UK	S3007
Phosphate Buffered Saline (PBS) tablets	Oxoid, UK	BR0014G
Absolute Ethanol	VWR, UK	20821.296
Endothelial Cell Growth Medium-2 (EGM-2) BulletKit (HUVEC)	Lonza, Switzerland	CC-3162
DetachKit	Promocell, Germany	C-41200
Trypsin/EDTA solution	ThermoFisher, UK	T4049
Interleukin-1beta (IL-1β)	Insight Biotechnology, UK	10-2012-C
Tissue necrotic factor alpha (TNFα)	Insight Biotechnology, UK	10-1034-C
Acridine Orange powder	FisherScientific, UK	1132794
2',7' –dichlorofluorescin diacetate (DCFDA) assay kit	Abcam, UK	Ab113851
3-(4,5-Dimethylthiazol-2-yl)-2,5-Diphenyltetrazolium Bromide (MTT) powder	Sigma Aldrich, UK	M5655
Dimethyl sulfoxide (DMSO) liquid	Sigma Aldrich, UK	D8418
Novex 10% Bis-Tris polyacrylamide gels	FisherScientific, UK	10184862
3-(N-Morpholino)propanesulfonic acid (MOPS) powder	Sigma Aldrich, UK	M1254
Trizma (Tris-base) crystalline powder	Sigma Aldrich, UK	93352

Ethylenediaminetetraacetic acid (EDTA) powder	Sigma Aldrich, UK	9884
Sodium dodecyl sulphate (SDS) powder	Sigma Aldrich, UK	75746
Bovine serum albumin (BSA) powder	FisherScientific, UK	11403164
Tween-20 liquid	Sigma Aldrich, UK	P1379
Luminol powder	Sigma Aldrich, UK	123072
p-Coumeric acid powder	Sigma Aldrich, UK	C9008
Hydrogen Peroxide (30% solution)	Santa Cruz Biotechnology	sc-203336
Antibodies	Refer to: 4.2.8.	

4.2.3. Cell Culture

Cells were purchased cryopreserved in cryogenic vials (500,000 cells) and stored in liquid nitrogen until use, as recommended. All experiments were carried out in a laminar flow hood under aseptic conditions using cells between passages 3 and 8. Cells were cultured in T75 flasks to 70-90% confluence prior splitting and plating.

Human Umbilical Vein Endothelial Cell Culture

HUVECs were cultured at 37ºC in a humidified atmosphere (5% CO_2) as recommended by Lonza using EGM-2 containing 2% FBS and all included supplements (per 500 ml): hydrocortisone (0.2 ml), hFGF-B (2 ml), VEGF (0.5 ml), R3-ICF-1 (0.5 ml), ascorbic acid (0.5 ml), hEGF (0.5 ml), GA-1000 (0.5 ml), and heparin (0.5 ml).

At 90% confluence, cells were dissociated from flasks using trypsin/EDTA and pelleted by centrifugation at 250 g for 4 minutes. Cells were then counted and plated at the following concentrations: T75 flask (1/10 dilution), T25 flask (1/6 dilution), 6-well plates (1 x 10^5 cells/ml), 12-well plate (5 x 10^4 cells/ml) and 96-well plate (5 x 10^4 cells/ml). Cells were cultured for a further 2 days at 37ºC/5% CO2 before carrying out assays.

4.2.4. Stimulations

Stock solutions, prepared in PBS, of IL-1β (0.3 and 1 μg/ml), TNFα (0.3 and 1 μg/ml) and hydrogen peroxide (3 and 10 mM) were diluted (1:100) directly into cell culture plate wells to obtain final concentrations: IL-1β (3 and 10 ng/ml), TNFα (3 and 10 ng/ml) and hydrogen peroxide (30 and 100 μM). Cells were stimulated for up to 48 h in 12-well plates

without any prior serum starving, although all stimulations were carried out after at least 2-days incubation without replacing media to minimise any serum-associated signalling effects.

4.2.5. Polypyrrole Coating Cell Culture

For PPy sample preparation see 2.2.3. and 2.2.4.

Conducting polymer coatings and uncoated samples (30 x 5 or 8 x 5 mm strips) were sterilised for 1 h in 70 % ethanol, then transferred with either 6-well (30 x 5) or 48-well (8 x 5) plates and allowed to air-dry for 1 h. Cells were seeded directly onto samples at the specific concentrations outlined previously (2.6.1-3.). Samples were incubated for up to 48 h, changing media every 24 h, before analysis.

4.2.6. Microscopy

After 24 and 48 hours, samples were transferred to new cell culture plates, and washed once with PBS. Adherent cells were fixed by adding ice-cold methanol and allowing fixation for 15 minutes at -20ºC. This was followed by further PBS washes, repeated 3 times. Cells were stained with acridine orange (20 µM in PBS) for 30 minutes at room temperature, and washed again with PBS, repeated 3 times. Stained cells were stored in PBS, with plates wrapped in foil to protect from light, for up to one week at 4 ºC before imaging.

Acridine orange is a fluorescent dye which binds to nucleic acid. Acridine orange binding with nucleic acid is non-selective but gives differential fluorescence after binding with DNA via intercalation, and with RNA by electrochemical attraction. Upon intercalating with DNA, acridine orange fluoresces green, whereas upon interacting with RNA, acridine orange fluoresces red. Acridine orange has also been shown to be sensitive to acidic environments and therefore has become a prominent tool for tracking cellular vesicles (Pierzynska-Mach, et al. 2014). In this study, the use of acridine orange is limited to imaging adherent cells, and providing morphological visualisation.

Fluorescence microscopy was carried out to image stained samples using a Nikon Eclipse E600 upright microscope and CoolLED light source. A generic FITC filter ($\lambda_{excitation}$ =457.5-492.5 nm, $\lambda_{emission}$ =508.5-551.5 nm) was chosen as the most suitable for imaging with acridine orange staining. This range matches suitably with the DNA-acridine orange fluorescence

peaks ($\lambda_{excitation}$ =500 nm, $\lambda_{emission}$ =526 nm), but does not correspond well with the RNA-acridine orange binding fluorescence ($\lambda_{excitation}$ =460 nm, $\lambda_{emission}$ =650 nm).

All post-imaging analysis was carried out using ImageJ (FIJI).

4.2.7. Cell Viability and Proliferation Assay

MTT (3-(4,5-Dimethylthiazol-2-yl)-2,5-Diphenyltetrazolium Bromide) assays were carried out to assess cell viability after stimulations and, attachment and proliferation of cells on coated samples.

Stimulants were added to cells in clear 96-well plates and incubated for up to 6 hours at 37ºC/5% CO_2, after which the media was replaced with 100 µl of media containing MTT reagent (0.5 mg/ml). Cells were incubated with MTT reagent for 2 hours, the MTT reagent was then carefully aspirated off and the remaining formazan product resuspended in 100 µl dimethyl sulphoxide (DMSO). Plates were incubated for a further 15 minutes to ensure proper formazan mixing and endpoint absorbance of the DMSO-formazan solution was read at 570 nm on a microplate reader (FlexStation3).

This protocol was modified for use for with stainless steel strips. After culture, strips were moved to new cell culture plates and washed once with PBS to remove any non-adherent cells. Media containing 0.5 mg/ml MTT was added to each well (6-well: 2 ml, 48-well: 200 µl) and samples were incubated for 2 hours. The media was then carefully removed and replaced with DMSO (6-well: 500 µl, 48-well: 200 µl). Plates were then mixed on a shaking platform (60 rpm) for 15 minutes to ensure formazan was properly mixed and removed from the coated surfaces. DMSO-formazan solutions were transferred to clear 96-well plates and endpoint absorbance of the solution was read at 570 nm on a microplate reader (FlexStation3).

Absorbance readings were used to calculate either: a percentage of the absorbance vs. the control wells (for use as a comparative measure of viability), or total cell number against a standard curve of known number of viable cells.

4.2.8. Bradford Protein Assays

Protein concentrations of cell lysates were calculated using a standard Bradford protein assay protocol from Sigma-Aldrich. 10 µl of lysate samples or buffer blanks were added to a clear 96-well plate, along with 10 µl of BSA standards to give a standard curve (0, 0.1, 0.25, 0.5, 0.75 and 1 mg/ml). 200 µl of Bradford reagent was added to each well. Bradford reagent contains Coomassie Blue G that reacts with protein to form a complex with high absorbance at 595 nm. This complex is stable for up to 60 minutes, but absorbance was measured between 5 and 10 minutes of adding Bradford reagent to ensure maximum stability of the complex. 595 nm absorbance values were measured for all samples using a microplate reader (BioRad) and buffer blanks subtracted from cell lysates to eliminate any detergent effects. Cell lysate concentrations were calculated by extrapolating the values against the linear region of the BSA standard curve.

Tissue homogenates were diluted (1:25, 1:50 and 1:75) to ensure the protein concentration in the assay fell within the linear range of the BSA standard curve. Final concentration extrapolated and homogenates diluted to 1 mg/ml for use as positive controls.

4.2.9. Immunoblotting

Cell lysates were prepared from confluent cell culture plates or flasks after stimulation. Confluent wells/flasks were washed once with PBS after stimulation and samples loaded in NuPAGE LDS sample buffer (+75 mM DTT, where proteins were separated under reducing conditions). The use of DTT is shown in table 1. An approximate concentration of 1 x 10^6 cells/ml was obtained by adding 150 µl buffer to 12-well plates and 300 µl to T25 flasks. Cells were scraped and homogenised with a needle (23 gauge) before boiling at 100ºC for 5 minutes. Protein expression was assessed by quantitative immunoblotting.

Separation of proteins was achieved by SDS-PAGE after loading samples and rat whole heart homogenates (5 µl, 1 mg/ml, positive control) into Novex 10% Bis-Tris polyacrylamide gels in MOPS running buffer (50 mM MOPS, 50 mM Tris-base, 0.1% SDS, 1 mM EDTA, pH 7.7). After separation, the proteins were transferred for 1 h in transfer buffer (25 mM Tris-base, 0.2 M glycine and 20% methanol) to nitrocellulose membranes and blocked with 5% BSA in Tris-buffered saline and Tween-20 (20 mM Tris-base, 150 mM NaCl, 0.1% Tween-20, pH 7.7) buffer (TBST).

Membranes were incubated in primary antibodies overnight at 4°C in 0.5% BSA in TBST at the concentrations outlined in Table 4.1.

Table 4.1. Primary antibodies, suppliers, secondary antibody species targets and concentrations for immunoblotting antibodies used in this study.

Antibody	Supplier and Catalogue Number	Species	Concentration	Number of Washes	Running Condition
CaMKIIδ	Custom Antibody (Eurogentec)	Rabbit	1:5000	3	Reducing
Oxidised-CaMKII	GeneTex #GTX36254	Rabbit	1:5000	5	Non-reducing
Phospho-CaMKII (HUVECs)	Thermo Fisher #MA1-047	Rabbit	1:1000	3	Non-reducing
Phospho-p65	Cell Signalling #3033	Rabbit	1:1000	3	Reducing
GAPDH	Abcam #ab8245	Mouse	1:100,000-300,000	3	Reducing and non-reducing

Primary incubation was followed by 3, 5-minute TBST washes, before secondary incubation for 2 h with either anti-mouse (1:5000, Sigma-Aldrich, #), or anti-mouse (1:7500, Sigma Aldrich, #) HRP-conjugated IgG, and a further set of 3 washes. Signals were developed using enhanced-chemiluminescence solution (0.1M Tris base, 2.5 mM luminol, 1.25 mM coumaric acid, 6 mM hydrogen peroxide) and signals visualised on radiographic film (UltraCruz, US). After development, signals of the scanned radiographs were quantified by densitometry using a GS-800 densitometer and Quantity One Image software (BioRad).

Aged whole rat homogenate was used as a positive control for all antibodies and was confirmed to display very high expression and activation of CaMKII (expression by both oxidation and phosphorylation) and p65 for each test. For simplication of the experimental results, these control results are not included alongside the data, but representative blots are included in Supplementary Figure S4.1.

4.2.10. Intracellular Reactive Oxygen Species Assay (DCFDA)

Intracellular oxidative stress was assessed in HUVECs (confluent black 96-well plate) with a (2',7'–dichlorofluorescin diacetate) DCFDA assay kit using the supplied protocol. Cells were washed with the supplied assay buffer and 25 μM DCFDA added to each well. Cells were incubated at 37ºC/5% CO_2 with the DCFDA for 45 minutes, during which the probe is internalised and cleaved by cellular esterases to form DCF. The cells were then washed again before stimulating as previously described in 2.6.4. Cells were stimulated for up to 6 h in foil; further incubation and longer time courses are not recommended with this kit due to the stability of the DCF probe and reduced specificity due to redox cycling reactions. The oxidised-DCF can be measured by fluorescence (λ_{ex} = 485 nm, λ_{em} = 535 nm) and this was measured after 1, 3 and 6 h (POLARstar, Omega) in separate wells to avoid photo bleaching. 55 mM Tert-Butyl Hydrogen Peroxide (TBHP) was used as a positive control and intracellular oxidative stress was expressed as a fold-change vs. unstimulated control cells.

4.2.11. Statistical Analysis

Graphs were created using GraphPad Prism 9 and regression and correlation analysis was performed using the built in tools. Specific curve fitting used is described for the data in Section 4.3. Statistical analysis was performed using Minitab (version 19.0). Unless otherwise stated, the statistical significance of data sets was determined using one-way analysis of variants (ANOVA) with post-hoc Dunnett's tests. The specific control groups used for these tests and details of other specific analysis are outlined with the relevant data in Section 4.3.

4.3. Results

4.3.1. Culture of HUVECs and effect of stimulation on cell viability

Before commencing experiments, cells were imaged to evaluate the morphology of the cells and the uniformity of the cell population. HUVECs obtained from Lonza were used as a relevant primary endothelial cell type. After the initial thaw, HUVECs were imaged using brightfield microscopy. Figure 4.1. (panel a and b) shows the images obtained for HUVECs (passage 2) at 40x and 100x magnification. Cells are visible with a slight elongated/spindle-shaped morphology and appear well spread across the tissue culture flask surface. Overall, the size and morphologies of these cells suggest that this culture of cells in phenotypically homogeneous. This gives confidence that the cells are representative of a macrovascular endothelial cell monoculture.

A MTT assay was used to assess the effects of stimulation on the viability of HUVECs. IL-1β, TNFα and hydrogen peroxide, as a positive control, were used and applied for up to 6 h at two concentrations for IL-1β and TNFα (3 and 10 ng/ml), and 100 μM for hydrogen peroxide. The results of this assay are shown in Figure 4.1. (panel c).

Exposure to IL-1β or TNFα led to no significant reduction in cell viability at 6 h (0 h: 100.00±3.02, vs. 3 ng/ml IL-1β: 96.47±2.99, 10 ng/ml IL-1β: 99.38±3.46, 3 ng/ml TNFα: 103.30±2.76, 10 ng/ml TNFα: 95.84±2.32; %mean(absorbance vs. control cells) ± S.E.M, $p>0.05$, n=3). Stimulation with hydrogen peroxide led to a clear time-dependant and significant loss in viability at every stimulation time (0 h: 100.00±3.02, vs. 1 h: 38.45±0.88, 3 h: 22.99±1.10 and 6 h: 8.84±1.23; %mean(absorbance vs. control cells)±S.E.M, $p<0.001$, n=3).

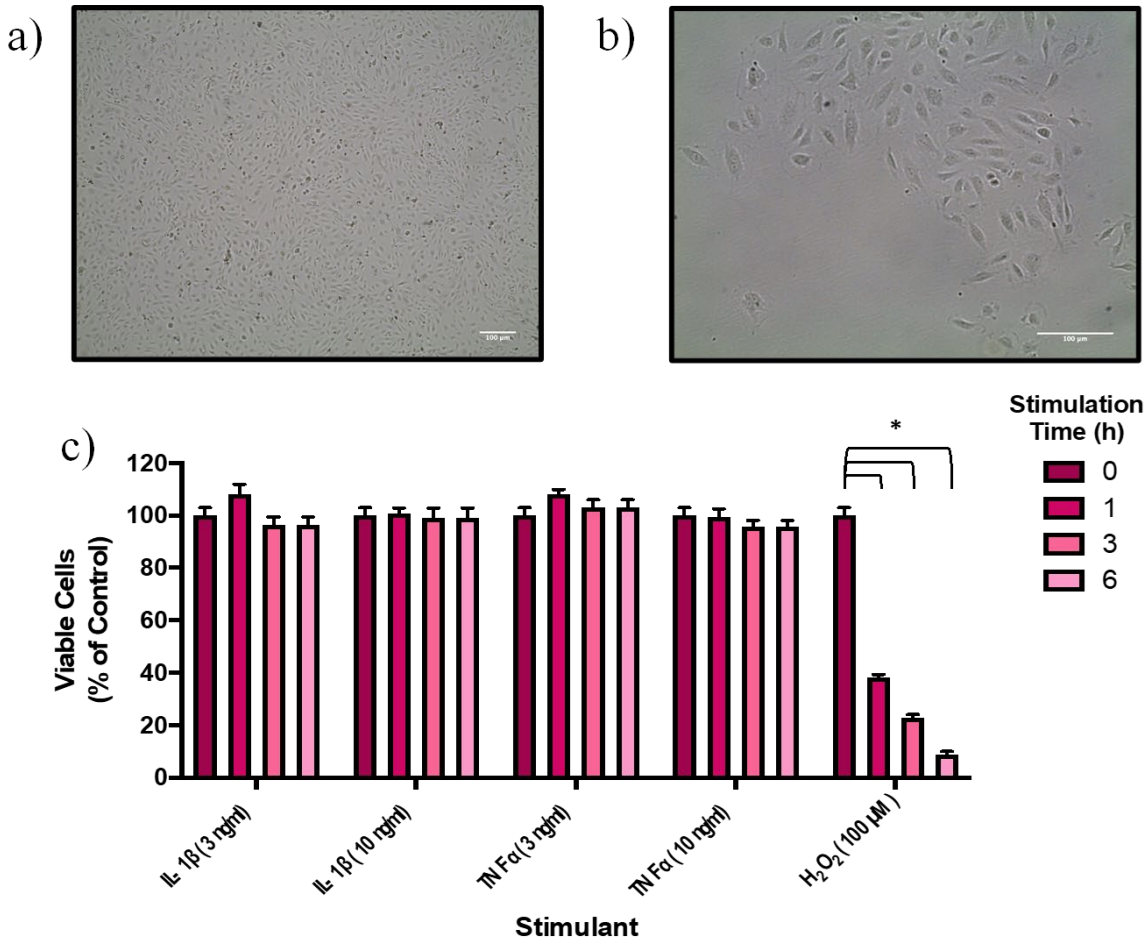

Figure 4.1. a and b) HUVECs (P2) imaged at 40x (a) and 100x (b) magnification. These images shown HUVECs at a high confluence (approximately 70%) and the cells shown a uniform morphology across the population. Images are representative of three independent repeats. c) MTT assay results showing the effects of IL-1β, TNFα and hydrogen peroxide stimulation on the viability of HUVECs. Each bar represents mean number of cells, as a percentage of the average control, error bars represent ±standard error of the mean. Only hydrogen peroxide stimulation induced significant loss in cell viability and this was observed at each time points. * $p<0.001$, n=3.

4.3.2. Effects of stimulation on pro-inflammatory signalling in HUVECs

The stimulatory effect of IL-1β and TNFα on pro-inflammatory signalling in HUVECs was assessed by measuring the activation of p65 using a specific antibody against phosphorylated p65 (phospho-p65). p65 is a subunit of the NF-κB complex and its activation, via phosphorylation, upregulates inflammatory cellular responses (Christian, et al. 2016). HUVECs were stimulated for up to 6 h with 10 ng/ml IL-1β and TNFα and the results of these experiments are shown in Figure 4.2.

Both stimulants were found to be capable of inducing pro-inflammatory signalling and this is presented as a fold-change vs. the unstimulated control (0 h). The fold-change stimulatory effects compared using a Dunnett's post-hoc test, where 0 h was set as the comparison control. With IL-1β, a gradual increase in phospho-p65 expression was observed until expression peaked at 1 h. Stimulation for 30 minutes and 1 h both resulted in a significant increase in phospho-p65 expression when compared against unstimulated HUVECs (0 h: 1.00 vs. 30 min: 5.74±1.01 and 1 h: 7.80±1.41; mean(fold-change)±S.E.M, $p<0.01$, $n=4$). After 1 h stimulation, phospho-p65 expression reduced to levels that remained elevated, but not significantly greater than the unstimulated control (0 h vs. 3 h: 4.09±1.04 and 6 h: 4.38±0.99; mean(fold-change)±S.E.M, $p>0.05$, $n=4$).

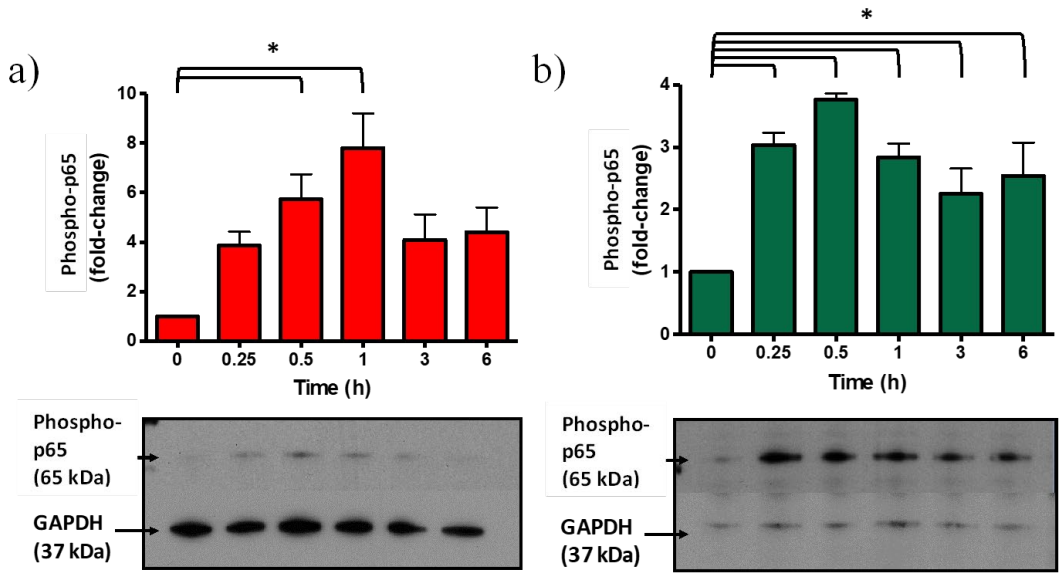

Figure 4.2. Effect on pro-inflammatory p65 signalling, as measured by phospho-p65 expression, of stimulation with: a) IL-1β, showing a significant increase in phospho-p65 expression after 30 minutes and 1 h, and b) TNFα, showing a significant increase in phospho-p65 expression at all time points. Bars represent mean fold-change, compared against unstimulated control HUVECs (0 h), error bars represent ±standard error of the mean. * $p<0.05$, n=4.

Despite seeding tissue culture plates with equal starting cell populations, and approximating confluence at approximately 70-80% at the time of stimulation, one issue with this data is the high variability in GAPDH loading control signal. This reduces the confidence of analysis when quantifying the outputs and limits comparison between the two stimulants.

This issue appears for all experiments utilising immunoblots, but fortunately appears to be less severe between lysates loaded on the same gel allowing the effects of different stimulation times to be assessed. Due to the saturation in the loading control signals used for normalisation control, the response is not shown to be linear, increasing variability. This is however worst-case since it decreases the statistical power and therefore a significant difference can still be established, but the validity of the result should be treated with caution. It is unclear what the cause of this variation is, but could result from inconsistent membrane washing, poor lysate preparation, improper buffer, sample or antibody storage, or irregular exposure time. The use of fluorescence secondary antibodies and LI-COR detection could mitigate some of these issues by providing a truer quantitative western blot protocol (Eaton, et al. 2014).

Upon stimulation with TNFα, a faster stimulatory effect was observed than with IL-1β. This was observed by significant increases in phospho-p65 expression at 15 minutes and peak stimulation at 30 minutes when compared against unstimulated control (0 h: 1.00, vs. 15 min: 3.04±0.19 and 30 min: 3.76±0.10; mean(fold-change)±S.E.M, $p<0.01$, $n=4$). Despite showing a lower magnitude of activation in fold-change terms, activation of p65 is shown to be faster and sustained up to 6 h with TNFα. After peak stimulation at 30 minutes, phospho-p65 expression falls but remains at significantly elevated levels when compared against the control (0 h, vs. 1 h: 2.84±0.22, 3 h: 2.25±0.40 and 6 h: 2.54±0.54; mean(fold-change)±S.E.M, $p<0.05$, $n=4$).

4.3.3. Effects of stimulation on ROS generation in HUVECs

After determining the pro-inflammatory effects of IL-1β and TNFα, it was necessary to determine whether this pro-inflammatory effect occurs in isolation or whether these stimulants were capable of also generating oxidative stress. For this preliminary work, DCFDA was considered a suitable assay for its simplicity and because it should give a clear indication of intracellular oxidative signalling.

The DCFDA assay was optimised using hydrogen peroxide at concentrations between 10 and 300 μM. The intracellular ROS present in HUVECs after 6 h stimulation with hydrogen peroxide is shown in Supplementary Figure S4.2. This data was analysed statistically using with a post-hoc Dunnett's test, with the unstimulated (0 μM) control cells used as the comparison control mean and there was a significant concentration-dependant increase in ROS generation after peroxide stimulation. This supports the use of DCFDA as it is shown to be capable of detecting increases in ROS generation in HUVECs.

After optimising the DCFDA assay with HUVECs stimulated with hydrogen peroxide for 6 hours, intracellular ROS generation in HUVECs stimulated with IL-1β and TNFα was assessed. ROS generation in response to these stimulants was assessed at 3 intervals (1, 3 and 6 h) and at 2 concentrations (3 and 10 ng/ml) to give more insight into the stimulatory effects of these inflammatory cytokines. For each stimulant, a two-way ANOVA with Tukey's post-hoc test was performed. This was set to compare differences between the stimulant concentrations at each time interval and differences between the same concentrations across the time course. The intracellular ROS generation in HUVECs in response to IL-1β and TNFα stimulation is shown in Figure 4.3.

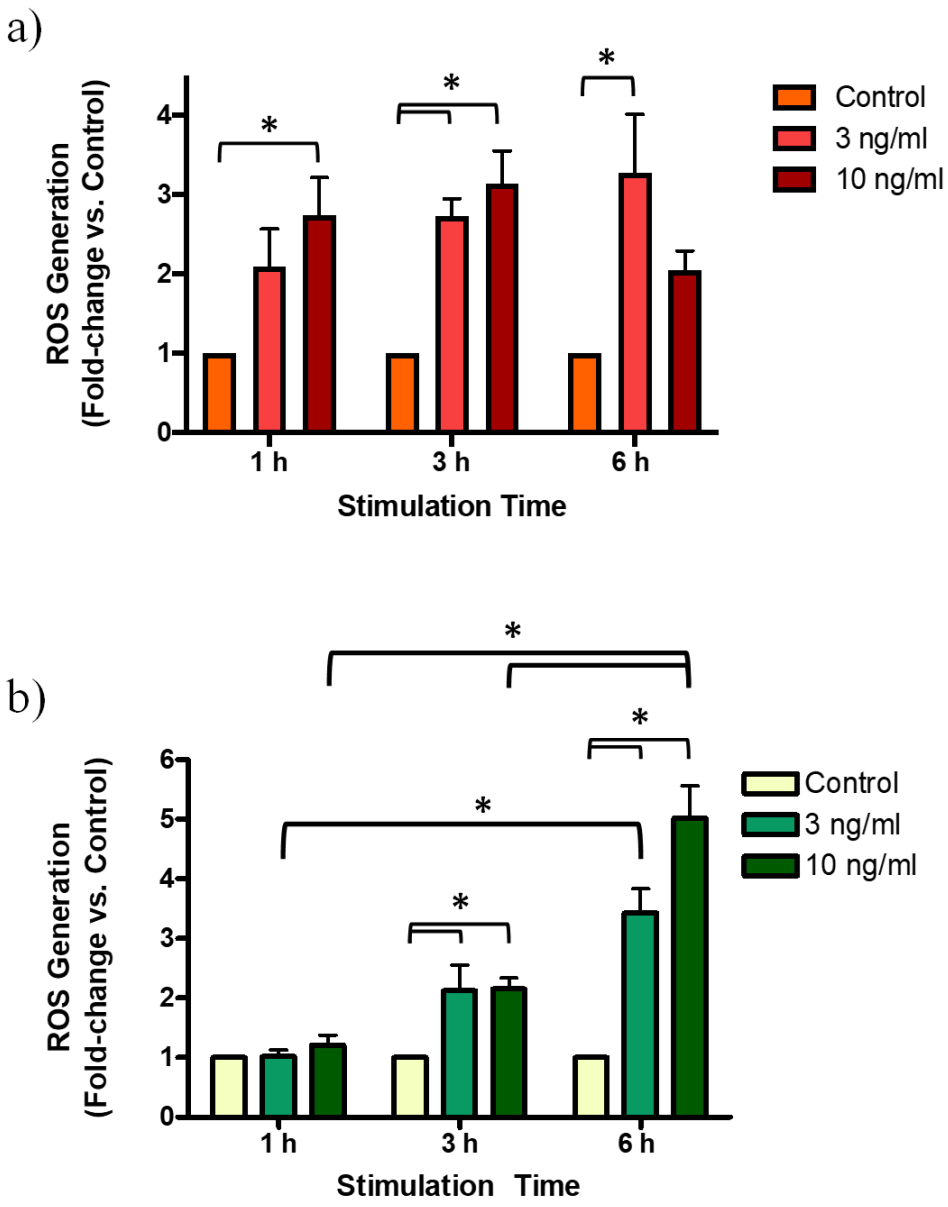

Figure 4.3. ROS generation in HUVECs stimulated for up to 6 h with IL-1β (a) and TNFα (b). When stimulating with IL-1β, 3 ng/ml stimulation was found to induce significant activation at 3 and 6 h, whereas 10 ng/ml stimulation was significant after 1 and 6 h. No statistically significant differences were observed between the time points. Both 3 and 10 ng/ml TNFα stimulation was found to induce significant ROS generation after 3 and 6 h, but neither were capable of stimulating ROS generation after 1 h. Statistically significant differences were observed between time points, with 10 ng/ml generating significantly increased effects at 6 h vs. 1 and 3 h, and 3 ng/ml generating significantly increased effects at 6 h vs. 1 h. Bars represent mean fold-change, compared against unstimulated control HUVECs, error bars represent ±standard error of the mean. * $p<0.05$, n=3.

Stimulation with 3 ng/ml IL-1β was found to be sufficient for significant stimulation of ROS generation at 3 h and 6 h (Control: 1.00±0.00, vs. 3 h: 2.73±0.22 and 6 h: 3.27±0.74; mean(fold-change) ± S.E.M, $p<0.01$, n=3). In contrast, 10 ng/ml was found to be capable of stimulating significant ROS generation at shorter intervals when comparing each stimulation time with the control HUVECs (Control vs. 1 h: 2.74±0.47 and 3 h: 3.14±0.4; mean(fold-change) ± S.E.M, $p<0.05$, n=3). From mean data, it appears that ROS generation increases over 6 h with 3 ng/ml IL-1β stimulation, but no significant difference was observed between the ROS generation at 1, 3 and 6 h time points ($p>0.05$). A decrease in ROS generation at 6 h is observed when stimulating HUVECs with IL-1β at 10 ng/ml, but overall, there was also no significant difference when assessing in ROS generation in HUVECs stimulated with 10 ng/ml IL-1β for 1, 3 or 6 h ($p>0.05$).

Compared with IL-1β stimulation, TNFα stimulation resulted in a clearer time and concentration dependent increase in ROS generation. Significant stimulation was only observed when using 3 ng/ml at 3 h and 6 h (3 h: 2.12±0.43, 6 h: 3.43±0.41, vs. Control: 1.00±0.00; mean(fold-change)±S.E.M, $p<0.01$, n=3), and similarly, 10 ng/ml TNFα stimulation induced significant ROS generation at 3 h (2.15±0.19, vs. Control; mean(fold-change)±S.E.M, $p<0.01$, n=3) and 6 h (5.12±0.54, vs. Control; mean(fold-change)±S.E.M, $p<0.01$, n=3). When comparing the effects of stimulation time, significant increases in ROS generation were observed with 3 ng/ml stimulation from 1 h to 6 h (1 h: 1.02±0.11, vs. 6 h: 3.42±0.41; mean(fold-change)±S.E.M, $p<0.01$, n=3). Significant increases were also observed with 10 ng/ml at 6 h vs. 1 h (1 h: 1.21±0.17, vs. 6 h: 5.12±0.54; mean(fold-change)±S.E.M, $p<0.01$, n=3) and 3 h (3 h: 2.15±0.19, vs. 6 h: 5.12±0.54; mean(fold-change)±S.E.M, $p<0.05$, n=3).

Overall, this data suggests IL-1β and TNFα are both capable of stimulating intracellular ROS generation and this occurs between after 1, 3 and 6 h stimulation for IL-1β and after 3 and 6 h for TNFα.

4.3.4. CaMKII expression in HUVECs and activation in response to cytokine stimulation

As previously noted, CaMKIIδ is a protein kinase of specific interest in this study as a novel target of oxidative stress in endothelial cells. Expression of CaMKIIδ was assessed in HUVECs using immunoblotting with a specific antibody raised against the C-terminus of the CaMKII-delta isoform and compared against CaMKIIδ expression in whole rat heart homogenate (WH), which has previously been shown to highly express the protein (McCluskey, et al. 2019).

Figure 4.4. shows an immunoblot, with the relevant area (50 – 60 kDa) for CaMKIIδ shown at the top of the figure and the relevant area (30 – 40 kDa) for GAPDH shown below. HUVEC lysate samples were loaded into the gel at 5, 10 and 15 µl, with normalisation of the protein concentration achieved by using a known concentration of cells (10^6 cells/ml). WH samples were normalised using a Bradford protein assay to achieve 1 mg/ml final protein concentration.

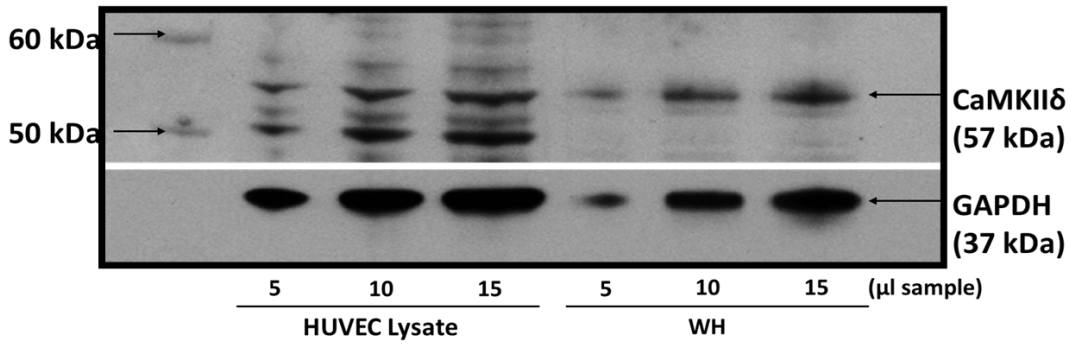

Figure 4.4. Immunoblot showing CaMKIIδ expression in HUVEC lysates (10^6 cells/ml) and whole rat heart homogenate (1 mg/ml). Bands for CaMKIIδ (57 kDa) are shown at the top of this figure, above bands for GAPDH (37 kDa), the loading control. This immunoblot shows that CaMKIIδ is expressed in the HUVECs used in this study.

For both HUVEC and WH samples, banding is visible between the 50 and 60 kDa marker bands that is representative of CaMKIIδ expression, suggesting that CaMKIIδ is high in HUVECs. GAPDH signals show that the protein loads are higher for the HUVEC lysates than WH, likely due to the different methods for normalising protein concentration. Based on the CaMKIIδ and GAPDH banding for the HUVEC lysate samples, it was decided that loading

10 µl of sample at this approximate cell concentration would be sufficient and appropriate for assessing CaMKII expression and activation via immunoblotting.

To assess the activation of CaMKII in HUVECs stimulated with IL-1β and TNFα (10 ng/ml), immunoblotting was used with specific antibodies against phosphorylated and oxidised forms of CaMKII. These blots were quantified using densitometry and analysed using a post-hoc Dunnett's test, with 0 h unstimulated control cells used as the statistical control. This is shown in Figures 4.5 and 4.6.

Only stimulation of HUVECs with IL-1β resulted in significant activation of CaMKII, as measured by an increase in oxidised-CaMKII expression. After IL-1β stimulation, a delayed increase in oxidised-CaMKII expression was observed, with significant activation after 1 h and a peak at 3 h (0 h: 1.0±0.0, vs. 1 h: 1.57±0.06, 3 h: 1.79±0.20 and 6 h: 1.60±0.15; mean(fold-change)±S.E.M, $p<0.05$, n=4). It was observed that at all stimulation times, TNFα stimulation led to a small measured increase in oxidised-CaMKII expression in HUVECs. This however was variable, less pronounced than with IL-1β stimulation and was not found to represent any statistically significant increase in oxidised-CaMKII expression (0 h: 1.0±0.0, vs. 0.25 h: 1.51±0.30, 0.5 h: 1.66±0.20, 1 h: 1.58±0.21, 3 h: 1.70±0.23 and 6 h: 1.55±0.23; mean(fold-change)±S.E.M, $p>0.05$, n=3).

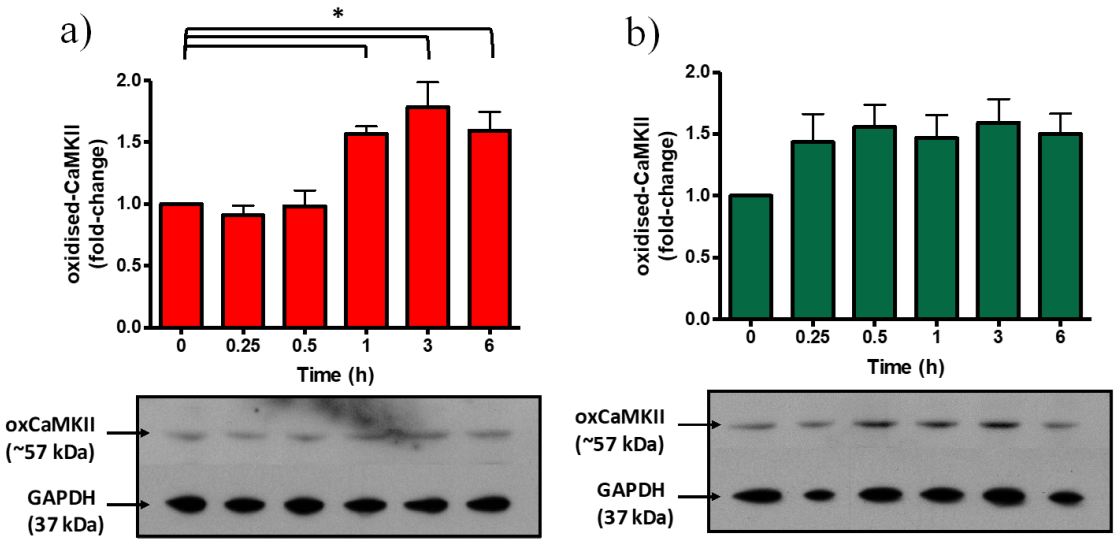

Figure 4.5. Effect on CaMKII activation signalling, as measured by oxidised-CaMKII (oxCaMKII) expression, of stimulation with: a) IL-1β, showing a significant increase in oxCaMKII expression after 1, 3 and 6 h, and b) TNFα, where no significant increase in oxCaMKII expression was observed. Bars represent mean fold-change, compared against unstimulated control HUVECs (0 h), error bars represent ±standard error of the mean. * $p<0.05$, n=4.

When assessing CaMKII activation via phosphorylation, neither stimulant was found to generate a clear increase in phospho-CaMKII expression in HUVECs compared to unstimulated control cells. IL-1β stimulation resulted in no significant increase in phosphor-CaMKII expression (0 h: 1.0±0.0, vs. 0.25 h: 1.15±0.19, 0.5 h: 1.15±0.07, 1 h: 0.98±0.10, 3 h: 1.01±0.19 and 6 h: 0.85±0.15; mean(fold-change)±S.E.M, $p>0.05$, n=3), and this observation was repeated after TNFα stimulation (0 h: 1.0±0.0, vs. 0.25 h: 1.11±0.11, 0.5 h: 0.96±0.15, 1 h: 1.11±0.20, 3 h: 1.15±0.07 and 6 h: 1.08±0.16; mean(fold-change)±S.E.M, $p>0.05$, n=3).

With both oxidised-CaMKII and phospho-CaMKII and across all experimental repeats, basal CaMKII activation was found to be high in the control unstimulated HUVEC samples. This may reflect in the low fold-change values obtained for these experiments compared with immunoblotting experiments for phospho-p65.

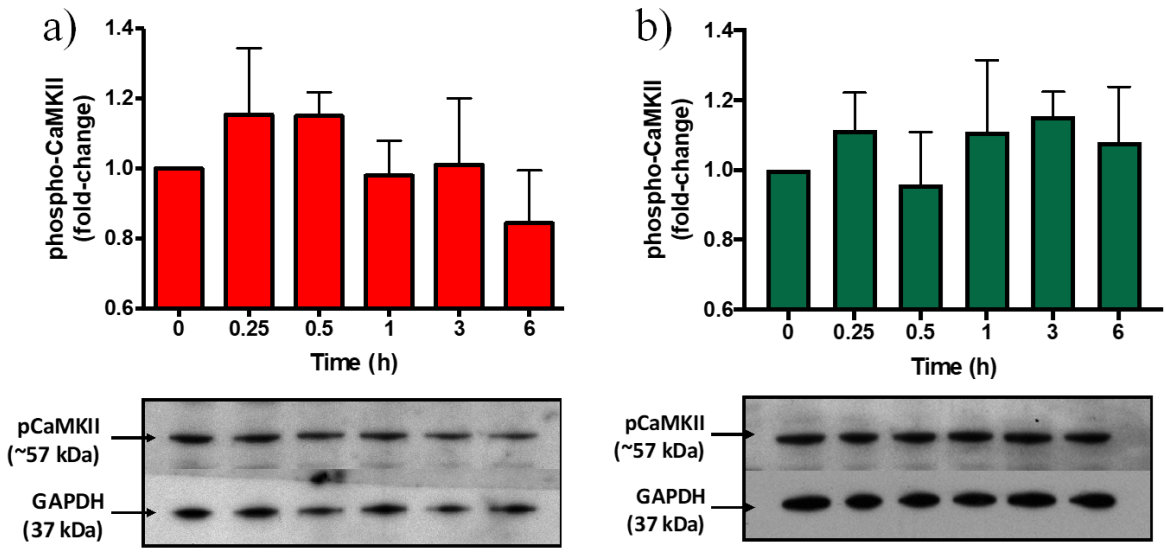

Figure 4.6. Effect on CaMKII activation signalling, as measured by phospho-CaMKII (pCaMKII) expression, of stimulation with: a) IL-1β, which did not induce an increase in pCaMKII signalling over 6 h, and b) TNFα, where no increase in pCaMKII expression over 6 h was also observed. Bars represent mean fold-change, compared against unstimulated control HUVECs (0 h), error bars represent ±standard error of the mean.

4.3.5. Assessing the suitability of PPy coatings for cell culture

Before considering the response of endothelial cells to PPy coated and uncoated 316L SS strips, the response of PPy coatings to sterilisation and incubation in endothelial cell culture media (Lonza EGM-2) was assessed. Figure 4.7. (panel a) shows the DPPH scavenging capacity of non-sterile and sterilised PPy coatings after 8 h incubation time. PPy wires, generated by potentiostatic electropolymerisation at 1.1 and 1.3 V, were sterilised using a pressurised steam autoclave (moist heat sterilisation) or 70% ethanol immersion for 24 h, as these are appropriate methods for use in this study. The effects of sterilisation were determined by performing a one-way ANOVA with Dunnett's post-hoc test, where non-sterile coatings were used as the control group.

Ethanol sterilisation was not found to have a significant adverse effect on the antioxidant capacity of PPy coatings generated at 1.1 V (Ethanol: 40.33±1.78 vs. Non sterile: 47.06±2.64; %mean(antioxidant activity)±S.E.M, $p>0.05$, $n=4$), or 1.3 V (Ethanol: 45.61±1.91 vs. Non sterile: 44.73±2.64; %mean(antioxidant activity)±S.E.M, $p>0.05$, $n=3$). This contrasted with the observed effect of the pressurised steam autoclave sterilisation. This sterilisation method was found to significantly reduce the antioxidant capacity of both coatings generated at 1.1 V (Moist heat sterilisation: 7.19±0.91 vs. Non sterile; %mean(antioxidant activity)±S.E.M, $p>0.05$, $n=3$) and 1.3 V (Moist heat sterilisation: 16.84±1.40 vs. Non sterile; %mean(antioxidant activity)±S.E.M, $p>0.05$, $n=4$). It was found that coatings generated at 1.3 V demonstrated significantly greater DPPH scavenging capacity after heat sterilisation than coatings generated at 1.1 V when compared using a t-test (1.1 V, vs. 1.3 V; %mean(antioxidant activity)±S.E.M, $p<0.01$, $n=3$).

Overall, these results suggest that ethanol sterilisation offers an approach to sterilise samples before cell culture experiments that retains the antioxidant activity of PPy coatings. It is clear that steam autoclaving is not suitable for this study.

To assess the effects of cell culture media on PPy coatings, coated wires and bare 316L SS were stored in EGM-2 and incubated at 37°C for up to 72 h. After incubation, DPPH scavenging capacity was again determined, and the results of this experiment are shown in Figure 4.7 (panel b). The change in antioxidant activity of PPy coatings and 316 L wires was modelled with hyperbola fits for each data set and a one-way ANOVA with Dunnett's post-

hoc test was used to compare the antioxidant activity at each time point vs. the control samples (0 h incubation) for each coating type.

PPy coatings were found to quickly lose their broad antioxidant capacity after EGM-2 incubation. Depletion of activity plateaued after 24 h for coatings generated under both conditions, with both coatings retaining approximately 20% of their DPPH scavenging after 24 h incubation. This represents a statistically significant loss of antioxidant capacity at 24 h for both coatings generated at 1.1 V (24 h: 17.40±0.86 vs. 0 h: 82.73±2.85; %mean(antioxidant activity)±S.E.M, $p<0.001$, n=3), and 1.3 V (24 h: 20.53±2.84 vs. 0 h: 85.43±1.46; %mean(antioxidant activity)±S.E.M, $p<0.001$, n=3). When comparing coatings generated at 1.1 and 1.3 V using t-tests, significant differences were observed between coatings at 1 h (1.1 V: 66.00±6.01, vs. 1.3 V: 85.22±1.20; %mean(antioxidant activity)±S.E.M, $p<0.05$, n=3) and 6 h (1.1 V: 27.56±0.91, vs. 1.3 V: 38.07±2.58; %mean(antioxidant activity)±S.E.M, $p<0.05$, n=3).

316L SS control samples demonstrated an increase in antioxidant activity over the 72 h period, particularly between 6 and 24 h. Although depleted at the endpoint, PPy coated samples retained significantly greater antioxidant capacity when compared against 316L at 72 h using a one-way ANOVA and Tukey post-hoc test (1.1 V: 38.07±2.58 and 1.3 V: 17.65±1.93, vs. 316L: 11.37±0.53; %mean(antioxidant activity)±S.E.M, $p<0.05$, n=3).

This data shows that incubation of PPy samples with EGM-2 depletes and limits antioxidant activity significantly and this effect must be considered when assessing the response of cells to PPy coatings.

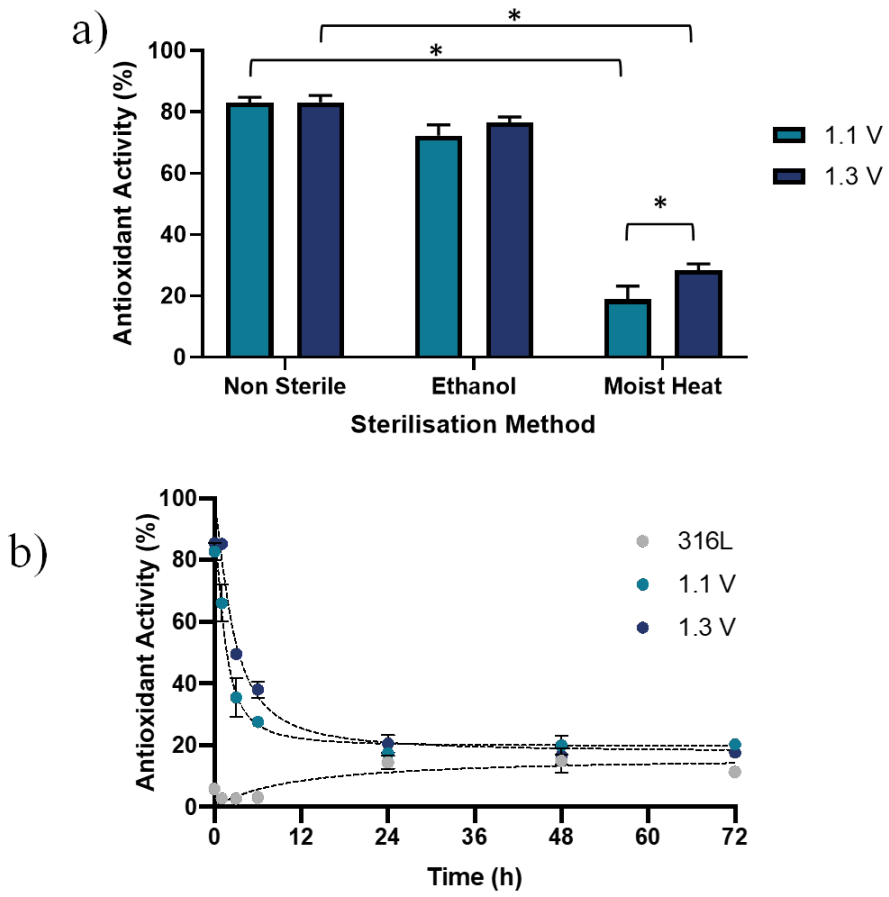

Figure 4.7. a) DPPH scavenging of potentiostatic electropolymerised PPy coatings after ethanol (24 h incubation in 70% ethanol), or moist heat (pressurised steam autoclave, 121°C) sterilisation, showing a significant reduction in antioxidant capacity after heat treatment (mean±S.E.M, n=4, *$p<0.05$). b) DPPH scavenging of potentiostatic electropolymerised PPy and uncoated SS coatings after incubation in EGM-2 endothelial cell culture medium (Lonza) for up to 72 h, showing a rapid loss (<24 h) in antioxidant capacity (n=3). Trendlines fitted using Graphpad Prism 9: hyperbola fit for SS and single-phase exponential decay for PPy coatings.

4.3.6. Influence of PPy surfaces on HUVEC attachment and proliferation

Basic compatibility of HUVECs with PPy and 316L SS was determined by assessing the attachment and proliferation of cells on coated and uncoated strips. Figure 4.8. shows the MTT absorbance from cells attached on PPy and SS surfaces after 24 and 48 h. Cell viability on each surface is estimated on each surface by normalising the MTT absorbance against the samples surface area. Although equal numbers of cells were seeding onto each sample, the number of cells attached may vary and therefore cell viability in this assay represents an estimated comparison of cell number. In this assay, 24 h was used as a measure of viable cell attachment and 48 h incubation was used as a measure of HUVEC proliferation in response to the different samples. Differences between the number of cells on each surface were assessed using a one-way ANOVA and Tukey post-hoc test.

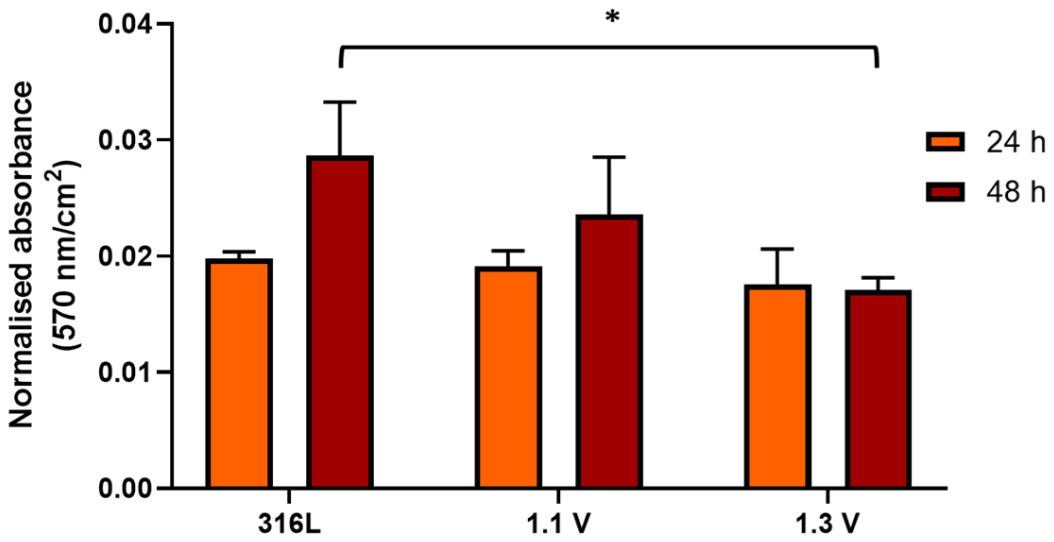

Figure 4.8. MTT assay results showing number of viable cells present on uncoated 316L SS strips and potentiostatic PPy strips. This data shows no significant difference in the samples at 24 h. Both 316L and +1.1 V coated samples demonstrated significant proliferation of HUVECs at 48 h and a significant difference in cell number on 316L vs. +1.3 V. Bars represent average MTT absorbance, normalised against sample surface area, error bars represent ±standard error of the mean, *$p<0.05$, n=3.

At 24 h, no significant difference was observed between 316L SS, 1.1 V PPy coatings and 1.3 V PPy coatings (316L SS: 0.02±0.001, 1.1V: 0.019±0.001, 1.3V: 0.018±0.003; mean(normalised absorbance)±S.E.M, $p>0.05$, $n=3$). Coatings generated at 1.3 V did not appear to promote proliferation and no increase in cell number between 24 and 48 h was observed with these samples. This led to a significant increase in the normalised absorbance at 48 h between 316 L and 1.3 V PPy coatings (316L: 0.029±0.001, vs. 1.3V: 0.017±0.001; mean(normalised absorbance)±S.E.M, $p<0.05$, $n=3$). The absorbance for 1.1 V samples did not significantly increase between 24 and 48 h (24 h, vs. 48 h: 0.024±0.001; mean(normalised absorbance)±S.E.M, $p>0.05$, $n=3$) and at 48 h was not significantly different when compared against the 316L and 1.3 V samples ($p>0.05$).

The MTT assay was followed by using acridine orange staining and fluorescence microscopy to provide further insight into the data that is presented in Figure 4.8. Adherent HUVECs on PPy coated and 316L SS strips were imaged at 40x and 100x magnification after 24 h incubation and this is shown in Figure 4.9.

Imaging on strips showed comparable cell number on all 3 samples, with no obvious differentiating observations or features. There is some indication that fewer cells were present on 316L samples, this observation does not reflect the MTT data and is not representative of the observations for all 3 repeat samples. Overall, high levels of variation were observed with all 3 samples when repeating this experiment.

However, a common observation that could be made was that cell attachment to 1.3 V samples was very patchy across the samples. Although the total number of cells appeared comparable, cells appeared to be more clustered than on 316L or 1.1 V coatings. At 100x magnification, the shape of cells can be observed and cells appear to show spreading on all 3 samples, but this appeared to be favourable with 1.1 V coatings.

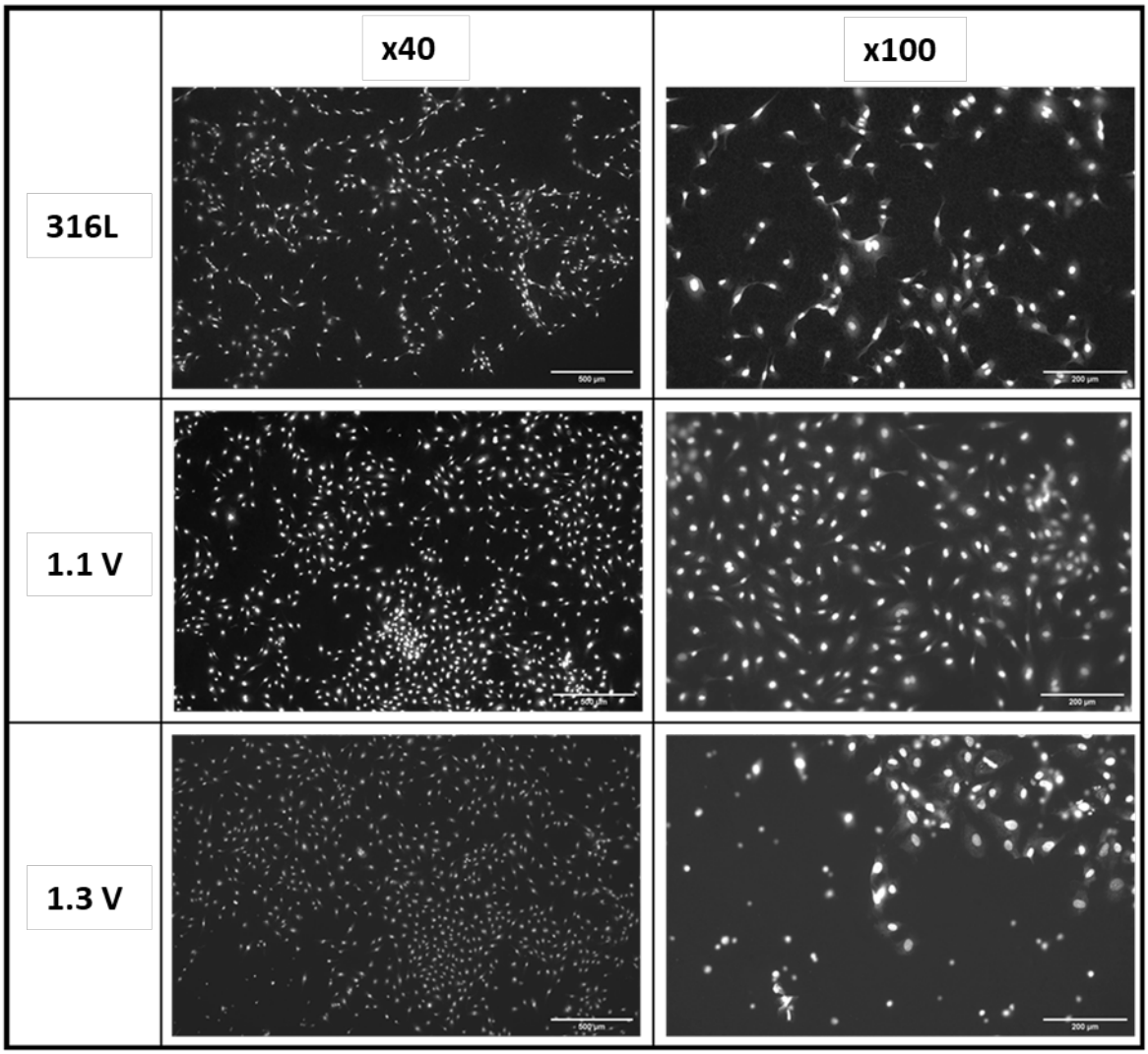

Figure 4.9. HUVECs stained with acridine orange and imaged, at 40x and 100x magnification on uncoated 316L SS strips and strips coated with PPy potentiostatically at +1.1 and 1.3 V. Images suggest that all 3 sample types are capable of supporting HUVEC attachment and cells are capable of spreading on the surfaces. Images representative of three repeat samples.

4.4. Discussion

The use of HUVECs as a model for assessing the biological response of the endothelium and endothelial cells to stenting or stent components has established applications (Campolo, et al. 2014; Tang, et al. 2011). With the incorporation of novel targets, such as CaMKIIδ, there is a need to specifically assess the appropriateness of HUVECs as an endothelial model. Based on the knowledge that more relevant primary cells offer fewer population doublings, assays that have limited suitability with HUVECs can be disregarded for this use. Here, the results presented will therefore be discussed in terms of the significance within the HUVEC model, but also their use for more complex in-vitro experiments.

4.4.1. *In vitro* culture of HUVECs and suitability in a restenosis-endothelial cell model

HUVECs used in this study were imaged to assess their cell morphology and the homogeneity of the cellular population and this is shown in Figure 4.1. (panels a & b). This was carried out to ensure confidence and it was found that the HUVECs represented a uniform cell population that was representative of macrovascular endothelial cells.

Although this method allowed some confidence in understanding the cell type, it does not indicate with certainty that the cells used were functional HUVECs. An improved method to assess the cellular phenotype using specific antibodies to stain for phenotypic cell markers would allow different cells with similar morphologies to be distinguished. Furthermore, endothelial to mesenchymal transition (EndMT) is a process whereby endothelial cells undergo a phenotypic switch to a myofibroblast phenotype and antibody staining would allow this to be quantified (Kovacic, et al. 2019). When repeating these in-vitro experiments with HCAECs and HCASMCs, it will be useful to implement immunocytochemistry to better understand the cells used.

HUVECs are not adult endothelial cells and are not derived from an arterial source, therefore there are issues with their use as indicators in a coronary endothelial context. Furthermore, when compared to the more relevant HCAECs, it has been shown that HUVECs respond differently to chemokines, specifically TNFα, TGF-β and IL-1α (Briones, et al. 2001). This presents a critical difference as the response to these mediators will have a considerable

influence on pro-inflammatory and oxidative stress, which has profound implications in the progression of restenosis in the clinical pathophysiology.

HUVECs offer an ideal model endothelial cell line for preliminary studies but should not be used in isolation to draw major conclusions about restenosis, re-endothelialisation, specific CaMKII signalling and vascular oxidative stress.

4.4.2. Suitability of stimulants in a restenosis-endothelial cell model

The use of stimulants in any in-vitro model to induce stress, must reflect the pathophysiological state *in vivo*. In this study, IL-1β and TNFα were used to determine their stimulatory effects, and their acute effect on cell viability alongside hydrogen peroxide, a positive control for oxidative stress. IL-1β and TNFα did not significantly reduce cell viability, as shown in Figure 4.1. (panel c), suggesting that the concentrations are not cytotoxic within the time course studied. This is useful as it gives confidence that the concentrations and times used here reflect only stimulation of pro-inflammatory and oxidative stress signalling and not apoptotic cell death.

A small, and non-significant, increase in the absorbance is observed at 1 hr with 3 ng/ml of both stimulants. Increased mitochondrial activity may result in increased MTT absorbance and provide a mechanism for IL-1β- and TNFα-induced ROS generation in HUVECs (Ott, et al. 2007). Six-hour stimulations were used in this study and led to significant hydrogen peroxide-induced cell death, but this time interval may be insufficient when considering p65 and CaMKII activation, which may require longer chronic stimulation (Maione, et al. 2017).

The concentrations and exposure times used in this study are based on previous research with other cardiovascular cell types (McCluskey, et al. 2018). Zen, et al. (1999) assessed the effects of IL-1β (0 – 10 ng/ml) and TNFα (0 – 100 ng/ml) stimulation for 24 h on HUVEC viability using MTT assays and found that neither cytokine significantly affected cell viability at any concentration. In contrast, Majewska, et al. (1997), found that 24 h stimulation with TNFα (10 ng/ml) led to a small, but significant reduction in HUVEC viability (approximately 20% loss of viable cells). This broadly reflects the observations made in this study with HUVECs at the lower time interval.

With an *in vitro* model, it is important to consider the relevance of clinical circulating levels of the stimulants used. Sardella, et al. (2006), found that BMS and DES stent placement induced small but significant elevation in circulating IL-1β, 20 minutes after placement, from approximately 3 pg/ml to 4 pg/ml. At 1 month after stenting, placement has been linked with elevations in circulating IL-1β levels only with BMS use. DES have instead been shown to reduce IL-1β levels after 24 h (Kochiadakis, et al. 2007). Similarly, TNFα levels are elevated after BMS placement, from 20 pg/ml to 50 pg/ml, 6 h after stent placement (Kozinski, et al. 2005). This TNFα elevation persisted up to 1 month after stent placement. This study compared TNFα elevation in patients who did and did not develop ISR and increased TNFα was unique to patients developing ISR, suggesting TNFα elevation may be a strong contributing factor to neointimal formation.

Pre-operative levels of circulating cytokines have also been considered as potential risk factors for ISR. Sun, et al. (2009) found pre-operative levels of TNFα to correlate strongly with risk of developing a neointimal lesion. The risks associated with different cytokines varied and pre-operative IL-1β did not correlate with increased restenosis rates. Although these studies present limited evidence that IL-1β presents a key driver of disease progression, IL-1β has been found to drive the progression of neointimal formation, via action on the IL-1 receptor in mice (Chamberlain, et al. 2006).

4.4.3. Effects of cytokine stimulation on pro-inflammatory signalling in HUVECs

The NF-κB pathway centres on the activation of the NF-κB protein complex. This signalling pathway allows for transcriptional control of DNA in response to multiple cellular stresses, for example: free radicals, cytokine binding and oxidised LDL. The NF-κB-dependent response of cells to stresses suggests an obvious connection to the vascular environment after stent placement.

p65 is one protein within the NF-κB complex. Phosphorylation of p65 is essential to canonical NF-κB activation and nuclear translocation (Christian, et al. 2016). This activation pathway has been associated with pro-atherosclerotic signalling in humans (Monaco, et al. 2004). Quantification of p65 phosphorylation provides a measure for pro-inflammatory signalling. Alternative measures for assessing inflammation include: IκBα degradation, NF-κB

translocation to the nucleus, or measuring other signalling molecules that are linked with pro-inflammatory effects, e.g. JNK or ERK.

In this study, both IL-1β and TNFα stimulated a significant increase in p65 phosphorylation, as demonstrated in Figure 4.2. Peak stimulation was observed with IL-1β at 1 hour and with TNFα at 30 minutes. This increase was in line with how stimulants were expected to effect HUVECs as they are known activators of the canonical pathway. Gao, et al. (2017), found that one-hour stimulation of HUVECs with both cytokines (20 ng/ml) led to significant p65 phosphorylation (approximately 3-fold and 5-fold respectively), but identified peak stimulation after 15 minutes. Pan, et al. (2011) also assessed phospho-p65 expression in HUVECs in response to TNFα (10 ng/ml) stimulation with a single 15-minute stimulation time. They found that TNFα induced significant stimulation in phospho-p65 expression after 15 minutes, supporting the findings of this study.

As previously discussed, TNFα release is upregulated after stent placement. This increase in TNFα has been shown to be critical in the activation of NF-κB in response to PCI (Pesarini, et al. 2010) and reduction in NF-κB signalling was shown to reduce late lumen loss, a measure of the stenotic lesion, in patients (Egashira, et al. 2008).

Although there is less obvious correlation between IL-1β and restenois, it has been shown to provide a positive feedback system for vascular inflammatory disease, via the NF-κB pathway (de Winther, et al. 2005). Despite the findings by Kochiadakis, et al. (2007), that circulating IL-1β levels are only transiently elevated after DES placement, it remains of interest as it upregulated in endothelial cells in response to mTOR-inhibitors released by DES (Chibana, et al. 2017).

4.4.4. Effects of peroxide stimulation on ROS generation in HUVECs

DCFDA was used as a preliminary assay to measure ROS generation in response to cytokine stimulation with hydrogen peroxide and TBHP used as positive controls. There are strong oxidising agents that can freely diffuse into the cell. The use of hydrogen peroxide in a restenosis model however is not appropriate as it does not reflect the mixed ROS environment after stent placement.

The preliminary optimisation of the DCFDA with H_2O_2 demonstrated that this assay can reliably detect increased intracellular ROS generation. H_2O_2 (100 and 300 μM) and TBHP stimulation resulted in very high ROS generation. This is shown in Supplementary Figure S4.2. TBHP is a more highly oxidising species than the hydrogen peroxide and would be expected to generate a greater increase in ROS. This observation indicates that the observed stimulatory effects of 100 and 300 μM hydrogen peroxide were very high – possibly disproportionately, due to the generation of mono 2-ethylhexyl phthalate and tetrabromobisphenil A from side reactions with media and serum, which lead to redox-cycling (Murphy, et al. 2022). Although DCF should be oxidised by products of downstream hydrogen peroxide reactions, the ability of hydrogen peroxide to freely diffuse into the cell means interference by hydrogen peroxide itself on the assay results cannot be dismissed.

4.4.5. Effects of cytokine stimulation on ROS generation in HUVECs

Stimulation of HUVECs with IL-1β or TNFα was found to generate significant increases in intracellular ROS production. This is shown in Figure 4.3. As previously discussed, the DCFDA assay is limited by redox cycling and therefore direct comparisons of IL-1β and TNFα with this data should be avoided. Observations made while performing these experiments further supported this effect, with IL-1β (10 ng/ml) stimulation leading to a visible loss in cell number after 6 h in the presence of DCFDA. This was not observed in the absence of DCFDA. Unfortunately, the 96-well plate format, time and light sensitivity of the DCFDA assay prevented imaging of the cells.

Although comparisons should be avoided, a stronger concentration and time-dependent effect on ROS generation was observed with TNFα stimulation than with IL-1β. Han, et al. (2017) observed significant increase in intracellular ROS (3.3-fold) after TNFα stimulation (10 ng/ml;6 h), supporting the finding of significant ROS generation with TNFα in HUVECs. Less data is present in the literature using IL-1β to stimulate ROS in vascular endothelial cells, especially HUVECs, with the DCFDA assay. Chang, et al. (2009) however used DCFDA in HUVECs pre-treated for 18 h with IL-1β and found IL-1β to stimulate significant ROS generation (approximately 20-fold increase).

The findings that IL-1β and TNFα both generate oxidative stress provides another route by which NF-kB may be activated, although this positive feedback mechanism of activation is

likely to have little effect in culture since peak p65 phosphorylation precedes peak ROS generation in HUVECs. When using HCAECs, it is key to confirm these effects and explore whether this reflects increases in specific ROS species.

4.4.6. CaMKII expression in HUVECs

Although HUVECs are known to express CaMKII (McClusky, et al. 2015), it was important to ensure sufficient expression in our endothelial cells. High CaMKIIδ expression was shown in our HUVECs (Figure 4.4.) and is comparable to previous observations, where CaMKIIδ, specifically CaMKIIδ_6, has been shown to be the predominant isoform (Wang, et al. 2010). If as suggested, the δ_6 isoform is predominant, this is not distinguished since our antibody is raised against the shared C-terminal. Importantly, the δ_6 isoform is not predominantly expressed in the heart or VSMCs and variants show varying functionality, through differences in their effects on calcium signalling (Zhang, et al. 2007).

One issue with this data is that HUVEC lysates were counted from cell suspensions to allow lysates to be prepared, whereas rat heart homogenates were prepared by homogenising rat hearts in sample buffer before normalising protein content using a Bradford protein assay. Both approaches provide a robust and reliable normalisation method, but the protein content is unlikely to be equal. Groups therefore cannot be directly compared, but normalisation to GAPDH is still possible across preparations.

4.4.7. Activation of CaMKII in response to cytokine stimulation

As with pro-inflammatory NF-κB signalling, cytokine stimulation was found to lead to CaMKII activation in HUVECs, but this effect was limited to IL-1β stimulation and only via oxidation, as demonstrated in Figures 4.5. & 4.6. This was in line with the peak stimulation of ROS generation observed and later than the peak phospho-p65 expression (1 h). Therefore, ROS generation and oxidative CaMKII activation appear to follow NF-κB activation. It is unclear where the pro-inflammatory signalling in HUVECs linked to the pro-oxidant signalling and CaMKII activation, but this could be clarified by inhibiting NF-κB signalling to discriminate any role it may have in pro-oxidant signalling.

Interactions between CaMKIIδ and NF-κB are widely reported, with CaMKII known to directly regulate NF-κB in cardiac fibroblasts through interactions with IKKβ (Martin, et al.

2018). Furthermore, CaMKII-mediated NF-κB activation contributes to pathological remodelling in the heart (Rusciano, et al. 2019). Antioxidants have been shown to mitigate against some of these pathological interactions in endothelial cells in ischaemic stroke models, suggesting ROS is a regulator of NF-κB and CaMKIIδ allowing it to act as a broad mediator of pathology (Gu, et al. 2016).

There is little reported use of IL-1β to stimulate CaMKII activation in HUVECs or other relevant cells, but IL-1β has been used in other systems, namely CaMKIIα in neurological applications. Stimulation of both rat astrocytes and macrophages with IL-1β has been shown to cause CaMKIIα activation, via phosphorylation (Wu, et al. 2009; Liu, et al. 2008). This response of CaMKIIα to IL-1β contrasts with the observations for CaMKII in HUVECs in this study, where no phosphorylation was observed.

Stimulation of HUVECs with TNFα (10 ng/ml) over 6 hours was not found to induce any significant activation of CaMKII, either by phosphorylation or oxidation. This lack of CaMKII activation contrasts with the previous stimulatory effects of increased phospho-p65 expression and ROS generation by TNFα. If ROS increases were reflected in CaMKII oxidation, it would be expected that increases in oxidised-CaMKII expression would be observed at 3 h and 6 h after stimulation, but this was not observed. If, as suggested by p65 phosphorylation and DCFDA data, the onset of stimulatory effects for TNFα are slower than IL-1β, 6 h stimulation may be insufficient to see the downstream effects of TNFα stimulation on CaMKII activation. Alternatively, these stimulants may generate different ROS, which DCFDA cannot discriminate between, with only IL-1β generating species that oxidise the CaMKII protein complex.

As with IL-1β, the finding that TNFα stimulation led to no significant increase in phospho-CaMKII expression is surprising. Gu, et al. (2016), assessed the effects of TNFα (2 ng/ml) stimulation on CaMKII in HUVECs and found at 4 hours, stimulation led to significant activation of CaMKII via phosphorylation. The same study also considered activation by oxidation and found that TNFα did not induce activation by oxidation.

One observation made frequently in our study was high basal control expression in HUVECs. This was not explicitly noted, or shown in immunoblot figures, in previously published studies. High basal signals may represent high levels of cellular stress and it would be expected for this to be represented in the basal phospho-p65 signal, this however was not observed.

Alternatively, this may result from the sensitivity of immunoblotting or, the specific antibodies used for detection.

4.4.8. Assessing the suitability of PPy coatings for cell culture

As presented in Chapter 3, ROS scavenging assays demonstrate the antioxidant capacity of PPy under simulated conditions. Before examining the compatibility of endothelial cells with these PPy surfaces and exploring any *in vitro* antioxidant actions, it was necessary to consider how the coatings may perform under *in vitro* cell culture conditions.

The effects of moist heat and ethanol sterilisation were assessed, and shown in Figure 4.7, as this study required sterilisation to be performed quickly and more complex approaches such as UV, gamma irradiation and ethylene oxide were not easily accessible. Ethanol sterilisation presented an appropriate technique for use as 24 h sterilisation resulted in no significant loss of DPPH scavenging capacity. In this experiment, samples were sterilised with 70% ethanol for 24 h, but for cell compatibility assays a shorter sterilisation time (1 h) was used. Shorter sterilisation times (30 minutes and 3 hours) have been reported to successfully sterilise PPy coatings for cell culture experiments (Li, et al. 2005; Lukasek, et al. 2019).

Moist heat sterilisation, via a steam autoclave, was unsuitable for sterilising coatings as it resulted in a significant loss in DPPH scavenging capacity that was more detrimental to PPy samples coated at 1.1 V. Steam autoclaving has been used for sterilising conducting polymer coatings, namely PEDOT, and found not to have a significant effect on cellular adhesion with the surface (Kim, et al. 2018). However, steam sterilisation has been shown to cause thermal damage and a loss in coating integrity (Uguz, et al. 2018). Because it is not possible to deduce what factor, e.g. heat, humidity or pressure, is negatively impacting the PPy coatings, future investigation could use dry heat sterilisation techniques to consider whether heat alone is imparting a significant effect.

The efficacy of sterilisation was not considered in this study, but in subsequent cell culture experiments, ethanol sterilisation, along with the gentamycin supplement included in the media was found to be sufficient in preventing infections. Further clinical application of PPy would require investigation of commercial sterilisation techniques. Gamma irradiation to has been shown to reduce the structural integrity of PPy (Kim, et al. 2018), presenting limitations in its future application.

In this study, it was also necessary to consider the effect of incubation in cell culture media on PPy antioxidant capacity. EGM-2 incubation significantly and rapidly depletes PPy antioxidant capacity and the rate and magnitude of loss in antioxidant capacity was more deleterious than the loss with PBS incubation at 37ºC. There are many components of the EGM-2 buffer that may react with PPy. Redox active compounds, such as ascorbic acid, may be more likely to react directly with the PPy coatings, resulting in the chemical modification of these coatings. Unfortunately, this data shows that incubating PPy samples with EGM-2 will result in the rapid loss of PPy antioxidant activity before 24 and 48 h, when assays are planned. There may be an early antioxidant benefit, but under our conditions it is not possible to assess this. The effect of media on antioxidant activity should be re-assessed when changing cell culture media.

The primary role of this study is to determine the potential therapeutic benefits of a PPy-based coating in coronary stent applications. It is not within the scope of this study to confirm those therapeutic benefits *in vivo*, however the finding that cell culture media can rapidly deplete the antioxidant capacity of PPy presents significant challenges if this response translates into an *in vivo* environment. If PPy is limited to <24 h of active antioxidant capacity, it is unlikely to offer the therapeutic benefit intended and will not provide any benefit over current DES technologies, which offer therapeutic effects up to 180 days. Furthermore, an *in vivo* environment is likely to be more challenging for the stent to tolerate compared with culture media due to its increased complexity. This study does not however explore the impact of other dopants or PPy doping levels, and these may provide further tunability to extend the active antioxidant period of PPy.

4.4.9. Influence of PPy surfaces on HUVEC attachment and proliferation

In this preliminary study, MTT and acridine orange staining were used as measures of HUVEC attachment to, and proliferation on PPy surfaces and compared against tissue culture wells and 316L SS. Although formazan generation by viable cells is a direct and proportional to the number of viable cells, it represents an indirect measure of cell number and proliferation.

From MTT data, as shown in Figure 4.8, normalised absorbance at 24 h was similar across 316L SS and PPy-coated strips and significantly lower when compared against tissue culture

plastic (TCP), suggesting that neither sample promotes cell attachment. Proliferation, assessed as by the increase in absorbance at 48 h, was variable, with HUVECs showing significant proliferation on 316L SS and strips coated with PPy at 1.1 V.

The application of using electrochemically-synthesised PPy coatings for cardiovascular applications is very novel. Proliferation of endothelial cells has however been assessed with PPy-coated polyester fibres, which were found to support the proliferation of aortic endothelial cells, with electrical conductivity correlating with improved endothelial cell growth (Jakubiec, et al. 1998). If, PPy generated by potentiostatic electropolymerisation at 1.3 V becomes over-oxidised, limiting its conductivity, this may result in the lack of endothelial proliferation observed. Mattioli-Belmonte, et al. (2005), found that overoxidised-PPy coatings changed topography in response to cell culture media and that cell attachment of keratinocytes was inhibited, but our data does not show inhibited HUVEC attachment. This same study also found that cells attached to regular PPy coatings displayed different morphologies to those attached to TCP, suggesting PPy can have a profound effect on cellular behaviour.

The presence of crystalline salicylate precipitation on the surface of 1.3 V PPy-coated samples was shown in Chapter 2. Salicylate solubility in ethanol is low, so it is likely that these crystals will not dissolve from the PPy until placed in cell culture media, causing high elution of salicylate into the media and locally at the coating surface. Controlled concentrations (<20 mM) of Sa have been shown to be non-cytotoxic to HUVECs (Shahidi, et al. 2014), but at these concentrations, proliferation may be inhibited.

An obvious advantage of using drug-free PPy coating is that the side effects related to high dosing are eliminated. In a pro-healing PPy design, it may not be possible to tightly control the dosage of drug elution due to the rapid drug-elution observed with PPy coatings in Chapter 3. Since it is hoped re-endothelialisation will be promoted when implanted, the drug elution may also be localised and concentrated to these cells resulting in difficulty when estimating the dosage rate. In a drug-free system where the electropolymerised PPy antioxidant capacity offers the only therapeutic effect, the benefit will be limited to the PPy surface and it is hoped will respond to the presence of elevated ROS species in a more targeted manner.

This assay was performed with large 30 x 5 mm strips in 6 well dishes. An improvement for this assay would be to reduce the coating size for use in a smaller well-plate format. If the

number of cells per mm^2 were kept constant, this would reduce the initial number of cells needed per sample and improve the overall sensitivity of the MTT assay.

Acridine orange staining supported the findings that cell attachment was comparable on 316L SS and PPy-coated samples and representative images are shown Figure 4.9. This technique overall was useful for easily imaging the adherent cells, but as expected, fluorescence was stronger for nuclear acridine binding than cytosolic binding. Some cytosolic fluorescence was observed giving an indication of the cellular morphology, but this was not easy to image or characterise on every sample. Additionally, samples were not imaged at 48 h, where MTT identified significant differences in the number of viable HUVECs. With more relevant cell types, this technique could be insightful if more broadly applied at each time point. Differences in cellular morphologies on each surface could be assessed with specific cell markers rather than using cytosolic acridine staining.

4.5. Conclusions

In conclusion, this chapter has achieved the aim of identifying a cell-based model to simulate the cellular stresses initiated immediately after stent placement. The use of HUVECs is effective as a preliminary cell type to demonstrate the ability for IL-1β and TNFα to generate intracellular inflammatory and oxidative stress. After stimulating HUVECs with IL-1β and TNFα, significant inflammatory stress was observed through an increase in p65 phosphorylation. Similarly, the increase of intracellular oxidative stress after stimulation with IL-1β and TNFα was observed using DCFDA and occurred at later time point to peak p65 phosphorylation.

When assessing the effect of both stimulants on CaMKII activation, activation was limited to oxidation and only after stimulation with IL-1β. This differentiate presents a potential route of stimulating inflammatory and oxidative stress with, or independently to, CaMKII activation. This may arise due to the activation of different oxidative signalling pathways after stimulation with IL-1β and TNFα and allow the effect of CaMKII activation on cell responses to PPy be explored further.

The ability to culture HUVECs on PPy-coated SS strips demonstrates the effectiveness of the strip format in a cell-based model. By using this technique and applying it with MTT and acridine orange assays, PPy was shown to allow endothelial cell attachment that for coatings generated potentiostatically at 1.1 V was comparable to uncoated 316L SS samples.

Although the results presented in this chapter identify a basic cell-based model for assessing the impact of PPy coatings on endothelial cell function, this needs to be explored and proven to translate into more relevant HCAECs and this will be explored in detail in Chapter 5.

5. *In vitro* characterisation of endothelial cell response to polypyrrole surfaces in the presence of oxidative stress

Chapter 5 explores the fourth and final aim of the study – validation of the *in vitro* model identified in Chapter 4 and application of this model to assess the biological antioxidant potential of polypyrrole (PPy) coated strips. This chapter begins by providing background context and outlines the key objectives. Further experimental methodology and materials to those used in Chapter 4 will also be described. Results of this work will then be presented, and key findings will be highlighted. Finally, this chapter will conclude with an in-depth discussion considering the significance of findings and future potential of this work.

5.1 Background and Aims

Previously, this study has established that TNFα and IL-1β are suitable stimulants for the induction of oxidative and inflammatory stress in HUVECs. It is however hoped that any cell-based model will utilise more relevant human coronary artery endothelial and smooth muscle cells (HCAECs and HCASMCs). Limited in-vitro work exists using HCAEC and HCASMCs in a restenosis model, but as discussed below, the clinical literature highlights the significance of p65 phosphorylation and the relevance of CaMKII as a novel-target for any potential antioxidant.

Firstly, endothelial cell activation in the coronary artery after PCI, particularly BMS placement, is associated with p65 phosphorylation and linked with increased restenosis rates (McNair, et al. 2010). This activation has been found in large part to be the result of TNFα upregulation, which is known to be triggered after all PCI and to correlate strongly with restenosis rates (Bittar, et al. 2005). Although modern everolimus-eluting stents have been shown to inhibit endothelial cell activation via this pathway (Fejes, et al. 2018), the potential for use of drug-free coatings with PPy reinforces the relevance of p65 activation.

p65 phosphorylation also has a clear role in the smooth muscle cell pathophysiology associated with restenosis, as the inflammatory response induced by stent placement similarly leads to p65 activation (Yang, et al. 2018). p65 activation in these cells has been shown to drive smooth muscle cells to a more synthetic and proliferative phenotype, driving neointimal formation.

Interestingly, this signalling was closely associated with NOX4-dependent redox signalling, further highlighting the potential benefit of a localised antioxidant (Wu, et al. 2019).

CaMKII activation has been implicated clinically in the development of restenosis, but it is less clearly linked than p65 phosphorylation and its activity is more strongly linked to smooth muscle cell dysfunction. House & Singer, (2008) explored CaMKIIδ expression in restenotic lesions and found increased protein expression and activation in smooth muscle cells after injury, which when downregulated or inhibited led to reduced cell proliferation. Unfortunately, this study used a rat model and the vessel injury in this model led to complete endothelial denudation preventing analysis in endothelial cells. However, it is known that CaMKII is expressed in the endothelium of human umbilical vein coronary arteries and eNOS is a downstream target of inflammation-induced CaMKII activation (Murthy, et al. 2017), suggesting a potential beneficial effect for both endothelial and neighbouring smooth muscle cells of CaMKII activity. Furthermore, CaMKII activity improves endothelial cell migration, which may improve the efficiency of re-endothelialisation (Meoli & White, 2009). Overall, the role of CaMKII in restenosis is more clearly associated with smooth muscle cell activity, but the scarcity of literature in endothelial cells highlights the need to explore the effects further in these cells.

In many respects, HCASMCs present the most relevant single cell model of restenosis since their phenotypic switch and resulting invasive proliferation are critical to neointimal formation. This can however be difficult to control and quantify *in vitro*, particularly since primary cells may be sourced from already diseased patients. This is further complicated since HCAEC and HCASMC communication, via paracrine mediators, extracellular vesicles, and contact-based factors, has a significant impact on HCASMC behaviour and requires a co-culture model (Mendez-Barbero, et al. 2021). Particularly relevant in this context is NO, a major paracrine signalling molecule between ECs and SMCs, which may be scavenged by PPy coatings, leading to undesirable consequences (Barbato, et al. 2005).

In vivo models provide the greatest anatomical and physiological comparisons, but *in vitro* work provides a protocol by which human physiology can be assessed and differences in PPy coatings can be observed quickly. It is also easier with these approaches to make interventions to assess the role of CaMKII in the vascular response, as measured by cell proliferation. Since the primary objective of our PPy coatings is to promote re-endothelialisation in order to

provide a resulting endogenous anti-proliferative effect to the underlying HCASMCs, it follows that the initial model should focus on the HCAEC response to our substrates.

Chapter 4 presented a model by which HUVECs could be stimulated to induce inflammatory and oxidative stress with and without CaMKII activation. This needs to be validated in the more relevant coronary artery cells, but also, considerations need to be made to translate the western blotting protocols used to allow for the incorporation of solid PPy coated substrates. This will likely be achieved by immunofluorescence, as imaging has been shown to be successful with acridine orange, and previously when accessing PPy in neurological device applications (George, et al. 2005).

This aim of the study can be separated and defined by four objectives as outlined below:

1. Validate the in-vitro inflammatory and oxidative stress model established in Chapter 4 in HCAECs and HCASMCs.
2. Re-optimise assay conditions, where necessary, for immunocytochemistry to allow their use with PPy coated strips.
3. Consider and quantify the effects of PPy and 316L surfaces on initial HCAEC and HCASMC characteristics, such as cell attachment, proliferation, and morphology.
4. Assess whether the ROS scavenging capacity of PPy translates to an inhibitory effect on oxidative or inflammatory signalling in this cell-based model, and thus whether the coatings impart a relevant biological effect.

5.2 Materials and Methods

5.2.1. Materials and Equipment

Material/Equipment	Supplier
Stainless Steel (316L wires and plates)	Goodfellow Cambridge Ltd, UK
Ag/AgCl Reference Electrode (KR5)	ThermoFisher Scientific, UK
Potentiostat/Galvanostat	Metrohm Autolab, UK
POLARstar Omega Plate reader	BMG LABTECH, UK
FlexStation3 Plate reader	Molecular Devices, UK
Plate reader	BioRad, UK
Human Coronary Artery Endothelial Cells (HCAEC)	Promocell, Germany
Human Coronary Artery Smooth Muscle Cells (HCASMC)	Promocell, Germany
Invitrogen Western Blot System	ThermoFisher Scientific, UK
Nitrocellulose	GE Healthcare, US
Autoradiography film	Santa Cruz Biotechnology, US
Calibrated Densitometer	BioRad, UK
EVOS M7000 Imaging System	ThermoFisher Scientific, UK

5.2.2. Chemicals

Chemical	Supplier	Catalogue Number
Pyrrole (98% solution)	Sigma Aldrich, UK	131709
Sodium Salicylate	Sigma Aldrich, UK	S3007
Phosphate Buffered Saline (PBS) tablets	Oxoid, UK	BR0014G
Absolute Ethanol	VWR, UK	20821.296
Endothelial Cell Growth Medium MV 2	Promocell, Germany	C-22121
Smooth Muscle Cell Growth Medium 2	Promocell, Germany	C22162
DetachKit	Promocell, Germany	C-41200
Trypsin/EDTA solution	ThermoFisher, UK	T4049
Interleukin-1beta (IL-1β)	Insight Biotechnology, UK	10-2012-C
Tissue necrotic factor alpha (TNFα)	Insight Biotechnology, UK	10-1034-C
Acridine Orange powder	FisherScientific, UK	1132794
2',7' –dichlorofluorescin diacetate (DCFDA) assay kit	Abcam, UK	Ab113851
3-(4,5-Dimethylthiazol-2-yl)-2,5-Diphenyltetrazolium Bromide (MTT) powder	Sigma Aldrich, UK	M5655
Dimethyl sulfoxide (DMSO) liquid	Sigma Aldrich, UK	D8418
Novex 10% Bis-Tris polyacrylamide gels	FisherScientific, UK	10184862
3-(N-Morpholino)propanesulfonic acid (MOPS) powder	Sigma Aldrich, UK	M1254

Trizma (Tris-base) crystalline powder	Sigma Aldrich, UK	93352
Ethylenediaminetetraacetic acid (EDTA) powder	Sigma Aldrich, UK	9884
Sodium dodecyl sulphate (SDS) powder	Sigma Aldrich, UK	75746
Bovine serum albumin (BSA) powder	FisherScientific, UK	11403164
Tween-20 liquid	Sigma Aldrich, UK	P1379
Luminol powder	Sigma Aldrich, UK	123072
p-Coumeric acid powder	Sigma Aldrich, UK	C9008
Hydrogen Peroxide (30% solution)	Santa Cruz Biotechnology	sc-203336
CellROX Green Solution	Invitrogen, UK	C10444
Hoechst 33342 Powder	Invitrogen, UK	H1399
Antibodies	Refer to: 5.2.8.	

5.2.3. Human Coronary Artery Endothelial Cell Culture

HCAECs were cultured at 37ºC in a humidified atmosphere (5% CO_2) as recommended by Promocell using Endothelial Cell Growth Medium MV2. Endothelial Cell Growth Medium MV2 contained 5% FBS and all included supplements (final concentration per ml media): hEGF (5 ng), hFGF (10 ng), R3-ICF-1 (20 ng), VEGF (0.5 ng), ascorbic acid (1 µg) and hydrocortisone (0.2 µg).

At 90% confluence, cells were dissociated from flasks using PromoCell DetachKit and pelleted by centrifugation at 1000 rpm for 3 minutes. Cells were then counted and plated at the following concentrations: T75 flask (6 x 10^4 cells/ml), T25 flask (3 x 10^4 cells/ml), 12-well plate (5 x 10^4 cells/ml), 48-well plate (5 x 10^4 cells/ml) and 96-well plate (1 x 10^4 cells/ml). Cells were cultured for a further 2 days at 37ºC/5% CO_2 before carrying out assays.

5.2.4. Human Coronary Artery Smooth Muscle Cell Culture

HCASMCs were cultured at 37ºC in a humidified atmosphere (5% CO_2) as recommended by Promocell using Smooth Muscle Cell Growth Medium 2 containing 5% FBS and all included supplements (final concentration per ml media): hEGF (0.5 ng), hFGF (2 ng) and insulin (5 µg).

At 90% confluence, cells were dissociated from flasks using PromoCell DetachKit and pelleted by centrifugation at 1500 rpm for 4 minutes. Cells were then counted and plated at the following concentrations: T75 flask (6 x 10^4 cells/ml), T25 flask (3 x 10^4 cells/ml), 12-well

plate (5 x 10^4 cells/ml). Cells were cultured for a further 2 days at 37ºC/5% CO_2 before carrying out assays.

5.2.5. Stimulations

In addition to TNFα and IL-1β stimulation (see 4.2.4), cells were stimulated with TGF-β (1-20 ng/ml) for 1-6 h. Stimulations were performed without any prior serum starving, although all stimulations were carried out after at least 2-days incubation without replacing media to minimise any serum-associated signalling effects.

5.2.6. Immunofluorescence

Cells were stained for common endothelial, smooth muscle cell and fibroblast markers to characterise cell phenotype, and separately stained for phosphorylated p65 and oxidised CaMKII to assess inflammatory and oxidative signalling. After culture and stimulation, samples were fixed with ice-cold methanol for 20 minutes and washed with PBS (x3). Cells were then permeabilised with 0.25% Triton X-100 for 10 minutes and washed a further three times. Before incubation with primary antibodies, cells were blocked for 30 minutes with BSA (1% in PBS). Samples were incubated in primary antibodies (diluted in blocking buffer) overnight at the concentrations listed in Table 5.1.

Table 5.1. Primary antibodies, suppliers, secondary antibody species targets and concentrations for immunofluorescence antibodies used in this study.

Antibody	Supplier and Catalogue Number	Species	Concentrations
Von Willibrand Factor	Abcam #ab6994	Rabbit	1:100
Vimentin	Sigma-Aldrich #V5255	Mouse	1:400
Alpha-Smooth Muscle Cell Actin	Abcam #ab7817	Mouse	1:200
Phospho-p65 - WB	Cell Signalling Technologies #3033	Rabbit	1:1500
Phospho-p65 - IF	Cell Signalling Technologies #3031	Rabbit	1:1500
Oxidised-CaMKII	GeneTex #GTX36254	Rabbit	1:100

After primary antibody incubation, samples were washed with PBS (x3) then blocked again. Alexa Fluor 488 secondary antibodies were added against the primary antibodies as listed above at a 1:100 dilution (in blocking buffer) for 60 minutes.

Before counter staining with DAPI, samples were washed with PBS (x3). DAPI (100 ng/ml in PBS) was added for 5 minutes then samples were washed again (x2). Coverslip samples were mounted to glass slides using mowiol and plated cells and uncoated and coated strips were imaged immediately.

Negative antibody controls were prepared by staining cells with primary or secondary antibodies only, and for all antibodies there was no discernible fluorescence signal. Negative antibody control images are shown in Figure 5.1. and 5.12.

5.2.7. Conducting Polymer Coating Cell Culture

Conducting polymer coatings and uncoated samples (8 x 5 mm strips) were sterilised for 1 h in 70 % ethanol, then transferred to 48-well plates and allowed to air-dry for 1 h. Cells were seeded directly onto samples and incubated for up to 48 h, changing media every 24 h, before analysis.

5.2.8. Cell Viability and Proliferation Assay

MTT (3-(4,5-Dimethylthiazol-2-yl)-2,5-Diphenyltetrazolium Bromide) assays and acridine orange staining was carried out to assess cell viability after stimulations and, attachment and proliferation of cells on coated samples.

Assays were carried out as outlined in 4.2.6 and 4.2.7. with the following alterations:

MTT assays were reoptimized for use with 8 x 5 mm strips and accordingly the volume of DMSO added to resolubilise was reduced to 100 µl.

Fluorescence microscopy was carried out using an EVOS M7000 inverted microscope. A generic GFP light cube ($\lambda_{excitation}$ =470 nm, $\lambda_{emission}$ =525 nm) was chosen as the most suitable for imaging with acridine orange staining.

5.2.9. Immunoblotting

The immunoblotting method and antibodies used in this part of the study are outlined in section 4.2.9.

5.2.10. Oxidative Stress Assays

Broad intracellular oxidative stress was assessed using CellROX Green. After stimulation, 200 µl of CellROX Green reagent (5 µM in PBS) was added to each sample well and incubated at 37°C for 30 minutes. After washing (x3) with PBS, cells were fixed for 15 minutes with 3.6% formaldehyde. Cell nuclei were counterstained with Hoechst 33342 (1 µg/ml) for 10 minutes at room temperature and washed again with PBS (x3).

Cells were imaged with the EVOS M7000 system using the GFP light cube for CellROX Green and DAPI light cube for Hoechst 33342. Quantification of fluorescence was performed using ImageJ.

5.2.11. Statistical Analysis

The data and statistical analyses methods used in this part of the study have been previously described in section 4.2.11

5.3. Results

5.3.1. Characterisation of Human Coronary Artery Endothelial and Smooth Muscle Cells

Previously, HUVECs were assessed morphologically to ensure the purity of the culture. Immunocytochemistry was identified as a more appropriate technique to verify the cell phenotype and ensure a homogenous population. α-Smooth muscle cell actin, vimentin and von Willibrand Factor were identified as appropriate markers that could be used to confirm endothelial and smooth muscle cell phenotypes.

Figure 5.1. shows HCAECs and HCASMCs stained for vWF, vimentin, αSMC-actin and DAPI. HCAECs were found to stain positive for vWF expression and very strongly for vimentin expression, but no αSMC-actin expression was observed in these cells. This profile of expression was uniform across the cell population. HCASMCs were found to express αSMC-actin and strongly express vimentin, but no expression of vWF was observed and this was uniform over the cell population. Cell morphology can also be observed and HCAECs are smaller and more rounded than HCASMCs, which are highly elongated.

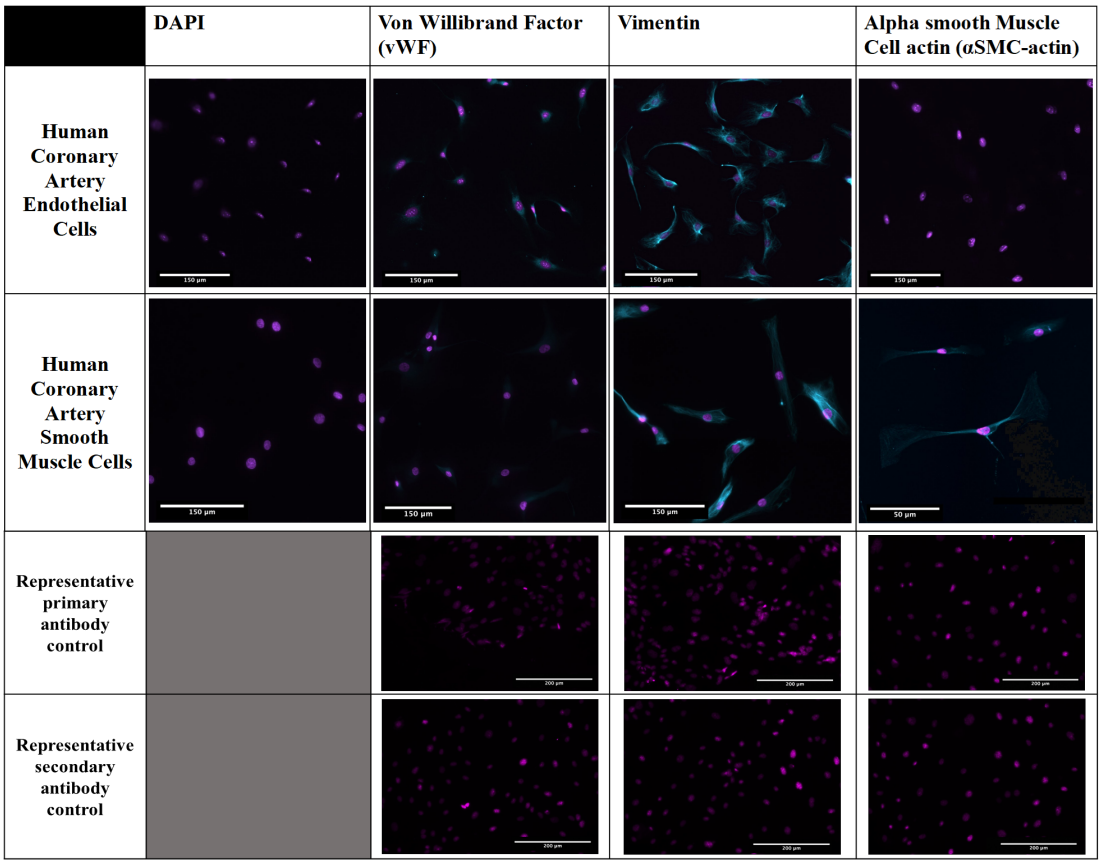

Figure 5.1. Immunofluorescent staining and imaging of HCAECs and HCASMCs for cell markers: von Willibrand Factor (vWF), vimentin and alpha-smooth muscle cell actin (αSMC-actin). Images show that HCAECs stain positive for vWF and strongly for vimentin, and HCASMCs stain positive for αSMC-actin and vimentin. Cyan: primary antibody target, Magenta: DAPI.

p65 and CaMKII were identified previously as relevant markers for inflammatory and oxidative stress, which in HUVECs could be activated, via oxidisation, by IL-1β or TNFα stimulation. Immunoblotting to confirm p65 and CaMKII expression in HCAEC and HCASMC is shown in Figure 5.2. p65 expression was comparable in all three cells with high expression observed in all cell types. CaMKII expression was found to be higher in HCASMC compared with endothelial cell types, particularly the band at the highest molecular weight position, which is predominant in these cells. In HCAECs, the lowest molecular weight band was predominant, matching the expression profile observed in HUVECs.

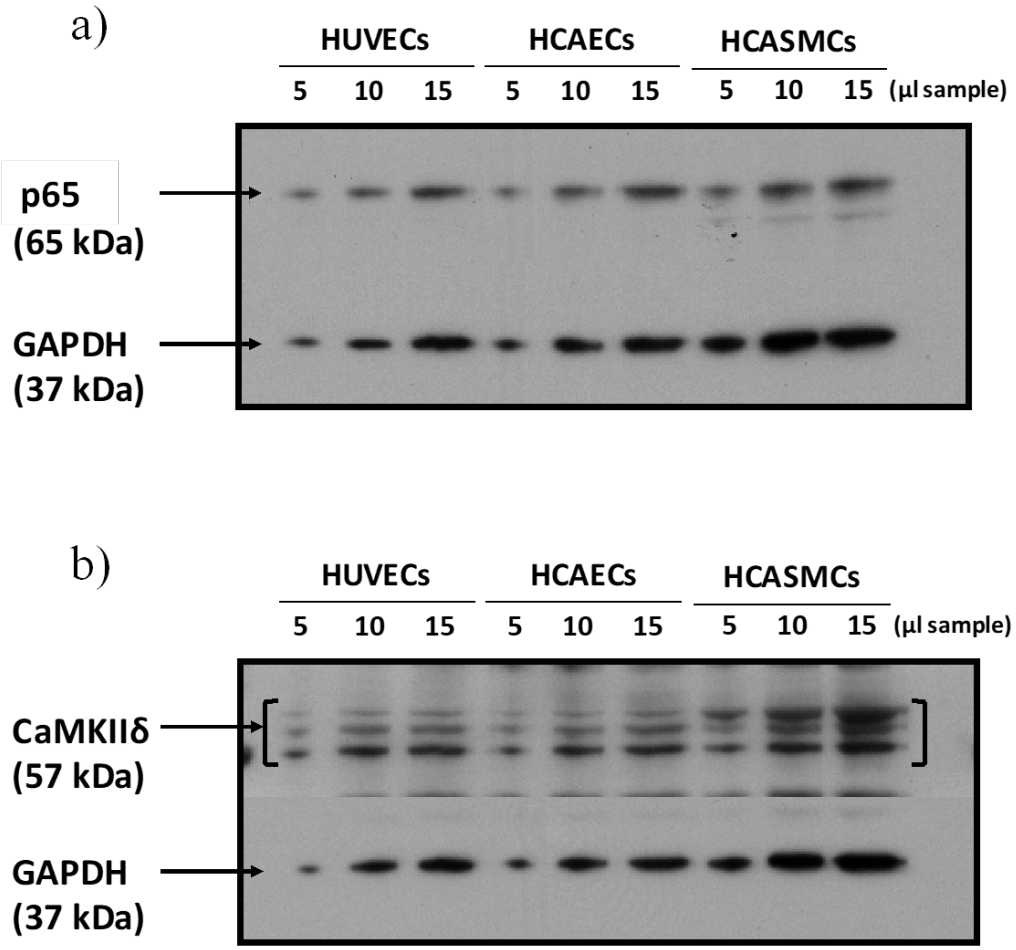

Figure 5.2. Expression of a) p65 and b) CaMKIIδ in HUVECs, HCAECs and HCASMCs, showing that both proteins are expressed in all three cell types. 5, 10 and 15 µl of cell lysates (approximately 10^6 cells/ml) were loaded for SDS-PAGE and GAPDH used as a loading control. p65 expression is comparable across the cell types, whereas CaMKIIδ expression appears to be greater in HCASMCs. Images representative of 3 independent blots.

The effects of cytokine stimulation on cell viability were assessed on HCAECs. This is shown in supplementary figure S5.1, with stimulation leading to broadly similar non-cytotoxic effects in HCAECs over the 6 h timepoint used. There was however a significant loss in HCAEC viability at the longest 6h timepoint with 10 ng/ml TNFα (6 h: 57.48±4.94, vs. unstimulated control: 100.00±13.82, mean% viable cells ± S.E.M, $p<0.01$, n=3, one-way ANOVA with post-hoc Dunnett's test).

5.3.2. p65 And CaMKII Activation in Human Primary Coronary Artery Cells

A central objective of this work was to validate the HUVEC cell-based model established in Chapter 4 in more relevant coronary artery cells. Initially, this focussed on activation of the inflammatory marker p65, and oxidation activated protein kinase CaMKII in HCAECs.

In HUVECs, phosphorylation of p65 was activated after 30-minute stimulation with both IL-1β or TNFα, and it was expected that HCAECs would mirror this activation response. This was confirmed by an initial six-hour stimulation of HCAECs with both stimulants, resulting in high p65 phosphorylation at 30-minutes and a similar overall activation profile to HUVECs. This is shown in Supplementary Figure S5.2. 30-minute stimulation was assessed more thoroughly and confirmed to significantly activate p65, via phosphorylation in HCAECs (Figure 5.3), with IL-1β (panel a) leading to a 1.93±0.29-fold increase in phospho-p65 expression, and TNFα stimulation (panel b) leading to a 1.54±0.15-fold increase (vs. unstimulated control cells, $n=4$, $p<0.05$, unpaired t-test).

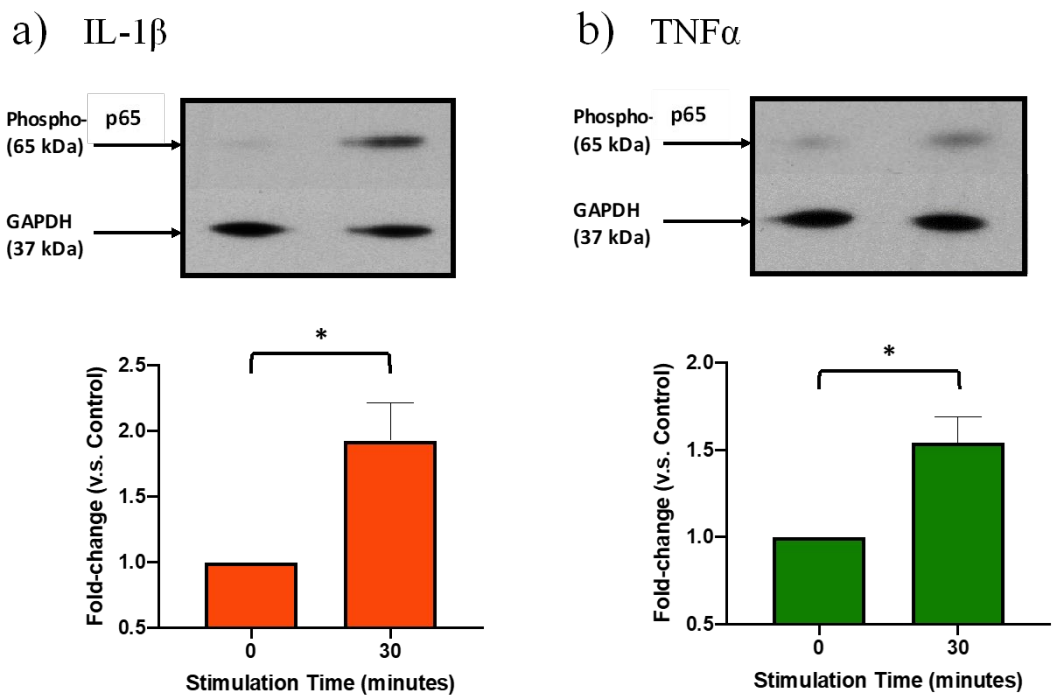

Figure 5.3. Expression change in phospho-p65 in HCAECs after stimulation with IL-1β (panel a) and TNFα (panel b) (both 10 ng/ml) for 30 minutes. Immunoblotting shows stimulation with both cytokines generates significant p65 activation, via phosphorylation, in HCAECs ($p<0.05$, n=4, unpaired t-test). This mirrors the response observed in HUVECs.

Unlike activation of p65 in HCAECs, CaMKII activation did not completely reflect the responses observed in HUVECs. Figure 5.4. shows phosphorylated-CaMKII expression after cytokine stimulation in HCAECs. Phospho-CaMKII expression was not significantly affected by either IL-1β (panel a) or TNFα (panel b) stimulation ($p>0.05$, n=4, One-way ANOVA), this mirrors the HUVEC response. Oxidation of CaMKII differed in these cells and Figure 5.5 shows oxidised-CaMKII expression after cytokine stimulation in HCAECs. Unlike in HUVECs, IL-1β (panel a) did not induce significant CaMKII activation, via oxidation within 6 h ($p>0.05$, n=4, One-way ANOVA). TNFα (panel b) stimulation however induced significant CaMKII oxidation at 6 h, when compared with unstimulated cells (6 h: 1.50±0.13, vs. 0 h: 1.00±0.00, $p<0.05$, n=4, One-way ANOVA with post-hoc Dunnett's test).

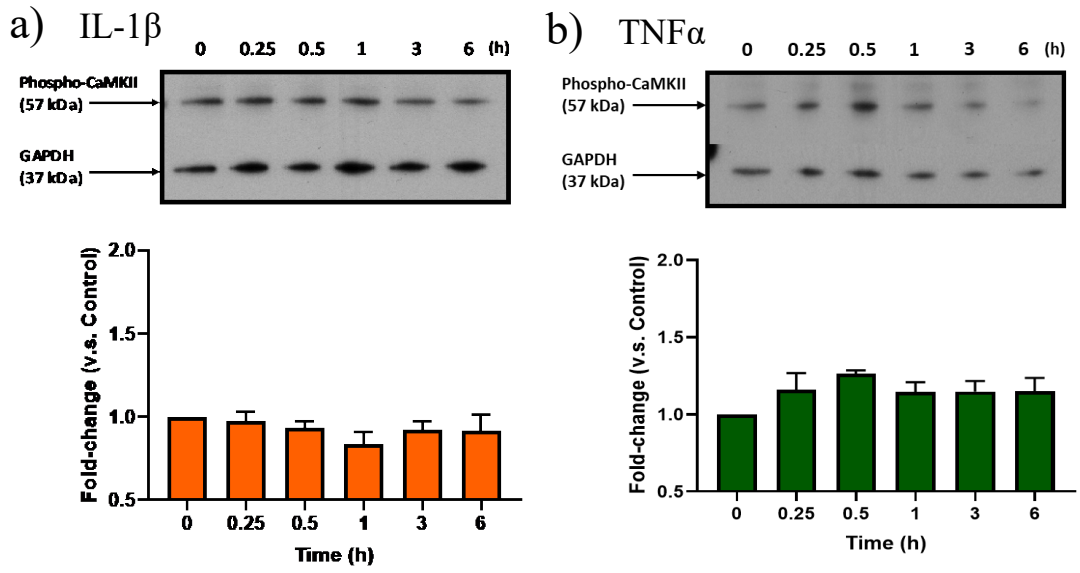

Figure 5.4. Expression change in phospho-CaMKII in HCAECs after stimulation with IL-1β (panel a) and TNFα (panel b) (both 10 ng/ml) for up to 6 hours. Immunoblotting shows stimulation with neither cytokine generated any significant change in phospho-CaMKII expression in HCAECs ($p>0.05$, $n=4$, One-way ANOVA). This suggests both cytokines do not induce CaMKII phosphorylation under the conditions studied.

Overall, HCAEC response to cytokine stimulation was broadly similar to HUVECs. p65 was activated in response to both IL-1β and TNFα, with 30-minute stimulation identified as a suitable time to initiate pro-inflammatory signalling. CaMKII phosphorylation was not triggered by either cytokine, but CaMKII oxidation occurred in response to TNFα only after 6 h, whereas this response was observed after IL-1β stimulation only in HUVECs.

HCASMCs were also considered for use with this cell-based model and p65 activation in these cells was also assessed. Supplementary Figures S5.3 shows the response of p65 in HCASMCs to cytokine stimulation. HCASMCs had a similar pro-inflammatory response to 10 ng/ml IL-1β stimulation, with significant peak activation after 30 minutes (0.5 h: 1.77±0.08, vs. 0 h: 1.00±0.00, $p<0.001$, n=4, One-way ANOVA with post-hoc Dunnett's test), but no significant increase was observed after TNFα (10 ng/ml) stimulation ($p>0.05$, n=4, One-way ANOVA). Due to issues associated with the difficulty of HCASMC culture, the lack of p65 activation after 10 ng/ml TNFα stimulation and time-constraints, it was decided that focus would be given in this study to further developing the endothelial cell-based model. This would allow focus on the PPy antioxidant benefit to be assessed in terms of the response of endothelial cells.

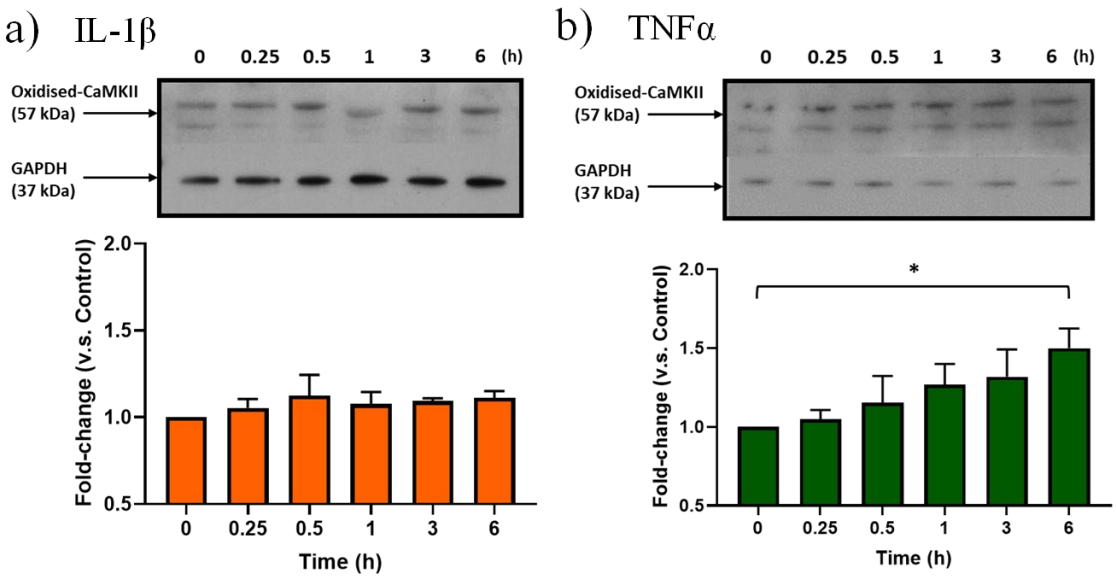

Figure 5.5. Expression change in ox-CaMKII in HCAECs after stimulation with IL-1β (panel a) and TNFα (panel b) (both 10 ng/ml) for up to 6 hours. Immunoblotting shows stimulation with TNFα (6 h) generated significant CaMKII oxidation in HCAECs ($p<0.05$, n=4, One-way ANOVA with post-hoc Dunnett's). This activation is in contrast with the response observed in HUVECs, where only IL-1β stimulation induced significant CaMKII oxidation.

5.3.3. Stability of polypyrrole antioxidant activity in cell culture media

In Chapter 4, HUVEC media was shown to reduce the DPPH scavenging capacity of PPy coated samples after incubation at 37°C, resulting in a rapid loss of the coating's broad antioxidant activity. In this study, the media used was changed for the culture of HCAEC and HCASMCs, so it was considered useful to reassess the effects these culture mediums may have on PPy antioxidant capacity.

Figure 5.6. shows the depletion of DPPH scavenging capacity of potentiostatic (panel a) and galvanostatic (panel b) PPy coatings in HCAEC media after incubation. Potentiostatic coatings produced at 1.1 V and 1.3 V both demonstrated a rapid loss in DPPH scavenging capacity. This loss was modelled for both coatings as a single-phase exponential decay reponse. The loss was more pronounced with 1.1 V coating with significantly lower mean antioxidant activity at 24 h (1.1 V: 35.17±1.97, vs. 1.3 V: 54.62±4.22, $p>0.05$, n=3, two-way ANOVA with post-hoc Šídák), but at 72 h, no significant difference was observed between the two potentiostatic coatings (1.1 V: 24.73±4.77, vs. 1.3 V: 33.79±3.02, $p>0.05$, n=3, two-way ANOVA with post-hoc Šídák).
Galvanostatic coatings produced at 0.5 mA and 1 mA also demonstrated a loss in DPPH scavenging capacity after incubation in HCAEC media, although 1 mA demonstrated a slower linear loss in capacity compared with the single-phase exponential decay response observed with 0.5 mA coatings. After 72 h, this depletion resulted in a significant difference between the DPPH scavenging capacities of 1 mA vs. 0.5 mA coatings (0.5 mA: 28.65±4.42, vs. 1 mA: 62.87±3.21, $p<0.05$, n=3, two-way ANOVA with post-hoc Šídák). For both coatings generated by potentiostatic and galvanostatic electropolymerisation, at time points used, all PPy coatings tested retained significantly greater DPPH scavenging capacity when compared against the bare 316L SS control ($p<0.05$, n=3, Šídák).

Loss of DPPH scavenging capacity was also assessed after incubation in HCASMC media and this is shown in Supplementary Figure S5.4. In this media, PPy samples exhibited a slower loss in scavenging capacity, with a linear depletion by 1.3 V potentiostatic and 0.5 and 1 mA galvanostatic coatings. A single-phase exponential decay was only observed with 1.1 V coatings, but due to the early plateau in this response, the DPPH scavenging capacity at 72 h was not significantly lower than 1.3 V coatings (1.1 V: 34.27±4.12, vs. 1.3 V: 37.11±1.99, $p>0.05$, n=3, two-way ANOVA with post-hoc Šídák). The reduced depletion in this medium

similarly led to all PPy coatings retaining significantly greater DPPH scavenging capacity compared against the bare 316L SS control ($p<0.05$, n=4, Šídák).

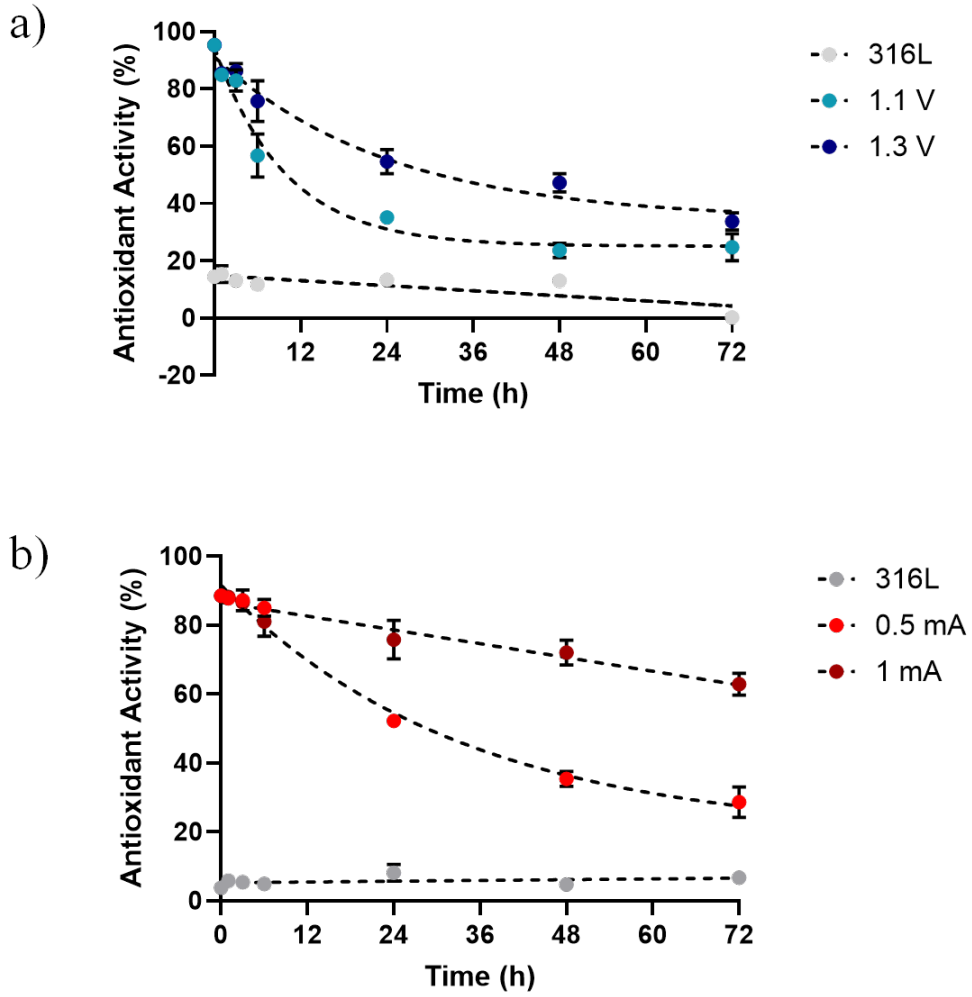

Figure 5.6. DPPH scavenging activity after incubation in HCAEC Media (EGM MV2) of potentiostatic (panel a) and galvanostatic (panel b) PPy coatings. At every time point, all PPy coatings tested demonstrate better scavenging capacity compared with the bare 316L SS. All but 1 mA galvanostatic coatings showed an exponential depreciation in DPPH scavenging capacity. 1 mA coatings retained the greatest DPPH scavenging capacity with a slow linear depreciation. Data points represents average DPPH scavenging activity ± S.E.M (n=3).

5.3.4. Endothelial Cell Compatibility of PPy coated stainless steel strips

Optimisation of cell assays, MTT and acridine orange, used to assess viability, attachment and proliferation are shown in Supplementary figure S5.5. Increasing cell densities were seeded on tissue culture plastic well plates (TCP) and 316L, and MTT and acridine orange used to assess cell attachment at 24 h. Increasing seeding density led to a linear increase in MTT absorbance with comparable viability observed on 316L and TCP. This is reflected in acridine orange imaging, although cells appear more spread on TCP than 316L SS surfaces. 5 $x10^4$ cells was chosen as an appropriate seeding density as it resulted in sufficient MTT absorbance, while imaging demonstrated high confluence with sufficient surface area remaining for proliferation.

MTT viability of HCAECs on PPy coated and 316L SS strips at 24 h, as a measure of initial attachment, and 48 h, as a measure of proliferation is shown in Figure 5.7. At 24 h, MTT absorbance was significantly lower on bare 316L SS and all PPy coated samples used when compared with the tissue culture plastic positive control (316L: 0.06±0.00; 1.1 V: 0.04±0.01; 1.3 V: 0.04±0.01; 1 mA: 0.05±0.01; 2 mA: 0.05±0.01, vs. TCP: 0.17±0.01, n=4, $p<0.001$, two-way ANOVA with post-hoc Tukey test). This suggests cell attachment was reduced on the coated and uncoated strips compared with TCP or that cell viability is diminished.

At 48 h however, a significant increase in MTT absorbance was observed on 316L SS samples (24 h: 0.06±0.00, vs. 48 h: 0.19±0.03, n=4, $p<0.001$, two-way ANOVA with post-hoc Šídák test) leading to no significant difference between this surface when compared with the TCP control (316L: 0.19±0.03, vs. TCP: 0.19±0.04, n=4, $p>0.05$, two-way ANOVA with post-hoc Tukey test). Comparable high increases in absorbance were not observed on PPy samples, resulting in significantly lower MTT absorbance compared with the 316L strips and TCP control (316L and TCP, vs. 1.1 V: 0.07±0.02; 1.3 V: 0.04±0.01; 1 mA: 0.09±0.00; 2 mA: 0.04±0.01, n=4, $p<0.01$, two-way ANOVA with post-hoc Tukey test). This suggests that significant cell proliferation or increase in cell viability occurred on 316L SS strips between the 24 and 48 h time points, which did not occur on any PPy surface used.

Images of acridine orange stained HCAECs attached to PPy coated and 316L SS strips, and TCP at 24 and 48 h are shown in Supplementary Figure 5.6. Similar observations are made when assessing attachment and proliferation from these images. There is a very clear and

substantial increase in the number of attached cells from 24 to 48 h on 316L strips and this confirms that the high seeding density used results in near confluent cell monolayer at 24 h with TCP, which is maintained at 48 h. These images do however show possible differences between PPy coatings, with a higher number of cells present at 48 h on 1 mA strips, suggesting that these coatings may be the most appropriate to use, although this does not reflect the cell viability data obtained from MTT assays.

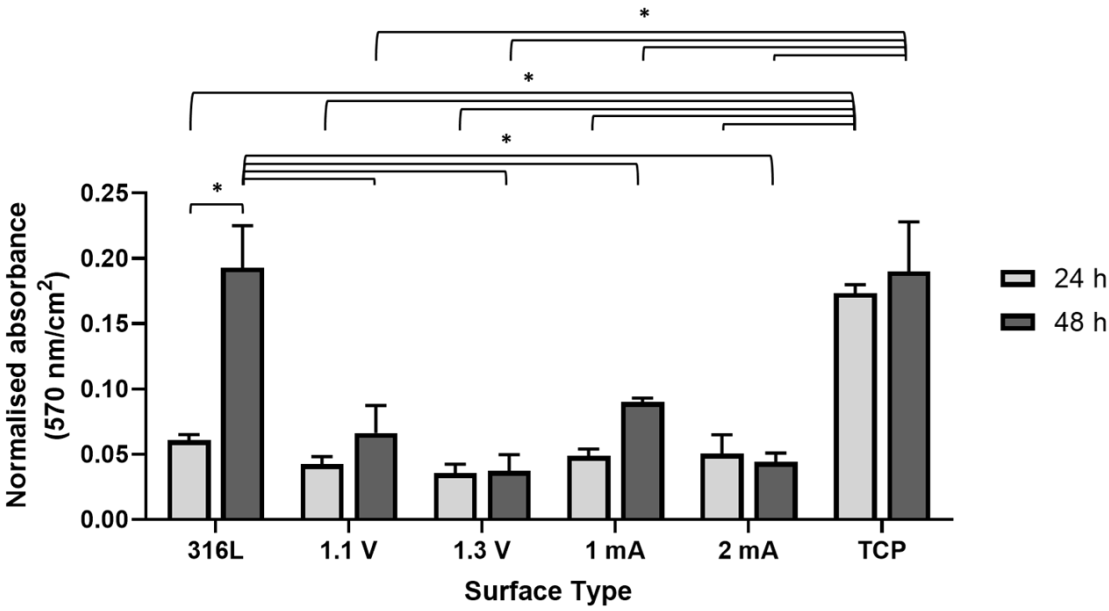

Figure 5.7. Normalised cell viability of HCAECs (5 x 10^4) seeded on PPy, 316L SS strips and tissue culture plastic (TCP). At 24 h, cell viability is low on SS and PPy substrates, indicating lower cell attachment than TCP. At 48 h, viability remains low on PPy samples, but cell viability is significantly increased on the SS substrate, suggesting significant proliferation between 24 and 48 h on this surface. ($p<0.05$, n=4, Two-way ANOVA with post-hoc Tukey (surface type) and Šídák (time) tests).

Due to the poor HCAEC attachment observed on PPy samples, further conditions were tested. PPy samples, generated potentiostatically at 1.1 V and galvanostatically at 1 mA, were tested again using the same experimental conditions, after an initial 24 h PBS salicylate release step. It was hoped that pre-releasing the salicylate dopant before cell seeding would enhance cell attachment and proliferation. The results of these tests are shown in Figure 5.8. and HCAECs attached to these PPy samples showed improved cell viability and notable improvements in cell number at 48 h compared with PPy samples without salicylate elution. PBS elution was therefore used as a pre-processing step before cell seeding in subsequent experiments.

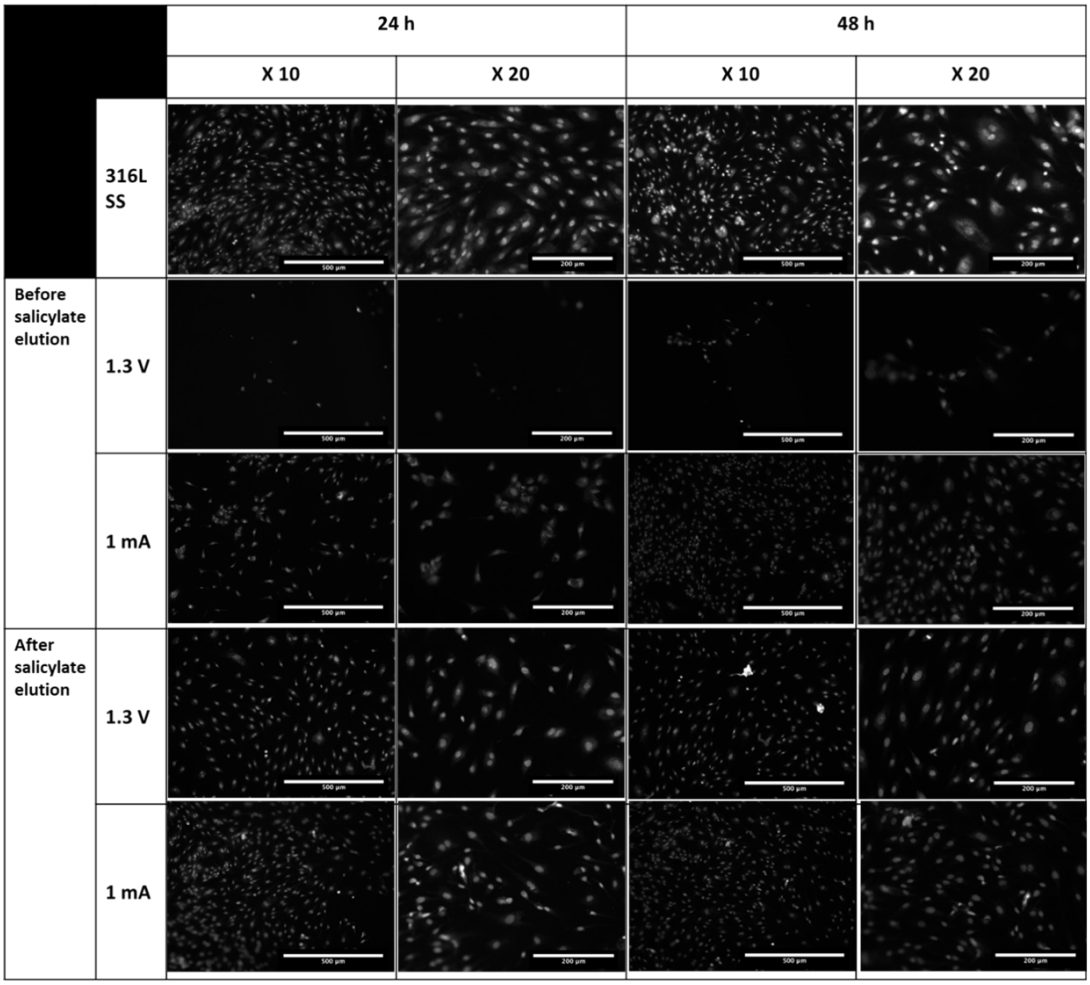

Figure 5.8. Acridine orange stained HCAECs attached to potentiostatically and galvanostatically PPy-coated and uncoated 316L SS strips. $1x10^5$ cells were seeded onto each coating and imaged after 24 and 48 h. Samples labelled "before salicylate elution" were sterilised in 70% ethanol without any pre-elution of salicylate. Samples labelled "after salicylate elution" were sterilised in 70% ethanol after 24 h elution of salicylate in sterile PBS. This figure shows that pre-elution of salicylate before cell seeding improved endothelial attachment. Each image is representative of 1 sample.

5.3.5. Oxidative Stress in PPy-attached human coronary artery endothelial cells

Oxidative stress was assessed in HCAECs attached to uncoated and PPy-coated 316L SS strips with and without TNFα stimulation by quantifying CellROX fluorescence and normalising this against Hoechst fluorescence obtained from the same area to correct for cell number differences. This assay was first optimised to find a suitable CellROX concentration and to validate the effectiveness of TNFα stimulation in generating intracellular oxidative stress in HCAECs. The results of these optimisations are shown in Supplementary Figures S5.7.

After trialling 1, 5 and 10 μM CellROX probes, 5 μM was selected as the optimal concentration as this concentration provided a visually detectable and quantifiable fluorescent signal, whereas the signal was poor when using 1 μM of the marker. Adding 10 μM resulted in a stronger fluorescent signal, but this also resulting in a higher basal signal, which could reduce the sensitivity of this assay. When using 5 μM CellROX, TNFα stimulation, along with hydrogen peroxide, were both shown to stimulate intracellular ROS generation in HCAECs. Significant increases in normalised fluorescence were observed for both hydrogen peroxide (control: 0.35±0.04, vs. 0.48±0.03) and TNFα (control vs. 0.47±0.00, $p<0.05$, $n=3$, One-way ANOVA with post-hoc Dunnett's.) stimulation. IL-1β stimulation was also tested but did not generate significant intracellular oxidative stress. Since only tissue culture plates were used, no background correction was applied.

When assessing oxidative stress in HCAECs on PPy coatings, cells were seeded on samples 48 h before TNFα stimulation. After quantifying CellROX and Hoechst fluorescence, normalised absorbance was calculated by subtracting background fluorescence taken from cell-free samples and normalising CellROX fluorescence against Hoechst fluorescence. Fold-changes were not used since the unstimulated control samples exhibited high variance in normalised ROS expression. Normalised absorbance values for ROS expression in HCAECs after TNFα is shown in Figure 5.9.

Differences in ROS expression between samples were initially compared with a two-way ANOVA and post-hoc Sidak, to compare within sample groups between stimulated and unstimulated samples, and Tukey tests, to compare both control and stimulated samples between sample groups. Using these tests, no significant differences were observed between

the groups or within the samples group. Due to visible differences in sample means, less powerful statistical tests were also performed. Repeat unpaired t-tests with Holm-Sidak correction were used to compare within sample groups between stimulated and unstimulated samples and two, one-way ANOVAs with post-hoc Tukey tests used to compare between sample groups. Repeated unpaired t-tests highlighted a significant increase in ROS generation after TNFα stimulation in HCAECs on the TCP control surfaces (control: 0.14±0.05, vs. TNFα: 0.39±0.01, $p<0.01$, n=4). One-way ANOVA on control samples showed no significant difference, but in TNFα stimulated cells did highlight a significant increase in ROS expression on 1.3 V PPy samples (0.69±0.14), vs. TCP (0.39±0.01, $p<0.05$, n=3), 316L (0.35±0.03, $p<0.05$, n=3) and 1 mA (0.26±0.06, $p<0.01$, n=3).

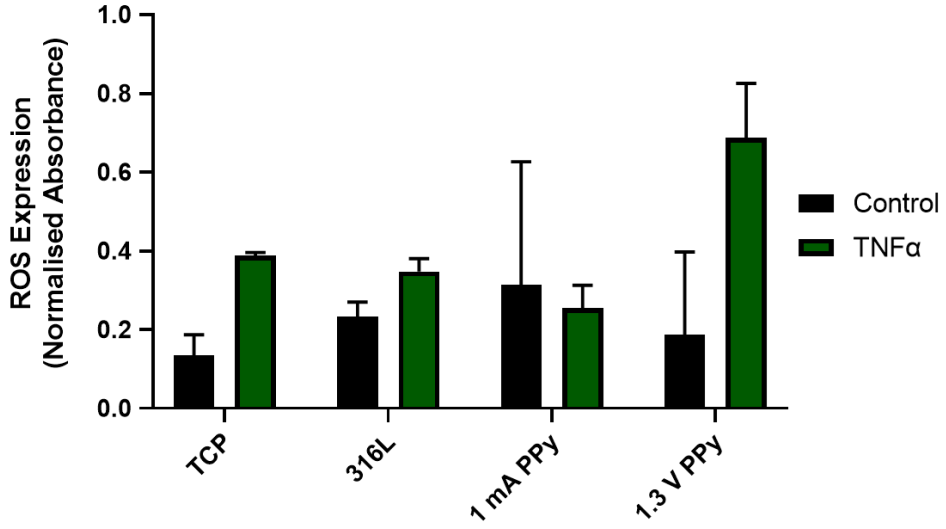

Figure 5.9. Quantification of CellROX fluorescence in HCAECs attached to tissue culture plastic (TCP), bare 316L SS strips and PPy coated strips. Expression was calculated by quantifying total image intensity for CellROX signal and normalised against total Hoechst intensity. Two-way ANOVA with post-hoc Tukey and Sidak tests were performed, with no significant difference between groups observed ($p > 0.05$, n=3/4).

Figure 5.10. shows representative fluorescence images of HCAECs attached to TCP, uncoated and PPy-coated SS samples stained with CellROX and Hoechst 33342 after TNFα (10 ng/ml; 6 h) stimulation. These images show very low fluorescence signals from HCAECs attached to all surfaces before stimulation and highlight the very high CellROX signal of HCAECs

attached to 1.3 V PPy samples after TNFα stimulation. Hoechst fluorescence is also visibly higher in HCAECs attached to 316L SS samples, and also 1.3 V PPy samples, although less so than SS. This highlights the need for normalising fluorescence measurements in this protocol.

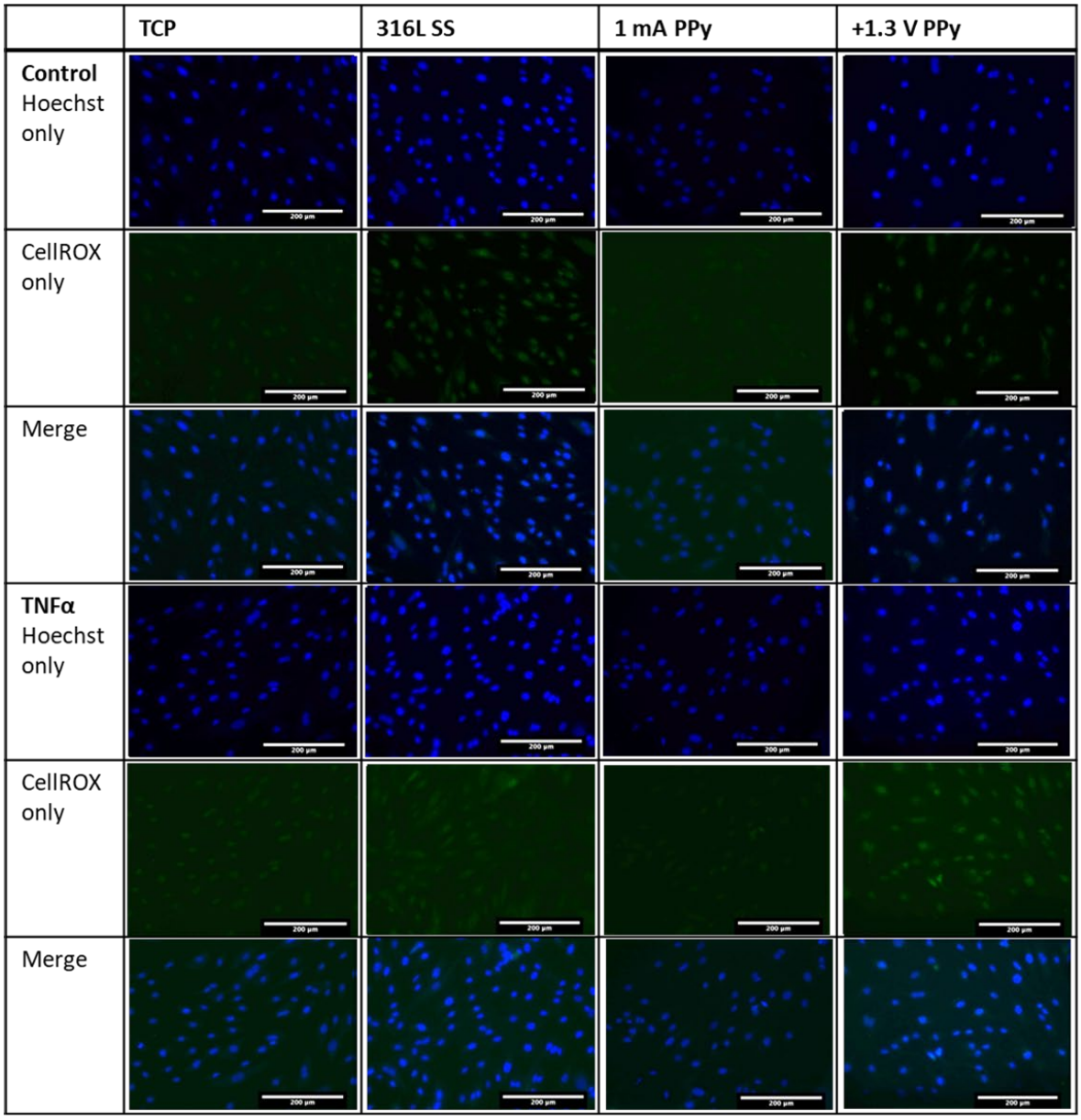

Figure 5.10. Representative images of CellROX and Hoechst fluorescence in HCAECs attached to tissue culture plastic (TCP), bare 316L SS strips and PPy coated strips, with and without TNFα (10 ng/ml; 6 h) stimulation. Images are representative of observed results for each samples type (n=4; 6 areas imaged per sample).

5.3.6. CaMKII oxidation in PPy-attached human coronary artery endothelial cells

As with the CellROX assay, to assess inflammatory and oxidative protein activation in HCAECs, cells were seeded 48 h before imaging and normalisation was carried out using the same process of background subtraction and Hoechst normalisation. Phosphorylated p65 was initially intended to be used as a model for pro-inflammatory signalling, as indicated in Figure 5.3. Optimisation of the immunocytochemistry staining for phospho-p65 in HCAECs is shown in Supplementary Figure S5.8. When used with immunocytochemistry, available antibodies raised against phospho-p65 were not found to provide a strong measurable signal, despite high phospho-p65 signal confirmed by WB. WB antibodies were found to provide a stronger, albeit weak signal, requiring a high concentration of antibody. Since the WB antibody is not certified for use with fluorescence microscopy, focus was given to the oxidised-CaMKII model of oxidative stress as this is the primary therapeutic target of interest in this study.

Oxidised-CaMKII antibodies were optimised for immunocytochemistry and immunofluorescence and quantification and representation images are shown in Supplementary Figure S5.9. Since only TCP was used in these experiments, no background correction was used. 1:200 antibody dilution was found to be most suitable and provide a suitable signal strength and under these conditions, significant increases in oxidised-CaMKII expression were observed after hydrogen peroxide (control: 0.31±0.01, vs. 0.76±0.03, $p<0.001$), TNFα (control: 0.31±0.01, vs. 0.72±0.04, $p<0.001$), and IL-1β (control: 0.31±0.01, vs. 0.50±0.01, $p<0.01$, n=3, One-way ANOVA with post-hoc Dunnett's) stimulation.

Oxidised-CaMKII expression was assessed in HCAECs attached to TCP and PPy-coated and uncoated 316L samples and this is shown as normalised absorbance in Figure 5.11. As with CellROX assessment, a two-way ANOVA and post-hoc Sidak was initially used to compare within sample groups between stimulated and unstimulated samples, and post-hoc Tukey tests, to compare both control and stimulated samples between sample groups. With this comparison, a significant reduction in oxidised-CaMKII expression in HCAECs attached to 1 mA after TNFα stimulation was observed compared with TCP (TCP: 1.93±0.19, vs. 1 mA: 0.75±0.06, $p<0.05$, n=4).

As with CellROX data, less powerful statistical tests were also performed. Repeat unpaired t-tests with Holm-Sidak correction were used to compare within sample groups and two, one-

way ANOVAs with post-hoc Tukey tests to compare between sample groups. Unpaired t-tests highlighted a significant increase in oxidised-CaMKII expression after TNFα stimulation with TCP control samples. (control: 1.02±0.13, vs. TNFα: 1.93±0.19, $p<0.01$, n=4), but no significant increase was observed in one-way ANOVAs of either the control or TNFα group ($p>0.05$).

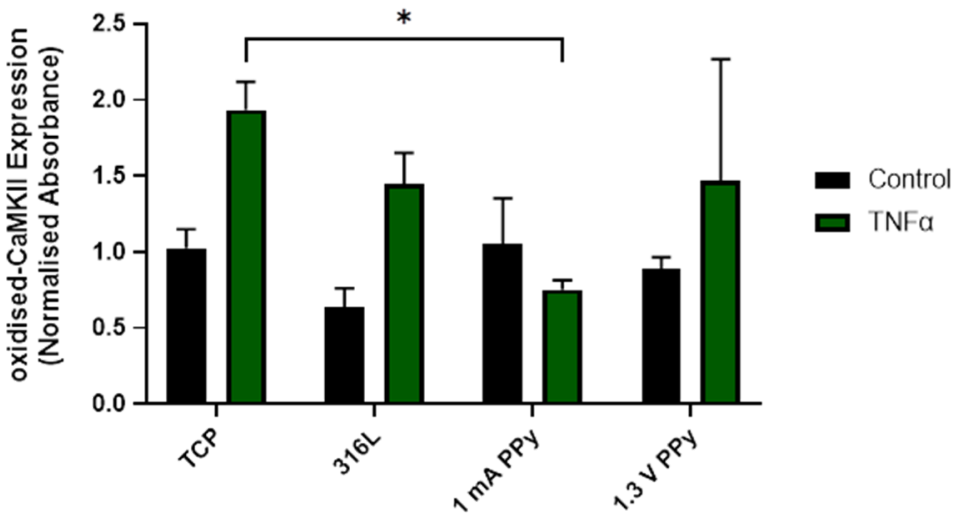

Figure 5.11. Quantification of oxidised-CaMKII fluorescence in HCAECs attached to tissue culture plastic (TCP), bare 316L SS strips and PPy coated strips. Expression was calculated by quantifying total image intensity for oxidisedCaMKII signal and normalised against total Hoechst intensity. Two-way ANOVA with post-hoc Tukey and Sidak tests were performed, with no significant difference between groups observed ($p > 0.05$, n=3/4).

Figure 5.12. shows representative fluorescence images of HCAECs attached to TCP, uncoated and PPy-coated SS samples stained with oxidised-CaMKII antibodies and Hoechst 33342 after TNFα (10 ng/ml; 6 h) stimulation. Overall, after stimulation, a clear increase in oxidised-CaMKII expression is observable over all sample surface types and this appears greatest on TCP and PPy surfaces generated potentiostatically at 1.3 V. As with CellROX samples, Hoechst fluorescence appeared visibly higher in HCAECs attached to 316L SS samples, although strong fluorescence was also observed in cells attached to TCP. From the Hoechst signal, a smaller number of attached cells is also visible on PPy surfaces compared with both TCP and uncoated 316L SS. This is similar, but more pronounced, than in the CellROX data.

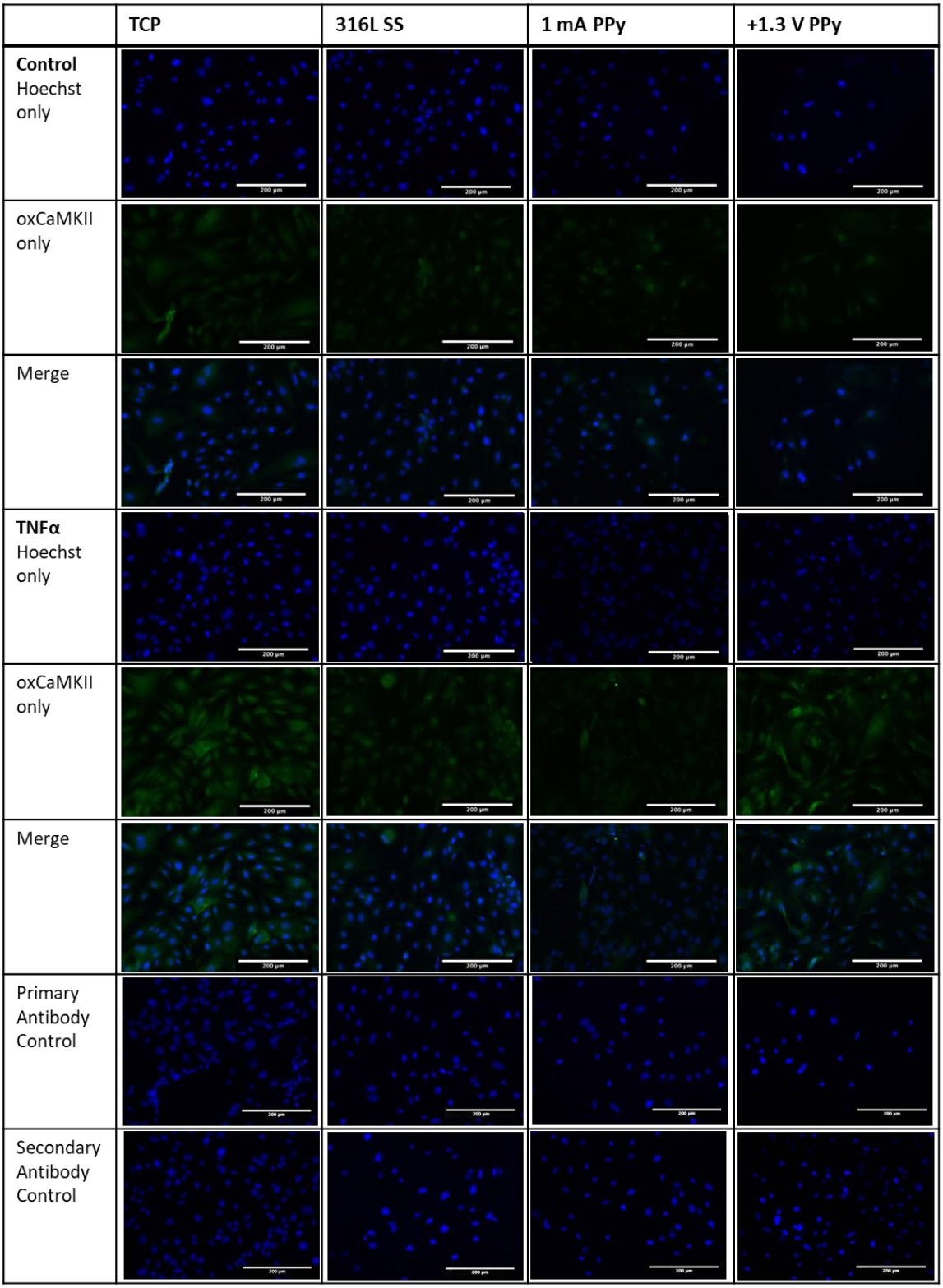

Figure 5.12. Representative images of oxidised-CaMKII (oxCaMKII) and Hoechst fluorescence in HCAECs attached to tissue culture plastic (TCP), bare 316L SS strips and PPy coated strips, with and without TNFα (10 ng/ml; 6 h) stimulation. Images are representative of observed results for each samples type (n=4; 6 areas imaged per sample).

5.4 Discussion

It has been shown in Chapter 4 of this present study that HUVECs offer a useful endothelial model of inflammatory and oxidative stress. It is however necessary to establish a model that is relevant to the biological environment in the coronary artery after stent placement. The results presented in this chapter examine the suitability of HCAECs in this application and this discussion will explore whether they can be reliably used. The potential to also incorporate HCASMCs was briefly considered, and this will also be discussed. Furthermore, HCAECs were used to assess the potential biological effects of PPy antioxidant activity and these effects will be explored and compared against reported PPy properties.

5.4.1. Characterisation of human coronary artery cells

Cell Characterisation

Previously, HUVEC morphology was assessed as a confirmatory test to confirm cell population heterogeneity and to give confidence that cells are representative of an endothelial cell type. It was concluded in Chapter 4, and from previous work in our laboratory (McMullen, et al. 2021), that immunocytochemistry with relevant cell markers could provide greater confidence in cell suitability. HCAECs were stained with von Willibrand Factor (vWF), alpha-SMC actin (aSMC-actin) and vimentin and this is shown in Figure 5.1.

Of these markers, the HCAECs used in this study stained positive for vWF and strongly for vimentin. Von Willibrand Marker is an important endothelial cell markers and HCAECs are also known to express vimentin (Lakota, et al. 2011), and this expression is representative of what would be expected from an endothelial cell population. Although vimentin expression is normal within HCAECs, high expression may also be an indicator of endothelial cells undergoing endothelial to meschchymal transition (EndMT) as vimentin is upregulated in this progress (Wang, et al. 2017). Since vWF is expressed, this cannot be confirmed, but could be identified by considering other markers specific to EndMT such as Snail, Slug and Twist. Interestingly, vimentin and EndMT are beginning to be considered more important as an indicator and propagator of vascular disease (van Engeland, et al. 2019; Chen, et al. 2020). As such, these factors could be explored when further developing an *in vitro* endothelial model.

The expression of these markers was also assessed for HCASMCs and these cells were found to stain positive for αSMC-actin and vimentin and these images are also shown in Figure 5.1.

As with endothelial cells, SMCs are known to abundantly express vimentin (Wang, et al. 2006). αSMC-actin is a key marker of SMC phenotype, but with SMCs in culture this becomes less useful since expression may change depending on the synthetic-contractile state of these cells (Rensen, et al. 2007). This may explain the lower expression in our cells, indicating a synthetic phenotype.

CaMKII and p65 expression

The high and uniform expression of total p65 is not surprising in either human endothelial or smooth muscle cells as p65 is known to be expressed in almost all cell type due to its fundamental role in the cell-stimuli response (Oeckinghaus & Ghosh, 2009). The high expression observed in this study does however confirm the suitability of our immunoblotting and sample preparation technique.

Basal CaMKII expression was also assessed and found to be high in both endothelial and vascular SMCs, as shown in Figure 5.2. CaMKII expression has been previously shown in cultured HCAECs by immunoblotting, with its activation linked to pro-inflammatory and pro-apoptotic effects (Ampem, et al. 2016). Ramirez-Sanchez, et al. (2010), also established the expression of CaMKII in HCAECs and links the activation in these cells to increased eNOS phosphorylation and NO production, ultimately leading to a vasodilatory and antioxidant effect.

CaMKII expression has also been identified in HCASMCs (Maione, et al. 2017), but this is less established than in HCAECs and is not widely reported. In VSMCs, expression and activation of CaMKII is linked with pathological H_2O_2 signalling (Bouallegue, et al. 2009), but unfortunately due to the sparse use of HCASMCs in CaMKII studies, this is not established in this specific cell type.

There was a clear difference in the observed protein expression profiles between HCAECs and HCASMCs. There is little reported on the specific CaMKII isoform expression in HCEACs, but in our immunoblots, these cells exhibit a very similar expression profile to HUVECs which are known to express predominantly CaMKIIδ_6 (Wang, et al, 2010). Similarly, HCASMC CaMKII isoforms are not reported, but in aortic SMCs, CaMKIIδ_2 is identified as a dominant isoform although, VSMCs also express γ isoforms (House, et al. 2007). This γ isoform expression may be responsible for the observed difference in expression profile. Unlike δ-

isoforms, these γ isoforms have an anti-proliferative and anti-atherogenic effect in SMCs (Saddouk, et al. 2015).

Cell Viability after Stimulation

As with HUVECs, the effect of stimulation on cell viability was assessed in HCAECs and shown in Supplementary Figure S5.1. Unlike HUVECs, HCAECs were found to be in some part sensitive to TNFα stimulation, resulting in a significant loss of viability at 6 h. This is different to what was observed in HUVECs, where there were potentially beneficial effects of TNFα stimulation, and this is supported in the literature (Wang, et al. 2017). The reduction in HCAEC viability observed after TNFα stimulation in this study has received little attention in the literature.

Stimulation times of 6 hours with 10 ng/ml TNFα were selected in this study for the confirmed stimulatory effects seen in HUVECs which are confirmed in the follow up optimisation data. Due to the loss of viability with HCAECs following TNFα stimulation, there is a risk of poor cell recovery, but this is not observed in protein recovery with western blotting or immunofluorescence. A more critical issue however is the relevance of our model. If TNFα is inducing cell death and apoptosis, this may reflect an oxidative environment in excess of that observed clinically. This may or may not be reflective of the physiological environment after stent placement, and due to the differences in patient response, this environment will also be different across patient groups and outcomes.

The use of highly stressed and potentially apoptotic cells is supported in the literature, since stent placement has been shown to induce apoptosis in the coronary endothelium (Cornelissen & Vogt, 2018). Furthermore, this apoptotic state is linked to reduced NO bioavailability and NO is shown to be directly downregulated by TNFα through post-translational downregulation, although this is unlikely to be captured by our acute stimulation (Yan, et al. 2008).

5.4.2. Human coronary artery endothelial cells as a model for endothelial inflammatory and oxidative stress

HCAECs were chosen in this study as they should provide the most relevant *in vitro* model for the stresses experienced after stenting which may drive restenosis. Furthermore, the use of HCAECs allows more comparable assessment of results obtained with this *in vitro* model to clinical data. As with HUVECs, the method of stimulation with these cells was considered carefully to ensure the suitability of any stimulant and relevance of any observed responses.

TNFα, IL-1β and hydrogen peroxide were used in this model based on the preliminary HUVEC data presented in Chapter 4, but also clinical evidence justifying their appropriateness. Specifically, TNFα was identified as the most relevant stimulant since increases in this cytokine after stent placement correlates strongly with restenosis (Bittar, et al. 2005). The effects of TNFα and IL-1β stimulation on p65 (Figure 5.3.) and CaMKII activation (Figures 5.4 & 5.5.) in HCAECs broadly reflect those observed in HUVECs although the oxidation of CaMKII was only observed after IL-1β stimulation in HUVECs and only after TNFα stimulation in HCAECs.

This response is expected since TNFα and IL-1β (10 ng/ml; 2h) have both been shown to promote NF-κB induction in HCAECs (Csiszar, et al. 2006). Interestingly, Csiszar, et al. (2006), found that intervention with resveratrol, a common antioxidant possessing strong HAT capacity, dampened the TNFα and IL-1β-induced NF-κB activation. CaMKII activation in HCAECs is however less established. In our study, improved activation in response to stimulants was expected since the EGM MV2 media used for HCAECs does not contain heparin, unlike the media used with HUVECs. Heparin is known to activate CaMKII (Li, et al. 2019). The expected reduction in basal activation of CaMKII was however not observed, nor was a strong increase in stimulatory effects, as demonstrated in Figures 5.4. & 5.5. Unfortunately, activation of CaMKII in HCAECs with TNFα or IL-1β is not well established in the literature.

Other stimulants have been demonstrated to activate CaMKII in HCAECs. Bradykinin (BK) is a pro-inflammatory protein with important vasodilatory roles and has been shown to activate CaMKII and eNOS (Ramirez-Sanchez, et al. 2011). Interestingly, the activation of eNOS after BK treatment, is almost entirely CaMKII dependent, making this a useful stimulant to

consider. Furthermore, it's relevance in the development of restenosis has been established, and BK antagonists and inhibitors have been shown to lower all-cause PCI complications (Rocha, et al. 2017; Xiao-Dong, et al. 2016).

Previous work using HCAECs, has shown that TNFα can downregulate eNOS expression, but CaMKII wasn't considered, and specifically 6 h was highlighted as being insufficient to see eNOS-associated stimulatory effects in HCAECs (Franscini, et al. 2004). HCAEC responses to smaller concentrations (2 ng/ml) of TNFα have been assessed and shown to have minimal effect on eNOS expression and activity (Jiang, et al. 2009), suggesting it may not be possible to extend stimulation time whilst using lower stimulant concentrations.

Endothelial dysfunction is known to be a combination of both inflammatory and oxidative stress, so it follows that an antioxidant would have the capacity to break the positive feedback cycle. (Rodríguez-Mañas, et al. 2009). The link between CaMKII and eNOS identifies CaMKII as a central mediator of the cycle. As such, it follows that any intervention targeting CaMKII should have an impact on oxidative signalling. This is particularly important in patients with Diabetes Mellitus who have a higher baseline of oxidative stress and where inflammation-induced oxidative stress can occur regularly in response to both hypo- and hyperglycaemia (Ceriello, et al. 2013).

For more advanced experiments, it was hoped that a more complex model could be developed incorporating the use of HCASMCs. The activation of NF-κB and CaMKII activation in HCASMCs is not well known, but in other VSMCs, IL-1β has been shown to activate the NF-κB pathway which in turn induces the phenotypic inflammatory switch of vascular smooth muscle cells (Alexander, et al. 2012). Furthermore, in SMCs, CaMKII activation is a posttranscriptional regulator of iNOS allowing NO production to be rapidly increased (Toussaint, et al. 2016). This CaMKII-associated increase in NO production reflects the response observed in HCAECs in this literature.

Overall, oxidised-CaMKII has been established as a useful marker of oxidative stress in the endothelium *in vivo* (Erickson, et al. 2008; McCluskey, et al. 2019). This however was not completely replicated in our study using our *in vitro* HCAEC model. This may support the idea that *in vitro* cell culture conditions are deleterious, or challenging, to the endothelial cells and under the conditions used in this study, do not reflect well the physiological scenario.

5.4.3. Human coronary artery endothelial cell compatibility with electropolymerized polypyrrole

Initially, before assessing the compatibility of antioxidant effects in HCAECs attached to PPy samples, the effect of cell culture media incubation on the antioxidant capacity of PPy-coated strips was re-assessed using HCAEC and HCASMC media, as shown in Figure 5.6. When incubated in the HCAEC media, a rapid loss in DPPH scavenging capacity was observed for all potentiostatic and galvanostatic coatings generated at 0.5 mA. This loss in activity limits the level of antioxidant activity that can be offered to attached cells *in vitro* and any high scavenging activity is limited to the very acute phase; before cells are stimulated in our model. This effect is further complicated since before adding cell suspension, PPy strips are sterilised for 1 h in ethanol, and in later experiments pre-treated with PBS for 24 h.

This rapid loss in scavenging capacity was not observed for galvanostatic coatings generated at 1 mA, which exhibited a linear depletion in DPPH scavenging capacity. Although 1 mA coatings exhibited poor topographical and mechanical properties, the longevity of antioxidant capacity in these samples does demonstrate that the loss in capacity is not an inherent property of PPy and electropolymerised coatings can be generated with predictable and stable antioxidant properties. The improved antioxidant properties of 1 mA coatings may suggest that salicylate incorporation and elution is involved in this process, due to the very high levels observed in these coatings. The loss of antioxidant capacity in PPy coatings exposed to cell culture media is surprising since these effects were not observed after PBS incubation, where coatings were further challenged in a shaking incubator. This may indicate that an active component within the cell culture media interferes with the coating leading to a loss in the redox sensitive chemistry and salicylate may protect against this or stabilise the chemistry.

When assessing loss in the HCASMC media, in addition to 1 mA galvanostatic coatings, 0.5 mA and 1.3 V potentiostatic coatings also exhibited a slower linear depletion in DPPH scavenging capacities. This further suggests that contents of each cell culture media uniquely affect the PPy chemistry. Unfortunately, the base buffer composition is not disclosed, but when comparing HCAEC and HCASMC supplements, the HCAEC media contains additional VEGF, ascorbic acid and hydrocortisone, of which only ascorbic acid is highly redox sensitive.

The effect of pH may also be considered, but all of the solutions used, including PBS, should be buffered at similar pH values. Zhang & Bai, (2003), found that a pH > 6.5 led to

deprotonation of polypyrrole coatings, which will lead to a loss of PPy HAT capacity. Overall however, this deprotonation effect was found to impart an overall negative charge to the PPy coatings, leading to an improvement in cell attachment responses. This demonstrates the interlink between different PPy properties and complexities in identifying one optimal PPy synthesis method.

An additional study of benefit would be to assess different PPy coatings compatibility with different salt solutions and different additives or supplements, at different pHs and temperatures for increasing time periods. This would allow the key factors that affect PPy antioxidant behaviour to be established and would indicate a better PPy composition or suitable applications to maintain antioxidant longevity.

As with HUVEC media, the observed rapid loss of PPy antioxidant capacity after incubation in cell culture media may limit its application *in vivo* and this should be assessed further before progressing with this technology in any application where an antioxidant benefit is sought. The difference in depletion between the three different media does however suggest that it may be possible to modify the PPy response to environmental challenge. When considering the effect *in vivo*, it will be important to identify a suitable medium that represents the challenge anticipated after stent placement, and ideally up to 180 days.

The attachment of HCAECs on PPy samples was assessed after 24 h and proliferation assessed at 48 h and shown in Figures 5.7. & 5.8. In their doped state, all PPy coatings tested demonstrated relatively poor cell attachment properties and no significant proliferation at 48 h. After 24 h pre-treatment of PPy samples with PBS however, cell attachment was noticeably improved, and proliferation observed up to 72 h. In the doped state and after PBS elution, 1 mA coatings appeared to offer better attachment properties leading to an increased number of cells at 48 h.

Cell attachment is a complex process driven by multiple cellular and protein processes and determined by surface topography, wettability and charge (Lister, et al. 2016). The observed improvements in cell attachment after salicylate elution in PBS suggests that either salicylate elution and de-doping of the polymer improves its attachment properties, or that salicylate released directly into the cell culture media impairs the ability of cells to attach or leads to cell death. Gelmi, et al. (2014), assessed the effect of PPy dopants on endothelial and cardiac progenitor cell viability, and although salicylate was not explored, it was found that the effects

of doping on cell viability was highly dependent on the cell type and dopant considered. This suggests that de-doping alone was not responsible for the improved cell attachment observed.

It is more likely that salicylate impairs cellular attachment, and in HUVECs, salicylate has been shown to diminish cell attachment by preventing integrin expression (Gerli, et al. 1998). It is however important to balance the benefits offered by salicylate elution, which are more relevant when these coatings are used clinically, such as its hydroxyl scavenging capacity (Grosser & Schröder, 2003) and effect on NF-kB inhibition (van der Heiden, et al. 2010).

Other studies have looked at methods to improve the cell attachment of PPy coatings by considering the different factors that contribute to it. Firstly, the hydrophobicity of PPy has been studied and hydrophilic coatings generated with naphthalenesulphonic acid dopants (Li, et al. 2016). Interestingly, the use of this dopant allows redox-controlled switching between hydrophobicity and hydrophilicity which is not observed with the use of other dopants. Topography also presents a strategy for improving attachment with novel coating parameters and micropatterning shown to be capable of modifying cell attachment and behaviour (Gomez, et al. 2007; Ateh, et al. 2006; Fonner, et al. 2008). Finally, coatings may also be chemically modified, either using surface functionalisation or by the use of selective pro-proliferative drugs as dopants.

Simple chemical functionalisation by modifying the surface with the amine groups has been shown to improve fibroblast attachment by the addition of inherently charged functional groups (Lee & Schmidt, 2015). VEGF functionalisation may present a more relevant target for endothelial cell attachment and has been demonstrated with PPy biosensors (Kwon, et al. 2010).

The most striking application of a selective pro-proliferative drug being used to promote endothelial cell attachment is heparin. Unlike amine and VEGF, this is incorporated directly during electropolymerisation and elution of heparin from these coatings has been shown to promote HUVEC attachment and supress human aortic SMC proliferation *in vitro* (Garner, et al. 1999 & Stewart, et al. 2012).

5.4.4. The effect of electropolymerized polypyrrole coatings on oxidative stress in surface-attached human coronary artery endothelial cells

CellROX and immunofluorescence were used to assess the oxidative stress of HCAECs attached to 316L and PPy-coated samples. HCASMCs were not considered in either attachment assay due to cell culture issues, preventing adequate cell populations to be obtained. Furthermore, lack of response after TNFα stimulation prevented further consideration of these cells.

Initially, the use of CellROX was optimised in HCAECs attached to tissue culture wells since this approach was not used in the preliminary HUVEC model. Although this was a new technique using HCAECs, the observed increase in oxidative stress broadly reflected the observations made with HUVECs using DCFDA. The finding that TNFα generates intracellular oxidative stress in HCAECs is supported by other studies. Uthman, et al. (2022) compared the stimulation of ROS by TNFα in both HUVECs and HCAECs and observed significant increases in both cell types, although with a higher fold-change with HCAECs. McGrath, et al. (2015) also observed significant activation when stimulating with 5 ng/ml for 3 hours, but both studies use DCFDA as their ROS probe.

When HCAECs were attached to PPy coatings and stimulated with TNFα, the antioxidant properties of PPy were found to have little beneficial effect on oxidative stress, as demonstrated in Figure 5.9. & 5.10. HCAECs attached to PPy coatings generated at 1.3 V exhibited a significant increase in intracellular oxidative stress compared with the unstimulated control. This increase was greater than the equivalent increase observed in the tissue culture well control. Since this elevation in oxidative stress is not observed in 1.3 V attached cells without stimulation, this suggests that HCAECs attached to these PPy coatings respond differently to stimulation.

The effect of TNFα on specific ROS generation in HCAECs has been previously explored. Chen, et al. (2008), showed using DHE that superoxide production was significantly increased after stimulation with TNFα concentrations as low as 2 ng/ml. Similarly, Yoshida & Tsunawaki, (2008), showed that stimulation with 10 ng/ml TNFα for 6 h led to a 1.8-fold increase in hydrogen peroxide generation. Similar superoxide scavenging capacities were observed chemically with 1.3 V potentiostatic and 1 mA galvanostatic, with only a slightly

higher mean for the potentiostatic coating. Chemically assessed hydrogen peroxide scavenging differed between the coatings with significant scavenging capacity only observed with 1.3 V potentiostatic coatings. In both cases, the *in vitro* chemical scavenging assays indicated that PPy could exhibit strong antioxidant activity, but this contradicts the detrimental effects observed, specifically for 1.3 V coatings in HCAECs *in vitro*.

It is worth noting, that the biological effects of PPy in this present study were only observed with less powerful statistical analysis techniques. The lack of significance when using a two-way ANOVA highlights the similarities in response between cells attached to samples surfaces, the weak statistical power of using four independent repeats for this test, and the weakness of performing the assay at only one fixed time point. The statistical power of this experiment could be improved by using a higher number of samples and improving the assay robustness; this may then provide more meaningful comparisons of the samples tested.

Differences in the experimental procedure between the chemical assays and this biological assessment of PPy effects, prevents direct comparison of the two data sets. Firstly, and likely more significantly, chemical assays are assessing scavenging of ROS within a homogeneous solution, whereas this biological assay is assessing the effect of PPy of intracellular ROS species within the attached cells. It is not clear whether having a PPy on the exterior of the cell will have any effect on the internal oxidative environment. Another difference is that when used for cell culture, PPy coatings were pre-treated with PBS and then sterilised in 70% ethanol, this was not replicated in chemical assays. This is however unlikely to factor into the outcome since the antioxidant capacity of PPy coatings was shown to be stable using DPPH after ethanol sterilisation and longer-term PBS storage.

One likely cause of the observed effects on cellular stress, is that the 1 mA coatings provide a more optimal attachment and beneficial substrate than 1.3 V coatings, independent of the antioxidant capacities of each coating. This is however speculative since this assay only explored oxidative stress and this justification is based on preliminary cell attachment work. This highlights the importance of also quantifying the inflammatory state. In such an assessment, 1 mA coatings may be shown to be less pro-inflammatory compared with 1.3 V coatings, which as shown has a downstream effect on oxidative stress. Another factor of 1.3 V likely to contribute to cellular stress and resulting ROS generation is delamination of the coating. This may contribute to cell death and particulate generation although, PPy particles

have been shown to be non-toxic *in vitro* and *in vivo* (Ramanaviciene, et al. 2007; Fahlgren, et al. 2015).

Finally, the CellROX Green probe, is less established than DCFDA within the literature. It is offered as a broad marker of ROS generation within the cytosolic space and has been shown to be superoxide sensitive (McBee, et al. 2017). Due to the significant difference in hydrogen peroxide scavenging between the PPy coatings used, it would be useful to consider their effects on intracellular peroxide generation, but this is not possible using CellROX (Choi, et al. 2015). Some issues have also been reported with this probe, such as poor regression and quantification, and high variability with small sample sizes (Celeghini, et al. 2019). As with all fluorescent probes it is sensitive to light and human use factors and localisation to nucleus limits the usefulness in a microscopy application. Overall, however CellROX still offers far better ROS detection than DCFDA (McBee, et al. 2017).

5.4.5. The effect of electropolymerized polypyrrole coatings on CaMKII activation in surface-attached human coronary artery endothelial cells

Following the fluorescence microscopy-based method to assess oxidative stress in HCAECs, it was hoped that this technique could be used with antibodies against phospho-p65 and oxidised-CaMKII to assess the impact of PPy coatings on these proteins. For both assays, optimisation was first performed to confirm that expression levels of the proteins using this technique reflected the activation observed with immunoblotting. This technique was not found to be effective for assessing p65 phosphorylation. The antibody used for immunoblotting is not approved for immunocytochemistry and the alternative immunocytochemistry was found to provide poor fluorescence intensity, preventing meaningful quantification. Despite the importance of assessing inflammatory stress in understanding the response of cells to the PPy coatings, it was decided that given the poor outcomes using this technique, it would be used only to assess CaMKII oxidation.

CaMKII oxidation was assessed using immunocytochemistry and the antibody provided was found to provide a very strong signal, that when quantified after TNFα stimulation, reflected the activation observed with immunoblotting. The oxidised-CaMKII antibody used in this study has no reported use in other studies using HCAECs, but McCluskey, et al. (2019) demonstrated it's use for western blotting and immunofluorescence in rat endothelial cells

(McCluskey, et al. 2019). Other oxidised-CaMKII antibodies have however been used for immunofluorescence in HCAECs to quantify CaMKII activation (Sanders, et al. 2013; He, et al. 2011).

When assessing the effect of PPy coatings on CaMKII oxidation in HCAECs, there was a significant impact observed between cells in the tissue culture well and attached to PPy coatings generated galvanostatically at 1 mA, as demonstrated in Figures 5.11. & 5.12. This significant dampening of CaMKII oxidation suggests that PPy is capable of offering a direct or indirect mechanism to inhibit CaMKII activation. Conversely, no significant reduction in TNFα-induced CaMKII oxidation was observed in cells attached to PPy coatings generated potentiostatically at 1.3 V. This suggests that the effect of PPy coatings is synthesis dependent, although there was very high variation in these samples, likely due to delamination of the coating from the underlying SS strip. This was also observed in the CellROX data.

Unlike the CellROX data, statistical significance was observed with the more powerful two-way ANOVA adding confidence to the meaningfulness of these differences. Interestingly, with the less powerful statistical tests, this difference was lost and no significant differences were observed between groups.

Overall, the results from this assay broadly align with the observed changes in oxidative stress, from which, it is difficult to conclude whether PPy has a direct antioxidant effect on the attached endothelial cells. The effect on oxidised-CaMKII is likely a downstream effect of the ROS changes observed in the CellROX, which may result from differences in the inflammatory response. Again, these results reiterate the positive effect of the 1 mA coatings, irrespective of their superoxide and peroxide scavenging activity, but highlight the need to understand the inflammatory response of attached HCAECs to PPy. Alternatively, the 1 mA coatings may have a direct on CaMKII activation. A ROS-dependent mechanism for targeting CaMKII may be obscured in this study by the limited ROS targets probed by CellROX and a ROS-independent mechanism of action is also possible. Fahlgren, et al. (2015), found that the activity of osteogenic proteins in osteoblasts varied between different PPy samples. Although osteoblasts and endothelial cells are substantially different, these cells are both highly responsive to different surfaces.

The ambiguity of the effect of PPy coatings on adherent endothelial cells highlights the need to explore the response of endothelial cells to these novel coatings in greater detail. As with the CellROX data, where exploring p65 phosphorylation may provide insight into the

contribution of inflammatory signalling, exploring CaMKII phosphorylation may also be helpful to observe whether the 1 mA coatings do impart a direct or topography-based anti-inflammatory benefit.

5.5 Conclusions

In conclusion, this chapter achieves the fundamental aim of assessing the effect of PPy coatings on the oxidative stress and CaMKII oxidation of adherent HCAECs. The use of HCAECs as a cell-based model is also established and the effectiveness of TNFα stimulation at promoting p65 phosphorylation, generating intracellular ROS and initiating CaMKII oxidation.

Unlike in HUVECs, the use of IL-1β to stimulate HCAECs did not lead to significant CaMKII oxidation and instead, this effect was observed after stimulation of the cells with TNFα. Higher sensitivity of HCAECs to eluted salicylate was also observed preventing cell attachment and proliferation on PPy surfaces. The pre-release of salicylate however eliminated this effect and demonstrated that PPy coatings can provide a suitable substrate for endothelial cell attachment and growth.

Although the scavenging capacity of PPy coatings to physiologically relevant ROS has been demonstrated in previous chapters, the beneficial effect of PPy was limited when assessed in terms of their ability to inhibit ROS generation and CaMKII oxidation after TNFα stimulation. Significant inhibition was only observed by coatings generated by galvanostatic electropolymerisation at 1 mA and limited to CaMKII oxidation, although there was some indication of a positive impact on ROS generation.

Due to experimental constraints, the scope of this study did not extend to exploring the effect of PPy coatings on pro-inflammatory signalling in HCAECs and wider signalling or coating compatibility with HCASMCs. As such, more work is required to establish the wider effectiveness of PPy coatings on vascular cells and over a longer period.

6. Discussion

Chapter 6 will discuss the overall findings and limitations of this study. This chapter will begin by summarising the key findings of each of the previous chapters before discussing the results in a wider context to consider the broader understanding provided by these results. Following this review of the study's findings, this chapter will outline some key limitations of the study and some future work that could be undertaken to advance the work. Finally, the conclusion presents an overall summary of the value and significance of this study to furthering the understanding of PPy and its potential application as a novel antioxidant stent platform.

Overall, this study successfully generated PPy coatings with demonstrable ROS scavenging capacity, which allowed endothelial cell attachment and proliferation. Using a cell-based model of oxidative stress, these PPy coatings were found to dampen CaMKII oxidation in adherent HCAECs.

6.1. Key Study Findings

Chapter 1 of this study presented an introduction to coronary artery stenting, oxidative stress, CaMKII and the electropolymerisation of conducting polymers. Through this review of the literature, the potential of PPy and electropolymerisation to reliably generate uniform coatings with antioxidant capacity was highlighted, but there were also areas where significant gaps in the available literature were identified. Specifically, there was limited evidence demonstrating the capacity of PPy to scavenge specific ROS that are most relevant to cardiovascular pathology, the effect that different electropolymerisation conditions would have on these properties, or the biological response of cells in contact with these novel stent coatings. Furthermore, there were no established methods utilising an *in-vitro* cell-based model to assess cell compatibility using HCAEC. Moreover, there is a general paucity of data on the role of oxidised CaMKII in vascular pathology and restenosis, with somewhat inconsistent findings observed in the small number of investigations published thus far These key areas where further knowledge is sought provided the rationale of this study's aims, which were subsequently explored in the subsequent chapters.

Electropolymerisation of Polypyrrole

The use of electropolymerisation as a means of reliably generating uniform PPy coatings was investigated in Chapter 2 of this study. Here, coatings were generated using either potentiostatic or galvanostatic electropolymerisation, with applied voltage and current, working electrode geometry, and salicylate dopant concentration all assessed to determine the optimum conditions for achieving uniform PPy films. Furthermore, the coatings generated were characterised using SEM, EIS, CV and FTIR to attempt to understand the oxidative state of PPy coatings generated. This analysis was therefore more comprehensive than many previously reported studies.

Based on the data presented in this chapter, it was determined that when coating 200 µm SS wires, the optimum electropolymerisation of uniform coatings with a typical 'cauliflower' morphology was achieved when using 0.1 M pyrrole and salicylate solutions, over a 10-minute polymerisation time, with 1.3 V applied voltage for potentiostatic, as shown in Figure 2.5, and 0.5 mA (2.65 $mA.cm^{-2}$) maintained current for galvanostatic electropolymerisation, as shown in Figure 2.6. Due to the low surface area of 200 µm SS wires, 30 x 5 mm SS strips were also coated and under this set-up 1.3 V was sufficient for potentiostatic electropolymerisation of PPy onto coated strips, as shown in Figure 2.7., but 1 mA (0.33 $mA.cm^{-2}$) was optimal for galvanostatic electropolymerisation, as shown in Figure 2.8.

Although the current-time profile for coatings generated at 1.3 V showed potential indication of overoxidation by an initial current peak followed by a slow loss in conductivity during the electropolymerisation cycle, there was no evidence of overoxidation observed in subsequent EIS, CV and FTIR analysis. This was indicated by EIS (Figures 2.16. and 2.17) through a very low charge transfer resistance at high frequencies (Marchesi, et al. 2011), by CV (Figure 2.18.) through observed reversible oxidation and reduction (Levi, et al. 2002), and FTIR (Figure 2.19.) by an absence of peaks related to C=O bonds in the pyrrole ring that occur during overoxidation (Li & Quan, 2000). For coated wires generated at 0.5 mA and strips generated at 1 mA, there was no evidence in the voltage-time profile to indicate the occurrence of overoxidation during electropolymerisation and this was reflected in EIS, CV and FTIR data. Scavenging has been previously demonstrated in oxidised and reduced PPy coatings (Hsu, et al. 2010; Upadhyay, et al. 2014), but this effect is dampened after overoxidation (Lee, et al. 2013). The absence of detectable overoxidation and the formation of consistent cauliflower morphologies, as observed by SEM, demonstrates the suitability of the electropolymerisation conditions used in this study.

The study fundamentally sought to generate PPy as a novel drug-free antioxidant stent coating platform, but the necessity to incorporate a dopant ion during electropolymerisation presents further opportunity for this platform as not only an antioxidant, but also as a drug elution platform. In this study, salicylate was incorporated due to its relatively small size, demonstrated suitability for PPy electropolymerisation (Arbizzani, et al. 2007; Cysewska, et al. 2016), and established anti-inflammatory effects (Marra, et al. 2000). The anti-inflammatory properties of salicylate have been shown to reduce smooth muscle cell proliferation, but this effect is non-selective and affects exposed endothelial cells (Gerli, et al. 1998) As such, the use of salicylate for DES should be carefully considered. Through modifying the potentiostatic voltage and galvanostatic currents, it was demonstrated, as shown in Figures 2.9. and 2.10., that the quantity of dopant incorporated could be controlled and some tunability of release rate was achieved. The elution properties observed reflected the behaviour of PPy-Sa coatings established by Arbizzani, et al. (2007). The replication of microtubular PPy structures (Figure 2.13), as described by Gonzales, et al. (2013), by changing dopant concentrations allowed for significantly greater incorporation of dopant and a more rapid release profile (Figure 2.15), further demonstrating the potential of PPy as a DES platform.

Antioxidant Activity of Electropolymerised Polypyrrole

As previously noted, the primary aim of this project was to generate PPy coatings to target pathological oxidative stress and as such, the antioxidant capacity of PPy was characterised in Chapter 3. Although there is evidence within the literature that PPy powders possess antioxidant activity, with Hsu et al, (2008), demonstrating this through scavenging of DPPH *in vitro*, there has been no characterisation of such activity for electropolymerized PPy coatings of the type generated in the present study. As shown in Figure 3.6., the optimal coated wires generated potentiostatically at 1.3 V and galvanostatically at 0.5 mA were found to demonstrate good resistance to repeated oxidative challenge and a moderate, but predictable loss in capacity after incubation in PBS.

The DPPH radical used can be reduced by both HAT and SET. As such, this assay cannot identify the mechanism of action for PPy antioxidant activity, and the linear depletion after repeated challenge could suggest either as the primary mechanism (Griesser, et al. 2018; Hristeac, et al. 2006). The presence of the amine functional group and delocalised electrons across the polypyrrole backbone indicate that either mechanism is theoretically plausible. It is important to understand the potential mechanism of action as it allows better prediction of how

PPy may behave *in vivo*. For example, although the most oxidative species such as hydroxyl radicals can be reduced by either mechanism, less oxidising species may only be reduced by one mechanism, such as peroxyl radicals which are reduced by HAT only. Due to their localisation within the cell and different oxidising power, different ROS can therefore have different targets and as such a specific antioxidant can be deploy targeted action.

Although the DPPH assay provides a simple indication of broad antioxidant abilities, it was more important in this study to establish the ROS scavenging capacity of PPy against oxidant species with physiological relevance. This was identified as a key priority in Chapter 1 as there are few studies that reported the specific ROS scavenging capacity of PPy. Table 6.1. shows the ROS scavenging capacity of pyrrole monomer, salicylate, optimal PPy coated strips generated at 1.3 V and 1 mA, and uncoated 316L SS. This summarises the findings presented in Figures 3.9. – 3.16.

Table 6.1. Specific ROS scavenging capacity of pyrrole monomer, salicylate, optimal PPy coated strips generated at 1.3 V and 1 mA, and uncoated 316L SS against superoxide, nitric oxide and peroxyl radicals, and hydrogen peroxide. Where scavenging capacity is indicated, this represents a significant scavenging capacity when compared against both the blank and uncoated controls as presented in Chapter 3.

	Superoxide	**Nitric Oxide**	**Hydrogen Peroxide**	**Peroxyl**
Pyrrole monomer	×	×	✓(negligible at high concentrations)	✓
Sodium salicylate	×	×	✓ (moderate at high concentrations)	✓
PPy (1.3 V)	✓	✓	✓	✓
PPy (1.3 V after electrochemical Sa-discharge)	✓ (higher capacity than 1.3 V coatings)	✓	✓	×
PPy (1 mA)	×	✓	×	✓
PPy (1 mA after electrochemical Sa-discharge)	×	✓	×	✓ (lower capacity than 1 mA coatings)
Uncoated SS	×	×	×	×

Despite the observed similarities between PPy coated strips generated at 1.3 V and 1 mA, there were differences between the samples in terms of their ROS scavenging capacities, particularly in terms of their superoxide and hydrogen peroxide scavenging capacity. 2 mA coatings were also assessed and found to exhibit significant scavenging capacity against superoxide radicals (before Sa-discharge) and hydrogen peroxide. This suggests that galvanostatic electropolymerisation alone isn't responsible for this difference.

Comparing the scavenging capacity of PPy coatings against the pyrrole monomer and aqueous salicylate provides insight into the mechanism of PPy antioxidant activity. Since the ORAC assay for peroxyl scavenging assesses only HAT, this in particular suggests that PPy may only offer minimal HAT scavenging activity. This can be observed by the complete loss for 1.3 V coatings and significant loss for 1 mA of peroxyl scavenging capacity after the loss of the salicylate dopant. This suggests that the salicylate dopant offered peroxyl scavenging capacity which is expected since it's a known scavenger of peroxyl and hydroxyl radicals (Rodríguez-Santiago, et al. 1999). Furthermore, the peroxyl scavenging capacity of the monomer suggests that the HAT source that is active in the monomer is lost or stabilised during electropolymerisation.

The superoxide scavenging capacity of 1.3 V coatings and nitric oxide scavenging capacity of both 1.3 V and 1 mA coatings demonstrates that electropolymerisation does however impart other mechanisms for scavenging, likely related to SET. Scavenging against these radicals can be achieved through SET or HAT (Lancaster, 2015; Li, et al. 2018) and the lack of scavenging by the monomer or dopant suggests that the delocalisation of electrons during electropolymerisation allows SET-based scavenging of these species that is not possible by the electron delocalisation, resulting from the N-H lone pair, in the monomer. By assessing the scavenging capacity of PPy before and after Sa-elution, it is shown that where the scavenging capacity isn't directly related to the dopant, the antioxidant activity is retained whether PPy is used as a drug-free or drug-eluting platform.

Developing a Cell-based Model of Inflammatory and Oxidative Stress

Although the assays described above measure the chemical capability of PPy to scavenge relevant biological ROS, these approaches do not demonstrate the ability of these coatings to offer a significant benefit to vascular cells and related corresponding downstream therapeutic benefit of minimising restenosis. In order to address this, our initial approach was to establish a cell-based model using HUVECs (Chapter 4). This demonstrated the capacity of TNFα to

stimulate pro-inflammatory and oxidative signalling in an endothelial setting. This was then studied further in Chapter 5 using the more relevant HCAECs. TNFα presents a particularly relevant cytokine for studying the response of vascular cells to PPy coatings since clinically expression of TNFα correlates strongly with post-stenting restenosis rates (Bittar, et al. 2005).

In HCAECs and as shown in Figure 5.3., p65 phosphorylation after TNFα (10 ng/ml) stimulation was observed as a marker of inflammatory stress, with an acute peak stimulation at 30 minutes. This correlated well with established data showing the stimulatory effects of TNFα on NF-κB activation (Csiszar, et al. 2016). Similarly, TNFα (10 ng/ml) was found to stimulate oxidative stress in HCAECs at 6 h (Figure 5.9.). Again, this aligns well with established data showing that TNFα stimulation leads to significant generation of both superoxide radicals and hydrogen peroxide (Chen, et al. 2008; Yoshida & Tsunawaki, 2008). There is a well-known link between pro-inflammatory signalling, in particular NF-κB activation, and oxidative stress, although this relationship is complicated as NF-κB activation has both pro-ROS and endogenous antioxidant downstream targets (Morgan & Liu, 2011). In the present study, the phosphorylation of p65 at 30 minutes precedes detectable increases in oxidative stress at 6 h, but it is not possible without further exploration of the specific downstream targets of NF-κB, such as xanthine oxidase or NOX2, to demonstrate that the increased phosphorylation of p65 is responsible for and mediating the increased intracellular oxidative stress.

Along with identifying antioxidant activity as a therapeutic mechanism for PPy coatings, the role of CaMKII in contributing to oxidative stress was also considered due to its role in mediating a number of key signalling pathways and its ability to be activated by both phosphorylation and oxidation (Rusciano, et al. 2019). CaMKII activation was assessed and TNFα was shown to stimulate CaMKII activation after 6 h by oxidation only (Figure 5.5.). This peak aligns with the peak intracellular oxidative stress observed, but there is limited reported data in the literature using TNFα to stimulate CaMKII in HCAECs.

Therapeutic Potential of Electropolymerised Polypyrrole Films

The suitability of the cellular stimulant and ability to reliably detect an increase in pro-inflammatory signalling and CaMKII oxidation allowed this technique to be applied in a cell-based model for assessing potential therapeutic benefits of the PPy coatings generated. Importantly, initial work assessed endothelial cell compatibility with PPy coated strips. Work in chapter 5 showed that in their doped state, PPy coatings limited HCAEC attachment and

inhibited proliferation. This was most likely due to the high initial elution of salicylate, a drug which is known to impair cell attachment (Gerli, et al. 1998). When a pre-elution step was added, thereby greatly diminishing subsequent salicylate release in the presence of cells, PPy was found to allow cell attachment and was not shown to inhibit proliferation (Figure 5.8.)

Wong, et al. (2004) and Jakubiec, et al. (1998) assessed the attachment of endothelial cells to PPy coatings. Wong, et al. found that good attachment of endothelial cells on oxidised PPy coatings, whereas Jakubiec, et al. observed that increases in PPy conductivity were associated with reduced cell viability. In the present study, it is difficult to assess the effect of conductivity since only 1.3 V and 1 mA coatings were studied and EIS was not performed on PPy coated strips.

In terms of the ability of PPy to impart a protective effect on to adherent cells subjected to oxidative stress, this was difficult to determine and showed limited evidence of the positive impact of PPy on the inflammatory signalling and oxidative stress of HCAECs. Firstly, due to the incompatibility of the phospho-p65 antibody with immunocytochemistry approaches, it was not possible to assess the anti-inflammatory potential of PPy. When assessing the antioxidant potential of PPy using CellROX, as shown in Figures 5.9 and 5.10, there was no significant reduction in intracellular ROS generation in HCAECs attached to PPy coatings. However, when assessing the ability of PPy to reduce CaMKII oxidation using immunofluorescence, as shown in Figures 5.11. and 5.12., there was a decrease in CaMKII oxidation observed in HCAECs attached to coated strips generated at 1 mA compared with cells attached to tissue culture plastic (TCP). With 1.3 V coatings, there was also a substantial increase in intracellular ROS expression, albeit there was high variation across the sample group. The ability of 1 mA to provide a comparable substrate to TCP by HCAECs in terms of ROS generation and the potential to inhibit CaMKII oxidation suggests that these coatings may offer significant benefits compared with current stent platforms which promote oxidative stress (Juni, et al. 2013).

When comparing the biological impact of PPy coatings on adherent HCAECs with the chemical scavenging capacities determined in Chapter 3, it is surprising that coated stips generated at 1 mA show the highest potential for offering therapeutic benefits when coatings generated at 1.3 V consistently offered greater scavenging capacity. This suggests that either the antioxidant capacity alone does not determine the biological impact, or that the chemical in vitro assays are poor indicators of potential biological effects. It is also worth noting that in

Figure 5.6. it was shown that the DPPH scavenging capacity of PPy is quickly lost after incubation in HCAEC media, so it is possible that PPy coatings offer little scavenging capacity whilst HCAECs are attached and during TNFα stimulation. Erickson, et al. (2008) demonstrated the capacity of hydrogen peroxide to oxidise CaMKII and as such its relevance as a key target for therapeutic antioxidants seeking to modulate CaMKII activity. Although other ROS explored in this study have not been explicitly implicated in CaMKII oxidation, they have not been eliminated from generating CaMKII oxidation either. If hydrogen peroxide is implicated, it is likely that hydroxyl and peroxynitrite species would be similarly effective, if not more effective, at oxidising CaMKII. This is supported by growing evidence of the capability of peroxynitrite to oxidise CaMKII (Zhou, et al. 2016).

Due to the longer half-life and corresponding stability of hydrogen peroxide, and the ability for vascular cells to secrete hydrogen peroxide as a paracrine mediator (Ardanaz & Pagano, 2006), this represents a logical target for an extracellular antioxidant such as the PPy films used in this study. This is however not reflected in the finding that coatings generated at 1 mA offer superior biological effects compared with 1.3 V coatings. It is therefore possible that the observed benefits to HCAECs offered by 1 mA coatings are mediated independently of ROS scavenging reactions.

6.2. Study Limitations

Limitations of this study are outlined for the individual strategies and techniques used in Chapters 2-5 and this section will provide a brief overview of the key limitations for the study overall.

Appropriateness of a wire and strip based model

Firstly, it was important to identify an appropriate substrate for generating PPy coatings to be characterised and studied. The use of 316L SS provided a logical and relevant material, but it was also critical to identify a suitable geometry. The use of an entire strut structure was eliminated due to the complexities of sourcing, post-processing for subsequent experiments (e.g. cutting or flattening), and the challenges posed in using this structure in a cell-based model. As such, wires were selected to mimic stent struts for characterisation of PPy electropolymerisation and strips were selected to provide an appropriate surface area for ROS scavenging assays and subsequent *in vitro* experiments.

This strategy presents a compromise to assess the potential of PPy in a cell-based model. It is unclear what, if any, impact this has on the resultant observations made in this study, but the use of two models does present limitations when attempting to compare the data. For any use of PPy as a stent coating, it is therefore important for the electropolymerisation to be validated with stent structures and in vivo animal studies to be performed.

Antioxidant Stability

In Figure 5.6., it was shown that there was limited stability of DPPH scavenging for PPy coatings after incubation in HCAEC media. This contrasts with the stability of PPy coatings after incubation in PBS shown in Chapter 3. Although the reason for this instability is unclear, if this were replicated under true physiological conditions, this presents a critical concern for the effectiveness of PPy as therapeutic stent coating.

After placement of a DES, systemic oxidative stress has been found to be highest in the following two days, but maintained up to 30 days after placement (Kochiadakis, et al. 2009). This may be lower with PPy coatings due to their potential drug-free nature, but is likely to be highly dependent on dopant and immune response. Misra, et al. (2008), found that markers of hydrogen peroxide-related oxidative stress were elevated until clinical diagnosis of restenosis. This suggests that the observed rapid loss of PPy antioxidant activity in biological media would limit its relevance in preventing restenosis.

Due to the novelty of PPy antioxidant activity against specific physiological ROS, it is not possible in the literature to determine the stability of the antioxidant activity observed for PPy against specific ROS and this was not assessed in this present study.

Clinical Relevance of ROS Scavenging

A further limitation presented by the chemical ROS scavenging assays is their relevance to the physiological context after stent placement. Due to the short half-life of ROS, it's not possible to determine the concentration present *in vivo*, this results in total blood peroxides being reported clinically. Kochiadakis, et al. (2009) investigated the total peroxides present after DES placements and found a peak level of 529 μM. Total serum peroxides relate most closely to hydroxyl and peroxyl radicals (Barrera, 2012) and poorly with superoxide, although this provides an indirect measure of superoxide since superoxide stoichiometrically generates downstream hydroxyl radicals (Ayala, et al. 2014).

It is hard to compare the concentrations of the assays used in this present study to total peroxides as each assay measures a different ROS target. For example, the DPPH uses a 64 μM challenge, whereas the hydrogen peroxide uses a 40 mM challenge far in excess of the physiological level and the ORAC uses 240 mM AAPH to continuously generate peroxyl. This highlights the need to consider the results of these assays as an indication of the potential for PPy coatings to scavenge the radicals and not to extrapolate this to a biological effect. Moreover, the high ROS scavenging capacity of PPy in the absence of adherent cells, but lack of detectable benefit to those cells may suggest that PPy scavenging capacity is limited to extracellular stresses and a reduction in this stress has limited benefit to the intracellular environment.

Use of Cell-based Models

This study specifically sought to use a cell-based model to explore the capacity of PPy to act as an antioxidant to impart a biological benefit to adherent vascular cells. Although this was achieved for HCAECs, it was not possible to achieve the same with HCASMCs, therefore it is not possible to determine the overall benefit of any effect by PPy to the vessel as a whole. This would be better assessed using an *in vivo* animal model, such as the pig coronary artery model that is recommended during the standard development of new stents.

Sterilisation of Polypyrrole

In this study, ethanol was used to sterilise PPy coated strips, due to the deleterious effect of steam sterilisation on the DPPH scavenging capacity of PPy shown in Figure 4.7. Although this was sufficient for this study, a process with higher throughput would be required to use PPy more widely. The use of electron beam sterilisation and gamma irradiation are likely to reduce polymer chain length and decrease mechanical properties (Bhadra & Khastgir, 2007). Consequently, this could also improve antioxidant properties by breaking bonds in the ring structure of the backbone, increasing the number of delocalised electrons and improving electron transfer or electrophilic substitution reactions. Gamma has been used with to achieve high sterilisation doses on PPy films without chemical modification, as assessed by CV and XPS, and shown to only cause some moderate oxidation of the films at high sterilisation doses and an increase in wettability (Kim, et al. 2018). This same study showed, using EIS, that larger dopants could limit this.

Although ethylene oxide has been shown to successfully sterilise conducting polymers, it has been shown to change their morphology and crystallinity, suggesting there are chemical

modifications during sterilisation (Valente, et al. 2016). Ethylene oxide may interfere with redox sensitive functional groups, for example polyethylene oxide has been shown to react with pyrrole during polypyrrole electrosynthesis (Khadka, et al. 2020). Other novel sterilisation strategies utilise ROS, such as vaporised H_2O_2 and NO_2 (McEvoy & Rowan, 2019), and as such are unsuitable in this application. Since the benefit of PPy may act independently of ROS scavenging, sterilisation may present fewer obstacles if PPy were to be used as a DES platform since its redox sensitivity can be sacrificed.

Biocompatibility of Polypyrrole

In this study, assessment of the biocompatibility of PPy was limited to endothelial cell cytocompatibility and only over an acute period. The long-term effects of PPy once implanted remain unclear as does the haemocompatibility of these coatings. Both of these properties are critical to the success of any stent coatings and present potentially significant obstacles to overcome. Furthermore, during this study, delamination of coatings was observed presenting potential issues relating to the mechanical properties of PPy. Delamination has been reported in PPy films and has been associated with doping issues (Kim, et al. 2016), but can also be an intrinsic property of thick coatings due to the poor interfacial adhesion strength with the underlying electrode (Kim & Kim, 2019). This may be minimised with modification of PPy coatings to improve chemical bonding or by using an intermediary at the interface (Jin, et al. 2019), changing the electrode surface topography (etching 316L to allow locking with cauliflower togography, changing substrate or changing electropolymerisation conditions.

6.3. Future Work

As the first study to explore the potential of PPy as an antioxidant stent coating, the study has revealed important novel insights that open up significant opportunities for further research. Firstly, this study only explored the use of salicylate as a dopant to generate PPy films by electropolymerisation. Exploration of a wider range of dopants could be explored, such as those investigated by Arbizzani, et al. (2007) and including other active pharmaceutical agents, or non-active dopants, will help reveal the optimal electropolymerisation strategy for this application. Additionally, known antioxidants could be incorporated as a dopant and subsequently eluted, although the release of antioxidants from traditional DES platforms has so far offered limited success (Tardif, et al. 2002; Watt, et al. 2013).

Another consideration is the influence that overoxidation has on PPy properties. Since none of the conditions used in this study generated overoxidised coatings, as assessed by EIS, CV and FTIR, it remains unclear what impact this modification would have. It is however known that overoxidation negatively impacts mechanical properties (Holze, 2022), and as such is unlikely to be a useful modification for medical PPy applications.

In addition to generating a wider range of PPy coatings, there are other techniques that may provide further insight into PPy's usability. Fonner, et al. (2008), demonstrated that coating conductivity could be used as a measure of salicylate release. This may present advantages over using PBS elution with spectrophotometry alone as it may indicate the quantity of residual dopant remaining after diffusion-related elution has concluded. Similarly, raman spectroscopy may provide further insight into the oxidative state of PPy or be used to monitor chemical changes *in situ* during polymerisation (Liu, 2004).

Future work should also aim to assess the capacity of PPy to scavenge a wider range of physiologically relevant ROS, such as hydroxyl and peroxyl radicals. As demonstrated in this study, these should be assessed using both chemical and biological assays. Furthermore, biological assays should be used to discriminate between intracellular and extracellular effects, this would demonstrate whether a localised extracelluar antioxidant can elicit a downstream intracellular benefit. Amplex Red, a probe for hydrogen peroxide, is one such assay that can provide this insight (Karakuzu, et al. 2019). Other assays may also be utilised in the biological context to assess irreversible oxidation products such as lipid peroxidation or generation of protein carbonyls (Colombo, et al. 2016), but work must also be done to consider the effectiveness of these assays when generating cell lysates from small culture surfaces such as PPy strips.

Alternatively, the lack of clear antioxidant benefit to adherent endothelial cells may justify the investigation of wider PPy properties or alternative strategies. For example, salicylate-doped PPy coatings have been demonstrated to exhibit antimicrobial properties against *S. aureus* (El Jaouhari, et al. 2017), and responsive ROS scavenging stent coatings have been generated by crosslinking cystamine with epigallocatechin gallate, which have been shown to scavenge hydrogen peroxide and induce non-inferior neointimal formation to bare 316L SS stents in a rat model of restenosis (Wang, et al. 2021).

6.4. Overall Conclusion

In conclusion, this study achieved the aim of utilising electropolymerisation to reliably generate uniform PPy coatings, which demonstrate ROS scavenging capacity. In parallel, this study also successfully achieved the aim of identifying and developing a cell-based model for testing the biological effects of PPy on oxidative signalling using p65 phosphorylation as a measure of inflammatory stress and oxidised-CaMKII as a marker of oxidative stress.

With coatings generated by galvanostatic electropolymerisation at 1 mA after salicylate elution, when using the HCAEC-based model developed in this study, PPy reduced the generation of intracellular ROS generation and CaMKII oxidation. This supports the continued investigation of PPy as a novel antioxidant coronary artery stent coating.

More work is however needed to understand the mechanism by which coatings generated by galvanostatic electropolymerisation at 1 mA impart this benefit and the role of CaMKII oxidation in propagating in-stent restenosis. Finally, work should be undertaken to establish the effect of PPy on vascular smooth muscle cells and vascular cells over a longer chronic time period.

References

Ahotupa, M. (2017) 'Oxidized lipoprotein lipids and atherosclerosis', *Free Radical Research*, 51(4), pp. 439–447.

Ahsan, H. (2013) '3-Nitrotyrosine: A biomarker of nitrogen free radical species modified proteins in systemic autoimmunogenic conditions', *Human Immunology*, 74(10), pp. 1392–1399.

Al-Amiery AA, Al-Majedy YK, Kadhum AAH, Mohamad AB. (2015) 'Hydrogen Peroxide Scavenging Activity of Novel Coumarins Synthesized Using Different Approaches', *PLOS ONE*, 10(7), p. e0132175.

Alexander MR, Murgai M, Moehle CW, Owens GK. (2012) 'Interleukin-1β modulates smooth muscle cell phenotype to a distinct inflammatory state relative to PDGF-DD via NF-κB-dependent mechanisms', *Physiological Genomics*, 44(7), pp. 417–429.

Almonacid Suarez AM, van der Ham I, Brinker MGL, van Rijn P, Harmsen MC. (2020) 'Topography-driven alterations in endothelial cell phenotype and contact guidance', *Heliyon*, 6(6), p. e04329.

Amann, R. and Peskar, B. A. (2002) 'Anti-inflammatory effects of aspirin and sodium salicylate', *European Journal of Pharmacology*, 447(1), pp. 1–9.

Ampem, P. T., Smedlund, K. and Vazquez, G. (2015) 'Pharmacological evidence for a role of the transient receptor potential canonical 3 (TRPC3) channel in endoplasmic reticulum stress-induced apoptosis of human coronary artery endothelial cells', *Vascular Pharmacology*, 76, pp. 42–52.

Anderson, H. D. I., Rahmutula, D. and Gardner, D. G. (2004) 'Tumor Necrosis Factor-α Inhibits Endothelial Nitric-oxide Synthase Gene Promoter Activity in Bovine Aortic Endothelial Cells', *Journal of Biological Chemistry*, 279(2), pp. 963–969.

Anderson, M. E. (2015) 'Oxidant stress promotes disease by activating CaMKII', *Journal of Molecular and Cellular Cardiology*, 89, pp. 160–167.

Annibaldi, V., Rooney, A. D. and Breslin, C. B. (2012) 'Corrosion protection of copper using polypyrrole electrosynthesised from a salicylate solution', *Corrosion Science*, 59, pp. 179–185.

Antolovich M, Prenzler PD, Patsalides E, McDonald S, Robards K. (2002) 'Methods for testing antioxidant activity', *Analyst*, 127(1), pp. 183–198.

Apak R. Ozyurek M, Guclu K, Capanoglu E. (2016) 'Antioxidant Activity / Capacity Measurement . 2 . Hydrogen Atom Transfer (HAT) -Based , Mixed-Mode (Electron Transfer (ET)/ HAT), and Lipid Peroxidation Assays', *Journal of Agricultural and Food Chemistry,* 64, pp. 1028-1045.

Arbizzani C, Mastragostino M, Nevi L, Rambelli L. (2007) 'Polypyrrole: A drug-eluting membrane for coronary stents', *Electrochimica Acta*, 52(9), pp. 3274–3279.

Ardanaz, N. and Pagano, P. J. (2006) 'Hydrogen peroxide as a paracrine vascular mediator: Regulation and signaling leading to dysfunction', *Experimental Biology and Medicine*, 231(3), pp. 237–251.

Arrieta Almario, A. A. and Tarazona Cáceres, R. L. (2009) 'Study of kinetic formation and the electrochemical behavior of polypyrrole films', *Journal of the Chilean Chemical Society*, 54(1), pp. 14–19.

Arteshi Y, Aghanejad A, Davaran S, Omidi Y. (2018) 'Biocompatible and electroconductive polyaniline-based biomaterials for electrical stimulation', *European Polymer Journal*. Elsevier, 108(August), pp. 150–170.

Asavapiriyanont S, Chandler GK, Gunawardena GA, Pletcher D. (1984) 'The electrodeposition of poly-N-methylpyrrole films from aqueous solutions', *Journal of Electroanalytical Chemistry and Interfacial Electrochemistry*, 177(1), pp. 245–251.

Ashrafi A. Golozar MA, Mallakpour S . (2003) 'Electropolymerization of Pyrrole and N-Methylpyrrole on Mild Steel Surface', *Iranian Polymer Journal*, 2(6), pp. 485–490.

Ateh, D. D., Navsaria, H. A. and Vadgama, P. (2006) 'Polypyrrole-based conducting polymers and interactions with biological tissues', *Journal of the Royal Society Interface*, 3(11), pp. 741–752.

Ayala, A., Muñoz, M. F. and Argüelles, S. (2014) 'Lipid peroxidation: Production, metabolism, and signaling mechanisms of malondialdehyde and 4-hydroxy-2-nonenal', *Oxidative Medicine and Cellular Longevity.*

Balint, R., Cassidy, N. J. and Cartmell, S. H. (2014) 'Conductive polymers: Towards a smart biomaterial for tissue engineering', *Acta Biomaterialia*, 10(6), pp. 2341–2353.

Balogh, E. (2018) 'Endothelial cell activation is attenuated by everolimus via transcriptional and post-transcriptional regulatory mechanisms after drug-eluting coronary stenting', pp. 1–20.

Banerjee S, Saikia JP, Kumar A, Konwar BK. (2010) 'Antioxidant activity and haemolysis prevention efficiency of polyaniline nanofibers', *Nanotechnology*, 21(4).

Barbato JE, Zuckerbraun BS, Overhaus M, Raman KG, Tzeng E (2005) 'Nitric oxide modulates vascular inflammation and intimal hyperplasia in insulin resistance and the metabolic syndrome', *American Journal of Physiology - Heart and Circulatory Physiology*, 289(1 58-1), pp. 228–236.

Barisci JN, Stella R, Spinks GM, Wallace GG.. (2000) 'Characterization of the topography and surface potential of electrodeposited conducting polymer films using atomic force and electric force microscopies', *Electrochimica Acta*, 46(4), pp. 519–531.

Barrera, G. (2012) 'Oxidative Stress and Lipid Peroxidation Products in Cancer Progression and Therapy', *ISRN Oncology*, 2012, pp. 1–21.

Bartsch, H. and Nair, J. (2006) 'Chronic inflammation and oxidative stress in the genesis and perpetuation of cancer: Role of lipid peroxidation, DNA damage, and repair', *Langenbeck's Archives of Surgery*, 391(5), pp. 499–510.

Bassous, N., Cooke, J. P. and Webster, T. J. (2016) 'Enhancing Stent Effectiveness with Nanofeatures', *Methodist DeBakey Cardiovascular Journal*, 12(3), pp. 163–168.

Battaglia, V., Salvi, M. and Toninello, A. (2005) 'Oxidative stress is responsible for mitochondrial permeability transition induction by salicylate in liver mitochondria', *Journal of Biological Chemistry*, 280(40), pp. 33864–33872.

Bedair TM, ElNaggar MA, Joung YK, Han DK. (2017) 'Recent advances to accelerate re-endothelialization for vascular stents', *Journal of Tissue Engineering*, 8, p. 204173141773154.

BelAiba RS, Djordjevic T, Petry A, Diemer K, Bonello S, Banfi B, Hess J, Pogrebniak A, Bickel C, Görlach A. (2007) 'NOX5 variants are functionally active in endothelial cells', *Free Radical Biology and Medicine*, 42(4), pp. 446–459.

Bendary E, Francis RR, Ali HMG, Sarwat MI, El Hady S. (2013) 'Antioxidant and structure–activity relationships (SARs) of some phenolic and anilines compounds', *Annals of Agricultural Sciences*. Faculty of Agriculture, Ain Shams University, 58(2), pp. 173–181.

Bergheanu, S. C., Bodde, M. C. and Jukema, J. W. (2017) 'Pathophysiology and treatment of atherosclerosis: Current view and future perspective on lipoprotein modification treatment', *Netherlands Heart Journal*, 25(4), pp. 231–242.

Bhadra, S. and Khastgir, D. (2007) 'Degradation and stability of polyaniline on exposure to electron beam irradiation (structure-property relationship)', *Polymer Degradation and Stability*, 92(10), pp. 1824–1832.

Bhatnagar P, Wickramasinghe K, Wilkins E, Townsend N. (2016) 'Trends in the epidemiology of cardiovascular disease in the UK', *Heart*, 102(24), pp. 1945–1952.

Bidez PR, Li S, MacDiarmid AG, Venancio EC, Wei Y, Lelkes PI. (2006) 'Polyaniline, an electroactive polymer, supports adhesion and proliferation of cardiac myoblasts', *Journal of Biomaterials Science, Polymer Edition*. 17, pp. 199-212

Bittar MN, Carey JA, Barnard JB, Pravica V, Deiraniya AK, Yonan N, Hutchinson IV. (2006) 'Tumor necrosis factor alpha influences the inflammatory response after coronary surgery', *Annals of Thoracic Surgery*, 81(1), pp. 132–137.

Bocchi V, Chierici L, Gardini GP, Mondelli R. (1970) 'On pyrrole oxidation with hydrogen peroxide', *Tetrahedron*, 26(17), pp. 4073–4082.

Boehler, C., Aqrawe, Z. and Asplund, M. (2019) 'Applications of PEDOT in bioelectronic medicine', *Bioelectronics in Medicine*, 2(2), pp. 89–99.

Boeva, Z. A. and Sergeyev, V. G. (2014) 'Polyaniline: Synthesis, properties, and application', *Polymer Science Series C*, 56(1), pp. 144–153.

Borges RS, Barros TG, Pereira GAN, Batista J, Filho RFGPB, Veiga AAS, Hamoy M, Mello VJ, da Silva ABF, Barros CAL (2014) 'A Structure and Antioxidant Activity Study of Paracetamol and Salicylic Acid', *Pharmacology & Pharmacy*, 05(13), pp. 1185–1191.

Borges, R. S. and Castle, S. L. (2015) 'The antioxidant properties of salicylate derivatives: A possible new mechanism of anti-inflammatory activity', *Bioorganic and Medicinal Chemistry Letters*. Elsevier Ltd, 25(21), pp. 4808–4811.

Bouallegue, A., Pandey, N. R. and Srivastava, A. K. (2009) 'CaMKII knockdown attenuates H2O2-induced phosphorylation of ERK1/2, PKB/Akt, and IGF-1R in vascular smooth muscle cells', *Free Radical Biology and Medicine*, 47(6), pp. 858–866.

Boyden TF, Nallamothu BK, Moscucci M, Chan PS, Grossman PM, Tsai TT, Chetcuti SJ, Bates ER, Gurm HS. (2007) 'Meta-Analysis of Randomized Trials of Drug-Eluting Stents Versus Bare Metal Stents in Patients With Diabetes Mellitus', *American Journal of Cardiology*, 99(10), pp. 1399–1402.

Bridges AB, Scott NA, Belch JJ. (1991) 'Probucol, a superoxide free radical scavenger in vitro', *Atherosclerosis*, 89(2-3), pp. 263-265

Briones MA, Phillips DJ, Renshaw MA, Hooper WC. (2001) 'Expression of chemokine by human coronary-artery and umbilical-vein endothelial cells and its regulation by inflammatory cytokines', *Coronary Artery Disease*, 12(3), pp. 179–186.

Buccheri D, Piraino D, Andolina G, Cortese B. (2016) 'Understanding and managing in-stent restenosis: A review of clinical data, from pathogenesis to treatment', *Journal of Thoracic Disease*, 8(10), pp. E1150–E1162.

Bueno DC, Canto RFS, de Souza V, Andreguetti RR, Barbosa FAR, Naime AA, Dey PN, Wüllner V, Lopes MW, Braga AL, Methner A, Farina M. (2020) 'New Probucol Analogues Inhibit Ferroptosis, Improve Mitochondrial Parameters, and Induce Glutathione Peroxidase in HT22 Cells', *Molecular Neurobiology*, 57(8), pp. 3273–3290.

Byon, C. H., Heath, J. M. and Chen, Y. (2016) 'Redox signaling in cardiovascular pathophysiology: A focus on hydrogen peroxide and vascular smooth muscle cells', *Redox Biology*, 9, pp. 244–253.

Byrne, R. A., Joner, M. and Kastrati, A. (2015) 'Stent thrombosis and restenosis: What have we learned and where are we going? the Andreas Grüntzig Lecture ESC 2014', *European Heart Journal*, 36(47), pp. 3320–3331.

Cai, H., Liu, D. and Garcia, J. G. N. (2008) 'CaM Kinase II-dependent pathophysiological signalling in endothelial cells', *Cardiovascular Research*, 77(1), pp. 30–34.

Campolo J, Vozzi F, Penco S, Cozzi L, Caruso R, Domenici C, Ahluwalia A, Rial M, Marraccini P, Parodi O. (2014) 'Vascular injury post stent implantation: Different gene expression modulation in Human Umbilical Vein Endothelial Cells (HUVECs) model', *PLoS ONE*, 9(2).

Cascalheira AC, Aeiyach S, Lacaze PC, Abrantes LM. (2003) 'Electrochemical synthesis and redox behaviour of polypyrrole coatings on copper in salicylate aqueous solution', *Electrochimica Acta*, 48(17), pp. 2523–2529.

Casscells, W. (1992) 'Migration of Smooth Muscle and Endothelial Cells Critical Events in Restenosis'. *Research Advances Series,* 86(3), pp. 723-729.

Cassese S, Byrne RA, Tada T, King LA, Kastrati A. (2012) 'Clinical impact of extended dual antiplatelet therapy after percutaneous coronary interventions in the drug-eluting stent era: A meta-analysis of randomized trials', *European Heart Journal*, 33(24), pp. 3078–3087.

Celeghini ECC, Alves MBR, de Arruda RP, de Rezende GM, Florez-Rodriguez SA, de Sá Filho MF. (2021) 'Efficiency of CellROX deep red® and CellROX orange® fluorescent probes in identifying reactive oxygen species in sperm samples from high and low fertility bulls', *Animal Biotechnology*, 32(1), pp. 77–83.

Ceriello A, Novials A, Ortega E, Canivell S, Sala LL, Pujadas G, Esposito K, Giugliano D, Genovese S. (2013) 'Glucagon-like peptide 1 reduces endothelial dysfunction, inflammation, and oxidative stress induced by both hyperglycemia and hypoglycemia in type 1 diabetes', *Diabetes Care*, 36(8), pp. 2346–2350.

Chaabane C, Otsuka F, Virmani R, Bochaton-Piallat ML (2013) 'Biological responses in stented arteries', *Cardiovascular Research*, 99(2), pp. 353–363.

Chamberlain J, Evans D, King A, Dewberry R, Dower S, Crossman D, Francis S. (2006) 'Interleukin-1β and signaling of interleukin-1 in vascular wall and circulating cells modulates the extent of neointima formation in mice', *American Journal of Pathology*, 168(4), pp. 1396–1403.

Chang WC, Chen CH, Lee MF, Chang T, Yu YM. (2010) 'Chlorogenic acid attenuates adhesion molecules upregulation in IL-1β-treated endothelial cells', *European Journal of Nutrition*, 49(5), pp. 267–275.

Chen C, Jamaluddin MS, Yan S, Sheikh-Hamad D, Yao Q. (2008) 'Human stanniocalcin-1 blocks TNF-α-induced monolayer permeability in human coronary artery endothelial cells', *Arteriosclerosis, Thrombosis, and Vascular Biology*, 28(5), pp. 906–912.

Chen X, Andresen BT, Hill M, Zhang J, Booth F, Zhang C. (2008) 'Role of reactive oxygen species in tumor necrosis factor-alpha induced endothelial dysfunction.', *Current hypertension reviews*, 4(4), pp. 245–255.

Chen, P. Y., Schwartz, M. A. and Simons, M. (2020) 'Endothelial-to-Mesenchymal Transition, Vascular Inflammation, and Atherosclerosis', *Frontiers in Cardiovascular Medicine*, 7(May), pp. 1–6.

Chepelev LL, Beshara CS, MacLean PD, Hatfield GL, Rand AA, Thompson A, Wright JS, Barclay RC. (2006) 'Polypyrroles as antioxidants: Kinetic studies on reactions of bilirubin and biliverdin dimethyl esters and synthetic model compounds with peroxyl radicals in solution. Chemical calculations on selected typical structures', *Journal of Organic Chemistry*, 71(1), pp. 22–30.

Cheranov, S. Y. and Jaggar, J. H. (2006) 'TNF-α dilates cerebral arteries via NAD(P)H oxidase-dependent Ca2+ spark activation', *American Journal of Physiology-Cell Physiology*. American Physiological Society, 290(4), pp. C964–C971.

Chibana H, Kajimoto H, Ueno T, Yokoyama S, Sasaki K, Ohtsuka M, Koiwaya H, Nakayoshi T, Mitsutake Y, Itaya N, Sasaki M, Yoshihiro Fukumoto 1. (2017) 'Interleukin-1β is associated with coronary endothelial dysfunction in patients with mTOR-inhibitor-eluting stent implantation', *Heart and Vessels*, 32(7), pp. 823–832

Chien S-CC, Tseng Y-HH, Hsu W-NN, Chu F, Chang S, Kuo H, Wang S. (2014) 'Anti-inflammatory and anti-oxidative activities of polyacetylene from Dendropanax dentiger.', *Natural Product Communications*, 9(11), pp. 1589–90.

Chikouche, I., Sahari, A. and Zouaoui, A. (2014) 'Influence of electropolymerization method on morphologies and capacitive properties of polypyrrole films growing on silicon', *Surface Review and Letters*, 21(6), pp. 1–8.

Cho JG, Lee A, Chang W, Lee MS, Kim J. (2018) 'Endothelial to mesenchymal transition represents a key link in the interaction between inflammation and endothelial dysfunction', *Frontiers in Immunology*, 9(FEB), pp. 3–5.

Choi, H., Yang, Z. and Weisshaar, J. C. (2015) 'Single-cell, real-time detection of oxidative stress induced in escherichia coli by the antimicrobial peptide CM15', *Proceedings of the National Academy of Sciences of the United States of America*, 112(3), pp. E303–E310

Choi WJ, Jung J, Lee S, Chung YJ, Yang C, Lee YK, Lee Y, Park JK, Ko HW, Lee J. (2015) 'Effects of substrate conductivity on cell morphogenesis and proliferation using tailored, atomic layer deposition-grown ZnO thin films', *Scientific Reports*, 5, pp. 1–9.

Chougule MA, Pawar SG, Godse PR, Mulik RN, Sen S, Patil VB. (2011) 'Synthesis and Characterization of Polypyrrole (PPy) Thin Films', *Soft Nanoscience Letters*, 01(01), pp. 6–10.

Christian, F., Smith, E. L. and Carmody, R. J. (2016) 'The regulation of NF-κB Subunits by Phosphorylation', *Cells*, 5(1).

Chung TW, Liu DZ, Wang SY, Wang SS. (2003) 'Enhancement of the growth of human endothelial cells by surface roughness at nanometer scale', *Biomaterials*, 24(25), pp. 4655–4661.

Cipolletta E, Monaco S, Maione AS, Vitiello L, Campiglia P, Pastore L, Franchini C, Novellino E, Limongelli V, Bayer KU, Means AR, Rossi G, Trimarco B, Iaccarino G, Illario M. (2010) 'Calmodulin-dependent kinase II mediates vascular smooth muscle cell proliferation and is potentiated by extracellular signal regulated kinase', *Endocrinology*, 151(6), pp. 2747–2759.

Collin, F. (2019) 'Chemical basis of reactive oxygen species reactivity and involvement in neurodegenerative diseases', *International Journal of Molecular Sciences*, 20(10).

Colombo G, Clerici M, Garavaglia ME, Giustarini D, Rossi R, Milzani A, Dalle-Donne I. (2016) ' A step-by-step protocol for assaying protein carbonylation in biological samples', *Journal of Chromatography B,* 1019. Pp. 178-190

Conti, V. *et al.* (2015) 'Aging-related changes in oxidative stress response of human endothelial cells', *Aging Clinical and Experimental Research*. Springer International Publishing, 27(4), pp. 547–553.

Contreras-Naranjo, J. E. and Aguilar, O. (2019) 'Suppressing non-specific binding of proteins onto electrode surfaces in the development of electrochemical immunosensors', *Biosensors*, 9(1).

Corda, S. *et al.* (2001) 'Rapid reactive oxygen species production by mitochondria in endothelial cells exposed to tumor necrosis factor-α is mediated by ceramide', *American Journal of Respiratory Cell and Molecular Biology*, 24, pp. 762-768.

Cornelissen, A. and Vogt, F. J. (2019) 'The effects of stenting on coronary endothelium from a molecular biological view: Time for improvement?', *Journal of Cellular and Molecular Medicine*, 23(1), pp. 39–46.

Costa D, Gomes A, Lima JLFC, Fernandes E. (2008) 'Singlet oxygen scavenging activity of non-steroidal anti-inflammatory drugs', *Redox Report*, 13(4), pp. 153–160.

Coyle, C. H. and Kader, K. N. (2007) 'Mechanisms of H2O2-induced oxidative stress in endothelial cells exposed to physiologic shear stress', *ASAIO Journal*, 53(1), pp. 17–22.

Csiszar A, Smith K, Labinskyy N, Orosz Z, Rivera A, Ungvari Z. (2006) 'Resveratrol attenuates TNF-α-induced activation of coronary arterial endothelial cells: Role of NF-κB inhibition', *American Journal of Physiology - Heart and Circulatory Physiology*, 291(4), pp. 1694–1699.

Csonka C, Páli T, Bencsik P, Görbe A, Ferdinandy P, Csont T. (2015) 'Measurement of NO in biological samples', *British Journal of Pharmacology*, 172(6), pp. 1620–1632.

Cysewska, K., Gazda, M. and Jasiński, P. (2017) 'Influence of electropolymerization temperature on corrosion, morphological and electrical properties of PPy doped with salicylate on iron', *Surface and Coatings Technology*, 328, pp. 248–255.

Cysewska, K., Karczewski, J. and Jasiński, P. (2019) 'Influence of the electrosynthesis conditions on the spontaneous release of anti-inflammatory salicylate during degradation of polypyrrole coated iron for biodegradable cardiovascular stent', *Electrochimica Acta*, 320.

Cysewska, K., Virtanen, S. and Jasiński, P. (2015) 'Electrochemical Activity and Electrical Properties of Optimized Polypyrrole Coatings on Iron', *Journal of The Electrochemical Society*, 162(12), pp. E307–E313.

Cysewska, K., Virtanen, S. and Jasiński, P. (2016) 'Study of the electrochemical stability of polypyrrole coating on iron in sodium salicylate aqueous solution', *Synthetic Metals*, 221, pp. 1–7.

Dalmolin C, Canobre SC, Biaggio SR, Rocha-Filho RC, Bocchi N. (2005) 'Electropolymerization of polyaniline on high surface area carbon substrates', *Journal of Electroanalytical Chemistry*, 578(1), pp. 9–15.

Daniele S, Ugo P, Bragato C, Mazzocchin GA. (1996) 'Use of Nafion® coated carbon disk microelectrodes in solution without and with different concentrations of supporting electrolyte', *Journal of Electroanalytical Chemistry*, 418(1–2), pp. 29–34.

Das, T. K. and Prusty, S. (2012) 'Review on Conducting Polymers and Their Applications', *Polymer - Plastics Technology and Engineering*, 51(14), pp. 1487–1500.

Das K. & Roychoudhury A. (2014) 'Reactive oxygen species (ROS) and response of antioxidants as ROS-scavengers during environmental stress in plants', *Frontiers in Environmental Science,* 2.

Dasgupta, Q., Chatterjee, K. and Madras, G. (2015) 'Controlled Release of Salicylic Acid from Biodegradable Cross-Linked Polyesters', *Molecular Pharmaceutics*, 12(9), pp. 3479–3489.

De Albuquerque JE, Mattoso LHC, Faria RM, Masters JG, MacDiarmid AG. (2004) 'Study of the interconversion of polyaniline oxidation states by optical absorption spectroscopy', *Synthetic Metals*, 146(1), pp. 1–10.

De Oliveira EM, Lima MAP, Bettega MHF, Sanchez SDA, Da Costa RF, Varella MTDN. (2010) 'Low-energy electron collisions with pyrrole', *Journal of Chemical Physics*, 132(20).

de Prado AP, Pérez-Martínez C, Cuellas-Ramón C, Gonzalo-Orden JM, Regueiro-Purriños M, Martínez B, García-Iglesias MJ, Ajenjo JM, Altónaga JR, Diego-Nieto A, de Miguel A, Fernández-Vázquez F. (2011) 'Time course of reendothelialization of stents in a normal coronary swine model: Characterization and quantification', *Veterinary Pathology*, 48(6), pp. 1109–1117

De Winther MPJ, Kanters E, Kraal G, Hofker MH. (2005) 'Nuclear factor κB signaling in atherogenesis', *Arteriosclerosis, Thrombosis, and Vascular Biology*, 25(5), pp. 904–914

Demirci B, Demir O, Dost T, Birincioglu M. (2014) 'Antioxidative effect of aspirin on vascular function of aged ovariectomized rats', *Age*, 36(1), pp. 223–229.

Di Mario, C. and Caiazzo, G. (2015) 'Biodegradable stents: The golden future of angioplasty?', *The Lancet*, 385(9962), pp. 10–12.

Dikalov, S. I. and Harrison, D. G. (2012) 'Methods for Detection of Mitochondrial and Cellular Reactive Oxygen Species', *Antioxidants & Redox Signaling*, 20(2), pp. 372–382.

Dong F, Zhang X, Wold LE, Ren Q, Zhang Z, Ren J. (2005) 'Endothelin-1 enhances oxidative stress, cell proliferation and reduces apoptosis in human umbilical vein endothelial cells: Role of ET B receptor, NADPH oxidase and caveolin-1', *British Journal of Pharmacology*, 145(3), pp. 323–333.

Douglas G, Van Kampen E, Hale AB, et al. (2013) 'Endothelial cell repopulation after stenting determines in-stent neointima formation: Effects of bare-metal vs. drug-eluting stents and genetic endothelial cell modification', *European Heart Journal*, 34(43), pp. 3378–3388.

Dröge, W. (2002) 'Free radicals in the physiological control of cell function', *Physiological Reviews*, 82(1), pp. 47–95.

Du, X. and Wang, Z. (2003) 'Effects of polymerization potential on the properties of electrosynthesized PEDOT films', *Electrochimica Acta*, 48(12), pp. 1713–1717.

Durand E, Zen AAH, Addad F, Brasselet C, Caligiuri G, Vinchon F, Lemarchand P, Desnos M, Bruneval P, Lafont A. (2005) 'Adenovirus-mediated gene transfer of superoxide dismutase and catalase decreases restenosis after balloon angioplasty', *Journal of Vascular Research*, 42(3), pp. 255–265.

Eaton SL, Hurtado ML, Oldknow KJ, Graham LC, Marchant TW, Gillingwater TH, Farquharson C, Wishart TM. (2014) 'A Guide to Modern Quantitative Fluorescent Western Blotting with Troubleshooting Strategies', *Journal of Visualised Experiments,* 93, pp. 52099.

Ebenebe, O. V., Heather, A. and Erickson, J. R. (2018) 'CaMKII in Vascular Signalling: "Friend or Foe"?', *Heart Lung and Circulation*, 27(5), pp. 560–567.

Ekstrand M, Trajkovska MG, Perman-Sundelin J, Fogelstrand P, Adiels M, Johansson M, Mattsson-Hultén L, Borén J, Levin M. (2015) 'Imaging of intracellular and extracellular ROS levels in atherosclerotic mouse aortas ex vivo: Effects of lipid lowering by diet or atorvastatin', *PLoS ONE*, 10(6), pp. 1–15.

El Jaouhari A, El Asbahani A, Bouabdallaoui M, Aouzal Z, Filotás D, Bazzaoui EA, Nagy L, Nagy G. (2017) 'Corrosion resistance and antibacterial activity of electrosynthesized polypyrrole', *Synthetic Metals*. Elsevier B.V., 226, pp. 15–24.

Elezi S, Kastrati A, Pache J, Wehinger A, Hadamitzky M, Dirschinger J, Neumann FJ, Schömig A. (1998) 'Diabetes mellitus and the clinical and angiographic outcome after coronary stent placement', *Journal of the American College of Cardiology*, 32(7), pp. 1866–1873

Elgrishi N, Rountree KJ, McCarthy BD, Rountree ES, Eisenhart TT, Dempsey JL. (2018) 'A Practical Beginner's Guide to Cyclic Voltammetry', *Journal of Chemical Education*, 95(2), pp. 197–206.

Erickson, J. R. (2014) 'Mechanisms of CaMKII activation in the heart', *Frontiers in Pharmacology*, 5 APR(April), pp. 1–5.

Erickson JR, Julie He B, Grumbach IM, Anderson ME. (2011) 'CaMKII in the cardiovascular system: Sensing redox states', *Physiological Reviews*, 91(3), pp. 889–915.

Erickson JR, Joiner MA, Guan X, Kutschke W, Yang J, Oddis CV, Bartlett RK, Lowe JS, O'Donnell SE, Aykin-Burns N, Zimmerman MC, Zimmerman K, Ham AL, Weiss RM, Spitz DR, Shea MA, Colbran RJ, Mohler PJ, Anderson ME. (2008) 'A dynamic pathway for calcium-independent activation of CaMKII by methionine oxidation', *Cell*, 133(3), pp. 462–474.

Erickson JR, He BJ, Grumbach IM, Anderson ME. (2019) 'CaMKII IN THE CARDIOVASCULAR SYSTEM ', *Physiol Rev,* (282), pp. 889–915.

Erickson JR, Nichols CB, Uchinoumi H, Stein ML, Bossuyt J, Bers DM. (2015) 'S -Nitrosylation Induces Both Autonomous Activation and Inhibition of Calcium / Calmodulin-dependent Protein Kinase.' 290(42):25646-25656.

Eruslanov, E. and Kusmartsev, S. (2010) 'Identification of ROS using oxidized DCFDA and flow-cytometry', *Methods in Molecular Biology*.

Evans, G. P. (2008) 'The Electrochemistry of Conducting Polymers', *Advances in Electrochemical Science and Engineering*. (Advances in Electrochemical Sciences and Engineering).

Everett SA, Kundu SC, Maddix S, Willson RL. (1995) 'MECHANISMS OF FREE-RADICAL SCAVENGING BY THE NUTRITIONAL ANTIOXIDANT β-CAROTENE', *Biochemical Society Transactions*, 23(2), pp. 230S-230S.

Fahlgren A, Bratengeier C, Gelmi A, Semeins CM, Klein-Nulend J, Jager EWH, Bakker AD. (2015) 'Biocompatibility of polypyrrole with human primary osteoblasts and the effect of dopants', *PLoS ONE*, 10(7), pp. 1–17.

Fantin SDS, Wainstein MV, Polanczyk CA, Ledur P, Lazzari CM, Klein C, Hackenhaar FS, Benfato MS, Schaan BD. (2011) 'Inflammatory and oxidative stress markers after intravenous insulin in percutaneous coronary intervention with stent in type 2 diabetes mellitus: A randomized controlled trial', *Journal of Clinical Endocrinology and Metabolism*, 96(2), pp. 478–485.

Fernandes E, Costa D, Toste SA, Lima JLFC, Reis S. (2004) 'In vitro scavenging activity for reactive oxygen and nitrogen species by nonsteroidal anti-inflammatory indole, pyrrole, and oxazole derivative drugs', *Free Radical Biology and Medicine*, 37(11), pp. 1895–1905.

Fernandez I, Trueba M, Nunez CA, Rieumont J. (2002) 'Electropolymerization of pyrrole from aqueous solutions on austenitic stainless steel electrodes', *Chemical Sciences Revisited*, 33(3): 121-125.

Finn A V., Nakano M, Narula J, Kolodgie FD, Virmani R. (2010) 'Concept of vulnerable/unstable plaque', *Arteriosclerosis, Thrombosis, and Vascular Biology*, 30(7), pp. 1282–1292

Finn A V., Nakazawa G, Joner M, Kolodgie FD, Mont EK, Gold HK, Virmani R. (2007) 'Vascular responses to drug eluting stents: Importance of delayed healing', *Arteriosclerosis, Thrombosis, and Vascular Biology*, 27(7), pp. 1500–1510.

Fonner JM, Forciniti L, Nguyen H, Byrne JD, Kou Y, Syeda-Nawaz J, Schmidt CE. (2008) 'Biocompatibility implications of polypyrrole synthesis techniques', *Biomedical Materials*, 3(3).

Foroughi J, Ghorbani SR, Peleckis G, Spinks GM, Wallace GG, Wang XL, Dou SX. (2010) 'The mechanical and the electrical properties of conducting polypyrrole fibers', *Journal of Applied Physics*, 107(10).

Förstermann, U., Xia, N. and Li, H. (2017) 'Roles of vascular oxidative stress and nitric oxide in the pathogenesis of atherosclerosis', *Circulation Research*, 120(4), pp. 713–735.

Foti, M. C. (2010) 'Antioxidant properties of phenols', *Journal of Pharmacy and Pharmacology*, 59(12), pp. 1673–1685

Foundation, B. H. (2019) 'UK Factsheet', *British Heart Foundation*, (April), pp. 1–21.

Fong, P. (2010) 'Increased Blood Flow Induces Oxidative Stress Through an Endothelium- and Nitric Oxide-Independent Mechanism' *Free Radic Biol Med,* 49(2), pp. 301-305.

Franscini N, Bachli EB, Blau N, Leikauf MS, Schaffner A, Schoedon G. (2004) 'Gene expression profiling of inflamed human endothelial cells and influence of activated protein C', *Circulation*, 110(18), pp. 2903–2909

Frey, R. S., Ushio–Fukai, M. and Malik, A. B. (2009) 'NADPH Oxidase-Dependent Signaling in Endothelial Cells: Role in Physiology and Pathophysiology', *Antioxidants & Redox Signaling*, 11(4), pp. 791–810.

Furmanik M, Chatrou M, Van Gorp R, Akbulut A, Willems B, Schmidt H, et al. (2020) 'Reactive Oxygen-Forming Nox5 Links Vascular Smooth Muscle Cell Phenotypic Switching and Extracellular Vesicle-Mediated Vascular Calcification', *Circulation Research*, 127(7), pp. 911–927.

Gao S, Zhao D, Wang M, Hara H, Chen P, Xu J, Tang J, Wei L, Li Z, Cooper DKC, Cai Z, Mou L. (2017) 'Human IL-6, IL-17, IL-1β, and TNF-α differently regulate the expression of pro-inflammatory related genes, tissue factor, and swine leukocyte antigen class I in porcine aortic endothelial cells', *Xenotransplantation*, 24(2), pp. 1–13.

Gao H, Liu L, Zhao Y, Zhao F, Han X, Qi Y, Liu J. (2017) 'Association Between Circulating Oxidized LDL and Atherosclerotic Cardiovascular Disease: A Meta-analysis of Observational Studies', *Canadian Journal of Cardiology*. Canadian Cardiovascular Society, 33(12), pp. 1624–1632.

Garner B, Georgevich A, Hodgson AJ, Liu L, Wallace GG. (1999) 'Polypyrrole-heparin composites as stimulus-responsive substrates for endothelial cell growth', *Journal of Biomedical Materials Research*, 44(2), pp. 121–129.

Gaudino M, Antoniades C, Benedetto U, Deb S, Di France A, Di Giammarco G, Fremes S, Glineur D, et al. (2017) 'Mechanisms, consequences, and prevention of coronary graft failure', *Circulation*, 136(18), pp. 1749–1764.

Gelmi A, Ljunggren MK, Rafat M, Jager EWH. (2014) 'Influence of conductive polymer doping on the viability of cardiac progenitor cells', *Journal of Materials Chemistry B*, 2(24), pp. 3860–3867.

Genies, E. M., Bidan, G. and Diaz, A. F. (1983) 'Spectroelectrochemical study of polypyrrole films', *Journal of Electroanalytical Chemistry and Interfacial Electrochemistry*, 149(1), pp. 101–113.

George CJ, Baim DS, Brinker JA, Fischman DL, Goldberg S, Holubkov R, Kennard ED, Veltri L, Detre KM. (1998) 'One-year follow-up of the stent restenosis (STRESS I) study', *American Journal of Cardiology*, 81(7), pp. 860–865.

George PM, Lyckman AW, Lavan DA, Hegde A, Leung Y, Avasare R, Testa C, Alexander PM, Langer R, Sur M. (2005) 'Fabrication and biocompatibility of polypyrrole implants suitable for neural prosthetics', *Biomaterials*, 26(17), pp. 3511–3519.

Gerli R, Paolucci C, Gresele P, Bistoni O, Fiorucci S, Muscat C, Belia S, Bertotto A, Costantini V. (1998) 'Salicylates inhibit adhesion and transmigration of T lymphocytes by preventing integrin activation induced by contact with endothelial cells', *Blood*, 92(7), pp. 2389–2398.

German, N., Ramanaviciene, A. and Ramanavicius, A. (2019) 'Formation of polyaniline and polypyrrole nanocomposites with embedded glucose oxidase and gold nanoparticles', *Polymers*, 11(2), pp. 19–24.

Ghebremariam YT, Huang NF, Kambhampati S, Volz KS, Joshi GG, Anslyn EV, Cooke JP. (2014) 'Characterization of a Fluorescent Probe for Imaging Nitric Oxide', *Journal of Vascular Research*, 51(1), pp. 68–79.

Giustarini D, Rossi R, Milzani A, Dalle-Donne I. (2008) 'Nitrite and Nitrate Measurement by Griess Reagent in Human Plasma: Evaluation of Interferences and Standardization', *Methods in Enzymology*, 440(07), pp. 361–380.

Gizdavic-Nikolaidis M, Travas-Sejdic J, Kilmartin PA, Bowmaker GA, Cooney RP. (2004) 'Evaluation of antioxidant activity of aniline and polyaniline', *Current Applied Physics*, 4(2–4), pp. 343–346.

Gizdavic-Nikolaidis M, Travas-Sejdic J, Bowmaker GA, Cooney RP, Thompson C, Kilmartin PA. (2004) 'The antioxidant activity of conducting polymers in biomedical applications', *Current Applied Physics*, 4(2–4), pp. 347–350.

Gomez N, Lee JY, Nickels JD, Schmidt CE. (2007) 'Micropatterned polypyrrole: A combination of electrical and topographical characteristics for the stimulation of cells', *Advanced Functional Materials*, 17(10), pp. 1645–1653.

González, M. B., Brugnoni, L. I. and Saidman, S. B. (2019) 'Salicylate release from a polypyrrole matrix', *Materials Today Communications*, pp. 119–123.

González MB, Brugnoni LI, Vela ME, Saidman SB. (2013) 'Silver deposition on polypyrrole films electrosynthesized in salicylate solutions', *Electrochimica Acta*, 102, pp. 66–71

González-Tejera, M. J., Carrillo, I. and Hernández-Fuentes, I. (1998) 'Influence of the electropolymerization parameters on the generation of polyfurane perchlorate doped films', *Synthetic Metals*, 92(3), pp. 187–195.

Gracia, K. C., Llanas-Cornejo, D. and Husi, H. (2017) 'CVD and oxidative stress', *Journal of Clinical Medicine*, 6(2).

Gray, C. B. B. and Brown, J. H. (2014) 'CaMKIIdelta subtypes: Localization and function', *Frontiers in Pharmacology*, 5 FEB(February), pp. 1–8.

Griesser, M., Chauvin, J. P. R. and Pratt, D. A. (2018) 'The hydrogen atom transfer reactivity of sulfinic acids', *Chemical Science.* Royal Society of Chemistry, 9(36), pp. 7218–7229.

Griffith, L. C. (2004) 'Regulation of calcium/calmodulin-dependent protein kinase II activation by intramolecular and intermodular interactions', *Journal of Neuroscience*, 24(39), pp. 8394–8398.

Grosser, N. and Schröder, H. (2003) 'Aspirin protects endothelial cells from oxidant damage via the nitric oxide-cGMP pathway', *Arteriosclerosis, Thrombosis, and Vascular Biology*, 23(8), pp. 1345–1351

Gu SX, Blokhin IO, Wilson KM, Dhanesha N, Doddapattar P, Grumbach IM, Chauhan AK, Lentz SR. (2016) 'Protein methionine oxidation augments reperfusion injury in acute ischemic stroke', *JCI Insight*, 1(7).

Gu, Y. and Chen, C. C. (2008) 'Eliminating the interference of oxygen for sensing hydrogen peroxide with the polyaniline modified electrode', *Sensors*, 8(12), pp. 8237–8247.

Guimard, N. K., Gomez, N. and Schmidt, C. E. (2007) 'Conducting polymers in biomedical engineering', *Progress in Polymer Science (Oxford)*, 32(8–9), pp. 876–921.

Gülçin, I. (2010) 'Antioxidant properties of resveratrol: A structure-activity insight', *Innovative Food Science and Emerging Technologies*, 11(1), pp. 210–218.

Gutierrez-Pineda, EG, Presa MJP, Gervasi CA, Bolzan AE. (2018) 'Tubular-structured polypyrrole electrodes decorated with gold nanoparticles for electrochemical sensing', *Journal of Electroanalytical Chemistry*, 812(August 2017), pp. 28–36.

Habib, A. and Finn, A. V. (2015) 'Endothelialization of drug eluting stents and its impact on dual anti-platelet therapy duration' *Pharmacol Res*. 93, pp. 22-7.

Halliwell, B. and Whiteman, M. (2004) 'Measuring reactive species and oxidative damage in vivo and in cell culture: how should you do it and what do the results mean?' *British Journal of Pharmacology,* 141, pp. 231-235.

Han BH, Yoon JJ, Choi ES, Jeong DH, Lee YJ, Kang DG, Lee HS. (2017) 'Inhibitory effect of brassinin on TNF-α-induced vascular inflammation in human umbilical vein endothelial cells', *Molecular Medicine Reports*, 16(5), pp. 6890–6895.

Han Q, Shea SM, Arleo T, Qian JY, Ku DN. (2022) 'Thrombogenicity of biomaterials depends on hemodynamic shear rate', *Artificial Organs,* 46(4), pp. 606-617

Haridas, K. K. and Bhat, P. (2008) 'Drug Eluting Stents – Do They Address the Problem of Restenosis?', *Medicine Update,* Chapter 8.

Hartman, J. and Frishman, W. H. (2014) 'Inflammation and atherosclerosis: A review of the role of interleukin-6 in the development of atherosclerosis and the potential for targeted drug therapy', *Cardiology in Review*.

Hasyim, M. R. & Rajagopalan, R. (2020) 'Prediction of Discharge Performances of Pseudocapacitors Using Their Impedance Characteristics', *Journal of The Electrochemical Society,* 167, 013536

He JB, Joiner MA, Singh MV, Luczak ED, Swaminathan PD, Koval OM, Kutschke W, Allamargot C, Yang J, Guan X, Zimmerman K, Grumbach IM, Weiss RM, Spitz DR, Sigmund CD, Blankesteijn WM, Heymans S, Mohler PJ, Anderson ME. (2012) 'Oxidation of CaMKII determines cardiotoxic effects of aldosterone', *Nat Med,* 17(12), pp. 1610-1618.

He J, Liu X, Su C, Wu F, Sun J, Zhang, Yang X, Zhang C, Zhou Z, Zhang X, Lin X, Tao J. (2019) 'Inhibition of Mitochondrial Oxidative Damage Improves Reendothelialization Capacity of Endothelial Progenitor Cells via SIRT3 (Sirtuin 3)-Enhanced SOD2 (Superoxide Dismutase 2) Deacetylation in Hypertension', *Arteriosclerosis, Thrombosis, and Vascular Biology*, 39(8), pp. 1682–1698.

He T, LF L, GJ D. (2012) 'Pro-opiomelanocortin gene delivery suppresses the growth of established Lewis lung carcinoma through a melanocortin-1 receptor-independent pathway', *Journal of Gene Medicine*, 14(1), pp. 44–53.

Hegyi, B., Bers, D. M. and Bossuyt, J. (2019) 'CaMKII signaling in heart diseases: Emerging role in diabetic cardiomyopathy', *Journal of Molecular and Cellular Cardiology*, 127(December 2018), pp. 246–259.

Herrera-Vásquez, A., Salinas, P. and Holuigue, L. (2015) 'Salicylic acid and reactive oxygen species interplay in the transcriptional control of defense genes expression', *Frontiers in Plant Science*, 6(MAR), pp. 1–9.

Holze, R. (2022) 'Overoxidation of Intrinsically Conducting Polymers', *Polymers*, 14(1584).

Hosseini, M G. Bagheri R, Najjar R. (2010) 'Electropolymerization of Polypyrrole and Polypyrrole-ZnO Nanocomposites on Mild Steel and Its Corrosion Protection Performance', *Journal of Applied Polymer Science,* 121, pp. 3159-3166.

House SJ, Ginnan RG, Armstrong SE, Singer HA. (2007) 'Calcium/calmodulin-dependent protein kinase II-δ isoform regulation of vascular smooth muscle cell proliferation', *American Journal of Physiology - Cell Physiology*, 292(6), pp. 2276–2287.

House, S. J. and Singer, H. A. (2008) 'CaMKII-δ isoform regulation of neointima formation after vascular injury', *Arteriosclerosis, Thrombosis, and Vascular Biology*, 28(3), pp. 441–447.

Hristea EN, Caproiu MT, Pencu G, Hillebrand M. (2006) 'and HOO – Radicals and Anions', *International Journal of Molecular Science*, 7, pp. 130–143.

Hsu CF, Peng H, Basle C, Travas-Sejdic J, Kilmartin PA. (2011) 'ABTS•+ scavenging activity of polypyrrole, polyaniline and poly(3,4-ethylenedioxythiophene)', *Polymer International*, 60(1), pp. 69–77

Hsu CF, Peng H, Basle C, Travas-Sejdic J, Kilmartin PA. (2008) 'Free radical scavenging properties of polypyrrole and poly(3,4-ethylenedioxythiophene)', *Current Applied Physics*, 8(3–4), pp. 316–319.

Htay, T. and Liu, M. W. (2005) 'Drug-eluting stent: a review and update.', *Vascular health and risk management*, 1(4), pp. 263–76.

Humpolíček P, Kašpárková V, Pacherník J, Stejskal J, Bober P, Capáková Z, Radaszkiewicz KA, Junkar I, Lehocký M. (2018) 'The biocompatibility of polyaniline and polypyrrole: A comparative study of their cytotoxicity, embryotoxicity and impurity profile', *Materials Science and Engineering C*, 91(May), pp. 303–310.

Humpolíček P, Kuceková Z, Kašpárková V, et al. (2015) 'Blood coagulation and platelet adhesion on polyaniline films', *Colloids and Surfaces B: Biointerfaces*, 133, pp. 278–285.

Hunjan MK, Panday S, Gupta A, Bhaumik J, Das P, Laha JK. (2021) 'Recent Advances in Functionalization of Pyrroles and their Translational Potential', *Chemical Record*, 21(4), pp. 715–780.

Hunter RA, Storm WL, Coneski PN, Schoenfisch MH. (2013) 'Inaccuracies of nitric oxide measurement methods in biological media', *Analytical Chemistry*.

Inoue T, Croce K, Morooka T, Sakuma M, Node K, Simon DI. (2011) 'Vascular inflammation and repair: Implications for re-endothelialization, restenosis, and stent thrombosis', *JACC: Cardiovascular Interventions*, 4(10), pp. 1057–1066.

Inzelt, G. (2012) 'Conducting polymers: a new era in electrochemistry', *Chemistry*.

Iqbal, J., Gunn, J. and Serruys, P. W. (2013) 'Coronary stents: Historical development, current status and future directions', *British Medical Bulletin*, 106(1), pp. 193–211

Jabs A, Göbel S, Wenzel P, Kleschyov AL, Hortmann M, Oelze M, Daiber A, Münzel T. (2008) 'Sirolimus-Induced Vascular Dysfunction. Increased Mitochondrial and Nicotinamide Adenosine Dinucleotide Phosphate Oxidase-Dependent Superoxide Production and Decreased Vascular Nitric Oxide Formation', *Journal of the American College of Cardiology*, 51(22), pp. 2130–2138.

Jadoun S, Riaz U, Budhiraja V. (2014) 'A novel electrochemically synthesized biodegradable thin film of polypyrrole–polyethyleneglycol–polylactic acid nanoparticles'. *Medical Devices and Sensors,* 4: e10141

Jakubiec B, Marois Y, Zhang Z, Sigot-Luizard MF, Dugré FJ, King MW, Dao L, Laroche G, Guidoin R. (1998) 'In vitro cellular response to polypyrrole-coated woven polyester fabrics: Potential benefits of electrical conductivity', *Journal of Biomedical Materials Research*, 41(4), pp. 519–526.

Jannati M, Navaei MR, Ronizi LG. (2019) 'A comparative review of the outcomes of using arterial versus venous conduits in coronary artery bypass graft (CABG)', *Journal of Family Medicine and Primary Care*, 8(9): 2768-2773.

Jeewandara, T. M., Wise, S. G. and Ng, M. K. C. (2014) 'Biocompatibility of coronary stents', *Materials*, 7(2), pp. 769–786.

Jiang J, Fu W, Wang X, Lin PH, Yao Q, Chen C. (2010) 'HIV gp120 induces endothelial dysfunction in tumour necrosis factor-α-activated porcine and human endothelial cells', *Cardiovascular Research*, 87(2), pp. 366–374.

Jiang JL, Li NS, Li YJ, Deng HW. (2002) 'Probucol preserves endothelial function by reduction of the endogenous nitric oxide synthase inhibitor level', *British Journal of Pharmacology*, 135(5), pp. 1175-1182.

Jin X, Wang H, Liu Y, Wang H, Wang W, Lin T. (2019) 'Hydrogen-bonding power interfacial load transfer of carbon fabric/polypyrrole composite pseudosupercapacitor electrode with improved electrochemical stability', *Applied Surface Science*, 470(November 2018), pp. 783–791.

Jones RJ, Jourd'heuil D, Salerno JC, Smith SME, Singer HA. (2007) 'iNOS regulation by calcium/calmodulin-dependent protein kinase II in vascular smooth muscle', *American Journal of Physiology - Heart and Circulatory Physiology*, 292(6), pp. 2634–2642.

Juni RP, Duckers HJ, Vanhoutte PM, Virmani R, Moens AL (2013) 'Oxidative stress and pathological changes after coronary artery interventions', *Journal of the American College of Cardiology*, 61(14), pp. 1471–1481.

Kalyanaraman B, Darley-Usmar V, Davies KJA, Dennery PA, Forman HJ, Grisham MB, Mann GE, Moore K, Roberts LJ, Ischiropoulos H. (2012) 'Measuring reactive oxygen and nitrogen species with fluorescent probes: Challenges and limitations', *Free Radical Biology and Medicine*.

Kamalesh S, Tan P, Wang J, Lee T, Kang ET, Wang CH. (2000) 'Biocompatibility of electroactive polymers in tissues', *Journal of Biomedical Materials Research*, 52(3), pp. 467–478.

Kandzari DE, Mauri L, Popma JJ, Fajadet J. (2011) 'Late-term clinical outcomes with zotarolimus- and sirolimus-eluting stents: 5-Year follow-up of the ENDEAVOR III (a randomized controlled trial of the Medtronic Endeavor Drug [ABT-578] eluting coronary stent system versus the cypher sirolimus-eluting coronary stent system in de novo native coronary artery lesions)', *JACC: Cardiovascular Interventions*, 4(5), pp. 543–550.

Kandzari DE, Leon MB, Meredith I, Fajadet J, Wijns W, Mauri L. (2013) 'Final 5-year outcomes from the endeavor zotarolimus-eluting stent clinical trial program: Comparison of safety and efficacy with first-generation drug-eluting and bare-metal stents', *JACC: Cardiovascular Interventions*, 6(5), pp. 504–512.

Karakuzu O, Cruz M, Liu Y, Garsin D. (2019) 'Amplex Red Assay for Measuring Hydrogen Peroxide Production from Caenorhabditis elegans', *Bio-Protocol*, 9(21), pp. 1–13.

Kattoor AJ, Pothineni NVK, Palagiri D, Mehta JL (2017) 'Oxidative Stress in Atherosclerosis', *Current Atherosclerosis Reports*. Current Atherosclerosis Reports, 19(11).

Kedare, S. B. and Singh, R. P. (2011) 'Genesis and development of DPPH method of antioxidant assay', *Journal of Food Science and Technology*, 48(4), pp. 412–422.

Kelly CR, Teirstein PS, Meredith IT, Farah B, Dubois CL, Feldman RL, Dens J, Hagiwara N, Rabinowitz A, Carrie D, Pompili V, Bouchard A, Saito S, Allocco DJ, Dawkins KD, Stone GW. (2017) 'Long-Term Safety and Efficacy of Platinum Chromium Everolimus-Eluting Stents in Coronary Artery Disease: 5-Year Results From the PLATINUM Trial', *JACC: Cardiovascular Interventions*, 10(23), pp. 2392–2400.

Khadka R, Zhang P, Tuan NN, Tamm T, Travas-Sejdic J, Otero TF, Kiefer R. (2020) 'Role of polyethylene oxide content in polypyrrole linear actuators', *Materials Today Communications*, pp. 100908.

Khan, W., Kapoor, M. and Kumar, N. (2007) 'Covalent attachment of proteins to functionalized polypyrrole-coated metallic surfaces for improved biocompatibility', *Acta Biomaterialia*, 3(4), pp. 541–549.

Kibos, A., Campeanu, A. and Tintoiu, I. (2007) 'Pathophysiology of coronary artery in-stent restenosis', *Acute Cardiac Care*, 9(2), pp. 111–119.

Kiemeneij F, Serruys PW, Macaya C, Rutsch W, et al. (2001) 'Continued benefit of coronary stenting versus balloon angioplasty: Five-year clinical follow-up of Benestent-I trial', *Journal of the American College of Cardiology*, 37(6), pp. 1598–1603

Kim K, Song H, Kim J, Chon J. (1988) 'Mechanism of Electropolymerisation of Pyrrole in Acidic Aqueous Solutions', *Bull. Korean Chem Soc*, 9(4), pp. 248-251.

Kim, K. G. and Kim, S. Y. (2019) 'Publisher Correction: Increase in Interfacial Adhesion and Electrochemical Charge Storage Capacity of Polypyrrole on Au Electrodes Using Polyethyleneimine Scientific Reports, 9, 1, (2169), 10.1038/s41598-019-38615-6)', *Scientific Reports*, 9(1), pp. 1–9.

Kim S, Jang LK, Park HS, Lee JY. (2016) 'Electrochemical deposition of conductive and adhesive polypyrrole-dopamine films', *Scientific Reports*, 6, pp. 1–8.

Kim S, Jeong JO, Lee S, Park J, Gwon H, Jeong SI, Hardy JG, Lim Y, Lee JY. (2018) 'Effective gamma-ray sterilization and characterization of conductive polypyrrole biomaterials', *Scientific Reports*, 8(1), pp. 1–10.

Kim, W., Cho, S. and Lee, J. S. (2020) 'Comparative study on the effect of protonation control for resistive gas sensor based on close-packed polypyrrole nanoparticles', *Applied Sciences (Switzerland)*, 10(5).

Kimura, K. (1997) 'Mechanisms of active oxygen species reduction by non-steroidal anti-inflammatory drugs', *Int. Journal of Biochemistry & Cell Biology,* 29(3), pp. 437-446

Kipshidze N, Dangas G, Tsapenko M, Moses J, Leon MB, Kutryk M, Serruys P. (2004) 'Role of the endothelium in modulating neointimal formation: Vasculoprotective approaches to attenuate restenosis after percutaneous coronary interventions', *Journal of the American College of Cardiology*, 44(4), pp. 733–739.

Kirchner, G. I., Meier-Weidenbach, I., Manns, M. P. (2004) 'Clinical pharmacokinetics of everolimus', *Clinical Pharmacokinetics,* 43(2), pp. 83-95.

Kladna A, Aboul-Enein HY, Kruk I, Lichszteld K, Michalska T. (2006) 'Scavenging of Reactive Oxygen Species by Some Nonsteroidal Anti-Inflammatory Drugs and Fenofibrate', *Biopolymers*, 82, pp. 99-105.

Kochiadakis GE, Arfanakis DA, Marketou ME, Skalidis EI, Igoumenidis NE, Nikitovic D, Giaouzaki A, Chlouverakis G, Vardas PE. (2010) 'Oxidative stress changes after stent implantation: A randomized comparative study of sirolimus-eluting and bare metal stents', *International Journal of Cardiology*, 142(1), pp. 33–37.

Kohn JC, Lampi M and Reinhart-King CA. (2015) 'Age-Related Vascular Stiffening: Causes and Consequences', *Frontiers in Genetics,* 06(112).

Koppara T, Cheng Q, Yahagi K, Mori H, Sanchez OD, et al.(2015) 'Thrombogenicity and early vascular healing response in metallic biodegradable polymer-based and fully bioabsorbable drug-eluting stents', *Circulation: Cardiovascular Interventions*, 8(6), pp. 1–9.

Korei N, Solouk A, Haghbin Nazarpak M, Nouri A. (2022) 'A review on design characteristics and fabrication methods of metallic cardiovascular stents', *Materials Today Communications*, p. 103467.

Kovacic JC, Dimmeler S, Harvey RP, Finkel T, Aikawa E, Krenning G, Baker AH. (2019) 'Endothelial to Mesenchymal Transition in Cardiovascular Disease: JACC State-of-the-Art Review', *Journal of the American College of Cardiology*, 73(2), pp. 190–209.

Koz, B., Kiskan, B. and Yagci, Y. (2008) 'Synthesis and characterization of polyacetylene with side-chain thiophene functionality', *International Journal of Molecular Sciences*, 9(3), pp. 383–393.

Kozinski M, Krzewina-Kowalska A, Kubica J, Zbikowska-Gotz M, Dymek G, Piasecki R, Sukiennik A, Grzesk G, Bogdan M, Chojnicki M, Dziedziczko A, Sypniewska G. (2005) 'Percutaneous coronary intervention triggers a systemic inflammatory response in patients treated for in-stent restenosis - Comparison with stable and unstable angina', *Inflammation Research*, 54(5), pp. 187–193.

Kufner S, Joner M, Thannheimer A, Hoppmann P, Ibrahim T, Mayer K, Cassese S, Laugwitz K, Schunkert H, Kastrati A, Byrne R. (2019) 'Ten-Year Clinical Outcomes From a Trial of Three Limus-Eluting Stents With Different Polymer Coatings in Patients With Coronary Artery Disease: Results From the ISAR-TEST 4 Randomized Trial', *Circulation*, 139(3), pp. 325–333

Kufner S, Ernst M, Cassere S, Joner M, Mayer K, Colleran R, Koppara T, Xhepa E, Koch T, Wiebe J, Ibrahim T, Fusaro M, Laugwitz KL, Schunkert H, Kastrati A, Byrne RA. (2020). '10-Year Outcomes From a Randomized Trial of Polymer-Free Versus Durable Polymer Drug-Eluting Coronary Stents', *Randomised Controlled Trial, Journal of American College of Cardiology,* 76(2): 146-58.

Kuroda M, Shinke T, Otake H, Sugiyama D, Takaya T, Takahashi H, Terashita D, Uzu K, Tahara N, Kashiwagi D, Kuroda K, Shinkura Y, Nagasawa Y, Sakaguchi K, Hirota Y, Ogawa W, Hirata K. (2016) 'Effects of daily glucose fluctuations on the healing response to everolimus-eluting stent implantation as assessed using continuous glucose monitoring and optical coherence tomography', *Cardiovascular Diabetology*, 15(1), pp. 1–14.

Kwon, O. S., Park, S. J. and Jang, J. (2010) 'A high-performance VEGF aptamer functionalized polypyrrole nanotube biosensor', *Biomaterials*, 31(17), pp. 4740–4747.

Kyung L, Hong YJ, Hachinoke D, Ahmed K, Jeong MH, Kim JH, Sim DS, et al. (2011) 'Effect of a dual drug-coated stent with abciximab and alpha-lipoic acid in a porcine coronary restenosis model', *Korean Circulation Journal*, 41(5), pp. 241–247.

Lakota K, Resnik N, Mrak-Poljak K, Sodin-Šemrl S, Veranič P. (2011) 'Colocalization of serum amyloid a with microtubules in human coronary artery endothelial cells', *Journal of Biomedicine and Biotechnology*, 2011

Lancaster, J. R. (2015) 'Nitric oxide: A brief overview of chemical and physical properties relevant to therapeutic applications', *Future Science OA*, 1(1), pp. 1–5.

Lange H, Suryapranata H, De Luca G, Borner C. (2004) 'Folate Therapy and In-Stent Restenosis after Coronary Stenting', *New England Journal of Medicine*, 350(26), pp. 2673–2681.

Lawton JS, Tamis-Holland JE, Bangalore S, Bates ER, Beckie TM, Bischoff JM, Bittl JA, Cohen MG, DiMaio JM, Don CW, Fremes SE, Gaudino MF, Goldberger ZD, Grant MC, Jaswal JB, Kurlansky PA, Mehran R, Metkus TS, Nnacheta LC, Rao SV, Sellke FW, Sharma G, Yong CM, Zwischenberger BA. (2022). '2021 ACC/AHA/SCAI Guideline for Coronary Artery Revascularization: A Report of the American College of Cardiology/American Heart Association Joint Committee on Clinical Practice Guidelines', *Journal of American College of Cardiology,* 79(2): e21-e129.

Lee J and Smith NP. (2012). 'The Multi-Scale Modelling of Coronary Blood Flow', *Annals of Biomedical Engineering,* 40(11), pp. 2399-413.

Lei, J. and Martin, C. R. (1995) 'Investigations of the Chemical Interactions between Molecular Oxygen and Pristine (Undoped) Polypyrrole', *Chemistry of Materials*, 7(3), pp. 578–584

Lebrin F, Deckers M, Bertolino P, Ten Dijke P. (2005) 'TGF-β receptor function in the endothelium', *Cardiovascular Research*, 65(3), pp. 599–608.

Lee YW, Kim PH, Lee WH, Hirani AA. (2010) 'Interleukin-4, Oxidative Stress, Vascular Inflammation and Atherosclerosis', *Biomolecules & therapeutics*, 18(2), pp. 135–144.

Lee, Y. W., Lee, W. H. and Kim, P. H. (2010) 'Oxidative mechanisms of IL-4-induced IL-6 expression in vascular endothelium', *Cytokine*, 49(1), pp. 73–79.

Lee, J. *et al.* (2013) 'Two formation mechanisms and renewable antioxidant properties of suspensible chitosan–PPy and chitosan–PPy–BTDA composites', *Synthetic Metals*, 164, pp. 6-11.

Lee, J. Y. and Schmidt, C. E. (2015) 'Amine-functionalized polypyrrole: inherently cell adhesive conducting polymer', *Journal of Biomedical Material Research A*, 103(6), pp. 165–165.

Leikert JF, Räthel TR, Müller C, Vollmar AM, Dirsch VM. (2001) 'Reliable in vitro measurement of nitric oxide released from endothelial cells using low concentrations of the fluorescent probe 4,5-diaminofluorescein', *FEBS Letters*, 506(2), pp. 131–134.

Leon MB, Nikolsky E, Cutlip DE, Mauri L, Liberman H, Wilson H, Patterson J, Moses J, Kandzari DE. (2010) 'Improved late clinical safety with zotarolimus-eluting stents compared with paclitaxel-eluting stents in patients with de novo coronary lesions: 3-year follow-up from the ENDEAVOR IV (Randomized Comparison of Zotarolimus- and Paclitaxel-Eluting Stents in Patients With Coronary Artery Disease) trial', *JACC: Cardiovascular Interventions*, 3(10), pp. 1043–1050.

Leopold, J. A. (2013) 'Prohealing endothelial progenitor cell capture stents do the cells captured explain the clinical outcomes?', *Circulation: Cardiovascular Interventions*, 6(5), pp. 494–495.

Levi MD, Lankri E, Gofer Y, Aurbach D, Otero T. (2002) 'The Behavior of Polypyrrole-Coated Electrodes in Propylene Carbonate Solutions', *Journal of The Electrochemical Society*, 149(6), p. E204.

Li CM, Sun CQ, Chen W, Pan L. (2005) 'Electrochemical thin film deposition of polypyrrole on different substrates', *Surface and Coatings Technology*, 198(1-3 SPEC. ISS.), pp. 474–477.

Li G, Yang P, Qin W, Maitz MF, Zhou S, Huang N. (2011) 'The effect of coimmobilizing heparin and fibronectin on titanium on hemocompatibility and endothelialization', *Biomaterials*, 32(21), pp. 4691–4703.

Li, H. and Sun, B. (2007) 'Toll-like receptor 4 in atherosclerosis', *Journal of Cellular and Molecular Medicine*, 11(1), pp. 88–95.

Li, H., Horke, S. and Förstermann, U. (2014) 'Vascular oxidative stress, nitric oxide and atherosclerosis', *Atherosclerosis*, 237(1), pp. 208–219.

Li X, Chen B, Xie H, He Y, Zhong D, Chen D.. (2018) 'Antioxidant structure–activity relationship analysis of five dihydrochalcones', *Molecules*, 23(5), pp. 1–13.

Li Y, Neoh KG, Cen L, Kang ET. (2005) 'Porous and electrically conductive polypyrrole- Poly (vinyl alcohol) composite and its applications as a biomaterial', *Langmuir*, 21(23), pp. 10702–10709

Li Y, Talotta-Altenburg LM, Silimperi KA, Ciabattoni GO, Lowe-Krentz LJ. (2020) 'Endothelial nitric oxide synthase activation is required for heparin receptor effects on vascular smooth muscle cells', *American Journal of Physiology - Cell Physiology*, 318(3), pp. C463–C475.

Li Y, Wei Y, Liao J, Hao Y, Ning C, Jiang L, Wang S. (2016) 'Surface Wettability Switched Cell Adhesion and Detachment on Conducting Polymer Nanoarray', *Advanced Materials Interfaces*, 3(19), pp. 1–4.

Li, Y. and Ouyang, J. (2000) 'Effect of nonionic surfactant additives on the electropolymerization of pyrrole in aqueous solutions', *Synthetic Metals*, 113(1), pp. 23–28.

Li, Y. and Qian, R. (2000) 'Electrochemical overoxidation of conducting polypyrrole nitrate film in aqueous solutions', *Electrochimica Acta*, 45(11), pp. 1727–1731.

Liang, N. and Kitts, D. D. (2014) 'Antioxidant property of coffee components: Assessment of methods that define mechanism of action', *Molecules*, 19(11), pp. 19180–19208

Lichtenberg, D. and Pinchuk, I. (2015) 'Oxidative stress, the term and the concept', *Biochemical and Biophysical Research Communications*, 461(3), pp. 441–444.

Liguori, I, Russo G, Curcio F, Bulli G, Aran L, Della-Morte D, Gargiulo G, Testa G, Cacciatore F, Bonaduce D, Abete1 P. (2018) 'Oxidative Stress, Aging and Diseases', *Clinical Intervention in Aging*, 13, pp. 757–772.

Lister, Z., Rayner, K. J. and Suuronen, E. J. (2016) 'How biomaterials can influence various cell types in the repair and regeneration of the heart after myocardial infarction', *Frontiers in Bioengineering and Biotechnology*, 4(JUL).

Liu, J. and Wan, M. (2001) 'Synthesis, characterization and electrical properties of microtubules of polypyrrole synthesized by a template-free method', *Journal of Materials Chemistry*, 11(2), pp. 404–407.

Liu J, Li M, Lu H, Qiao W, Xi D, Luo T, Xiong H, Guo Z. (2015) 'Effects of probucol on restenosis after percutaneous coronary intervention a systematic review and meta-analysis', *PLoS ONE*, 10(4), pp. 1–13

Liu X, Chen R, Shang Y, Jiao B, Huang C. (2009) 'Superoxide radicals scavenging and xanthine oxidase inhibitory activity of magnesium lithospermate B from Salvia miltiorrhiza', *Journal of Enzyme Inhibition and Medicinal Chemistry*, 24(3), pp. 663–668.

Liu X, Yao M, Li N, Wang C, Zheng Y, Cao X. (2008) 'CaMKII promotes TLR-triggered proinflammatory cytokine and type I interferon production by directly binding and activating TAK1 and IRF3 in macrophages', *Blood*, 112(13), pp. 4961–4970

Liu, Y. C. (2004) 'Characteristics of vibration modes of polypyrrole on surface-enhanced Raman scattering spectra', *Journal of Electroanalytical Chemistry*, 571(2), pp. 255–264.

Livingston, M. and Tan, A. (2019) 'Coating techniques and release kinetics of drug-eluting stents', *Journal of Medical Devices*, 10(1), pp. 1–21.

Loos A, Rohde R, Haverich A, Barlach S. (2007) 'In vitro and in vivo biocompatibility testing of absorbable metal stents', *Macromolecular Symposia*, 253, pp. 103–108.

Losito I, Malitesta C, Sabbatini L, Zambonin PG. (1994) 'Pristine and Overoxidized Polypyrrole by XPS', *Surface Science Spectra*, 3(4), pp. 375–383.

Lubos, E., Loscalzo, J. and Handy, D. E. (2011) 'Glutathione peroxidase-1 in health and disease: From molecular mechanisms to therapeutic opportunities', *Antioxidants and Redox Signaling*, 15(7), pp. 1957–1997.

Luczak, E. D. and Anderson, M. E. (2014) 'CaMKII oxidative activation and the pathogenesis of cardiac disease' *J Mol Cell Cardiol,* August, pp. 112-116.

Ludman, P. F. and Bradley, A. (2015) 'National Audit of Percutaneous Coronary Interventions Annual Report', (October), p. 5.

Lukášek J, Hauzerová Š, Havlíčková K, Strnadová K, Mašek K, Stuchlík M, Stibor I, Jenčová V, Řezanka1 M. (2019) 'Cyclodextrin-polypyrrole coatings of scaffolds for tissue engineering', *Polymers*, 11(3).

Lum, K. and Roebuck, K. A. (2001) 'Oxidant stress and endothelial dysfunction', *Am J Physiol Cell Physiol*, 280, pp. C719-C741.

Luo SC, Ali EM, Tansil NC, Yu H, Gao S, Kantchev EAB, Ying JY. (2008) 'Poly(3,4-ethylenedioxythiophene) (PEDOT) nanobiointerfaces: Thin, ultrasmooth, and functionalized PEDOT films with in vitro and in vivo biocompatibility', *Langmuir*, 24(15), pp. 8071–8077.

MacDiarmid, A. G. and Epstein, A. J. (1989) 'Polyanilines: A novel class of conducting polymers', *Faraday Discussions of the Chemical Society*, 88, pp. 317–332.

MacLean PD, Chapman EE, Dobrowolski SL, Thompson A, Barclay LRC. (2008) 'Pyrroles as antioxidants: Solvent effects and the nature of the attacking radical on antioxidant activities and mechanisms of pyrroles, dipyrrinones, and bile pigments', *Journal of Organic Chemistry*, 73(17), pp. 6623–6635.

Maeng M, Jensen LO, Kaltoft A, Tilsted H, Christiansen EH, Thayssen P, Madsen M, Sørensen HT, Lassen JF, Thuesen L. (2012) 'Comparison of zotarolimus-eluting and sirolimus-eluting coronary stents: A study from the Western Denmark Heart Registry', *BMC Cardiovascular Disorders*, 12, pp. 15–17.

Mahmood A, Saqib M, Ali M, Abdullah MI, Khalid B. (2013) 'Theoretical investigation for the designing of novel antioxidants', *Canadian Journal of Chemistry*, 91(2), pp. 126–130.

Mahmoudinezhad, H. M., Karkhaneh, A. and Jadidi, K. (2018) 'Effect of PEDOT:PSS in tissue engineering composite scaffold on improvement and maintenance of endothelial cell function', *Journal of Biosciences*, 43(2), pp. 307–319.

Maione AS, Cipolletta E, Sorriento D, Borriello F, Soprano M, Rusciano MR, D'Esposito V, et al. (2017) 'Cellular subtype expression and activation of CaMKII regulate the fate of atherosclerotic plaque', *Atherosclerosis*, 256, pp. 53–61

Majewska E, Paleolog E, Baj Z, Kralisz U, Feldmann M, Tchórzewski H. (1997) 'Role of tyrosine kinase enzymes in TNF-α and IL-1 induced expression of ICAM-1 and VCAM-1 on human umbilical vein endothelial cells', *Scandinavian Journal of Immunology*, 45(4), pp. 385–392

Mani G, Feldman MD, Patel D, Agrawal CM. (2007) 'Coronary stents: A materials perspective', *Biomaterials*, 28(9), pp. 1689–1710.

Marchesi, LF, Simoes FR, Pocrifka LA, Periera EC. (2011) 'Investigation of Polypyrrole Degradation Using Electrochemical Impedance Spectroscopy', *The Journal of Physical Chemistry B*, 115, pp. 9570–9575.

Maron BA, Tang SS, Loscalzo J. (2013) 'S-Nitrosothiols and the S-Nitrosoproteome of the Cardiovascular System', *Antioxidants & Redox Signalling,* 18(3), pp. 270-287

Maroudas, N. G. (1975) 'Adhesion and spreading of cells on charged surfaces', *Journal of Theoretical Biology.*

Marra, D. E., Simoncini, T. and Liao, J. K. (2000) 'Inhibition of vascular smooth muscle cell proliferation by sodium salicylate mediated by upregulation of p21(Waf1) and p27(Kip1)', *Circulation*, 102(17), pp. 2124–2130.

Martin TP, McCluskey C, Cunningham MR, Beattie J, Paul A, Currie S. (2018) 'CaMKIIδ interacts directly with IKKβ and modulates NF-κB signalling in adult cardiac fibroblasts', *Cellular Signalling*, 51(April), pp. 166–175.

Maruthapandi M, Saravanan A, Luong JHT, Gedanken A. (2020) 'Antimicrobial properties of polyaniline and polypyrrole decorated with zinc-doped copper oxide microparticles', *Polymers*, 12(6).

Mathis BJ, Kato H, Matsuishi Y, Hiramatsu Y. (2022) 'Endogenous and exogenous protection from surgically induced reactive oxygen and nitrogen species', *Surgery Today.*

Mattioli-Belmonte M, Gabbanelli F, Marcaccio M, Giantomassi F, Tarsi R, Natali D, Callegari A, Paolucci F, Biagini G. (2005) 'Bio-characterisation of tosylate-doped polypyrrole films for biomedical applications', *Materials Science and Engineering: C,* 25, pp. 43-49.

Mauler-Wittner, S. & Garot, P. (2021) 'The Biolimus A9-coated BioFreedom ™ stent: from clinical efficacy to real-world evidence', *Future Cardiology*, 17(2), pp. 239-255.

McBee ME, Chionh YH, Sharaf ML, Ho P, Cai MWL, Dedon PC. (2017) 'Production of superoxide in bacteria is stress- and cell state-dependent: A gating-optimized flow cytometry method that minimizes ROS measurement artifacts with fluorescent dyes', *Frontiers in Microbiology*, 8(MAR), pp. 1–17.

McCluskey C, Mooney L, Paul A, Currie S. (2019) 'Compromised cardiovascular function in aged rats corresponds with increased expression and activity of calcium/calmodulin dependent protein kinase IIδ in aortic endothelium', *Vascular Pharmacology*, 118–119(April), p. 106560.

McEvoy, B. and Rowan, N. J. (2019) 'Terminal sterilization of medical devices using vaporized hydrogen peroxide: a review of current methods and emerging opportunities', *Journal of Applied Microbiology*, 127(5), pp. 1403–1420

McGinty, S. (2014) 'A decade of modelling drug release from arterial stents', *Mathematical Biosciences,* 257, pp. 80-90

McGrath KCY, Li XH, McRobb LS, Heather AK. (2015) 'Inhibitory Effect of a French Maritime Pine Bark Extract-Based Nutritional Supplement on TNF-α-Induced Inflammation and Oxidative Stress in Human Coronary Artery Endothelial Cells', *Evidence-based Complementary and Alternative Medicine*, 2015.

McKittrick CM, Kennedy S, Oldroyd KG, McGinty S, McCormick C. (2016) 'Modelling the Impact of Atherosclerosis on Drug Release and Distribution from Coronary Stents', *Annals of Biomedical Engineering*, 44(2), pp. 477–487.

McKittrick CM. McKee S, Kennedy S, Oldroyd K, Wheel M, Pontrelli G, Dixon S, McGinty S, McCormick C. (2019) 'Combining mathematical modelling with in vitro experiments to predict in vivo drug-eluting stent performance', *Journal of Controlled Release*, 303, pp. 151-161.

McMullen CJ, Chalmers S, Wood R, Cunningham MR, Currie S.. (2021) 'Sunitinib and Imatinib Display Differential Cardiotoxicity in Adult Rat Cardiac Fibroblasts That Involves a Role for Calcium/Calmodulin Dependent Protein Kinase II', *Frontiers in Cardiovascular Medicine*, 7(February), pp. 1–15.

McNair ED, Wells CR, Mabood Qureshi A, Basran R, Pearce C, Orvold J, Devilliers J, Prasad K. (2010) 'Soluble receptors for advanced glycation end products (sRAGE) as a predictor of restenosis following percutaneous coronary intervention', *Clinical Cardiology*, 33(11), pp. 678–685.

Melly L, Torregrossa G, Lee T, Jansens J, Puskad JD. (2018) 'Fifty years of coronary artery bypass grafting', *Journal of Thoracic Disease*, 10(3), pp. 1960-1967.

Méndez-barbero, N., Gutiérrez-muñoz, C. and Blanco-Colio, L. M. (2021) 'Cellular crosstalk between endothelial and smooth muscle cells in vascular wall remodeling', *International Journal of Molecular Sciences*, 22(14).

Meoli, D. F. and White, R. J. (2009) 'Thrombin induces fibronectin-specific migration of pulmonary microvascular endothelial cells: Requirement of calcium/calmodulin-dependent protein kinase II', *American Journal of Physiology - Lung Cellular and Molecular Physiology*, 297(4), pp. 706–715.

Milenković D, Dorović J, Jeremić S, Dimitrić Marković JM, Avdović EH, Marković Z. (2017) 'Free Radical Scavenging Potency of Dihydroxybenzoic Acids', *Journal of Chemistry*, 2017.

Milatovic D. Gupta RC, Yu Y, Zaja-Milatovic S, Aschner M. (2011) 'Protective effects of antioxidants and anti-inflammatory agents against manganese-induced oxidative damage and neuronal injury', *Toxicol Appl Pharmacol,* 256(3), pp. 219-226.

Mindroiu M, Pirvu C, Popescu S, Demetrescu I. (2009) 'Polypyrrole as conducting polymer coating on Ti6A17Nb alloy', *Materiale Plastice*, 46(4), pp. 394–398.

Misra P, Reddy PC, Shukla D, Caldito GC, Yerra L, Aw TY. (2008) 'In-stent stenosis: Potential role of increased oxidative stress and glutathione-linked detoxification mechanisms', *Angiology*, 59(4), pp. 469–474.

Mollova MY, Katus HA, Backs J. (2015) 'Regulation of CaMKII signaling in cardiovascular disease', *Frontiers in Pharmacology*, 6, pp. 178

Monaco C, Andreakos E, Kiriakidis S, Mauri C, Bicknell C, Foxwell B, Cheshire N, Paleolog E, Feldmann M. (2004) 'Canonical pathway of nuclear factor κB activation selectively regulates proinflammatory and prothrombotic responses in human atherosclerosis', *Proceedings of the National Academy of Sciences of the United States of America*, 101(15), pp. 5634–5639.

Montorfano I, Becerra A, Cerro R, Echeverría C, Sáez E, Morales MG, Fernández R, Cabello-Verrugio C, Simon F. (2014) 'Oxidative stress mediates the conversion of endothelial cells into myofibroblasts via a TGF-b1 and TGF-b2-dependent pathway', *Laboratory Investigation*, 94(10), pp. 1068–1082.

Moreno, R., Schultz, C. and Schmitz, M. L. (2010) 'Specification of the NF- i B transcriptional response by p65 phosphorylation and TNF-induced nuclear translocation of IKK e', 38(18), pp. 6029–6044.

Morgan, M. J. and Liu, Z. G. (2011) 'Crosstalk of reactive oxygen species and NF-κB signaling', *Cell Research*, 21(1), pp. 103–115.

Morgan, S. (2017) 'Bioactive Surfaces for Improved Coronary Stent Performance' *University of Strathclyde,* Doctoral Thesis.

Mostany, J. and Scharifker, B. R. (1997) 'Impedance spectroscopy of undoped, doped and overoxidized polypyrrole films', Synthetic Metals, 87(3), pp. 179–185.

Muñoz E, Valero RA, Quintana A, Hoth M, Núñez L, Villalobos C. (2011) 'Nonsteroidal anti-inflammatory drugs inhibit vascular smooth muscle cell proliferation by enabling the Ca2+-dependent inactivation of calcium release-activated calcium/Orai channels normally prevented by mitochondria', *Journal of Biological Chemistry*, 286(18), pp. 16186–16196.

Munzel T, Camici GG, Maack C, Bonetti NR, Fuster V, Kovacic JC. (2017) 'Impact of Oxidative Stress on the Heart and Vasculature Part 2 of a 3-Part Series' *Journal of American College of Cardiology*, 70(2), pp. 212-229.

Murthy S, Koval OM, Diaz JMR, Kumar S, Nuno D, et al. (2017) 'Endothelial CaMKII as a regulator of eNOS activity and NO-mediated vasoreactivity', pp. 1–23.

Murphy, MP, Bayir H, Belousov V, et al. (2022) 'Guidelines for measuring reactive oxygen species and oxidative damage in cells and in vivo', *Nature Metabolism,* 4, pp. 651-662

Musialik M, Kuzmicz R, Pawlowski TS, Litwinienko G. (2009) 'Acidity of hydroxyl groups: An overlooked influence on antiradical properties of flavonoids', *Journal of Organic Chemistry*, 74(7), pp. 2699–2709.

Mohammed Nabeeluddin, S. (2016) 'A Facile Novel Method to Control Surface Topography of Conducting Polymer for Improved Coronary Stent Performance', *Biophysical Journal*. Biophysical Society, 110(3), p. 337a.

Nakano, H. and Kuwahara, Y. (2005) 'Formation of Poly(2-vinylpyridine) Films on Zn by Galvanostatic Electropolymerization,' pp. 780–786.

Nakatani M, Takeyama Y, Shibata M, Yorozuya M, Suzuki H, Koba S, Katagiri T. (2003) 'Mechanisms of restenosis after coronary intervention: Difference between plain old balloon angioplasty and stenting', *Cardiovascular Pathology*, 12(1), pp. 40–48.

Nakazawa G, Finn A V., Joner M, Ladich E, Kutys R, Mont EK, Gold HK, Burke AP, Kolodgie FD, Virmani R. (2008) 'Delayed arterial healing and increased late stent thrombosis at culprit sites after drug-eluting stent placement for acute myocardial infarction patients: An autopsy study', *Circulation*, 118(11), pp. 1138–1145.

Nazarzadeh Zare E, Mansour Lakouraj M, Mohseni M. (2014) 'Biodegradable polypyrrole/dextrin conductive nanocomposite: Synthesis, characterization, antioxidant and antibacterial activity', *Synthetic Metals*. Elsevier B.V., 187(1), pp. 9–16.

Ndunda P, Vindhyal MR, Muutu T, Fanari Z. (2020) 'Clinical Outcomes of the Dual-Therapy CD34 Antibody-Covered Sirolimus-Eluting Stent Versus Standard Drug-Eluting Coronary Stents: A Meta-Analysis', *Cardiovascular Revascularization Medicine,* 21(2), pp. 213-221.

Nguyen EK, Koval OM, Noble P, Broadhurst K, Allamargot C, Wu M, Strack S, Thiel WH, Grumback IM. (2018) 'CaMKII (Ca2+/calmodulin-dependent kinase II) in mitochondria of smooth muscle cells controls mitochondrial mobility, migration, and neointima formation', *Arteriosclerosis, Thrombosis, and Vascular Biology*, 38(6), pp. 1333–1345.

Nicola F, B. BE, Nenad B, Maria-Sybille L, Andreas S, Gabriele S. (2004) 'Gene Expression Profiling of Inflamed Human Endothelial Cells and Influence of Activated Protein C', *Circulation*, 110(18), pp. 2903–2909.

Nidhin, J. *et al.* (2016) 'Conducting Polymers: Biomedical Applications', *Biomedical Applications of Polymeric Materials and Composites*, pp. 37–89.

Noad, R. L., Hanratty, C. G. and Walsh, S. J. (2011) 'Clinical Impact of Stent Design', *Interventional Cardiology Review, 9(2), p. 89*

Nolfi-Donegan D, Braganza A, Shiva S. (2020) 'Mitochondrial electron transport chain: Oxidative phosphorylation, oxidant production, and methods of measurement', *Redox Biology*, 37:1010674

Noonan J, Grassia G, MacRitchie N, Garside P, Guzik TK, Bradshaw AC, Maffia P. (2019) 'A Novel Triple-Cell Two-Dimensional Model to Study Immune-Vascular Interplay in Atherosclerosis', *Frontiers in Immunology*, 10(849).

Novack GV, Galeano P, Castano EM, Morelli L. (2020) 'Mitochondrial Supercomplexes: Physiological Organization and Dysregulation in Age-Related Neurodegenerative Disorders', *Frontiers in Endocrinology*, 11, p600

Nozaki A, Kawakita J, Kuroda S, Sakamoto Y. (2010) 'Growth Mechanism of Polypyrrole through Electrochemical Polymerization', *Electrochemistry,* 2, pp. 140-142.

Oelßner, W., Berthold, F. and Guth, U. (2006) 'The iR drop - Well-known but often underestimated in electrochemical polarization measurements and corrosion testing', *Materials and Corrosion*, 57(6), pp. 455–466.

Ohtsuki T, Satoh K, Omura J, Kikuchi N, Satoh T, Kurosawa R, Nogi M, Sunamura S, Yaoita N, Aoki T, Tatebe S, Sugimura T, Takahashi J, Miyata S, Shimokawa H. (2017) 'Prognostic impacts of plasma levels of cyclophilin a in patients with coronary artery disease', *Arteriosclerosis, Thrombosis, and Vascular Biology*, 37(4), pp. 685–693.

Okner R, Oron M, Tal N, Mandler D, Domb AJ. (2007) 'Electrocoating of stainless steel coronary stents for extended release of Paclitaxel', *Materials Science and Engineering C*, 27(3), pp. 510–513.

Okner R, Oron M, Tal N, Mandler D, Domb AJ. (2009) 'Electrocoating of stainless steel coronary stents for extended release of paclitaxel', *Journal of Biomedical Materials Research - Part A*, 88(2), pp. 427–436.

Oparka M, Walczak J, Malinska D, van Opeen LMPE, Szczepanowska J, Koopman WJH, Wieckowski MR. (2016) 'Quantifying ROS levels using CM-H2DCFDA and HyPer', *Methods*, 109, pp. 3–11.

Otero, T. F. and Martinez, J. G. (2011) 'Activation energy for polypyrrole oxidation: Film thickness influence', *Journal of Solid State Electrochemistry*, 15(6), pp. 1169–1178.

Otsuka F, Yahagi K, Ladich E, Kutys R, Alexander R, Fowler D, Virmani R, Joner M. (2015) 'Hypersensitivity Reaction in the US Food and Drug Administration–Approved Second-Generation Drug-Eluting Stents', *Circulation,* 131, pp. 322-324.

Ott M, Gogvadze V, Orrenius S, Zhivotovsky B. (2007) 'Mitochondria, oxidative stress and cell death', *Apoptosis*, 12(5), pp. 913–922.

Pache J, Kastrati A, Mehilli J, Schühlen H, Dotzer F, Hausleiter J, et al. (2003) 'Intracoronary stenting and angiographic results: Strut thickness effect on restenosis outcome (ISAR-STEREO-2) trial', *Journal of the American College of Cardiology*, 41(8), pp. 1283–1288.

Pacher, P., Beckman, J. S. and Liaudet, L. (2007) 'Nitric Oxide and Peroxynitrite in Health and Disease', *Physiological Reviews*. American Physiological Society, 87(1), pp. 315–424.

Pacher, P. and Szabo, C. (2006) 'Role of peroxynitrite in the pathogenesis of cardiovascular complications of diabetes' *Curr Opin Pharmacol,* 6(2), pp. 136-141

Pan LL, Liu XH, Gong QH, Wu D, Zhu YZ. (2011) 'Hydrogen sulfide attenuated tumor necrosis factor-α-induced inflammatory signaling and dysfunction in vascular endothelial cells', *PLoS ONE*, 6(5).

Panday A, Sahoo MK, Osorio D, Batra S.. (2015) 'NADPH oxidases: An overview from structure to innate immunity-associated pathologies', *Cellular and Molecular Immunology*, 12(1), pp. 5–23.

Pandey D, Gratton JP, Rafikov R, Black SM, Fulton DJR. (2011) 'Calcium/calmodulin-dependent kinase II mediates the phosphorylation and activation of NADPH oxidase 5', *Molecular Pharmacology*, 80(3), pp. 407–415.

Paolo, C., T., W. J. and T.H., Y. E. (2003) 'Inflammatory Cytokines Stimulated C-Reactive Protein Production by Human Coronary Artery Smooth Muscle Cells', *Circulation*, 108(16), pp. 1930–1932.

Patel S, Kumar S, Jyoti A, Srinag BS, Keshari RS, Saluja R, Verma A, Mitra K, Barthwal MK, Krishnamurthy H, Bajpai VK, Dikshit M. (2010) 'Nitric oxide donors release extracellular traps from human neutrophils by augmenting free radical generation', *Nitric Oxide*, 22(3), pp. 226–234.

Pelliccia F, Cianfrocca C, Rosano G, Mercuro G, Speciale G, Pasceri V. (2010) 'Role of Endothelial Progenitor Cells in Restenosis and Progression of Coronary Atherosclerosis After Percutaneous Coronary Intervention.' *JACC: Cardiovascular Interventions*, 3, pp. 78-86

Pepke S, Kinzer-Ursem T, Mihalas S, Kennedy MB. (2010) 'A dynamic model of interactions of Ca2+, calmodulin, and catalytic subunits of Ca2+/calmodulin-dependent protein kinase II', *PLoS Computational Biology*, 6(2).

Perkins LEL, Boeke-Purkis KH, Wang Q, Stringer SK, Coleman LA. (2009). 'XIENCE V™ Everolimus-Eluting Coronary Stent System: A Preclinical Assessment', *Journal of International Cardiology,* 22: S28-S40.

Pesarini G, Amoruso A, Ferrero V, Bardelli C, Fresu L, Perobelli L, Scappini P, De Luca G, Brunelleschi S, Vassanelli C, Ribichini F. (2010) 'Cytokines release inhibition from activated monocytes, and reduction of in-stent neointimal growth in humans', *Atherosclerosis*, 211(1), pp. 242–248

Pham-Huy LA, He H, Pham-Huy C. (2008) 'Free Radicals, Antioxidants in Disease and Health', *InternatIonal journal of Biomedical science*, 4(2), pp. 89–96.

Pierzynska-Mach S, Janowki PA, Dobrucki JW. (2014) 'Evaluation of Acridine Orange, LysoTracker Red, and Quinacrine as Fluorescent Probes for Long-Term Tracking of Acidic Vesicles' *Cytometry A,* 85A: 729-737

Piskareva AI, Korshak Y V, Mezhuev YO, Shtil MI. (2013) 'The kinetics of single-electron transfer from a pyrrole molecule to a persulphate ion', *Plasticheskie Massy*, 5, pp. 25–27.

Poverenov E, Li M, Bitler A, Bendikov M. (2010) 'Major effect of electropolymerization solvent on morphology and electrochromic properties of PEDOT films', *Chemistry of Materials,* 22(13), pp. 4019–4025.

Prabhakar PK, Raj S, Anuradha PR, Sawant SN, Doble M. (2011) 'Biocompatibility studies on polyaniline and polyaniline-silver nanoparticle coated polyurethane composite', *Colloids and Surfaces B: Biointerfaces*, 86(1), pp. 146–153.

Pradhan A, Vishwakarma P, Vankar S, Sethi R. (2019) '"The Unpredictable ABSORB" – Very Late Stent Thrombosis of Bioresorbable Vascular Scaffold', *Heart Views,* 20(2): 65-69.

Qiu, Y.-J. and Reynolds, J. R. (1992) 'Electrochemically initiated chain polymerization of pyrrole in aqueous media', *Journal of Polymer Science Part A: Polymer Chemistry*, 30(7), pp. 1315–1325.

Quirk, K., McCormick, C. and Kazakidi, A. (2021) 'A biphasic diffusion model of drug release from medical implant coatings', *University of Strathclyde, Department of Biomedical Engineering,* Masters Thesis.

Raggi P, Genest J, Giles JT, Rayner KJ, Dwivedi G, Beanlands RS, Gupta M. (2018) 'Role of inflammation in the pathogenesis of atherosclerosis and therapeutic interventions', *Atherosclerosis*, 276, pp. 98–108.

Rahman, S. U. and Ba-Shammakh, M. S. (2004) 'Thermal effects on the process of electropolymerization of pyrrole on mild steel', *Synthetic Metals*, 140(2–3), pp. 207–223

Ramanaviciene A, Kausaite A, Tautkus S, Ramanavicius A. (2010) 'Biocompatibility of polypyrrole particles: an in-vivo study in mice', *Journal of Pharmacy and Pharmacology*, 59(2), pp. 311–315

Ramanavicius A, Finkelsteinas A, Cesiulis H, Ramanaviciene A. (2010) 'Electrochemical impedance spectroscopy of polypyrrole based electrochemical immunosensor', *Bioelectrochemistry*, 79(1), pp. 11–16.

Ramezanian, M. S., Padmaja, S. and Koppenol, W. H. (1996) 'Nitration and hydroxylation of phenolic compounds by peroxynitrite', *Chemical Research in Toxicology*, 9(1), pp. 232–240.

Ramirez-Sanchez I, Maya L, Ceballos G, Villarreal F. (2010) '(-)-Epicatechin activation of endothelial cell endothelial nitric oxide synthase, nitric oxide, and related signaling pathways', *Hypertension*, 55(6), pp. 1398–1405.

Ramirez-Sanchez I, Maya L, Ceballos G, Villarreal F. (2011) '(-)-Epicatechin induces calcium and translocation independent eNOS activation in arterial endothelial cells', *American Journal of Physiology - Cell Physiology*, 300(4), pp. 880–887.

Rathore, S. (2010) 'Small coronary vessel angioplasty: Outcomes and technical considerations', *Vascular Health and Risk Management*, 6(1), pp. 915–922.

Ravichandran R, Sundarrajan S, Venugopal JR, Mukherjee S, Ramakrishna S. (2010) 'Applications of conducting polymers and their issues in biomedical engineering', *Journal of the Royal Society Interface*, 7(SUPPL. 5).

Rebeiz AG, Zoghbi E, Harb R, Youhanna S, Skouri HN, Dimassi A, Abou-Nader G, Nasrallah A, Sawaya J, Gharzuddine W, Alam S. (2009) 'Comparison of the systemic levels of inflammatory markers after percutaneous coronary intervention with bare metal versus sirolimus-eluting stents', *Journal of Interventional Cardiology*, 22(2), pp. 169–174.

Rees MD, Kennett EC, Whitelock JM, Davies MJ. (2008) 'Oxidative damage to extracellular matrix and its role in human pathologies', *Free Radical Biology and Medicine*, 44(12), pp. 1973–2001

Reiss, A. B., Siegart, N. M. and De Leon, J. (2017) 'Clinical Lipidology Interleukin-6 in atherosclerosis: atherogenic or atheroprotective? Interleukin-6 in atherosclerosis: atherogenic or atheroprotective?', *CliniCal lipidology*, 12(1), pp. 14–23.

Rellos P, Pike ACW, Niesen FH, Salah E, Lee WH, Delft F Von. (2010) 'Structure of the CaMKII d / Calmodulin Complex Reveals the Molecular Mechanism of CaMKII Kinase Activation', 8(7).

Rensen, S. S. M., Doevendans, P. A. F. M. and Van Eys, G. J. J. M. (2007) 'Regulation and characteristics of vascular smooth muscle cell phenotypic diversity', *Netherlands Heart Journal*, 15(3), pp. 100–108.

Rizas, K. D. and Mehilli, J. (2016) 'Stent polymers: Do they make a difference?', *Circulation: Cardiovascular Interventions*, 9(6), pp. 1–13.

Rocha LA, Piccinato CE, Ribiero MS, Becari C, Joviliano RD, Joviliano EE. (2017) 'The role of the kallikrein-kinin system, matrix metalloproteinases, and tissue inhibitors of metalloproteinases in the early restenosis of covered stents in the femoropopliteal arterial segment', *Journal of Vascular Surgery*, 65(1), pp. 119–127.

Rodríguez-Mañas L, El-Assar M, Vallejo S, López-Dóriga P, Solís J, Petidier R, Montes M, Nevado J, Castro M, Gómez-Guerrero C, Peiró C, Sánchez-Ferrer CF. (2009) 'Endothelial dysfunction in aged humans is related with oxidative stress and vascular inflammation', *Aging Cell*, 8(3), pp. 226–238.

Rodríguez-Santiago L, Sodupe M, Oliva A, Bertran J. (1999) 'Hydrogen atom or proton transfer in neutral and single positive ions of salicylic acid and related compounds', *Journal of the American Chemical Society*, 121(38), pp. 8882–8890.

Roos, D. and de Boer, M. (2014) 'Molecular diagnosis of chronic granulomatous disease', *Clinical and Experimental Immunology*, 175(2), pp. 139–149.

Ross, R. (1999) 'Atherosclerosis--an inflammatory disease.', *N Engl J Med*.

Rusciano MR, Sommariva E, Douin-Echinard V, Ciccarelli M, Poggio P, Maione AS. (2019) 'CaMKII activity in the inflammatory response of cardiac diseases', *International Journal of Molecular Sciences*, 20(18), pp. 1–15.

Roy J, Galano JM, Durand T, Le Guennec JY, Lee JCY. (2017) 'Physiological role of reactive oxygen species as promoters of natural defenses', *The FASEB Journal*

Saddouk FZ, Sun LY, Liu YF, Jiang M, Singer DV, Backs J, Riper DV, Ginnan R, Schwarz JJ, Singer HA (2016) 'Ca2+/calmodulin-dependent protein kinase II-γ (CaMKIIγ) negatively regulates vascular smooth muscle cell proliferation and vascular remodeling', *FASEB Journal*, 30(3), pp. 1051–1064.

Sadki S, Schottland P, Brodie N, Sabouraud G. (2000) 'The mechanisms of pyrrole electropolymerization', *Chemical Society Reviews*, 29(5), pp. 283–293.

Saidman, S. and Vela, M. (2005) 'Electropolymerisation of pyrrole onto aluminium from alkaline solutions containing a surfactant', *Thin Solid Films*

Sakakura K, Nakano M, Otsuka F, Ladich E, Kolodgie FD, Virmani R. (2013) 'Pathophysiology of atherosclerosis plaque progression', *Heart Lung and Circulation*, 22(6), pp. 399–411.

Sakr, S. A., Ramadan, M. M. and El-Gamal, A. (2016) 'The inflammatory response to percutaneous coronary intervention is related to the technique of stenting and not the type of stent', *Egyptian Heart Journal*, 68(1), pp. 37–43

Salisbury D & Bronas U. (2015) 'Reactive Oxygen and Nitrogen Species: Impact on Endothelial Dysfunction', *Nursing Research,* 64, pp 53-66.

Sanders PN, Koval OM, Jaffer OA, Businga TR, Scott JA, Hayden PJ, et al. (2013) 'Asthma: CaMKII is essential for the proasthmatic effects of oxidation', *Science Translational Medicine*, 5(195), pp. 1–28.

Sardella G, Mariani P, D'Alessandro M, Luca LD, Pierro M, Mancone M, Porretta A, Accapezzato D, Fedele F, Paroli M. (2006) 'Early elevation of interleukin-1β and interleukin-6 levels after bare or drug-eluting stent implantation in patients with stable angina', *Thrombosis Research*, 117(6), pp. 659–664.

Satoh, K., Nigro, P. and Berk, B. C. (2010) 'Oxidative Stress and Vascular Smooth Muscle Cell Growth: A Mechanistic Linkage by Cyclophilin A', *Antioxidants and Redox Signaling*, 12(5), pp. 675–682

Scheschowitsch K, de Sordi R, de Moraes JA, Barja-Fidalgo C, Assreuy J. (2013) 'Vascular smooth muscle cell activation depends on NOS-1-derived NO and consequent peroxynitrite generation', *Critical Care*, 17(4), p. P82.

Schmidt HHHW, Stocker R, Vollbracht C, Paulsen G, Riley D, Daiber A, Cuadrado A. (2015) 'Antioxidants in Translational Medicine', *Antioxidants and Redox Signaling*, 23(14), pp. 1130–1143.

Sehgal, S. N. (2003) 'Sirolimus: Its discovery, biological properties, and mechanism of action', *Transplantation Proceedings*, 35(3 SUPPL.), pp. S7–S14.

Senoner, T. and Dichtl, W. (2019) 'Oxidative stress in cardiovascular diseases: Still a therapeutic target?', *Nutrients*, 11(9).

Shah SAA, Firlak M, Berrow SR, Halcovitch NR, Baldock SJ, Yousafzai BH, Hathout RN, Hardy JG. (2018) 'Electrochemically enhanced drug delivery using polypyrrole films', *Materials*, 11(7), pp. 1–16

Shahidi M, Barati M, Hayat P, Tavasoli B, Bakhshayesh M. (2014) 'The in vitro effects of sodium salicylate on von Willebrand factor and C-reactive protein production by endothelial cells', *Inflammopharmacology*, 22(6), pp. 367–372

Sharma DK, Pareek K, Chowdhury A. (2013) 'In vitro antibacterial and free radical scavenging activity of green hull of Juglans regia', *Journal of Pharmaceutical Analysis*, 3(4), pp. 298–302.

Sharma PS, Pietrzyk-Le, D'Souza FD, Kutner W. (2012) 'Electrochemically synthesized polymers in molecular imprinting for chemical sensing', *Analytical and Bioanalytical Chemistry,* 402(10), pp. 3177-3204.

Shi, C. and Zhitomirsky, I. (2010) 'Electrodeposition and capacitive behavior of films for electrodes of electrochemical supercapacitors', *Nanoscale Research Letters*, 5(3), pp. 518–523.

Shi X, Ding M, Dong Z, Chen F Ye J, Wang S, Leonard SS, Castranova V, Vallyathan V.. (1999) 'Antioxidant properties of aspirin: Characterization of the ability of aspirin to inhibit silica-induced lipid peroxidation, DNA damage, NF-κB activation, and TNF-α production', *Molecular and Cellular Biochemistry*, 199(1–2), pp. 93–102.

Shimokawa, H. (2013) 'Reactive oxygen species promote vascular smooth muscle cell proliferation', *Circulation Research*, 113(9), pp. 1040–1042.

Shiomi R, Shigetomi K, Inai T, Sakai M, Ikenouchi J.. (2015) 'CaMKII regulates the strength of the epithelial barrier', *Scientific Reports*, 5, pp. 1–11.

Shtivelband MI, Juneja HS, Lee S, Wu KK. (2003) 'Aspirin and salicylate inhibit colon cancer medium- and vegf-induced endothelial tube formation: Correlation with suppression of cyclooxygenase-2 expression', *Journal of Thrombosis and Haemostasis*, 1(10), pp. 2225–2233.

Shustak G, Gadzinowski M, Slomkowsli S, Domb AJ, Mandler D. (2007) 'A novel electrochemically synthesized biodegradable thin film of polypyrrole–polyethyleneglycol–polylactic acid nanoparticles', *New Journal of Chemistry,* 31, pp. 163-168.

Sikora A, Zielonka J, Lopez M, Joseph J, Kalyanaraman B. (2009) 'Direct oxidation of boronates by peroxynitrite: Mechanism and implications in fluorescence imaging of peroxynitrite', *Free Radical Biology and Medicine,* 47(10), pp. 1401-1407.

Silva, B. R., Pernomian, L. and Bendhack, L. M. (2012) 'Contribution of oxidative stress to endothelial dysfunction in hypertension', *Frontiers in Physiology*, 3 DEC(December), pp. 1–5.

Simoncini S, Sapet C, Camoin-Jau L, Bardin N, Harlé J, Sampol J, Dignat-George F, Anfosso F. (2005) 'Role of reactive oxygen species and p38 MAPK in the induction of the pro-adhesive endothelial state mediated by IgG from patients with anti-phospholipid syndrome', *International Immunology*, 17(4), pp. 489–500.

Sim DS, Jeong MH, Hong YJ, Kin JH, Ahn Y, Park KH, et al. (2018) 'Safety and Efficacy of the Endeavor Resolute® Stent in Patients with Multivessel Disease: The HEART (Honam EndeAvor ResoluTe) Prospective, Multicenter Trial', *Chonnam Medical Journal*, 54(1), p. 55.

Skopalová, K. (2019) 'In-Vitro Hemocompatibility of Polyaniline', *Polymers,* 11, pp. 1–9.

Sochor J, Dobes J, Krystofova O, Ruttkay-Nedecky B, Babula P, Pohanka M, Jurikova T, Zitka O, Adam V, Klejdus B, Kizek R. (2013) 'Electrochemistry as a tool for studying antioxidant properties', *International Journal of Electrochemical Science,* 8(6), pp. 8464–8489.

Solecka J, Guśpiel A, Postek M, Ziemska J, Kawęcki R, Lęczycka K, Osior A, Pietrzak B, Pypowski K, Wyrzykowska A. (2014) 'New derivatives of 3,4-dihydroisoquinoline-3-carboxylic acid with free-radical scavenging, d-amino acid oxidase, acetylcholinesterase and butyrylcholinesterase inhibitory activity', *Molecules*, 19(10), pp. 15866–15890.

Souilhol C, Harmsen MC, Evans PC, Krenning G. (2018) 'Endothelial–mesenchymal transition in atherosclerosis', *Cardiovascular Research*, 114, pp. 565-577.

Spiteller, G. (2001) 'Lipid peroxidation in aging and age-dependent diseases', *Experimental Gerontology*, 36(9), pp. 1425–1457.

Sroka, Z. and Cisowski, W. (2003) 'Hydrogen peroxide scavenging, antioxidant and anti-radical activity of some phenolic acids', *Food and Chemical Toxicology*, 41(6), pp. 753–758.

Steigerwald K, Merl S, Kastrati A, Wieczorek A, Vorpahl M, Mannhold R, Vogeser M, Hausleiter J, Joner M, Schömig A, Wessely R. (2009) 'The pre-clinical assessment of rapamycin-eluting, durable polymer-free stent coating concepts', *Biomaterials*, 30(4), pp. 632–637.

Stewart EM, Liu X, Clark GM, Kapsa RMI, Wallace GG. (2012) 'Inhibition of smooth muscle cell adhesion and proliferation on heparin-doped polypyrrole', *Acta Biomaterialia*, 8(1), pp. 194–200.

Su, W. and Iroh, J. O. (1997) 'Formation of polypyrrole coatings on stainless steel in aqueous benzene sulfonate solution', *Electrochimica Acta*, 42(17), pp. 2685–2694.

Sudhir K, Hermiller JB, Ferguson JM, Simonton CA.. (2013) 'Risk Factors for Coronary Drug-Eluting Stent Thrombosis: Influence of Procedural, Patient, Lesion, and Stent Related Factors and Dual Antiplatelet Therapy', *ISRN Cardiology*, 2013, pp. 1–8.

Sugden PH. & Clerk A. (2006) 'Oxidative stress and growth regulating intracellular signaling pathways in cardiac myocytes' *Antioxidants & Redox Signaling*, 8(11-12), pp. 2111–2124

Sun J, Yu H, Liu H, Pu D, Gao J, Jin X, Liu X, Yan A. (2020) 'Correlation of pre-operative circulating inflammatory cytokines with restenosis and rapid angiographic stenotic progression risk in coronary artery disease patients underwent percutaneous coronary intervention with drug-eluting stents', *Journal of Clinical Laboratory Analysis*, 34(3), pp. 1–12.

Sun HJ, Wu ZY, Cao L, Zhu MY, Nie XW, Huang DJ, Sun MT, Bian JS. (2020) 'Role of nitroxyl (HNO) in cardiovascular system: From biochemistry to pharmacology', *Pharmacological Research,* 159, pp. 104961

Suyani E, Derici UB, Sahin T, Ofluoglu E, Pasaoglu H, Erdem O, Barit G, Reis KA, Erten Y, Arinsoy T, Sindel S. (2009) 'Effects of everolimus on cytokines, oxidative stress, and renal histology in ischemia-reperfusion injury of the kidney', *Renal Failure*, 31(8), pp. 698–703.

Szabo, C. (2002) 'Multiple pathways of peroxynitrite cytotoxicity', *Toxicology Letters,* 140, pp. 105-112

T. Baltazar M, J. Dinis-Oliveira R, A. Duarte J, L. Bastos M, Carvalho F. (2011) 'Antioxidant Properties and Associated Mechanisms of Salicylates', *Current Medicinal Chemistry*, 18(21), pp. 3252–3264.

Tang C, Wang G, Wu X, Li Z, Shen Y, Lee JC, Yu Q. (2011) 'The impact of vascular endothelial growth factor-transfected human endothelial cells on endothelialization and restenosis of stainless steel stents', *Journal of Vascular Surgery*, 53(2), pp. 461–471.

Tansey MG, Luby-Phelps K, Kamm KE, Stull JT. (1994) 'Ca-dependent phosphorylation of myosin light chain kinase decreases the Ca sensitivity of light chain pshosphorylation within smooth muscle cells.' *Journal of Biological Chemistry,* 269(13), pp. 9912-9920.

Tardif, J. C., Grégoire, J. and L'Allier, P. L. (2002) 'Prevention of restenosis with antioxidants: Mechanisms and implications', *American Journal of Cardiovascular Drugs*, 2(5), pp. 323–334

Tardif JC, Grégoire J, Schwartz L, Title L, Laramee L, et al. (2003) 'Effects of AGI-1067 and probucol after percutaneous coronary interventions', *Circulation*, 107(4), pp. 552–558

Taverne YJHJ, Bogers AJJC, Duncker DJ, Merkus D. (2013) 'Reactive Oxygen Species and the Cardiovascular System', *Oxidative Medicine and Cellular Longevity.*

Thalla PK, Fadlallah H, Liberelle B, Lequoy P, De Crescenzo G, Merhi Y, Lerouge S. (2014) 'Chondroitin sulfate coatings display low platelet but high endothelial cell adhesive properties favorable for vascular implants', *Biomacromolecules*, 15(7), pp. 2512–2520.

Thomas C, Mackey MM, Diaz AA, Cox DP. (2009) 'Hydroxyl radical is produced via the Fenton reaction in submitochondrial particles under oxidative stress: Implications for diseases associated with iron accumulation', *Redox Report*, 14(3), pp. 102–108.

Tishchenko GA, Dybal J, Stejskal J, Kůdela V, Bleha M, Yu E, Rosova. Elyashevich GK.. (2002) 'Electrical resistance and diffusion permeability of microporous polyethylene membranes modified with polypyrrole and polyaniline in solutions of electrolytes', *Journal of Membrane Science,* 196, pp. 279-287.

Tourillon, G. and Garnier, F. (1983) 'Effect of dopant on the physicochemical and electrical properties of organic conducting polymers', *Journal of Physical Chemistry*, 87(13), pp. 2289–2292.

Toussaint F, Charbel C, Blanchette A, Ledoux J. (2015) 'CaMKII regulates intracellular Ca2+dynamics in native endothelial cells', *Cell Calcium*, 58(3), pp. 275–285.

Toussaint F, Charbel C, Allen BG, Ledoux J. (2016) 'Vascular CaMKII: heart and brain in your arteries', *American Journal of Physiology - Cell Physiology*, 311(3), pp. C462–C478.

Tousoulis Di, Oikonomou E, Economou EK, Crea F, Kaski JC. (2016) 'Inflammatory cytokines in atherosclerosis: Current therapeutic approaches', *European Heart Journal*, 37(22), pp. 1723–1735.

Touyz RM, Anagnostopoulou A, Camargo LL, Rios FJ, Montezano AC. (2019) 'Vascular Biology of Superoxide-Generating NADPH Oxidase 5 - Implications in Hypertension and Cardiovascular Disease', *Antioxidants and Redox Signaling*, 30(7), pp. 1027–1040

Trivedi, M. K., Dahryn, A. B. and Khemraj, H. S. (2015) 'Fourier Transform Infrared and Ultraviolet-Visible Spectroscopic Characterization of Biofield Treated Salicylic Acid and Sparfloxacin', *Natural Products Chemistry & Research*, 03(05).

Tzafriri AR, Vukmirovic N, Kolachalama VB, Astafieva I, Edelman ER. (2010) 'Lesion complexity determines arterial drug distribution after local drug delivery', *Journal of Controlled Release*, 142(3), pp. 332–338.

Tsui J, Inagaki M, Schulman H. (2005) 'Calcium/calmodulin-dependent protein kinase II (CaMKII) localization acts in concert with substrate targeting to create spatial restriction for phosphorylation', *Journal of Biological Chemistry,* 280(10), pp. 9210-6.

Uguz I, Ganji M, Hama A, Tanaka A, Inal S, Youssef A, Owens RM, Quilichini PP, Ghestem A, Bernard C, Dayeh SA, Malliaras GG. (2016) 'Autoclave Sterilization of PEDOT:PSS Electrophysiology Devices', *Advanced Healthcare Materials*, 5(24), pp. 3094–3098

Upadhyay J, Kumar A, Gogoi B, Buragohain AK. (2014) 'Biocompatibility and antioxidant activity of polypyrrole nanotubes', *Synthetic Metals*, 189, pp. 119–125.

Uppu RM, Nossaman BD, Greco AJ, Fokin A, Murthy SN, Fonseca VA, Kadowitz PJ. (2007) 'CARDIOVASCULAR EFFECTS OF PEROXYNITRITE', *Clinical and Experimental Pharmacology and Physiology*, 34(9), pp. 933–937.

Uthman L, Li X, Baartscheer A, Schumacher CA, Baumgart P, Hermanides J, Preckel B, Hollmann MW, Coronel R, Zuurbier CJ, Weber NC. (2022) 'Empagliflozin reduces oxidative stress through inhibition of the novel inflammation/NHE/[Na+]c/ROS-pathway in human endothelial cells', *Biomedicine and Pharmacotherapy*, 146, p. 112515.

Valente TAM, Silva DM, Gomes PS, Fernandes MH, Santos JD, Sencadas V. (2016) 'Effect of sterilization methods on electrospun poly(lactic acid) (PLA) fiber alignment for biomedical applications', *ACS Applied Materials and Interfaces*, 8(5), pp. 3241–3249.

Van Der Heiden K, Cuhlmann S, Luong LA, Zakkar M, Evans PC. (2010) 'Role of nuclear factor κB in cardiovascular health and disease', *Clinical Science*, 118(10), pp. 593–605.

Van Domburg RT, Foley DP, Breeman A, Van Herwerden LA, Serruys PW. (2002) 'Coronary artery bypass graft surgery and percutaneous transluminal coronary angioplasty: Twenty-year clinical outcome', *European Heart Journal*, 23(7), pp. 543–549

van Engeland NCA, Suarez Rodriguez F, Rivero-Müller A, Ristori T, Duran CL, et al. (2019) 'Vimentin regulates Notch signaling strength and arterial remodeling in response to hemodynamic stress', *Scientific Reports*, 9(1), pp. 1–14.

Varenhorst C, Lindholm M, Sarno G, Olivecrona G, Jensen U, Nilsson J, Carlsson J, James S, Lagergvist. (2018) 'Stent thrombosis rates the first year and beyond with new- and old-generation drug-eluting stents compared to bare metal stents', *Clinical Research in Cardiology*. Springer Berlin Heidelberg, 107(9), pp. 816–823.

Vasile, C. (2018) 'Polymeric nanocomposites and nanocoatings for food packaging: A review', *Materials*, 11(10).

Vega-Avila, E. and Pugsley, M. K. (2011) 'An Overview of Colorimetric Assay Methods Used to Assess Survival or Proliferation of Mammalian Cells', *Proc . West . Pharmacol . Soc*, 54(January), pp. 10–14.

Verdecchia P, Reboldi G, Angeli F, Mazzotta G, Lip GYH, Brueckmann M, Kleine E, Wallentin L, Ezekowitz MD, Yusuf S, Connolly SJ, Pasquale GD. (2018) 'Dabigatran vs. warfarin in relation to the presence of left ventricular hypertrophy in patients with atrial fibrillation-the Randomized Evaluation of Long-term anticoagulation therapY (RE-LY) study', *Europace*, 20(2), pp. 253–262.

Veredas, F. J., Cantón, F. R. and Aledo, J. C. (2017) 'Methionine residues around phosphorylation sites are preferentially oxidized in vivo under stress conditions', *Scientific Reports*, 7(July 2016), pp. 1–14.

Vichova, T. and Motovska, Z. (2013) 'Oxidative stress: Predictive marker for coronary artery disease', *Experimental and Clinical Cardiology*, 18(2), pp. 88–91.

Vlachojannis GJ, Puricel S, Natsuaki M, Morimoto T, Smits PC, Kimura T. (2017) 'Biolimus-eluting versus everolimus-eluting stents in coronary artery disease: a pooled analysis from the NEXT (NOBORI biolimus-eluting versus XIENCE/PROMUS everolimus-eluting stent) and COMPARE II (Abluminal biodegradable polymer biolimus-eluting stent versus durable polymer everolimus-eluting stent) randomised trials', *EuroIntervention*, 12(16), pp. 1970-1977.

Vo TTN, Morgan S, McCormick C, McGinty S, McKee S, Meere M. (2018) 'Modelling drug release from polymer-free coronary stents with microporous surfaces', *International Journal of Pharmaceutics*, 544(2), pp. 392–401.

Vu D, Huang D Bin, Vemu A, Ghosh G. (2013) 'A structural basis for selective dimerization by NF-κB RelB', *Journal of Molecular Biology*, 425(11), pp. 1934–1945.

Wainstein M V., Gonçalves SC, Zago AJ, Zenker R, Burttet R, Couto GdB, Tomazi F, Ribeiro JP. (2003) 'Plasma endothelin-1 levels after coronary stenting in humans', *American Journal of Cardiology*, 92(10), pp. 1211–1214.

Walch L, Massade L, Dufilho M, Brunet A, Rendu F. (2006) 'Pro-atherogenic effect of interleukin-4 in endothelial cells: Modulation of oxidative stress, nitric oxide and monocyte chemoattractant protein-1 expression', *Atherosclerosis,* 187(2), pp. 285–291.

Walford GA, Moussignac RL, Scribner AW, Loscalzo J, Leopold JA. (2004) 'Hypoxia Potentiates Nitric Oxide-mediated Apoptosis in Endothelial Cells via Peroxynitrite-induced Activation of Mitochondria-dependent and -independent Pathways', *Journal of Biological Chemistry*, 279(6), pp. 4425–4432.

Wang J, He W, Xu X, Guo L, Zhang Y, Han S, Shen D. (2017) 'The mechanism of TGF-β/miR-155/c-Ski regulates endothelial–mesenchymal transition in human coronary artery endothelial cells', *Bioscience Reports*, 37(4), pp. 1–10.

Wang K, Shang T, Zhang L, Zhou L, Liu C, Fu Y, Zhao Y, Li X, Wang J. (2021) 'Application of a Reactive Oxygen Species-Responsive Drug-Eluting Coating for Surface Modification of Vascular Stents', *ACS Applied Materials and Interfaces*, 13(30), pp. 35431–35443.

Wang, R., Li, Q. and Tang, D. D. (2006) 'Role of vimentin in smooth muscle force development', *American Journal of Physiology - Cell Physiology*, 291(3), pp. 483–489.

Wang Z, Ginnan R, Abdullaev IF, Trebak M, Vincent PA, Singer HA. (2010) 'Calcium/calmodulin-dependent protein kinase II delta 6 (CaMKIIδ 6) and RhoA involvement in thrombin-induced endothelial barrier dysfunction', *Journal of Biological Chemistry*, 285(28), pp. 21303–21312

Watt J, Kennedy S, McCormick C, Agbani EO, McPhaden A, Mullen A, Czudaj P, Behnisch B, Wadsworth RM, Oldroyd KG. (2013) 'Succinobucol-eluting stents increase neointimal thickening and peri-strut inflammation in a porcine coronary model', *Catheterization and Cardiovascular Interventions*, 81(4), pp. 698–708.

Watt J, Wadsworth R, Kennedy S, Oldroyd KG. (2008) 'Pro-healing drug-eluting stents: A role for antioxidants?', *Clinical Science*, 114(3–4), pp. 265–273.

Weaver, B. A. (2014) 'How Taxol/paclitaxel kills cancer cells', *Molecular Biology of the Cell*, 25(18), pp. 2677–2681.

Weintraub, W. S. (2007) 'The Pathophysiology and Burden of Restenosis', *American Journal of Cardiology*, 100(5 SUPPL.).

Włodarczyk K, Singer F, Jasiński P, Virtanen S. (2014) 'Solid state conductivity of optimized polypyrrole coatings on iron obtained from aqueous sodium salicylate solution determined by impedance spectroscopy', *International Journal of Electrochemical Science*, 9(12), pp. 7997–8010.

Wood BM, Simon M, Galice S, Alim CC, Ferrero M, Pinna NN, Bers DM, Bossuyt J. (2018) 'Cardiac CaMKII activation promotes rapid translocation to its extra-dyadic targets', *Journal of Molecular and Cellular Cardiology*, 125(October), pp. 18–28.

Wong, J. Y., Langer, R. and Ingber, D. E. (1994) 'Electrically conducting polymers can noninvasively control the shape and growth of mammalian cells.', *Proceedings of the National Academy of Sciences.*

Wong, J. Y., Leach, J. B. and Brown, X. Q. (2004) 'Balance of chemistry, topography, and mechanics at the cell – biomaterial interface : Issues and challenges for assessing the role of substrate mechanics on cell response', *Surface Science,* 570, pp. 119–133.

Wright, E., Scism-Bacon, J. L. and Glass, L. C. (2006) 'Oxidative stress in type 2 diabetes: The role of fasting and postprandial glycaemia', *International Journal of Clinical Practice*, 60(3), pp. 308–314.

Wu, A., Venancio, E. C. and MacDiarmid, A. G. (2007) 'Polyaniline and polypyrrole oxygen reversible electrodes', *Synthetic Metals*, 157(6–7), pp. 303–310.

Wu CY, Hsieh HL, Sun CC, Yang CM. (2009) 'IL-1β induces MMP-9 expression via a Ca2+-dependent CaMKII/JNK/c-Jun cascade in rat brain astrocytes', *Glia*, 57(16), pp. 1775–1789

Wu W, Zhang W, Choi M, Zhao J, Gao P, Xue M, Singer HA, Jourd'heuil D, Long X. (2019) 'Vascular smooth muscle-MAPK14 is required for neointimal hyperplasia by suppressing VSMC differentiation and inducing proliferation and inflammation', *Redox Biology*, 22(February), p. 101137.

Xiao-Dong Z, Fei-Fei L, Zhan-Peng W, Xin-Xue L, Zhi-Min D. (2016) 'Renin-angiotensin system inhibitors in patients with coronary artery disease who have undergone percutaneous coronary intervention', *Therapeutic Advances in Cardiovascular Disease*, 10(3), pp. 172–177.

Yan G, You B, Chen SP, Liao JK, Sun J. 'TNF-alpha Downregulates Endothelial Nitric Oxide Synthase mRNA Stability via Translation Elongation Factor 1-alpha 1', *Circulatory Research*, 103(6), pp. 591–597.

Yang D, Sun C, Zhang J, Lin S, Zhao L, Wang L, Lin R, Lv J, Xin S. (2018) 'Proliferation of vascular smooth muscle cells under inflammation is regulated by NF-κB p65/microRNA-17/RB pathway activation', *International Journal of Molecular Medicine*, 41(1), pp. 43–50.

Yang X, Dai T, Zhu Z, Lu Y. (2007) 'Electrochemical synthesis of functional polypyrrole nanotubes via a self-assembly process', *Polymer*, 48(14), pp. 4021–4027.

Yang Y, Qi P, Wen F, Li X, Xia Q, Maitz MF, Yang Z, Shen R, Tu Q, Huang N. (2014) 'Mussel-inspired one-step adherent coating rich in amine groups for covalent immobilization of heparin: Hemocompatibility, growth behaviors of vascular cells, and tissue response', *ACS Applied Materials and Interfaces,* 6(16), pp. 14608-14620.

Yang ZJ, Xie Y, Bosco GM, Chen C, Camporesi EM. (2010) 'Hyperbaric oxygenation alleviates MCAO-induced brain injury and reduces hydroxyl radical formation and glutamate release', *European Journal of Applied Physiology*, 108(3), pp. 513–522.

Yeh RW, Silber S, Chen L, Chen S, Hiremath S, Neumann F, Qiao S, Saito S, Xu B, Yan Y, Mauri L. (2017) '5-Year Safety and Efficacy of Resolute Zotarolimus-Eluting Stent: The RESOLUTE Global Clinical Trial Program', *JACC: Cardiovascular Interventions*, 10(3), pp. 247–254.

Yerokun, BA, Williams JB, Gaca J, Smith PK, Roe MT. (2016) 'Indications, algorithms, and outcomes for coronary artery bypass surgery in patients with acute coronary syndromes', *Coron Artery Dis,* 27(4), pp. 319-326.

Maeng Y, Min J, Kim JH, Yamagishi A, Mochizuki N, Kwon J, Park Y, Kin Y, Kwon Y. (2006) 'ERK is an anti-inflammatory signal that suppresses expression of NF- κ B-dependent inflammatory genes by inhibiting IKK activity in endothelial cells', *Cellular Signallling*, 18, pp. 994–1005.

Yoshida, L. S. and Tsunawaki, S. (2008) 'Expression of NADPH oxidases and enhanced H2O2-generating activity in human coronary artery endothelial cells upon induction with tumor necrosis factor-α', *International Immunopharmacology*, 8(10), pp. 1377–1385.

Yussuf A, Al-Saleh M, Al-Enezi S, Abraham G. (2018) 'Synthesis and Characterization of Conductive Polypyrrole: The Influence of the Oxidants and Monomer on the Electrical, Thermal, and Morphological Properties', *International Journal of Polymer Science*, 2018.

Zalka D, Kovács N, Szekeres K, Ujvari M, Vesztergom S, Eliseeva S, Kondratiev V, Lang GG. (2017) 'Determination of the charge transfer resistance of poly(3,4-ethylenedioxythiophene)-modified electrodes immediately after overoxidation', *Electrochimica Acta*, 247, pp. 321–332.

Zen K, Karsan A, Stempien-Otero A, Yee E, Tupper J, Li X, Eunson T, Kay MA, Wilson CB, Winn RK, Harlan JM. (1999) 'NF-κB activation is required for human endothelial survival during exposure to tumor necrosis factor-α but not to interleukin-1β or lipopolysaccharide', *Journal of Biological Chemistry*, 274(40), pp. 28808–28815.

Zhang, P. (2017) 'CaMKII: The molecular villain that aggravates cardiovascular disease (review)', *Experimental and Therapeutic Medicine*, 13(3), pp. 815–820.

Zhang T, Kohlhaas M, Backs J, Mishra S, Phillips W, Dybkova N, Chang S, Ling H, Bers DM, Maier LS, Olson EN, Brown JH. (2007) 'CaMKIIδ isoforms differentially affect calcium handling but similarly regulate HDAC/MEF2 transcriptional responses', *Journal of Biological Chemistry*, 282(48), pp. 35078–35087.

Zhang, X. and Bai, R. (2003) 'Surface electric properties of polypyrrole in aqueous solutions', *Langmuir*, 19(26), pp. 10703–10709.

Zhang Z, Roy R, Dugre FJ, Tessier D, L Dao H.. (2001) 'In vitro biocompatibility study of electrically conductive polypyrrole-coated polyester fabrics', *Journal of Biomedical Materials Research*, 57(1), pp. 63–71

Zhang Z, Li G, Yan F, Zheng X, Li X.. (2012) 'Towards understanding of protein adsorption behaviour on plasma polymerized pyrrole film', *Central European Journal of Chemistry*, 10(4), pp. 1157–1164.

Zhen J, Lu H, Wang XQ, Vaziri ND, Zhou XJ. (2008) 'Upregulation of endothelial and inducible nitric oxide synthase expression by reactive oxygen species', *American Journal of Hypertension*, 21(1), pp. 28–34.

Zhou C, Ramaswamy SS, Johnson DE, Vitturi DA, Schopfer FJ, Freeman BA, Hudmon A, Levitan ES. (2016) 'Novel Roles for Peroxynitrite in Angiotensin II and CaMKII Signaling', *Scientific Reports*, 6, pp. 1–9.

Zhao, J., Fujita, K. and Sakai, K. (2007) 'Reactive oxygen species, nitric oxide, and their interactions play different roles in Cupressus lusitanica cell death and phytoalexin biosynthesis', *New Phytologist*, 175(2), pp. 215–229.

Zhou P, Lu S, Luo Y, Wang S, Yang K, Zhai Y, Sun G, Sun, X. (2017) 'Attenuation of TNF-α-induced inflammatory injury in endothelial cells by ginsenoside Rb1 via inhibiting NF-κB, JNK and p38 signaling pathways', *Frontiers in Pharmacology*, 8(AUG), pp. 1–13.

Zhou, M. and Heinze, J. (1999) 'Electropolymerization of Pyrrole and Electrochemical Study of Polypyrrole. 3. Nature of "Water Effect" in Acetonitrile', *The Journal of Physical Chemistry B,* 103, pp. 8451-8457.

Ziberna L, Martelanc M, Franko M, Passamonti S. (2016) 'Bilirubin is an Endogenous Antioxidant in Human Vascular Endothelial Cells', *Scientific Reports*, 6, pp. 1–6.

Zima AV. & Mazurek SR. (2016) 'Functional Impact of Ryanodine Receptor Oxidation on Intracellular Calcium Regulation in the Heart', *Review of Physiological and Biochemical Pharmacology*, 171, pp. 39-62.

Supplementary Figures

Chapter 2

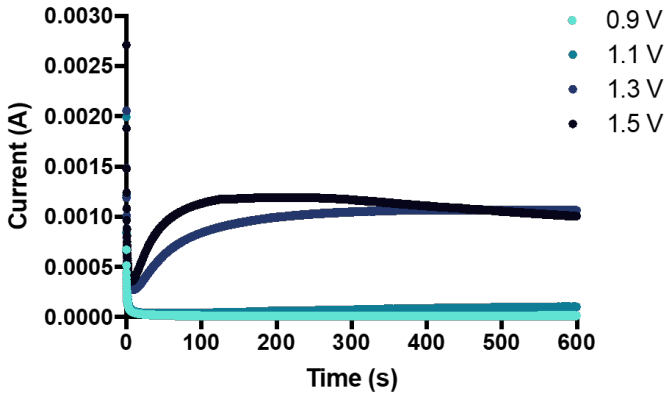

Supplementary Figure S2.1. Preliminary current-time profiles for potentiostatic electropolymerisation of pyrrole on 1 mm 316L SS wires, coated for 10 minutes over a range of applied voltages between +0.9 and +1.5 V. Data is representative of the mean current from 3 coatings per applied voltage.

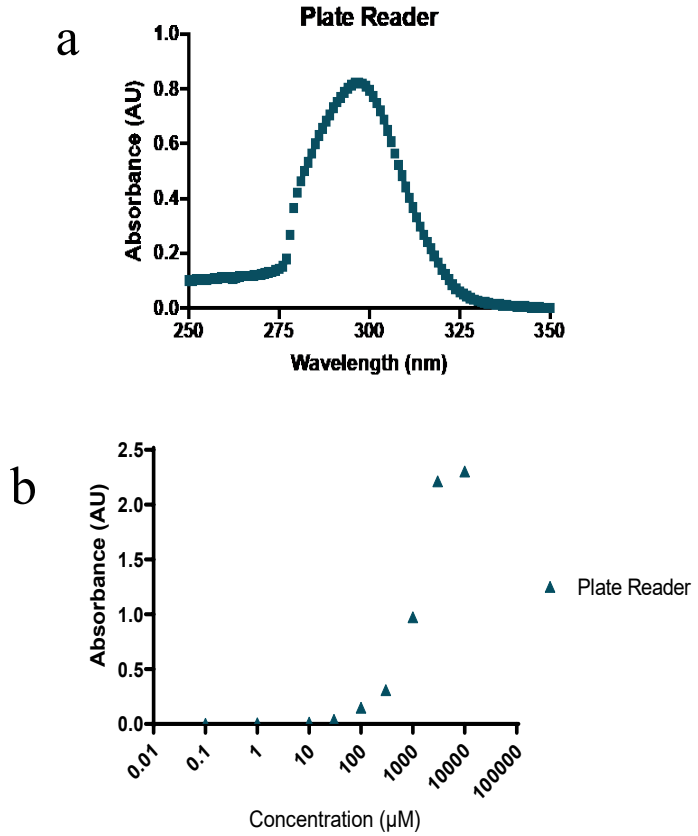

Supplementary Figure S2.2. a) 250 – 350 nm absorbance spectrum for 1 M sodium salicylate in PBS as measured using a plate reader. c) 296.5 nm absorbance of sodium salicylate in PBS, measured using a plate reader (100 μM – 10 M).

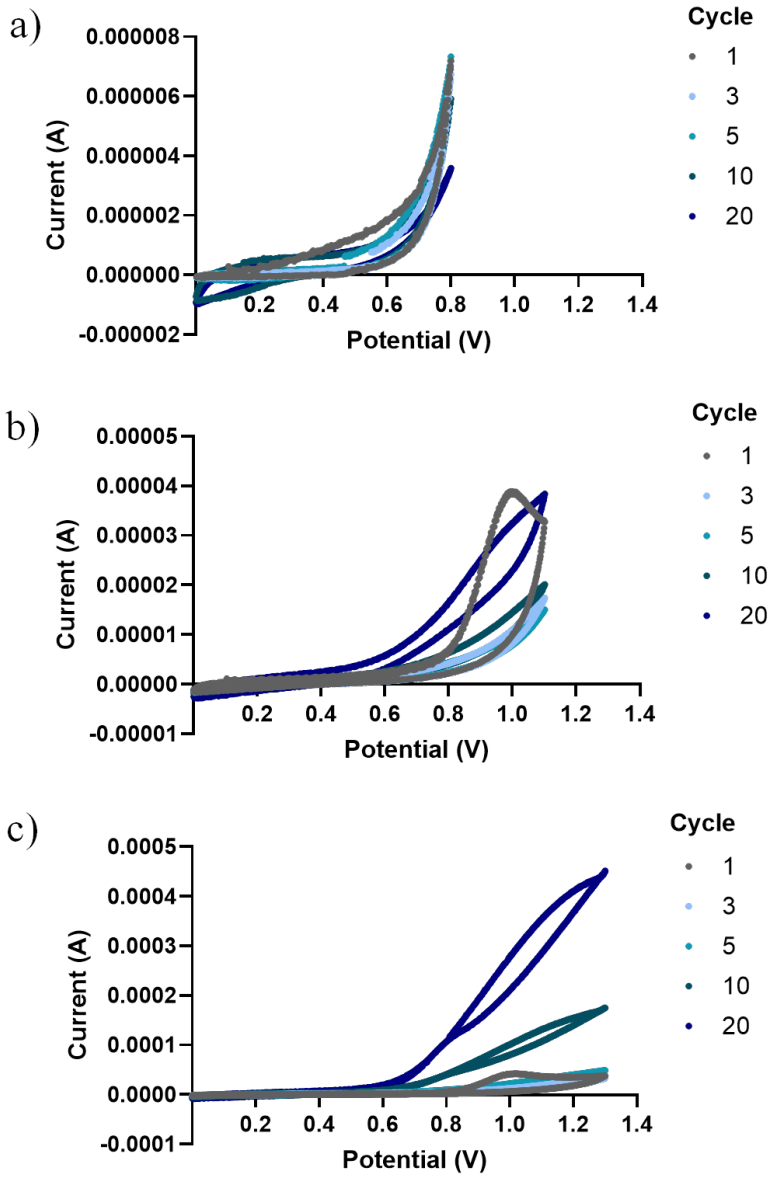

Supplementary Figure S2.3. Potentiodynamic electropolymerisation of PPy coatings on 200 µm diameter SS wires at applied voltages ranges: a) 0 - +0.8 V, b) 0 - +1.1 V, and c) 0 - +1.3 V. Each graph represents a single coating.

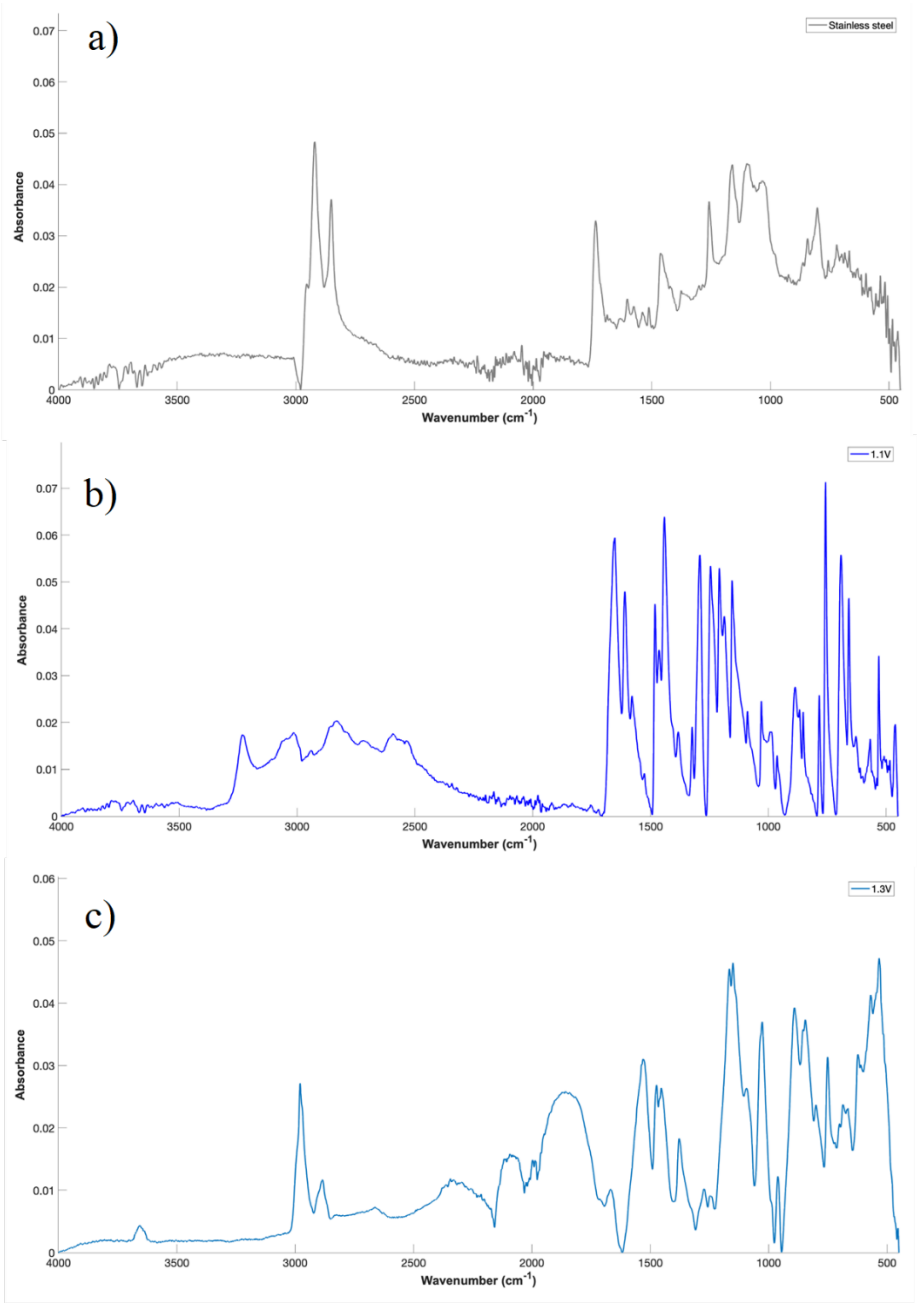

Supplementary Figure S2.4. FTIR spectra for a) uncoated 316L SS, b) PPy generated by potentiostatically electropolymerisation at 1.1 V, c) PPy generated by potentiostatically electropolymerisation at 1.3 V. Spectra represent average traces from 3 repeat measurements from 3 independent samples with a baseline correction applied.

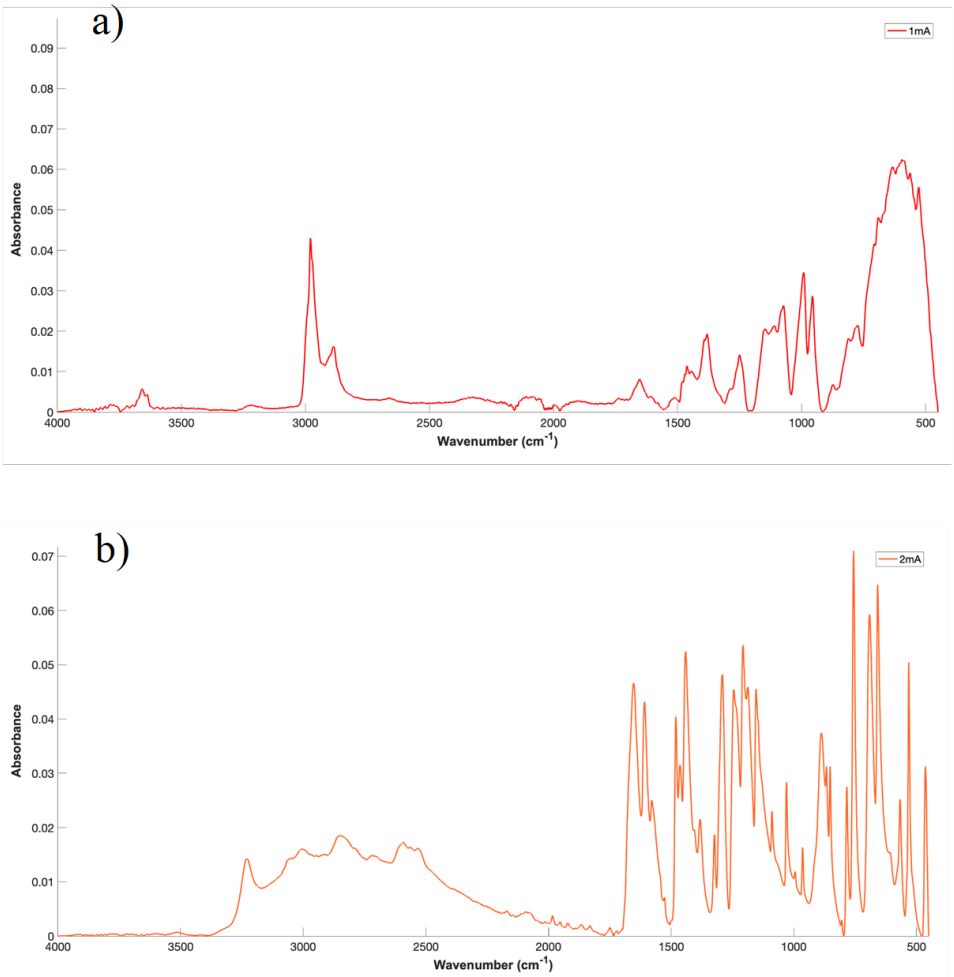

Supplementary Figure S2.5. FTIR spectra for PPy generated by galvanostatic electropolymerisation at a) 1 mA and b) 2 mA. Spectra represent average traces from 3 repeat measurements from 3 independent samples with a baseline correction applied.

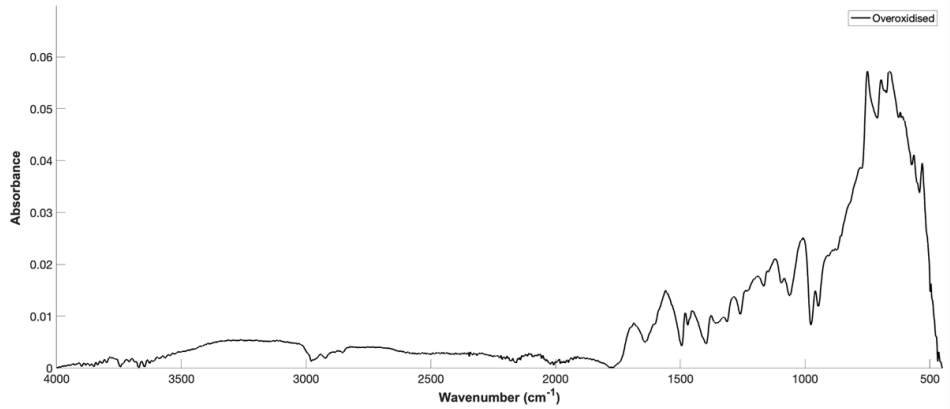

Supplementary Figure S2.6. FTIR spectra for overoxidised PPy coatings generated by galvanostatic electropolymerisation at 1 mA followed by CV (20 cycles, 0 - +1.5 V, 20 $mV.s^{-1}$). Spectra represent average traces from 3 repeat measurements from 3 independent samples with a baseline correction applied.

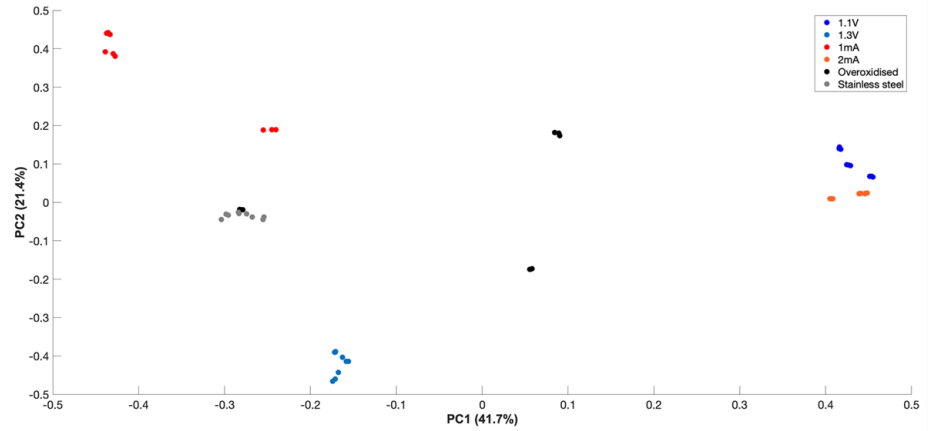

Supplementary Figure S2.7. Principal component analysis (PCA) of FTIR spectra for uncoated 316L SS, PPy coatings and overoxidised PPy. Due to the low sample size, high variability was observed between groups, with some clustering of coatings 1.1 V potentiostatic coatings and 2 mA galvanostatic coatings.

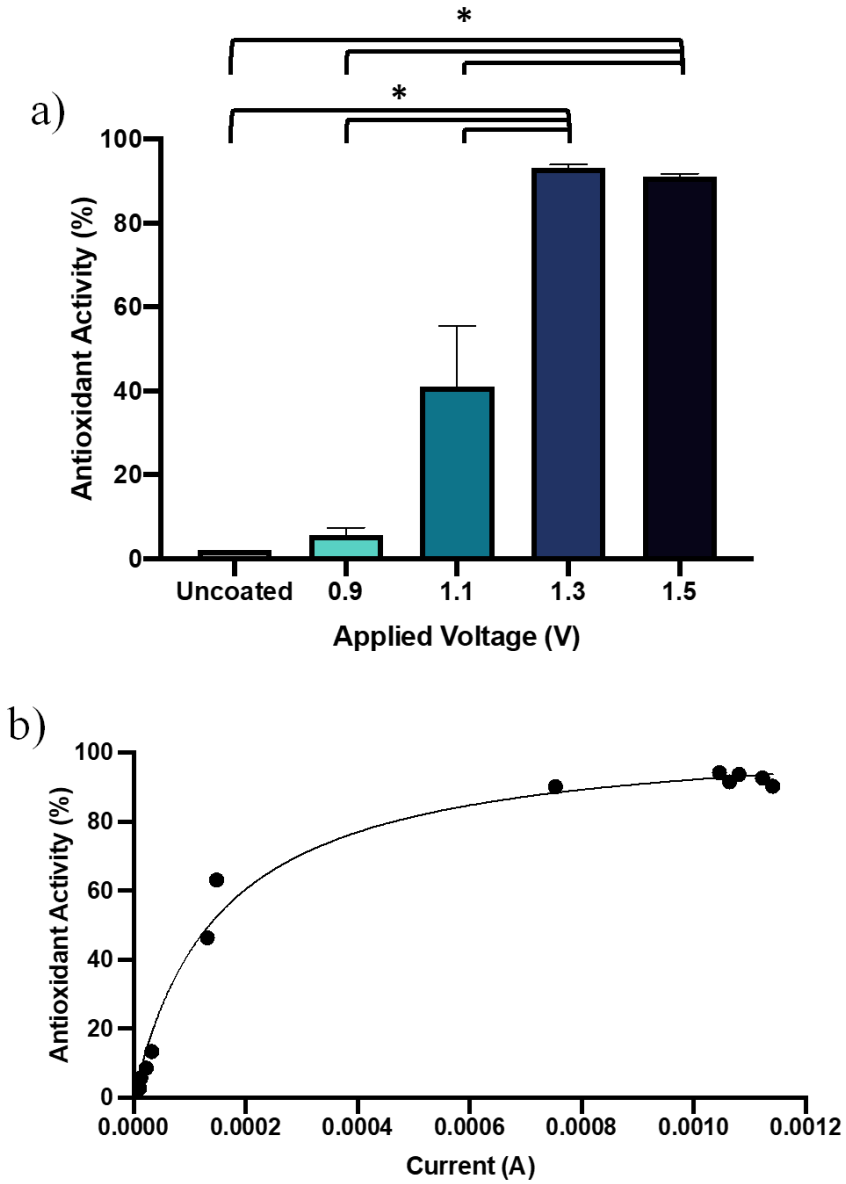

Supplementary Figure S3.1. a) DPPH scavenging activity of potentiostatic electropolymerised PPy on 1 mm wires after 24 h incubation, showing strong antioxidant potential (mean±S.E.M, n=3, *$p<0.05$). b) Correlation between DPPH scavenging activity of 1 mm µm coated wires and terminal current during electropolymerisation (r^2 = 0.9872). As the current at the end of the electropolymerisation process increases, the DPPH scavenging capacity of 1 mm PPy-coated wires also increases.

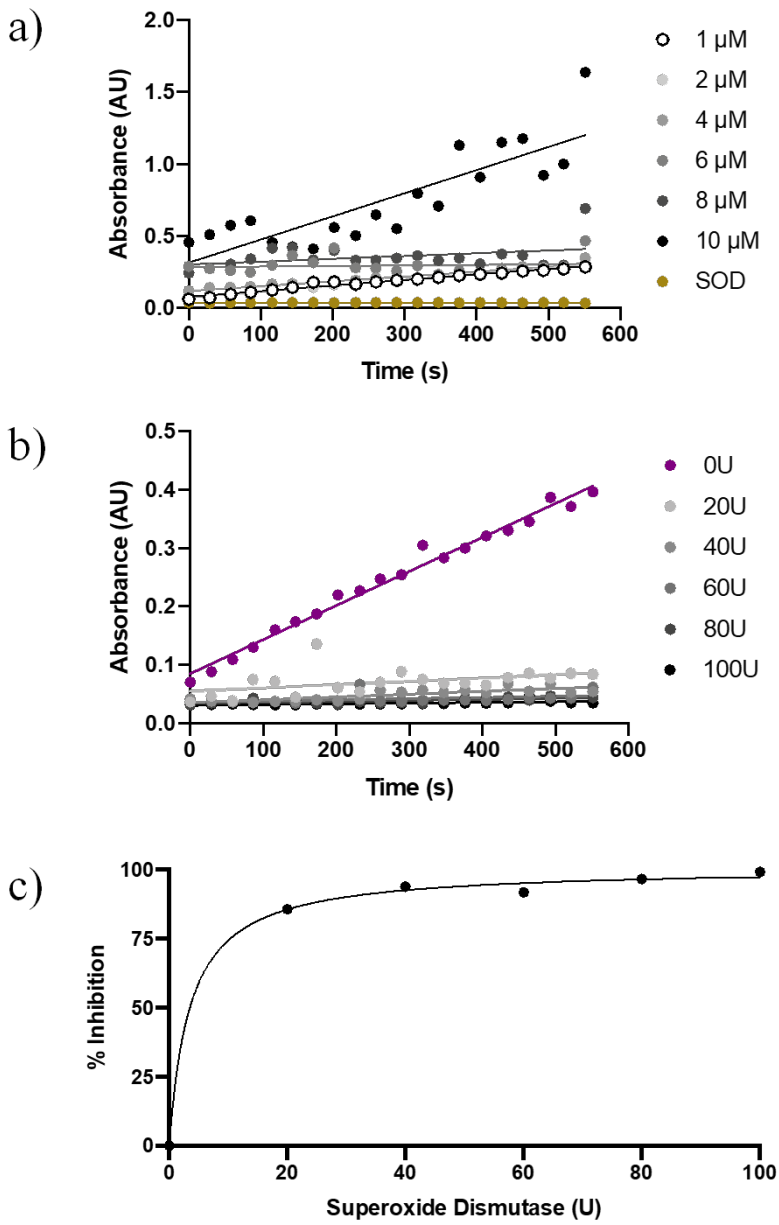

Supplementary Figure S3.2. Optimisations for the superoxide scavenging assay: a) Superoxide assay reaction (NBT reduction by superoxide) kinetics when initiated with increased concentrations of hypoxanthine, suggesting 1 or 2 µM as optimal for this reaction. b) Inhibition of NBT reduction by superoxide, as measured by 605 nm absorbance, in the presence of increasing superoxide dismutase. c) Percentage inhibiton of the superoxide-NBT reaction, suggesting SOD > 400 U/ml as sufficient for complete inhibition. All data represents an average (mean) of three independent samples.

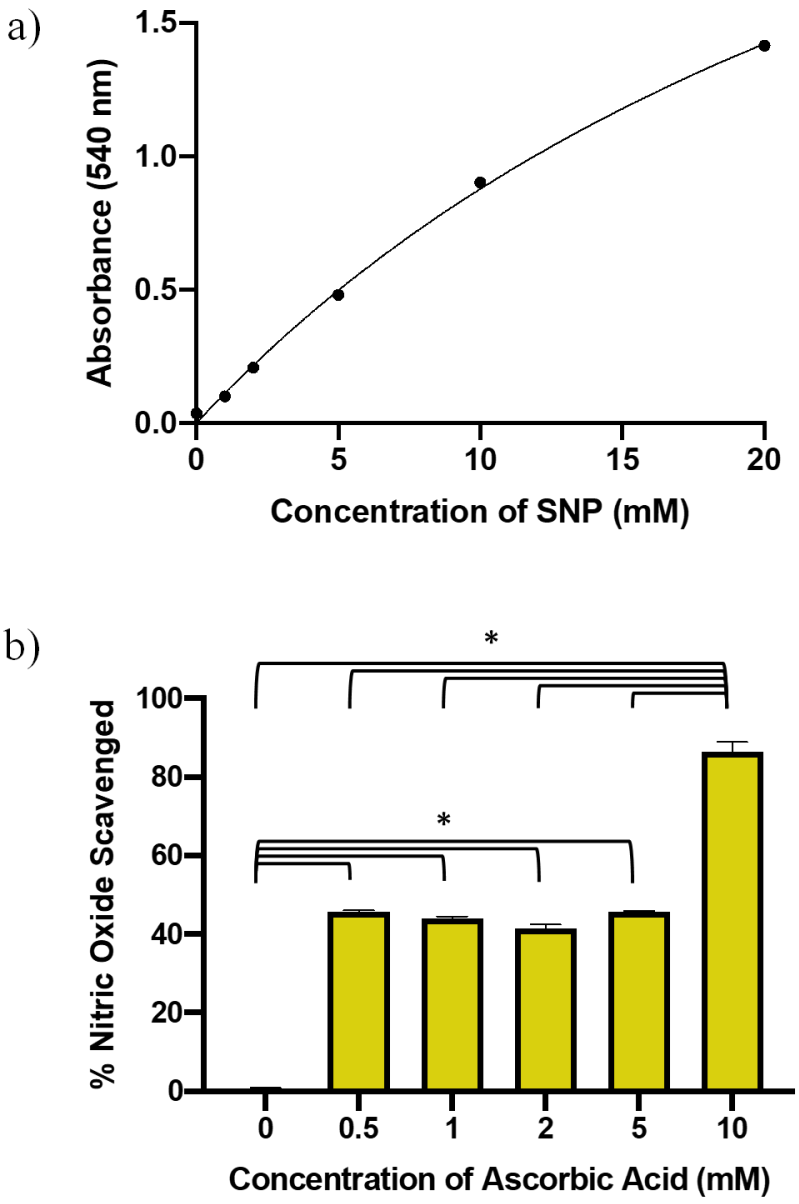

Supplementary Figure S3.3. a) Griess absorbance standard curve with increasing concentrations of SNP (1-20 mM) as a nitric oxide generator. b) Optimisation of the L-ascorbic acid positive control. 5 mM SNP was incubated with increasing concentrations of ascorbic acid (0.5-10 mM) for 150 minutes and the % of NO scavenged was calculated. 10 mM ascorbic acid demonstrated significantly greater NO scavenging capacity than all other concentrations and the blank (mean ± S.E.M, n=3, *$p<0.05$).

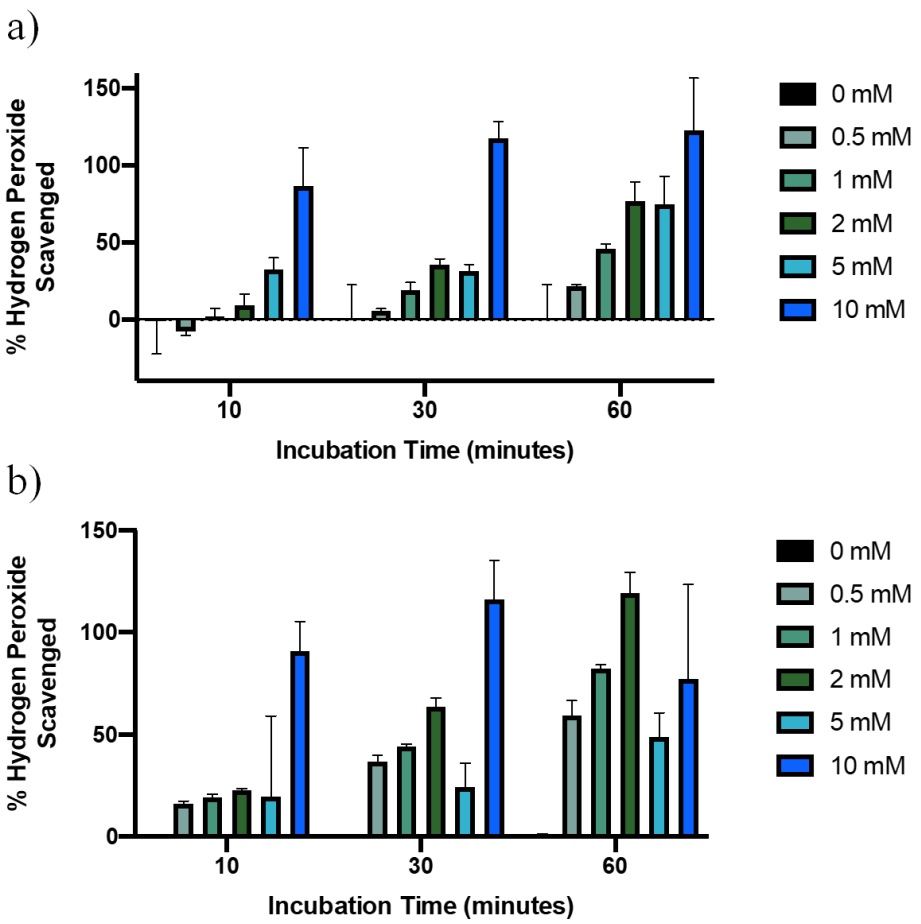

Supplementary Figure S3.4. Optimisation of the hydrogen peroxide scavenging assay using a) 40 mM and b) 20 mM hydrogen peroxide. The L-ascorbic acid positive control was incubated with both peroxide concentrations for 10, 30 or 60 minutes at increasing concentrations (0.5-10 mM). Bars represent mean % of hydrogen peroxide scavenged ± S.E.M. Significance not shown to improve legibility. Based on this data, 40 mM hydrogen peroxide and 10-minute incubation times were chosen as optimal conditions.

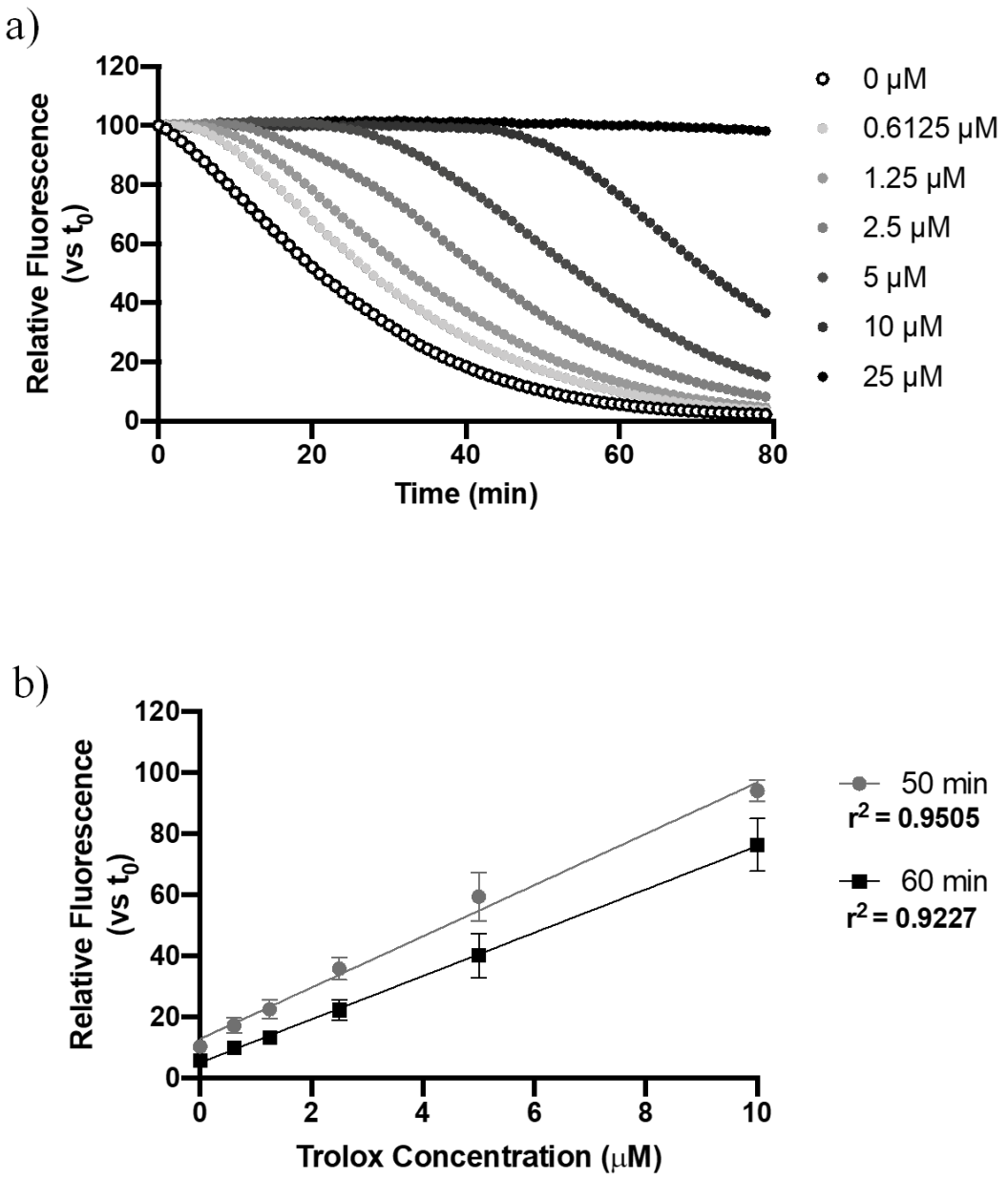

Supplementary Figure 3.5. Optimisations for the oxygen radical absorbance capacity (ORAC) assay: a) Loss of fluorescence due to peroxyl radical generation in the presence of increasing Trolox concentrations. b) Relative fluorescence for Trolox standards at 50 and 60 minutes from panal a, showing strong postive correlation at both time intervals, suggesting 50 minutes as an appropriate time to measure peroxyl scavenging capacity (mean±S.E.M, n=3).

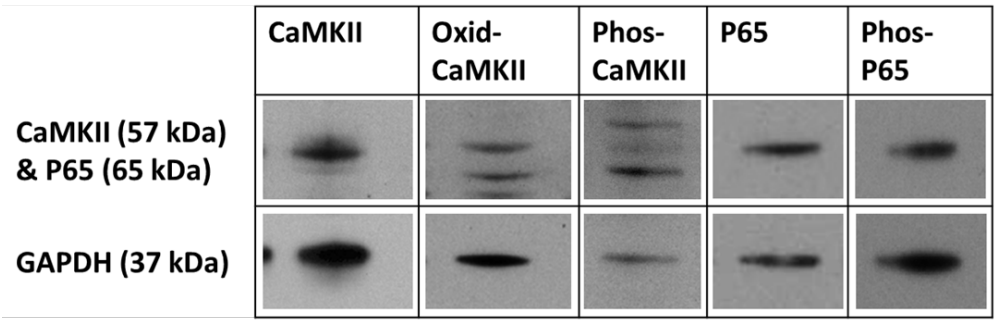

Supplementary Figure S4.1. Aged heart homogenate immunoblotting controls for primary antibodies against CaMKII, oxidised-CaMKII (oxid-CaMKII), phosphorylated-CaMKII (phos-CaMKII), P65 and phosphorylated-P65 (phos-P65).

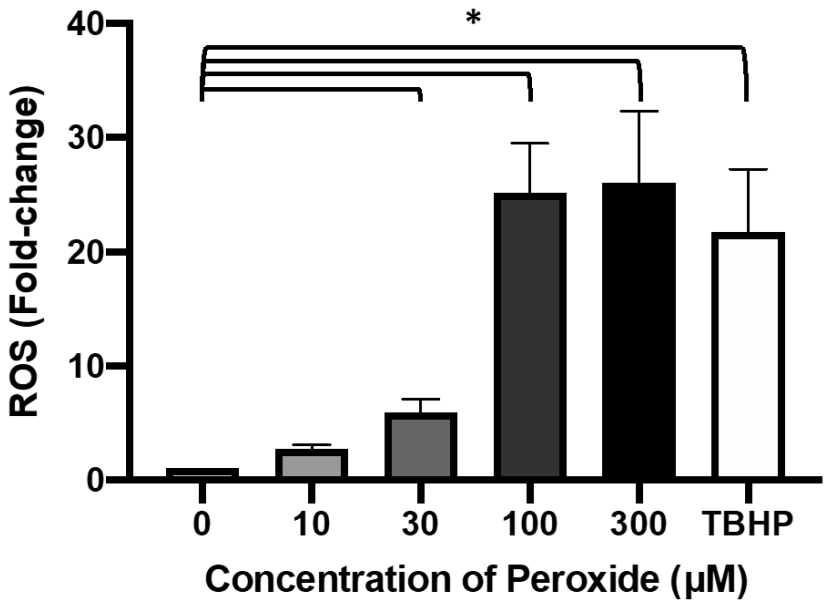

Supplementary Figure S4.2. Effect of 6 h hydrogen peroxide (10 -300 µM) stimulation on ROS generation in HUVECs. Stimulation with 30, 100 and 300 µM hydrogen peroxide was found to induce significant ROS generation in HUVECs. TBHP is shown as a positive control and also induce significant ROS generation. Bars represent mean fold-change, compared against unstimulated control HUVECs (0 µM), error bars represent ±standard error of the mean. * $p<0.05$, n=4.

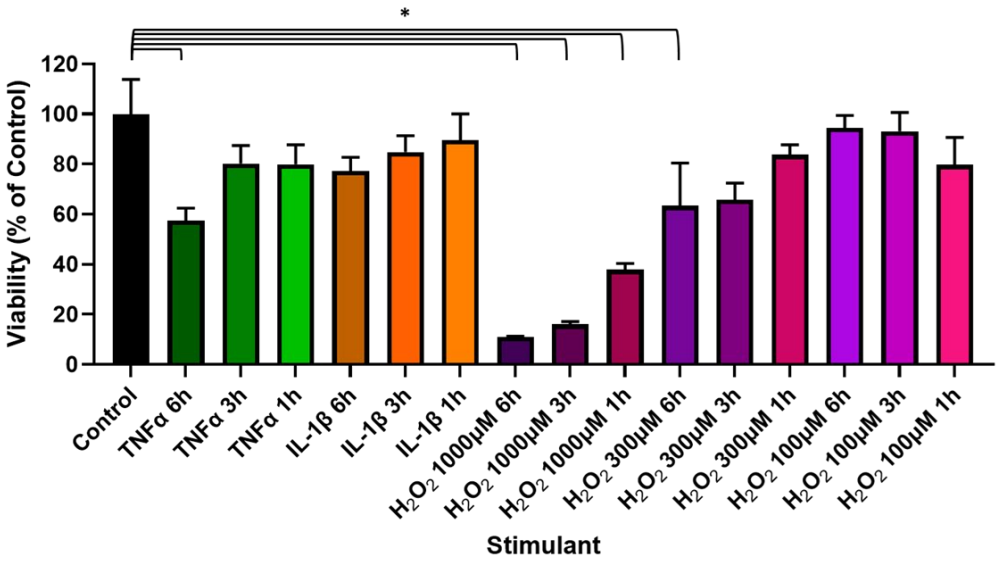

Supplemental Figure S5.1. MTT assay results showing the effects of IL-1β, TNFα (both 10 ng/ml) and hydrogen peroxide stimulation on the viability of HCAECs. Each bar represents mean number of cells, as a percentage of the average control, error bars represent ± S.E.M. High concentrations (>300μM) hydrogen peroxide stimulation induced significant loss in cell viability. Significant loss of viability was also observed after 6h TNFα stimulation. * $p<0.05$, n=3.

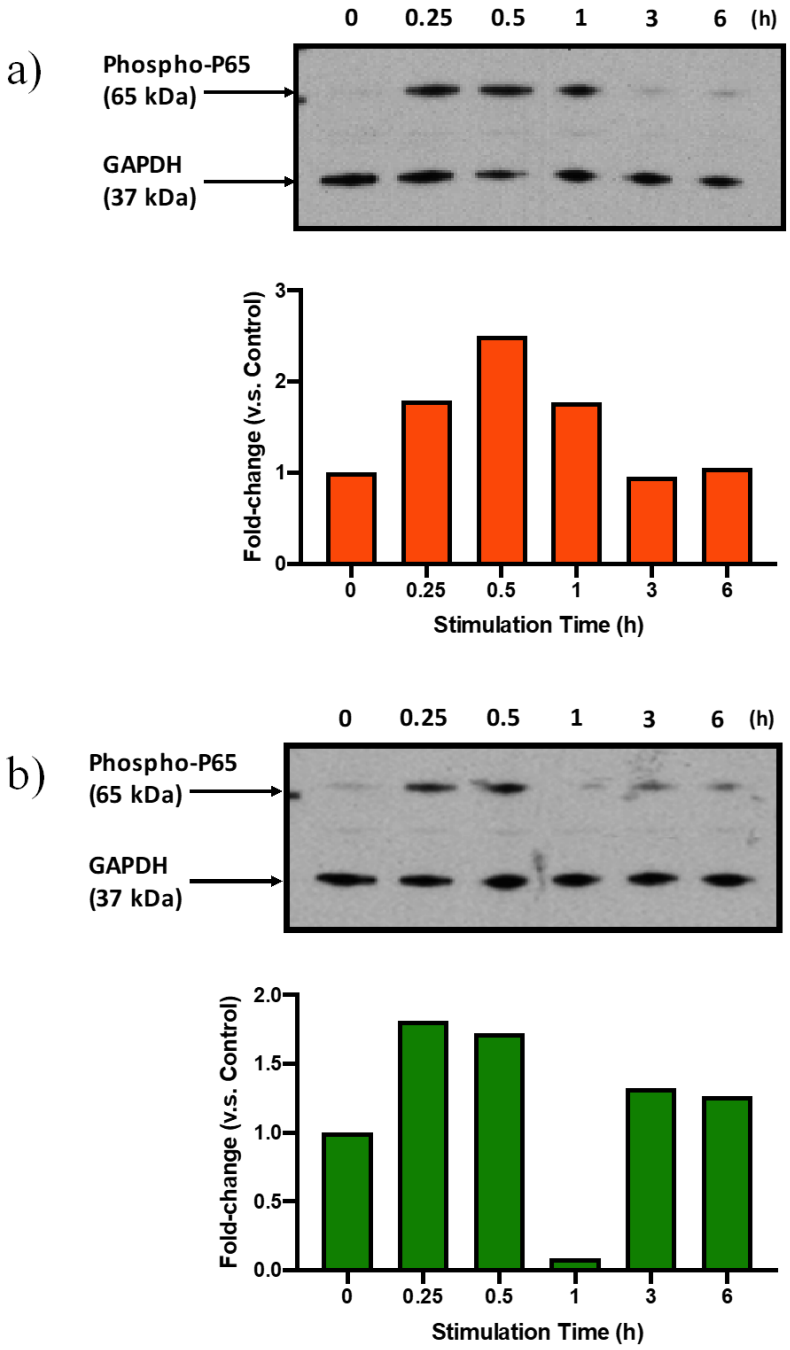

Supplementary Figure S5.2. Expression change in phospho-P65 in HCAECs after stimulation with IL-1β (panel a) and TNFα (panel b) (both 10 ng/ml) for up to 6 hours. Immunoblotting shows both cytokines generate P65 activation in HCAECs when used at the same concentrations and incubation times used for optimisation in HUVECs. This supports the use of exploring further 10 ng/ml stimulation for 30 minutes with both cytokines in HCAECs. Data shown obtained from a single experiment (n=1)

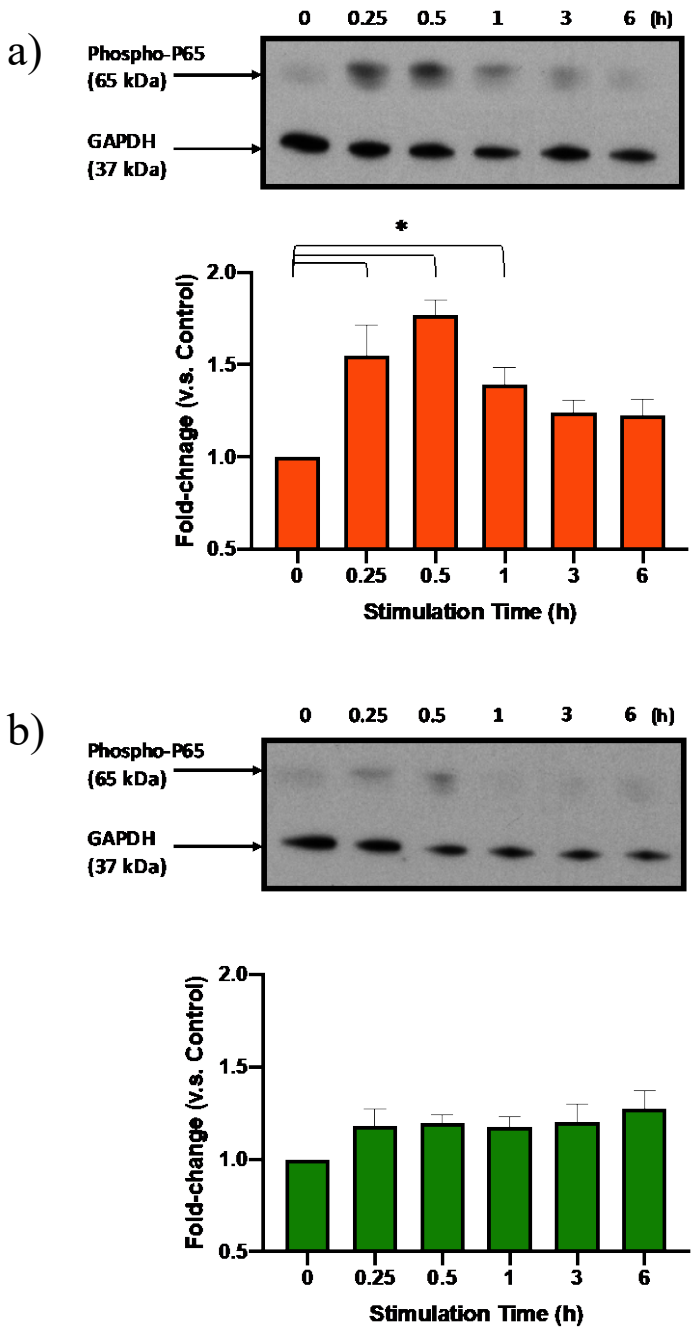

Supplementary Figure S5.3. Expression change in phospho-P65 in HCASMCs after stimulation with IL-1β (panel a) and TNFα (panel b) (both 10 ng/ml) for up to 6 hours. Immunoblotting shows IL-1β stimulation generates significant P65 activation in HCAECs between 15 minutes and 1 h (*$p<0.05$, n=4, One-way ANOVA with post-hoc Dunnett's), whereas TNFα stimulation was not found to significantly induce P65 activation (*$p>0.05$, n=4, One-way ANOVA). This suggests IL-1β triggers pro-inflammatory signalling in HCASMCs under the conditions studied, but TNFα does not.

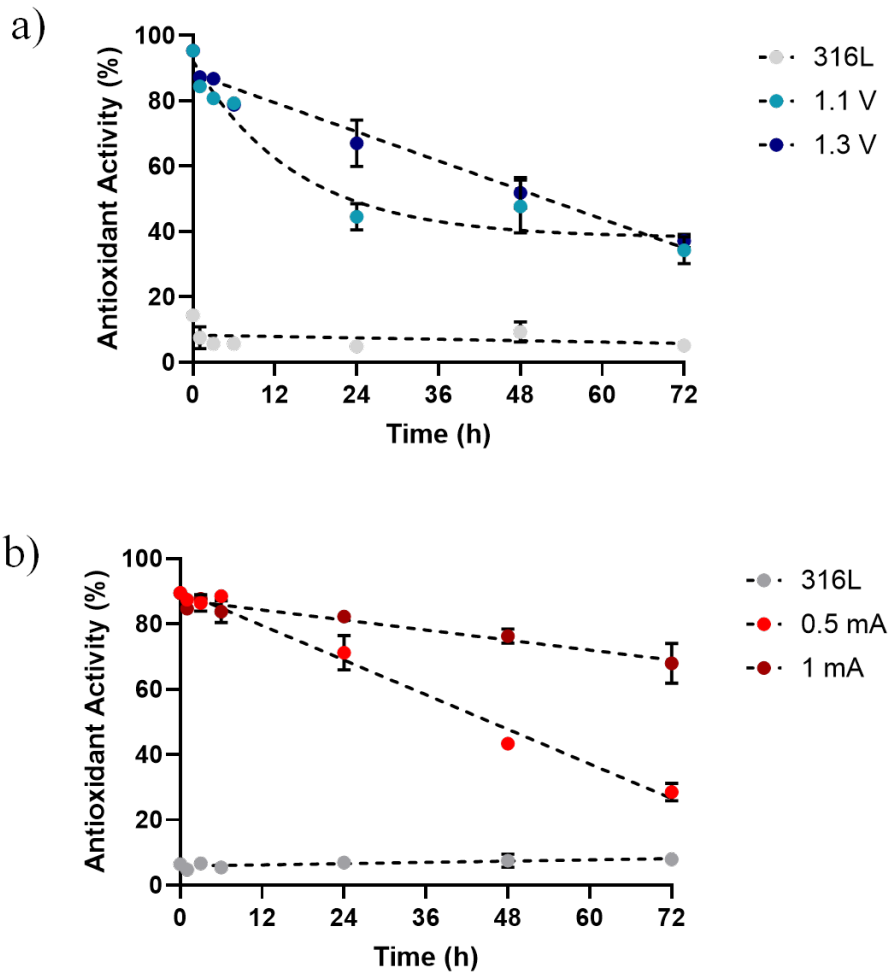

Supplementary Figure S5.4. DPPH scavenging activity after incubation in HCASMC Media of potentiostatic (panel a) and galvanostatic (panel b) PPy coatings. At every time point, all PPy coatings tested demonstrate better scavenging capacity compared with the bare 316L SS. All but 1.1 V potentiostatic coatings showed a linear depreciation in DPPH scavenging capacity. 1.1 V coatings exhibited an exponential decay in DPPH scavenging capacity. 1 mA coatings retained the greatest DPPH at 72 h. Data points represents average DPPH scavenging activity ± S.E.M (n=3).

a)

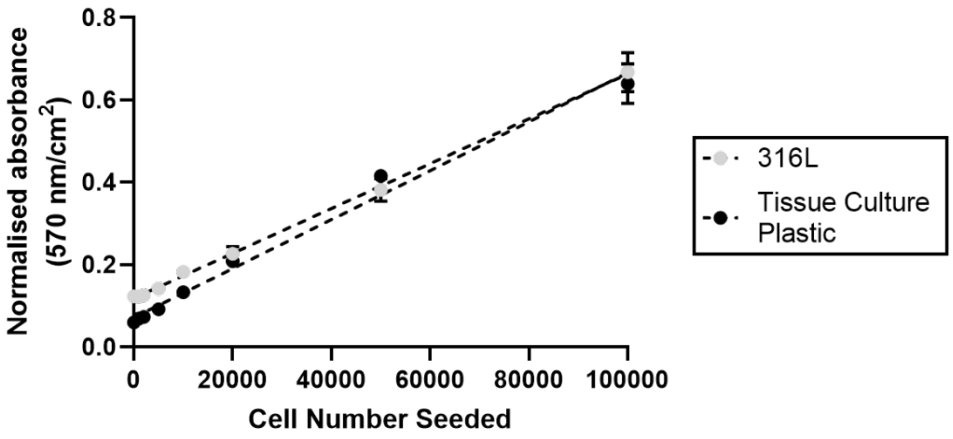

b)

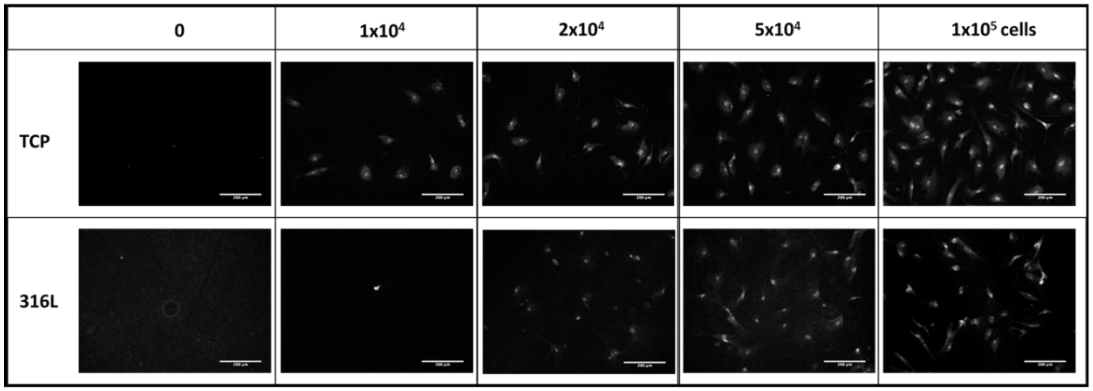

Supplementary Figure 5.5. Optimisation of cell viability assays with HCAECs. a) MTT assay of 316L SS and tissue culture plastic (TCP) attached cells after 24 h with increasing cell densities. Cell viability is comparable on both surfaces at all densities. b) Acridine orange staining of attached cells after 24 h on 316L SS and TCP. The number of attached cells increases comparably on both surfaces as seeding density is increased. This supports the MTT assay data.

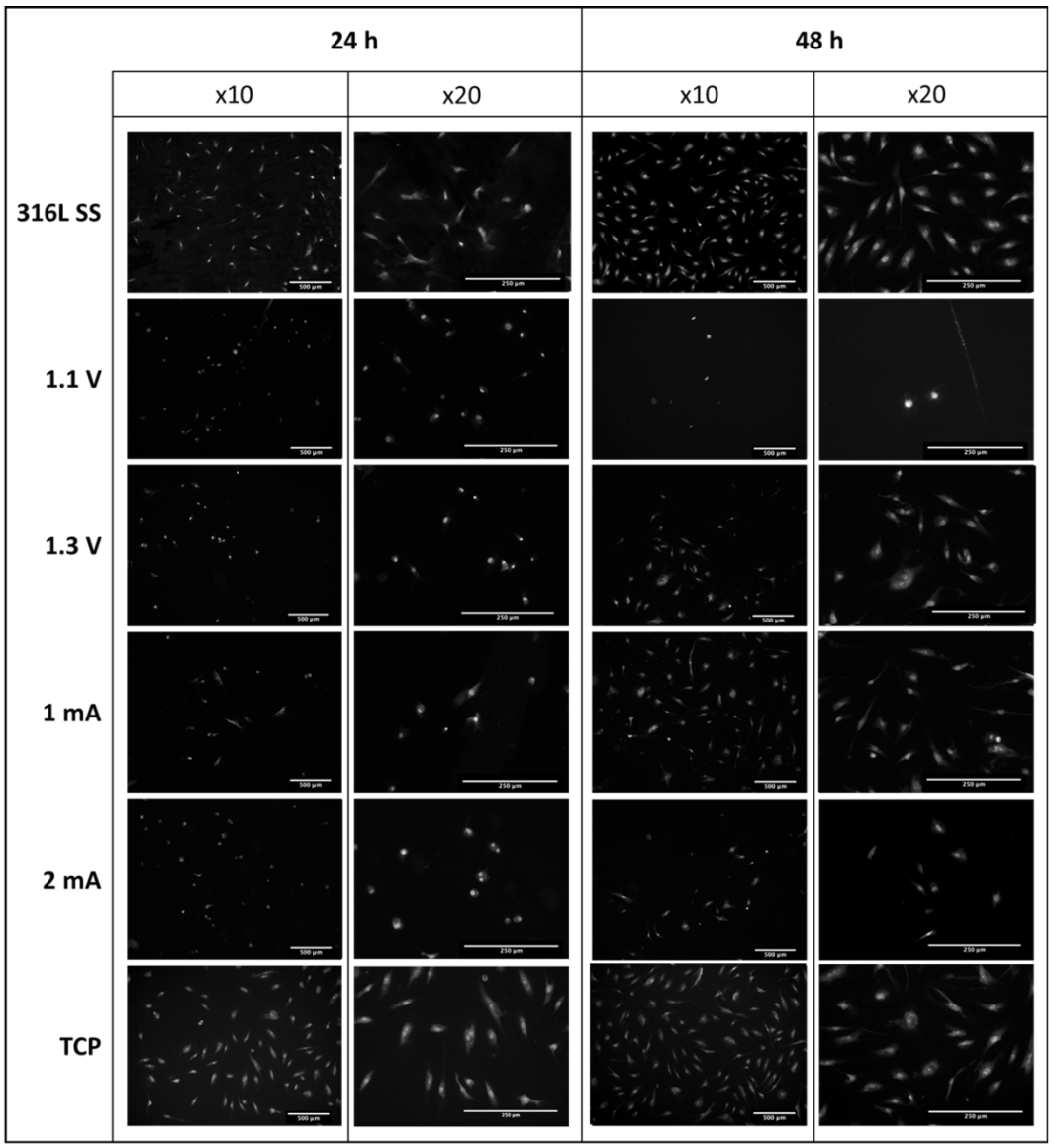

Supplementary Figure S5.6. Acridine orange staining of of HCAECs (5 x 10^4) seeded on PPy, 316L SS strips and tissue culture plastic (TCP). HCAECs show improved attachment on SS and TCP substrates than PPy and a high increase in cell density is observed on SS at 48 h, suggesting this surface is conducive to HCAEC proliferation. HCAEC attachment at 24 h appears reduced on PPy surfaces and attached cells are more rounded. At 48 h, an increased cell number was observed on 1 mA galvanostatic coatings and 1.3 V potentiostatic coatings. Images are taken from one experiment and representative of three independent samples.

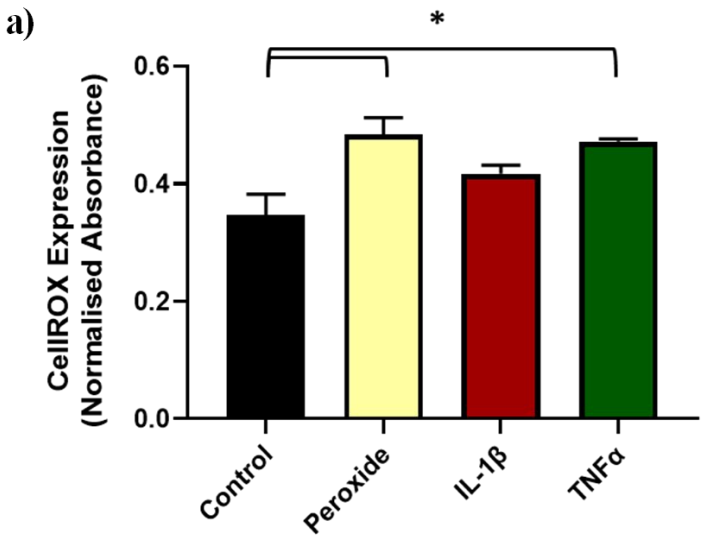

b)

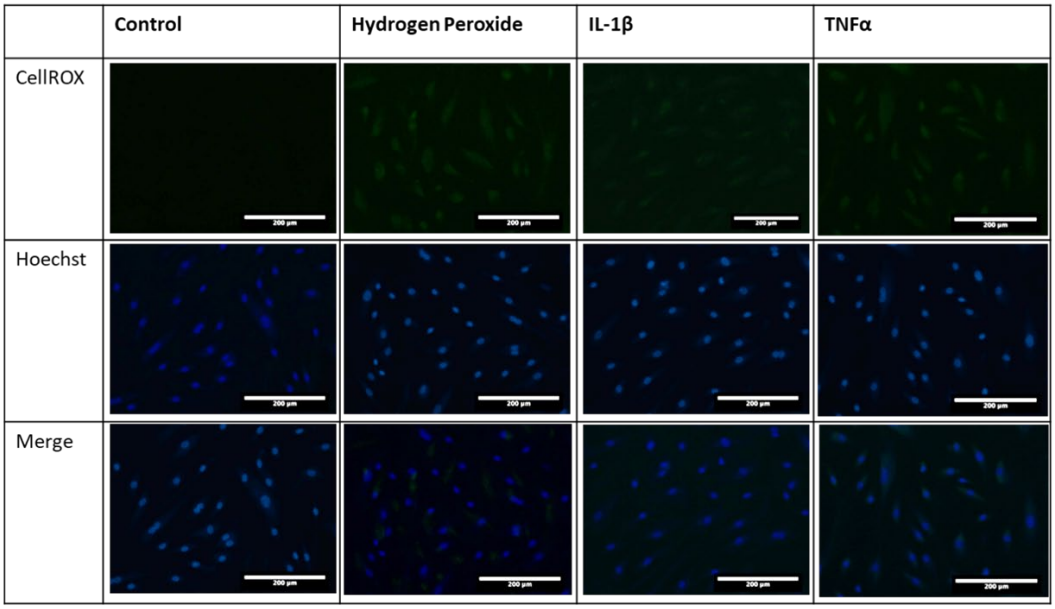

Supplementary Figure S5.7. Optimisation of the CellROX ROS generation assay. HCAECs were stimulated with 100 μM hydrogen peroxide, 10 ng/ml IL-1β and TNFα for 6 h and treated with CellROX Green for 30 minutes before fixing and counterstaining with Hoechst. a) Quantification of the CellROX signal normalised against Hoechst signal showing significant increases in intracellular ROS generation after stimulation with peroxide and TNFα (Control: 0.35±0.04, vs. Peroxide: 0.48±0.03, and TNFα: 0.47±0.00, One-way ANOVA and post-hoc Dunnett's, $p<0.05$, n=3). b) Representative immunofluorescence images of HCAECs stained with CellROX and Hoechst.

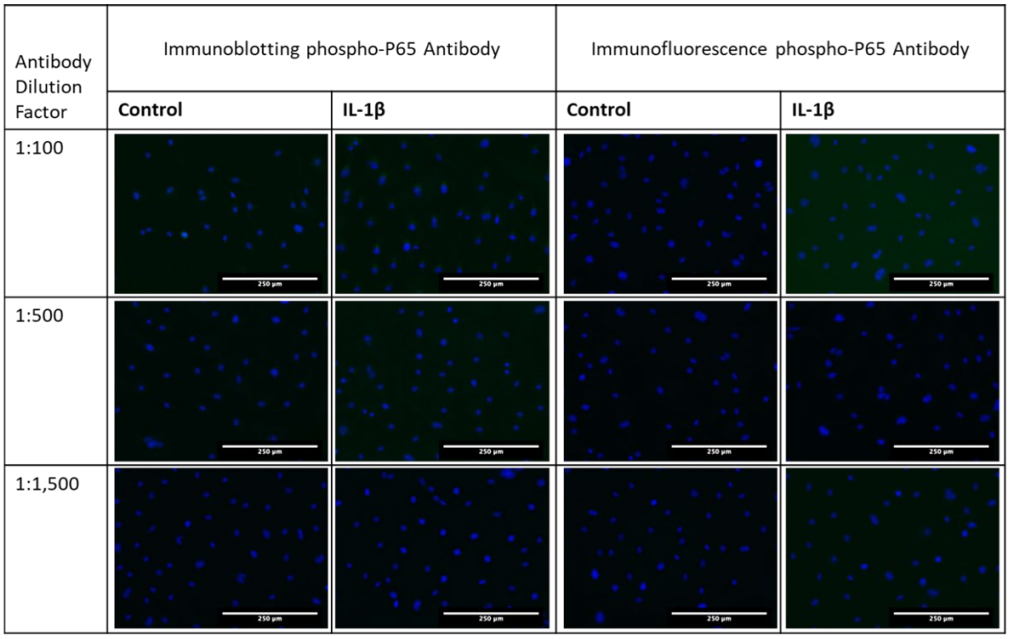

Supplementary Figure S5.8. Optimisation of the phosphorylated-P65 immunofluorescence. HCAECs were stimulated with 10 ng/ml IL-1β for 30 minutes and stained for phospho-P65 and Hoechst. Representative immunofluorescence images of cells stained using phospho-P65 certified for immunoblotting (Cell Signalling #3031) and immunofluorescence (Cell Signalling #3033) at 1:100, 1:500, 1:1,500 dilutions. Neither antibody offered strong fluorescent signals, but a stronger more specific signal was observed when using the immunoblotting certified antibody.

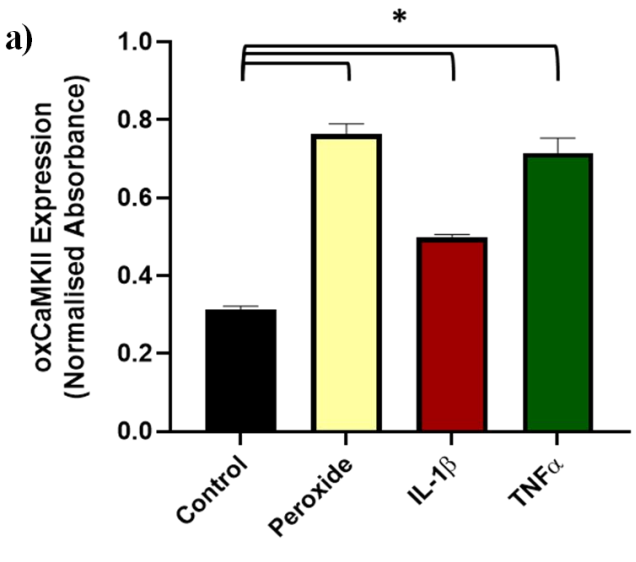

b)

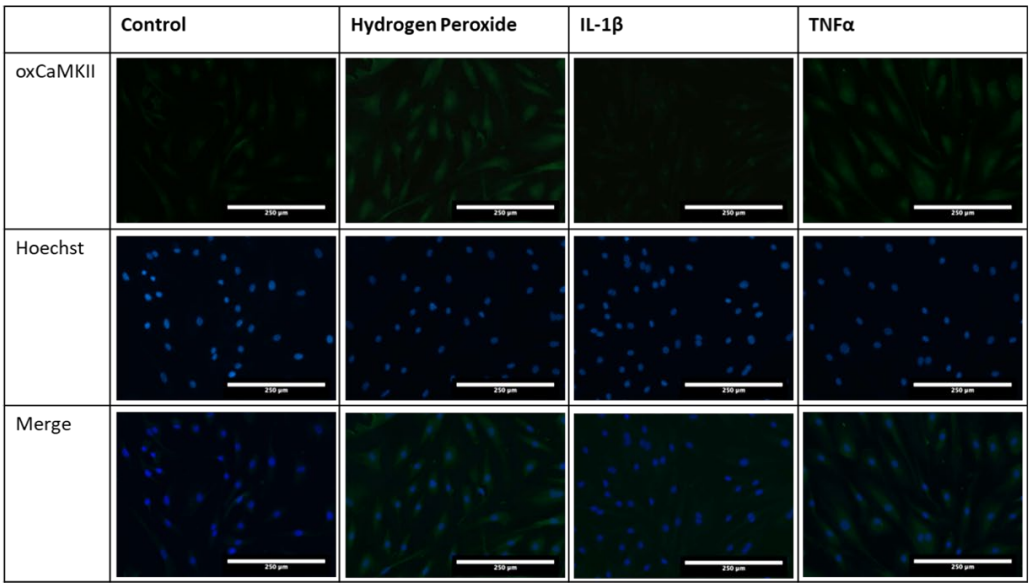

Supplementary Figure S5.9. Optimisation of the oxCaMKII immunofluorescence. HCAECs were stimulated with 100 μM hydrogen peroxide, 10 ng/ml IL-1β and TNFα for 6 h and stained for oxCaMKII and DAPI. a) Quantification of the oxCaMKII signal normalised against DAPI signal showing significant increases in CaMKII oxidation after stimulation with peroxide and TNFα (Control: 0.31±0.01, vs. Peroxide: 0.76±0.03, and TNFα: 0.71±0.04, One-way ANOVA and post-hoc Dunnett's, $p<0.05$, n=3). b) Representative immunofluorescence images of HCAECs stained for oxCaMKII and DAPI.